Standards, Applications and Quality Assurance in Medical Radiation Dosimetry (IDOS)

Proceedings of an International Symposium Vienna 9–12 November 2010

Vol. 2

ORGANIZED BY THE

International Atomic Energy Agency

IN COOPERATION WITH THE

American Association of Physicists in Medicine

Asia-Oceania Federation of Organizations for Medical Physics

Asociación Latinoamericana de Física Médica

Bureau International des Poids et Mesures

European Commission

European Federation of Organisations for Medical Physics

European Society for Therapeutic Radiology and Oncology

International Commission on Radiological Protection

International Commission on Radiation Units and Measurements

International Organization for Medical Physics

Institute of Physics and Engineering in Medicine

Society of Nuclear Medicine

United Nations Scientific Committee on the Effects of Atomic Radiation

World Federation of Nuclear Medicine and Biology

World Health Organization

STANDARDS, APPLICATIONS AND QUALITY ASSURANCE IN MEDICAL RADIATION DOSIMETRY (IDOS)

VOLUME 2

The Agency's Statute was approved on 23 October 1956 by the Conference on the Statute of the IAEA held at United Nations Headquarters, New York; it entered into force on 29 July 1957. The Headquarters of the Agency are situated in Vienna. Its principal objective is "to accelerate and enlarge the contribution of atomic energy to peace, health and prosperity throughout the world''.

PROCEEDINGS SERIES

STANDARDS, APPLICATIONS AND QUALITY ASSURANCE IN MEDICAL RADIATION DOSIMETRY (IDOS)

PROCEEDINGS OF AN INTERNATIONAL SYMPOSIUM ON STANDARDS, APPLICATIONS AND QUALITY ASSURANCE IN MEDICAL RADIATION DOSIMETRY (IDOS)
ORGANIZED BY THE INTERNATIONAL ATOMIC ENERGY AGENCY
IN COOPERATION WITH THE
AMERICAN ASSOCIATION OF PHYSICISTS IN MEDICINE,
ASIA–OCEANIA FEDERATION OF ORGANIZATIONS FOR MEDICAL PHYSICS,
ASOCIACIÓN LATINOAMERICANA DE FÍSICA MÉDICA,
BUREAU INTERNATIONAL DES POIDS ET MESURES,
EUROPEAN COMMISSION,
EUROPEAN FEDERATION OF ORGANISATIONS FOR MEDICAL PHYSICS,
EUROPEAN SOCIETY FOR THERAPEUTIC RADIOLOGY AND ONCOLOGY,
INTERNATIONAL COMMISSION ON RADIOLOGICAL PROTECTION,
INTERNATIONAL COMMISSION ON RADIATION UNITS AND MEASUREMENTS,
INTERNATIONAL ORGANIZATION FOR MEDICAL PHYSICS,
INSTITUTE OF PHYSICS AND ENGINEERING IN MEDICINE,
SOCIETY OF NUCLEAR MEDICINE,
UNITED NATIONS SCIENTIFIC COMMITTEE ON
THE EFFECTS OF ATOMIC RADIATION,
WORLD FEDERATION OF NUCLEAR MEDICINE AND BIOLOGY
AND THE WORLD HEALTH ORGANIZATION
AND HELD IN VIENNA, 9–12 NOVEMBER 2010

In two volumes

VOLUME 2

INTERNATIONAL ATOMIC ENERGY AGENCY
VIENNA, 2011

COPYRIGHT NOTICE

Marketing and Sales Unit, Publishing Section
International Atomic Energy Agency
Vienna International Centre
PO Box 100
1400 Vienna, Austria
fax: +43 1 2600 29302
tel.: +43 1 2600 22417
email: sales.publications@iaea.org
http://www.iaea.org/books

Printed by the IAEA in Austria
November 2011
STI/PUB/1514

IAEA Library Cataloguing in Publication Data

International Symposium on Standards, Applications and Quality Assurance in Medical Radiation Dosimetry (2010 : Vienna, Austria) Standards, applications and quality assurance in medical radiation dosimetry (IDOS) : proceedings of an international symposium, Vienna, 9–12 November 2010. — Vienna : International Atomic Energy Agency, 2011.
2 v. ; 24 cm. — (Proceedings series, ISSN 0074–1884)
STI/PUB/1514
ISBN 978–92–0–116210–6
Includes bibliographical references.

1. Radiation dosimetry — Congresses. 2. Radiation dosimetry — Standards. 3. Diagnostic imaging — Safety measures. 4. Radiation protection. I. International Atomic Energy Agency. II. Series: Proceedings series (International Atomic Energy Agency).

IAEAL 11–00712

FOREWORD

Ionizing radiation is employed in a wide variety of applications and processes in technologically advanced countries. Dosimetry is the science of measuring ionizing radiation and understanding it is essential for the safe and effective use of nuclear technology. Medical radiation dosimetry deals with those applications in which patients are irradiated.

These proceedings embody a selection of refereed papers that were presented at the International Symposium on Standards, Applications and Quality Assurance in Medical Radiation Dosimetry held in Vienna from 9 to 12 November 2010. More than 370 delegates representing 66 Member States, 45 observers and 12 international and professional organizations attended the meeting, at which 75 oral presentations were delivered, 4 round table discussions were held and 187 posters were presented.

Owing to its dual role in disseminating radiation measurement standards and verifying the accuracy of dosimetry applied at the hospital level, the IAEA is well positioned to convene international meetings focused on dosimetry. The previous meeting was held in Vienna in November 2002. Since then, three major developments have helped progress medical radiation dosimetry. Firstly, Member States have rapidly adopted new treatment technologies, e.g. intensity modulated radiotherapy (IMRT), and they have continued to acquire sophisticated diagnostic capabilities, e.g. computed tomography (CT) and positron emission tomography scanning. Unfortunately, the adoption of these technologies has not always been trouble-free. News stories in various countries have highlighted radiation accidents during IMRT due to dosimetric errors. In addition, overuse of CT scanning and failure to adopt clinical protocols appropriate to patient size, particularly in paediatric cases, have caused concern. Measurement of radiation dose properly necessitates adoption of new technologies and, consequently, much research has been devoted to improving dosimetry, particularly for the small fields typically used in IMRT.

Secondly, dosimetry protocols based on standards of absorbed dose to water, which simplified the translation of basic dosimetry from the standards laboratory to the hospital level, are 10 years old and need reviewing. There have been advances in dosimetry for both graphite and water calorimetry for external beam therapy and the strengthening of dosimetry for beams of protons and light ions, as their use is implemented clinically. Advances have also been made at primary laboratories to develop absorbed dose to water standards for brachytherapy sources that are inserted directly into patients. All these issues were addressed during the symposium.

Thirdly, there has been a rapid expansion in the level of diagnostic information for therapy planning, delivery and patient follow-up. New paradigms

have been created for more comprehensive quality assurance. Since auditing physical dosimetry is an integral part of quality auditing for the whole process of treating patients, one session focused on it. The ongoing need to optimize radiation doses justified a session on radiation protection dosimetry.

In addition to oral and poster presentations, four interactive, round table discussions were held, focusing on the consequences of dosimetry errors, dosimetry knowledge gaps for new technologies, the role of education and training to improve dosimetric understanding and the meaning of traceability in the dosimetric chain. A CD-ROM of the contributed papers accompanies these proceedings.

The IAEA gratefully acknowledges the contributions made by the Programme Committee, the collaborating organizations, and the session chairs, co-chairs and scientific reviewers.

EDITORIAL NOTE

CONTENTS OF VOLUME 2

CLINICAL DOSIMETRY IN X RAY IMAGING (Session 4)

EXTERNAL QUALITY AUDITS (Session 7)

CLINICAL DOSIMETRY X RAY IMAGING

(Session 4)

Chairpersons

A. TORRESIN
K. FAULKNER
European Federation of Organisations for Medical Physics

J. BOONE
International Commission on Radiation Units and Measurements

Co-Chairpersons

D.R. DANCE
European Federation of Organisations for Medical Physics

F. SHANNOUN
World Health Organization

D. McLEAN
IAEA

CALIBRATION OF KERMA AREA PRODUCT METERS WITH A PATIENT DOSE CALIBRATOR

P. TOROI*, M. HUSSO**, A. KOSUNEN*

* Radiation and Nuclear Safety Authority (STUK),
Helsinki
Email: paula.toroi@stuk.fi

** University Hospital of Kuopio,
Kuopio

Finland

Abstract

Kerma area product (KAP) meters used in X ray imaging for monitoring patient exposure were calibrated using different reference meters. Typically, the reference KAP value is the product of the air kerma and the X ray field size. In the tandem method, the reference value is measured with another KAP meter; in this study, a large KAP meter of novel type, the patient dose calibrator (PDC), was used for this purpose. The properties of the PDC meter were studied and the use of the meter as a reference meter was reviewed throughout the whole train of events from calibration in a secondary standard dosimetry laboratory to using the meter in clinical situations. Compared to conventional KAP meters, the advantages of the PDC are the lower energy dependence of response and the possibility to use larger field sizes. In laboratory measurements, the properties of the PDC meter were proved suitable to be used as a reference meter. The uncertainty related to the differences in X ray tube output used in calibration at the laboratory and in measurements at the clinic is highlighted. The calibration coefficients for field KAP meters calibrated by the PDC meter and by other meters were congruent on the average within 4%. Clinical measurements emphasized the need for in situ calibration of clinical KAP meters. Particularly in the under-couch situation, the calibration should be performed with the couch in the beam.

1. INTRODUCTION

Kerma area product (KAP) meters are used for monitoring patient exposure during X ray imaging. In many studies, it has been observed that there is a real need for a calibration of KAP meters [1–7]. Field KAP meters are attached to the X ray system, and their calibration should preferably be performed using this clinical set-up [3, 8]. Internationally, a relative uncertainty not higher than 7%

(confidence level 95%) is recommended for air kerma and KAP measurements [8, 9]. To achieve an appropriate measurement accuracy and comparable results, the use of an adequate calibration method is essential.

The IAEA introduces three options for calibrations of field KAP meters [9]:

(i) Calibration of a KAP meter in laboratory;
(ii) Calibration of a KAP meter in situ using a reference air kerma meter;
(iii) Calibration of a KAP meter in situ using a reference KAP meter.

The use of a reference KAP meter was studied by Toroi et al. and named as a tandem calibration method [3]. The main drawback of the tandem method is the relatively large uncertainty produced by the pronounced energy dependence of the response of conventional type of KAP meters used as a reference instrument [4]. The patient dose calibrator (PDC) meter has a lower energy dependence, and a reduced uncertainty can be expected for the calibration of field KAP meters when using a PDC as a reference instrument [10]. In this study, the use of a large, novel PDC meter as a reference KAP meter in tandem method is studied and compared to the other calibration methods.

2. MATERIALS AND METHODS

2.1. Reference meters

The patient dose calibrator PDC (Radcal, USA) version 1.10 is a large transmission ionization chamber with a cross-sectional area of 30 cm × 30 cm that can be used to measure either the air kerma or the KAP. In this study, only the KAP measurement mode was used. The transmission windows of the PDC are not light transparent. The meter is designed to be used for quality assurance measurements of the X ray equipment, without the patient. The PDC detects radiation both from the front and the rear sides so it cannot be used directly on the patient couch without the effect of backscatter from the support. The meter has separate measurement modes for low and high KAP rates, and the technical specifications of the PDC (manual 2008) quote a rated KAP rate range of 1–11 040 $\mu Gy \cdot m^2 \cdot min^{-1}$ for the low rate mode and from 2103 to 910 500 $\mu Gy \cdot m^2 \cdot min^{-1}$ for the high rate mode. The other types of reference meters in this study were a cylindrical ionization chamber (Radcal, model 10X5-6, 6 cm^3) and a conventional type of KAP meter (PTW, Diamentor M4, dimensions 15 cm × 15 cm). For the reference PDC and the conventional KAP meter, the central electrode of the chamber was used as the reference plane for the measurements

2.2. Calibration of reference meters

All reference meters were calibrated for incident beam in the secondary standards dosimetry laboratory (SSDL) of STUK. The X ray system at the laboratory consists of a Seifert Isovolt 160 HS X ray generator and an MB 161/4 X ray tube with a tungsten anode of 20º target angle and an inherent filtration of 1 mm Be. The system includes also a set-up for added filtration and a transmission monitor chamber (PTW 786). The reference distance from the focal spot is one meter and the diameter of the radiation beam, without separate KAP collimation, at this distance is 14.5 cm. Radcal 10X5-6 air kerma chamber was calibrated at that distance and in an open field. The reference air kerma rates at 1 m focus distance were measured using STUK's working standard, an A3 Exradin Shonka-Wyckoff spherical ionization chamber (Standard Imaging, USA) with a calibration traceable to PTB (Germany).

An additional set-up was used for calibration of PDC and Diamentor meters. More details on the calibration method for conventional KAP meters can be found in other publications [3, 9]. For the calibration of the PDC reference chamber, an additional 5 mm thick lead collimator (KAP collimator) was used at the distance of 100 cm from the focal spot. The distance between the KAP collimator and the front surface of the PDC chamber was 5 cm. The diameter of the circular aperture of the KAP collimator was 56.6 mm. For the PDC, apertures of 40 mm and 80 mm and larger, and 10 cm and 20 cm collimator–detector separations, were also used to study the effects of the field size. In these measurements, the diameter of the circular X ray field on the surface of the PDC ranged from 42 mm to 96 mm. The scatter to the PDC meter from outside the collimated X ray beam was measured with closed beam aperture at the KAP collimator.

High KAP rates could not be reached in the calibration laboratory and all laboratory measurements were made using the low KAP rate mode of the PDC. The calibration was performed with IEC standard RQR radiation qualities [11], with tube voltages from 40 kV to 150 kV and filtrations from 2.6 mm Al to 4.5 mm Al. Clinical radiation qualities were produced by using two fixed filtrations: of 5 mm Al and 4 mm Al + 0.2 mm Cu with tube voltages of 50, 70, 90, 120 and 150 kV. To test the repeatability of the PDC meter, the measurement with the radiation quality RQR 5 were repeated ten times. RQR 5 radiation quality was also used for the measurements with different field sizes.

2.3. Calibrations of clinical KAP meters

2.3.1. Methods

Reference meters were used for calibrations of the field KAP meters of clinical X ray equipment. Three field KAP meters in three clinical type X ray equipment were investigated and different calibration methods were compared.

The laboratory method was applied for a portable field KAP meter, which was calibrated in the laboratory for transmitted beam, and a correction for extra focal scattered radiation and specific to the clinical X ray unit was used. This correction requires measurements with the KAP chamber attached to the clinical X ray system in the position where it is normally used and in another position further down the beam (in this case at 30 cm distance from the focus). In this paper, only the unit specific corrected results from the previous study [3] were used.

In a beam area method, the KAP reference value was determined as a product of the measured air kerma and the beam area at the same focus distance. The air kerma was measured at the centre of the radiation field with the Radcal 10X5-6 chamber, and the beam area was obtained from a digital image. A scale rod was used to calculate the beam size from the resized image. The inverse square law was applied to convert the beam area and air kerma values to their values in the reference plane.

As the tandem method was used, the reference KAP value was either measured with the Diamentor KAP meter or with the PDC and the X ray beam was centred inside the collecting area of the reference meter used.

2.3.2. Clinical systems

2.3.2.1. STUK system

A clinical type of X ray equipment was used in the SSDL of STUK. The X ray equipment has a CPI, Indico 100 generator with a Comet DI 10 HS-22/52-150 X ray tube. The type of the field KAP meter was a Diamentor M4 (PTW, Germany). In the previous study by Toroi et al. [3], the calibration for this meter was performed with laboratory and beam area methods and the tandem method with a conventional KAP meter as a reference meter. In this study, the calibration is performed for the same set-up with the tandem method, but now using the PDC meter as a reference meter.

The total filtration of all radiation qualities was 4.8 mm Al, and tube voltages were in the range 40–150 kV. The tube current was 100 mA and the irradiation times varied from 20–400 ms generating KAP rates in the range

770–23400 μGy·m^2·min^{-1}. The distance between the central electrodes of the field KAP chamber and the reference chamber was 30 cm. For the PDC the field size was 10 cm × 10 cm at the reference chamber position. For X ray tube voltages from 60 kV to 100 kV, the PDC was used in both the low and the high KAP rate modes.

To determine the repeatability of the PDC measurements in the low and high KAP rate modes, the measurements with a 80 kV radiation quality were repeated ten times in both modes. The KAP rate was close to 6000 μGy·m^2·min^{-1}, which is according to the manufacturer's instructions, a suitable rate to be measured with both modes. In these measurements, the field meter was used to monitor the X ray beam stability.

Compared to the previous work by Toroi et al., the field size dependence test was extended to larger field sizes [3], as square fields from 2.5 cm to 25 cm were used. The field size was varied by the collimator aperture, while keeping the distance between the chambers at 30 cm. The tube voltage was 80 kV.

The effects of the distance between the field KAP chamber and the reference PDC were studied over a range from 1.7 cm to 100 cm. At a 30 cm distance from the field meter, the field size was 10 cm × 10 cm. For comparison, the attenuation in air was estimated using the Spektripaja program [12]. The low KAP rate mode and a tube voltage of 80 kV were used in these measurements.

2.3.2.2. KUH 1

The measurements were performed at the University Hospital of Kuopio (KUH) using an interventional X ray system, Siemens Axion Artis Zee Ceiling, which is mainly used for peripheral angiography and vascular interventions. The typical tube voltage range is 70–125 kV. The fixed filtration is 2.5 mm Al, and the available additional filtrations range is 0.1–0.9 mm Cu. Typically, the system is used in under-couch conditions in which vase the beam is attenuated and filtered by the couch and the mattress. The Diamentor KAP meter (PTW, Germany) is included and fixed into the system.

The calibration was performed with the beam area method and the tandem method with the PDC. Tube voltages of 60, 70, 81 and 96 kV with no additional copper filtration and with a small focal spot size were used. Measurements were made in the low KAP rate mode of the PDC. The calibration with this system was performed in the under-couch position with the table and mattress between the field and the reference meter, and in horizontal beam direction when the couch was not in the beam. The foam support provided together with the PDC meter was used to place the PDC meter at 17 cm distance from the table top. The focal spot to the reference chamber distance was 70 cm.

For the beam area method, the field size (12.3 cm × 12.3 cm) was measured with a CR cassette placed on the table at a distance of 53 cm from the focal spot. The field size was converted to that at the distance of air kerma measurements using the geometry from the focus. In the calibration without the patient couch, the distance of the reference meter from the focal spot was 78 cm.

2.3.2.3. KUH 2

The other clinical system at KUH was the Kodak Directview DR 7500 direct digital X ray equipment with an X ray tube of type Varian RAD-60. This system is used for general native X ray examinations. The fixed filtration was 3.34 mmAl and additional filtrations of 0, 1 mm Al, 1 mmAl + 0.1 mm Cu and 1 mm Al + 0.2 mm Cu were available and in use. In this system, the KAP meter (Diamentor, PTW) is permanently built into the system.

The calibration was performed with the beam area method and the tandem method using the PDC and the Diamentor as reference meters. In the calibration with the PDC all available filtrations and tube voltages of 50, 70, 90 and 120 kV were used. The PDC was used in the high KAP rate mode. Calibration with other reference meters was performed with the same tube voltages and no added filtration. The distance of the reference meter was 60 cm from the focal spot and 30 cm from the front window of the collimator housing. The field size at this distance was 10 cm × 10 cm.

3. RESULTS

3.1. Calibration and properties of PDC

In laboratory measurements, the repeatability of the PDC measurements with a RQR 5 radiation quality is 0.1%.

When measuring with the closed beam aperture, the scattered radiation outside the KAP collimator area has an effect on the large area PDC ionization chamber. The contribution by the scattered radiation to the reference KAP value is 2.5–5.5%, depending on the radiation quality. All results were corrected based on these measurements.

The maximum difference of the calibration coefficients of the PDC is 1.2% when using different distances between the KAP collimator and the meter. However, when the distance from the collimator is increased, the air attenuation will also affect the results. At a 5 cm distance and at different apertures, the maximum difference in calibration coefficients is 0.3%, which is within the uncertainty of the measurement.

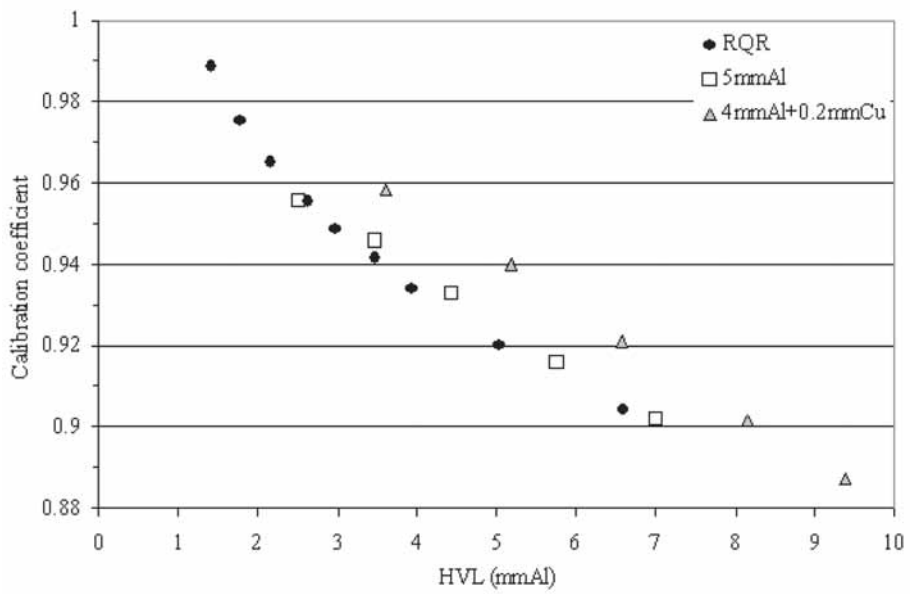

FIG. 1. Calibration coefficients for PDC meter for incident X ray beam as a function of the HVL and with different beam qualities.

The calibration coefficients of the PDC are presented in Fig. 1 for different radiation qualities. Within the presented range of radiation qualities, interpolations based on the half value layer (HVL) can be made with a maximum deviation of 2%.

3.2. Calibrations of clinical KAP meters

3.2.1. STUK

In the repeated measurements, the field KAP meter of STUK system gives almost constant results; it can therefore be assumed that the output the X ray system is stable from one shot to another. The maximum deviation for these KAP values is 0.02 $\mu Gy \cdot m^2 \cdot min^{-1}$ and the relative standard deviation for 20 measurements is 0.06%. Concerning the PDC, it was observed that the average KAP value is 2% higher for the high KAP rate mode (10.40 $\mu Gy \cdot m^2 \cdot min^{-1}$) than for the low KAP rate mode (10.19 $\mu Gy \cdot m^2 \cdot min^{-1}$). Also, the standard deviation is higher for high KAP rate mode (2.4%) than for low KAP rate mode (0.1%).

In Fig. 2, the calibration coefficients of the field KAP meter from the calibration with the PDC are compared with the previous results of the other

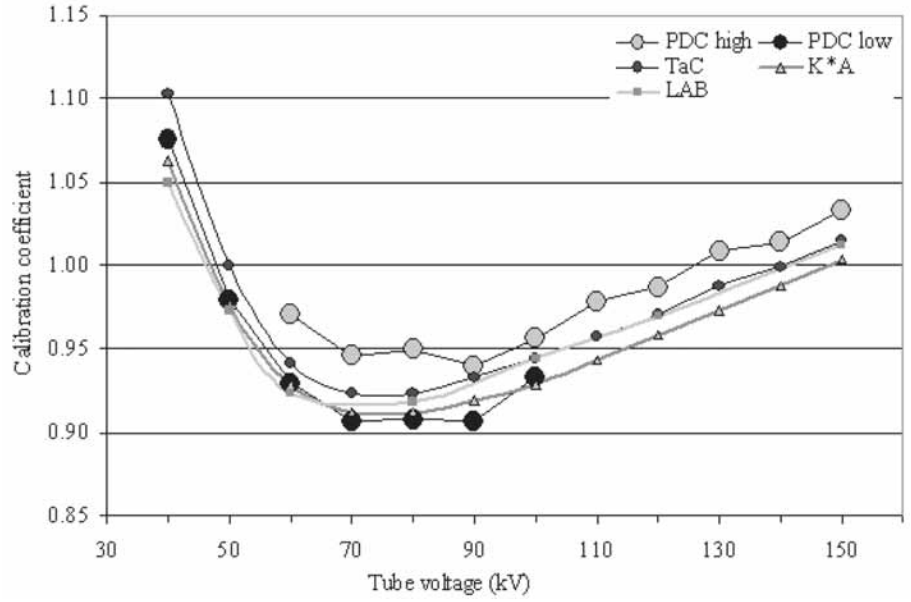

*FIG. 2. Calibration coefficients for a field KAP meter (Diamentor) calibrated with different methods: tandem method with a conventional KAP meter as a reference meter (TaC), beam area method (K*A) and laboratory method (LAB) (see description of the equipment and methods in the text). Results for the PDC were obtained in this study and the other results are from a previous study [3]. Calibration was performed in the low and high KAP rate modes of PDC, total filtration is 4.8 mm Al.*

calibration methods. For the intermediate KAP rates (2103–11 040 $\mu Gy \cdot m^2 \cdot min^{-1}$), either of the selectable the KAP rate modes can be used for the PDC. The calibration in the low KAP rate mode gives very similar results with respect to other methods, while the results for high rate mode are on the average 4% higher. The PDC meter was calibrated in the SSDL laboratory in the low rate mode; the calibration coefficients obtained in this mode were also used for the high rate mode.

The variation of the calibration coefficients of a field KAP with field size when using the PDC as a reference instrument is presented in Figure 3. The standard and maximum deviations are 1.4% and 6.2%, respectively. In these measurements, the air kema rate is relatively constant, but the KAP rate is changing. The field size dependence of the calibration coefficient is affected both by the reference and the field instruments. With the largest field size (25 cm × 25 cm), a large variation (8%) was observed, which may be related to small differences in placement of the PDC. With the largest field size, the

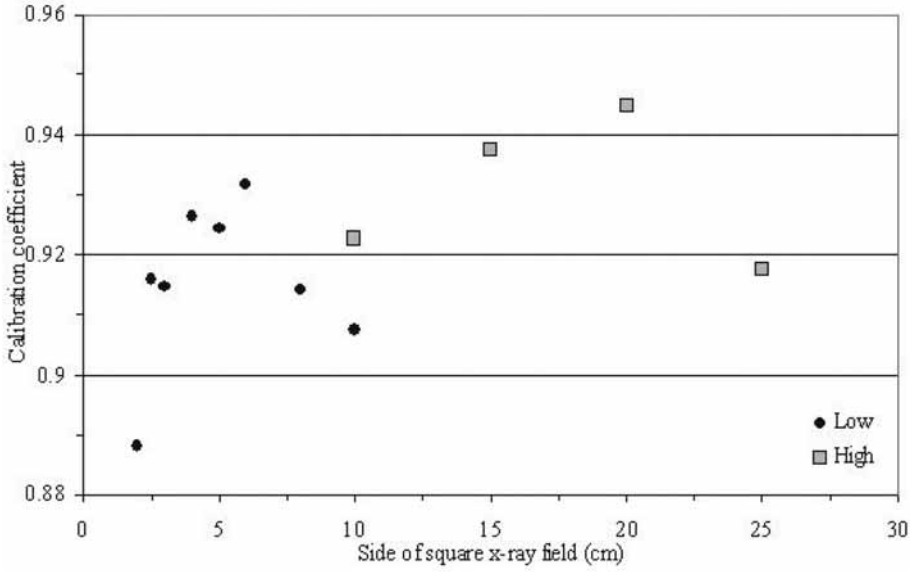

FIG. 3. Calibration coefficients of field KAP meter (Diamentor) for different field sizes. Low and high KAP rate modes are used for the reference meter (PDC). Tube voltage is 80 kV and total filtration is 4.8 mm Al.

penumbra area and possible other tails in the beam may easily lay outside of the collective area of the PDC.

The results at different distances between the field KAP meter and the PDC are shown in Fig. 4. For both the field KAP meter and the PDC, the KAP value decreases with increasing distance, as expected because of the decrease of scattering between the meters. The effect of backscattering from the PDC to the field meter is <1% at 30 cm and negligible at a distance of 50 cm. The decrease of the value with the PDC meter is a combination of decreased scattering and the attenuation in air.

3.2.2. KUH 1

The results of the calibration at the KUH 1 system with the beam area method and the tandem method with the PDC as a reference are presented in Fig. 5. The difference of calibration coefficients of the field KAP meter between the two methods is 3.5% on the average. The calibration coefficients are close to 0.5 with the X ray tube in under-couch position and close to 0.8 in over-couch situation, indicating air kerma attenuation of 35–40%.

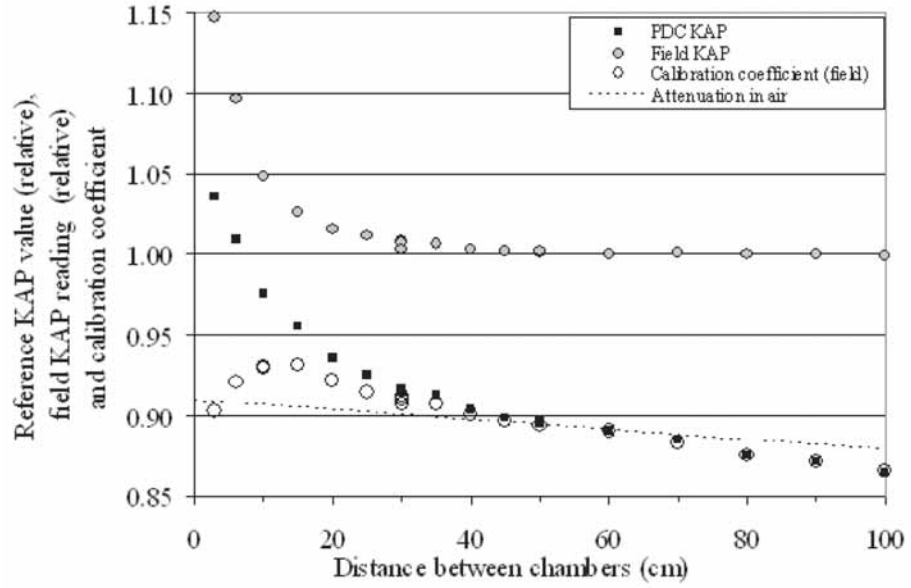

FIG. 4. Calibration results of KAP meters for different distances between the field (Diamentor) and reference chamber (PDC). KAP values are normalized by 9.68 μGy·m^2. The STUK system with a tube voltage of 80 kV and total filtration of 4.8 mm Al is used. The field size is 10 cm × 10 cm at 30 cm distance from field meter.

3.2.3. KUH 2

The calibration coefficients for field KAP meter of KUH 2 system obtained with three different methods for a large range of clinical radiation qualities are presented in Fig. 6. The maximum difference between the methods, when no additional filtration is used, is on average 3.1%. The results for different filtrations and PDC as a reference meter highlight the energy dependence of the response of the field KAP meter.

3.3. Uncertainties

The estimated uncertainties are expressed as expanded total relative uncertainties, k = 2 (confidence level 95%) [13]. The estimated uncertainties for different methods are summarized in Table 1. Individual numbers are discussed here only as a comparison to the previous estimation [3].

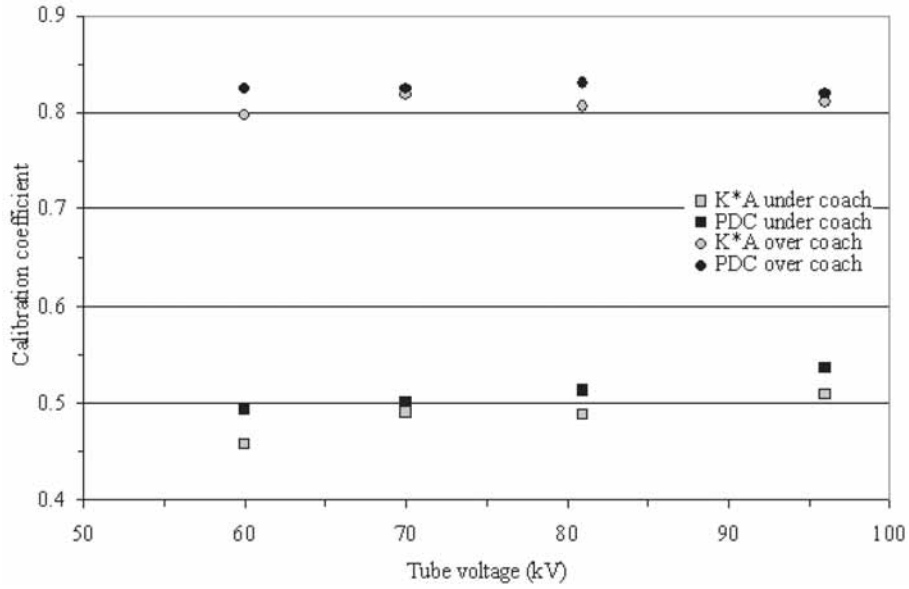

FIG. 5. Calibration coefficients for the field KAP meter (Diamentor) of KUH 1 system for under- and over-couch X ray tube positions. Calibration was performed with the beam area method and the tandem method using the PDC as a reference meter.

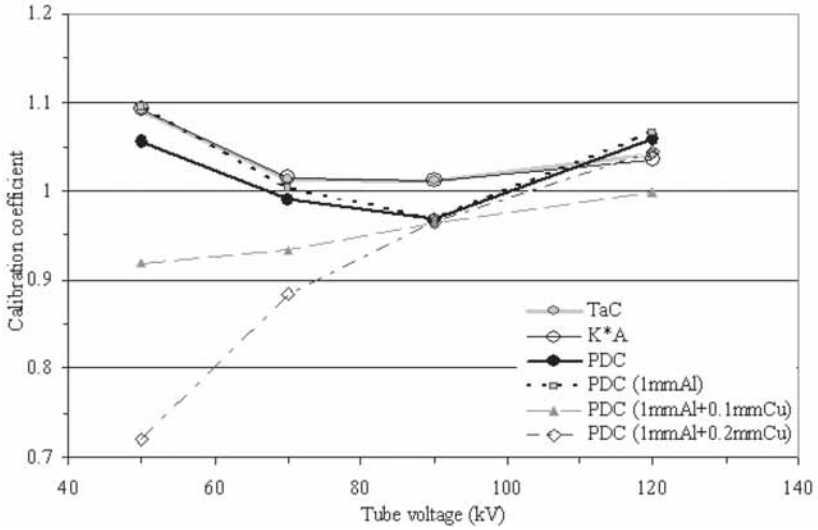

*FIG. 6. Calibration coefficients for KUH 2 field KAP meter (Diamentor) with different additional filtrations (in brackets) and tube voltages. With no additional filtration, the calibration was performed with the beam area method and with the tandem method using both the PDC meter and the conventional KAP meter as a reference. TaC: tandem method with a conventional KAP meter as a reference meter, K*A: kerma area method.*

TABLE 1. RELATIVE UNCERTAINTIES FOR THE CALIBRATION OF THE FIELD KAP METERS WITH DIFFERENT METHODS

	Relative uncertainty (%) k = 2		
Source of uncertainty	Tandem method: PDC	Tandem method: Conventional KAP meter	Beam area method
Calibration coefficient of the reference meter	3.0	3.0	3.0
Difference between the radiation qualities in the calibration and use of the reference meter	3	5	1
Reading of the reference meter	1.5	1.5	1.5
Reading of the field KAP meter	1.5	1.5	1.5
Deviations from the applied air density corrections (two different chambers)	2	2	2
Field area measured from the digital image			4
Distance correction factor			2
Effects of field inhomogeneities			4
Stray radiation and other uncontrolled factors of the method	1.5	1.5	1.5
Total relative expanded uncertainty	5.4	6.7	7.5

Note: See main text for full description of the methods and equipment.

Based on the previous calculations [3], the relative uncertainty of the calibration coefficient for the PDC is 3%. The results of this study confirm this estimation. The calibration coefficients and the energy dependence pertain only

to low KAP rate mode. To be able to estimate the uncertainties for the high KAP rate mode, more measurements are needed.

Indicated by the results, the HVL can be used as a radiation quality specifier for the PDC with an uncertainty of 2%. However, in clinical situations, the HVL is not necessarily known, and the determination of the calibration coefficient may need to also take into account the total filtration and the X ray tube voltage. This determination is not straightforward. For example, the filtration and beam hardening effects due to the patient couch are not well known. Therefore, it is estimated that the difference between the radiation qualities in the laboratory and in clinical situation produces an uncertainty of 3% when selecting the appropriate calibration coefficient for the PDC meter. For the tandem method with a conventional KAP meter, the uncertainty associated with differences in calibration and clinical radiation qualities is estimated at 5% for the entire range of radiation qualities. However, to achieve this accuracy level with a conventional KAP meter, a comprehensive calibration for clinical radiation qualities is needed. This does not include the uncertainties related to interpolations by HVL alone as the radiation quality specifier.

For the beam area method, all the uncertainty values are the same as in the previous study [3]. However, in clinical situations, accurate measurements of the distance and the beam area are not always very accurate. For an assessment of the uncertainty of a measurement, the uncertainties associated with these input parameters need to be considered appropriately.

4. DISCUSSION

4.1. Calibration and properties of PDC

Based on the measurements at the SSDL, the basic dosimetric properties of the PDC indicate that the meter is suitable for reliable dosimetry. However, only characteristics of one individual PDC were studied.

The energy dependence of the response is similar to what was found previously [10]. The dependence is much lower than that of conventional KAP meters, and the HVL can be used to interpolate the calibration coefficient with uncertainties within 2%. This means that measurements with an acceptable uncertainty can be performed for practically all clinically used radiation qualities with an instrument calibrated for standard radiation qualities and performing the required interpolations of calibration coefficients based on HVL. However, for use in clinical radiation, qualities with higher energies extended over an energy range of radiation qualities are needed [14].

There are some special issues in the calibration of the large PDC meter compared to that of air kerma meters and conventional KAP meters. In this study, a small range of field sizes was used and the range of the field size should be expanded to be able to test the large ionization chamber of the PDC meter more comprehensively. The uniformity of the response of the PDC meter could be tested with a smaller field moved to various locations. However, these results should not be used as a basis for a calibration because, typically, the X ray beam is centered in the KAP ionization chamber and the possible variations in response at the border area of the chamber could influence the measured KAP value only in a minor way.

Owing to the large area of the PDC chamber, it has also strengthened sensitivity to scattered radiation. Although the air kerma rate is low outside the primary beam, this may cause up to a 5.5% effect on measurements. The size of the KAP collimator or the distance between collimator and PDC should be larger than that used in this study to avoid this scattered radiation. Furthermore, the scattered radiation produced by the whole X ray facility should be minimized.

4.2. Calibrations of clinical KAP meters

The proper set-up parameters for the geometry used in tandem calibration with the PDC were studied with the STUK X ray system. In calibrations at different distances between the field and reference meter, it was observed that the field KAP meter detects backscattered radiation from the PDC even at a 30 cm distance. Using larger distances, e.g. 50 cm, would reduce the influence of scattered radiation. In a previous study, 30 cm was recommended as a minimum distance for conventional reference KAP meters. The higher amount of backscatter with the PDC meter than with the conventional KAP meter as a reference meter could be due to larger field sizes used for PDC and differences of materials and dimensions of these two types of KAP ionization chamber. Because the same X ray beam passes through both the field and the reference KAP chambers, the nominal size of the beam in the calibration is not critical for the accuracy of calibration. However, it is important to ensure that the whole beam, including the penumbra area, is inside the effective area of the PDC meter. The generally recommended field size of 10 cm × 10 cm is an appropriate choice for this meter.

For intermediate KAP rates, up to 5% difference was detected between the results of the high and low KAP rate modes. This must be considered by the user in the actual clinical measurements. The effect may even be larger for KAP rates under calibration conditions in a laboratory and in clinical situations. As a consequence, in the high KAP rate mode, several repeated measurements may be required for lower KAP rates to get an acceptable statistical uncertainty.

Generally, the calibration coefficient for a dosimeter is valid only for the specified range or mode and this fact applies also to the PDC and the KAP rate mode used.

In all clinical calibrations, the results with different methods were congruent within 4%. For calibrations of a field KAP meter, the use of a reference KAP meter allows to decrease the uncertainty of the calibration coefficient below 7% (2 SD), and with the PDC, even lower due to the relatively low energy dependence of the response of the PDC.

Independently of the calibration method and the reference dosimeter, the recommended accuracy of 7% [8, 9] may be difficult to achieve in the actual clinical KAP measurements. The need for in situ calibration is highlighted. Large enhancement in accuracy is achieved in measurements if the calibration is performed at least with one radiation quality in situ. In the KUH 1 system, and for a radiation quality with 60 kV, the presence of the couch in the beam caused up to 40% air kerma attenuation. For the under-couch position, the calibration coefficient was close to 0.5. This system is typically used as an under-couch system, but since the KAP meter of the system was not adjusted to this situation, the patient exposure is overestimated. A proper adjustment of the KAP range prior to the patient exposure is especially important if the KAP is used as a limiting value for the irradiation of the patient.

For the KUH 2 system, the adjustment of the meter was performed in such a way that the calibration coefficient was close to one. The energy dependence of the response of this field meter was about 20% for the range of clinically used radiation qualities. If more accurate results are required in calculations of patient exposure, the use of different calibration coefficient for different radiation qualities is needed.

5. CONCLUSIONS

Three different calibration methods gave similar results. The need for clinical in situ calibrations of KAP meters is emphasized and a more extensive calibration with a range of calibration coefficients is needed for accurate calculation. In calibrations of field KAP meters with the PDC the field size could be extended to larger sizes. Also, for the tandem method and for comparing the use of conventional KAP meter as a reference instrument, a larger distance between the field and the reference PDC meter should be chosen. The effect of differences in the air kerma and the KAP rates under calibration and in clinical use should be studied at greater depth for this PDC and other KAP meter types.

ACKNOWLEDGEMENT

This work is a contribution to the IAEA collaborative research project E2.10.08, the objective of which is the development of advanced dosimetry techniques for diagnostic and interventional radiology.

REFERENCES

[1] LARSSON, J.P., PERSLIDEN, J., SANDBORG, M., ALM CARLSSON, G., Transmission ionization chambers for measurements of air collision kerma integrated over beam area. Factors limiting the accuracy of calibration, Phys. Med. Biol. **41** (1996) 2381–2398.

[2] LARSSON, J.P., PERSLIDEN, J., SANDBORG, M., ALM CARLSSON, G., Ionization chambers for measuring air kerma integrated over beam area. Deviations in calibration values using simplified methods, Phys. Med. Biol. **43** (1998) 599–607.

[3] TOROI, P., KOMPPA, T., KOSUNEN, A., A tandem calibration method for kerma area product meters, Phys. Med. Biol. **53** (2008) 4941–4958.

[4] TOROI, P., KOMPPA, T., KOSUNEN, A., TAPIOVAARA, M., Effects of radiation quality on the calibration of kerma area product meters in x-ray beams, Phys. Med. Biol. **53** (2008) 5207–5221.

[5] JANKOWSKI, J., DOMIENIK, J., PAPIERZ, S., PADOVANI, R., VANO, E., FAULKNER, K., An international calibration of kerma–area product meters for patient dose optimisation study, Rad. Prot. Dosim. **129** (1–3) (2008) 328–332.

[6] HETLAND, P.O., FRIBERG, E.G., ØVREBØØ, K.M., BJERKE, H.H., Calibration of reference KAP-meters at SSDL and cross calibration of clinical KAP-meters, Acta Oncologica **48**(2) (2009) 289–294.

[7] LARSSON, J.P., Calibration of ionization chambers for measuring air kerma integrated over beam area in diagnostic radiology, Factors influencing the uncertainty in calibration coefficients, PhD Thesis, Linköping University, Sweden (2008).

[8] INTERNATIONAL COMMISSION ON RADIATION UNITS AND MEASUREMENTS, Patient dosimetry for x-rays used in medical imaging, ICRU Report 74, J. ICRU **5**(2) (2005) 1–113.

[9] INTERNATIONAL ATOMIC ENERGY AGENCY, Dosimetry in Diagnostic Radiology: An International Code of Practice, Technical Reports Series No. 457, IAEA, Vienna (2007).

[10] TOROI, P., KOSUNEN, A., The energy dependence of the response of a patient dose calibrator, Phys. Med. Biol. **54** (2009) N151–N156.

[11] INTERNATIONAL ELECTROTECHNICAL COMMISSION, Medical diagnostic X-ray equipment — Radiation Conditions for use in the determination of characteristics, IEC 61267, IEC, Geneva (2005).

[12] TAPIOVAARA, M., TAPIOVAARA, T., The validation and user's manual of the Spektripaja (2.0) program, STUK-TR 3, STUK, Helsinki (2008) (in Finnish).

[13] INTERNATIONAL ORGANIZATION FOR STANDARDIZATION, Guide to the expression of uncertainty in measurement, ISO, Switzerland (1995).

[14] TOROI, P., Patient exposure monitoring and radiation qualities in two-dimensional digital x-ray imaging, PhD Thesis, STUK-A239, STUK, Helsinki (2009).

CALIBRATION OF PENCIL TYPE IONIZATION CHAMBERS AT VARIOUS IRRADIATION LENGTHS AND BEAM QUALITIES

C.J. HOURDAKIS, A. BOZIARI, E. KOUMPOULI
Greek Atomic Energy Commission,
Athens, Greece
Email: khour@gaec.gr

Abstract

Pencil type ionization chambers are being used in several diagnostic radiology applications, for the measurement of the air kerma length product, P_{KL}. This work investigates several aspects of the pencil chamber calibration. The air kerma behind the apertures that are used for the partial irradiation of the pencil chambers depends on the irradiation set-up and equals to the air kerma free in air only under 'good geometry' irradiation conditions. Appropriate correction factors, k_w, may be needed for this. The residual signal of four pencil chamber models was measured using various apertures widths. The residual signal should be subtracted from chamber signal in order to improve accuracy. Twenty-three commercial pencil type chambers were calibrated at RQT radiation qualities. The variation of performance between chambers of the same model and between different models is discussed, while the energy dependence of their response is presented. Finally, a comparison of the two calibration methods (total and partial irradiation of chamber) showed that both methods deduce similar calibration coefficients. The uncertainties of the measurements are assessed and discussed.

1. INTRODUCTION

Pencil type ionization chambers are being used in several diagnostic radiology applications for the measurement of the air kerma length product, P_{KL}. For the last few decades, these chambers have mainly been used in computed tomography (CT) dosimetry. Recently, in the light of new CT technologies, the standards of CT dosimetry and methods have been reviewed, and new types of detector have been proposed to be used, replacing the pencil type chambers [1]. However, before these new standards will be fully reviewed, adopted and implemented, the pencil type chambers will remain in use. Furthermore, pencil type chambers are being or could be used for dose measurement in other applications, such as orthopantomograph dental (OPG) systems and cone beam CT, bone densitometry fan beams.

In practice, two methods for calibration of the pencil type ionization chambers are applied at calibration laboratories:

Method A: The whole sensitive volume of the pencil chamber is irradiated by a uniform X ray beam with a cross section that totally covers the chamber dimensions. The calibration coefficient, $N_{P_{KL}}$ is determined by means of the equation $N_{P_{KL}} = K_i \times L/R$, where K_i is the reference value of the air kerma pertaining to the point of measurement (i.e. at the point where the centre of the pencil chamber is placed), L is the rated length of the pencil chamber, and R, its reading corrected for all influence quantities (i.e. temperature, pressure, etc.). The main disadvantage of this method is that the limits of the sensitive volume are not precisely known, because they do not always coincide with the markers on the chamber body; therefore, the quantity L may not be determined accurately. However, the absence of apertures close to the pencil type chamber eliminates the influence of the scattered radiation.

Method B: This method is proposed in the IAEA TRS 457 Code of Practice as the standard method for pencil type chambers calibration [2] and has been applied in several studies [3, 4]. A fraction of the effective chamber length is irradiated by placing a rectangular lead aperture with a width perpendicular to the chamber axis in front of the pencil chamber. The width of the aperture parallel to the chamber axis, w, is between 20 mm and 50 mm and known to within 0.01 mm. The calibration coefficient, $N_{P_{KL}}$ is determined by means of Eq. (1)

$$N_{P_{KL}} = \frac{K_i \cdot w \cdot (d_r / d_a)}{R} \tag{1}$$

where

K_i is the reference air kerma behind the aperture;
d_r is the distance between the focal spot and the point of test (1000 mm);
d_a is the distance between the focal spot and the plane of aperture;
and the term $w(d_r/d_a)$ corresponds to the chamber irradiation length.

The main advantages of this method are that the reference value of $P_{KL} = K_i w(d_r/d_a)$ is determined according to its metrological definition, and all the quantities used are derived from measurements and therefore their values may be accurately determined and the associated uncertainties are known. Furthermore, the partial irradiation of the chamber resembles the clinical irradiation conditions in which the pencil chamber is used (e.g. CT, OPG, etc.).

However, there are a few practical problems and drawbacks associated with this method. First, the air kerma may not always be directly measured behind the aperture, due to the small X ray field size at this point, and it may not completely

cover the reference ionization chamber used. Normally, the air kerma, K_i, is determined in the plane of measurement in the absence of the aperture, *w*, and this value are used for the air kerma, $K_{i,w}$ behind the aperture. Theoretically, K_i and $K_{i,w}$ should be the same under 'good geometry' irradiation conditions. However, in practice, $K_{i,w}$ may include scattered radiation from the aperture that K_i does not, or the slit may absorb extrafocal radiation or scattered radiation from other components of the X ray system, which may contribute to K_i but not to $K_{i,w}$. Second, not being irradiated, the remaining volume of the chamber is sensitive to scattered radiation from the apertures and contributes to the chamber signal. The situation is similar to the stem effect for conventional ionization chambers, but on a larger scale. For this extra signal, often referred to as 'residual signal', an appropriate correction must be introduced [3].

This work presents the calibration results of a number of commercial pencil type chambers and demonstrates the variation of performance between chambers of the same model and between different models. It also explores the chambers' performance in various irradiation conditions and highlights some specialties of their calibration. The tests and measurements were performed at the Ionizing Radiation Calibration Laboratory of the Greek Atomic Energy Commission, which is a secondary standards dosimetry laboratory network run by the IAEA. It has been accredited since 2003 under the terms of ISO 17025 by the Hellenic Accreditation System.

2. MATERIALS AND METHODS

The calibrations of the pencil type chambers were performed with radiation qualities of the RQT series of IEC 61267 [4] following the above mentioned method B, at the PANTAK 225 HF high frequency X ray system. The X ray beam cross-section was defined by three apertures (each 10 mm thick): (a) the initial permanent circular aperture of the X ray tube housing, 100 mm in diameter placed at a distance of 226 mm from the focal spot of the X ray tube (FAD), (b) the first removable circular aperture (A1), 50 mm in diameter at FAD = 335 mm, and (c) the second removable rectangular aperture (A2), 33.5 mm × 33.5 mm at FAD = 501 mm. For the partial irradiation of the pencil chambers, additional 5 mm thick apertures were used (hereafter 'slits'), rectangular in shape, which were placed at a distance d_a of 950 mm from the focal spot. This distance, d_a, was determined by measuring the distance, d_{ic}, between the aperture end plane and the centre of the chamber using a caliper with an uncertainty of 0.005 mm; then $d_a = d_r - d_{ic}$. Six slits with different widths were available. The slit widths, i.e. the dimension that was parallel to the pencil chamber axis, were 10, 20, 30, 50, 80 and 100 mm, while the other slit dimension

(vertical to pencil chamber) was 50 mm for all slits. The pencil chambers were placed vertically to the X ray anode to cathode direction in order to eliminate the influence of the heel effect.

2.1. Measurement of the air kerma $K_{i,w}$ behind the slits

The air kerma behind the slit, $K_{i,w}$ may differ from the air kerma free in air, K_i. Therefore, corrections factors, k_w, should be introduced to convert K_i to $K_{i,w}$ by means of the relation $K_{i,w} = K_i \times k_w$, where the factor k_w depends on the irradiation set-up. In order to quantify the k_w factors, the PTW 31014 therapy PinPoint ionization chamber with an effective volume of 0.015 cm^3 and an inner diameter of the cavity of 2 mm was used to measure the air kerma behind the slits. The size of this chamber was small enough that even the narrowest X ray field produced by the 10 mm slit had a much larger cross-section than the chamber's dimension. The irradiation was performed with the RQT9 beam quality [4] for all available slits, under three aperture arrangements: (a) no aperture in place, i.e. with the presence of the initial tube housing aperture only, (b) aperture A1 in place but without the aperture A2, and (c) apertures A1 and A2 in place. For each aperture arrangement and slit size, k_w, was determined as the ratio of $K_{i,w}$ and K_i, where K_i was the respective pinpoint chamber reading without the presence of the slit.

2.2. Residual signal of the pencil chambers

Following Ref. [3], the residual signal of a pencil chamber was determined by partially irradiating the chamber for various lengths of the X ray field. Four models of commercial pencil chambers were tested: PTW (TM 30009) RADCAL (20x5-3CT), RTI (DCT 10) and VICTOREEN (660, 500). The irradiations were performed with the RQT9 beam quality, with the apertures A1 and A2 in place, using the 10, 20, 30, 50, 80 and 100 mm slits. A graph of the chamber reading, R, versus irradiation length was obtained. The extrapolation of this graph intercepted the ordinate at a positive value R_0, which corresponded to the residual chamber signal.

2.3. Calibration of pencil type chambers

Twenty-three pencil chambers have been calibrated at RQT series beam qualities [5]; five from PTW (TM 30009), eight from RADCAL (20x5-3CT), five from RTI (DCT 10) and five from VICTOREEN (660, 500). All chambers had an active volume with a length of 100 mm. They were connected to their electrometer/measuring device. All PTW devices measured P_{KL} in mGy·cm. One of the Radcal instruments measured P_{KL}; instead, they measured either the

exposure, in mR, or the air kerma, in mGy. The RTI devices measured P_{KL} in mGy·cm or μGy·m. The Victoreen instruments measured P_{KL} in μGy·m, the air kerma in mGy or the exposure in mR. Given the diversity of the measurement quantities and units of the test objects, all instruments were calibrated in terms of the air kerma length product in units of mGy·cm.

The calibrations were performed in 'good geometry' with apertures A1 and A2 in place, while the 50 mm slit was placed close to the pencil chamber. The reference value of K_i was measured using the A3 Exradin ionization chamber connected to PTW UNIDOS electrometer. For the determination of $K_{i,w}$, the readings of the A3 reference ionization chamber, R_{ref}, were corrected for the influence of beam quality, k_Q, air density, k_{PT}, slit presence, k_w and ion recombination, k_s; P_{KL}^{ref} was obtained by $P_{KL}^{ref} = K_{i,w} \cdot w \cdot (d_r/d_a) = R_{ref} \cdot N_K \cdot k_Q \cdot k_{PT} \cdot k_s \cdot k_w \cdot w \cdot (d_r/d_a)$, where the N_K is the calibration coefficient of the reference chamber for the RQT9 beam quality.

The calibration coefficient of the pencil chamber being tested was obtained by means of the relation $N_{P_{KL}} = P_{KL}/(R\text{-}R_0)$ where R was the reading of the instrument corrected for the influence of air density, k_{PT}.

Furthermore, the energy dependence of response of few pencil chamber models was determined at the RQT and RQR (50–150 kV) series beam qualities through the k_Q correction factor; k_Q is defined as the ratio of the calibration coefficients at radiation quality Q to that of the radiation quality RQT9 (for the RQT series) or RQR5 (for the RQR series). By definition, k_Q equals 1 at RQR 5 or RQT9.

2.4. Comparison of the calibration methods A and B

Seven pencil chambers incorporating measuring devices that measured the air kerma in mGy (i.e. not P_{KL}) were calibrated with both methods A (total irradiation of chamber) and B (partial irradiation) at RQT9 quality. In method A, the calibration coefficient, $N_{P_{KL}}$ in terms of P_{KL} was deduced from the ratio of the product $K_i \times L$ and the chamber reading, where L was the rated effective chamber length, 10 cm. The calibration coefficients deduced by each method were compared to each other.

3. RESULTS AND DISCUSSION

3.1. Measurement of the air kerma $K_{i,w}$ behind the slits

Figure 1 presents the k_w correction factors, for the three different irradiation geometries.

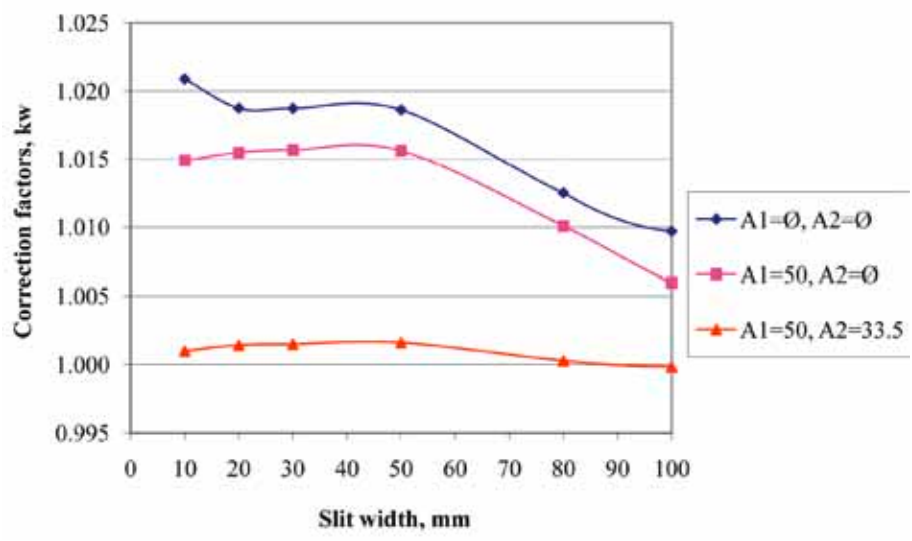

FIG. 1. The k_w correction factors for various irradiation lengths for the three different aperture arrangements.

The results showed that when appropriate collimation was used, i.e. both apertures A1 and A2 in place, the air kerma behind the slit, $K_{i,w}$ was equal to the air kerma K_i free in air without the slit. Under this 'good geometry' irradiation condition, no correction was needed (k_w = 1.000). However, an associated uncertainty of 0.2% was incorporated in the evaluation of the calibration coefficient uncertainty. When 'good geometry' was not realized, differences up to 2% between $K_{i,w}$ and K_i were observed. In such cases, correction factor k_w was applied.

The energy dependence of response of the PinPoint chamber did not influence the measurement of the primary beam. However, since the energy of scattered X rays was not known, associated corrections were not feasible. An uncertainty of 0.5 % (at 1 SD) was assigned to the influence of this effect.

The overall uncertainty of the k_w factors was 1.2% at 2 SD (at about 95% confidence level, k = 2) and took into account the stability of the X ray output, changes of temperature and pressure, the reproducibility of measurement, the energy dependence of chamber response, the resolution of the display and the geometrical conditions (slit widths, distances, etc.).

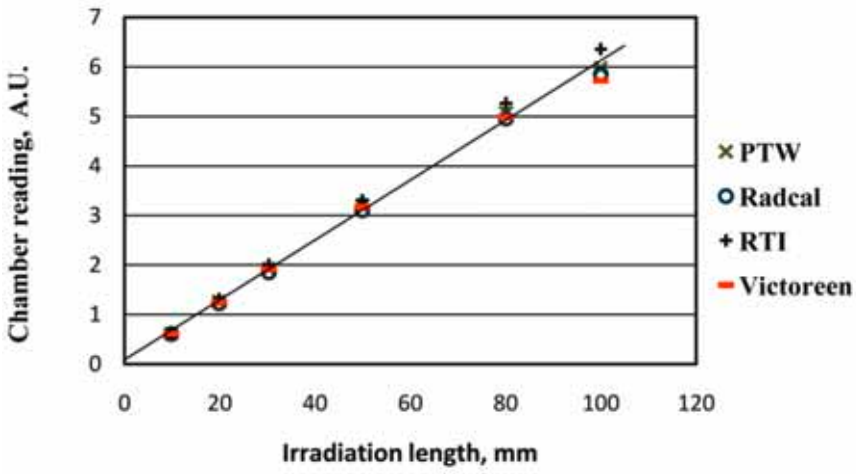

FIG. 2. The relationship of the pencil chamber readings in arbitrary units versus the chamber irradiation length for the four models: PTW (TM 3000), RADCAL (20X5-3CT), RTI (DCT 10) and VICTOREEN (660-6). The ordinate interception of each extrapolated curve represents the residual signal of the chamber (the curve for the PTW chamber is shown as an example).

3.2. Residual signal of the pencil chambers

Figure 2 shows the chamber reading versus the irradiation length (mm) for the four models of pencil chambers: PTW (TM 30009, RADCAL (20X5-3CT), RTI (DCT 10) and VICTOREEN (660-6). The relationships were linear for all chamber models; the regression coefficient R^2 was better than 0.995 in all cases.

The residual signals of the four commercial pencil chamber models being studied are presented in Table 1. The ratios (as percentages) of the residual signal to the chambers' signal for 100 mm and 50 mm irradiation lengths are also shown.

It appears that the residual signal depends on the pencil chamber design and performance characteristics. According to Table 1, the Victoreen 660-6 shown larger residual signal than for the other chambers, due to its larger effective chamber volume (10 cm^3) and inner cavity radius, which result in higher chamber sensitivity. The other chambers had similar residual signal values due to their construction similarities (6 cm^3 volume, same radius and length).

The residual signal depends on the irradiation geometry as well and mostly on the 'shadow' of the slits and the subsequent 'penumbra' on the pencil chamber plane.

TABLE 1. THE RESIDUAL SIGNAL OF THE PENCIL TYPE CHAMBER/ METER MODELS

Chamber model	Residual signal	Residual to actual signal (%)	
	(A.U.)	100 mm slit	50 mm slit
PTW TM 3000	0.060	1.0	1.9
RADCAL 20X53-CT	0.067	1.2	2.2
RTI DCT 10	0.053	0.8	1.6
VICTOREEN 660-6	0.141	2.5	4.4

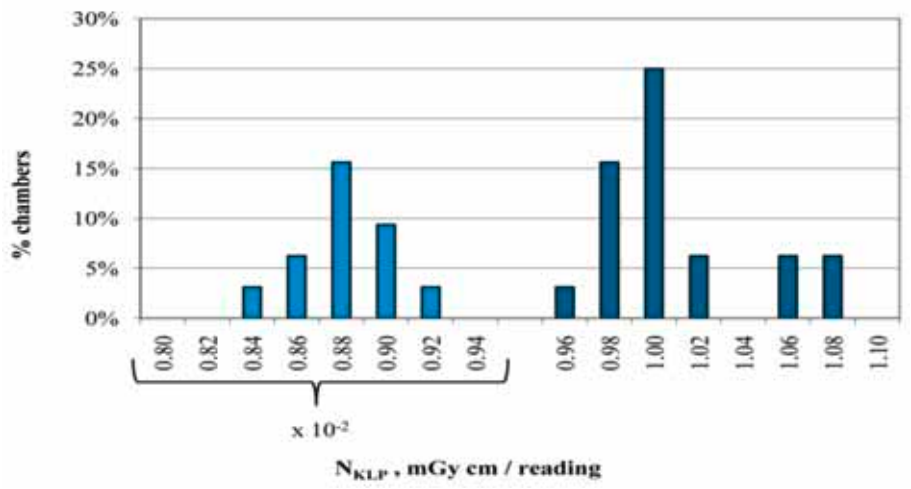

FIG. 3. The distribution of the calibration coefficients at RQT9 beam quality of the 23 pencil chambers being tested. The left distribution applies to chambers measuring exposure, and the right one to those measuring air kerma.

During the calibration, the residual signal R_0 should be measured and subtracted from the chamber reading, R, that is used for the calculation of the calibration coefficient. The percentage values of the third and fourth columns of Table 1 corresponded to the error that would be introduced to the calibration coefficient if the residual signal had not been taken into account.

3.3. Calibration of pencil type chambers

The calibration results of the tested dosimeters (pencil chamber and electrometer) are presented in Fig. 3.

Due to the differences of the units displayed by the tested dosimeters, the reading of the dosimeters that measured in units of roentgens were converted to air kerma by applying the conversion factor of 8.76×10^{-3} mGy/mR; the multiplication factor $\times 10^{-2}$ has not been taken into account. Accordingly, the average values together with the relative standard deviations of the calibration coefficients $N_{P_{KL}}$ of the pencil chamber models at RQT9 beam quality are given in Table 2.

The energy dependence of response of the pencil chamber models being tested in terms of the k_Q correction factors at the RQT and RQR series beam qualities are presented in Fig. 4 and Table 2 (for RQT series).

The typical combined relative uncertainty of the calibration coefficient N_{PKL} was 3.7% with coverage factor k = 2. The major contribution was the uncertainty of the X ray irradiation length determination (1.4% with k = 1). Other influence quantities were: the calibration coefficient and the energy dependence of the reference chamber; temperature and pressure; the reproducibility of

TABLE 2. THE CALIBRATION COEFFICIENTS FOR THE RQT9 BEAM QUALITY AND THE ENERGY DEPENDENCE OF RESPONSE OF THE PENCIL CHAMBER MODELS BEING TESTED

	All chambers	PTW	RADCAL	RTI	VICTOREEN
Mean N_{PKL} (± sd)	0.982 ± 0.117	0.983 ± 0.009	0.934 ± 0.089	0.899 ± 0.030	1.005 ± 0.120
Median	0.976	0.984	0.923	0.896	1.005
Energy dependence	—	3.7%	19%	.8%	1.5%

Note: The energy dependence is given in terms of peak-to-peak values.

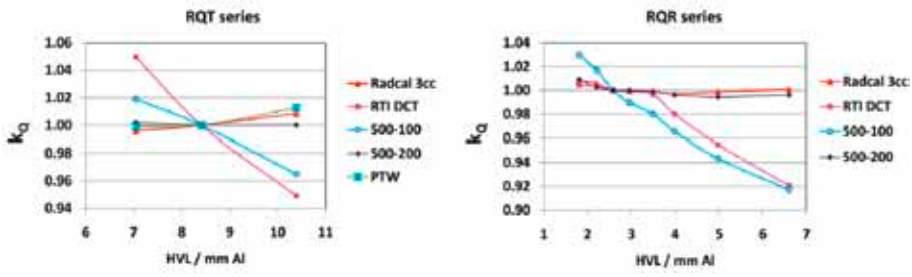

FIG. 4. The k_Q correction factors of the pencil chambers as a function of beam quality (half value layer) at the RQT and RQR series; this relationship corresponds to the energy dependence of response of the pencil chambers.

measurements; the stability of the X ray output; the uniformity of the X ray beam; the positioning of the reference and the pencil chamber at the same distance from the focal spot; and the resolution of the display of the instruments.

3.4. Comparison of the calibration methods A and B

Table 3 presents the calibration coefficients of the seven pencil chambers, which were deduced by applying the calibration methods A and B, as described in Section 2.4. The uncertainties (with k = 2) as well as the percentage difference of the calibration coefficients are also shown.

In method A, the uncertainty of the rated effective length of the chamber was not known because it was not stated in the chamber specifications and manuals. Chamber manufacturers are advised to include the effective length uncertainty in the chamber specification data, since some calibration laboratories follow this calibration method. Another way to deduce the effective length is by taking a radiograph, which was not performed in this study. For purposes of comparison, a reasonable arbitrary value of 1.0% (at 1 SD) was assigned to it, resulting to an overall combined uncertainty of the calibration coefficient of 2.6% (with k = 2).

According to Table 3, methods A and B were comparable. The resulting calibration coefficients differed by less than their uncertainties (2.6% and 3.7%, respectively). Table 3 provides the relative comparison of the two methods

TABLE 3. COMPARISON OF THE CALIBRATION METHODS A AND B FOR SEVEN OF THE PENCIL CHAMBERS

Chamber	$N_{P_{KL}}$ (method A) total irradiation (mGy·cm/reading)	$N_{P_{KL}}$ (method B) partial irradiation (mGy·cm/reading)	Difference (%)
RADCAL	1.00 ± 0.03	1.01 ± 0.04	1.19
RADCAL	0.99 ± 0.03	0.97 ± 0.04	2.36
RADCAL	1.06 ± 0.03	1.07 ± 0.04	1.30
RADCAL	0.97 ± 0.03	0.99 ± 0.04	2.17
RADCAL	0.97 ± 0.03	0.98 ± 0.04	1.08
VICTOREEN	1.32 ± 0.03	1.30 ± 0.05	1.29
VICTOREEN	1.07 ± 0.03	1.09 ± 0.04	1.38

performed for the purposes of this study and does not refer to the manufacturer calibration data.

4. CONCLUSION

The calibration of the pencil type ionization chambers in terms of P_{KL} by partial irradiation of the chamber is the method suggested by several scientific committees and organizations. Special attention should be paid to the determination of the air kerma in the plane of measurement behind the apertures as well as to the evaluation of the residual signal of the pencil chambers. The energy dependence of the chamber response may need to be considered in case the chamber is used in beams of significantly different radiation quality.

REFERENCES

[1] AMERICAN ASSOCIATION OF PHYSICSTS IN MEDICINE, Comprehensive Methodology for the Evaluation of Radiation Dose in X-Ray Computed Tomography, Report of AAPM Task Group 111: The Future of CT Dosimetry, AAPM Report 111 (2010).

[2] INTERNATIONAL ATOMIC ENERGY AGENCY, Dosimetry in Diagnostic Radiology: An International Code of Practice, Technical Reports Series No. 457, IAEA, Vienna (2007).

[3] BOCHUD, F.O., GRECESCU, M., VALLEY, J.F., Calibration of ionization chambers in air kerma length, Phys. Med. Biol. **46** (2001) 2477–2487.

[4] INTERNATIONAL ELECTROTECHNICAL COMMISSION, Medical Diagnostic X-Ray Equipment – Radiation Conditions for Use in the Determination of Characteristics, IEC 61267, IEC, Geneva (2005).

PERFORMANCE TEST OF MULTI-PARAMETER MEASURING DEVICES USED FOR QUALITY ASSURANCE IN DIAGNOSTIC RADIOLOGY

L. BÜERMANN, R. BÖTTCHER
Physikalisch-Technische Bundesanstalt,
Braunschweig, Germany
Email: ludwig.bueermann@ptb.de

Abstract

The results are presented of a performance test of four different types of semiconductor based, multi-parameter measuring devices used for measurements in the technical quality assurance of X ray diagnostic radiology. The response of such instruments was determined with respect to the parameters dose, the X ray tube voltage, the half-value layer and the total filtration as a function of selected reference radiation qualities typical of conventional diagnostic radiology and mammography. The results are compared with the technical specifications given by the manufacturers and with requirements defined in international standards. It resulted that a remarkably high amount of all measured data points (20–50%) fall beyond the limits of accuracy stated by the manufacturers. The measured dose results of the four devices comply with the requirements in international standard IEC 61674, but only half the measured X ray tube voltage measurements were within the limits required by international standard IEC 61676. The results of this performance test suggest that possible users should be careful with the application of such devices if quantities other than dose are measured. Furthermore, it has become obvious that there is a need for the international standardization of the performance of semiconductor based, multi-parameter measuring devices, especially for those quantities that are essential for quality assurance in diagnostic radiology.

1. INTRODUCTION

Semiconductor based multi-parameter measuring devices (MMD) are frequently used for measurements necessary in the quality assurance (QA) of medical X ray imaging devices, e.g. for acceptance and constancy tests. Such instruments are capable of measuring the X ray tube voltage, the exposure time, the dose, the dose rate, the half-value layer (HVL) and the total filtration (TF) from a single shot exposure when placed in the beam of a radiographic or a mammographic X ray unit. The requirements on the performance of such instruments with respect to the parameters dose and the dose rate are given in international standard IEC 61674 [1] and those for the non-invasive

measurements of X ray tube voltage in IEC 61676 [2]. Unfortunately, there are no standards that define requirements on the performance of measurements of the total filtration or HVL. The purpose of this work is to examine the performance of MMDs with respect to their indication of the dose in terms of air kerma, the X ray tube voltage, the HVL and the total filtration as a function of reference radiation qualities as defined in IEC 61267 [3] and used for studies in general radiography and mammography. The question was how these systems comply with the manufacturers' technical specifications and with requirements of international standards.

2. MATERIALS AND METHODS

Frequently used MMDs from four different manufacturers were bought: RTI Piranha S/N CB2-09050138 (A), Quardt dido 2100 — S/N 02065 (B), Unfors Xi Platinum with Base 8201011-B–S/N 157751 and detector 8202031-C Xi RF&MAM — S/N 157039 (C) and Radcal Rapidose Model RAPD-W–S/N 01B-09-10238 and Model RAPD-M — S/N 01B-09-20205 (D). These devices, in the following referred to as A, B, C and D, were examined at the X ray facilities of the Physikalisch-Technische Bundesanstalt (PTB). These facilities are otherwise used for the calibration of secondary standard dosimeters and non-invasive meters of the X ray tube voltage. Table 1 summarizes the specifications given in the manuals for the measuring quantities of dose, tube voltage, HVL and total filtration. Selected radiation qualities listed in Table 2 according to IEC 61267 [3] and additional mammographic qualities based on W-, Mo- and Rh-anode X ray tubes operated with constant potential high voltage generators were used. The X ray tube voltage was measured by means of voltage dividers produced and calibrated at PTB. The photon fluence spectra of all PTB radiation qualities were measured with a high purity germanium detector. The measured spectra were used to calculate parameters characterizing the beam quality, such as the mean photon energy and the first and second aluminium HVLs with respect to air kerma rate.

Air kerma rates were measured with the PTB primary standard free-air chambers for low and medium energy X rays. The relative expanded uncertainties (k = 2) of the measured air kerma rates were less than 1% and those of the measured X ray tube high voltages, less than 0.3%. Aluminium HVLs were determined from the measured photon fluence spectra with expanded uncertainties (k = 2) of less than 0.02 mm Al. The thicknesses of the filters used for the radiation qualities were measured with an uncertainty of less than 1 μm. The homogeneities of the filters were measured with a digital X ray imaging device and were found to be within less than 1% for all the aluminium filters,

TABLE 1. SPECIFICATIONS OF THE LIMITS OF ACCURACY STATED IN THE MANUALS OF THE TESTED DEVICES

Quantity	Application	Device A	Device B	Device C	Device D
Air kerma	R&F[a], MAM[b]	5%	2%	5%	5%
Tube voltage	R&F	1.5%	5%	2%	2%
	MAM	2% or 1 kV	5%	2% or 0.5 kV	2%
HVL/(mm Al)	R&F	10% or 0.2 mm	n.s.[c]	10% or 0.2 mm	10% or 0.5 mm
	MAM	—	—	5%	—
Total filtration	R&F	10% or 0.3 mm	n.s.[c]	—	10% or 0.5 mm

[a] RF: Radiography and fluoroscopy.
[b] MAM: Mammography.
[c] Not specified.

TABLE 2. RADIATION QUALITIES USED FOR THE PERFORMANCE TEST

Quality code	Tube Voltage	Total filtration		1st HVL	Mean energy (fluence)
W-anode	kV	mm Al		mm Al	keV
RQR 2	40	2.49		1.42	28.4
RQR 5	70	2.83		2.57	40.3
RQR 8	100	3.36		3.96	50.8
RQR 10	150	4.38		6.55	64.5
RQA 3	50	12.5		3.74	39.1
RQA 5	70	23.8		6.73	52.4
RQA 7	90	33.2		9.21	63.5
RQA 10	150	49.4		13.23	88.6
Mo-anode	kV	mm Mo	mm Al	mm Al	keV
MMV 25[a]	25	0.03		0.29	16.1
MMV 28	28	0.03		0.32	16.7

TABLE 2. RADIATION QUALITIES USED FOR THE PERFORMANCE TEST (cont.)

Quality code	Tube Voltage	Total filtration		1st HVL	Mean energy (fluence)
MMV 30	30	0.03		0.33	17.1
MMV 35	35	0.03		0.37	18.1
MMH 25[b]	25	0.03	2.0	0.56	18.8
MMH 28	28	0.03	2.0	0.61	19.8
MMH 30	30	0.03	2.0	0.64	20.7
MMH 35	35	0.03	2.0	0.73	23.2
W-anode	kV	mm Rh	mm Al	mm Al	keV
WRV 25	25	0.05		0.48	18.6
WRV 28	28	0.05		0.51	19.1
WRV 30	30	0.05		0.52	19.4
WRV 35	35	0.05		0.56	20.5
WRH 25	25	0.05	2.0	0.73	20.4
WRH 28	28	0.05	2.0	0.77	20.9
WRH 30	30	0.05	2.0	0.80	21.4
WRH 35	35	0.05	2.0	0.92	23.8
Rh-anode	kV	mm Rh		mm Al	keV
RRV 28	28	0.025		0.37	18.1

[a] MMV series identical to IEC 61267 RQR-M series.
[b] MMH series identical to IEC 61267 RQA-M series.

0.7 µm for the molybdenum filter, and 2.4 µm for the rhodium filter. These uncertainties of the conventional true values of the corresponding quantities are only about a tenth of the limits of accuracies shown in Table 1 and therefore sufficiently low for the intended performance test.

3. MEASUREMENTS AND RESULTS

The single shot calibration factors, N_q, of the four MMDs were determined for the quantities dose, X ray tube voltage, HVL and total filtration as a function

of the radiation qualities listed in Table 2. At least five repeated measurements of N_q were performed at each radiation quality using an exposure time of 15 s for each single measurement, and the mean value was taken as the result. The relative standard deviation of the mean of the repeated measurements was always less than 1%. The relative percentage deviation of the calibration factor from unity, $\Delta_q = (1 - N_q)100$, was determined for the quantities: dose in terms of air kerma, designated as Δ_{dose}, Al HVL, designated as Δ_{HVL}, X ray tube voltage, designated as Δ_{kV} and total filtration, designated as Δ_{filter}. Results of the deviations measured for the four devices at different radiation qualities are shown in Figs 1–3. The data for Δ_{filter} are not shown because only two instruments were designed to measure the total filtration for only a small subset of the radiation qualities shown in Table 2.

From the figures, it can already be concluded that a large number of the indicated values deviate from the conventional true values by more than the limits of accuracy given by the manufacturers (see Table 1). Since it was not the aim of this work to compare different types of MMDs, but rather, to determine their general performance with respect to given specifications, a statistical evaluation of the frequency distributions of the combined results of all devices with respect

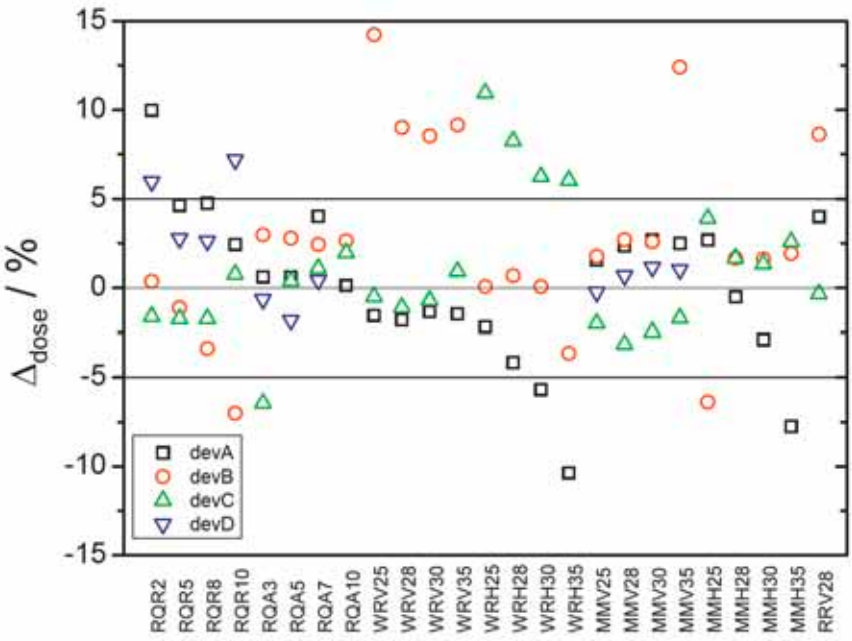

FIG. 1. Percentage deviation, Δ_{dose}, of the devices A, B, C and D at different radiation qualities.

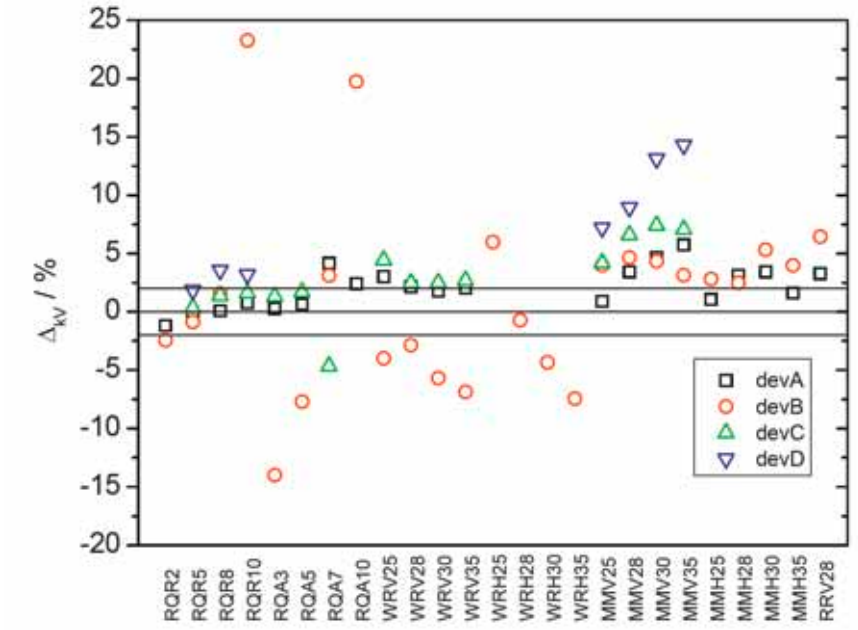

FIG. 2. Percentage deviation, Δ_{kV}, of the devices A, B, C and D at different radiation qualities.

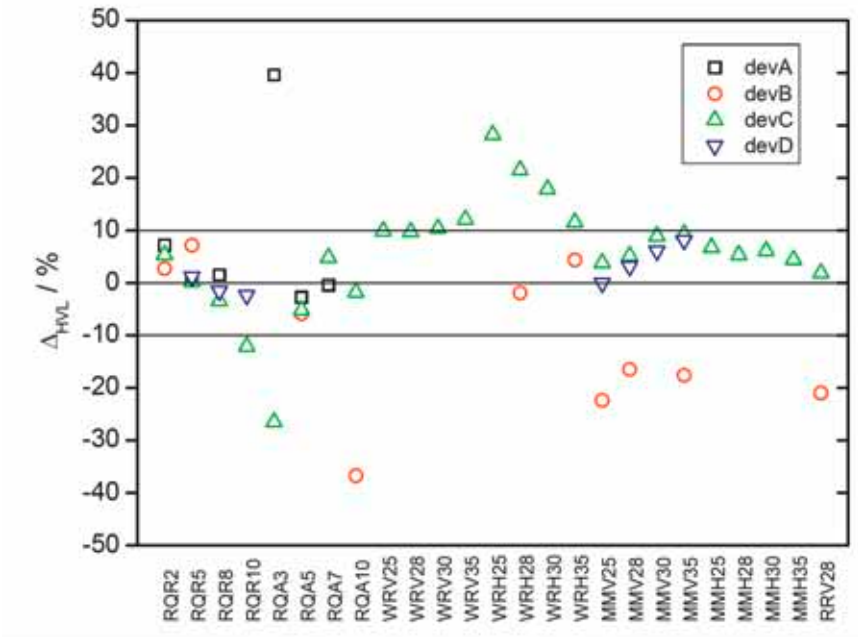

FIG. 3. Percentage deviation, Δ_{HVL}, of the devices A, B, C and D at different radiation qualities.

to deviation classes was undertaken and the results for all types of measurements are shown in Fig. 4. The total number of measured calibration factors was 86 for dose, 67 for X ray tube voltage, 47 for HVL and 19 for total filtration. The reason for the decreasing numbers is that all devices can measure dose for nearly all selected radiation qualities, but X ray tube voltage and HVL measurements are only possible for a subset of them. Measurements of the total filtration were not possible with two of the devices, and the other two offered this possibility for only a small subset of the selected radiation qualities.

From the frequency distributions it was evaluated that the relative standard deviations were 4.4, 5.6, 13 and 14% for the deviations in dose, X ray tube voltage, HVL and total filtration measurements, respectively. Accordingly, if a confidence level of approximately 95% is needed, one has to accept limits of accuracy of about 9, 12, 26 and 28% for dose, X ray tube voltage, HVL and total filtration measurements. Only a small number of points could be measured for the total filtration, which limits the validity of the statistical results.

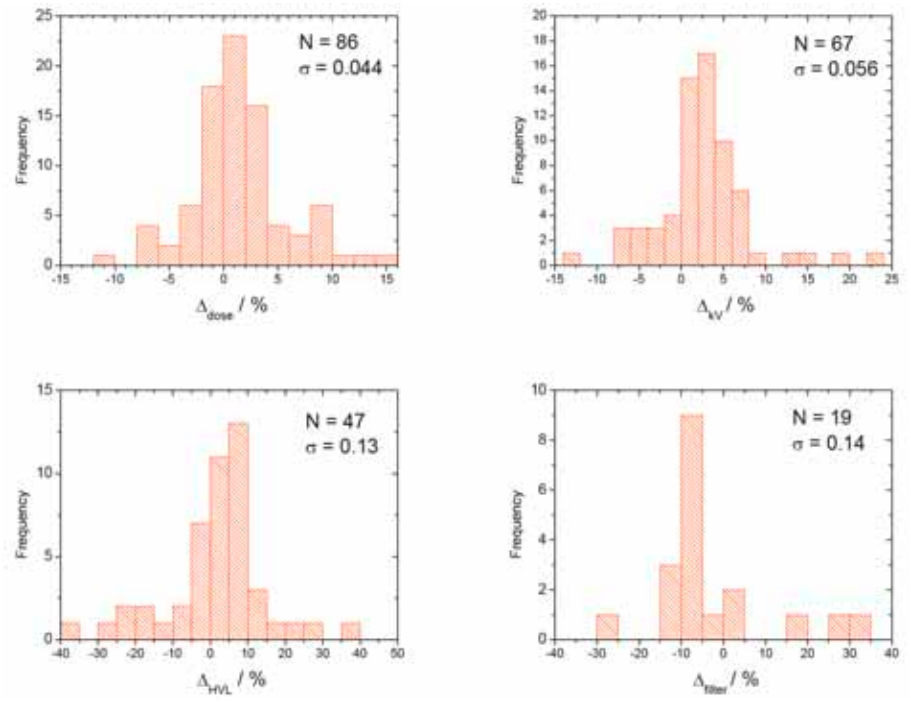

FIG. 4. Frequency distributions of the combined results of all devices with respect to deviation classes of 2% (upper diagrams) and 5% lower diagrams.

It was evaluated that about 20% of all dose measurements fall beyond the specified 5% limit of accuracy given by the manufacturers. Most of the outliers for dose measurements are located at either end of a given series. These radiation qualities are not used very frequently. The situation is worse for the non-invasive measurements of the X ray tube voltage where about half the measured points do not fulfil the manufacturers' specification of 2% or 5% limits of accuracy. About 30% of the HVL and total filtration measurements did not meet the specified limits of 10%. In conclusion, a remarkably high amount of the measured data falls beyond the limits of accuracy stated by the manufacturers.

Another question is whether the results comply with the requirements of international standards. Standard IEC 61674 [1] defines requirements for air kerma measurements with dosimeters with semi-conductor detectors, as used in X ray diagnostic imaging. Part 5 of this standard sets limits of performance characteristics and part 6, limits of variation for effects of influence quantities. The relative intrinsic error for air kerma measurements for air kerma rates as used in the current performance tests must not exceed 5%. The limits of the variation for the effects of the radiation qualities within the rated range must not exceed 5%. The other influence quantities were kept at reference conditions during the dose measurements of this performance test. The combined effect of intrinsic error and limits of variation for the effect of radiation quality allows a maximum deviation from the conventional true value of 10%. From Figs 1 and 4, it becomes obvious that about 95% of the results fall within these limits, and it can be concluded that the measured dose results of the four devices comply with international standard IEC 61674 [1].

Standard IEC 61676 [2] defines performance requirements for dosimetric instruments used for the non-invasive measurement of X ray tube voltage in diagnostic radiology. This standard requires a maximum relative intrinsic error for measurements of voltages above 50 kV at 2%, and for voltages below 50 kV in absolute terms at 1 kV. Since all the performance test measurements of this work were undertaken close to standard test conditions as defined in Table 2 of IEC 61674, the defined intrinsic errors can be regarded as the approximate performance limits set by the standard. The relative intrinsic error for the mammographic qualities (close to 30 kV) can roughly be estimated at 3.5%. If ones uses these values, only about 50% of the measured points are within the limits. Consequently, it can be stated that the degree of compliance with the standard is low and needs significant improvement. Unfortunately, there are no standards with requirements for the single shot HVL and total filtration measurements.

4. CONCLUSIONS

In general, it can be concluded that for the quantities dose, X ray tube voltage, HVL and total filtration, a remarkably high number of the values indicated by the four multi-parameter measuring devices go beyond the limits of accuracy stated in the corresponding manuals. Only the results for dose measurements are acceptable, although some improvements are still required. It seems that the other quantities, X ray tube voltage, HVLs and total filtration are intended to promote sales, but they cannot really be recommended for use in quality assurance measurements. If non-invasive measurements of the X ray tube voltage are needed, it is recommended that the device be calibrated at radiation qualities close to those for which measurements are needed. HVLs should preferentially be measured by using well established conventional methods based on the use of calibrated ionization chambers and sets of appropriate aluminium absorbers [4]. The results of this work demonstrate the need for international standards that define further requirements on the performance of semiconductor based, multi-parameter measuring devices, especially for those quantities that are essential for quality assurance in diagnostic radiology.

REFERENCES

[1] INTERNATIONAL ELECTROTECHNICAL COMMISSION, Medical Electrical Equipment — Dosemeters with Ionization Chambers and/or Semiconductor Detectors as Used in X-ray Diagnostic Imaging. IEC Publication 61674 (Geneva: International Electrotechnical Commission) (1997).

[2] INTERNATIONAL ELECTROTECHNICAL COMMISSION, Medical Electrical Equipment — Dosimetric Instruments for Non-Invasive Measurements of X-ray Tube Voltage in Diagnostic Radiology. IEC Publication 61676 (Geneva: International Electrotechnical Commission) (1996)

[3] INTERNATIONAL ELECTROTECHNICAL COMMISSION, Medical Diagnostic X-ray Equipment — Radiation Conditions for Use in the Determination of Characteristics. IEC Publication 61267 (Geneva: International Electrotechnical Commission) (2005).

[4] INTERNATIONAL ATOMIC ENERGY AGENCY, Dosimetry in Diagnostic Radiology: An International Code of Practice, Technical Reports Series No. 457, IAEA, Vienna (2007).

REFERENCE X RAY FIELD FOR MAMMOGRAPHY DOSIMETRY IN JAPAN

T. TANAKA, T. KUROSAWA, R. NOUDA, T. MATSUMOTO, N. SAITO
National Institute of Advanced Industrial Science and Technology,
Tokyo
Email: takahiro-tanaka@aist.go.jp

S. MATSUMOTO, K. FUKUDA
Chiyoda Corporation,
Yokohama

Japan

Abstract

The mammography radiation qualities, which are produced using a molybdenum anode X ray tube and a molybdenum filter, are different from those of other X ray diagnostics such as a chest X ray system. Because a mammography air kerma standard was not disseminated in Japan, dosimeters used as quality control of mammography were calibrated in the soft X ray reference field produced using a tungsten anode X ray tube and an aluminium filter. To minimize and manage radiation dose precisely in mammography, the authors have developed the mammography reference field. At this mammography reference field, a glass dosimeter used for quality control of mammography in many hospitals was evaluated.

1. INTRODUCTION

Recently, the importance of early detection and early treatment of breast cancer has been emphasized, which has resulted in an increase in the number of mammography examinations in breast cancer screening since 2000 in Japan. Since the number of mammography examinations has steadily increased, more attention has been focused on the quality control of the mammography equipment. The quality control requires hospitals to measure the air kerma emitted from the mammography equipment. This air kerma measurement in hospitals is normally performed using a plane-parallel ionization chamber [1]. In Japan, the Central Committee on Quality Control of Mammographic Screening audit mammography systems in hospitals and use a glass dosimeter to check the X ray dose in terms of mean glandular dose (MGD). For low energy X rays such as mammography X rays, calibration coefficients of a plane-parallel ionization

chamber and a glass dosimeter normally depend strongly on the X ray beam quality. Therefore, dosimeters used as quality control of mammography should be calibrated for those radiation qualities used in clinical mammography.

The National Metrology Institute of Japan (NMIJ) maintains the national standards for radiation dosimetry in Japan. NMIJ has also developed, maintains and disseminates the soft X ray air kerma standard using a tungsten (W) anode X ray tube and an aluminium filter (W/Al target/filter combination). The irradiation and calibration of soft X ray are performed in terms of air kerma or exposure. The soft X ray air kerma standard mainly plays a role in the quality control of radiography. Currently, radiation dose has been evaluated in accordance with the national air kerma standard for radiography such as chest X ray imaging.

However, mammography radiation qualities from a molybdenum (Mo) anode X ray tube differ from those emitted from a W anode X ray tube in typical X ray systems. Because a mammography air kerma standard was not disseminated in Japan, dosimeters used for quality control in mammography were calibrated in the soft X ray reference fields, which are traceable to the NMIJ soft X ray air kerma standard.

The development of the mammography air kerma standard using a Mo anode X ray tube has become necessary because mammography radiation qualities are different from those of other X ray diagnostics.

In order to meet such a demand, the authors have developed the mammography reference field. In this mammography reference field, a glass dosimeter used for quality control of mammography in many hospitals was evaluated.

2. MAMMOGRAPHY REFERENCE FIELD

The soft X ray standards for air kerma or exposure at NMIJ are realized by means of a free-air ionization chamber. Figure 1 shows a cross-sectional view of the free-air ionization chamber. The measurement volume is defined by the product of the area of the diaphragm of the free-air ionization chamber and the length of the collector plate in the free-air chamber. The reference plane in which the air kerma rate is determined is defined by the diaphragm. Several correction factors are described briefly below.

At low X ray energies, the air attenuation due to the air path between the reference plane and the collector centre is the largest correction factor. This correction is determined by measuring the ratio of the ionization currents with the free-air ionization chamber at two positions: the normal position and the position

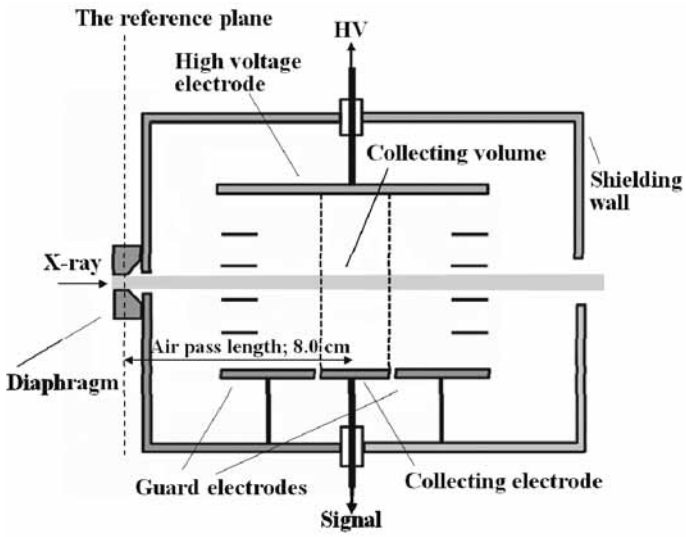

FIG. 1. Schematic of the free-air ionization chamber.

closer to the source by a distance equal to the air path length between the diaphragm and the centre of the measuring electrode. The attenuation correction factors are corrected for a pressure of 101.325 kPa and temperature of 293.15 K (the reference conditions). For mammography X rays, the attenuation correction factors are about 2%.

For the chamber shown in Fig. 1 and for mammography radiation qualities, the second largest correction factor is the correction for the electric charge generated by scattered X rays inside the free-air ionization chamber. This includes the effect of fluorescence radiation. This correction is evaluated using the Monte Carlo technique of EGS5.

A schematic diagram of the mammography calibration system is given in Fig. 2. The mammography reference field consists of a Mo anode X ray tube, a Mo filter and the free-air ionization chamber. The X ray source is a Gulmay generator and a RTW Mo anode X ray tube. The inherent filtration is 1 mm beryllium. IEC 61267 revised in 2005 [2] recommended that the thickness of additional Mo filter is 32 μm. Two kinds of Mo filters with thicknesses of 30 μm and 32 μm were used.

In addition to the Mo filter, compression paddle can be used (3 mm thick polycarbonate) to evaluate its effect on the radiation qualities. The calibration distance is 60 cm: the distance between the focal spot of the X ray tube and the reference plane. The reference plane of the free-air ionization chamber is set at

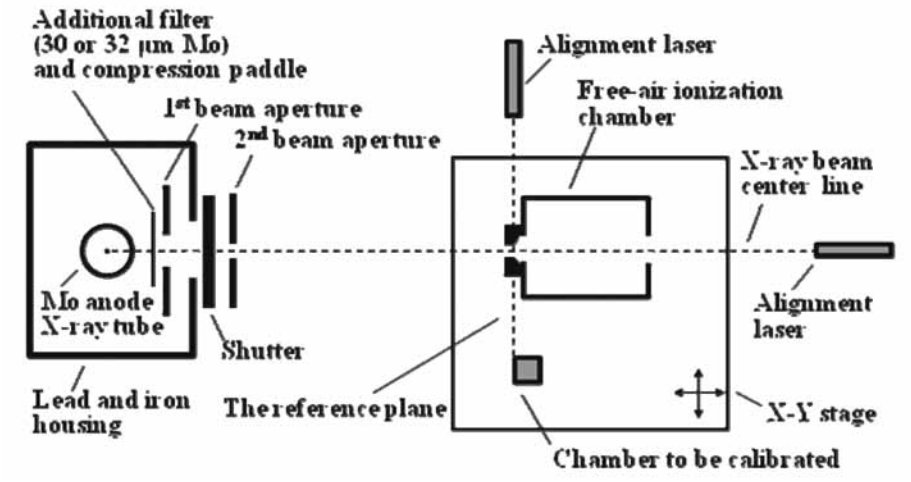

FIG. 2. Schematic of the mammography calibration system (not to scale).

the fixed position using laser light beams. The voltage applied to the free-air ionization chamber is +2500 V.

Two kinds of scopes are available for dosimeter calibrations: one is the soft X rays generated by the W anode X ray tube at constant potentials of 10–50 kV. The radiation qualities are the CCRI qualities [3], ISO 4037 narrow spectrum series [4] and Japanese (quality index, E_{eff}/E_{max}) qualities, where E_{eff} is the effective X ray energy (the energy of monoenergetic X ray beam that has the same HVL as the spectrum in question) and E_{max} is the maximum X ray energy. The E_{max} value was determined from the highest energy edge of the X ray spectrum measured with a low energy lithium drifted silicon X ray detector.

The other are the mammography radiation qualities generated using the Mo anode X ray tube at constant potentials between 20 kV and 35 kV. Table 1 shows the characteristics of some mammography radiation qualities.

3. EVALUATION OF GLASS DOSIMETERS

Reference to the general characteristics of glass dosimeters used is made in the reference list.

Figure 3 shows an overview of the glass dosimeter for mammography radiation. This glass dosimeter is specially designed to measure mammography X rays and is used for quality control of mammography in hospitals. The glass dosimeter consists of photoluminescent glass [5–7] and four aluminium filters with different thicknesses. A photoluminescent glass is a silver activated

TABLE 1. CHARACTERISTICS OF SOME MAMMOGRAPHY RADIATION QUALITIES

Tube voltage (kV)	Additional filtration (mm)	Compression paddle	1st HVL (mm Al)
20	0. 030 Mo	Without	0.211
		With	0.247
	0.032 Mo	Without	0.220
		With	0.255
28	0.030 Mo	Without	0.306
		With	0.360
	0.032 Mo	Without	0.322
		With	0.369
35	0.030 Mo	Without	0.364
		With	0.415
	0.032 Mo	Without	0.376
		With	0.422

FIG. 3. Photograph of a glass dosimeter for mammography radiation: glass plate (left) and case (right).

phosphate glass, which has the advantage of a low background signal of photoluminescence and long term stability. The thickness of a photoluminescent glass is 1 mm. The thicknesses of the Al filters are 0.3, 0.4, 0.6 and 1.0 mm, and their purity is above 99.9%. The glass dosimeter simultaneously measures the air kerma and an attenuation curve. Tube voltage and half value layer (HVL) are estimated from the attenuation curve. According to the Japanese protocol for mammography quality control, MGD is estimated from a set of air kerma, tube voltage and HVL. Therefore, this glass dosimeter provides air kerma, tube voltage, HVL and MGD.

The glass dosimeters were evaluated in the mammography reference field. The radiation qualities used in this evaluation were 24, 26, 28, 30 and 32 kV with the Mo filter of 30 μm and the compression paddle. For these five radiation

FIG. 4. Evaluation of glass dosimeters at the National Insitute of Advanced Industrial Science and Technology (AIST).

qualities, air kerma, tube voltage and HVL measured by the glass dosimeters were evaluated.

The three glass dosimeters were arranged vertically to evaluate measurement uncertainty. The middle of the three glass dosimeters was set on the X ray beam axis. The reference plane for the glass dosimeters was taken to be on the middle of the casing, i.e. on a 3 mm depth from the casing surface. The glass dosimeters were fixed in the expanded polystyrene (shown in Fig. 4) to eliminate scattering radiation. The compression paddle was set in front of the glass dosimeters. According to the Japanese protocol for mammography quality control, the distance between the compression paddle and the centre of the glass dosimeters is set at 5 mm. The value of air kerma was obtained by a monitor ionization chamber (PTW 23344) calibrated against the free-air chamber using the same radiation qualities. The field size is set at 240 mm × 180 mm. The air kerma rate was set at about 0.3mGy/s.

First, the air kerma rate was measured using the ionization chamber for a given radiation quality. Second, the glass dosimeters were irradiated for a certain time (typically ~30s). Finally, the air karma rate was checked after irradiation to the glass dosimeters. The air kerma with which the glass dosimeters were irradiated was evaluated by multiplying the air kerma rates by the irradiation time. The three sets of glass dosimeters were irradiated separately three times for

one radiation quality. The first set of irradiation data was used for making calibration curves. The second and third sets of the irradiation data were evaluated using these calibration curves.

Table 2 shows some measurement results of the X ray tube voltage, HVL and air kerma by means of the glass dosimeters compared to the corresponding reference values. The tube voltages were calibrated by measuring the X ray spectra with a Si(Li) detector. The reference HVLs were measured using the free-air chamber with 99.999% purity of Al attenuation filters. The uncertainty of all the reference values is about 1.0% at the confidence level of about 95%.

The comparison made in Table 2 is very informative Furthermore, the uncertainty will be expressed at least for the reference instrument (free-air chamber).

The uncertainties in the determination of air kerma with the glass dosimeters for all Mo/Mo radiation qualities are given in Table 3. The relative expanded uncertainty is ±3.8% at the about 95% confidence level. It was confirmed that the glass dosimeter can measure air kerma, tube voltage and HVL with an uncertainty of about 4%.

4. SUMMARY

The reference mammography field was developed. The reference mammography field consists of a Mo anode X ray tube, a Mo filter and the free-air ionization chamber. Two kinds of Mo filters were used, with different

TABLE 2. COMPARISON OF RESULTS OBTAINED WITH IONIZATION CHAMBER AND GLASS DOSIMETERS

Tube voltage (kV)		HVL (mm Al)		Air kerma (mGy)	
NMIJ/AIST	Glass dosimeters	NMIJ/AIST	Glass dosimeters	NMIJ/AIST	Glass dosimeters
24.0 (2nd)	24.3	0.310	0.314	8.67	8.67
24.0 (3rd)	24.0		0.313	8.64	8.65
28.0 (2nd)	27.7	0.359	0.356	8.77	8.90
28.0 (3rd)	27.7		0.357	8.79	8.90
32.0 (2nd)	31.7	0.393	0.390	9.79	9.87
32.0 (3rd)	32.0		0.388	9.71	9.82

TABLE 3. UNCERTAINTIES IN THE DETERMINATION OF AIR KERMA WITH THE GLASS DOSIMETERS

Source of uncertainty	Standard uncertainty (%)
Positioning	0.14
Air kerma	0.5
Lot-to-lot variation	0.58
Radiophotoluminescent signal measurements	0.6
Calibration coefficients	1.6
Quadratic sum	1.9
Relative expanded uncertainty (k = 2)	3.8

thickness of 30 μm and 32 μm. In addition to a Mo filter, we can put the compression paddle into the beam to evaluate the effect on radiation quality. For these radiation qualities, the authors evaluated the values of air kerma, tube voltage and HVL measured by the glass dosimeters.

Consequently, it was confirmed that the values of air kerma, tube voltage and HVL measured by the glass dosimeters were in agreement with those measured by the ionization chamber within their uncertainty of about 4%.

The glass dosimeters can provide the precise quality control for mammography equipment in hospitals.

Since the energy dependence of the glass dosimeter is relatively flat (see also Table 2), it is also expected that there will not be much of a difference in response between the Mo/Mo versus W/Al fields. Therefore, it is not clear what the benefit is of performing irradiations in a Mo/Mo X ray field. This suggests the same level of accuracy could be achieved through the calibrations in W/Al fields if the HVL is used as a beam quality specifier.

Furthermore, this could also extend to the common use of Rh/Rh fields as an alternative to Mo/Mo fields.

REFERENCES

[1] INTERNATIONAL ATOMIC ENERGY AGENCY, Dosimetry in Diagnostic Radiology: An International Code of Practice, Technical Reports Series No. 457, IAEA, Vienna (2007).

[2] INTERNATIONAL ELECTROTECHICAL COMMITTEE, IEC61267, Medical diagnostic X ray equipment-Radiation conditions for use in the determination of characteristics.
[3] BIPM, Qualités de rayonnement, CCEMRI(I) (1972) R15.
[4] INTERNATIONAL ORGANIZATION OF STANDARDIZATION, ISO4037, X and γ reference radiations for calibrating dosemeters and dose ratemeters and for determining their response as a function of photon energy.
[5] KASTNER, J., EGGENBERGER, D., LOGNECKER, A., KING, D., SCHUTT, D., "UV Laser Excitation for Ultra-Sensitive Photoluminescent Dosimetry", Solid State and Chemical Radiation Dosimetry in Medicine and Biology (Proc. Int. Symp. Vienna, 1966), IAEA, Vienna (1967) 115–120.
[6] YOKOTA, R., MUTO, Y., KOSHIRO, Y., SUGAWARA, H., "New Type of High-sensitive and Soil-Insensitive RPL Glass Dosimetry", (Proc. 3rd Int. Conf. on Luminescence Dosimetry. Risö) Report No. 279, Part II (1971) 709–717.
[7] PIESCH, E., BURGKHARDT, B., FISCHER, M., ROBER, H.G., UGI, S., Properties of radiophotoluminescencent glass dosemeter systems using pulsed laser UV excitation. Radiat. Prot. Dosim. **17** (1986) 293–297.

DIGITAL BREAST TOMOSYNTHESIS: COMPARISON OF DIFFERENT METHODS TO CALCULATE PATIENT DOSES

A. JACOBS*, L. COCKMARTIN*, D.R. DANCE**, H. BOSMANS*

* Radiology Department, Leuven University Hospitals,
Leuven, Belgium
Email: annelies.jacobs@uzleuven.be

** NCCPM, Royal Surrey County Hospital,
Guildford, United Kingdom

Abstract

Different methods have been proposed in the literature to calculate the dose to the patient's breast in 3-D mammography. The methods described by Dance et al. and Sechopoulos et al. have been compared in this study using the two tomosynthesis systems available in the authors' hospitals (Siemens and Hologic). There is a small but significant difference of 23% for the first X ray system and 13% for the second system between dose calculations performed with Dance's method and Sechopoulos' method. These differences are mainly due to the fact that the two sets of authors used different breast models for their Monte Carlo calculations. For each system, the calculated breast doses were compared with the dose values indicated on the system console. Good agreement was found when the method of Dance et al. was used for a breast glandularity based on the patient age. For the Siemens system, the calculated doses were 5% lower than the indicated dose and for the Hologic system, the calculated doses were 12% higher. Finally, the 3-D dose values were compared with the doses found in a large 2-D dosimetry study. The dose values for tomosynthesis on the Siemens system were almost double the doses in one view 2-D digital mammography. For a typical breast of thickness 45 mm, the dose of one 2-D view was 0.83 mGy and for one 3-D view 1.79 mGy.

1. INTRODUCTION

Digital breast tomosynthesis (DBT) has been proposed as a promising new development in the field of breast imaging. This pseudo 3-D technique provides images with reduced structure noise from overlaying tissues. While clinical studies are ongoing to evaluate the clinical performance of DBT systems, the associated radiation dose should also be examined. It is important to survey the dose delivered to the patient, especially when it is aimed to use DBT systems in a

breast screening programme. Different methods for calculating the dose delivered to the patient are available in the literature.

2. MATERIALS AND METHODS

Data collection was performed on two systems at the University Hospital in Leuven, a Siemens MAMMOMAT Inspiration TOMO breast tomosynthesis system (Siemens, Erlangen, Germany) and a Hologic Selenia Dimensions tomosynthesis system (Hologic, Bedford, USA). Data from 100 clinical cases in the age ranges 34–84 years were collected for both medio-lateral-oblique (MLO) and cranio-caudal (CC) views on the Siemens tomosynthesis system. On the Hologic tomosynthesis system, data from only 18 clinical cases in the age range 43–82 years were available. These data were used for the calculation of the average glandular dose (AGD) within the patient's breast. Different approaches were used, two based on the work of Dance et al. ([1–3] (method 1, below), and the other based on the work of Sechopoulos et al. ([4, 5] (method 2, below).

2.1. Method 1

In the method of Dance et al. [1–3], the breast is represented as a semicircular cylinder with a diameter of 16 cm. The structure comprises a central region which is a homogeneous mixture of adipose and glandular tissues with an adipose layer of 5 mm surrounding the central region on all sides except at the chest wall. The breast is simulated for an examination in the CC view, but the data are also used for the estimation of the breast dose for the MLO view. The AGD is calculated using an extension of the formula used for 2-D mammography. It is given by:

$$AGD = kgcs\sum t(a), \tag{1}$$

where K is the incident air kerma for a single projection, measured at zero degree projection angle and the remaining factors were obtained from Monte Carlo simulations. The g factor is the incident air kerma to average glandular dose conversion factor for 50% glandularity breasts, the c factor allows a correction for different glandularities and the s factor corrects for the use of different spectra. These factors are the same as those used for 2-D breast dose calculations. Term $t(\alpha)$ is the tomo-factor which is dependent on the projection angle, α, measured

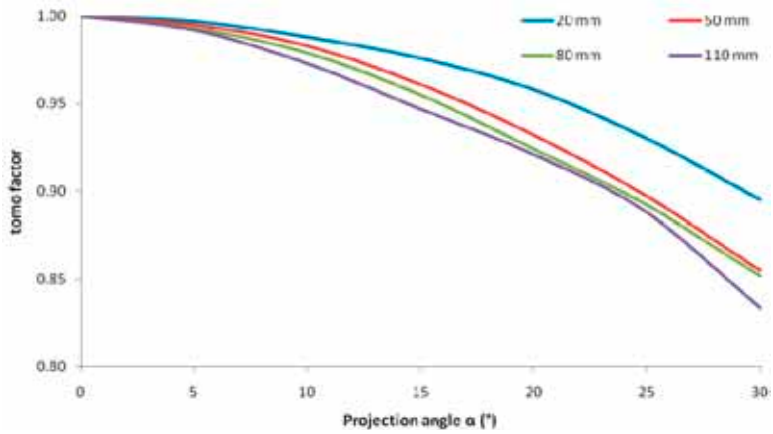

FIG. 1. Tomo-factor as a function of projection angle for different breast thicknesses. The values are an average of the minimum and maximum values of t(α) for different spectra (Mo/Mo, Mo/Rh, Rh/Rh, W/Rh, W/Ag, W/Al (0.7mm) and W/Al (0.5mm)) and different breast glandularities [3].

from the centre of rotation. Figure 1 represents the tomo-factor *t(α)* as a function of the projection angle for different breast thicknesses. These values are the average values of the minimum and maximum values of *t(α)* obtained for different spectra and different breast glandularities [3]. The tomo-factor is almost unity for small projection angles and will not differ much from the original dose calculation method for 2-D mammography but decreases slightly for larger projection angles. Although the individual values of *t(α)* are quite different for MLO and CC compression, when they are integrated, the results are very similar. The individual dose was calculated, once based on an average glandularity deduced from the age of the patient which is available in the DICOM header of the image and a second time based on the individual glandularity of the patient's breast. The information about breast glandularities was provided by the radiologists.

The air kerma is measured at the breast support plate, at 4 cm from the chest wall side, with the compression paddle in contact with the dosimeter. The multipurpose detector of RTI (Sweden) was used for the tube output measurements. On the Siemens system, the measurements were done in 2-D mode because the same target–filter combination is used in 2-D and in 3-D modes. On the Hologic system, the static 3-D mode is used because the target–filter (W/Al) is not available in 2-D. The inverse square law was applied to calculate the incident air kerma at the upper surface of the breast. No allowances for the heel effect were made in the Monte Carlo simulations. Equation (1) can

only be used when the tube current–time product is the same for every projection. This was the case for the systems used in this work.

2.2. Method 2

The second method is described by Sechopoulos et al. [4, 5]. In this work, both CC and MLO views of the breast are simulated. In the MLO view, part of the pectoral muscle is included. Breast specific parameters are: chest to nipple distance (7–19 cm in steps of 3 cm), compressed breast thickness (2–8 cm in steps of 1 cm) and glandularity (1, 25, 50, 75 and 100%). For both views, the breast is surrounded by a skin layer of 4 mm thickness and the breast is composed of a mixture of glandular and adipose tissue. A different formula is used for the dose calculations:

$$AGD = X_{CR} D_g N_0 \sum_{\alpha=\alpha_{MIN}}^{\alpha_{MAX}} RGD(\alpha) \tag{2}$$

where AGD is the average glandular dose, X_{CR} is the 'free in air' exposure of a single projection measured at a reference point on the breast support plate (expressed in röntgen) without the compression plate. This reference point is the point where the central X ray meets the support plate. D_gN_0 is the normalized glandular dose per unit exposure for the zero degree projection and RGD(α) is the relative glandular dose coefficient which is calculated for every tomosynthesis projection angle (α) measured from the support plate. It is equivalent to the quantity *t(α)* in Eq. (1). The summation is performed over the entire range of projection angles. The RGD(α) factors were calculated following the formulae for CC view or MLO view:

$$RGD_{cc} = a + b\alpha + c\delta + d\alpha^2 + e\delta^2 + f\alpha\delta + g\alpha^3 + h\delta^3 + i\alpha\delta^2 + j\alpha^2\delta \tag{3}$$

$$RGD_{MLO} = \frac{a + c\alpha + e\delta + g\alpha^2 + i\delta^2 + k\alpha\delta}{1 + b\alpha + d\delta + f\alpha^2 + h\delta^2 + j\alpha\delta} \tag{4}$$

The coefficients *a,b,… k* are fitted coefficients which are tabulated [4] and δ is the compressed chest-to-nipple distance (expressed in cm).

3. RESULTS AND DISCUSSION

The different methods were used to calculate the doses of the two X ray systems. In a first step, the different methods are compared for the same system. Then, the calculated AGD values are compared with the doses indicated on the tomosynthesis systems. Finally, the 3-D doses are compared with 2-D doses from a large patient dosimetry study.

3.1. Comparison of different methods

The AGD calculation methods described by Dance et al. and Sechopoulos et al. were compared. In the case of the first method, the calculations were performed twice, once based on the age of the patient, the other based on the individual breast glandularity. Afterwards, a comparison of the three methods is presented. Figure 2 shows the dose distribution for the three methods as a function of the compressed breast thickness for the Siemens tomosynthesis system along with the 2-D acceptable and achievable dose levels [6]. Data from both the CC and MLO views are included. The doses calculated using the Dance et al. method for individual estimates of glandularity varied between 0.69 mGy and 4.67 mGy for the range of compressed breast thicknesses from 33 mm to 95 mm. The AGD values obtained by the method of Sechopoulos et al. varied

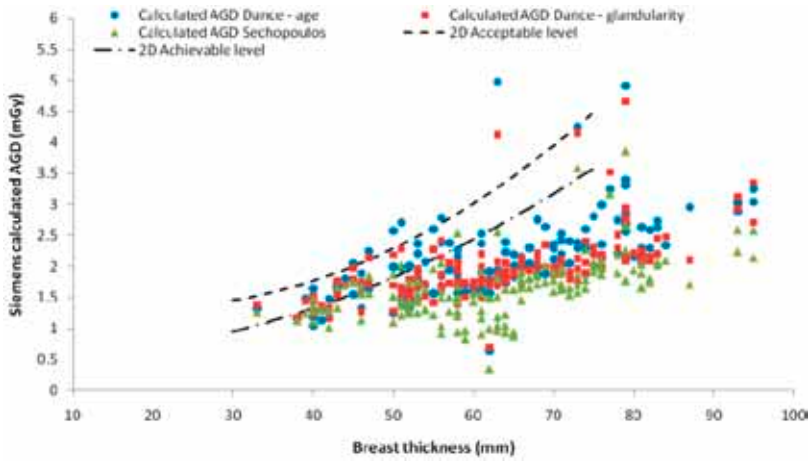

FIG. 2. Calculated AGD as a function of breast thickness for the Siemens tomosynthesis system. The blue dots represent the AGD values based on the age of the patient, the red squares are the data based on the glandularity of the breast (both using the Dance et al. method)and the green triangles are the AGD values calculated by the method of Sechopoulos et al. The 2-D acceptable and achievable dose levels of the European guidelines are also shown [6].

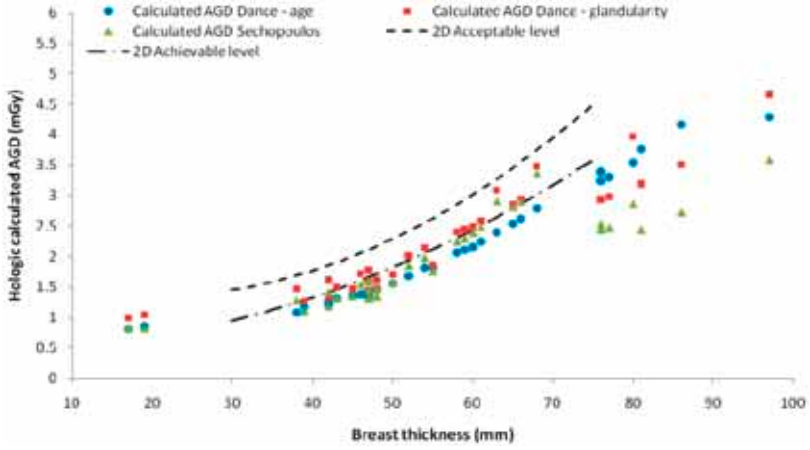

FIG. 3. Calculated AGD as a function of compressed breast thickness for the Hologic tomosynthesis system. The blue dots represent the data calculated with the Dance et al. method based on patient age, the red squares are the data calculated with patient glandularity and the green triangles are the dose values calculated by the method of Sechopoulos et al. The 2-D acceptable and achievable dose levels of the European guidelines are also shown [6].

between 0.35 mGy and 3.87 mGy. The equivalent results for the Hologic tomosynthesis system are shown in Fig. 3, where the AGD values based on individual estimates of glandularity information varied between 1.26 mGy and 3.48 mGy. When applying the

Sechopoulos et al. method, the doses varied between 1.11 mGy and 3.38 mGy. Tables 1 and 2 give an overview of the AGD values for the different methods and the different compressed breast thicknesses for both tomosynthesis systems.

For the Dance et al. method, the calculation method based on the individual glandularity of the patient's breast is chosen for the comparison of the two methods because glandularity information is also used in Sechopoulos' method. The ratio of AGD values from the two approaches has been calculated, along with the mean value of this ratio, the standard deviation and the maximum deviation from the mean value. This is done for all views and for CC and MLO views separately. Figures 4 and 5 show for each patient the ratio between the two AGD values for the Siemens system and the Hologic system, respectively. Table 3 summarizes the mean ratio, standard deviation and maximum deviation from the mean for both systems. The mean ratio between the two calculation methods for all views is 1.23 for the first system and 1.13 for the second system. This difference of 23% and 13% is mainly due to differences in the breast model and

TABLE 1. OVERVIEW OF THE MEAN AGD VALUES FOR DIFFERENT METHODS AND FOR DIFFERENT RANGES OF COMPRESSED BREAST THICKNESS FOR THE SIEMENS TOMOSYNTHESIS SYSTEM

Compressed breast thickness (mm)	AGD Dance: Age (mGy)	AGD Dance: Glandularity (mGy)	AGD Sechopoulos (mGy)
20–30	—	—	—
31–40	1.32	1.35	1.26
41–50	1.67	1.62	1.49
51–60	1.84	1.74	1.43
61–70	2.07	1.94	1.52
71–80	2.59	2.36	2.08
>80	2.64	2.44	2.02

TABLE 2. OVERVIEW OF THE MEAN AGD VALUES FOR DIFFERENT METHODS AND FOR DIFFERENT RANGES OF COMPRESSED BREAST THICKNESS FOR THE HOLOGIC TOMOSYNTHESIS SYSTEM

Compressed breast thickness (mm)	AGD Dance: Age (mGy)	AGD Dance: Glandularity (mGy)	AGD Sechopoulos (mGy)
20–30	—	—	—
31–40	1.13	1.36	1.19
41–50	1.39	1.59	1.43
51–60	1.97	2.27	2.13
61–70	2.52	2.99	2.90
71–80	3.21	3.02	2.46
>80	2.71	2.47	2.51

the fact that method 2 (Sechopoulos et al. method) takes the heel effect into account whereas method 1 (Dance et al. method) does not. The mean ratio for the CC view is 1.15 for system 1 and 1.10 for system 2 with a maximum deviation from the mean of 5% for the first system and 10% for the second.

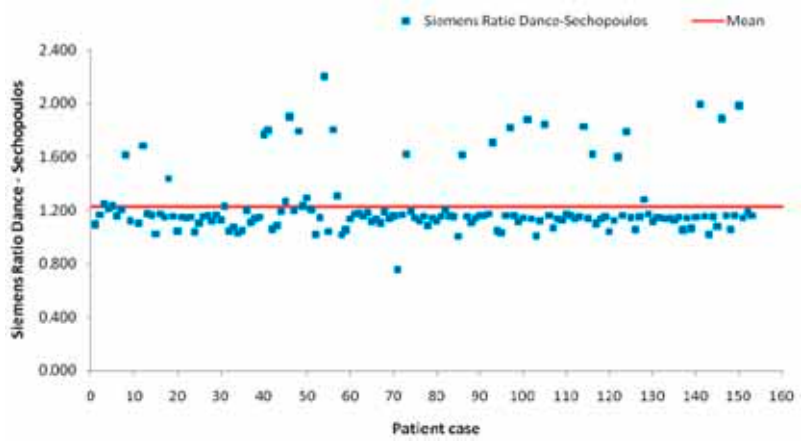

FIG. 4. Ratio of AGD values calculated by the Dance et al. method based on breast glandularity and Sechopoulos' method for the Siemens tomosynthesis system. The mean ratio is indicated by the red line.

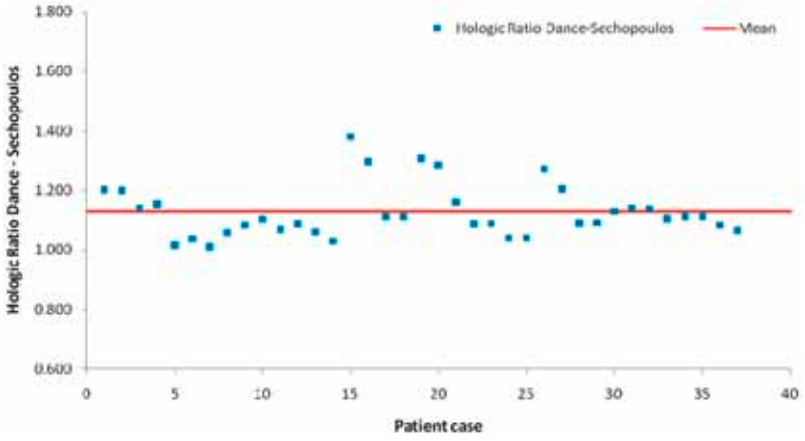

FIG. 5. Ratio of dose values calculated based on the Dance et al. method and glandularity information and Sechopoulos' method for the Hologic system. The mean ratio is indicated by the red line.

3.2. Comparison with dose indicated on the system

In a second step, the dose indicated on the system is compared with the calculated AGD values in order to know whether the dose indicated on the system is a good estimation of the doses calculated with the two methods described here.

TABLE 3. MEAN RATIO OF AGD VALUES CALCULATED BY METHOD 1 AND METHOD 2, FOR ALL VIEWS AND CC AND MLO VIEW SEPARATELY (*the standard deviation and maximum deviation from the mean value are also shown*)

	System 1			System 2		
	All	CC	MLO	All	CC	MLO
Mean ratio	1.23	1.15	1.27	1.13	1.10	1.14
Standard deviation	0.244	0.014	0.293	0.088	0.048	0.099
Maximum deviation	0.976	0.053	0.937	0.253	0.101	0.243

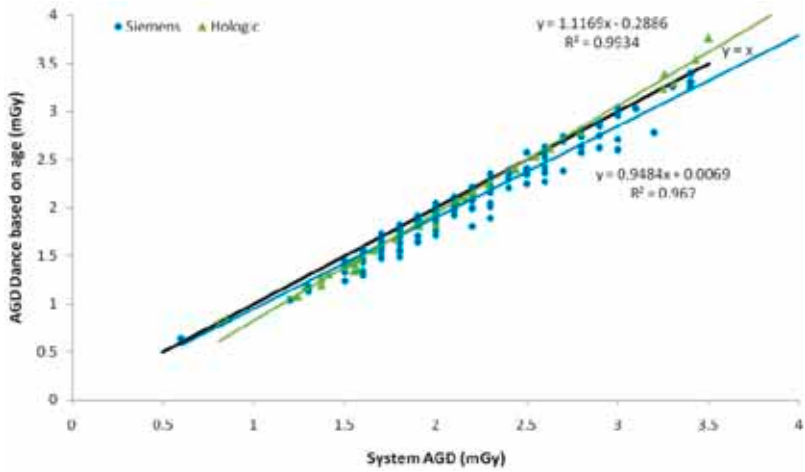

FIG. 6. Comparison between AGD indicated on the system and AGD calculated based on the age of the patient.

The comparison was done for the three methods and the two X ray systems. In Fig. 6, the results of the Dance et al. method based on age, which was the closest compared to the system AGD, are shown. For both systems, the method of Dance et al. based on age provided the best results with only a difference of 5% between the indicated and the calculated value for the Siemens tomosynthesis system and a 12% difference for the Hologic tomosynthesis system. The differences are larger when the other methods are used, up to 40% for the

comparison of the Sechopoulos method with the AGD of the Siemens X ray system. Siemens confirmed that they use the 2-D approach of Dance et al. to estimate the AGD on their systems. Because the difference between the 2-D and 3-D formula is not that large (*t*-factors are close to unity), there is a good agreement in the authors' calculations. Hologic does not use any of these three methods, but instead applies the ACR method described by Boone et al. [7, 8]. Therefore, larger deviations are expected between calculated and indicated AGD values.

It can be concluded that the dose calculation based on patients' age gives the best correlation with the indicated AGD.

3.3. Comparison of 2-D and 3-D AGD values

On the Siemens system, a comparison was made between the calculated 3-D AGD values and the 2-D dose values from a large patient dosimetry study. The 2-D doses were calculated for about 1000 patients collected on the same system, during the same period of data collection of the DBT patient doses. The 2-D dose calculation is based on the formula of Dance et al. using the age of the patient and therefore the same method is used for the 3-D doses. Figure 7 shows both the 2-D and 3-D dose values as a function of the compressed breast thickness. An exponential curve is fitted through the data, the acceptable and achievable dose levels for 2-D mammography are also shown. The 3-D doses varied between 0.64 mGy and 4.98 mGy for a compressed breast thickness ranging from 33 mm to 95 mm. The AGD values for 2-D varied between 0.25 mGy and 3.30 mGy for a compressed breast thickness of between 20 mm and 90 mm. For a typical breast of 45 mm, the AGD of one 2-D view is 0.83 mGy and for one 3-D view the dose is 1.79 mGy. Table 4 presents an overview of the 2-D and 3-D AGD values for different ranges of compressed breast thickness. From Table 4, it can be seen that doses in one view DBT are almost doubled compared to doses in one view 2-D digital mammography. However, studies are ongoing to compare 2-D mammography in two views with one view DBT. If for DBT, image acquisition could be restricted to only one view, the radiation dose to the women will stay the same for these tomosynthesis systems compared to 2-D digital mammography.

4. CONCLUSION

The methods proposed to calculate the 3-D AGD were applied and compared on the available dataset in the hospital. It is possible to calculate the

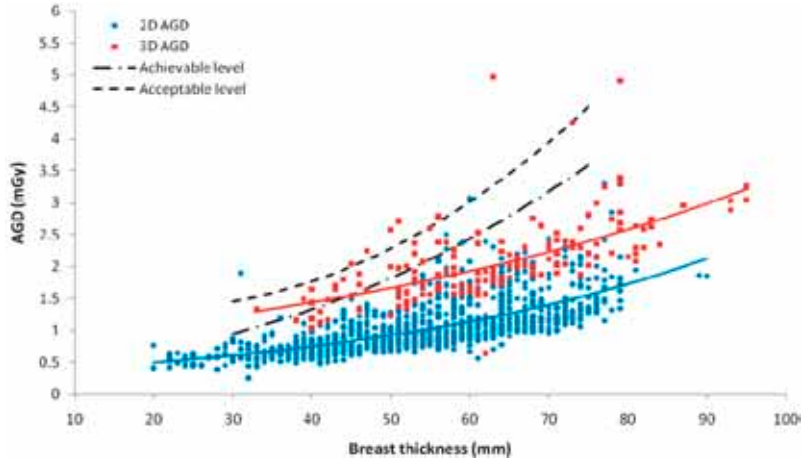

FIG. 7. Comparison between 2-D and 3-D doses in function of breast thickness. The blue dots represent the 2-D AGD values and the red squares represent the 3-D dose values based on the age of the patient. The 2-D acceptable and achievable dose levels are also shown. Doses in one view DBT are almost double the doses in one view 2-D digital mammography.

TABLE 4. OVERVIEW OF 2-D AND 3-D AGD VALUES FOR DIFFERENT RANGES OF COMPRESSED BREAST THICKNESS

Compressed breast thickness (mm)	2-D AGD (mGy)	3-D AGD (mGy)
20–30	0.58	—
31–40	0.70	1.32
41–50	0.86	1.67
51–60	1.11	1.84
61–70	1.29	2.07
71–80	1.57	2.59
>80	1.90	2.64

3-D AGD in a similar way as for 2-D mammography using different methods that could be considered relatively easy and applicable on a larger dataset. However, when glandularity information is to be included, the dose calculations become more complex due to the fact that the input information of the glandularity is obtained from the radiologists and is not available in the DICOM header of the images. The same applies for the distance from the chest wall to the nipple.

There is a small but significant difference between the two methods which can be explained by the different breast models used in the simulations and by the fact that the heel effect was taken into account in Sechopoulos' method but not in the method of Dance et al.

The calculated dose values were compared with the system AGD. Good agreement was found between the latter method based on the age of the patient and the indicated dose for both tomosynthesis systems with only a bias of 6% in the case of Siemens and 12% in the case of Hologic. The deviation is much larger when the other methods are compared.

Finally, the authors demonstrated that, on the Siemens system, doses in one view DBT are almost double those in one view 2-D digital mammography.

ACKNOWLEDGEMENTS

This work was funded by the OPTIMAM project which is supported by CR-UK & EPSRC Cancer Imaging Programme, in association with the MRC and Department of Health (United Kingdom).

REFERENCES

[1] DANCE, D.R., SKINNER, C.L., YOUNG, K.C., BECKETT, J.R., KOTRE, C.J., Additional factors for the estimation of mean glandular breast dose using the UK mammography dosimetry protocol, Phys. Med. Biol. **45** (2000) 3225–3240.

[2] DANCE, D.R., YOUNG, K.C., VAN ENGEN, R.E., Further factors for the estimation of mean glandular dose using the United Kingdom, European and IAEA breast dosimetry protocols, Phys. Med. Biol. **54** (2009) 4361–4372.

[3] DANCE, D.R., YOUNG, K.C., VAN ENGEN, R.E., Estimation of mean glandular breast dose for digital tomosynthesis: factors for use with the UK, European and IAEA breast dosimetry protocols. Phys. Med. Biol. **56** (2011) 453–471.

[4] SECHOPOULOS, I., SURYANARAYANAN, S., VENDANTHAM, S., D'ORSI, C.J., KARELLAS, A., Computation of the glandular radiation dose in digital tomosynthesis of the breast, Med. Phys. 34 (1), January 2007, 221–232.

[5] SECHOPOULOS, I., D'ORSI, C.J., Glandular radiation dose in tomosynthesis of the breast using tungsten targets, Journal of Applied Clinical Medical Physics, Volume 9, Number 4, Fall 2008, 161–171.

[6] VAN ENGEN, R.E., YOUNG, K.C., BOSMANS, H., THIJSSEN, M., Addendum on digital mammography, version 1.0, addendum to chapter 3 of the European guidelines for quality assurance in mammography screening, November 2003, 18.

[7] BOONE, J.M., Glandular breast dose for monoenergetic and high-energy X-ray beams: Monte Carlo assessment. Med. Phys. Volume 213, Number 1, 1999, 23–37.

[8] BOONE, J.M., Normalized glandular dose (DgN) coefficients for arbitrary x-ray spectra in mammography: Computer-fit values of Monte Carlo derived data, Med. Phys. 29 (5) May 2002, 869–875.

COMPLIANCE OF FULL FIELD DIGITAL MAMMOGRAPHY SYSTEMS WITH THE EUROPEAN PROTOCOL FOR IMAGE QUALITY AND DOSE

P.J. BARNES, D. TEMPERTON
Regional Radiation Physics and Protection Service,
University Hospital Birmingham NHS Foundation Trust,
Kings Norton,
United Kingdom
Email: david.temperton@uhb.nhs.uk

Abstract

The European Guideline for Breast Cancer Screening recommends methods to assess the contrast to noise ratio (CNR) and mean glandular dose (MGD) for full field digital mammography systems and provides limiting values that should be achieved. The performance of six integrated digital systems and three computed radiography (CR) systems was compared with these limiting values. Only one of the integrated systems and all three CR systems required adjustment to meet the CNR standards. For an equivalent breast thickness of 53 mm, the MGD varied between 1.1 mGy and 1.6 mGy for the integrated systems and between 2.0 mGy and 2.4 mGy for the CR systems. The range in doses increased with increasing breast thickness. Integrated systems consistently performed better than the CR systems against the European Protocol across a range of equivalent breast thicknesses.

1. METHOD

The performance of the mammography systems described in Tables 1 and 2 was assessed against the European Protocol [1] in terms of contrast to noise ratio (CNR) and mean glandular dose (MGD).

Polymethyl methacrylate (PMMA) with thicknesses between 20 mm and 70 mm (placed on the bucky) and spacers were used to simulate a range of breast thicknesses. Exposures were made under automatic exposure control (AEC) allowing the kV and target/filter combination to alter automatically. MGD was calculated for the simulated breasts as described in the European Protocol [1]. Air kerma measurements were undertaken using a Radcal 20X5-6M ion chamber with calibration traceable to national standards.

The CNR was measured for each PMMA thickness. An aluminium square (10 mm × 10 mm × 0.2 mm) was positioned on the patient platform with its right hand edge on the mid-line and 60 mm from the chest wall edge; the required

TABLE 1. LIST OF INTEGRATED EQUIPMENT

Manufacturer/model	Detector type	Detectorsize	Pixel pitch (μm)	Target/filter combination
GE Senographe DS software version ADS 53.10.1.1	a-Si (CsI)	19 × 23	100	Mo/Mo, Mo/Rh, Rh/Rh
GE Senographe DS software version ADS 43.10.1 (older model)	a-Si (CsI)	19 × 23	100	Mo/Mo, Mo/Rh, Rh/Rh
GE Senographe Essential software version ADS 53.30	a-Si (CsI)	24 × 31	100	Mo/Mo, Mo/Rh, Rh/Rh
Lorad Selenia	a-Se (Hologic)	24 × 29	70	W/Rh, W/Ag
Siemens Mammomat Inspiration	a-Se (Anrad)	24 × 30	85	Mo/Mo, Mo/Rh, W/Rh
Sectra L30 software version 8.3	Scanning silicon Technology	24 × 26	50	W/Al

TABLE 2. LIST OF COMPUTED RADIOGRAPHY (CR) EQUIPMENT

CR system[a]	Image plate	Detector size	Equivalent pixel pitch (μm)[b]	Target/filter combination available[c]
Fuji FCR FCR 5000 mA CR; software version A10	Fuji HR BD	18 × 24	50	Mo/Mo, Mo/Rh
Carestream Elite CR; software version 5.2	Kodak EHR M3	18 × 24	50	Mo/Mo, Mo/Rh
Konica Minolta Regius 170 CR; software version 2.32	Konica RP-7M	18 × 24	87	Mo/Mo, Mo/Rh

[a] Siemens Nova 3000 X ray units were used with all CR systems.
[b] Equivalent pixel pitch: determined from the CR reader scan resolution.
[c] W/Rh target/filter combination not in use.

PMMA thickness was placed on top. The mean pixel values (MPV) and standard deviations of the pixel values (σ) were assessed in four small regions of interest (ROIs) over the aluminium, and four over the PMMA. For CR systems, the pixels' values and their standard deviations were linearized against the image plate entrance surface air kerma. The ROI size was kept small (approximately 1.5 mm × 1.5 mm) to reduce any bias that may result from the heel effect [2]. The CNR was calculated using the following formula:

$$CNR = \frac{MPV_{PMMA} - MPV_{Al}}{\sqrt{\frac{\sigma^2_{PMMA} + \sigma^2_{Al}}{2}}} \quad (1)$$

where

MPV_{PMMA} is the average of the 4 MPVs for the PMMA ROIs;
MPV_{Al} is the average of the 4 MPVs for the aluminium ROIs;
$\sigma_{Al/PMMA}$ is the average of the standard deviations in the four relevant ROIs.

Threshold contrast (TC) was assessed using the CDMAM phantom (version 3.4, UMC St. Radbound, Nijmegen University, Netherlands) and 40 mm of PMMA; 20 mm of PMMA was placed above and below the phantom. This arrangement is equivalent to 50 mm of PMMA or 60 mm equivalent breast thickness. Sixteen exposures were made under manual control using the exposure factors determined previously under AEC control for 60 mm equivalent breast thickness. Contrast detail measurements were taken from the 16 images using a combination of the CDCOM software (version 1.5.2) [3, 4] and Young's automated readout software (version 2.4) [5].

Image analysis was performed on the pre-processed images. The limiting CNR for 50 mm of PMMA (based on the acceptable threshold contrast for a 0.1 mm diameter detail) was calculated using the relationship:

$$CNR_{\text{limiting value (50 mm of PMMA)}} = (TC_{\text{measured}} \times CNR_{\text{measured}})/TC_{\text{limiting value, acceptable}}$$
$$TC_{\text{limiting value, acceptable}} = 23\% \text{ as given in the Protocol.} \quad (2)$$

The $CNR_{\text{limiting value}}$ for different breast thicknesses were then calculated by multiplying the $CNR_{\text{limiting value}}$ for 50 mm of PMMA by the limiting values for relative CNR (expressed as a percentage) for different thicknesses given in the European Protocol.

Optimization should ideally ensure that for each equivalent breast thickness, the normalized CNR value (i.e. $CNR_{measured}/CNR_{limiting\ value}$) is greater than 1.0 and the normalized MGD ($MGD_{measured}/MGD_{limit}$) is less than 1.0. Table 3 gives the MGD limit for each thickness and the relative CNR values from the European Protocol.

The older GE Senographe DS (software version ADS 43.10.1) did not initially meet the $CNR_{limiting\ value}$ in the European Protocol in the standard dose mode. The dose to the digital detector was therefore increased in order to meet the $CNR_{limiting\ value}$. Similarly, the $CNR_{measured}$ for all CR systems initially fell below the $CNR_{limiting\ value}$. Adjustments to the AEC were required to increase the dose and alter the spectra at different thicknesses based on the optimization method described by Young et al. [6]. For the 53 mm breast equivalent thickness, the dose had to be increased by approximately 50% compared with the previous film screen system. The CNR results presented are those obtained after the dose and spectra adjustments. The target filter combinations used for different equivalent breast thickness are given in Table 4.

2. RESULTS

The resultant doses and normalized measured CNR values for a range of PMMA thicknesses are shown in Figs 1 and 2, respectively. The error in the MGD is estimated at 8% and for the normalized CNR, the error is estimated at 20% (‘two standard error of the mean’).

TABLE 3. MGD LIMITS FOR EACH THICKNESS OF PMMA OR EQUIVALENT BREAST THICKNESS [1]

Thickness of PMMA (mm)	Equivalent breast thickness (mm)	MGD limit (mGy)	Relative CNR (%)
20	21	1.0	115
30	32	1.5	110
40	45	2.0	105
45	53	2.5	103
50	60	3.0	100
60	75	4.5	95
70	90	6.5	90

TABLE 4. TUBE VOLTAGE (kV) AND TARGET/FILTER USED FOR EACH BREAST EQUIVALENT THICKNESS

System	Breast equivalent thickness (mm)						
	21	32	45	53	60	75	90
GE Essential	25 kV Mo/Mo	26 kV Mo/Mo	29 kV Rh/Rh	29 kV Rh/Rh	29 kV Rh/Rh	29 kV Rh/Rh	31 kV Rh/Rh
GE DS	26 kV Mo/Mo	26 kV Mo/Rh	29 kV Rh/Rh	29 kV Rh/Rh	29 kV Rh/Rh	30 kV Rh/Rh	31 kV Rh/Rh
GE DS (older model)	26 kV Mo/Mo	26 kV Mo/Rh	27 kV Rh/Rh	29 kV Rh/Rh	29 kV Rh/Rh	29 kV Rh/Rh	29 kV Rh/Rh
Lorad Selenia (Hologic)	25 kV W/Rh	26 kV W/Rh	27 kV W/Rh	28 kV W/Rh	29 kV W/Rh	27 kV W/Ag	30 kV W/Ag
Inspiration (Siemens)	26 kV W/Rh	27 kV W/Rh	28 kV W/Rh	29 kV W/Rh	30 kV W/Rh	31 kV W/Rh	32 kV W/Rh
Sectra L30	29 kV W/Al	29 kV W/Al	32 kV W/Al	32 kV W/Al	32 kV W/Al	32 kV W/Al	32 kV W/Al
Siemens Nova 3000; Fuji	26 kV Mo/Mo	26 kV Mo/Mo	27 kV Mo/Mo	27 kV Mo/Rh	27 kV Mo/Rh	29 kV Mo/Rh	29 kV Mo/Rh
Siemens Nova 3000; Kodak	26 kV Mo/Mo	27 kV Mo/Mo	27 kV Mo/Rh	27 kV Mo/Rh	27 kV Mo/Rh	29 kV Mo/Rh	29 kV Mo/Rh
Siemens Nova 3000; Konica	26 kV Mo/Mo	27 kV Mo/Mo	27 kV Mo/Rh	29 kV Mo/Rh	29 kV Mo/Rh	29 kV Mo/Rh	29 kV Mo/Rh

The error in the MGD was estimated from the quadrature sum of the errors in the ionization chamber calibration (5%), HVL assessment (2%) and variations in PMMA (2%), dosimeter position (2%) and the reference cassette (2%). The 20% error in the normalized CNR is estimated from the combined errors of the CNR readings (12%) and the threshold contrast scores (16%).

3. DISCUSSION

The results indicate that integrated digital mammography systems perform better in terms of image quality and dose than CR systems. Only the modern

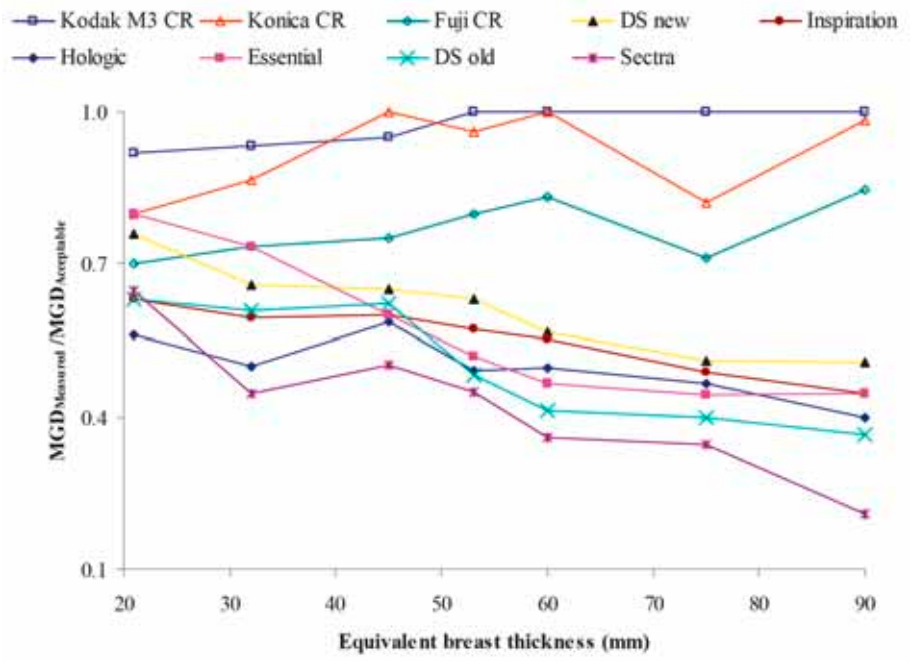

FIG. 1. Measured MGD normalized to the dose limits in the European protocol.

integrated systems achieve a normalized CNR above 1.2 across the full range of breast thicknesses, thus demonstrating compliance with the European Protocol even allowing for errors. For CR systems, the normalized dose for all breast thicknesses is at least 0.7, so the units are operating close to the European dose limits. This agrees with data published in NHSBSP equipment reports [7] and a recent study in France [8]. In this investigation, the target filter combinations available for the CR systems were Mo/Mo and Mo/Rh, which may lower the overall performance. Improvements have been seen in units fitted with Rh/Rh [9] and W/Rh [10] target filter combinations. Nonetheless, the CR results provide a relative comparison using a Mo/Rh target/filter combination. There is some scope to improve the CNR values for Fuji CR systems, but this will result in an increase in dose.

Optimization of the modern integrated systems was not carried out in this investigation. Improved image quality of these systems may be achieved by either adjusting the dose, the choice of beam quality or both. However, a dose increase is not currently possible for the Sectra because it is operating at the maximum dose mode.

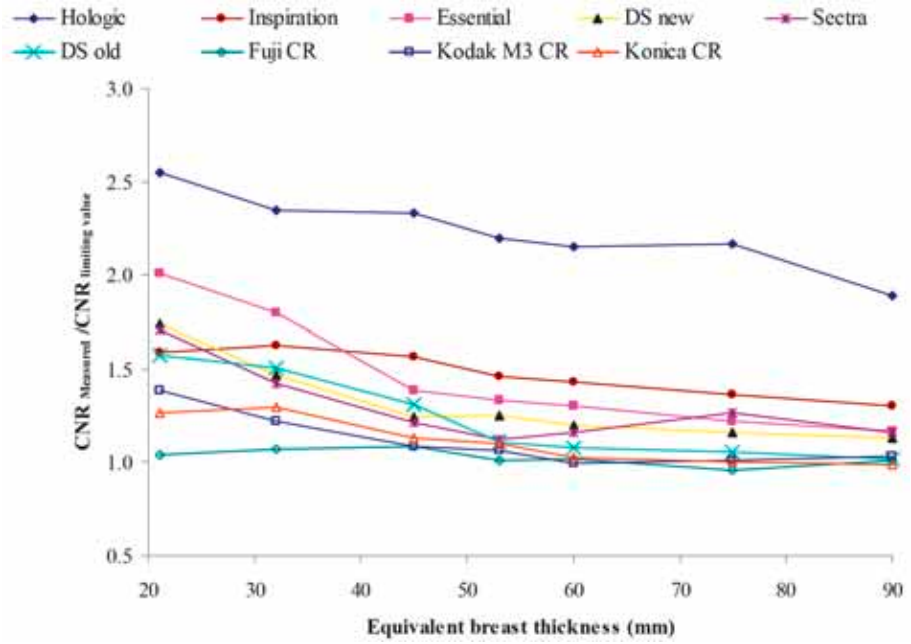

FIG. 2. Measured CNR normalized to the limiting values in the European Protocol.

The Sectra has a curved patient platform that gives a maximum 17 mm air gap at the centre when performing tests with the CDMAM. This may introduce blurring of the detail diameters in the images, reducing the threshold contrast score. Further investigation is required.

4. CONCLUSION

Most integrated digital systems performed better in terms of image quality and all delivered lower doses relative to CR systems.

All modern integrated digital systems required no adjustment to comply with the European standards, but the older model of the GE Senographe DS used in this study needed adjustments in order to comply. All three CR systems required adjustments to the AEC to meet the standards. With an equivalent breast thickness of 60 mm, the highest MGD estimated on an integrated system was 1.7 mGy. The lowest MGD at the same thickness measured on an optimized CR system using Mo/Rh was 2.5 mGy. Thus, a dose reduction of at least 50% can be achieved by using an integrated system (even without in-house optimization) compared with an optimized CR system. At equivalent breast thickness of

90 mm, the highest dose for an integrated system was 3.3 mGy, and the lowest dose for an optimized CR system was 5.5 mGy, which is a 70% difference in dose.

REFERENCES

[1] VAN ENGEN, R., YOUNG, K.C., BOSMANS H.,THIJSSEN, M.., "The European protocol for the quality control of the physical and technical aspects of mammography screening, Part B: Digital mammography", European Guidelines for Breast Cancer Screening, 4th edn, Luxembourg: European Commission (2006).

[2] ALSAGER, A., YOUNG, K.C., ODUKO, J.M., Impact of heel effect and ROI size on the determination of contrast-to-noise ration for digital mammography systems. Proceedings of SPIE medical Imaging, 2008 6913, 691341

[3] VISSER, R., KARSSEMEIJER, N., CDCOM Manual: software for automated readout of CDMAM 3.4 images.

[4] KARSSEMEIJER, N., THIJSSEN, M.A.O., "Determination of contrast-detail curves of mammography systems by automated image analysis", Digital Mammography '96. (Proc. of the 3rd International Workshop on Digital Mammography) (1996) 155–160.

[5] YOUNG, K.C., ENNE, J., Automated determination of threshold contrast: Software and instruction manual v2.6.

[6] YOUNG, K.C., COOK, J.J.H., ODUKO, J.M., Use of the European protocol to optimise a digital mammography system (ASTLEY, S.M., BRADEY, M., ROSE, C., ZWIGGELAAR, R., Eds) (Proc. of the 8th Int. Workshop on Digital mammography, Berlin Germany) Springer-Verlag, Lecture Notes in Computer Science **4046** (2006) 362–369.

[7] YOUNG, K.C., ODUKO, J.M., GUNDOGDU, O., ALSAGER, A., Technical evaluation of the Konica Minolta Regius 190 CR mammography system and three types of image plates, NHSBSP equipment report 0806.

[8] HEID, P., Impact of the introduction of CR and DR in a National Screening Programme, symposium mammographicum conference, Liverpool (2010).

[9] YOUNG, K.C., ODUKO J.M., Technical Evaluation of the Kodak Directview Mammography Computerised Radiography System using EHR-M2 Plates, NHSBSP equipment report 0706.

[10] BARNES, P.J., BIRD, E.M., ANTOINE, C., Optimisation of Computed Radiography Based Mammography Systems — Can a Tungsten Anode Reduce Dose? (in preparation).

TEST AND CALIBRATION OF A HOME-MADE IONIZATION CHAMBER FOR DOSE MEASUREMENTS IN COMPUTED TOMOGRAPHY

V.S. BARROS*, M.P.A. POTIENS**, M. XAVIER**,
H.J. KHOURY*, M.E. DE ANDRADE*, L.V.E. CALDAS**

* Nuclear Energy Department,
Federal University of Pernambuco,
Recife

** Instituto de Pesquisas Energeticas e Nucleares,
Comissão Nacional de Energia Nuclear,
São Paulo
Email: lcaldas@ipen.br

Brazil

Abstract

This paper describes the results of the calibration of a home-made, pencil shaped CT chamber, designed and manufactured by the Instituto de Pesquisas Energéticas e Nucleares (IPEN/CNEN-SP). The response of the chamber was evaluated at clinical dosimetry conditions, and was compared with the response of a comercial ionization chamber. The results obtained showed a good agreement between the response of both chambers with a difference lower than 5%.

1. INTRODUCTION

Computed Tomography (CT) is an important, widely used diagnostic imaging method. It is based on the acquisition of thin axial images of the patient body, resulting in little overlap of anatomical structures, providing high quality images. These advantages come at a price, because patient dose in CT procedures is much larger than in conventional radiological procedures.

The dosimetry for CT medical equipment differs from the methods applied to conventional radiodiagnostic dosimetry mainly because of the tube rotation around the patient. According to IAEA TRS-457 [1], the currently recommended quantities for CT dosimetry are the volume CT air kerma index (C_{VOL}) and the air

kerma length product ($P_{KL,CT}$). C_{VOL} is a useful indicator of CT dose, considering specific information on each acquisition protocol. The $P_{KL,CT}$ represents the total CT scan air kerma length product [2] and is measured using a CT ionization chamber calibrated in 'air kerma length product', in units of mGy·cm. The air kerma length product is defined [3] as the integral of the air kerma along a line. This quantity is useful in CT where the line is chosen to be parallel to the axis of rotation of the CT scanner.

This paper describes the results of the characterization and calibration of a homemade pencil shaped CT chamber, designed and manufactured by the Instituto de Pesquisas Energéticas e Nucleares (IPEN), Brazil.

2. MATERIALS AND METHODS

A diagram and a photographic image of the CT chamber are shown in Fig. 1. The wall material of the sensitive volume of the chamber is polyvinyl chloride plastic (PVC) coated with graphite and its electrode material is aluminum with a thickness of 1.2 mm. The PVC is cheap, durable, and easy to assemble. The internal diameter is 6.7 mm, and the wall thickness and the sensitive length of the chamber are 0.26 mm and 100 mm, respectively.

The chamber was calibrated in the Metrology Laboratory of Ionizing Radiation of Nuclear Energy Department (LMRI-DEN/UFPE) which is located in Recife, Brazil. The radiation exposure was performed on a Pantak 420 X ray system using the radiation qualities established according to IEC 61267 [2] and a reference ionization chamber.

The ionization chambers were irradiated with their axis perpendicular to the anode–cathode axis of the X ray tube, at a distance of 100 cm from the focal spot. Using lead collimators with a rectangular aperture, the field dimension at the ionization chamber was adjusted to 8 cm × 8 cm. The chamber was

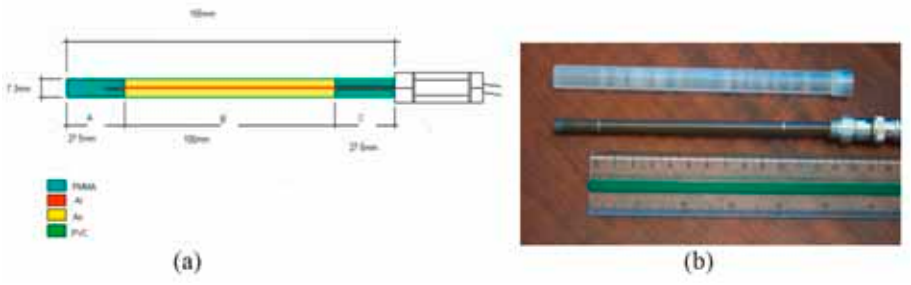

FIG. 1. Diagram (a) and image (b) of the IPEN-CNEN-SP CT chamber.

connected to a PTW electrometer UNIDOS E and the current was measured by irradiating the chamber at known air kerma rates with RQT-8, RQT-9 and RQT-10 X ray qualities. The standard ionization chamber Radcal model RC3CT serial 8769, calibrated in the German primary standard laboratory Physikalisch-Technische Bundesanstalt, was used as a reference. For comparison, measurements were also made with the Radcal CT chamber, model RC3CT (serial no. 8849), from the laboratory. The calibration factor, in units of $Gy \cdot cm \cdot C^{-1}$, was then determined on the basis of the quotient between the air kerma length product determined by the standard chamber and the ionisation current of the chamber under study.

After calibration, the response of the IPEN CT chamber was evaluated at clinical dosimetry conditions. For this evaluation, measurements of the CT air kerma index, $C_{a,100}$, were made with the ionization chamber at a Toshiba Asteion single slice CT scanner, installed at an university hospital. The $C_{a,100}$ was measured for a single rotation with the ionization chamber in air, along a line parallel to the axis of rotation of the CT scanner. The CT air kerma index was also measured inside a PMMA head phantom and the notation; this air kerma index is $C_{PMMA,100}$. Measurements were made with the ionization chamber in the centre ($C_{PMMA,100,c}$) and at four locations around the periphery of the phantom ($C_{PMMA,100,p}$). These measurements provide an indication of the average air-kerma in phantom over a single rotation. The weighted CT air kerma index, C_w, was calculated by:

$$C_w = 1/3\ (C_{PMMA,100,c} + 2C_{PMMA,100,p}) \quad (1)$$

where $C_{PMMA,100,c}$ and $C_{PMMA,100,p}$ are the CT air kerma indices in the centre, *c*, and at the periphery, *p*, of the phantom.

To compare the response of the home-made ionization chamber and a commercial CT chamber, the $C_{a,100}$ and the C_w values were determined using a previously calibrated PTW CT ion chamber, serial no. 30009-0666.

The chamber response was tested in relation to its stability (short and medium term stabilities). The CT chamber was repeatedly exposed to a $^{90}Sr + ^{90}Y$ check source positioned at an acrylic support, under reproducible geometric conditions.

3. RESULTS

Table 1 shows the results of the values of the calibration coefficient N_K ($Gy \cdot cm \cdot C^{-1}$), with respect to the beam quality RQT-9 [2], and energy correction factors k_Q obtained with the IPEN home-made CT chamber, the

TABLE 1. N_K AND k_Q VALUES FOR THE TESTED IONIZATION CHAMBERS

Ionization chamber	X ray quality	N_K ($Gy \cdot cm \cdot C^{-1}$)	k_Q	U (%) (k = 2)
Standard Radcal C3CT-8769	RQT-8	9.57×10^7	0.997	1.5
	RQT-9		1.000	1.5
	RQT-10		1.005	1.5
IPEN	RQT-8	7.733×10^7	0.990	2.2
	RQT-9		1	2.2
	RQT-10		1.010	2.2
Commercial Radcal RCSCT-8849	RQT-8	9.57×10^7	0.996	2.2
	RQT-9		1.000	2.2
	RQT-10		1.006	2.2

TABLE 2. $C_{A,100}$ AND $_NC_{A,100}$ VALUES DETERMINED WITH THE IPEN/CNEN AND PTW CHAMBERS

Ionization chamber	$C_{a,100}$ (mGy)	$_nC_{a,100}$ (mGy/mAs)	Standard deviation (%)
PTW	28.06	0.281	0.2
IPEN	27.43	0.274	0.2

standard chamber (Radcal RC3CT-8769) and the Radcal chamber RCSCT-8849. The values of the expanded uncertainties (U) (k = 2) estimated according to the IEC/ISO Guide, 1995 [4], are also presented in Table 1.

The results indicate that the IPEN ionization chamber response is around 24% higher than that of the Radcal chambers, and has greater energy dependence than the Radcal CT chambers.

Table 2 presents the results of the $C_{a,100}$ values measured with the PTW and the IPEN chambers. The values of the CT air kerma index normalized by the tube current time product are also presented.

The results show a good agreement between the values of the CT kerma index determined with both ionization chambers. The deviation of the $C_{a,100}$ values obtained with the IPEN/CNEN chamber in relation to the PTW chamber is 2.1%. The results of the values of CT air kerma index measured with both ionization chambers inside a PMMA head phantom are shown in Table 3. The calculated values of the weighted CT air kerma index, C_w, and their normalized values to tube current–exposure time product values are also presented in Table 3.

TABLE 3. $C_{PMMA,100,C}$, $C_{PMMA,100,P}$, C_W AND ${}_nC_W$ VALUES DETERMINED WITH THE IPEN/CNEN AND PTW CHAMBERS FOR A CT TOSHIBA SCANNER (MODEL ASTEION)

Ionization chamber	$C_{PMMA,100,c}$ (mGy)	$C_{PMMA,100,p}$ (mGy)	C_W (mGy)	${}_nC_W$ (mGy/mAs)
PTW	15.53	16.77	16.36	0.164
IPEN	14.83	15.67	15.39	0.154
Deviation	4.54%	6.57%	5.93%	5.93%

To evaluate the stability of response of the ionization chamber, short term and medium term stability tests were performed. The short term stability test was obtained by ten readings of charge, during time intervals of 60 s and using a voltage of +100 V, under reproducible conditions. The highest variation coefficient obtained was 0.2%, within the recommended limit of IEC 61674 [5], which is 1% for CT specific chambers.

The medium term stability test was obtained by taking the medium value of the ten measurements of the short term stability tests during a period of one month. The coefficient variation of the results during this period was lower than 1% and, as per the IEC 61674 [5] recommendation, 3%.

The uncertainty values associated with the measurement of the CT kerma index considering the components Type A (reproducibility, stability, calibration factor of the ionization chamber) and Type B (stability of the CT scanner, calibration electrometer, geometry of irradiation) is 11%, with 95% confidence interval. This value is considered in accordance with the values presented by the IAEA, i.e. 14%.

4. CONCLUSIONS

This study shows that the IPEN home-made chamber with aluminum electrode material has a sensitivity of around 24% higher than the Radcal CT chambers and an energy dependence of the response of 2% between RQRT-8 to RQRT-10, which is higher than the observed variation with respect to the Radcal chamber. The stability response test showed that the ionization chamber reaches the recommended limits of IEC 61674. The uncertainty in the measurements of the CT kerma index using this ionization chamber can be considered satisfactory in terms of IAEA [1] and ICRU [3] international requirements.

ACKNOWLEDGEMENTS

The authors acknowledge the financial support of Fundação de Amparo à Pesquisa do Estado de Pernambuco (FACEPE), Conselho Nacional de Desenvolvimento Científico e Tecnológico (CNPq), Brazil, Fundação de Apoio à Pesquisa do Estado de São Paulo (FAPESP) and the INCT project, Radiation Metrology in Medicine.

REFERENCES

[1] INTERNATIONAL ATOMIC ENERGY AGENCY, Dosimetry in Diagnostic Radiology: An International Code of Practice, Technical Reports Series No. 457, IAEA, Vienna (2007).

[2] INTERNATIONAL ELECTROTECHNICAL COMMISSION, Medical diagnostic X ray equipment — Radiation conditions for use in the determination of characteristics, IEC 61267, Geneva (2005).

[3] INTERNATIONAL COMMISSION ON RADIATION UNITS AND MEASUREMENTS, Patient dosimetry for X Rays used in Medical Imaging, ICRU Report 74, Oxford University Press, Oxford, UK, Vol. 5, No. 2 (2005).

[4] INTERNATIONAL ORGANIZATION FOR STANDARDIZATION, Guide to the expression of uncertainty in measurement. ISO-GUM, Geneva (1995).

[5] INTERNATIONAL ELECTROTECHNICAL COMMISSION, Medical electrical equipment-dosimeters with ionization chambers and/or semi-conductor detectors as used in X ray diagnostic imaging, Geneva (1997).

PATIENT SPECIFIC KERMA AREA PRODUCT AS AN EXPOSURE ESTIMATOR IN COMPUTED TOMOGRAPHY: THE CONCEPT AND TYPICAL VALUES

A. MALUSEK*, E. HELMROT**, G. ALM CARLSSON*

* Division of Radiological Sciences,
Department of Medical and Health Sciences
Email: alexandr.malusek@liu.se

** Department of Radiation Physics,
Linköping University Hospital

Linköping, Sweden

Abstract

Monitoring of exposure levels in computed tomography is important from the radiation safety point of view. In this paper, the concept suggested by Huda of using the patient specific kerma area product as an exposure estimator is extended by providing both a rigorous definition of this quantity and a method for its evaluation. The method was demonstrated on an axial scan of the standard CT dosimetry head phantom taken with a Siemens Somatom Open CT scanner. The resulting patient specific kerma area product was 0.25 Gy cm^2 for the X ray tube voltage of 120 kV, tube current of 100 mA, scanning time of 1 s, and beam width at the isocentre of 1.2 cm. To implement this method, the CT scanner must be equipped with a KAP meter, and the calculation procedure must be added to the scanner's software. Alternatively, the patient specific kerma area product can be calculated by the CT scanner without using a KAP meter. In this case, however, the extra safety feature provided by the direct monitoring of the X ray beam by the KAP meter is lost.

1. INTRODUCTION

Computed tomography (CT) is a large contributor to the irradiation of population from medical radiation sources [1, 2] and thus monitoring of patient doses and knowledge of associated risks are of great importance. As thousands of projections are performed in a single CT X ray tube rotation, effective doses from, for instance, abdomen examinations often exceed 5 mSv [2]. CT dosimetry for quality control has been performed via CTDI measurements using CT phantoms, and patient specific doses have been estimated from CT scanner

settings [3]. Applicability of the original definition of CTDI [3] is, however, problematic for CT scanners using wide (cone) beams. New quantities were proposed in Ref. [4] to mitigate the problem, but the concept remains the same. An alternative approach is to use the patient specific kerma area product as an exposure estimator. In this case, the kerma area product for radiation impinging on the patient is measured for each projection, and a total value from a complete scan is reported and shown on the user console. The concept was suggested by Huda in Ref. [1] but no detailed information on how to evaluate this quantity in practice was given. A simplified version was applied in dental radiology in Ref. [5]. The kerma area product was estimated as a product of the kerma length product and the average width of the patient jaw. A correction factor that accounted for beam attenuation by the bowtie filter was applied. The aim of this article is to extend the idea by proposing: (a) a rigorous definition of patient specific kerma area product, and (b) a method for its evaluation by a CT scanner. To demonstrate the performance of the method, the Siemens Somatom Open CT scanner was used to obtain patient specific kerma area product values (here denoted as P_{PSKA}) for the standard CT dosimetry head phantom.

2. THEORY

Let patient specific kerma area product of a CT examination be defined as a sum over all projection specific kerma area products $P_{KA,i}$

$$P_{PSKA} = \sum_i P_{KA,i} \tag{1}$$

where $P_{KA,i}$ is determined for the projection i and neglects photons passing beside the patient. It can be calculated by a CT scanner from values measured by a KAP meter mounted downstream of the bowtie filter (see Fig. 1a), as follows. For each projection, detector elements shaded by the patient are identified. For simplicity, it is assumed here that the corresponding region at an isocentre crossing plane perpendicular to the beam axis is given by an interval (x_a, x_b) (see Fig. 1). Then $P_{KA,i}$ is evaluated as:

$$P_{KA,i} = \Delta t_i \dot{P}_{KA}(I) \frac{P_{KL}(0)}{P_{KA}} \int_{x_a}^{x_b} \frac{P_{KL}(x)}{P_{KL}(0)} dx \tag{2}$$

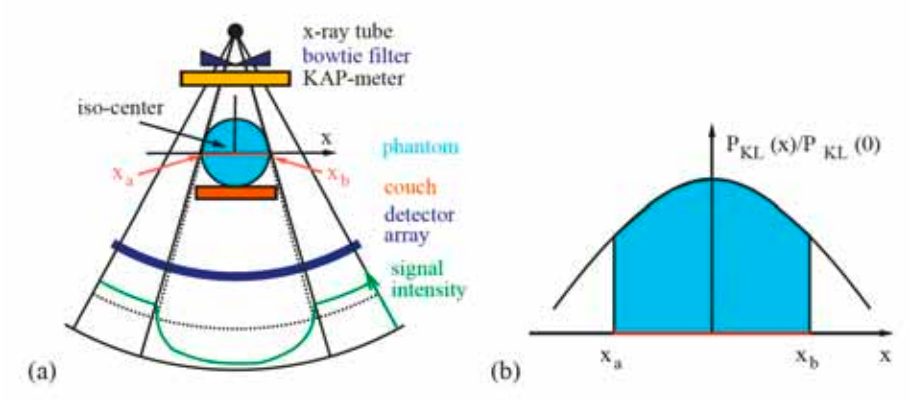

FIG. 1. (a) Schematic view of the integration interval (x_a, x_b), which can be defined as a region where the signal intensity drops below a certain threshold level. To avoid attenuation in the couch, the signal can be calculated from reconstructed images. (b) The interval (x_a, x_b) is used to evaluate the integral in Eq. (2); the integral equals the area below the curve $P_{KL}(x)/P_{KL}(0)$.

where

$\dot{P}_{KA}(I)$ is the kerma area product rate measured by the KAP meter, which depends on the tube current I,

Δt_i is the acquisition time for projection i,

and $P_{KL}(x)$ and $P_{KL}(0)$ are the kerma length products taken at positions x and 0, respectively.

The ratios $P_{KL}(x)/P_{KL}(0)$ and $P_{KL}(0)/P_{KA}$, where P_{KA} is the kerma area product measured by the KAP meter, can be determined during manufacturing or maintenance of the CT scanner as a part of the calibration procedure. The integral in Eq. (2) must be evaluated separately for each projection during a patient scan. If a polynomial is used to fit the measured $P_{KL}(x)/P_{KL}(0)$ ratio, then the primitive function can be found analytically and the calculation of the definite integral simplifies to a calculation of a difference between two functional values of the primitive function. The calculation of Eq. (1) can be performed 'on the fly' and the resulting value can be displayed on the operator's console in real time; the delay caused by the need to obtain reconstructed images to determine the integration ranges may be made sufficiently short.

3. METHODS

To date, clinical CT scanners have not been equipped with KAP meters, and thus the solution described in Section 2 was not directly applicable. To demonstrate the concept for a Siemens Somatom Open CT scanner, the authors considered an axial scan of the standard CT dosimetry head phantom (a PMMA cylinder with a diameter of 16 cm) and calculated the P_{PSKA} value using a simplified method. The measurement of the kerma area product rate, $\dot{P}_{KA}(I)$, was replaced with the measurement of the kerma length product rate, $\dot{P}_{KL}(I; x = 0)$, at the isocentre. It simplified Eq. (2) to:

$$P_{KA,i} = \Delta t_i \dot{P}_{KL}(I; x = 0) \int_{x_a}^{x_b} \frac{P_{KL}(x)}{P_{KL}(0)} dx \tag{3}$$

Owing to the axial symmetry of the imaged object,

$$\dot{P}_{KL}(I; x = 0)$$

did not depend on the viewing angle. Both the kerma length rate $\dot{P}_{KL}$ and the ratio $P_{KL}(x)/P_{KL}(0)$ were measured using a pencil ionization chamber (model WD CT 10 manufactured by Wellhöfer). As the X ray spectrum became harder for larger distances x from the beam axis due to the increased path length through the bowtie filter, corrections to the chamber's measured calibration coefficient had to be applied (see Section 3.1). They were determined from calculated calibration coefficients of the chamber (see Section 3.2). Corrected values of the $P_{KL}(x)/P_{KL}(0)$ ratio were fitted with polynomials of degree 8. The definite integral on the right hand side of Eq. (3) was calculated analytically for these polynomials. As the geometry was rotationally symmetric, the patient specific kerma area product defined by Eq. (1) was calculated as:

$$P_{PSKA} = \left(\sum_i \Delta t_i \right) \dot{P}_{KL}(I; x = 0) 2 \int_0^{x_c} \frac{P_{KL}(x)}{P_{KL}(0)} \mathrm{dx} \tag{4}$$

where

$$\sum_i \Delta t_i$$

is the total time of the axial scan and x_c is the integration interval bound for a cylinder with radius of 8 cm positioned in the isocentre.

3.1. Measurement of the kerma length product

The WD CT 10 chamber was positioned free in air inside the gantry of the CT scanner using a computer controlled positioning table. Uncorrected kerma length values $P^{*}_{KL,m}(x;U)$ were obtained at 16 equally spaced distances in the interval [0, x_b] (see Fig. 1(a)) from the measured charge $Q(x;U)$ as $P^{*}_{KL,m}(x;U) = Q(x;U)N_{KL,Q_0}$, where the calibration coefficient N_{KL,Q_0} = 24.2 mGy·cm·nC^{-1} was obtained at a secondary standards laboratory for the tube voltage of 120 kV and filtration of 2.5 mm Al (half value layer = 4.05 mm). Since the corrected kerma length values can be calculated as:

$$P_{KL,m}(x;U) = P^{*}_{KL,m}(x;U)\frac{N_{KL}(x;U)}{N_{KL,Q_0}} \tag{5}$$

where $N_{KL}(x;U)$ is the calibration coefficient for position x and tube voltage U, the corrected ratio $r_m(x;U)$ was calculated as:

$$r_m(x;U) = \frac{P_{KL,m}(x;U)}{P_{KL,m}(0;U)} = \frac{P^{*}_{KL,m}(x;U)}{P^{*}_{KL,m}(0;U)}\frac{N_{KL}(x;U)}{N_{KL}(0;U)} = r^{*}_{m}(x;U)\frac{N_{KL}(x;U)}{N_{KL}(0;U)} \tag{6}$$

where $r^{*}_{m}(x;U) = P^{*}_{KL,m}(x;U)/P^{*}_{KL,m}(0;U)$ is the uncorrected ratio. The calibration coefficient $N_{KL}(x;U)$ was calculated using the Monte Carlo method (see section 3.2). The dependence of the calibration coefficient on the filter thickness, t, was approximated using linear regression as:

$$\frac{N_{KL}}{\text{mGy cm nC}^{-1}} = a_0 + a_1\frac{t}{\text{mm}} \tag{7}$$

By inserting Eq. (7) into (6), the corrected ratio was expressed as:

$$r_m(x;U) = r^{*}_{m}(x;U)\frac{a_0(U) + a_1(U)\left[t(x)/\text{mm}\right]}{a_0(U) + a_1(U)\left[t(x=0)/\text{mm}\right]} \tag{8}$$

where the bowtie filter thickness, $t(x)$, as a function of position x was obtained from a technical drawing of the bowtie filter. The drawing was provided under a

non-disclosure agreement, which prevented the authors from showing the function here.

3.2. Calculation of the calibration coefficient

The calibration coefficient of the WD CT 10 pencil ionization chamber was calculated as:

$$N_{KL} = \frac{P_{KL}}{Q} = \frac{wK_{air}}{\varepsilon/\left(W_i/e\right)} \tag{9}$$

where

Q is the collected charge;
K_{air} is the air kerma in the centre of the ion chamber;
w is the beam width at the axis of the pencil chamber;
W_i is the average energy loss per elementary charge produced [6];
e is the electric charge of electron; and
ε is the energy imparted to the air cavity of the chamber.

The ratio W_i/e = 33.97 J/C was taken from Ref. [7]; K_{air} was calculated analytically as:

$$K_{air} = \int E\Phi_E\left(E,r\right)\left(\mu_{tr}/\rho\right)_{air} dE \tag{10}$$

where $\Phi_E(E, r)$ is the distribution of fluence with respect to energy at the point r, and $(\mu_{tr}/\rho)_{air}$ is the mass energy transfer coefficient for air. A contribution of scattered photons to the value of K_{air} was neglected as it is typically less than 1% in this calibration setup. The energy imparted to the air cavity, ε, was calculated using the PENCYL program of the PENELOPE-2008 Monte Carlo code [8]. The geometry consisted of a point source emitting photons to a cylindrical fan beam and three concentric cylinders modelling the pencil ionization chamber. Radii of these cylinders were: 0.5 mm for the metallic inner electrode, 4.0 mm for the inner radius of the outer electrode made of carbonated epoxy resin, and 4.5 mm for the outer radius of the outer electrode. Length of all cylinders was 100 mm. Densities and elemental compositions of the metallic and epoxy resin electrodes were set according to a qualified guess as the manufacturer could not provide accurate data. Spectra for X ray tube voltages of 80, 100, 120 and 140 kV were

obtained from Siemens and analytically filtered with aluminum filters of thicknesses varying from 0 to 45 mm. Inherent filtration of the X ray tube had already been taken into account in the provided X ray spectra. Cut-off energies for the transport of photons and electrons were set to 50 eV in the air cavity, 100 eV in the chamber walls, and 1 keV in the surrounding air. Individual electron collisions were simulated in the air cavity by setting PENELOPE's simulation parameters to $C_1 = C_2 = 0$. In other regions, the condensed history method with $C_1 = C_2 = 0.5$ was used.

4. RESULTS

Calibration coefficients of the WD CT 10 pencil ionization chamber as a function of the aluminium filter thickness for X ray tube voltages of 80, 100, 120 and 140 kV are plotted in Fig. 2(a). The relative difference of 4% between measured and calculated calibration coefficients (24.2 and 23.2 mGy·cm·nC^{-1}, respectively) for the tube voltage of 120 kV was most likely caused by inaccurate elemental composition of materials used in simulations and, to a lesser degree, by differences in used X ray spectra. Fitting lines in Fig 2(a) were obtained via linear regression for thicknesses from 0 to 25 mm as only these were applicable for distances up to 150 mm from the central axis.

Corresponding coefficients of linear regression, a_0 and a_1, given in Table 1 were used to correct the ratio $r_m^*(x; U)$ of measured P_{KL} values (see Eq. (8)), for the beam hardening that increased with increasing distance from the central axis. The corrected ratio $r_m(x;U)$ as a function of filter thickness for tube voltages of 80, 100, 120, and 120 kV is plotted in Fig. 2(b).

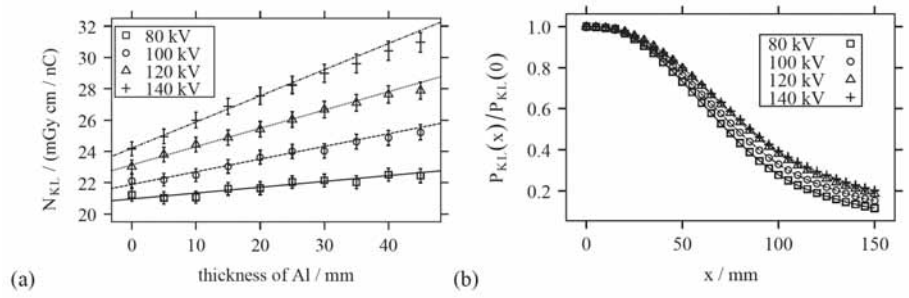

FIG. 2. (a) Calculated calibration coefficient, N_{KL}, of the WD CT 10 chamber as a function of aluminium filter thickness. (b) The normalized kerma length product, $P_{KL}(x)/P_{KL}(0)$, as a function of position, x, for X ray tube voltages of 80, 100, 120, and 140 kV and the head bowtie filter.

TABLE 1. COEFFICIENTS OF LINEAR REGRESSION OF THE CALIBRATION COEFFICIENT[a] FOR X RAY TUBE VOLTAGES OF 80, 100, 120 AND 140 kV WITH STANDARD UNCERTAINTIES

	80 kV	100 kV	120 kV	140 kV
a_0	20.97 ± 0.16	21.89 ± 0.13	23.13 ± 0.071	24.209 ± 0.086
a_1	0.037 ± 0.011	0.0809 ± 0.0091	0.1169 ± 0.0049	0.1671 ± 0.0061

[a] See Eq. (7).

TABLE 2. VALUES OF THE DEFINITE INTEGRAL FOR THE STANDARD CT DOSIMETRY HEAD PHANTOM (X_C = 80.8 mm) SCANNED BY THE SIEMENS SOMATOM OPEN CT SCANNER

Voltage:	80 kV	100 kV	120 kV	140 kV
$\int_0^{x_C} \frac{P_{KL}(x)}{P_{KL}(0)} dx$:	63.6 mm	65.6 mm	67.8 mm	68.1 mm

Values of the definite integral on the right hand side of Eq. (3) calculated for the cylindrical head phantom are shown in Table 2. For the tube voltage of 120 kV, scanning time of 1 s, tube current–time product of 100 mAs, and beam width of 1.2 cm at the isocentre, the total kerma length product measured free in air at the isocentre was P_{KL} = 18.8 mGy·cm. The corresponding value of the patient specific kerma area product was then P_{PSKA} = 18.8 mGy·cm × 2 × 6.78 cm = 0.25 Gy·cm^2. For a sequential 10 cm scan of the head cylinder with pitch 1, the value was 10/1.2 = 8.3 times larger, i.e. P_{PSKA} = 2.1 Gy·cm^2.

5. DISCUSSION

Formulas in Section 2 assume that the interval (x_a, x_b) fully describes the shadow of the scanned object. For wide beams and objects with strongly varying cross sections in the axial direction, however, this assumption may not be fulfilled. Nevertheless, it is still possible to apply the described algorithm to individual rows of the detector array (and sum up the individual contributions) or replace the integration of P_{KL} in one dimension with an integration of K_{air} in two dimensions. It should also be noted that the calculation of P_{PSKA} can be

implemented in the CT scanner software without the use of the KAP meter. In this case, however, the extra safety feature provided by the direct monitoring of the X ray beam by the KAP meter is lost.

6. CONCLUSIONS

A method using the patient specific kerma area product, P_{PSKA}, as an exposure estimator in CT was described. Contrary to the currently used method based on CTDI measurements, it is patient specific and it takes into account all radiation incident on the patient. These are clear advantages from the radiation safety point of view. To implement this method: (a) the CT scanner must be equipped with a KAP meter, (b) the calculation procedure must be added to the scanner's software, and (c) a calibration to determine the ratio $P_{KL}(0)/P_{KA}$ and the effect of the bowtie filter expressed as the function $P_{KL}(x)/P_{KL}(0)$ must be performed. There are several issues to address: since currently available commercial KAP meters are not well suited for this purpose, a KAP meter able to withstand high radiation doses and centrifugal forces is needed; and an analgorithm is needed that can quickly determine the integration range from reconstructed images. The $P_{KL}(0)/P_{KA}$ and $P_{KL}(x)/P_{KL}(0)$ ratios can be determined by the manufacturer and occasionally checked at the clinics.

REFERENCES

[1] HUDA, W., Time for unification of CT dosimetry with radiography and fluoroscopy, Radiation Protection Dosimetry, Vol. 128, No. 2 (2008), 129–132.

[2] UNITED NATIONS, 2008 Report to the General Assembly, with scientific annexes, Volume I (Report to the General Assembly), Scientific Committee on the Effects of Atomic Radiation (UNSCEAR), UN, New York (2010).

[3] INTERNATIONAL ATOMIC ENERGY AGENCY, Dosimetry in Diagnostic Radiology: An International Code of Practice, Technical Reports Series No. 457, IAEA, Vienna (2007).

[4] DIXON, R., BOONE, J., Cone beam CT dosimetry: A unified and self-consistent approach including all scan modalities — with or without phantom motion. Med. Phys. **37**(6) (2010) 2703–2718.

[5] HELMROT, E., THILANDER-KLANG, A., Methods for monitoring patient dose in dental radiology, Radiation Protection Dosimetry(2010), Vol. 139, No. 1–3, 303-305.

[6] INTERNATIONAL ORGANIZATION FOR STANDARDIZATION, Quantities and Units — Part 10: Atomic and nuclear physics, ISO 80000-10 (2009), IDT.

[7] INTERNATIONAL COMMISSION ON RADIATION UNITS AND MEASUREMENTS (ICRU), Dosimetry of beta rays and low-energy photons for brachytherapy with sealed sources, ICRU Report 72, J. ICRU 4(2).

[8] SALVAT, F., FERNÁNDEZ-VAREA, J., SEMPAU, J., “PENELOPE-2008: A code system for Monte Carlo simulation of electron and photon transport”, (Workshop Proc., Barcelona, Spain, 30 June — 3 July 2008) (2008).

REGIONAL DIAGNOSTIC REFERENCE LEVELS AND COLLECTIVE EFFECTIVE DOSES FROM COMPUTED TOMOGRAPHY (CT) SCANNERS IN INDIA

R.S. LIVINGSTONE, P.M. DINAKARAN
Department of Radiology,
Christian Medical College, Vellore,
Tamil Nadu, India
Email: roshanlivingstone@gmail.com

Abstract

Diagnostic examinations performed using computed tomography (CT) are on the increase, and the use of this modality needs to be monitored periodically. The aim of this study was to formulate regional diagnostic reference levels (DRLs) and assess collective effective doses from CT scanners in Tamil Nadu, India. In-site CT dose measurements were performed for 127 CT scanners in Tamil Nadu as a part of the Atomic Energy Regulatory Board (AERB) funded project for a period of two years. Regional DRLs were formulated at third quartile level for three CT protocols such as thorax, abdomen and pelvis and were found to be 557 mGy·cm, 521 mGy·cm and 294 mGy·cm, respectively. The collective effective dose in Tamil Nadu was found to be 14.93 man Sv per day.

1. INTRODUCTION

Since the 1970s, computed tomography (CT) has played a vital role in diagnosing diseases than with other radiological procedures, although it imparts high radiation doses to patients. Owing to the current increase in the collective doses for medical usage, it is important to periodically monitor radiation doses to patients undergoing radiological procedures. Technological developments have improved the speed and quality of images, which has encouraged the increase in CT practice worldwide [1]. In a regional survey on CT scanners in India, it was found that there has been an increase of 35% in the number of multislice CT scanners compared to single slice CT scanners since 2000 [2]. The regional diagnostic reference levels (DRLs) presented in the study would be the first step towards the optimization of CT doses in the Indian context.

2. METHODS AND DISCUSSION

On-site CT dose measurements were performed for 127 CT scanners in 20 regions in Tamil Nadu, through a survey performed over a period of two years. The DRLs were formulated for three CT scanning protocols, namely thorax, abdomen and pelvis. A questionnaire used for data collection included: the type and model of the scanner; the location of the installation; exposure parameters used routinely; the number of scans performed daily; and the availability of dose reduction techniques and dose derivatives in the console. Radiation dose measurements were performed using routine exposure parameters for thorax, abdomen and pelvis as practised in each installation. CT dose index (CTDI) was measured using a 32 cm polymethyl methacrylate (PMMA) body phantom. The weighted CTDI ($CTDI_w$) values were calculated using the formula:

$$CTDI_w = 1/3\ CTDI_{100,c} + 2/3\ CTDI_{100,p}$$

The dose length product (DLP) was calculated using volume CT dose index ($CTDI_{vol}$) and scan length. The effective dose (E) was estimated using DLP values and a conversion factor from the European criteria for measurement of CT doses [3]. The collective effective doses were calculated from the mean effective dose from CT examinations and the corresponding number of examinations performed each day. An average of 2107 CT examinations are performed each day in the region. Of the 127 CT scanners evaluated, 13 were conventional, 11 refurbished conventional, 53 single slice helical scanners, six refurbished single slice helical scanners and 44 multidetector CT units. Fifty-four per cent of CT installations were in the hospitals, 13% in residential areas and 33% in commercial areas. Table 1 shows the mean scan lengths and regional DRLs for CT examinations of specific anatomical regions. The mean effective dose per day per individual in the region was 7.95 ± 2.1 mSv (5.61–15.18) and the collective effective dose per day in Tamil Nadu was 14.93 man Sv.

Variations in doses could be attributed to the differences in dose efficiency between scanner models, the use of obsolete scanners and variation in protocols. This study is the first step in the country to establish DRLs for CT scanners. Twenty-five per cent of the scanners had radiation doses above the third quartile values required for the establishment of DRLs in Tamil Nadu. The study reveals that the DRLs are within the reference level for CT scanners, as reported in the literature [3]. Since the number of CT examinations performed in the country is on the increase, it is imperative to audit CT examinations in order to ensure that doses do not deviate from the formulated regional DRLs. In light of this study, it is necessary that every CT user be trained to interpret the dose descriptors such as $CTDI_{vol}$, DLP or effective dose values available on the CT console in order to

TABLE 1. MEAN AND THIRD QUARTILE DLP VALUES FOR CT EXAMINATIONS OF THORAX, ABDOMEN AND PELVIS

CT examination (Mean scan length)	DLP in mGy·cm	
	Mean ± SD (Range)	Third quartile
Thorax (36.1 cm)	476 ± 191.7 (113.7–1465.4)	557
Abdomen (33.8 cm)	445.8 ± 179.5 (106.5–1372)	521
Pelvis (19.1 cm)	251.9 ± 101.4 (60.2–775.3)	294

keep doses as low as reasonably practicable. In India, there is a need for standardizing clinical protocols for optimizing exposure parameters and scan lengths for desired anatomical regions.

REFERENCES

[1] HATZIIOANNOU, K., PAPANASTASSIOU, E., DELICHAS, M., BOUSBOURAS, P., A contribution to the establishment of diagnostic reference levels in CT, B. J. Radiol. **76** (2003) 541–545.

[2] LIVINGSTONE, R.S., DINAKARAN, P., Regional survey of CT dose indices in India, Radiat. Prot. Dosim. **136**(3) (2009) 222–227.

[3] EUROPEAN COMMISSION. European guidelines on quality criteria for computed tomography, Report EUR 16262, European Community, Brussels (1998).

VARIATIONS OF DOSE TO THE LUNG DURING COMPUTED TOMOGRAPHY (CT) THORAX EXAMINATIONS: A MONTE CARLO STUDY

R. SCHMIDT, J. WULFF, L. CASTRA, K. ZINK
Institut für Medizinische Physik und Strahlenschutz,
University of Applied Sciences, Gießen, Germany
Email: ralph.schmidt.123@gmail.com

Abstract

This study determined the influence of patient individuality on lung organ doses for chest computed tomography (CT) examinations, viewed in the context of the recommendation of the ICRP 103. Within this current recommendation, a more individualized dose estimation is emphasized. The new ICRP 110 voxelized adult phantom was used and compared to calculation of lung doses for chest CT studies with identical scan parameters (120 kV, 135 mAs, 100 mm collimation, 1.5 pitch). For all patient images, the lung was contoured, and the scanning geometry was simulated using the Monte Carlo method. The lungs were completely included in the scan area. A user code was developed for the Monte Carlo package EGSnrc, which enables the simulation of a CT examination procedure and allows an efficient dose scoring within a patient geometry. All simulations were calculated with the same CT source model and calibrated to a realistic CTDIair value. Simulation values were grouped into 1 mSv classes. The organ dose classes fit well to a Gaussian distribution (adjusted correlation coefficient $R^2 = 0.95$). The mean value of the fit was 10 mSv, with a standard deviation of 2 mSv. The variability was about ±30% with a minimum of 8 mSv and maximum of 13 mSv. The calculated lung dose of the ICRP adult female phantom was approximately 11 mSv and thus within the calculated standard deviation of the patient pool. The correlation between lung volume and dose was weak (adjusted correlation coefficient $R^2 = 0.33$). Gender specific differences between the ICRP male and female phantoms were about 17%. In comparison, the differences between the female and a limited set of male patient studies were not statistically significant. Further, the relation between the HU values of CT scans and material/density necessary for the Monte Carlo simulations was investigated. It resulted that the simple but commonly employed relationship leads to significant deviations compared to definite materials in the ICRP phantoms. In conclusion, the present study demonstrates the expected variance in dose estimation due to the individual patient anatomy based on Monte Carlo simulations. The new ICRP phantoms properly represent the mean of the investigated patient pool. Nevertheless, a more individualized approach should be aimed for in the future.

1. INTRODUCTION

The International Commission on Radiological Protection (ICRP) recommends a more accurate and individualized risk assessment in diagnostic

radiology [1]. As a consequence, the recommendations introduce a change in dose estimation from simplified, 'mathematical' to 'voxelized' phantoms. This demand is also supported by the International Commission on Radiation Units and Measurements (ICRU) [2]. Phantoms are to be developed that will best represent the population for various ages and gender. In addition, phantoms in various stages of pregnancy should allow dose calculation in the foetus. As a first step, the ICRP 110 published two voxelized phantoms in 2009 [3]: adult male and adult female. A future aim is a more accurate dose assessment in diagnostic radiology with the help of these two phantoms. First organ dose calculations with monoenergetic electrons and photons were presented by Hadid et al. [4].

For a further individualization of the dose calculation, two approaches are conceivable: the direct dose calculation on real patient data [5] or the adaptation of a phantom to the patient's anatomy. The latter approach can be achieved with a phantom from a 'family', as mentioned above, or by a deformable phantom fit to the actual patient anatomy. The advantage of these two methods is that the needed exact segmentation of organs for the effective dose calculation already exists. The first approaches of deformable phantoms were published by Na et al. [6] and Xu et al. [7].

The importance of a precise estimation of the individual risk in radiology can be observed particularly in computed tomography (CT), where the examination number has grown steadily in recent years and the trend is likely to be continued [1, 8, 9] .

The aim of this study was the investigation of patient individuality and its influence on changes in organ doses. The variability within the patient pool can serve as a measure of dose estimation uncertainty due to the missing individuality for a generalized phantom such as the ICRP phantom. The organ dose to the lung for chest CT examination studies was analysed using a Monte Carlo (MC) simulation. Comparisons were made to the ICRP 110 phantoms. In addition, possible uncertainties in the calculation of real CT examinations considering the Hounsfield unit (HU) to density and material conversion were investigated. This conversion is a necessary step for an MC simulation.

2. METHODS

2.1. MC simulation environment

The EGSnrc MC code system was used for particle transport and dose calculations [10]. EGSnrc was demonstrated to be suitable for simulations in the keV range and is equipped with the necessary physical models, such as bound Compton-scattering, atomic relaxations, electron impact ionization etc. [10]. A

new C++ user code CTDOSPP was developed for simulating a computed tomography examination. The user code is based on the egspp-application classes and takes full advantage of flexible geometry and source definitions [11]. All simulations were performed with kerma approximation to improve simulation efficiency. For further variance reduction in kerma calculations, a track length estimator, as described by Williamson, was implemented in CTDOSPP [12]. For simulations, Rayleigh scattering, atomic relaxations, Sauter photon angular sampling and bound Compton scattering were turned on. For details on the implementation of these physics models, the reader is referred to the EGSnrc documentation [10]. Cut-off energies for photons were set to 1 keV.

All simulations were handled within a developed graphical user interface (GUI) called GMctdospp (Fig. 1). The program allows loading of patient studies and ICRP phantoms, defining calculation grid size and CT scan area, steering of simulation runs and analysis of the calculation results. All simulations were calibrated in GMctdospp for better handling and visualization to a $CTDI_{air}$ value of 22.9 mGy. This value corresponds to a typical CT chest examination similar to the virtual CT parameters.

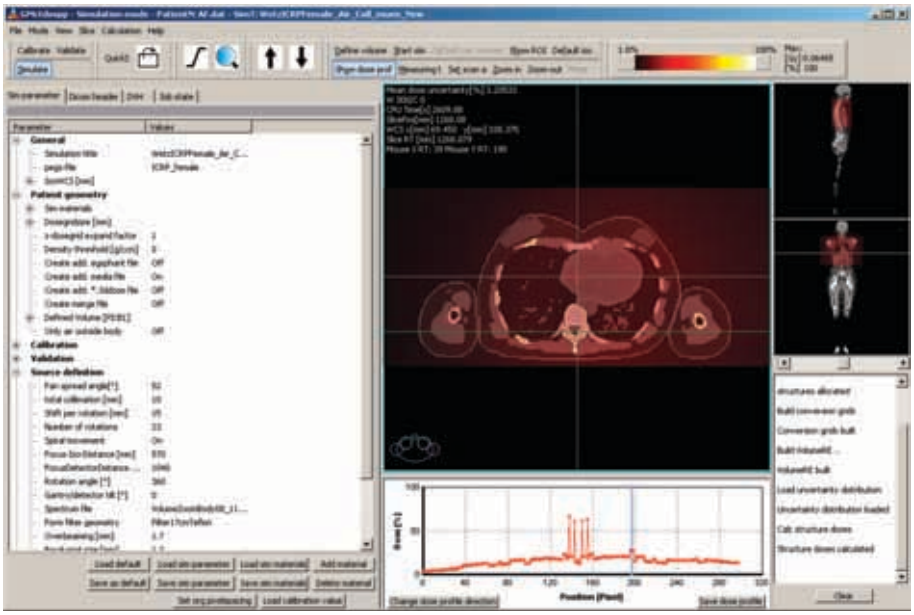

FIG. 1. Screenshot of the developed program GMctdospp. The colour coded relative dose distribution is shown for a simulation of the ICRP adult female phantom in slices of different orientation (transversal, frontal and sagital). On the left side, parameter selection is visible. In the lower plot, a horizontal profile of the dose distribution is shown.

2.2. Examined patient studies

A statistical analysis was performed for a total of 61 female patient simulations. All patient studies were originally used for radiotherapy planning. They were taken from a radiation oncology clinic (Wetzlar, Germany), and each study contained contour information of both lungs and body outline in the DicomRT struct format [13]. The body and lungs structures were contoured within a treatment planning system by a threshold based contouring tool and the outcome controlled by the operator. In all simulations, the chest area of the patient's body was completely within the CT scan area. A virtual CT was created (120 kV, 10 mm collimation, 135 mAs, spiral movement, 1.5 pitch, 2.5 mm Al + 1.2 mm Ti primary filter, a shaped bowtie filter adapted from a Siemens Volume Zoom CT, 1.7 mm overbeaming, 1.2 mm focal spot size of the particle source) to ensure that all patient studies were simulated with an identical source model. Every voxel outside the patients' body was assumed to be air, avoiding influences from different patient tables. The voxel grid for dose calculation and the pixel resolution of the original CT study were kept identical in order to exclude influences from interpolation of the HU values. Typical voxel grid values for a patient study were 1 mm × 1 mm × 5 mm. For the mapping between the HU values and corresponding densities and materials, a piecewise linear fit was employed. The materials used were air, lung, tissue and bone with boundaries as seen in Fig. 1 and defined by [10], respectively. Possible correlations between lung volume and lung dose of the patient pool were also analysed. Further, a limited set of 26 male patient studies was simulated identically, as described above for an analysis of the influence of gender.

2.3. ICRP phantoms

The density and material composition of all organs of the ICRP phantoms were directly taken from the corresponding ICRP publication [3]. This density and material information for every voxel present in the phantom was saved in a three dimensional file compiled by GMctdospp. The patient table as well as the bed and pillow were assumed to be air in order to be the same within the patient pool. The simulations were run in original voxel size of 1.775 mm × 1.775 mm × 4.834 mm. Either the ICRP adult male phantom was implemented to compare lung dose values to see gender specific differences.

2.4. Uncertainty estimation of the HU value to material and density conversion

As mentioned above, the materials within the ICRP phantom are given by a defined composition. In a simulation based on the CT of a patient, there is a certain uncertainty. This results from the conversion of the HU value to a corresponding material and density with the above mentioned function. In order to estimate the uncertainty of this conversion for the ICRP adult female phantom, the following method was applied: a HU value for each material defined within the ICRP adult female phantom was calculated (a total of 141 materials). This was achieved with the material's specific mass attenuation coefficient according to Eq. (1).

$$V_M = \frac{\mu_M - \mu_W}{\mu_W} 1000 HU \quad (1)$$

where

V_M is the calculated HU value of the material;
μ_M is the mean mass attenuation coefficient of the material;
μ_W is the mean mass attenuation coefficient of water.

The mean mass attenuation coefficients were derived from EGSnrc internal data for monoenergetic photons weighted by the initial spectrum of the X ray source. Afterwards, the HU values for the different materials were assigned to the phantom geometry, and the same conversion was employed as for patient studies (Fig. 2).

3. RESULTS

Each simulation took roughly three hours on a Xeon 2.5 GHz single core, resulting in a mean statistical uncertainty in the lungs of 2–3.5%. The ICRP simulation was two hours less, which can be attributed to the more homogenous material/density distribution.

The total number of 61 simulation results for the female chest was grouped into 1 mSv classes (Fig. 3). As shown in Fig. 3, the organ dose classes fit well to a Gaussian distribution with an adjusted correlation coefficient of $R^2 = 0.95$. The

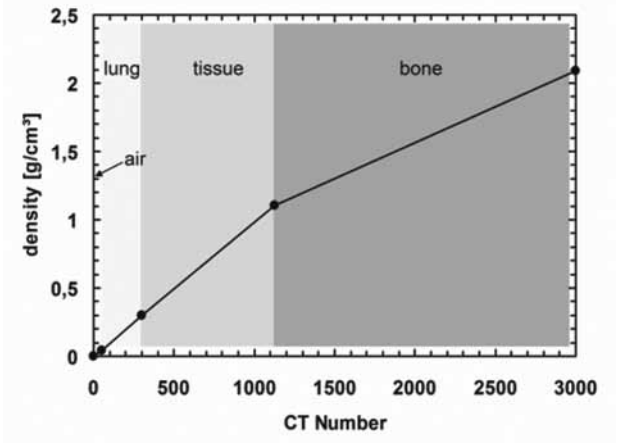

FIG. 2. Ramp function used to convert HU values to materials (air, lung tissue, bone) and mass density defined by Ref. [10].

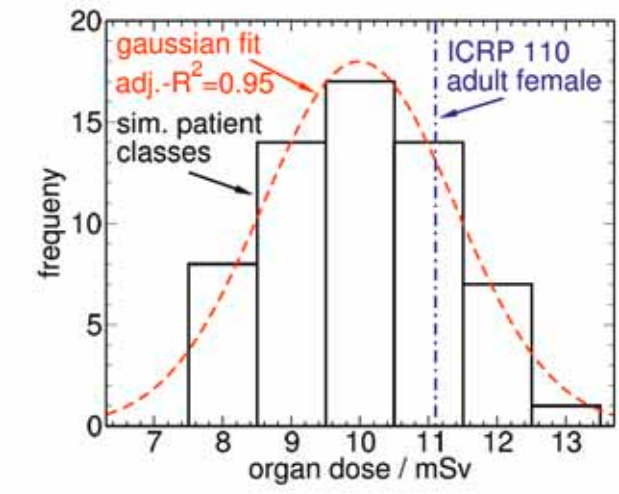

FIG. 3. Variations in dose to the lung of 61 patients (black bars), the Gaussian fit through the simulated classes (red dotted line) and the lung dose of the ICRP adult female phantom (blue dotted line).

mean value of the fit is 10 mSv, with a standard deviation of 2 mSv. The variability is about ±30%, with a minimum value of 8 mSv and maximum of 13 mSv. The calculated lung dose of the ICRP adult female phantom is 11 mSv and thus within the calculated standard deviation of the patient pool.

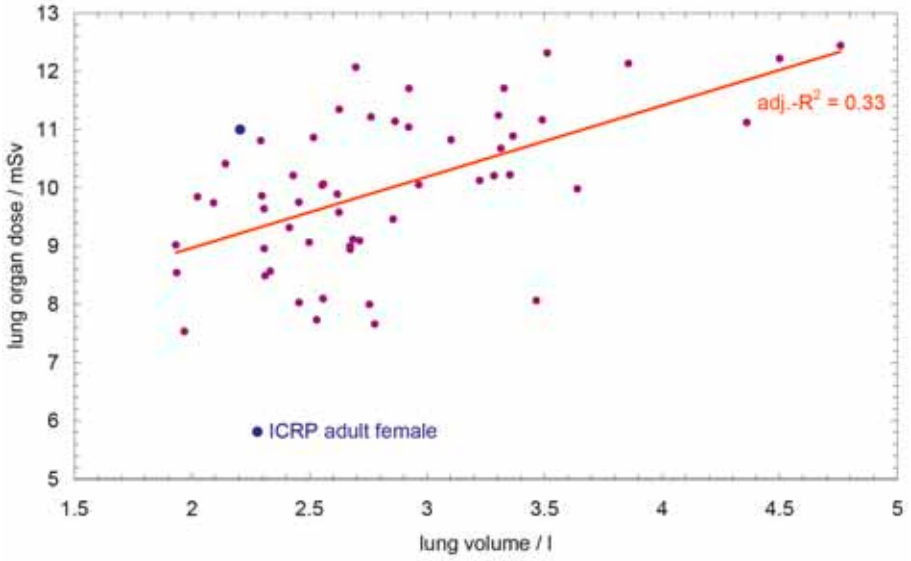

FIG. 4. The organ doses to the lung volume of the examined patients as function of the lung volume (purple dots) and the linear fit (red line). The lung volume of the ICRP adult female phantom is also shown (large blue dot).

A possible explanation of the remaining difference between ICRP phantom and mean value is the mentioned uncertainty within the HU conversion (see section 2.4). The difference between the fixed media definition and the conversion from estimated HU values is about 10%. The latter method results in a lung dose of 9.9 mSv, which almost equals the mean value of the patient pool.

The influence of lung volume on the lung dose is shown in Fig. 4. A linear regression can also be observed, but as is apparent, the correlation is weak (adjusted correlation coefficient $R^2 = 0.33$). The lung volume of the ICRP adult female phantom is about 2.2 L, which is in the lower part of the distribution.

Gender specific differences were determined between the ICRP adult female and adult male phantom. The male phantom determined a lung dose of 9.4 mSv, which is about 17% lower than the female phantom. However, a preliminary and limited test with 26 male studies simulated under the same conditions as the female patients showed no significant difference. The calculated mean value of the male patient pool was 9.8 mSv, and hence both mean values are identical within the confidence interval of about 1.5 mSv.

4. DISCUSSION AND CONCLUSION

The examined lung dose study shows a statistical verification of the 30% assumption in uncertainty caused by patient individuality [14]. However, it cannot be parameterized in terms of lung volume. If one accepts a 30% uncertainty in dose estimation, the ICRP phantoms clearly represent the mean patient. In a similar examination of 30 CT chest studies, Angel et al. showed a similar variance in lung doses of about 40% [15]. Gender specific differences that were observed for the two ICRP phantoms could not be confirmed for the patient pools; the reason might be the wide spread of the distribution, which probably covers any specific effects.

As demonstrated, a more detailed conversion from HU units to density/material within the MC simulation is needed if individual patient dose estimation should be based completely on the patient's CT image. This is different from radiotherapy applications where the stopping power is due to higher beam qualities that are less dependent on different materials.

The described method is a valid and reliable alternative to measurements in phantoms and the comparison between other phantoms [2]. The influence of individuality is demonstrated in the distribution of lung doses and provides an insight into possible variances of further individualized phantom calculation. The developed program GMctdospp allows a statistical evaluation of organ doses to patients and the comparison to the new ICRP phantoms.

ACKNOWLEDGEMENT

D. Theis of the Wetzlar Hospital is acknowledged for compiling the patient studies.

REFERENCES

[1] INTERNATIONAL COMMISSION ON RADIOLOGICAL PROTECTION, The 2007 Recommendations of the International Commission on Radiological Protection, Publication 103, Ann. ICRP **37** (2007) 2–4 .

[2] INTERNATIONAL COMMISSION ON RADIATION UNITS AND MEASUREMENTS, Patient Dosimetry for X Rays used in Medical Imaging, Journal of the ICRU, Vol. 5, No. 2, Report 74 (2005).

[3] INTERNATIONAL COMMISSION ON RADIOLOGICAL PROTECTION, Adult Reference Computational Phantoms, ICRP Publication 110, Elsevier Ltd. (2009).

[4] HADID, L., DESBREE, A., SCHLATTL, H., FRANCK, D., BLANCHARDON, E., ZANKL, M., Application of the ICRP/ICRU reference computational phantoms to internal dosimetry: calculation of specific absorbed fractions of energy for photons and electrons". Phys. Med. Biol. **55** 13 (2010) 3631–3641.

[5] DEAK, P., VAN STRATEN, M., SHRIMPTON, P.C., ZANKL, M., KALENDER, W.A., "Validation of a Monte Carlo tool for patient-specific dose simulations in multi-slice computed tomography", Eur. Radiol. **18** 4 (2008) 759–772.

[6] NA, Y.H., ZHANG, B., ZHANG, J., CARACAPPA, P.F., XU, X.G. "Deformable adult human phantoms for radiation protection dosimetry: anthropometric data representing size distributions of adult worker populations and software algorithms", Phys. Med. Biol. 55 13 (2010) 3789–3811.

[7] XU, X.G., TARANENKO, V., ZHANG, J., SHI, C., A boundary-representation method for designing whole-body radiation dosimetry models: pregnant females at the ends of three gestational periods–rpi-p3, -p6 and -p9, Phys. Med. Biol. **52** 23 (2007) 7023–7044.

[8] THE AMERICAN ASSOCIATION OF PHYSICISTS IN MEDICINE, The Measurement, Reporting, and Management of Radiation Dose in CT, Report 96, College Park, AAPM (2008).

[9] UNITED NATIONS SCIENTIFIC COMMITTEE ON THE EFFECTS OF ATOMIC RADIATION, Effects of ionizing radiation, Vol. I, Report to the General Assembly with Scientific Annexes A and B, Vienna, United Nations Office (2008).

[10] KAWRAKOW, I., ROGERS, D., The EGSnrc Code System: Monte Carlo Simulation of Electron and Photon Transport. NRCC Report No. PIRS-701, National Research Council of Canada (2010).

[11] WULFF, J., KEIL, B., AUVANIS, D., HEVERHAGEN, J., KLOSE, K., ZINK, K., Dosimetrische evaluation von Augenlinsen-Protektoren in der Computertomographie — Messungen und Monte-Carlo-Simulationen, Z Med Phys **18** (2007) 9–26.

[12] WILLIAMSON, J.F., Monte Carlo evaluation of kerma at a point for photon transport problems, Med Phys **14** 4 (1987) 567–576.

[13] DIGITAL IMAGING AND COMMUNICATIONS IN MEDICINE at http://medical.nema.org

[14] NAGEL, H., Ed., Radiation Exposure in Computed Tomograph, European Coordination Committee of the Radiological and Electromedical Industries, Frankfurt (2000).

[15] ANGEL, E., YAGHMAI, N., JUDE, C.M., DEMARCO, J.J., CAGNON, C.H., GOLDIN, J.G., McCOLLOUGH, C.H., PRIMAK, A.N., CODY, D.D., STEVENS, D.M., McNITT-GRAY, M.F., Dose to radiosensitive organs during routine chest CT: Effects of tube current modulation, AJR Am J Roentgenol **193** (2009) 1340–1345.

APPLICATION OF DOSIMETRIC METHODS FOR OBTAINING DIAGNOSTIC REFERENCE LEVELS IN PANORAMIC DENTAL RADIOGRAPHY

L.V. CANEVARO*, M.M. NUNES**, C.D. ALMEIDA*

* Instituto de Radioproteção e Dosimetria/Comissão Nacional de Energia Nuclear, Jacarepaguá
Email: luciacanevaro@yahoo.com

** Instituto de Física, Universidade Federal do Rio de Janeiro

Rio de Janeiro, Brazil

Abstract

The goals of the present study were to verify the viability of using a kerma area product (P_{KA}) meter and a pencil ionization chamber to evaluate the P_{KA} and P_{KL} (kerma length product) in a panoramic X ray unit as feasible methods to obtain dosimetric reference values for panoramic examinations. Two methods for obtaining P_{KA} in panoramic devices have been tested in this study. The two methods evaluated found similar values, making it possible to include these tests in the quality control routine demanded by the regulations. Considering the results of this study, it is possible to conclude that both methods of measurement can be used simply and directly obtain diagnostic reference values for this practice. Using on dosimetric reference values in this type of examination is a better way to evaluate the exposition of patients.

1. INTRODUCTION

Dental radiography is one of the most frequently performed X ray procedures. Radiological techniques in dentistry have been developing rapidly and the panoramic dental radiology equipment (PDR) has been used increasingly [1]. PDR is a complex procedure [2], where the doses are higher than in the simplest dental procedures, such as periapical X ray. Although exposure associated with dental radiography is relatively low (if compared with CT or angiography), all radiological examinations should be justified and optimized to meet the ‘as low as reasonably achievable’ principle [3]

In PDR, radiosensitive organs can be irradiated by the primary beam or can receive scattered radiation [3]. Recently, the United Nations Scientific Committee

on the Effects of Atomic Radiation [1] has been paying increasing attention to cancers of the salivary glands, which were recently introduced as an organ of interest by international bodies such as ICRP [3]. In Brazil, reference levels for panoramic radiography have not been adopted, mainly because there are few dosimetric researches in PDR.

Technical Reports Series No. 457 [4] suggests the use of the quantity kerma length product (P_{KL}) to measure the dose in PDR. Another quantity that can be used is the kerma area product (P_{KA}). Some factors make it difficult to measure these values. For instance, the fact that the system moves during the emission of X rays and that the irradiation fields are small, etc., make it difficult to perform the dose measurement and identify the field size. The point is to determine the most appropriate method considering its practicality and uncertainty.

The goals of this study were to verify the viability of a P_{KA} meter and a CT ionization chamber to assess P_{KA} and P_{KL} in a panoramic X ray unit as feasible methods of obtaining dosimetric values to quantify patient exposure and to identify typical values for this type of examination.

2. MATERIALS AND METHODS

In this work, two methods for obtaining P_{KA} were tested in panoramic devices (Rotographic Plus, Villa Sistemi Medicali, Fig. 1). The items used were a Diamentor M4-KDK P_{KA} meter, a Radcal 9015 dosimetric system with electrometer model 9015 with a CT ionization chamber (10X5-3CT), and a thimble chamber (10X5-6).

2.1. Measurements with P_{KA} meter

P_{KA} meters are calibrated by the manufacturer, traceable to a primary measure of air kerma area product in a geometry different from the one to be used in practice. Thus, the meter must be calibrated in situ. In PDR, the distances are fixed, the X ray tube rotates during the exposure, the radiation beam is extremely narrow and the collimator is fixed. To overcome these difficulties, the meter was calibrated in cephalometric mode, since the beam quality does not depend on the mode of use, but on the tube voltage and on total filtration.

To calibrate the P_{KA} meter, the real value of P_{KA} was estimated from the measurement of air kerma (at certain distance from the focus) and the irradiated area (on a film exposed at the same point where the air kerma was measured). This value, $P_{KAcalculated}$, is compared with the value measured by the P_{KA} chamber,

FIG. 1. Rotographic Plus (Villa Sistemi Medicali) panoramic dental equipment.

$P_{KAmeasured}$, thus obtaining a calibration factor. All values of P_{KA} measured later were corrected by multiplying by this factor.

The P_{KA} calibration procedure was performed as follows:

— An 18 cm × 24 cm radiographic film was placed within the primary beam (Fig. 2(b)). In order to obtain an image without scattering, the film was put into an envelope without intensifying screen. Once exposed, it was developed, and the irradiated area was calculated. The irradiation parameters were 60 kVp, 10 mA and 0.6 s.
— The P_{KA} ionization chamber was placed in front of the exit of the first collimator (Fig. 2(a)). At the same time, the 6 cm^3 ionization chamber (Radcal 10X5-6) was placed at the same point where the film had been placed before (Fig. 2(b)). Subsequently, an irradiation was made. Measured values were recorded.

In order to calculate the area, its edges were defined by measuring the optical density of the film to determine the point where there was a 50% reduction in its value. The dimensions of the rectangle were measured with an accurate ruler. With all the measured values, the following comparison was made (Eq. (1)):

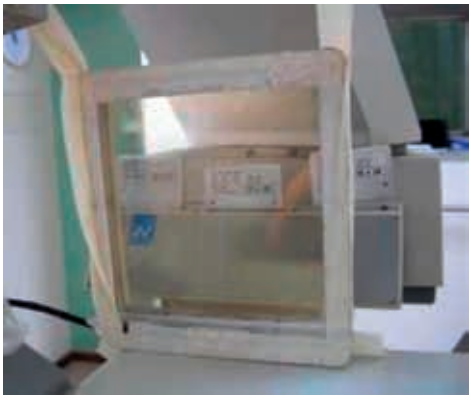

a

b

FIG. 2. (a) Set-up of the P_{KA} ionization chamber. (b) Set-up of the film and 6 cm^3 ionization chamber.

$$K \times Area = \alpha \times P_{KA\,measured} \quad (1)$$

where

K is the measured air kerma;
Area is the irradiated area on the film;
α is the calibration factor;

and $P_{KAmeasured}$ is the P_{KA} value measured with the P_{KA} meter.

2.2. Measurements with a CT pencil chamber

For each value of voltage and current of the tube, dosimetric measurements were performed with the P_{KA} ionization chamber positioned in front of the first collimator and CT chamber in front of the second collimator (Fig. 3). The procedure was repeated using other collimators on the equipment (e.g. collimators for children). The height of the radiation beam at the entrance of the second collimator was measured on an exposed radiographic film at the same point where the CT chamber had been placed.

The values obtained with the P_{KA} meter were compared with the values calculated from CT chamber data using Eq. (2)

FIG. 3. Set up of CT pencil chamber.

$$P_{KAcalculated} = P_{KL} \times h \quad (2)$$

where

P_{KL} is the kerma length product measured with a CT chamber;
h is the height of the radiation beam at the entrance of the second collimator.

3. RESULTS

In the film used to calibrate the *PKA* meter, the uncertainty of length of the irradiated area was estimated at 1 mm. Measurements were: width = 90 ± 1 mm; height = 93 ± 1 mm The area of the rectangle and its uncertainty were calculated using Eq. (3) thus:

Area = 8370 ± 131 mm^2

$$\delta A = A \times \sqrt{\sum_{i}^{n} \left(\frac{\delta A_n}{A_n} \right)^2} \quad (3)$$

TABLE 1. MEASUREMENTS PERFORMED DURING THE P_{KA} METER CALIBRATION (mA = 10)

kVp	Time (s)	Air kerma (μGy)	$P_{KA\text{calculated}}$ (cGy·cm^2)	$P_{KA\text{measured}}$ (cGy·cm^2)	Calibration factor
70	1.0	46.0	0.37	0.46	0.81
70	2.5	112.0	0.92	1.12	0.82
70	3.0	135.0	1.09	1.35	0.81
75	1.0	59.0	0.48	0.60	0.80
75	2.5	146.0	1.18	1.48	0.80
75	3.0	178.0	1.45	1.79	0.81
80	1.0	70.0	0.57	0.70	0.81
80	2.5	178.0	1.39	1.78	0.78
80	3.0	206.0	1.67	2.11	0.79
85	3.0	247.0	2.00	2.56	0.78
Average P_{KA} calibration factor					0.80

Table 1 shows the results of measurements (average of 3 expositions) performed for obtaining the P_{KA} meter calibration factor. The air kerma measurement associated uncertainty was 6.4% (k = 2). The P_{KA} measurement associated uncertainty was 11% (k = 2).

The average P_{KA} calibration factor obtained was 0.80 ± 0.13. Similar values were obtained for other equipment. This value was used to calculate de actual P_{KA} value, measured during the simulated examinations.

Table 2 shows the P_{KA} and P_{KL} values obtained during simulation tests in a panoramic equipment evaluated. The height of the field was constant and the value found was 11.8 ± 0.1 cm. The associated uncertainty related to the CT chamber was 13% (k = 2).

Both evaluated methods found similar values when compared. The values of P_{KA} and P_{KL} in the authors' work were similar to those found in the literature [5–7]. For example, Helmrot and Carlsson [6] found a P_{KA} value equal to 0.04 Gy·cm² at 64 kV, which is very close to the value 0.034 Gy·cm² found in this study. Differences in values can be justified for small differences in the techniques used. Since published papers do not always have the associated uncertainties, it is difficult to compare values obtained with those of other authors.

TABLE 2. RESULTS OF P_{KA} AND P_{KL} MEASUREMENTS IN ROTOGRAPHIC PLUS X RAY EQUIPMENT *(mA = 10, area = 83.7 ± 1.3 cm²)*

kVp	Time (s)	$P_{KA\text{measured}}$ (cGy·cm²)	CL (Pencil chamber measure) (μGy)	P_{KL} (μGy·cm)	$P_{KA\text{calculated}}$ cGy·cm²)	Δ (%)
60	14	2.64 ± 0.30	224 ± 29	2240 ± 290	2.64 ± 0.30	0
65	14	3.36 ± 0.35	290 ± 38	2900 ± 380	3.42 ± 0.45	–2
70	17	5.14 ± 0.56	429 ± 55	4296 ± 550	5.07 ± 0.66	1
75	17	7.09 ± 0.78	580 ± 75	5802 ± 750	6.85 ± 0.90	3
80	17	8.27 ± 0.90	677 ± 88	6770 ± 880	7.99 ± 1.03	3
85	17	10.71 ± 0.95	838 ± 100	8384 ± 1000	9.89 ± 1.30	8

4. CONCLUSION

Both measurement methods can be employed as simple and direct ways to measure patient doses for this type of examination. Relying on dosimetric values in this type of oral examinations promotes greater control of patients' exposure.

The calculations required are simple, quick and easy, thus did not introduce many sources of uncertainty in the measurement process. This makes it possible to include these tests in the quality control routine.

This methodology is being applied in other panoramic equipment in order to have enough dosimetric information. So, mechanisms for optimization of this practice can be proposed and, in the long run, reference levels for PDR in Rio de Janeiro and elsewhere in Brazil can be established.

REFERENCES

[1] UNITED NATIONS, Effects of ionizing radiation: 2006 Report Vol. 1 (Report to the General Assembly), Scientific Committee on the Effects of Atomic Radiation (UNSCEAR), UN, New York (2008) 17–322.

[2] WHITE, S., PHAROAH, M., et al., Radiologia Oral: Fundamentos e Interpretação. Elsevier (2007).

[3] INTERNATIONAL COMMISSION ON RADIOLOGICAL PROTECTION, "Recommendations of the International Commission on Radiological Protection". ICRP Publication 103, Pergamon Press (2007).

[4] INTERNATIONAL ATOMIC ENERGY AGENCY, Dosimetry in Diagnostic Radiology: An International Code of Practice, Technical Reports Series No. 457, IAEA, Vienna (2007).
[5] WILLIAMS, J.R., MONTGOMERY, A. Measurement of dose in panoramic dental radiology, The British Journal of Radiology **73**, (2000) 1002–1006, The British Institute of Radiology.
[6] HELMROT, E., CARLSSON, G.A. "Measurement of Radiation Dose in Dental Radiology", Radiat. Prot. Dosim., Vol. 114, Nos· 1–3 (2005) 168–171.
[7] POPPE, B., et al., "Dose area product measurements in panoramic dental radiology", Radiat. Prot. Dosim, September 2006, Nos 1–4 (2006).

ASSESSMENT OF TRIGGER LEVELS TO PREVENT TISSUE REACTION IN INTERVENTIONAL RADIOLOGY PROCEDURES

A. TRIANNI, R. PADOVANI
Medical Physics Department,
University Hospital
Email: trianni.annalisa@aoud.sanita.fvg.it

D. GASPARINI
Radiology Department,
University Hospital

Udine, Italy

Abstract

It is well known that the large use of fluoroscopy in interventional radiology procedures may induce unintended injuries to the patients' skin. For this reason, assessment of skin dose for these procedures is becoming increasingly important. This study aims to investigate the role of cumulative air kerma (CK) as an on-line dose indicator and to evaluate the possibility of defining a local CK trigger level that can help operators identify situations with high probability to exceed a peak skin dose of 2 Gy, the threshold dose for transient skin erythema. Cerebral angiography, aneurysm embolization and chemoembolization of liver cancer have been identified as the interventional procedures where high skin doses could be delivered. Dosimetric data — CK, air kerma area product (KAP) and fluoroscopy time — have been collected in a sample of procedures. The peak skin dose (PSD) has been measured with large area radiochromic films (Gafchromic, IPS, USA) located between the tabletop and the patient. PSD varied in very wide range, and in a few cases, were close to the threshold for main erythema and epilation (6 Gy). The correlations between PSD and CK have been assessed for each procedure type. A trigger level for CK has been derived to alert the interventionalist on the probability to have reached a PSD of 2 Gy. In the authors' medical centre, trigger levels of 5200 mGy and 2500 mGy have been established for brain aneurysm embolization and chemoembolization procedures, respectively.

1. INTRODUCTION

The extensive use of fluoroscopy in interventional radiology procedures may induce unintended injuries to the patients' skin varying from erythema to necrosis. Some cases have been described in a review paper by Koenig et al. [1, 2].

As stated by the European Directive 97/43/Euratom, patient dose should be periodically evaluated to guarantee optimisation and justification of the practice. Moreover, the International Commission on Radiological Protection recommends providing an adequate follow-up and eventual treatment of these injuries, for patients whose skin dose has been 3 Gy or greater [3].

The maximum skin dose (MSD) could be directly measured using film or thermoluminescent dosimeters [4, 5]. In this way, the operator does not have an immediate knowledge of the amount of dose received by a patient. It is important to perform an 'on-line' evaluation (e.g. during the procedure) of the patient's skin dose to optimize the procedure in which the skin dose could be greater than the threshold for deterministic effects. Therefore, dosimetric indicators for estimating and monitoring patient skin dose in routine practice should be identified.

For interventional radiology procedures, kerma air product (KAP) and cumulative air kerma (CK) at the interventional reference point could be used as dosimetric indicators for skin dose.

The aim of this work is to investigate the correlation between these parameters and the directly measured skin dose for a sample of interventional procedures.

The dosimetric indicator that better correlate with the MSD should then be used to define trigger levels that indicate doses over the threshold for deterministic effects and the necessity of medical follow-up for possible radiation injuries, respectively.

2. MATERIALS AND METHODS

From October 2007 to October 2008, dosimetric data from procedures, both diagnostic and interventional, performed in two interventional rooms in Udine University Hospital (Udine, Italy) were collected. The procedures were performed by four experienced radiologists with two angiographic systems (Axiom Artis dFa, Siemens, Germany), equipped with a digital flat panel detector. The peak skin dose (PSD) was measured with radiochromic films (Gafchromic XR-typeR, IPS, USA), placed between the patient and the couch in a sample of 61 procedures. The radiochromic films were calibrated under an angiographic beam for comparison with an ionization chamber (Radcal,

Model 2026C 6cc ion cahmber). Films were read with a flatbed scanner (Epson 1680pro) in reflective mode. Images obtained were evaluated in terms of dose with a Matlab homemade routine The overall uncertainty associated with MSD measurement was estimated at around 16%. The correlations between PSD and KAP and PSD and CK have been investigated for each procedure type.

3. RESULTS

Data collected are summarized in Table 1, shows: type of procedure, number of patients, mean values of fluoroscopy time (FT), KAP and CK at the interventional reference point.

TABLE 1. MEAN AND STANDARD DEVIATION FOR FT, KAP AND CK FOR A SAMPLE INTERVENTIONAL PROCEDURE PERFORMED AT UDINE UNIVERSITY HOSPITAL, OCTOBER 2007 TO OCTOBER 2008

Procedure	Number	FT (min)	KAP ($Gy \cdot cm^2$)	CK (mGy)
Cerebral angiography	197	6.1 ± 8.2	1.1 ± 49.2	770.9 ± 887.4
Aneurysm embolization	76	26.6 ± 13.5	5.4 ± 60.8	2153.7 ± 1345.3
Chemoembolization	144	14.1 ± 7.7	210.5 ± 138.6	1136.3 ± 767.9
Embolizations	57	22 ± 41.6	269.7 ± 320.8	1384.7 ± 1472.0
Peripheral angiography	145	1.4 ± 1.9	43.4 ± 29.3	154.5 ± 106.1
Lower limb angioplasty	44	15.6 ± 9.9	24.7 ± 37.6	149.0 ± 237.6
Carotid angioplasty	73	9.4 ± 5.5	53.7 ± 26.0	247.3 ± 135.7
Iliac angioplasty	45	11.4 ± 9.8	80.5 ± 89.5	401.9 ± 293.8
Below-knee angioplasty	27	17.9 ± 10.4	8.9 ± 14.3	101.8 ± 326.0
Renal angioplasty	12	7.7 ± 3.5	48.8 ± 54.8	308.6 ± 270.3
AAA/AAT	13	11.6 ± 5.1	87.6 ± 50.3	495.7 ± 248.6
Brachyteraphy	9	22.6 ± 19.8	16.4 ± 14.6	104.1 ± 94.5
Cavography	7	7.5 ± 6.5	66.1 ± 53.8	273.3 ± 216.4

TABLE 1. MEAN AND STANDARD DEVIATION FOR FT, KAP AND CK FOR A SAMPLE INTERVENTIONAL PROCEDURE PERFORMED AT UDINE UNIVERSITY HOSPITAL, OCTOBER 2007 TO OCTOBER 2008 (cont.)

Procedure	Number	FT (min)	KAP ($Gy \cdot cm^2$)	CK (mGy)
Fibrinolysis	10	19.9 ± 11.0	28.1 ± 29.6	113.2 ± 102.9
Caval filter	10	7.0 ± 7.3	64.1 ± 98.3	236.7 ± 282.7
Fistolography	10	4.6 ± 4.0	4.5 ± 14.6	28.4 ± 109.2
Flebography	26	6.5 ± 16.1	28.4 ± 58.9	300.2 ± 803.9
HVPG measurement	10	9.1 ± 7.1	29.2 ± 18.1	167.0 ± 100.1
TIPS	13	20.5 ± 13.3	117.3 ± 74.1	827.5 ± 609.5
Epiaortic trunk angiography	13	3.6 ± 3.3	40.9 ± 30.5	221.3 ± 150.4
Vertebroplasty	13	13.0 ± 16.1	51.4 ± 26.0	392.7 ± 157.3

TABLE 2. PSD (MEAN VALUES, STANDARD DEVIATION AND RANGE) FOR A SAMPLE OF SELECTED INTERVENTIONAL PROCEDURES

Procedure	No.	PSD (mGy)	Range (mGy)
Cerebral angiography	25	352.4 ± 145.4	98.8 ± 561.9
Aneurysm embolization	18	1072.5 ± 1085.2	332.2 ± 4941.9
Chemoembolization	38	1343.8 ± 915.7	343.4 ± 4135.5

Mean values of FT, KAP and CK indicate that cerebral angiography, aneurysm embolization and chemoembolization of liver cancer are procedures where high skin doses could be delivered. PSD has been measured in a sample of these procedures (see Table 2).

The correlation between PSD and KAP and CK was investigated. Results for cerebral angiography are represented in Figs 1 and 2 for KAP and CK, respectively.

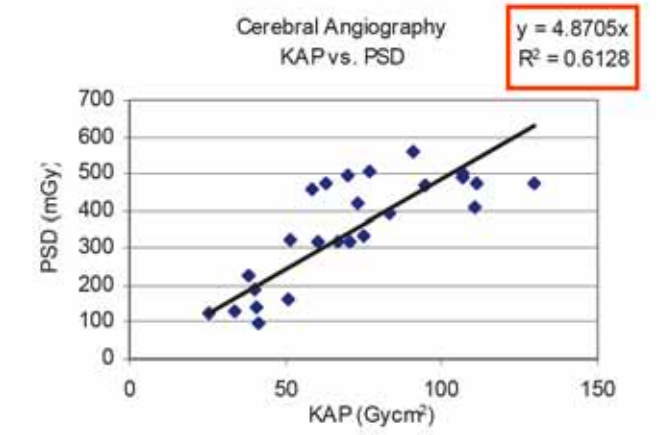

FIG. 1. Correlation between KAP and PSD for cerebral angiography.

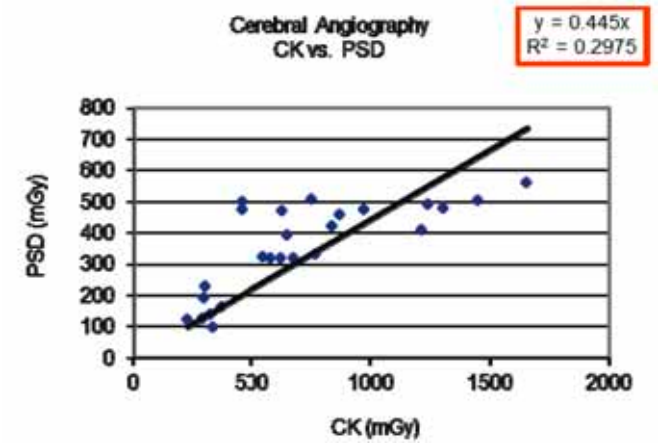

FIG. 2. Correlation between CK and PSD for cerebral angiography.

Results for aneurysm embolization are reported in Figs 3 and 4 for KAP and CK, respectively.

Results for chemoembolization are reported in Figs 5 and 6 for KAP and CK, respectively.

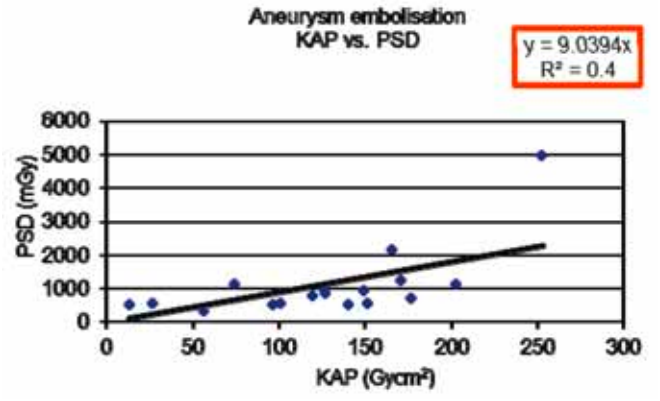

FIG. 3. Correlation between KAP and PSD for aneurysm embolization.

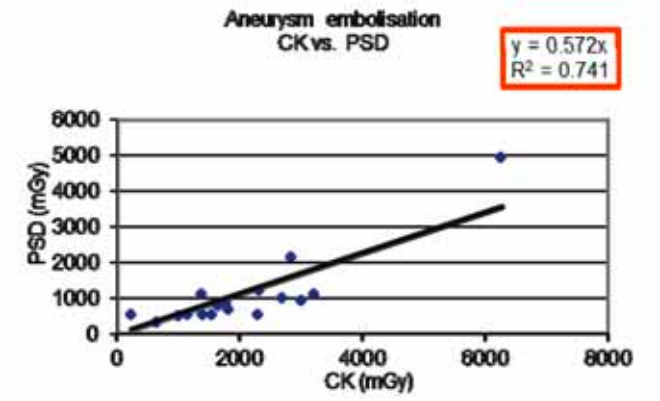

FIG. 4. Correlation between KAP and PSD for aneurysm embolization.

4. DISCUSSION

Registered values of KAP, CD and FT are high and suggest high doses to the patient's skin, in particular for cerebral angiography, aneurysm embolization and chemoembolization for liver cancer.

Therefore, it is important to understand the meaning of these values in terms of skin dose. Moreover, it is important to allow the operator to have an immediate knowledge of the amount of dose received by the patient and to recognize those procedures in which the dose could be greater than the threshold for deterministic effects.

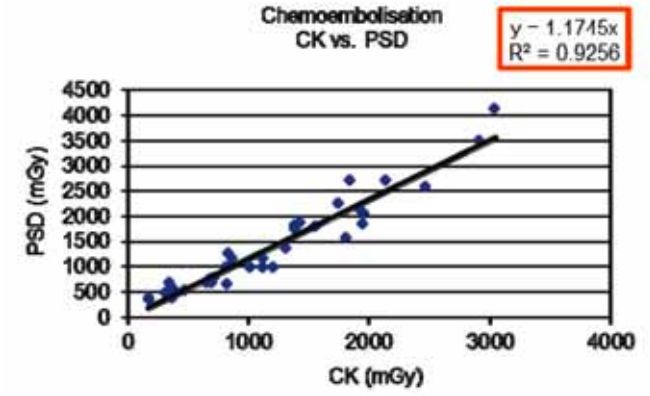

FIG. 5. Correlation between KAP and PSD for chemoembolization.

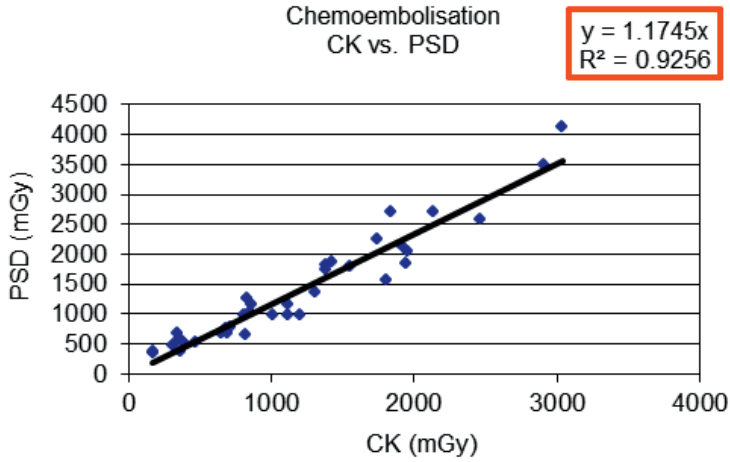

FIG. 6. Correlation between CK and PSD for chemoembolization.

For this reason, the correlation between dosimetric indicators such as KAP and CK given by the equipment and directly measured PSD has been assessed, and the possibility to establish trigger levels to be used in routinely practice has been investigated for cerebral angiography, aneurysm embolization and chemoembolization.

4.1. Cerebral angiography

For cerebral angiography procedures, correlation between PSD and both dosimetric indicators is weak ($R^2 = 0.61$ and $R^2 = 0.3$, respectively, for KAP and CK). This is probably due to the high number of the projections at different angles used in these procedures. As a consequence, the definition of a trigger level was not possible. However, doses measured in the sample are quite low (maximum value of 561.9 mGy).

A comparison was performed between FT, KAP and CK of the sample in which PSD has been measured and the values of the entire October 2007 to October 2008 database: mean values were not statistically different. Thus, it can be asserted that doses delivered in this type of procedure are generally not high, and the definition of trigger levels in this case is not relevant.

4.2. Aneurysm embolization

For aneurysm embolization procedures, correlation between PSD and KAP is weak ($R^2 = 0.4$), instead correlation between PSD and CK is quite strong ($R^2 = 0.74$), as reported in Figs 3 and 4.

A retrospective analysis on the entire database was carried out using the linear coefficient to estimate PSD from CK. Estimated PSD exceeded the threshold for transient erythema (2 Gy) by ten times (13% of procedures) and two times the threshold for temporary epilation (3 Gy). Therefore, it is necessary in this case to define a trigger level that indicates the possible exceeding of 3 Gy for PSD. The value established in terms of CK for that type of procedure in the authors' medical centre is 5200 mGy.

4.3. Chemoembolization for liver cancer

For chemoembolization procedures, there was a good correlation of PSD ($R^2 = 0.68$) with KAP and very strong correlation with CK ($R^2 = 0.93$) (Figs 5 and 6). Also, for these procedures, a retrospective analysis on the entire database was conducted using the linear coefficient between PSD and CK, which found that PSD exceeded the threshold for transient erythema (2 Gy) in 25 procedures (17% of the total number) and in one procedure, PSD was estimated at higher than 5 Gy. Therefore, also in this case, it is necessary to define a trigger level that indicates the possible exceeding of 3 Gy for PSD. The value established in terms of CK for chemoembolization procedures in the authors' medical centre is 2500 mGy.

5. CONCLUSION

Doses delivered to the patient's skin during some interventional procedures could be very high and exceed the threshold for tissue reactions.

The study proposes a methodology to assess trigger levels for interventional radiology. This trigger level might be a useful instrument for alerting the physician for high skin dose procedures. CK appears to be a better dose indicator than KAP for the type of procedure analysed. Consequently, the relationship established between CK and MSD could be used to derive trigger levels. It does not represent the general relationship between CK and MSD because it is strictly dependent on many different parameters such as procedure, the physician's experience, calibration and reading of films, and KAP meter calibration.

CK trigger level is not a dose constraint or dose limit, but it is a useful instrument for the identification of unusually high levels of radiation that require investigation if substantially exceeded.

In our centre, these levels are 5200 mGy and 2500 mGy, respectively, for aneurysm embolization and chemoebolization.

REFERENCES

[1] KOENIG, T.R., WOLFF, D., METTLER, F.A., WAGNER, L.K., Skin injuries from fluoroscopically guided procedures: Part I, Characteristics of radiation injury, Am J Roentgenol **177** (2001) 3–11.

[2] KOENIG, T.R., METTLER, F.A., WAGNER, L.K., Skin injuries from fluoroscopically guided procedures: Part 2, review of 73 cases and recommendations for minimizing dose delivered to patient, J Roentgenol **177** (|2001) 13–20.

[3] INTERNATIONAL COMMISSION ON RADIOLOGICAL PROTECTION, Recommendations of the International Commission on Radiological Protection. Publication 85: Avoidance of radiation injuries from medical interventional procedures. Ann. ICRP, Oxford, UK: Pergamon Press (2000).

[4] VANO, E., GONZALEZ, L., TEN, J.I., FERNANDEZ, J.M., GUIBELALDE, E., MACAYA, C., Skin dose and dose-area product values for interventional cardiology procedures. Br J Radiol. **74** (2001) 48–55.

[5] TRIANNI, A., CHIZZOLA, G., TOH, H., QUAI, E., CRAGNOLINI, E., BERNARDI, G., PROCLEMER, A., PADOVANI, R., Patient skin dosimetry in haemodynamic and electrophysiology interventional cardiology, Radiat Prot Dosimetry 117 (2005) 241–246.

RADIATION DOSE MEASUREMENTS FOR PAEDIATRIC PATIENTS AND COMFORTERS DURING MICTURATING CYSTOURETHROGRAPHY

A. SULIEMAN, F.N. ABD-ALRAHMAN, B.M. HUSSAIN,
M. HAMADELNEEL
College of Medical Radiologic Science,
Sudan University of Science and Technology,
Khartoum, Sudan
Email: abdelmoneim_a@yahoo.com

Abstract

The study was carried out in Soba University Hospital, Khartoum with the objectives to: (a) determine the entrance surface dose (ESD), organ dose and effective dose (*E*) associated with paediatric patients undergoing micturating cystourethrography (MCUG), and (b) to evaluate the technique applied to reduce the dose to patients and comforters. A total of 60 thermoluminescence dosimeter (TLD) circular chips of lithium fluoride (LiF: Mg, Cu, P) were used in this study. The TLD signal was read using an automatic TLD reader (Fimel PCL3, France) in an atmosphere of inert nitrogen. The ESD was determined by TLDs for 33 children. Moreover, the surface dose was evaluated for the comforter, who helped in support and comfort of the children during the examination. ESD was used to estimate *E* using the National Radiological Protection Board (NRPB SR279) software. The mean ESD and *E* resulting from MCUG procedure was estimated at 5.51 mGy and 0.22 mSv, respectively. The mean ESD results for all patients were greater than previous studies, which indicate the need for radiation dose optimization. The results of this study provide baseline data to establish reference dose levels for MCUG examination in young patients in Sudan.

1. INTRODUCTION

Micturating cystourethrography (MCUG) or voiding cystourethrography is the definitive method of assessing the lower urinary tract and accounts for 40% of all fluoroscopic procedures performed on children in Europe [1, 2]. It is particularly valuable for the assessment of vesicoureteric reflux (VUR), a common abnormality found in children with urinary tract infection (UTI), which causes renal damage [3]. UTI incidence during childhood has been estimated at 8% for girls and 2% for boys, and the incidence of VUR estimated at 52% [4], mostly occurring in the first year of life [5, 6]. MCUG involves inevitable radiation dose to the paediatric patients as well as to the comforter, i.e.

individuals helping in the support, care and comfort of the children during the examination.

Radiation doses to children undergoing fluoroscopy examinations are of concern due to their higher risk of developing radiation induced malignancies than adults. During MCUG procedures, the comforter is usually located close to the radiation field and is exposed to scattered radiation. The Council of the European Union has adopted Directive 97/43/EURATOM [6], which requests Member States to ensure that dose constraints are established for exposure of those individuals (voluntary helpers) knowingly and willingly helping patients undergoing medical diagnosis or treatment. As the number of examinations procedures performed in paediatrics and children worldwide continues to increase, growing concerns have been raised about the radiation exposures to pediatric patients and their comforters. Several studies have been published [7–13] on patient doses during MCUG procedure that stress the importance to use the lowest radiation dose necessary without compromising clinical diagnosis.

The objectives of this study are to: (a) determine the entrance surface dose (ESD), organ and thyroid surface dose, effective dose (E) and relevant radiogenic risks associated with paediatric patients undergoing MCUG, and (b) evaluate the technique applied in order to reduce patient and co-patient dose.

2. MATERIAL AND METHODS

2.1. Dosimeter

The dosimeters used in this work were TLD-GR-200 circular chips, 4.5 mm in diameter and 0.8 mm thick. These TLDs were calibrated under reproducible reference condition using a Phillips Duo Diagnost X ray machine (Phillips Medical Systems, Hamburg, Germany) and a PTW CONNY II ionization chamber connected to radiation monitor controller at 100 cm SSD, using 75 kV and 20 mA. Both the chamber and electrometer were calibrated for the energy ranges 30–120 kVp at the national standards laboratory. TLDs were irradiated on a perspex calibration test bed which had been constructed with the dimensions of 25 cm × 25 cm × 10 cm. Each TLD was identified by its position in the array. Individual calibration factors were obtained by irradiating the entire group to the same dose. The measured signal of each TLD obtained by the reader was divided by the mean signal of the group this process was repeated three times to minimize the effect of statistical variations. The TLD signal was read using an automatic TLD reader (Fimel PCL3, France) in an atmosphere of inert nitrogen.

The time–temperature profile was divided into:

— Pre-heat temperature: (pre-readout) is done by heating to 155°C, to ensure consistency of the reading and to remove unwanted peaks;
— Acquisition: the signal is acquired up to 260°C with a heating rate of 1°C/s to obtain the glow curve.

Prior to each irradiation, all dosimeters were annealed (as recommended by the manufacturer) in an annealing oven (TLDO, PTW, Freiburg, Germany), with accuracy better than 1% used to anneal the detectors at 240°C for 10 min.

2.2. X ray machine

An under couch fluoroscopy unit and over couch intensifying screen made in 2005 (Toshiba, KXO-15E (Toshiba Corporation, Japan)) was used. The minimum tube filtration was 2.5 mm aluminium. The kV and mA ranges are 150–40 and 640–20, respectively. The machine had already passed the routine quality control tests performed by the Sudan Atomic Energy Commission.

2.3. MCUG procedure

An MCUG examination is a specific radiological procedure performed under fluoroscopic screening to visualize the bladder by filling it with contrast media and to evaluate the urethral morphology during voiding.

Catheterization was performed under strict aseptic conditions. Intermittent fluoroscopy was performed to detect VUR or other abnormality. Radiographic images were taken as follows:

— Scout radiograph of the kidneys and bladder before contrast is injected;
— Right and left oblique views of the bladder when full in order to show the vesicoureteral regions;
— The urethra while voiding;
— Post-void radiograph of the bladder and kidneys.

More radiographs may be taken when an abnormality is discovered.

2.4. Dosimetry of patients and comforters

A total of 33 children were examined in the Radiology Department of Soba University Hospital in Khartoum. Radiation doses were measured by directly

placing a labelled TLD envelope on the skin at the centre of the field of view and on the thyroid.

For comforters of the patient helpers, two envelopes were used: one at the chest level above the lead apron (0.5 mm thick lead equivalent), and the other, at the level of the waist under the lead apron. The comforter dose, *E*, was estimated by using the following formula [14]:

$$E = 0.06(H_{OS} - H_U) + H_U \quad (1)$$

where H_{OS} is the dose measured by the dosimeter at the neck (shallow depth) and H_U is the dose measured under the apron at waist level (deep).

For each patient, the following parameters were recorded: radiographic data (kV, mA·s and exposure time), fluoroscopic data (minimum and maximum kV and mA and total exposure time) and patient data (name, gender, age, weight, height, date of birth, clinical indication, radiologist, start and end time of the procedure).

2.5. Patient effective and organ dose estimation

ESD was used to assess the equivalent organ dose for selected organs during MCUG procedure. Organ dose (mGy) estimation was performed by using the National Radiological Protection Board (NRPB-SR279) [15] computer software.

3. RESULTS

Thirty-three children, seven girls and 26 boys, with an age range of 48 d to ten years were examined. Of the 33 children, 15 patients had positive VUR and 18 had negative VUR. Characteristics for male patients are presented in Table 1, which demonstrates large variations.

TABLE 1. MEAN VALUES FOR MALE PATIENT CHARACTERISTICS, SCREENING TIME AND NUMBER OF RADIOGRAPHIC IMAGES

Age group	*N*	Patient age (year)	Height (m)	Weight (kg)	BMI (kg/m^2)	Screening time (min)	Number of images
All	33	4.21 (0.13–10)	0.96 (0.5–1.5)	13 (3–35)	13.40 (6.45–21.05)	2.8 (1.1–9)	5 (3–8)

Mean kV and mA·s obtained during the examinations were 56 kV and 9.9 mA·s, respectively, as shown in Table 2.

For all patients the mean, minimum, median, 3rd quartile and maximum values of ESD obtained by TLD for MCUG examination are presented in Table 3.

The organ equivalent dose (mSv) to the skin, testes, urinary bladder, uterus and ovaries for all patients are presented in Table 4.

Finally, for comforters, the mean, minimum, median, third quartile and maximum of radiation dose (mGy) as well as the effective dose values are presented in Table 5.

TABLE 2. MEAN VALUES OF RADIOGRAPHIC AND FLUOROSCOPIC EXPOSURE FACTORS

Radiography		Fluoroscopy	
kVp	mA·s	kVp	mA·s
56 (44–70)	9.9 (4–30)	56.34 (50–74)	0.55 (0.2–1)

TABLE 3. MINIMUM, MEDIAN, MEAN, THIRD QUARTILE AND MAXIMUM VALUES OF THE ESD AND THYROID DOSES (mGy) FOR PATIENTS

Patient	Mean	Minimum	Median	3rd quartile	Maximum
ESD	5.51	0.39	4.75	8.89	16.12
Thyroid	0.30	0.13	0.24	0.27	1.53

TABLE 4. MEAN ORGAN RADIATION EQUIVALENT DOSE (mSv per MCUG PROCEDURE)

Organ	Skin	Testes	Urinary bladder	Ovaries	Uterus	Effective dose
Organ equivalent dose (mSv)	0.43	0.27	0.35	0.54	0.49	0.22

TABLE 5. MINIMUM, MEAN, MEDIAN, THIRD QUARTILE AND MAXIMUM VALUES OF COMFORTERS RADIATION DOSES (mGy) AND EFFECTIVE DOSE (mSv)

Co-patients	Mean	Minimum	Median	3rd quartile	Maximum
Chest	0.27	0.18	0.21	0.24	1.60
Waist	0.21	0.14	0.20	0.24	0.30
Effective dose	0.21	0.15	0.20	0.23	0.38

4. DISCUSSION

This study intended to provide a detailed evaluation of radiation dose during MCUG and to analyse factors that might affect the radiation dose for both patients and comforters.

4.1. Patient body characteristic data

The patient body characteristic data (age, height, weight and BMI) in Table 1 are comparable to mean values reported in the literature [7–10]. The Screening time ranged from 1.1 min to 9 min. The mean screening time, as shown in Table 1, was greater than that previously reported, which ranged from 0.4 to 8.9 min [8]. Perisinakis et al. [9] reported a mean fluoroscopy time and number of radiographs during MCUG as 0.73 min and 2.3 min for female patients, and 0.91 min and 3.0 min for male paediatric patients, respectively. The number of radiological views depends on the technique used at various radiological centres. In this study, the mean number of radiographs per MCUG examination ranged from 3 to 8, which is lower than that reported by Sulieman et al. [7] (see Table 6).

4.2. Exposure factors

The exposure factors (kVp, mA) for all patients were comparable to exposure factors reported in previous studies [7–10, 16]. In general, high kVp increases the scatter radiation and thus also the patients' dose, while decreasing the contrast of the image. The quality of the radiation depends on the tube voltage and the total filtration of the X ray beam. Radiographic exposure factors used in this study ranged from 44 kVp to 70 kVp and time current product from 4 mA·s to 32 mA·s during the examination. Fluoroscopic applied voltage ranged from 50 kVp to 74 kVp and tube current from 0.2 mA to 1 mA (see Table 2).

TABLE 6. THE MEAN PATIENT PARAMETERS, SCREENING TIME, NUMBER OF RADIOGRAPHIC IMAGES, ESD AND EFFECTIVE DOSE IN VARIOUS STUDIES

Author	*N*	Age (year)	BMI (kg/m^2)	Screening time (min)	Number of radiographic images	Dose area product ($Gy \cdot cm^2$)	ESD (mGy)	Effective dose (mSv)
Present study	33	4.21	13.40	2.8	5	NR[a]	5.51	0.22
Suleiman et al. [7]	52	0.0–2	15.35	0.75	1.18	NR	1.13	0.20
Perisinaks et al. [9]	19	0–1	16.9	0.73	6.3	0.41	NR	(0.12–1.67)[b] (0.15–1.45)[c]
Fotakis et al. [10]	30	NR	NR	3	NR	NR	4.58	(0.76 ± 0.28)[b] (0.86 ± 0.31)[c]
Travassos et al. [16]	37	3	18.8	8.5	11	7.94	113.5	NR

[a] NR: not reported.
[b] Girls.
[c] Boys.

Sulieman et al. [7] reported that MCUG with digital equipment and fluoroscopy captured image technique could reduce the dose to a patient by up to 50%. Ward et al. [13] reported that, grid controlled variable rate pulsed fluoroscopy reduce the radiation dose to a patient at least eight times lower than continuous fluoroscopy during MCUG.

No significant correlation was found between patient dose, patient characteristics, and exposure factors, but it should be noted that the patient dose depends on the complexity of the procedure. In general, variations in patient morphology and exposure factors influence the patient dose and image contrast.

4.3. Patient absorbed and effective dose

The mean ESD and *E* resulting from MCUG procedure have been estimated at 5.51 mGy and 0.22 mSv, respectively, for the patient population (see Table 5). The mean ESD result for all patients was higher than previous studies, as shown in Table 6. Considerable variations were observed among patient populations in

terms of radiation dose and fluoroscopic time (Tables 1–3). These variations are due to the different indications, patient characteristics and clinical indications.

Since MCUG involves direct irradiation of some of the internal and in radiosensitive organs, equivalent doses for specific organs were estimated, as shown in Table 4. Ovaries and testes dose, which are of concern due to the hereditary effect of radiation, were estimated at 0.54 mGy and 0.27 mGy, respectively. In comparison with Sulieman et al. [7], the mean equivalent doses for ovaries and testes were significantly higher, at 0.44 mSv and 0.33 mSv, respectively. The equivalent dose for brain, eye lenses, thyroid and thymus were very low values because they were not in the field of view (pelvis region).

4.4. Dose to the patient comforters

The measured doses to the comforter (mGy) are presented in Table 5. The mean and range of effective doses to them were 0.21 mSv and 0.15–0.38 mSv, respectively. As expected, the comforters were exposed to scatter radiation, while their radiation dose was high because they were always near to the primary beam.

The radiation dose inside the lead apron is insignificant, and the examiners are adequately protected. The results this study are comparable with those of a previous study [7], where it was reported that a mean dose to the comforter was 0.14 mGy, with a range from 0.03 mGy to 0.5 mGy.

5. CONCLUSION

This study indicates the need for radiation exposure reduction to patients and comforters, and underlines the importance of the protection for pediatric patients. The mean patient dose for MCUG is high compared to the other studies found in the literature. The mean effective dose for comforters to the comforters is well within established safety limits. The results of this study provide baseline data to establish reference dose levels for MCUG examination in very young patients in Sudan.

REFERENCES

[1] HARDY, M., BOYNES, S., Paediatric Radiology, 1st ed. Blackwell Science Ltd., USA (2003).

[2] SCHNEIDER, K., KRUGER-STOLLFUB, I., ERNST, G., Paediatric Fluoroscopy: A survey of children hospitals in Europe, Paediatr. Radiol. (1) (2001) 238–246.

[3] COULTHARD, M.G., LAMBERT, H.J., KEIR, M.J., Occurrence of renal scars in children after their first referral for urinary tract infection, BMJ **315** (1997) 918–9.
[4] EUROPEAN COMMISSION, Quality Criteria for Diagnostic Radiographic Images in Paediatrics, Report EUR 16261, Luxembourg: Office for Official Publications of the European Communities (1996) 1–35.
[5] JAUKOVIC, L., AJDINOVIC, B., DOPUDJA, M., KRSTIC, Z., Renal Scintigraphy in Children with Vesicoureteral Reflux, Indian Journal of Paediatrics. **76** 10 (2009) 1023–1026.
[6] EUROPEAN UNION, Council Directive 97/43 Euratom on Health Protection of Individuals Against The Dangers of Ionizing Radiation in Relation to Medical Exposure. Official Journal of the European Communities No. L 180, 9 July 22–27 (1997).
[7] SULIEMAN, A., THEODOROU, K., VLYCHOU, M., T TOPALTZIKIS, T., KANAVOU, D., FEZOULIDIS, I., KAPPAS, C., Radiation dose measurement and risk estimation for paediatric patient**s** undergoing micturating cystourethrography Br J Radiol. (2007) 731–737.
[8] WARD, V., Patient dose reduction during voiding cystourethrography**,** Paediatr Radiol. 36(2) 168–172 (2006).
[9] PERISINAKIS, K., RAISSAKI, M., DAMILAKIS, J., STRATAKIS, J., NERATZOULAKIS, J., GOURTSOYIANNIS, N., Fluoroscopy-controlled voiding cystourethrography in infants and children: Are the radiation risks trivial? Eur Radiol **16**(4) (2006) 846–51.
[10] FOTAKIS, M., MOLYVDA ATHANASOPOULOU, E., PSARRAKOS, K., ECONOMOU, I., Radiation doses to paediatric patients up to 5 years of age undergoing micturating cystourethrography examinations and its dependence on patient age, Br J Radiol 76(911) (2003) 812–7.
[11] SCHULTZ, F.W., GELEIJNS, J., HOLSCHER, H.C., WESTSTRATE, J., ZONDERLAND, H.M., ZOETELIEF, J., Radiation burden to paediatric patients due to micturating cystourethrography examinations in a Dutch children's hospital. Br. J. of Radiol. **72** 860 (1999) 763–772.
[12] LEE, R., THOMAS, K., CONNOLLY, B., FALKINER, M., GORDON, C., Effective dose estimation for paediatric voiding cystourethrography using an anthropomorphic phantom set and metal oxide semiconductor field-effect transistor (MOSFET) technology, Paediatr Radiol. **39**(6) (2009) 608–15.
[13] WARD, V.L., STRAUSS, K.J., BARNEWOLT, C.E., ZURAKOWSKI, D., VENKATAKRISHNAN, V., FAHEY, F.H., LEBOWITZ, R.L., TAYLOR, G.A., Paediatric radiation exposure and effective dose reduction during voiding cystourethrography, Radiology **249** (3) (2008) 1002–9.
[14] PADOVANI, R., RODELLA, C.A., Staff dosimetry in interventional cardiology. Radiat. Prot. Dosim. **94** (2001) 99–103.
[15] HART, D., JONES, D.G., WALL, B.F., Normalized organ dose for paediatric X ray examinations calculated using Monte-Carlo techniques, NRPB Chilton (1996).
[16] VIEIRA TRAVASSOS, L., BASTOS BOECHAT, M.C., NUNEZ SANTOS, E., DE OLIVEIRA, S.R., DA SILVA, M.O., PIRES CARVALHO, A.C., Evaluation of radiation dose in voiding cystourethrography in children, Radiol. Bras. **42**(1) (2009) 21–25.

ON THE INFLUENCE OF PATIENT POSTURE ON ORGAN AND TISSUE ABSORBED DOSES CAUSED BY RADIODIAGNOSTIC EXAMINATIONS

R. KRAMER, V.F. CASSOLA
Computational Dosimetry,
Department of Nuclear Energy,
Federal University of Pernambuco,
Recife, Brazil
Email: rkramer@uol.com.br

Abstract

Virtual human phantoms, frequently used for organ and tissue absorbed dose assessment in radiology, normally represent the human body either in standing or in supine posture. This raises the question as to whether it matters dosimetrically if the postures of the patient and of the phantom do not match. This study uses the recently developed FASH2_sta (Female Adult meSH) and FASH2_sup phantoms which represent female adult persons in standing and supine posture. The effect of the posture on organ and tissue absorbed doses will be studied using the EGSnrc Monte Carlo code for simulating abdominal radiographs and special attention will be directed to the influence of body mass on the results. For the exposure conditions considered here, posture-dependent absorbed dose differences by up to a factor of two were found.

1. INTRODUCTION

In X ray diagnosis, depending on the protocol of the radiological procedure to be carried out, patients have to take up a specific posture relative to the X ray beam. For examinations of organs and tissues located in the human trunk, the standing and the supine (lying on the back) postures are those most frequently used in routine X ray diagnosis. Owing to the gravitational force, a number of anatomical effects occur when a standing person takes up a supine posture, such as cranial (towards the head) and dorsal (towards the back) shifts of organs, compression of the lungs and change of the fat distribution. Consequently, the question is whether such anatomical effects could significantly influence the absorbed dose to radiosensitive organs and tissues caused by radiological examinations.

Often, methods to determine absorbed dose to organs and tissues use phantoms, which normally represent human bodies either in standing or in supine posture. Consequently, one has to develop a human phantom representing both postures in order to find an answer to the question raised above. Using male and

female adult phantoms, such an approach has recently been reported by Cassola et al. [1]. In their study, the MASH2 (Male Adult meSH) and the FASH2 (Female Adult meSH) phantoms have been designed in the standing as well as in the supine posture. Using 3-D modelling software, the standing phantoms have been developed based on anatomical atlases. Their organ and tissue masses, whole body mass and body height correspond to the reference data given by ICRP89. Then, the standing phantoms were transformed into supine phantoms by shifting organs and deforming fat based on anthropometric and medical data, such as sagittal diameters for different postures, cranial and dorsal shifts of organs and posture dependent lung volumes found in the medical research papers cited by Cassola et al. [1]. Monte Carlo calculations of organ and tissue absorbed doses were carried out for various exposure scenarios. For simulated X ray exposures of the thorax and the abdomen, posture dependent differences between organ and tissue absorbed doses of more than 60% were found. Cassola et al concluded that with increasing body mass the 'posture effect' on organ and tissue absorbed dose is expected to increase, because the lateral shift of more fat would increase the difference between the sagittal diameters for the two postures. This paper aims to verify this expectation.

2. MATERIALS AND METHODS

For the purpose of this study, the whole body masses of both versions of the FASH2 phantom (Figs 1 and 2) have been increased by 5 kg of subcutaneous fat. Frontal and lateral views of the heavier FASH2+5kg_sta and FASH2+5kg_sup phantoms are shown in Figs 3 and 4, respectively. Compared to the standing FASH+5kg_sta phantom, the supine phantom FASH2+5kg_sup has a smaller sagittal diameter, a greater lateral diameter, flatter breasts, broader shoulders and a different position of the arms. Internally, organs are shifted cranially and dorsally in the supine phantom to be shown later with the results. The comparison between Figs 1 and 2, on the one hand, and Figs 3 and 4, on the other hand, clearly reflects the increase of body mass.

After voxelization [1], all four phantoms were coupled to the EGSnrc Monte Carlo code [2] and abdominal radiographs were simulated using the following exposure conditions: tube voltage of 90 kVcp, total filtration of 2.5 mm Al, anterior-posterior (AP) projection, field size in detector plane of 35 cm × 40 cm and focus-to-detector distance (FDD) of 115 cm. For all four phantoms, the field was centred on the body at the height of the iliac crest. Deposition of radial energy in organs and tissues was calculated based on coupled transport of photons and electrons in all segmented organs and tissues, and

FIG. 1. FASH2_sta and FASH2_sup: frontal view of surfaces[1].

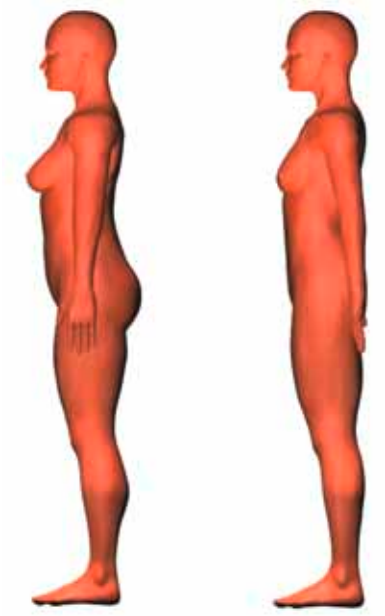

FIG. 2. FASH2_sta and FASH2_sup: lateral view of surfaces [1].

FIG. 3. FASH2+5kg_sta and FASH2+5kg_sup: frontal view of surfaces.

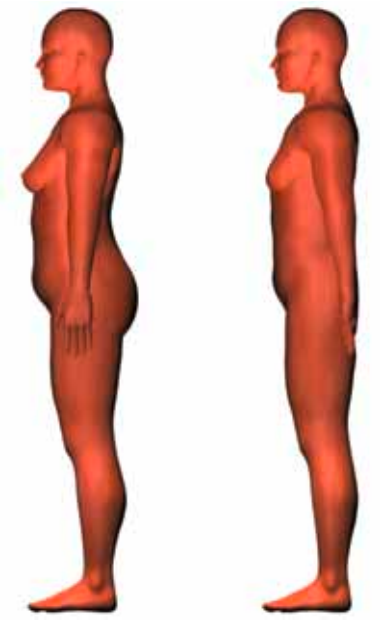

FIG. 4. FASH2+5kg_sta and FASH2+5kg_sup: lateral view of surfaces.

additionally using microCT images of human spongiosa for the determination of absorbed dose to radiosensitive skeletal tissues [3]. Absorbed doses to organs and tissues were normalized to incident air kerma (INAK) [4], which was calculated simultaneously based on the air kerma to fluence conversion function for photons [5] during radiation transport of the photons through the phantoms, i.e. that the results were determined as conversion coefficients (CCs). Cut-off energies for photons were 2 keV for photons in all tissues, 20 keV for electrons in tissues located outside the skeleton and 5 keV for electrons in skeletal tissues.

3. RESULTS

In the case of external whole body exposure, all radiosensitive organs and tissues are located in the radiation field, so that for a given exposure situation, the average organ or tissue absorbed dose is primarily a function of the depth of the tissue of interest below the body surface in the direction of the radiation. Taking up a supine posture, causes the above mentioned changes, such as compression of the lungs, cranial and dorsal organ shifts, and a change of the subcutaneous fat distribution. As a consequence, organ absorbed doses for the supine posture can become greater or smaller than for the standing posture depending on the net effect of all the anatomical changes on the position of the organ under consideration. An X ray radiograph, however, usually represents a partial body exposure by which the position of an organ or tissue relative to the radiation field additionally becomes an influential parameter for the absorbed dose, which is especially important here because organ shifts due to posture change can move organs more into or more out of the radiation field.

Exposure geometries for abdominal radiographs are shown for the FASH2_sta, the FASH2_sup, the FASH2+5kg_sta and the FASH2+5kg_sup phantoms in Figs 5–8, respectively. The field size was 35 cm × 40 cm in the detector plane, shown by the blue rectangle. The black rectangle represents the field size at the entrance plane. As the field position is the same with respect to the pelvis for all phantoms, the cranial organ shifts can easily be recognized in the figures. For example, in the supine posture the urinary bladder is partly shifted into the radiation field, while the liver, the stomach, the spleen are partly shifted out of the radiation field. The sagittal diameter across the field is smaller for the supine phantoms than the standing versions and larger for the heavier phantoms than the original phantoms due to the increase of body mass.

For selected radiosensitive organs and tissues, Table 1 shows the results of the Monte Carlo simulation for FASH2_sta and FASH2_sup, called here the ‘Base’ phantoms, and for FASH2+5kg_sta and FASH2+5kg_sup, termed here the

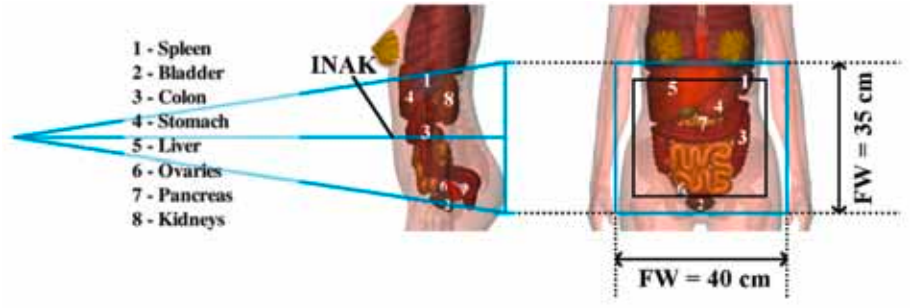

FIG. 5. Abdominal exposure of the standing FASH2_sta phantom. 90 kVcp, 2.5 mm Al, FDD = 115 cm, field size in detector plane = 35 cm × 40 cm, AP.

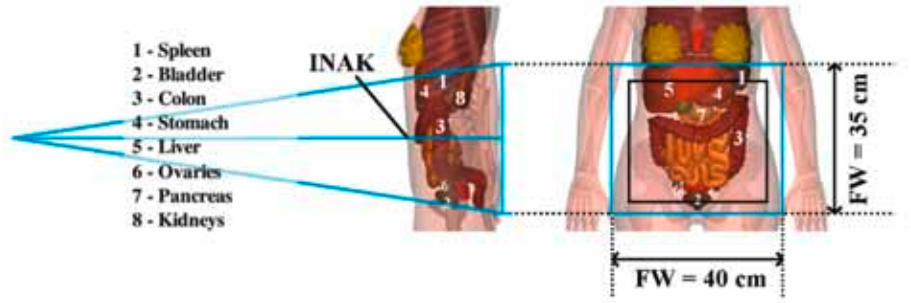

FIG. 6. Abdominal exposure of the supine FASH2_sup phantom. 90 kVcp, 2.5 mm Al, FDD = 115 cm, field size in detector plane = 35 cm × 40 cm, AP.

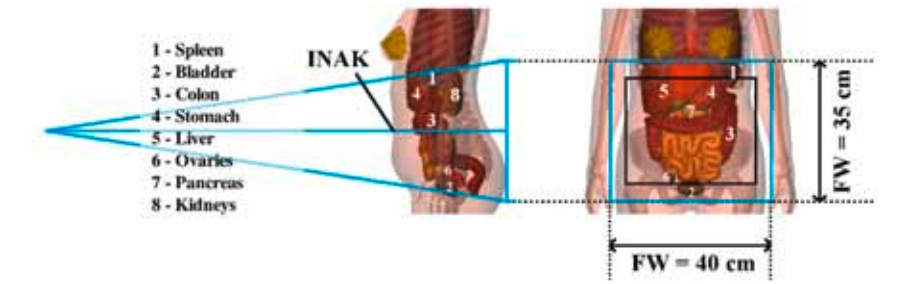

FIG. 7. Abdominal exposure of the standing FASH2+5kg_sta phantom. 90 kVcp, 2.5 mm Al, FDD = 115 cm, field size in detector plane = 35 cm × 40 cm, AP.

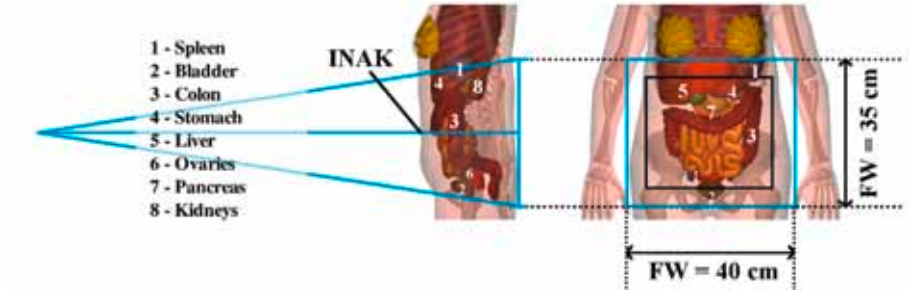

FIG. 8. Abdominal exposure of the supine FASH2+5kg_sup phantom. 90 kVcp, 2.5 mm Al, FDD = 115 cm, field size in detector plane = 35 cm × 40 cm, AP.

'+5 kg' phantoms. The data represent the CCs between the average organ absorbed dose and the INAK in Gy/Gy, the statistical error in per cent and the ratio between the supine and the standing CCs for the 'Base' as well as for the '+5kg' phantoms.

In the supine posture, for AP projection, the reduction of the sagittal diameter increases organ absorbed dose, while the dorsal organ shift decreases organ absorbed dose. Consequently, the net effect of the two parameters can lead to supine organ absorbed doses that are either greater or smaller than the standing organ absorbed doses. Additionally, the supine absorbed dose is influenced by a possible change of the organ position relative to the radiation field.

The 'Base' ratios in column 6 of Table 1 show an increase of absorbed dose for the bladder wall, the colon wall, the ovaries, the small intestine wall, the uterus, the red bone marrow and the bone surface cells, because for these organs and tissues, the above mentioned net effect causes a reduction of the shielding when the phantom's posture changes from standing to supine. For the small intestine wall, the supine absorbed dose is 15.5% greater than the standing absorbed dose, for example. In addition, the bladder is shifted into the radiation field in the supine posture, which increases the absorbed dose even further to reach 45.5%. The dorsal shift of the pancreas more than compensates the reduction of the sagittal diameter and the organ is shifted out of the field centre where the particle fluence has its maximum, which leads to a net decrease of the supine organ dose by 11.5%. For organs such as the kidneys, the liver, the spleen and the stomach, a significant shift out of the radiation field occurs in the supine posture. Therefore, the absorbed dose for these organs decreases, for example, for the spleen, by 27.7%.

The '+5 kg' ratios in the last column reflect the impact of 5 kg additional subcutaneous fat. At the field centre, the sagittal diameter difference between standing and supine posture is 0.7 cm and 1.6 cm for the 'Base' and the '+5 kg'

TABLE 1. CONVERSION COEFFICIENTS BETWEEN AVERAGE ORGAN OR TISSUE ABSORBED DOSE (*D*) AND INAK AND RATIOS BETWEEN THEM FOR THE FASH2 BASE PHANTOMS AND THE FASH2+5kg PHANTOMS IN STANDING (STA) AND SUPINE (SUP) POSTURE FOR ABDOMINAL RADIOGRAPHS.

FASH2	Base	Base	Base	Base	Base	+5 kg	+5 kg	+5 kg	+5 kg	+5 kg
	STA D/INAK	STA error	SUP D/INAK	SUP error	SUP/STA ratio	STA D/INAK	STA error	SUP D/INAK	SUP error	SUP/STA ratio
Organ/tissue	(Gy/Gy)	(%)	(Gy/Gy)	(%)		(Gy/Gy)	(%)	(Gy/Gy)	(%)	
Bladder wall	0.268	1.3	0.390	1.1	1.455	0.184	1.5	0.377	1.1	2.049
Colon wall	0.522	0.3	0.573	0.3	1.098	0.407	0.3	0.545	0.3	1.339
Kidneys	0.171	0.6	0.137	0.7	0.801	0.136	0.7	0.141	0.7	1.037
Liver	0.462	0.2	0.359	0.2	0.777	0.384	0.2	0.352	0.2	0.917
Ovaries	0.326	2.2	0.343	2.2	1.052	0.210	2.7	0.316	2.2	1.505
Pancreas	0.453	0.6	0.401	0.6	0.885	0.357	0.6	0.384	0.6	1.076
Sm. intestine wall	0.483	0.3	0.558	0.2	1.155	0.356	0.3	0.513	0.2	1.441
Spleen	0.357	0.6	0.258	0.8	0.723	0.297	0.7	0.261	0.7	0.879
Stomach wall	0.589	0.5	0.479	0.5	0.813	0.477	0.5	0.471	0.5	0.987
Uterus	0.234	1.0	0.265	0.9	1.132	0.160	1.2	0.241	1.0	1.506
RBM max.	0.147	1.0	0.165	0.9	1.122	0.094	1.2	0.153	1.0	1.628
BSC max.	0.219	1.1	0.243	1.1	1.110	0.139	1.4	0.223	1.1	1.604

Note: Exposure parameters: 90 kVcp, 2.5 mm Al, FDD = 115 cm, field in detector plane = 35 cm × 40 cm, field centred on the body at the height of the iliac crest. Error = statistical error of the Monte Carlo calculation.

phantoms, respectively. The greater difference between the fat layers of the '+5 kg' phantoms and their distributions cause an additional increase of the absorbed dose difference between supine and standing posture for the bladder wall, the colon wall, the ovaries, the small intestine wall, the uterus, the red bone marrow and the bone surface cells; from 15.5% to 44.1% for the small intestine wall, for example. The kidneys, the liver, the pancreas, the spleen and the stomach experience the same fat layer difference in the '+5 kg' phantoms, but as their supine absorbed doses were decreasing in the 'Base' phantoms, the net effect in the '+5 kg' phantoms is a decrease of the difference between supine and standing absorbed dose; from 22.7% to 8.3% for the liver or from 18.7% to 1.3% for the stomach wall, for example.

4. CONCLUSION

Dosimetric assessments of organ and tissue absorbed doses for patients submitted to radiographic examinations require the use of human phantoms that correctly reflect the posture of the patient according to the protocol of the medical procedure to be simulated. Ignoring the anatomical differences between the standing and the supine posture in organ absorbed dose calculations can introduce errors of up to 45.5% for the abdominal radiograph simulated here for the ICRP89-based FASH phantom. This investigation has demonstrated that with increasing body mass, some of the absorbed dose errors also increase. As shown in Table 1, the error can arrive at a factor of two for the urinary bladder wall, for example. For some organs, posture dependent absorbed dose differences may become smaller with increasing body mass. This occurs especially for organs that are (partly) shifted out of the radiation field in the supine posture, such as the liver. However, with further increasing body mass, an increase of the posture dependent absorbed dose difference is to be also expected for these organs.

The posture dependent MASH2 and FASH2 phantoms are available to the scientific community and can be downloaded free of charge from www.grupodoin.com following the link 'Caldose'.

ACKNOWLEDGEMENTS

The authors would like to thank the Conselho Nacional de Desenvolvimento Científico e Tecnológico and the Fundação de Amparo à Ciência do Estado de Pernambuco for financial support.

REFERENCES

[1] CASSOLA, V.F., KRAMER, R., BRAYNER, C., KHOURY, H.J., Poster-specific phantoms representing female and male adults in Monte Carlo-based simulations for radiological protection, Phys. Med. Biol. **55** (2010) 4399–4430.

[2] KAWRAKOW, I., ROGERS, D.W.O., The EGSnrc code system: Monte Carlo simulation of electron and photon transport, NRC Report PIRS-701 (2003).

[3] KRAMER, R., CASSOLA, V.F., KHOURY, H.J., VIEIRA, J.W., DE MELO LIMA, V.J., ROBSON BROWN, K., FASH and MASH: female and male adult human phantoms based on polygon mesh surfaces: II. Dosimetric calculations, Phys Med Biol **55** (2010) 163–189.

[4] INTERNATIONAL COMMISSION ON RADIATION UNITS AND MEASUREMENTS, Patient dosimetry for X-rays used in medical imaging ICRU Report No. 74 International Commission on Radiation Units and Measurements, Bethesda, MD, USA (2005).

[5] INTERNATIONAL COMMISSION ON RADIOLOGICAL PROTECTION, Conversion Coefficients for Use in Radiological Protection against External Radiation. ICRP Publication 74 (Oxford: Pergamon) (1996).

CLINICAL DOSIMETRY IN RADIOTHERAPY

(Session 5)

Chairpersons

G.S. IBBOTT
American Association of Physicists in Medicine

J. VAN DYK
IAEA

ASSESSING HETEROGENEITY CORRECTION ALGORITHMS USING THE RADIOLOGICAL PHYSICS CENTER ANTHROPOMORPHIC THORAX PHANTOM

D.S. FOLLOWILL*, S. DAVIDSON**, A. MOLINEU*, P. NITSCH**, G. FISHER*, P. ALVAREZ*, G.S. IBBOTT*

* Department of Radiation Physics,
M.D. Anderson Cancer Center,
The University of Texas
Email: dfollowi@mdanderson.org

** Department of Radiation Physics,
Methodist Hospital

Houston, Texas,
United States of America

Abstract

The Radiological Physics Center's (RPC) mission is to assure the US National Cancer Institute and the cooperative clinical trial groups that participating institutions deliver radiation treatments that are clinically comparable. The RPC credentials institutions to participate in advanced technology trials using several anthropomorphic quality assurance phantoms. Owing to the recent implementation of several lung protocols requiring heterogeneity-corrected target doses, the RPC, through credentialing activities, evaluated numerous heterogeneity correction algorithms from various treatment planning systems. The thorax phantom was sent to nearly 200 institutions since 2004. Institutions were requested to image, plan and treat the phantom as if a patient. The institutions submitted both homogeneous and heterogeneity corrected treatment plans, using the same number of monitor units. Initial evaluation of the target doses comparing the ratio of the homogeneous dose to heterogeneity corrected dose revealed a difference of 5–10% between doses calculated by the Clarkson and pencil beam (PB) algorithms and those calculated by the superposition convolution (SC), anisotropic analytical algorithm (AAA), and Monte Carlo (MC) algorithms. This difference was not obvious when considering the ratio of the thermoluminescent dosimeter (TLD) dose to the calculated heterogeneity corrected doses in the centre of the target where the average TLD/target dose ratio was 0.97 ± 0.025 (SD) except for the Accuray MultiPlan Ray Tracing algorithm (ratio of 0.87 ± 0.018). The dose profiles and binary agreement map (±5%/3 mm) comparisons of dose distributions near and in the target showed differences between classes of heterogeneity correction algorithms. The differences were due to the lack of lateral electron scatter in the PB and Clarkson type algorithms. The SC/AAA/MC algorithms accounted for the lateral scatter

and the agreement between measurement and calculation was good. In conclusion, various heterogeneity correction algorithms are more accurate at calculating doses to targets in the lung and these algorithms are being required for clinical trials treating lung tumours.

1. INTRODUCTION

The Radiological Physics Center (RPC) was established in 1968 to assure the National Cancer Institute (NCI) and the cooperative study groups that institutions participating in NCI sponsored cooperative clinical trials deliver prescribed radiation doses that are clinically comparable and consistent. The RPC accomplishes this by assessing each institution's radiation therapy programmes through off-site, remote auditing and on-site dosimetry reviews. Mailable anthropomorphic quality assurance (QA) phantoms, which include pelvic, head and neck, spine and thorax phantoms, are used as an end to end test to verify the accuracy of tumour dose delivery for special treatment techniques, such as intensity modulated radiation therapy and stereotactic body radiation therapy (SBRT). The RPC is the only QA group to use these phantoms to credential institutions to participate in specific advanced technology clinical trials. The QA phantoms verify the complete treatment process, from imaging and treatment planning, to set-up and dose delivery for institutions participating in clinical trials sponsored by the NCI.

QA for conventional therapy techniques and treatment planning dose calculations is described in American Association of Physicists in Medicine Task Group reports 40 and 53 [1, 2]. Unlike with conventional radiation therapy, treatment of the thorax presents additional unique QA problems. Target motion and heterogeneities in the beam path can complicate the delivery of dose to both target and normal tissues. Of particular concern is the accuracy of heterogeneity corrected dose calculations from various treatment-planning computers in clinical use today in tissues of low density such as the lung. Whether the algorithm is pencil beam (PB) based, superposition convolution (SC), Monte Carlo (MC) or Clarkson scatter corrected, dose calculations for the lungs should be verified in a clinically representative manner prior to clinical implementation and before use in clinical trials where consistency is of utmost importance.

The accuracy of dose calculations using heterogeneity corrections has mostly been evaluated along the central axis and in the penumbral regions based on simple beam geometries using slab phantoms [3, 4]. Other studies have compared the accuracy of treatment planning systems to MC calculations from patient CT data sets [4–6]. However, there are very little data for advanced treatment planning systems designing heterogeneity corrected treatment plans using anthropomorphic phantoms [7–9]. The accuracy of dose calculations using

various heterogeneity correction algorithms delivered to an anthropomorphic phantom has yet to be studied in depth for multiple treatment planning systems, as indicated by the American Association of Physicist in Medicine Task Group Report No. 65 [10].

Owing to the large incidence and associated mortality of lung cancer, the NCI has made the treatment of lung cancer a high priority. As such, more sophisticated clinical trials are being developed requiring image guidance and accurate calculations of the dose distributions so that normal tissues can be avoided while delivering large stereotactic body radiation therapy doses with high dose gradients to the tumour. The 'credentialing' of institutions to participate in these lung trials is conducted by the RPC to ensure that all of the participating institutions deliver consistent radiation doses and in doing so, use heterogeneity correction algorithms that calculate the dose distribution as accurately and consistently as possible.

Verification of an overall treatment procedure should include patient image acquisition, treatment planning and dose delivery. Therefore, to verify the safety and accuracy of a complicated treatment delivery, the simple transfer of the dose distribution to a homogeneous cubic or cylindrical phantom [11] or a hypothetical benchmark case may be inadequate. However, an anthropomorphic phantom QA system that offers humanoid external shape, heterogeneities, targets and critical structures will allow a more complete evaluation of the overall treatment procedure. To this end, the RPC has developed, commissioned and used an anthropomorphic thorax QA phantom, which is similar to the RPC head and neck phantom described previously [12].

The goal of this work was to quantify and show the differences between measured and calculated photon doses delivered to an anthropomorphic thorax phantom, based on clinically relevant radiation therapy heterogeneity corrected treatment plans from several current generation treatment planning systems employing different heterogeneity correction algorithms.

2. MATERIALS AND METHODS

2.1. Anthropomorphic thorax phantom

Since the anthropomorphic thorax QA phantoms are mailed to institutions participating in clinical trials for credentialing purposes, they were designed to be lightweight and durable. The phantom's overall physical dimensions were determined from a sampling of patient cases to simulate an average patient. The phantom, shown in Fig. 1, consists of a PVC shell filled with water that contains a simulated heart made of nylon, a spine made of PBT-polyester, lungs

constructed of compressed cork particles material, and a nylon lung tumour. The shell has an angled anterior surface that simulates the slope of the chest. The thorax phantom has a removable imaging/dosimetry insert within the left lung (seen in Fig. 1). The materials selected for each component were of similar density and CT number to actual tissues. The phantom was built to simulate actual patient anatomy, as shown in the CT images in Fig. 2. The superior side of the phantom provides access to the insert containing anatomical structures as well as thermoluminescent dosimeters (TLDs) and film dosimeters (Fig. 1). Two acrylic rods, each containing a TLD capsule at the tip, are inserted into hollow acrylic tubes that extend through the centre of the heart and spine to provide point dose measurements within these critical structures. A large acrylic tube in the left lung accepts the imaging/dosimetry insert. This insert locks into an alignment notch located at the end of the tube in a unique orientation to ensure positioning reproducibility. This alignment notch also ensured that the film dosimeters were always located in the coronal and sagittal planes.

The imaging/dosimetry insert is split in half along the axial plane corresponding to the centre of the target to allow access to the film and TLD locations. The target is embedded in the lung substitute material so that a single insert serves as both the imaging insert and dosimetry insert. The two halves slide along two threaded nylon guide rods that maintain proper alignment of the superior and inferior film planes and TLDs. The dosimetry insert accommodates

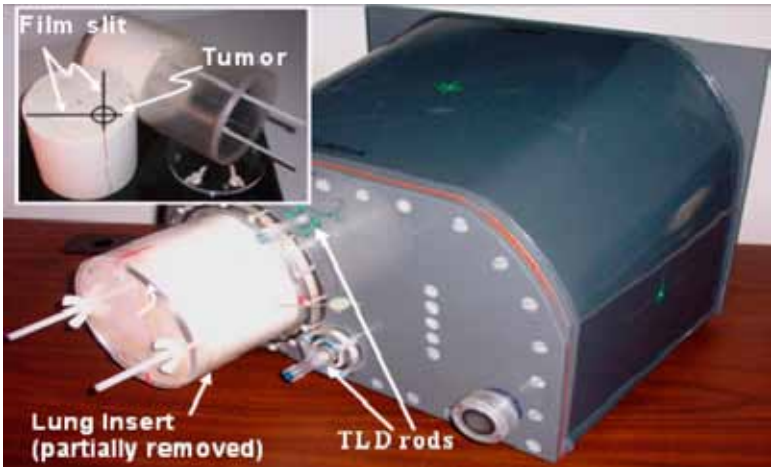

FIG. 1. Thorax anthropomorphic phantom shown in the supine position with superior end exposed. For clarity, the lung insert is shown partially removed. The inset shows the lung insert disassembled with the superior lung section removed showing insert cross section with tumour and film slits.

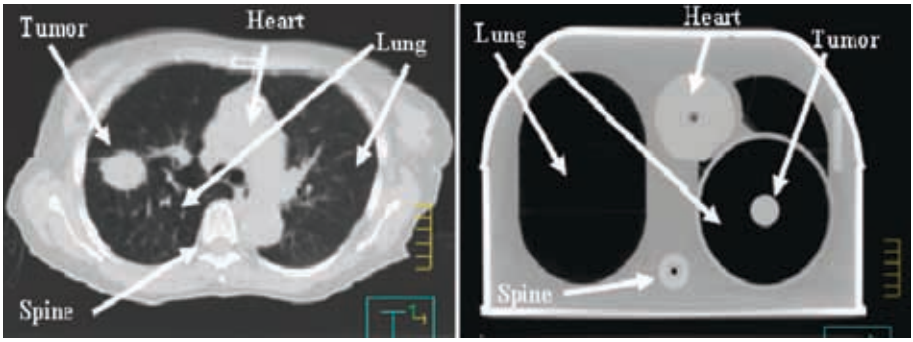

FIG. 2. Tranverse axial CT scan of the thorax phantom (right) and patient (left). Phantom anatomy compares well with patient anatomy.

TLD capsules in the superior and inferior halves of the target and radiochromic film in the axial, sagittal and coronal planes. Each insert contains registration guide holes that are drilled through the outer acrylic sleeve and lung material to provide registration pinholesn the axial, sagittal and coronal films [12].

2.2. Dosimeters

The selection of dosimeters for use within the phantom was based on compatibility with the TLD and radiochromic film dosimetry systems used at the RPC [13–18]. These two dosimeters have been shown to be suitable for use within the phantoms due to their well characterized dose response, quantifiable fading and a spatial resolution of ±2 mm in high dose gradient regions [17–22]. Radiochromic film is approximately tissue equivalent and insensitive to light, and has no significant angular dependence [16, 23]. A more detailed description of the dosimeters used in the RPC QA phantoms and their analysis has been described by Molineu et al. [19]. The TLDs are used as an absolute dosimeter within the phantom and are located near the centre of the target and in the organs at risk. The film dosimeters are used as relative dosimeters that are normalized at a point to the corresponding TLD dose.

2.3. Phantom irradiation

The thorax phantom was irradiated at over 200 institutions wishing to be credentialed for specific lung clinical trials. Institutions were initially asked to image the phantom as if it were a patient and then to develop a treatment plan assuming it to be a homogeneous phantom, but after approximately 100 irradiations, the homogeneous plan was no longer required. Using the same

number of monitor units as calculated from the homogeneous plan, the institution recalculated the dose distribution using the heterogeneity correction algorithm. The institution was asked to submit both plans for comparison to the measurements. Only photon beams with energies ranging from 4 MV to 10 MV were used. The prescription was to deliver 6 Gy to at least 95% of the PTV with a minimum dose of 5.4 Gy to 99% of the PTV to a homogeneous phantom (not using the heterogeneity correction). The maximum dose to any point 2 cm from the PTV was to be less than or equal to 3.5 Gy. Less than 10% of the total volume of the whole lung could receive a dose greater than 2 Gy. No point in the spinal cord and heart was to receive a dose ≥1.8 Gy and ≥3 Gy, respectively. The phantom irradiation dose was delivered in one fraction.

Various planning systems and heterogeneity correction algorithms were used to plan the thorax treatment. These systems included Philips Pinnacle (Philips Medical Systems, Andover, MA) SC (adaptive convolve and collapsed cone) algorithms, Varian Eclipse (Varian Medical Systems, Palo Alto, CA) PB and anisotropic analytical algorithm (AAA) algorithms, TomoTherapy (TomoTherapy, Inc., Madison, WI) planning station SC, Accuray (Accuray, Sunnyvale, CA) Multiplan Ray Tracing and MC algorithms, Nomos (Best Medical International, Inc., Springfield, VA) Corvus PB, CMS (Computerized Medical Systems, Inc., St. Louis, MO) XiO SC, BrainLab (BrainLab North America, Westchester, IL) PB and Elekta (Elekta, Inc., Norcross, GA) PrecisePlan Clarkson algorithm.

2.4. Comparison of treatment plan calculations and measurements

Point dose calculations from the treatment planning systems at the locations of the TLD were compared to the measured TLD doses. The institution was asked to contour the powder within the TLD capsule and determine the mean dose to the powder for comparison. Treatment plan isodose distributions and 3-D dose matrices from each phantom plan were submitted from which profiles and 2-D dose distributions were obtained and compared to the data from the film dosimeters in the sagittal and coronal planes. The 2-D film and dose calculation distributions were compared using a binary agreement map (BAM), discussed by Davidson et al. [24] Briefly, the planes of dose data were aligned using reference points marked on the films and by registering the calculated dose distribution coordinate system to the film coordinate system. The BAM applied a ±5%/3 mm criterion level. Unlike the gamma index comparison, the BAM required that each point of comparison be within the ±5% criterion or that there be a dose point within ±5% within a ±3 mm distance from the point of comparison. Unlike the gamma index method, the BAM does not provide the level of detail of the regions that are near or far from a specified criterion as do gamma maps.

2.5. Results

The thorax phantom was initially sent to any institution requesting the phantom regardless of the heterogeneity correction algorithm used. In addition, several controlled experiments were conducted by the RPC to evaluate the accuracy of specific treatment planning algorithms that would be used for clinical trial patients. From these studies and institution irradiations of the thorax phantom, the data in Table 1 were generated.

Although there have been over 200 irradiations, the number of irradiations in Table 1 is less than 200, because at one point, institutions were no longer asked to submit the homogeneous treatment plan since it was not useful in the comparison of the phantom measured data and the plan calculation.

The initial evaluation of the target doses comparing the ratio of the homogeneous dose to heterogeneity corrected dose revealed a difference between

TABLE 1. COMPARISON OF THE RATIO OF HETEROGENEITY CORRECTED DOSE TO THE HOMOGENEOUS CALCULATED DOSE AT THE CENTRE OF THE PTV FOR VARIOUS HETEROGENEITY CORRECTION ALGORITHMS[a]

TPS	Heterogeneity correction algorithm	No. of irradiations	Ctr. of target (avg.) D_{hetero}/D_{homo}	Ctr. of target (avg.) D_{TLD}/D_{hetero}
Pinnacle	Adap. conv./CC conv	24	1.14	0.98
Hi-Art	SC	9	1.15	0.99
XiO	SC	10	1.13	0.97
Accuray Multiplan	MC	6	1.10	0.98
Eclipse	AAA	14	1.14	0.96
Eclipse	PB	21	1.18	0.95
XiO	Clarkson	3	—	0.93
Brain Lab	PB	5	1.20	0.96
PrecisePlan	Clarkson	2	1.19	0.99
Accuray Multiplan	PB	6	—	0.87

[a] The TLD to heterogeneity calculated dose ratio to the centre of the PTV is also shown.

several of the planning system algorithms. There was a 5–10% difference between the Clarkson/PB algorithms calculated corrected heterogeneity doses compared to the SC/AAA/MC corrected heterogeneity doses. The average value of the centre of target ratio D_{hetero}/D_{homo} for the five algorithms in the black box and the remaining PB/Clarkson algorithms was 1.14 and 1.19, respectively. The values in the black box come from the more accurate heterogeneity correction algorithms. This difference was not obvious when considering the ratio of the TLD dose to the calculated heterogeneity corrected doses in the centre of the target where the average TLD/target dose ratio was 0.97 ± 0.025 (SD), with the exception of the Accuray MultiPlan algorithm (0.87 ± 0.018) and the XiO Clarkson algorithm (0.93 ± 0.009). The significant deficiency in the Accuray Multiplan PB heterogeneity calculation resulted in the company implementing its MC algorithm which calculates dose in a low density region accurately. The XiO Clarkson algorithm used a Batho correction and is known to overestimate doses in the low density lung region. Several of the algorithms selected for initial analysis were chosen based on an RTOG lung heterogeneity correction survey containing responses from 114 participating institutions of the heterogeneity correction algorithms used most often by clinical trial participants. The three heterogeneity correction photon algorithms most often utilized clinically in clinical trials were the SC [25, 26], PB [27] and the Clarkson with a heterogeneity correction.

However, when observing the dose profiles and binary agreement maps (BAMs) (±5%/3 mm) of the dose distributions going through and around the target, there were clear differences between classes of heterogeneity correction algorithms, as seen in Fig. 3. The dose profile distributions representative of the Pinnacle SC data, MultiPlan MC, XiO Clarkson, BrainLab PB and Eclipse PB are compared in Fig. 3. The comparison of the measured phantom dose profiles with the TPS calculated profiles are in excellent agreement for the SC and MC heterogeneity correction algorithms. However, the agreement between the Clarkson and PB heterogeneity correction algorithms were not in good agreement. As noted in Table 1, the doses agree fairly well at the centre of the PTV, but at the edges of the profiles, the measured profiles differ from the calculated profiles using the Clarkson and PB algorithms at the edges of the PTV. The reason for this observed difference at the edges of the PTV was due to the lack of accounting for lateral electron transport in the PB and Clarkson type algorithms. The SC/AAA/MC algorithms all accounted for this lateral scatter, and as such, the agreement between measurement and calculation was excellent. The incorporation of the lack of lateral scatter component to the heterogeneity correction algorithm plays a significant role in accurately calculating the dose in low density materials.

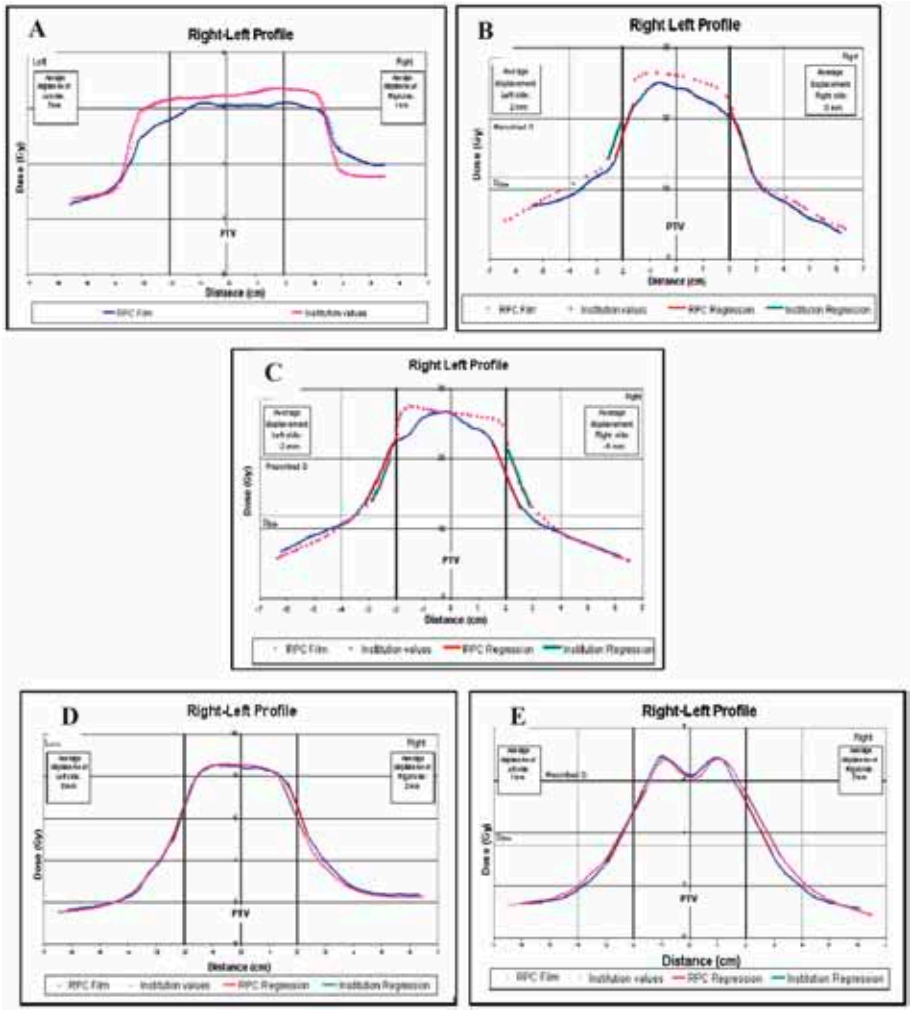

FIG. 3. Comparison of dose profiles between measurements and the heterogeneity corrected dose calculations for XiO Clarkson (A), Eclipse PB (B), BrainLab PB (C), Philips Pinnacle SC (D) and MultiPlan MC (E) algorithms.

A BAM analysis using criteria of ±5%/3 mm was performed on a subset of the irradiations for each TPS heterogeneity correction algorithm used to plan the treatments. An example of the BAM plots can be seen in Fig. 4 for the Pinnacle SC, Eclipse PB and Eclipse AAA algorithms. As mentioned above, the SC and AAA algorithm calculations show excellent agreement with the measurements from the thorax phantom, but the PB dose calculations do not agree as well, particularly in the region of the PTV edges. Areas shown in grey fell outside of

FIG. 4. BAM plots for Pinnacle SC (A), Eclipse PB (B) and Eclipse AAA (C) heterogeneity corrected dose calculations compared to measured dose distributions in a thorax phantom using a ±5%/3 mm criteria.

the ±5%/3 mm criteria and areas in black fell outside of a ±7%/7 mm criteria. The gamma analysis of the Clarkson heterogeneity correction algorithm (data not shown) was similar to the Eclipse PB results shown in Fig. 4, whereas the other SC and MC algorithms had very similar results to the Pinnacle results shown in Fig. 4.

The percentage of pixels within the films for each phantom irradiation that passed the ±5%/3 mm gamma criteria comparing the dose calculations and measurements were tabulated for the various heterogeneity correction algorithms, as shown in Fig. 5. As noted earlier, the SC, AAA and MC heterogeneity correction algorithms were in better agreement with the measured dose values in the thorax phantom, ranging from 85 to 96% of the pixels passing the criteria. The Clarkson and PB algorithms performed rather poorly with agreement being as poor as 31% of the pixels passing for the MultiPlan Ray Tracing algorithm to 61% for the Corvus PB algorithm. These data suggest that there are two distinct classes of heterogeneity correction algorithms, one that performs very well compared to measurement, and one that performs poorly for dose calculations in the low density regions of the lung.

Based on the authors' analysis of comparisons between various types dose calculation algorithms using TLD and radiochromic film measurements in an anthropomorphic thorax phantom, it is concluded that the SC, AAA, MC algorithms perform more consistently and more accurately than the Clarkson and ray tracing algorithms when applied to treatment planning and dose calculations in the low density regions of the lung.

In regions of low density, it was found that the use of the SC, AAA, and MC algorithms consistently met the ±5%/3 mm gamma criteria while the Clarkson, PB and ray tracing algorithms usually overestimated the dose in the PTV and

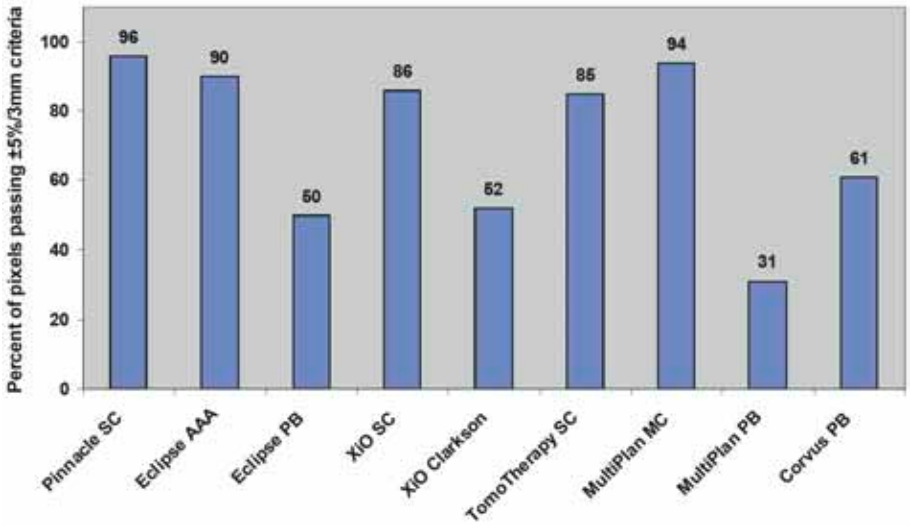

FIG. 5. Histogram of the percentage of pixels passing the ±5%/3 mm BAM criteria for the various heterogeneity correction algorithms in various treatment planning systems.

underestimated the penumbral broadening. This pattern of disagreement reflects the limitation of the one dimensional heterogeneity correction based algorithms. Numerous other studies have agreed with the above observation [10, 28–37] that the Clarkson and PB algorithms perform poorly in the lung as compared to the other algorithms tested. In addition to the work presented by Davidson et al. [21, 24], another study by Schiefer et al. [9] also performed a comprehensive study of heterogeneity correction algorithms in multiple planning system in clinical use today using anthropomorphic phantoms. The work by Schiefer et al. came to the same conclusions as presented in this work. Based on our findings, using the thorax anthropomorphic QA phantom as one of the RPC's quality audit tools, new radiation therapy clinical trials of lung tumours require participating institutions to use either SC, AAA or MC heterogeneity correction algorithms to calculate the target and lung doses. The use of these more accurate algorithms should result in more consistent patient radiation doses resulting in steeper dose response curves increasing the effectiveness of the clinical trial in answering the trial question.

ACKNOWLEDGEMENT

This work was supported by Public Health Service Grants CA 10953 and CA 81647 awarded by the National Cancer Institute, Department of Health and Human Services.

REFERENCES

[1] AMERICAN ASSOCIATION OF PHYSICISTS IN MEDICINE Radiation Therapy Committee Task Group 40, Comprehensive QA for Radiation Oncology: Report of the AAPM Radiation Therapy Committee Task Group 40, Med. Phys. **21** (1994) 581–618.

[2] AMERICAN ASSOCIATION OF PHYSICISTS IN MEDICINE Radiation Therapy Committee Task Group 53, "Quality assurance for clinical radiotherapy treatment planning," Med. Phys. **25** (1998-a) 1773–1829.

[3] WONG, J.W., PURDY, J.A. "On methods of inhomogeneity corrections for photon transport," Med. Phys. **17** (5) (1990) 807–814.

[4] INTERNATIONAL COMMISSION ON RADIATION UNITs and Measurement ICRU, Determination of Absorbed Dose in a Patient Irradiated by Beams of X or Gamma Rays in Radiotherapy Procedures, ICRU Report **24** (1976) 22–23.

[5] SONTAG, M.R., CUNNINGHAM, J.R., Corrections to absorbed dose calculations for tissue inhomogeneities, Med. Phys. **4** (5), 431–436 (1977).

[6] SONTAG, M.R., CUNNINGHAM, J.R., "The equivalent tissue–air ratio method for making absorbed dose calculations in a heterogeneous medium," Radiology. 129 (3) (1978) 787–794.

[7] MACKIE, T.R., SCRIMGER, J.W., BATTISTA, J.J., A convolution method of calculating dose for 15-MV x rays, Med. Phys. **12** (2) (1985) 188–196.

[8] GRAHAM, M.V., et al., Clinical dose-volume histogram analysis for pneumonitis after 3-D treatment for non-small cell lung cancer (NSCLC), Int J Radiat Oncol Biol Phys **45** (2) (1999) 323–329.

[9] SCHIEFER, H., et al., The Swiss IMRT dosimetry intercomparison using a thorax phantom, Med Phys **37** (2010) 4424–4431.

[10] PAPANIKOLAOU, N., et al., "Tissue Inhomogeneity Corrections for Megavoltage Photon Beams," AAPM Task Group #65 Radiation Therapy Committee (2004).

[11] LOW, D.A., MUTIC, S., Abutment region dosimetry for sequential arc IMRT delivery, Phys. Med. Biol. 42 (1997) 1465–1470.

[12] FOLLOWILL, D.S., et al., Design, Development, and Implementation of the Radiological Physics Center's Pelvis and Thorax Anthropomorphic Quality Assurance Phantoms, Med. Phys. **34** (2007) 2070–6.

[13] KIRBY, T.H., et al., Mailable TLD system for photon and electron therapy beams, Int. J. Radiation Oncology Biol. Phys. **12** (1986) 261–265.

[14] KIRBY, T.H., et al., Uncertainty analysis of absorbed dose calculations for thermoluminescence dosimeters, Med. Phys. 19 (1992) 1427–1433.

[15] AGUIRRE, J.F., et al., Thermoluminescence Dosimetry as a tool for remote verification of output for radiotherapy beams: 25 years of experience, Standards and Codes of Practice in Medical Radiation Dosimetry 2 (2002) 191–9.
[16] NIROOMAND–RAD, A., et al., American Association of Physicists in Medicine Radiation Therapy Committee Task Group 55, Radiochromic film dosimetry: Recommendations of AAPM Radiation Therapy Committee Task Group 55, Med. Phys 25 (1998) 2093–2115.
[17] RADFORD, D.A., FOLLOWILL, D.S., HANSON, W.F., "Design of an anthropomorphic intensity modulated radiation therapy quality assurance phantom", (Proceedings of the 2000 World Congress on Medical Physics and Biomedical Engineering, MO-CXH-1, IEEE, July 2000) (2000).
[18] CHERRY, C.P., FOLLOWILL, D.S., HANSON, W.F., "Design of a heterogeneous thoraxphantom for remote verification of three-dimensional conformal radiotherapy", (Proceedings of the 2000 World Congress on Medical Physics and Biomedical Engineering) (2000).
[19] MOLINEU, A., et al., Design and Implementation of an Anthropomorphic Quality Assurance Phantom for Intensity-Modulated Radiation Therapy for the Radiation Therapy Oncology Group, Int. J Radiat. Oncol. Biol. Phys 63 (2005) 577–583.
[20] FISHER, G., et al., The accuracy of 3-D inhomogeneity photon algorithms in commercial treatment planning systems using a heterogeneous lung phantom, Med. Phys. 30 (2003) 1507.
[21] DAVIDSON, S., et al., The Evaluation of Several Commercial IMRT Treatment Planning Systems Heterogeneity Dose Calculation Algorithms Using An Anthropomorphic Thorax Phantom, Med. Phys. **32** (2005) 1988.
[22] ALVAREZ, P., et al., Evaluation of Doses Delivered by SBRT to the Lung of An Anthropomorphic Thorax Phantom, Medical Physics **32** (2005) 2043.
[23] MEIGOONI, A.S., et al., Dosimetric Characteristics of an Improved Radiochromic film. Medical Physics **23** (1996) 1883–1888.
[24] DAVIDSON, S.E., et al., Accuracy of two heterogeneity dose calculation algorithms for IMRT in treatment plans designed using an anthropomorphic thorax phantom, Med. Phys. 34 (5) (2007) 1850–1857.
[25] MACKIE T.R., SCRIMGER, J.W., BATTISTA, J.J., A convolution method of calculating dose for 15-MV x rays, Med. Phys. **12** (1985b) 188–196.
[26] AHNESJÖ, A., Collapsed cone convolution of radiant energy for photon dose calculation in heterogeneous media, Med. Phys. **16** (1989) 577–92.
[27] MOHAN, R., CHUI, C.S., LIDOFSKY, L., Differential pencil beam dose computation model for photons, Med. Phys. **13** (1983) 64–73.
[28] JERAJ, R., KEALL, P.J., SIEBERS, J.V., "The effect of dose calculation accuracy on inverse treatment planning," Phys Med Biol **47** (3) 391–407 (2002).
[29] JONES, A.O., DAS, I.J., "Comparison of inhomogeneity correction algorithms in small photon fields," Med Phys **32** (3) (2005) 766–776.
[30] KNOOS, T., et al., Comparison of dose calculation algorithms for treatment planning in external photon beam therapy for clinical situations, Phys Med Biol **51** (22) (2006) 5785–5807.

[31] MA, C.M., et al., Monte Carlo verification of IMRT dose distributions from a commercial treatment planning optimization system, Phys Med Biol **45** (9) (2000) 2483–2495.

[32] McDERMOTT, P.N., HE, T., DEYOUNG, A., Dose calculation accuracy of lung planning with a commercial IMRT treatment planning system, J Appl Clin Med Phys **4** (4) (2003) 341—351.

[33] METCALFE, P.E., WONG, T.P., HOBAN, P.W., Radiotherapy X-ray beam inhomogeneity corrections: the problem of lateral electronic disequilibrium in lung, Australas Phys Eng Sci Med. **16** (4) (1993) 155–167.

[34] PAWLICKI, T., MA, C.M., "Monte Carlo simulation for MLC-based intensity-modulated radiotherapy," Med Dosim **26** (2) (2001) 157–168.

[35] VANDERSTRAETEN, B., et al., Accuracy of patient dose calculation for lung IMRT: A comparison of Monte Carlo, convolution/superposition, and pencil beam computations, Medical Physics **33** (9) (2006) 3149–3158.

[36] CARRASCO, P., et al., Comparison of dose calculation algorithms in phantoms with lung equivalent heterogeneities under conditions of lateral electronic disequilibrium, Med Phys **31** (10) (2004) 2899–2911.

[37] STERPIN, E., et al., Monte Carlo evaluation of the AAA treatment planning algorithm in a heterogeneous, http://online.medphys.org/resource/1/mphya6/v34/i5/p1665_s1?isAuthorized=no.

LITHIUM FORMATE FILM DOSIMETERS FOR SKIN DOSIMETRY

S. LELIE*,**, B. SCHAEKEN*,**,***, T. LENNERTZ*,
B. BOGDANOV+, M. DUCHATEAU++, E. BRESSERS+++,
S. SCHREURS*, W. SCHROEYERS*, D. VERELLEN**,++

* Nuclear Technological Centre,
XIOS Hogeschool Limburg, Diepenbeek
Email: steven.lelie@xios.be

** Vrije Universiteit Brussel, Jette

*** Department of Radiotherapy, ZNA Middelheim, Antwerp

+ Orfit Industries, Wijnegem

++ Oncologisch Centrum, UZ Brussel, Jette

+++ Limburgs Oncologische Centrum, Jessa Hospital, Hasselt

Belgium

Abstract

In radiotherapy, accurate skin dose determination is a very important aspect to help reduce early and late skin effects. Planning system skin dose determinations are in general less reliable due to difficulties in beam modelling of the buildup zone in combination with accurate patient contour definition on CT images. Lithium formate monohydrate (LiFo) is already under investigation as an electron magnetic resonance dosimeter for radiotherapy. We present a feasibility study on the use of a LiFo film dosimeter for skin dose determination during radiotherapy. Pure LiFo was mixed with a low melting point polymer and shaped into rectangular, flat dosimeters. Irradiated films are read out using a Bruker EMR^{micro} spectrometer. The dosimetric properties of the dosimeters were studied and preliminary clinical experiments were performed. The dosimeters showed great potential to be used as skin dosimeter for clinical irradiations.

1. INTRODUCTION

The absence of charged particle equilibrium, the lack of accurate knowledge of the percentage depth dose curve in the first few millimetres of tissue, electron contamination and the partial volume effect are challenges to the current clinically used treatment planning systems (TPS). Skin dose, however, is an important factor during radiation therapy, especially when superficial tumours are being treated. High doses might lead to early and late skin effects (e.g. telangiectasia and erythema [1, 2]), and low doses might compomise tumour control. At the time of writing, skin dose measurements were impractical and time consuming. Film dosimeters are possible candidates for replacing the more classic measurement techniques.

Electron magnetic resonance (EMR) film dosimeters can be produced using different radiosensitive materials. L-a-alanine is the most common EMR dosimeter used today and alanine dosimetry is already used in clinical dosimetry, as stated by Schaeken et al. [3] and Anton [4]. Alanine has the disadvantage that relative high doses (4 Gy) are necessary to reduce the measurement uncertainty to an acceptable level for radiotherapy. Common radiotherapy treatments consist of approximately 2 Gy fractions, increasing the measurement uncertainty.

Lithium formate monohydrate (LiFo) dosimeters are new in the EMR dosimetry domain. LiFo has a theoretical sensitivity that is up to a factor of 7 higher than alanine [5]. This can result in even smaller dosimeters than alanine, but can also decrease the dose necessary for reliable dose measurements in radiotherapy. LiFo has already been used for clinical dose determinations by Waldeland [6] and Gustafsson [7]. This work presents a feasibility study using LiFo as a dosimetric material in films to measure skin dose.

2. MATERIALS AND METHODS

2.1. LiFo dosimeters

LiFo was obtained from Sigma-Aldrich N.B./S.A. and was melted with a low melting point polymer binder (ε-polycaprolactone). The mixtures (35 wt% LiFo and 65 wt% binder) were extruded using a twin-screw extruder and pressed to shape rectangular sheets of desired thickness (0.5 mm and 1 mm) by Orfit Industries NV (Wijnegem, Belgium). The sheets were cut into rectangular strips to fit into the spectrometer's resonant cavity quartz tubes (20 mm × 4 mm). Here, it is assumed that the LiFo is homogeneously distributed within the cut out dosimeter and the effective point of measurement was assumed to be half the thickness of the dosimeter. The average mass of the dosimeter batch was

103.64 mg with a relative standard deviation of 7.23%. In total, more than 100 LiFo film dosimeters were irradiated for calibration and clinical situations. The calculated effective atomic number [8] is 6.66, compared to 7.23 for pure LiFo and 7.42 for soft tissue.

2.2. Irradiations

Dosimeters were irradiated with different irradiation units at different radiotherapy departments.

The set of LiFo dosimeters for calibration and monitoring fading was irradiated at ZNA Middelheim, Antwerp, Belgium, with an Elektra SLi-3 linac. The photon beam energy used was 6 MV with a source–surface distance of 100 cm and a field size of 10 cm × 10 cm. The dosimeters were positioned at d_{max} = 1.5 cm, between solid water plates, and were centred at the beam axis. Irradiated LiFo-films were stored in a room with controlled humidity (below 50%) at room temperature and shielded from direct sunlight.

Some of the film dosimeters were placed on the skin during the complete course of clinical breast irradiations. The irradiations were performed at three different radiotherapy departments using different irradiation techniques (see Section 2.8).

2.3. EMR measurement

The LiFo film dosimeters were read out using an X-band spectrometer (Bruker EMX^{micro}) equipped with a high sensitivity resonant cavity (Bruker ER4119HS). To correct for fluctuations in spectrometer sensitivity, the dosimeters were read out simultaneously with a reference nuclide (Bruker ER4119HS-2100). The spectrometer settings for LiFo-films were optimized for alanine [2]: centre magnetic field = 350 mT; sweep width = 30 mT; microwave power = 0.252 mW; field modulation = 0.5 mT; modulation frequency = 100 kHz; conversion time = 40.96 ms, and a sweep time = 83.89 s. To correct for rotational dependencies, each dosimeter's reading was expressed as the average for two orientations: parallel (0°) and perpendicular (90°) to the magnetic field.

2.4. Dose calculation

The dose was calculated using the intensity of the LiFo absorption in the EMR spectrum (Fig. 2) (A), corrected for mass (A_m) and for fluctuations in

spectrometer sensitivity using the reference substance (A_m^{ref}, Eq. 1). Absorbed dose to water is calculated using a linear fit into the dose–response curve:

$$\overline{A_m^{ref}} = \frac{1}{n}\sum_{i=1}^{n}\left(\frac{1}{m}\frac{A_i}{A_{reference,i}}\right) \text{ with } n = 2, \text{ number of rotations} \quad (1)$$

2.5. Rotational dependency

Film dosimeters are rectangular shaped, and consequently, rotational dependency of the dosimeter signal was expected. Rotational dependency was checked by acquiring absorption spectra after subsequent rotation of the dosimeter over 360° in steps of 45 ± 2°. The dosimeter was positioned without dedicated holder. This allowed the dosimeter to tilt slightly in the quartz tube.

2.6. Signal fading

Signal fading might occur and can depend on environmental conditions such as humidity, temperature and UV exposure. The evolution of the signal intensity in time was monitored with a dosimeter irradiated to 15 Gy in a 6 MV photon beam.

The influence of UV was investigated by exposing the film to UV light with a QUV accelerated Weathering Tester (Q-lab Corporation, Ohio, USA). Previous tests with the Weathering Tester indicated that 200 hours in the QUV corresponds to one year of direct sunlight in Europe. The light intensity is 0.59 W/m^2 and the UV spectrum contained wavelengths in the range of 365 nm down to 295 nm.

Irradiated LiFo films were also exposed to higher temperatures (37°C) to investigate the influence of temperature on fading behaviour.

2.7. Signal optimization

The signal strength obtained from the spectrum depends on the microwave power and magnetic field in the cavity. A higher microwave power and magnetic field increases the signal amplitude, but one should be aware of signal saturation at high microwave powers. In this experiment, a high dose (40 Gy) film dosimeter was read out simultaneously with the reference substance. Both microwave power and modulation amplitude of the spectrometer were altered to determine an optimized spectrometer setting for the LiFo film dosimeters.

2.8. Clinical irradiation

Integral skin doses were measured in vivo during the entire treatment for two different radiation techniques: (case 1) irradiation of brain metastasis with two lateral opposed large fields (30 Gy in 12 fractions); (case 2) breast conserving radiotherapy with forward intensity modulated radiation therapy tangential fields (target dose of 50 Gy in 25 fractions). In addition, LiFo film dosimeters were irradiated with the tomotherapy treatment modalities at UZ Brussel, Jette, Belgium. A treatment plan was created based on contours drawn on a cylindrical solid water phantom (TomoPhant, Gammex Inc., Middleton, USA) using MIMvista (MIMvista Corp., Cleveland, USA). Two contours were drawn (Fig. 8), one representing the breast and the other a lung as an organ at risk (OAR).

In the irradiation plan, a 5 cm wide field with a pitch of 0.280 and a planning modulation factor of 2 was used. A dose calculation grid of 0.390 cm × 0.390 cm was used. A dose of 20 Gy was prescribed to the target volume (breast) and the OAR was completely blocked resulting in a tangential radiation of the target volume. The dose was delivered in ten fractions, and the dosimeters were in place during the complete treatment.

The LiFo film dosimeters were fixed on the phantom using tape, and a MVCT scan of the phantom with the dosimeters attached was acquired prior to treatment to ensure correct positioning of the phantom. For dose estimations in the treatment plan, the MVCT scan was registered with the planning CT, and the LiFo dosimeters were contoured on the MVCT image set. To derive dose statistic at the location of the LiFo film volume, a recalculation of the dose volume histogram was performed using MIMvista.

To check the dose measurements with LiFo films, the irradiation was repeated using TLD-700 dosimeters. These were irradiated with one fraction and positioned at the centre location of the LiFo film dosimeter plane.

3. RESULTS

3.1. Calibration

A dose response curve was obtained by irradiating four dosimeters per dose point (Fig. 1). The dosimeters were irradiated to doses in the range of 5–50 Gy with an uncertainty of 1% (NCS18) [9]. The graph shows a linear relationship between the mass corrected amplitude and absorbed dose. At a dose of 10 Gy, the measurement uncertainty is of the order of 3.6%.

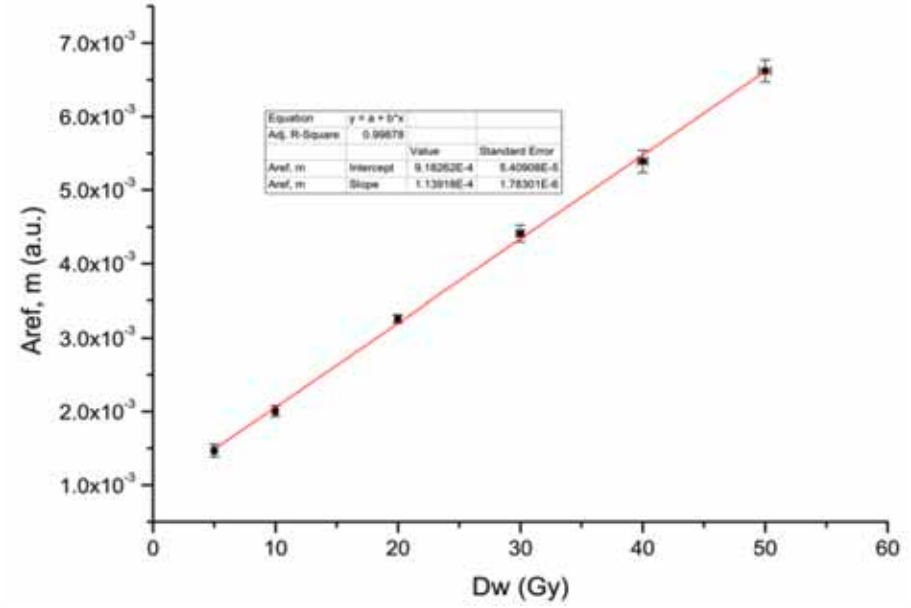

FIG. 1. Calibration curve. A linear regression was performed between dose and EMR response. The measurements are corrected for mass and fluctuations in spectrometer sensitivity.

The LiFo film spectrum (Fig. 2) shows a background signal. In this study, no background manipulation was performed. Background correction is still a topic under investigation.

3.2. Rotational dependency

The rotational dependency was checked using dosimeters irradiated to 20 Gy. The dosimeter aligned with the magnetic field was defined as 0°. The results for angular dependency are shown in Fig. 3, and the signal intensity shows a maximum when the dosimeter is orientated perpendicularly to the magnetic field. The standard deviation of the mean value is 3.2%, but differences between maximum and minimum can reach up to 8.5%. This deviation is not acceptable, and care should be taken of the orientation of the dosimeters in the cavity.

The shape of the dosimeter can easily explain the significant rotational dependency. Standard EMR dosimeters are cylindrical in shape, having a homogeneous mass distribution in the cavity. This film has a rectangular shape and will cut through the magnetic field lines differently at each orientation in the cavity.

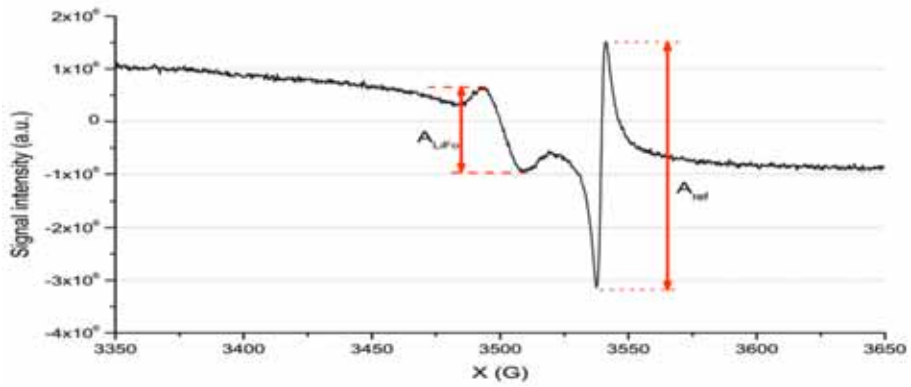

FIG. 2. LiFo film spectrum for 20 Gy. The left peak represents the LiFo absorption peak (A_{LiFo}); the right peak is the reference signal (A_{Ref}).

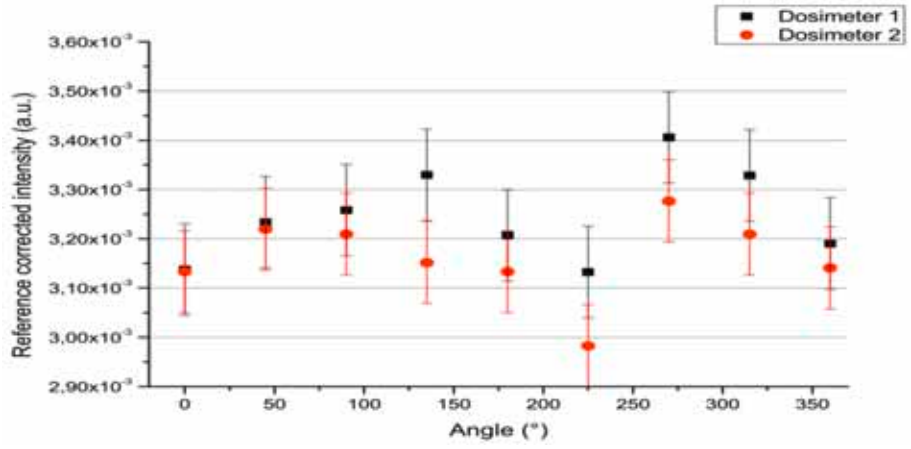

FIG. 3. Rotational dependency of the LiFo film dosimeters. The orientation where the film is aligned with the magnetic field is defined as 0°. 90° corresponds to a perpendicular orientation relative to the magnetic field. The squares and circles represent two different dosimeters.

3.3. Spectrometer settings

The spectrometer settings were optimized by adjusting the microwave power and modulation amplitude of the spectrometer. In Fig. 4, the signal intensity is plotted as a function of the magnetic field strength and microwave power for both the LiFo film signal intensity (A) and reference signal (B). Both the LiFo and reference signals show an increase in amplitude when a higher microwave power and magnetic field are applied. The reference amplitude shows

a decrease in amplitude when maximum power is applied. This effect is not observed for the LiFo amplitude. The optimized parameters for LiFo film dosimeters are shown in Table 1 and compared with the L-a-alanine parameters as used in the lab.

3.4. Fading

Time dependency of the signal over a large period of time was studied using four dosimeters irradiated to 15 Gy, as shown in Fig. 5. The reference and mass corrected amplitudes were recorded during 21 weeks in regular time intervals. No fading was observed in the first few weeks after irradiation, in accordance with Vestad [5]. After 15 weeks, a significant drop in the signal was observed (10%); after 21 weeks, the signal fading increased to approximately 20%.

The influence of UV light was checked using four dosimeters irradiated to 50 Gy and was measured before and after exposure to UV light. After 30 min of exposure, no fading of the signal was found for the dosimeters. After 150 min of exposure, a fading of 5% (SD = 1.4%) was observed. During the UV exposure,

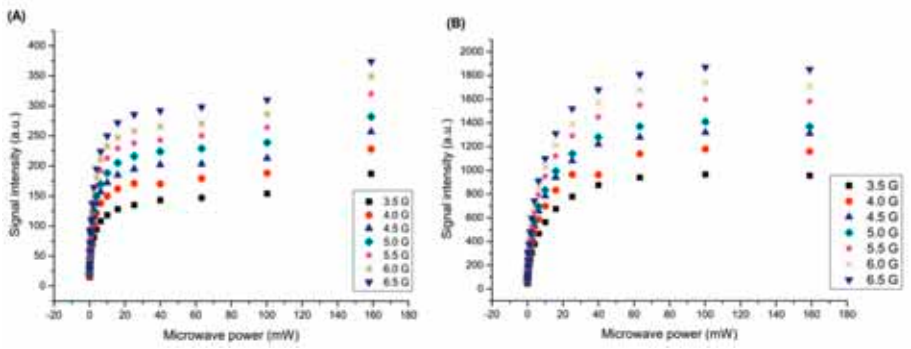

FIG. 4. Optimization of the parameters. (A) shows the intensity of the LiFo signal, (B) shows the intensity for the reference substance.

TABLE 1. EMR SPECTROMETER PARAMETER SETTINGS[a]

Parameter	L-a-alanine	LiFo-film
Modulation amplitude (mT)	0.5	0.6
Microwave Power (mW)	0.252	1

[a] The L-a-alanine system of the Nuclear Technological Centre is compared to the preferred parameters for lifo film dosimetry.

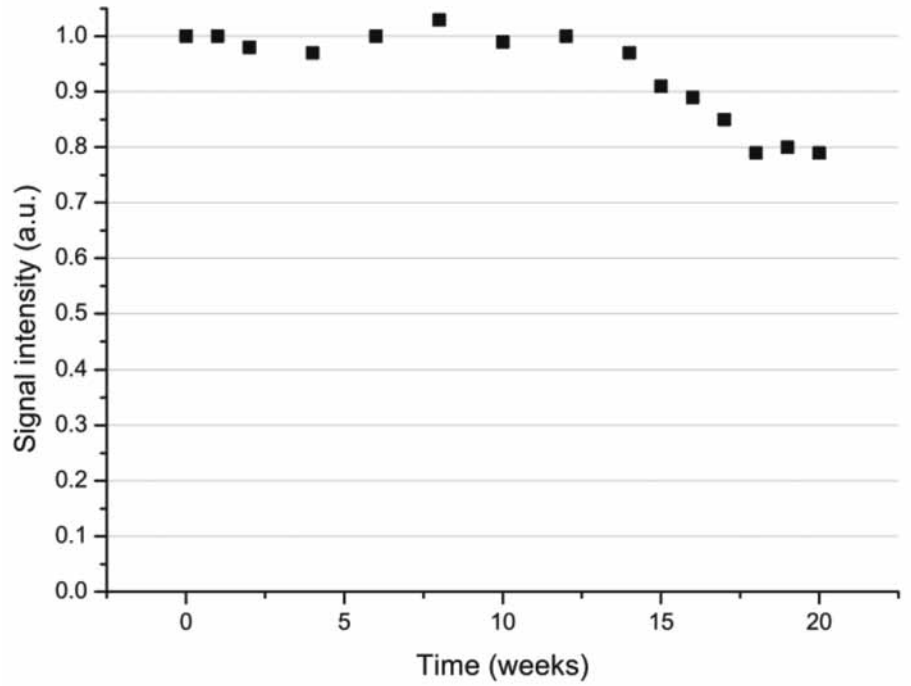

FIG. 5. EMR signal of dosimeter as a function of time. Dosimeters were stored at room temperature with relative humidity below 50%.

the temperature of the dosimeter increased to 37°C and the fading effect could be induced by both UV-light exposure and temperature. However, additional experiments with heating the dosimeters to a controlled temperature of 37 ± 1°C revealed no signal fading.

3.5. Clinical measurement

Clinical irradiations were performed using different irradiation techniques. For each dose point, two dosimeters were placed at positions likely to have high doses during treatment. Owing to the limited sensitivity of the current film dosimeters, the integral dose was measured to increase the absorbed dose to a level with acceptable uncertainty. The estimated doses were calculated with the TPS by the local medical physicists. The results are summarized in Table 2, which show an overestimation of the dose calculated with the TPS.

Case 1 involved the cranial irradiation of the whole brain is shown in Fig. 6. Four dosimeters, placed in pairs, were incorporated in the head fixation mask. The dose was delivered with two opposed 6 MV photon beams of field size

TABLE 2. RESULTS OF CLINICAL IRRADIATIONS FOR TWO TANGENTIAL BEAMS[a]

Position	D_{skin} (Gy)	SD (%)	Estimated dose TPS with 4 mm slice (Gy)
Above nipple	18.9	7.98	24.5
Right breast fold	17.2	4.95	19.3
Under nipple	17.8	7.00	21.4
Left breast fold	17.8	9.63	20.6

[a] Skin doses are consistently lower than dose calculations performed by the TPS.

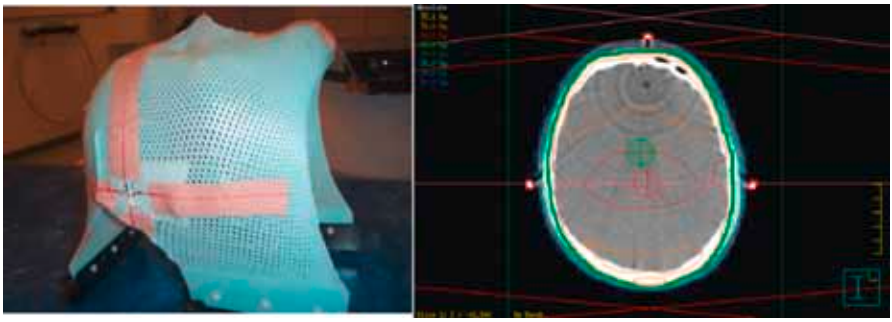

FIG. 6. Set-up for a cranial irradiation. Left: the head fixation mask with the LiFo film dosimeters in the centre of the red cross. Right: the TPS calculated isodose lines. The red circled dots at the side of the head indicate the dosimeter position.

16 cm × 21 cm. The treatment consisted of 12 fractions of 2.5 Gy at the centre of the brain. At each side, two LiFo film dosimeters were positioned at the central axis of the beam. Skin doses for the left and right side of the head were measured to be 6.4 Gy. The TPS isodose lines show doses between 10 Gy and 20 Gy, overestimating the actual skin dose.

Case 2, a breast tumour, was irradiated with two tangential 6 MV beams. The relative weight of the beam was divided equally for both beam angles. The medial and lateral gantry angles were 308° and 118°, respectively, with source–surface distances of 95.48 cm and 83.96 cm, respectively. The treatment was delivered in 25 fractions of 2 Gy. The skin dose was compared at four locations with treatment planning calculations. The dosimeters packages were made as illustrated in Fig. 7. This allowed extrapolation of the measurement data to calculate the dose at a depth of 70 μm in the skin [10].

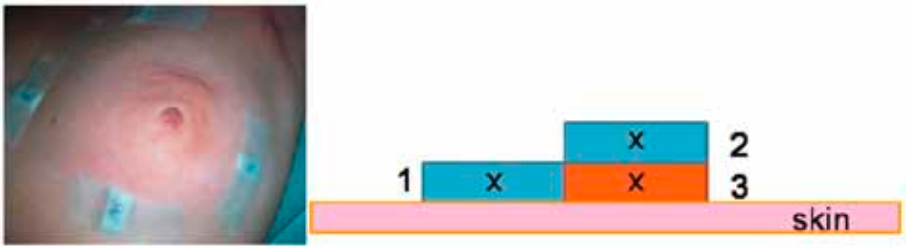

FIG. 7. Tangential breast irradiation. Left: the positioning of the dosimeters at the breast. Right: set-up dosimeters in the packages. The stacking of the two dosimeters allows estimation of the skin dose by extrapolation.

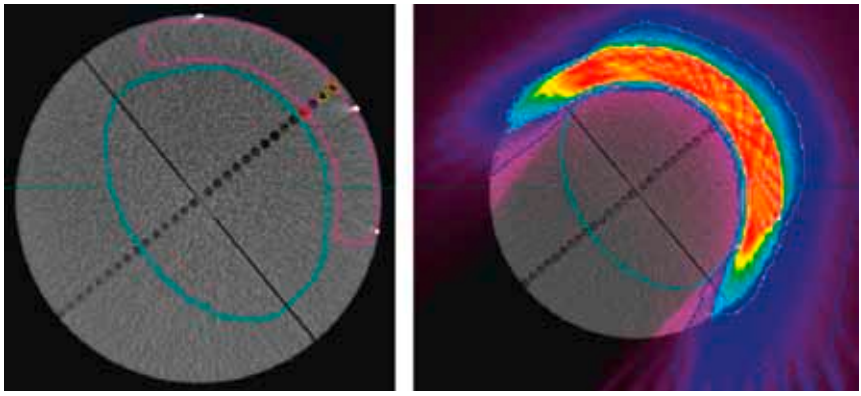

FIG. 8. Irradiation plan TomoPhant. A dose of 20 Gy was given to the target volume. The blue lines show the border of the OAR, which had a prescribed dose of 0 Gy. Consequently, the dose is delivered by tangential irradiation. The dosimeters are stuck to the phantom where the CT image colours white.

Additional irradiations were performed on the tomotherapy treatment modalities with a cylindrical solid water phantom (see Section 2.8 and Fig. 8) to verify the skin dose at a more uniform tumour volume and without day to day removal of the dosimeter at the skin. The dosimeters were read out nine days after irradiation in order to avoid fading corrections. The dosimeters were read out in the presence of the reference substance, and doses were calculated with Eq. 1 in combination with the calibration curve of Fig. 1.

Preliminary results (Table 3) show that the skin dose measured with the LiFo films are lower than the doses calculated with the Tomotherapy ® TPS, which is in accordance with the findings for the tangential breast irradiations.

TABLE 3. RESULTS OF THE TOMOTHERAPY SKIN DOSE MEASUREMENT[a]

	TPS (Gy)	LiFo-film (Gy)	TLD-700 (Gy)
LiFo 1	14.12 ± 1.45	4.40 ± 0.37	6.2 ± 0.83
LiFo 2	15.34 ± 1.01	3.90 ± 0.46	8.4 ± 1.2
LiFo 3	13.93 ± 1.42	2.91 ± 0.26	6.2 ± 0.85

[a] The TPS dose estimation is compared with both lifo-films and tld dosimeters. both dosimeters show a substantial lower skin dose than the TPS.

The same measurement was repeated using TLD-700 dosimeters. LiFo films 1 and 3 were replaced with three TLD dosimeters, while LiFo film 2 was replaced by 4 TLDs. The results show lower doses for the TLD measurement, but higher than LiFo measurements. The difference in results between the LiFo and TLD measurements could not be explained at the time of writing and is subject for further investigation.

4. DISCUSSION AND CONCLUSION

Dosimetric behaviour of LiFo films was studied for use in patient dosimetry. Preliminary results show that the dosimeters could be used, but the low LiFo concentration in the film implies that relative high radiation doses should be administered to ensure clinically accepted uncertainties. Fractionated doses of 2 Gy are too low, but this could be overcome by measuring integral doses.

Homogeneity of the LiFo films was not specifically studied, but visual inspection revealed a gradient in the optical transmission of the film. This is a downside of the current production process of the film dosimeters. Homogeneity of the LiFo film could be improved by manufacturing the film as a composite of thin layers, which is a topic for further investigation.

Fading experiments show little fading in the first weeks after irradiation when the dosimeter are stored in ambient conditions with a controlled relative humidity kept below 50%. The sudden drop in sensitivity observed after 15 weeks is unexpected and is subject to further research. Fading of the dosimeter signal is influenced by UV exposure. As a consequence, the films should be stored out of direct light.

The signal intensity was strongly dependent on the orientation of the dosimeter in the spectrometer cavity. This suggests the need for the development of a dedicated (quartz) dosimeter holder allowing accurate and reproducible positioning of the film dosimeter within the cavity.

Skin dose measurements during clinical irradiations show that the measured skin dose is considerably lower than the TPS calculated skin dose, stressing the importance of dose calculations algorithms taking into account the dose variation in the first few millimetres of tissue. In addition, the absence of a smooth transition between skin and air in a CT scan increases the uncertainty on skin dose calculations.

ACKNOWLEDGEMENTS

This work was supported by grants of the institute for the promotion of Innovation through Science and Technology in Flanders (IWT-Vlaanderen). ORFIT is also acknowledged for producing the dosimeter batch.

REFERENCES

[1] LOPER, E., GUERREO, R., NUNEZ, M., DEL MORAL, R., Early and late skin reactions to radiotherapy for breast cancer and their correlation with radiation induced DNA damage in lymphocytes, Breast Cancer Research, Vol. 7 (2005) 690–698.

[2] ENAMI, B., LYMAN, J., BROWN, A., COIA, L., GOITEIN, M., MUNZENRIDER, J.E., SHANK, B., SOLIN, L.J., WESSON, M., Tolerance of normal tissue to therapeutic irradiation, Int. J. Onc. Bil. Phys. **21** (1991) 109–122.

[3] SCHAEKEN, B., LELIE, S., Meijnders, P., Van den Weyngaert, D., Janssens, H., Verllenen, D., "Alanine/EPR dosimetry applied to the verification of a total body irradiation protocol and treatment planning dose calculation using a humanoid phantom", Med. Phys., Accepted [DOI: 101118/1.3496355] (2010).

[4] ANTON, M., Development of a secondary standard for the absorbed dose to water based on the alanine EPR dosimetry system, Appl. Rad. Isot. 62 (2005) 779–795.

[5] VESTAD, T.A., MALINEN, E., LUND, A., HOLE, E.O., SAGSTUEN, E., "EPR dosimetric properties of formates", Appl. Rad. Isot. 59 (2003) 181–188.

[6] WALDELAND, E., HÖRLING, M., HOLE, E.O., SAGSTUEN, E., MALINEN, E., Dosimetry of stereotactic radiosurgery using lithium formate EPR dosimeters, Phys. Med. Biol. 55 (2008) 4667–4682.

[7] GUSTAFSSON, H., LUND, E., OLSSON, S., Lithium formate EPR dosimetry for verifications of planned dose distributions prior to intensity modulated radiation therapy, Phys. Med. Biol. 53 (2008) 4667–4682.

[8] MURTY, R.C., Effective atomic numbers of heterogeneous materials, Nature 207 (1965) 298–399.

[9] EMAMI, B., LYMAN, J., BROWN, A., COIA, L., GOITEIN, M., MUNZENRIDER, J.E., SHANK, B., SOLIN, L.J., WESSON, M., Tolerance of normal tissue to therapeutic irradiation, Int. J. Rad. Onc. Biol. Phys. 21 (1991) 109-122.

[10] KRON, T., BUTSON, M., HUNT, F., DENHAM, J., TLD extrapolation for skin dose determination in vivo, Radiother. Oncol., Vol. 41 (1996) 119–123.

A DOSIMETRIC PROTOCOL FOR THE USE OF RADIOCHROMIC FILM IN RADIOTHERAPY QUALITY ASSURANCE IN NORWAY

A. MAURING
Norwegian Radiation Protection Authority,
Østerås, Norway
Email: alexander.mauring@nrpa.no

Abstract

In 2008, a project was initialized at the Norwegian Radiation Protection Authority in order to relate the established dosimetric methods using ionization chamber measurements in a water phantom to 2-D dosimetry with radiochromic film. The measurement set-ups were designed to be simple and reproducible, while shedding light on different areas of interest. In particular, the project looked at a standard reference field, abutted fields, collimator rotation and overtravel field techniques. Measurements were carried out at all ten radiotherapy hospitals in Norway. Results from the ionization chamber and film measurements indicate that all hospitals have good control of their standard reference field, both with regard to relative and absolute dosimetry. Set-ups with abutted fields show over- or underdosages of over 30% in border areas due to overlaps or gaps between fields. Errors were magnified further in cases with collimator rotation. Analysis of small overtravel fields show that although the fields are successfully reproduced geometrically, in some cases there are large discrepancies between planned dose and the dose actually given. Radiochromic film shows promise as a useful tool in radiotherapy. The project was finished in May 2009, and published results were disclosed to all participating hospitals.

1. INTRODUCTION

At present, there are ten hospitals in Norway that offer external beam radiotherapy. Since 2001, the number of patients receiving radiation treatment steadily grown over the last few years, and the number of annual treatment field exposures has more than doubled, according to the internet portal, http://kvist.nrpa.no. Continual development and improvements in high energy external beam radiotherapy have required a revision in the dosimetric quality controls at Norwegian hospitals, especially regarding newer modalities such as IMRT. Existing quality assurance (QA) routines are mainly concerned with ionization chamber measurements in a water phantom, and often exclude planar dose distributions and advanced treatment techniques.

In late 2007, a Master's thesis project was defined at the University of Oslo in collaboration with the NRPA. The purpose was to develop a method using radiochromic film for relating the absolute standard dosimetry of the secondary standards dosimetry laboratory [1] to 2-D film dosimetry. Experimental set-ups were designed to shed light on different areas where existing QA routines might be inadequate. The project was later expanded under the Norwegian QA in radiotherapy [2] dosimetry working group to include field measurements at all ten radiotherapy hospitals. All results have been made anonymous, but with hospitals having full access to their own results.

Participating hospitals were: Ullevål University Hospital, Haukeland University Hospital, Stavanger University Hospital, St. Olavs Hospital, University Hospital of Northern Norway (Tromsø), Nordland Hospital (Bodø), Ålesund Hospital, Sørlandet Hospital (Kristiansand), Gjøvik Hospital and the Norwegian Radium Hospital.

2. EXPERIMENTAL METHODS AND THEORY

2.1. Use of radiochromic film

2.1.1. GafChromic® EBT film

The GafChromic® EBT (International Specialty Products, Wayne, NJ) type film has several advantageous properties for applications in high energy photon dosimetry. It is near tissue-equivalent in chemical composition, with an effective atomic number close to that of water. It changes colour spontaneously upon exposure to doses between 1 cGy and 8 Gy, with energy independent response for photons. The lateral resolution is high with typical scanning resolution corresponding to about 3 pixels per mm, and scanning can be performed on a regular flat-bed scanner [3, 4].

2.1.2. Film processing

After exposure, the films were stored in a lightproof envelope for 15–24 hours before scanning because of previously reported post-irradiation coloration [5]. Films were then scanned on an Epson Perfection V750 flatbed scanner (Seiki Epson Corp., Nagano, Japan) using a custom-made fitted frame so light scattering conditions would be equivalent for all scans. The software used was Epson Scan, running in professional mode with 72 dpi resolution at 48 bit. Each film was scanned five times in landscape mode, with the last three scans averaged for further analysis as recommended by Paelinck et al. (2007) [6]. All

resulting images were processed using self-written software based on Matlab 7 (Mathworks Inc, Natick, MA). The red channel was extracted and a 5 × 5 pixel Wiener filter was applied to the resulting image to reduce random noise. The pixel values from the film were converted into optical density (OD) values using Eq. 1, which was first suggested by Devic et al. (2003) [4]:

$$OD = \log_{10}\left(\frac{PV_0}{PV}\right) \quad (1)$$

where PV is the pixel value from the exposed film and PV_0 is the corresponding pixel value from an unexposed film from the same batch, scanned in the same area on the scanner. The subtraction of the signal from an unexposed film causes a de facto correction for inhomogeneity in the scanning field. Further investigation of the properties of the film showed no need for any additional scanner flatness correction as reported by Lewis (2007) [7] and Menegotti et al. (2008) [8].

2.1.3. Absolute dose calibration

In order to relate optical density to absolute dose, a calibration of the film's dose–response was carried out using a GammaBeam® X200 ^{60}Co-source (Best Theratronics Ltd, Ottawa, Canada) at the secondary standards dosimetry laboratory. In addition, 3.0 cm × 12.7 cm strips of film were fixed in a water phantom at 5 g/cm^2 depth and 95 cm SSD, and exposed to a range of doses from 0.13–3.50 Gy. All doses were previously determined by ionization chamber dosimetry at identical conditions. Calibration films were scanned using a fitted frame to ensure equivalent light scattering, and dose was plotted against the resulting OD values. It has been shown that the relationship between absolute dose (D) and OD can be approximated by Eq. 2:

$$D(OD) = a \cdot (OD)^n + b \cdot (OD) \quad (2)$$

In Eq. 2, a, b and n are empirically determined constants. The coefficient of determination (R^2) correlation between the fitting functions and experimental measurements was approximately 1 for both film batches used in the project. It was observed during the clinical measurements that conditions may differ between linear accelerators in such a way that even films from the same batch

may differ slightly in response. A post-adjustment correction as shown in Eq. 3 was applied to the calibration curve for each set of measurements:

$$D'(OD) = \frac{D_{isoc,chamber}}{D_{isoc,film}} \cdot D(OD) \quad (3)$$

where $D_{isoc,chamber}$ is the 'true' value of the dose as measured with the ionization chamber set-up. $D_{isoc,film}$ is the empirically determined dose value from the film at identical exposure conditions for the same linear accelerator.

2.1.4. Uncertainty assessment

The factors that contribute to the film's measurement uncertainty can be divided into three main categories; the chemical composition of the film, scanning and absolute dose calibration. Works carried out by Saur and Frengen (2008) [9] and Martisikova et al. (2008) [10] was used as a base for the uncertainty analysis conducted in this project. Assessment of all the proponents of uncertainty showed that the uncertainty is approximately inversely proportional to dose, and that the 2σ dose uncertainty at 2 Gy is approximately 3.5%. A more comprehensive treatment of calculations and full uncertainty budgets relating to this project can be found in a previous report [11].

2.2. Clinical measurements

Clinical measurement set-ups were designed to be as simple as possible in order to be successfully replicated at all hospitals, but they still yield interesting results and shed light on areas with known challenges in high energy photon radiotherapy QA.

2.2.1. Ionization chamber set-up

After the implementation of TRS 398 protocol in the early 2000s at all Norwegian hospitals, absolute dose is realized through ionization chamber measurements in a water phantom [12]. Ionization chamber measurements were carried out using 15 MV photon beams, and 6 MV beams where applicable. A Wellhöfer FC-65G (Scanditronix Wellhöfer, Schwarnbruck, Germany) ionization chamber was positioned in the Bjerke phantom [13] at the hospitals reference conditions. The number of monitor units given to the chamber corresponded to a requested dose of 2 Gy at 10 g/cm^2 depth and 90 cm SSD, using a 10 cm × 10 cm.

2.2.2. Film set-ups

All films were placed into a slit under a water phantom at an equivalent depth of 10 g/cm^2 of water, with a 90 cm SSD 5 cm of solid water plates were placed underneath this set-up for backscatter. Final adjustments were made using the hospital's positioning lasers, backpointer and ruler. Five different film set-ups were used for each of the linear accelerators, and each field was given the same number of monitor units as the ionization chamber set-up (generally 200 MU). A detailed diagram of each film set-up is shown in Fig. 1. Film set-ups were planned using the hospital's treatment planning software in order to compare planned dose distributions with experimentally measured dose distributions from the radiochromic film. Minor adjustments had to be made to the experimental set-ups at certain hospitals due to set limitations and restrictions, but it is assumed that these have no impact on final results.

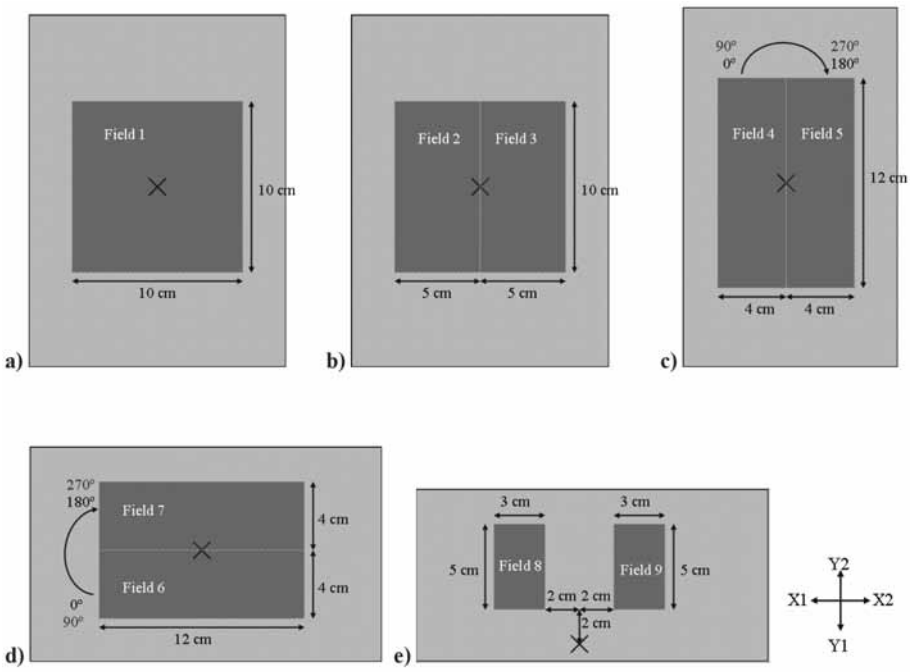

FIG. 1. Beam's eye view of the five different field set-ups used for film measurements. The coordinate scheme is in accordance with IEC 1217 standard, where the gantry is located in the Y2 direction. The location of the isocentre is denoted by '×'. Collimator rotation is denoted for both Siemens/Elekta (black font) and Varian units (grey font). (a) standard reference field set-up, (b) abutted field set-up, (c) abutted fields with collimator rotation 1, (d) abutted fields with collimator rotation 2, and (e) overtravel field set-up.

2.3. Data analysis

Most of the image analysis was carried out using a self-written Matlab based software package named ProcessEBT. This software has built-in algorithms to calculate parameters such as max dose, reference dose, field size, penumbra widths, field flatness and symmetry, as well as display line profiles, isodose lines, 2-D and 3-D representations of the lateral dose distribution. Dose measurements were calculated as the median value over a 3 × 3 pixel ROI defined in the image. Linear accelerator 10 experienced technical errors on the day of the measurements, and results cannot be considered representative.

Planned doses from treatment planning software were compared to film measurements using gamma evaluation methods according to Low et al. (2003) [14] and Depuydt et al. (2003) [15]. IDL based 'VerA' software (created by E. Wasbø, used with permission) was used for these evaluations, with tolerance levels 5 mm distance-to-agreement and 5% dose difference. Areas extending to 1 cm outside the 50% isodose of the fields were evaluated.

3. MEASUREMENT RESULTS AND ANALYSIS

Clinical measurements were performed on a total of 19 linear accelerators at ten hospitals. Each linear accelerator was given a unique identification number in order to make the results anonymous. Nine Varian (linear accelerators Nos 1, 2, 5, 6, 7, 8, 13, 14, 19), six Elekta (Nos 3, 4, 11, 12, 15, 16) and four Siemens (Nos 9, 10, 17, 18) treatment units were included. All hospitals were told which identifier numbers corresponded to their linear accelerators.

3.1. Ionization chamber measurements

Results of the absolute dose measurements on all linear accelerators can be seen in Fig. 2. The error bars correspond to the implicit uncertainty of these measurements, calculated to be 2% at 2σ. Three or more measurements were made to ensure repeatability and assess the standard deviation of the measurement. A number of monitor units corresponding to a requested dose of 2 Gy was given to the ionization chamber. Owing to time constraints, no absolute measurements were carried out on linear accelerator 9. Results have a mean of 2.00 Gy with a standard deviation of 0.02 Gy, and range between 1.98 Gy and 2.03 Gy.

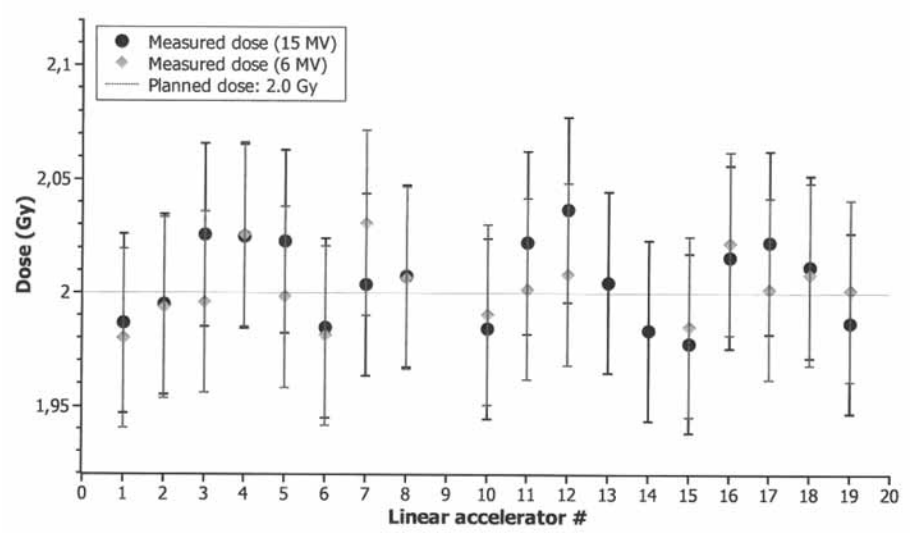

FIG. 2. Measurement results from absolute dose measurements on all linear accelerators, using 15 MV photon beams and 6 MV photon beams where applicable.

3.2. Film measurements

All general procedures concerning the storage, handling, exposure, scanning and processing of the radiochromic film were carried out as described in Sections 2.1 and 2.2.

3.2.1. Reference field set-up

Measurements of field size and penumbra using radiochromic film for the hospital's reference field set-up can be seen in Figs 3 and 4, respectively. Field size measurements have a mean of 10.02 cm with a standard deviation of 0.08 cm which indicates that the hospitals are successful in reproducing their standard field geometrically. Penumbra measurements have a mean of 0.53 cm with a standard deviation of 0.07 cm, a much higher relative standard deviation than for the field size results.

3.2.2. Abutted fields

Measurements were carried out for abutted fields both with and without collimator rotation. Gamma evaluation shows strong disagreement between measurements and treatment planning software in the border regions between two

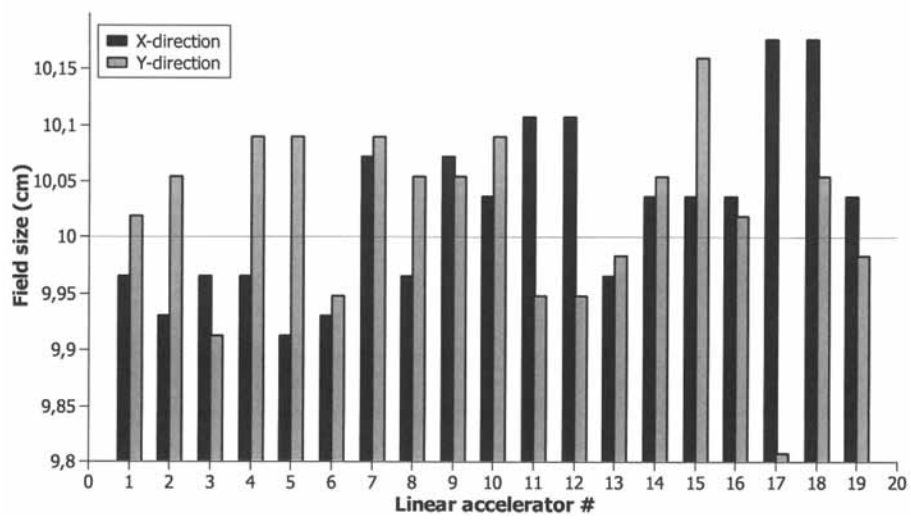

FIG. 3. Field size measurements for standard reference field.

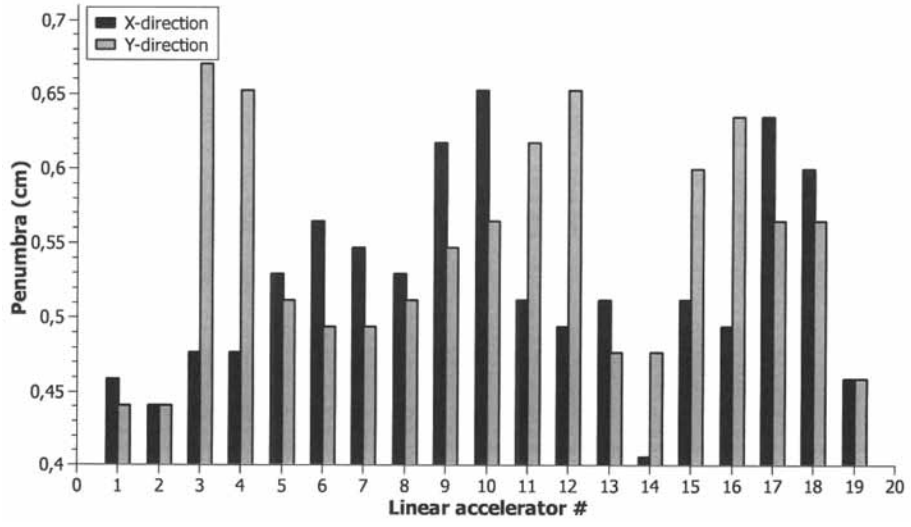

FIG. 4. Penumbra measurements for the standard reference field.

fields in both cases. This is due to overlaps or gaps that occur when the secondary collimator/MLC travels too far or too short when adjusting the field sizes. Sometimes when rotating the collimator the error is doubled as a result. Fig. 5 shows the dose difference between the border area and the flattened area of the

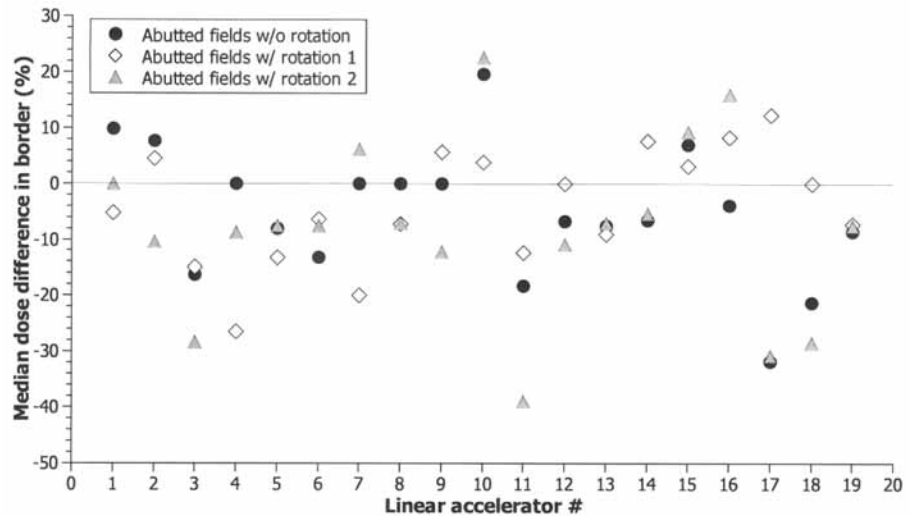

FIG. 5. Relative dose difference in border areas for all field set-ups.

fields. The average dose difference is 11% with a standard deviation of 9%, and the set-ups utilizing collimator rotation exhibit the largest dose difference.

3.2.3. Overtravel fields

For the overtravel set-up, doses to the two fields were calculated using the median value of a 3 × 3 pixel ROI in the centre of each field. The results can be seen in Fig. 6. Fields were also analysed to determine their actual field sizes. An overview of these results is shown in Fig. 7.

Dose measurements have a mean of 1.88 Gy and a standard deviation of 0.04 Gy for field 8, and a mean of 1.92 Gy with a standard deviation of 0.04 Gy for field 9. These values indicate a notable variation in field centre doses between linear accelerators and, in some cases, between the two fields on the same linear accelerator. Gamma evaluation also showed that many treatment planning systems erroneously predicted the doses to these fields (see Fig. 8). However, from the field size measurements, it is evident that the field is successfully reproduced geometrically at all hospitals. Measured field sizes have a mean of 2.98 cm and a standard deviation of 0.10 cm in the x-direction, and mean 5.03 cm with standard deviation 0.08 cm in the y-direction.

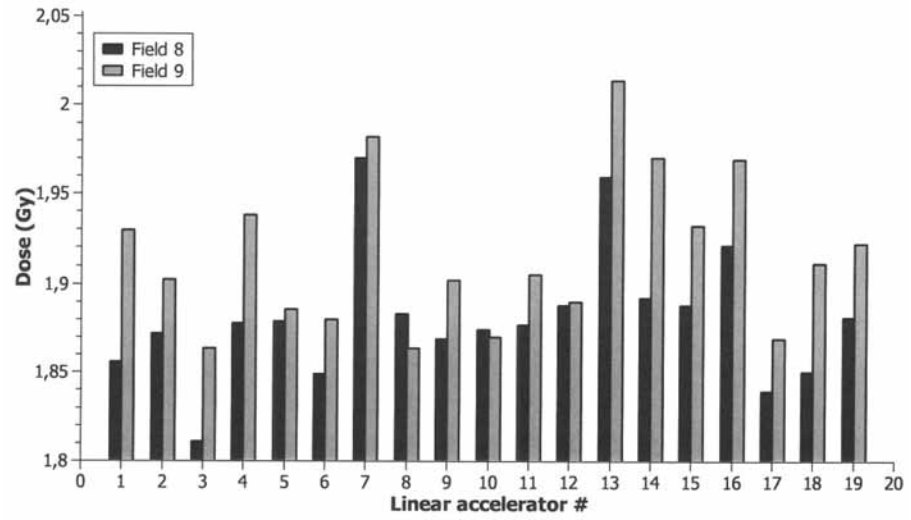

FIG. 6. Field centre dose measurements for the overtravel field set-up.

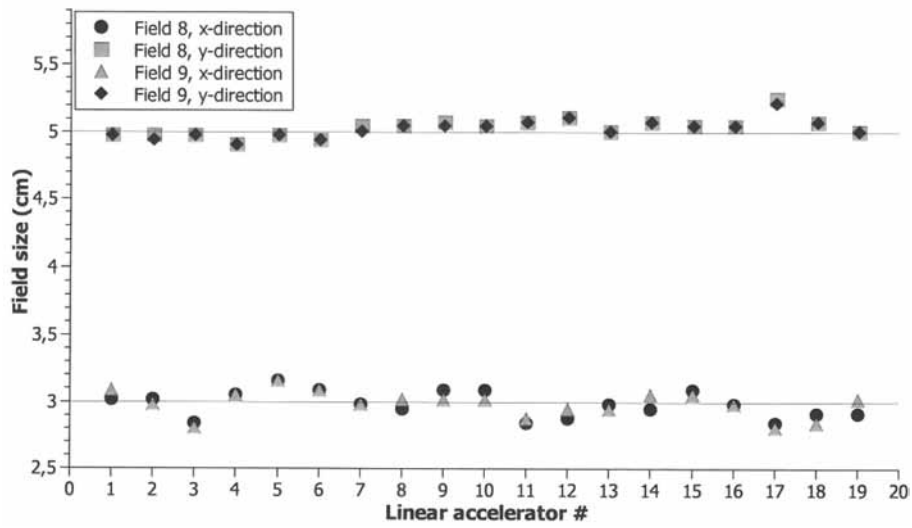

FIG. 7. Field size measurements for the overtravel field set-up.

3.2.4. Gamma evaluation

Film measurements from linear accelerators 1, 2, 5, 6, 7, 8, 13, 14, 15, 16 and 19 were compared to planned dose distributions from treatment planning software using gamma evaluation. The discrete gamma distribution was used to

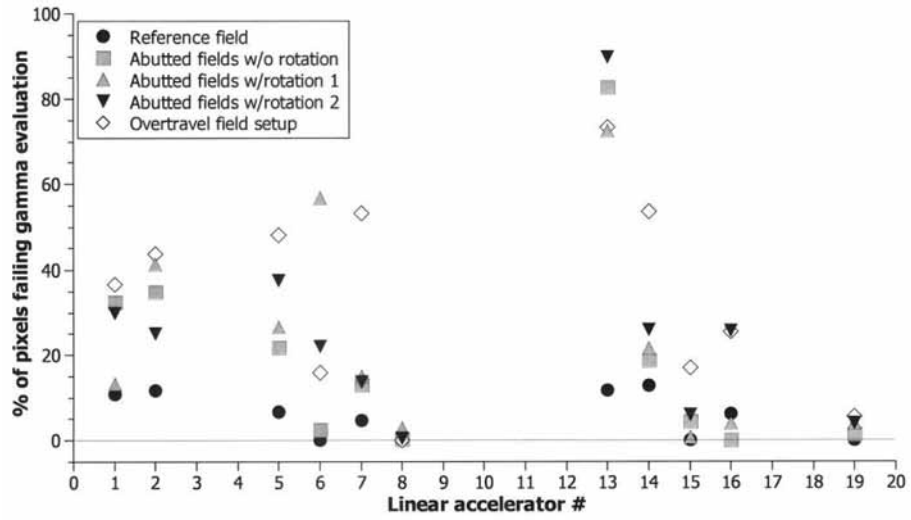

FIG. 8. Results of gamma evaluation on selected treatment units for all field set-ups.

determine the fraction of pixels failing the evaluation, and results can be seen in Figure 8. Twenty-two per cent of pixels fail the gamma evaluation on average for all field set-ups. The overtravel fields have the largest discrepancies (on average, 34% of failing pixels), while the standard reference field has the highest agreement (on average, 6% of failing pixels).

4. CONCLUSIONS

Results from this project are presented 'as is' and it is up to the individual hospitals to decide how to interpret them. In general, they show that all hospitals have good control of their standard reference field, with regard to both absolute and relative dosimetry. Absolute dose measurements show an improvement over the last dosimetric audit conducted in 2002 [16]. Geometric measurements of penumbra and field size are generally also in agreement with planned values. A notable difference in the penumbra in the x- and y-directions on Varian linear accelerators was observed. This discrepancy is not routinely corrected for at some affected hospitals.

Abutted fields are commonly encountered in, for example, head and neck treatments. Border areas between the abutted fields are a challenge because a small error in the collimator position may give relatively high over- or underdosages. Traditional radiotherapy QA using ionization chamber arrays do

not have the resolution to fully uncover this type of error because the affected area can be very small. Overall, discrepancies detected in this project will not contribute significantly to the total dose distribution of a radiation treatment. However, such errors can easily be avoided with the right equipment. Since set-ups with rotated abutted fields are rarely encountered in conventional radiotherapy, their clinical relevance is limited.

Small fields with collimator overtravel are often used as booster fields, and their weighting is usually very low. Results from this project indicate that these fields are successfully reproduced geometrically at all hospitals, but treatment planning software is not always successful in predicting the dose distribution for overtravel fields. It would be worthwhile to compare how different algorithms perform when planning doses to these fields.

GafChromic EBT® film has proven a useful tool in radiotherapy QA, with time efficient analysis of the planar dose distribution. A new generation of film has recently been released [17], which the producer claims offers several improvements over the original film. It is likely that this type of film will become more prominent in clinical QA routines.

ACKNOWLEDGEMENTS

The author wishes to thank all participating hospitals for their cooperation. Gratitude is also extended to H. Bjerke and P.O. Hetland of the Norwegian dosimetry laboratory at the NRPA for their support throughout the project.

REFERENCES

[1] NORWEGIAN RADIATION PROTECTION AUTHORITY, Dosimetrilaboratoriet ved Statens Strålevern, NRPA, Østerås, Norway, SrålevernInfo 4, (2003).

[2] NORWEGIAN RADIATION PROTECTION AUTHORITY, Quality assurance in radiotherapy — 8 years outcome, Østerås, Norway, NRPABulletin 8 (2008).

[3] INTERNATIONAL SPECIALTY PRODUCTS, GafChromic® EBT: Self-developing film for radiotherapy dosimetry, Wayne, NJ (2007), http://online1.ispcorp.com/_layouts/ Gafchromic/content/products/ebt/pdfs/ EBTwhitepaper.pdf.

[4] DEVIC, S., et al., Precise radiochromic film dosimetry using a flatbed document scanner, Med Phys 32 (2005) 2245.

[5] CHEUNG, T., BUTSON, M.J., YU, P.K.N., Postirradiation colouration of Gafchromic EBT radiochromic film, Phys. Med. Biol. 50 (2005) 281.

[6] PAELINCK, L., et al., Precautions and strategies in using a commercial flatbed scanner for radiochromic film dosimetry, Phys. Med. Biol. 52 (2007) 231.
[7] LEWIS, D.F., New developments in scanning radiochromic film, International Specialty Products, Wayne, NJ (2007).
[8] MENEGOTTI, L., DELANA, A., MARTIGNANO, A., Radiochromic film dosimetry with flatbed scanners: a fast and accurate method for dose calibration and uniformity correction with single film exposure, Med. Phys. 35 (2008) 3078.
[9] SAUR, S., FRENGEN, J., GafChromic EBT film dosimetry with flatbed CCD scanner: a novel background correction method and full dose uncertainty analysis, Med Phys 35 (2008) 3094.
[10] MARTISÍKOVÁ, M., ACKERMANN, B., JÄKEL, O., Analysis for uncertainties in GafChromic(R) EBT film dosimetry of photon beams, Phys Med Biol 53 (2008) 7013.
[11] MAURING, A., Radiochromic film for characterization of the radiation field: A protocol for the practical use of GafChromic® EBT for dosimetric purposes in radiotherapy, Østerås, Norway, StrålevernRapport 9, NRPA (2009).
[12] INTERNATIONAL ATOMIC ENERGY AGENCY, Absorbed Dose Determination in External Beam Radiotherapy: An International Code of Practice for Dosimetry Based on Standards of Absorbed Dose to Water, Technical Reports Series No. 398, IAEA, Vienna (2000).
[13] BJERKE, H., HULT, E.A., A water phantom for cross calibration and reference dose determination in high energy photon beams, IAEA-96-34P (2002) 68.
[14] LOW, D.A., et al., A technique for the quantitative evaluation of dose distributions, Med. Phys. 25 (1998) 656.
[15] DEPUYDT, T., VAN ESCH, A., HUYSKENS, D.P., A quantitative evaluation of IMRT dose distributions: refinement and clinical assessment of the gamma evaluation, Radiother Oncol 62 (2002) 309.
[16] BJERKE, H., Dosimetry in Norwegian radiotherapy: Implementation of the absorbed dose to water standard and code of practice in radiotherapy in Norway, Strålevernrapport 11, NRPA, Østerås, Norway (2003).
[17] INTERNATIONAL SPECIALTY PRODUCTS, GafChromic® EBT2: Self-developing film for radiotherapy dosimetry, Wayne, NJ (2009), http://online1.ispcorp.com/_layouts/Gafchromic/content/products/ebt2/pdfs/GAFCHROMICEBT2TechnicalBrief-Rev1.pdf

QUALITY ASSURANCE IN RADIOTHERAPY WITH ANTHROPOMORPHIC PHANTOMS

P. ALVAREZ, A. MOLINEU, D.S. FOLLOWILL, G.S. IBBOTT
MD Anderson Cancer Center,
Radiological Physics Center, University of Texas,
Houston, Texas,
United States of America
Email: palvarez@mdanderson.org

Abstract

Modern conformal treatment planning and delivery, using techniques such as 3-D conformal radiotherapy, intensity modulated radiotherapy and stereotactic body radiotherapy require multiple procedures before the delivery of the prescribed dose. Imaging of the patient, identification of target volumes and organs at risk, calculation of the optimal dose distribution and even quality assurance procedures before the treatment are part of this process. Each step as well as the delivery of the final plan is vulnerable to errors. Anthropomorphic phantoms have been designed to simulate patient anatomy to evaluate treatment planning and delivery. They are mailable, filled with water on site, and contain targets and organs at risk with densities and dimensions similar to human anatomy. Dosimeters are included for the analysis of dose distributions. An analysis of irradiations performed at multiple institutions that failed to meet acceptance criteria is presented. With five distinct designs to perform tests at different body sites and almost ten years of experience, the use of these phantoms allows the identification of errors in the modelling of the beam by the treatment planning system, inaccuracies in dose calculation methods when heterogeneities are taken into account and positioning errors. These phantoms are powerful tools for quality assurance and verification of the treatment delivered to a patient from CT table to treatment couch.

1. INTRODUCTION

The Radiological Physics Center (RPC) participates in the ‘credentialing’ of institutions wishing to participate in certain National Cancer Institute sponsored clinical trials. When advanced technologies are involved, the institution must demonstrate its ability to successfully irradiate an anthropomorphic phantom to be able to enter patients into these clinical trials. Phantoms were built by the RPC to simulate actual patient anatomy, including lesions to be treated, and mimic the head and neck (H&N), prostate, liver, spine or lung, and allow verification of 3-D conformal radiotherapy (3-D CRT), stereotactic body radiotherapy and intensity modulated radiotherapy (IMRT)

plans. A reciprocating table, which is able to reproduce different breathing cycles, is also included when a technique to account for target motion is required for the 'credentialing' process. In the case of the thorax phantom, which is used for verification of treatments in the lung or the spine, fiducial markers were included to allow the use of image guided radiotherapy techniques. Instructions sent with the phantom specify the prescribed dose to the target, limits of dose to organs at risk (OAR), delivery technique to be used, energies accepted, and requirements for the design of the plan. All parameters of the treatment plan are defined to be consistent with the clinical trial under evaluation. The phantom is sent to institutions requesting to be 'credentialed' for the trial. The institutions are instructed to treat the phantom as if it were a patient: they have to image the phantom, develop a treatment plan following written guidelines, perform the quality assurance procedures normally used in the clinic and deliver the plan to the phantom. The analysis of each irradiation is done at the RPC. A comparison is performed between measurements from the RPC dosimetry systems located within the phantom and data from the treatment planning system (TPS) sent by the institution. The Advanced Technology Consortium, of which the RPC is a member, and the Radiation Therapy Oncology Group (RTOG) agreed upon criteria for the acceptance of phantom results. The criteria were based on the result of irradiations of each phantom performed at an initial group of institutions. There are two aspects of this evaluation process. Being able to meet the criteria is an indication of the capability of the institution to accomplish the technical and knowledge requirements to enter patient in a specific clinical trial with the primary goal to reduce the deviation rate for the data submitted for this study. Not being able to meet the criteria may indicate problems with planning or delivery. In either case, the process is an opportunity to educate the institution regarding use of the technology being tested. This paper presents an analysis of the errors found through irradiation of the anthropomorphic phantom as part of the RPC's 'credentialing' programmes.

2. METHODS AND MATERIALS

The phantoms have an anthropomorphic outer plastic shell, are lightweight and water-fillable for mailing purposes and contain imageable targets as well as OAR. Densities and dimensions provide realistic conditions for dose constraints used during the planning and delivery process. Thermoluminescent dosimeters (TLDs) and radiochromic films are used for the analysis of dose distribution [1, 2]. The analysis of the irradiation is a two step process. TLD-100 powder placed in capsules is used as absolute dosimeter. The capsules are cylinders of 1.5 cm height and 0.4 cm diameter with 0.1 cm wall thickness. The capsules are

located near the centre of the target as well as within the OAR. The locations of the capsules are identified based on a coordinate system whose centre agrees with the centre of the target. This coordinate system is also used to localize the edges of the target and OAR inside the phantom. The TLD capsules in the target area are expected to receive a dose with uniform distribution over their volume. The dose is calculated from the TLD signal following the method developed by the RPC for the remote monitoring programme [3]. The TLD dose and the dose calculated by the TPS at the same point inside the target must agree within ±7% (the exception is the lung and spine phantoms with a ±5% criterion). Radiochromic film is placed in orthogonal planes through the centre of the target. Marks are included on each film to establish geometrical references based on the coordinate system described above. Films are scanned using a charge-couple device densitometer (CCD100 Microdensitometer, Photoelectron Corporation) with a light emitting diode based diffused light source operated at 636 nm. The optical density from the scanner is converted to dose through a dose response curve defined for each batch of film [4]. The dose to the film is normalized to the dose to the TLD located in the target area. These films allow the evaluation of the dose distribution over the target area and into the surrounding OAR. The RPC uses the Computational Environment for Radiotherapy Research (CERR, Washington University, St. Louis, MO) for film analysis. Registration of the film, conversion from optical density to dose, and normalization to TLD dose are done with this software. Institutions are asked to submit an electronic version of the plan designed for the phantom to the Image-Guided Therapy Center, another member of the Advanced Technology Consortium. RTOG or DICOM format are required. The software allows the registration of the CT data set based on the coordinate system defined in the phantom. A comparison can be made of the dose distribution between the film and TPS data. A set of profiles is taken through three different axes from the films as well as from the TPS data. Profiles are compared in the high dose gradient regions. The agreement must be ≤4 mm. (This value is 5 mm for the lung phantom.) A 2-D analysis of the dose distribution is performed over areas defined around the target. The gamma index method is used to evaluate the agreement between the film dosimetry and the TPS data. This method is used to evaluate irradiations of the thorax phantom for both lung and spine tumours. In Table 1, the number of phantoms available as well as the year when each was introduced is presented.

The H&N and the pelvis phantoms were designed for IMRT plans only. Figure 1 shows images of these phantoms and CT slices over the axial plane.

TABLE 1. NUMBER OF EACH MODEL OF PHANTOM AVAILABLE AND YEAR IN WHICH USE STARTED

Phantom	H&N	Pelvis	Liver	Lung	Spine
#	31	10	2	10	3
Year	2001	2004	2005	2004	2008

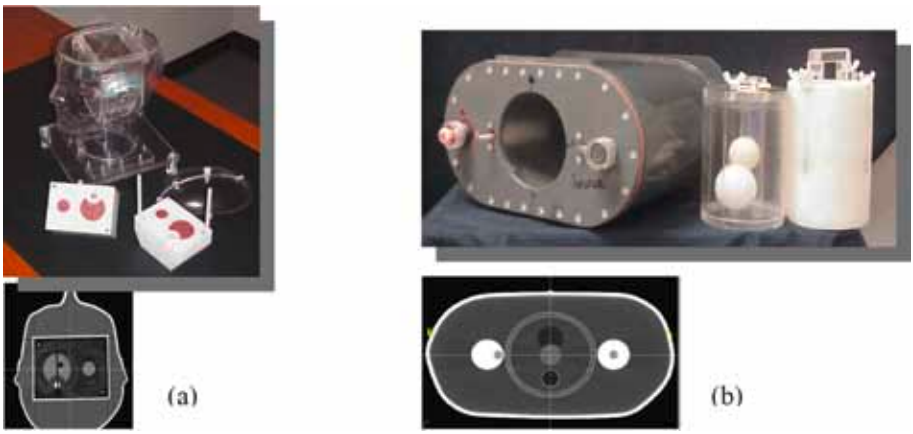

FIG. 1. Picture and CT slices of H&N (a) and prostate (b) phantoms.

The thorax phantom ws developed for use with a clinical trial of stereotactic body radiotherapy treatment of the lung. The phantom is used for IMRT and 3-D CRT plans and also for deliveries where tracking, gating or breath hold techniques are used to account for motion of the target. The liver phantom is a unique design. This phantom was developed for a specific protocol known as RTOG 0438 [5]. The design includes two targets of different size and location. A reciprocating table is used during the phantom test. Four different breathing cycles are available. The first is a free breathing cycle with a total motion of 2 cm within the longitudinal and sagittal planes. Two types of breath-hold cycle are available. These consist of a regular free breathing cycle with a pause for 20 seconds to simulate breath hold at expiration or inspiration. Finally, an option defined as ‘abdominal compression’ allows the phantom to move in the longitudinal and sagittal plane a total of only 0.5 cm. The spine phantom was developed most recently. The phantom was designed specifically for RTOG 0631 [6]. The complexity of this test derives from the dimensions of the target and OARs, their relative locations and the highly conformal dose distribution

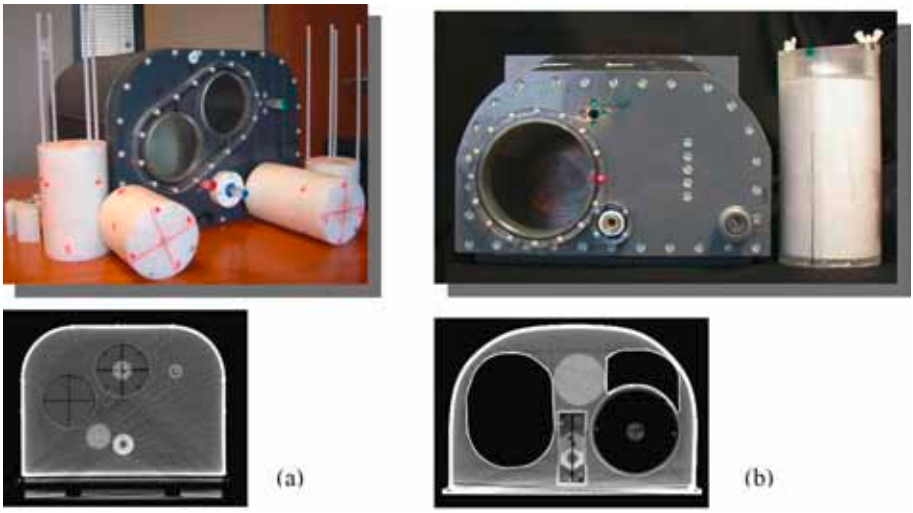

FIG. 2. Images and CT slices of liver (a) and lung (b) phantoms.

required to meet the constraints of the clinical trial [7]. Figure 2 shows images of the liver as well as the lung phantom used for lung as well as spine cases.

3. RESULTS

Since 2001, when the programme started with the H&N phantom, more than 1200 cases have been analysed. The complexity of the delivery process has increased considerably since then. Institutions are now encouraged to use advanced imaging techniques to better identify the target and total motion as well as to assure correct positioning of the phantom on the treatment couch. New delivery techniques are also currently available. The initial testing of the phantom programme was performed with doses delivered from conventional linear accelerators. Now delivery systems such as Tomotherapy, CyberKnife and volumetric modulated arc therapy are available and acceptable for use on clinical trials. When heterogeneities are taken into account, new versions of TPS software are available with significant changes to the algorithm for dose calculation. The failure rate with the RPC phantoms is an indication of the ability of the institutions to manage the requirements of advanced technology clinical trials as well as to handle the new technology in the clinic. The number of irradiations that failed to meet the criteria and the total number of irradiations performed is shown on Table 2.

TABLE 2. RESULTS FROM IRRADIATION OF PHANTOMS *(percentage of failures is given in parentheses)*

Phantom	Non-acceptable irrad./irrad. analysed	Inst. failed on first attempt /total inst.
H&N	175/805 (22%)	133/582 (23%)
Prostate	33/188 (18%)	31/166 (19%)
Liver	11/23 (48%)	8/16 (50%)
Spine	10/29 (34%)	10/26 (38%)
Lung	58/216 (27%)	43/153 (28%)

In 2008, the failure rate reported for the H&N phantom was 30% [8]. However, the failure rate has decreased each year since the programme started, especially for the H&N and pelvis phantoms. A significant number of errors were discovered to have contributed to the failing irradiations of these phantoms. These include incorrect data entered into the TPS during the commissioning process; errors in couch indexing for intensity modulated arc therapy delivery leading to 15% hot spots in the longitudinal plane; and positioning errors of up to 3.0 cm due to misinterpreting set-up instructions provided by the TPS. A number of systematic errors resulted from inappropriate beam modelling of the penumbra below rounded multileaf collimator leaves [9]. This error led to dose discrepancies of up to 12%. A 20% dose discrepancy resulted from a software error that filled the expansion region from the GTV to the PTV with material of zero density. The failure rate remains at about 30% for the lung and spine phantom irradiations. Most of the failures in the irradiation of the lung phantom resulted from the use of inadequate heterogeneity correction algorithms. The pencil beam algorithm and the Clarkson algorithm overestimate the dose in the PTV and underestimate penumbra broadening resulting from the presence of low density regions. The convolution superposition algorithm and the analytical anisotropic algorithm take into account lateral scatter and electron transport and are better able to perform accurate dose calculations [10, 11]. Based on these results, the Clarkson and pencil beam calculation algorithms are not allowed tobe used on lung clinical trials. Preliminary results with the Monte Carlo dose calculation algorithm show very good agreement between the dose delivered to the phantom and the dose calculated by the TPS. Another reason for the failure with this phantom was the use of incorrect conversions from CT number to electron density. Incorrect calibration of the CT unit used for lung patients at an institution was responsible for an 8–10% dose difference in at least three cases.

Many plans were designed with beams going through the treatment couch. The results of dose comparisons improved when the treatment couch was included in the TPS calculation. So far, the use of a reciprocating table to simulate respiratory motion with the lung phantom has not led to an increase in the number of failures, as was expected. The failure rate for the spine phantom is under analysis. Initial results were presented at AAPM 2010 [12] and reflect the complexity of the case. The failure rate of 50% for the irradiation of the liver phantom was related to the fact that two targets with motion are treated at the same time. Unfortunately, the low accrual of the trial did not allow the authors to send the phantom to a sufficient number of institutions to yield good statistics in the results.

4. CONCLUSIONS

The phantoms provide a comprehensive evaluation of new external beam treatment technologies currently used in radiotherapy. The existence of a quality assurance programme that audits the entire treatment process is very important. The analysis of these phantom results allows the RPC to detect and resolve important planning and delivery problems. Feedback to the institutions contributes to their education regarding use of the advanced technology being evaluated. 'Credentialing' with phantoms helps to improve the quality of the data used by the clinical trial groups by resolving any errors discovered. This audit programme benefits not only trial patients, but also all the patients treated under similar conditions at the participant institutions.

ACKNOWLEDGEMENT

This work was supported by PHS CA010953 and CA081647 awarded by the National Cancer Institute, DHHS.

REFERENCES

[1] FOLLOWILL, D., et al., "Design, development and implementation of the Radiological Physics Center's pelvis and thorax anthropomorphic quality assurance phantoms", Med. Phys, Vol. 34 (6) (2007) 2070–2076.

[2] MOLINEU, A., et al, Design and implementation of an anthropomorphic quality assurance phantom for intensity-modulated radiation therapy for the Radiation Therapy Oncology Group, International Journal of Radiation Oncology Biology Physics, Vol. 63, Issue 2, (2005) 577–583.

[3] KIRBY, T., et al., Mailable TLD system for photon and electron dose calculation for thermoluminescence dosimeters, International Journal of Radiation Oncology Biology Physics, Vol. 12, (1986) 261–265.
[4] ALVAREZ, P., et al., Characterization of EBT versus MD-55 Gafchromic films for relative dosimetry measurements, Med. Phys Vol. 33 (2006) 2217.
[5] KATZ, A., A phase i trial of highly conformal radiation therapy for patients with liver metastasis, http://www.rtog.org/members/protocols/0438/0438.pdf
[6] RYU, S., Phase ii/iii study of image-guide radiosurgery/sbrt for localized spine metastasis, http://www.rtog.org/members/protocols/0631/0631.pdf
[7] CARUTHERS, D., et al., Commissioning and anthropomorphic spine and lung phantom for remote quality assurance of spinal radiosurgery, Med. Phys. Vol. 37 (6) (2010) 3314.
[8] IBBOTT, G., et al., Challenges in credentialing institutions and participants in advance technology multi-institutional clinical trials, International Journal of Radiation Oncology Biology Physics, Vol. 71, Issue 1 (2008) S71–S75.
[9] CADMAN, P., et al., Dosimetric considerations for the validation of sequential IMRT process with a commercial treatment planning system, Phys Med. Biol., Vol. 47 (2002) 3001–3010.
[10] DAVIDSON, S., et al., Heterogeneity dose calculation accuracy in IMRT: Study of five commercial treatment planning systems using an anthropomorphic thorax phantom, Med. Phys. Vol. **35**(12) (2008) 5434–5439.
[11] ALVAREZ, P., et al., A comparison of heterogeneity correction algorithms, Med. Phys. Vol. **35** (6) (2008) 2888.
[12] MOLINEU, A., et al., Initial results from multiple irradiations of an anthropomorphic spine phantom, Med. Phys., Vol. **37** (6) (2010) 3400.

DEVELOPMENT OF IN-HOUSE PROCESS QA IN MODERN RADIATION THERAPY

L.J. SCHREINER*,**, T. OLDING*, J. DARKO*,**

* Department of Physics,
Queen's University

** Medical Physics Department,
Cancer Centre of Southeastern Ontario
Email: John.Schreiner@krcc.on.ca

Kingston, Ontario,
Canada

Abstract

Modern radiation therapy is a complex process, with conformal and intensity modulated radiation therapy (IMRT) becoming the standard of care. Typically, these therapies are used via image guided radiation therapy to ensure localization for precise treatment. These advances have also initiated moves to adaptive approaches (IGART) in which patient treatment is modified at various points taking advantage of information acquired during the treatment course. Current physics quality assurance (QA) typically validates individual steps (e.g., through machine QA) or operates in well controlled but somewhat artificial environments (e.g. IMRT fluence pattern measurements by physics staff to test dose delivery for individual patients). Such QA does not validate the treatment process as actually implemented in the clinic. In this paper, a schema is described for IGART process control in which a test phantom is handed over to appropriate clinic staff (medical radiation therapy technicians and dosimetrists) to be treated as if it were a patient. The test object is evaluated by physics staff at the end of the QA run. An example of the implementation is given. The aim is to develop a system under which compliance to a clinic's IGART policies and procedures can be regularly monitored and validated, in a setting reflecting how they are applied to patients.

1. INTRODUCTION

Radiation therapy has improved recently through the development of three dimensional (3-D) conformal radiation therapy techniques such as achieved by intensity modulated radiation therapy (IMRT). These techniques have become standard practice, and experience indicates that patients benefit from their use [1]. The dose distributions resulting from 3-D conformal therapy are designed to fit

tightly about the specific target volumes. Therefore, the possibility of missing the target increases, because of patient set-up errors, organ motion, or even machine malfunctions during treatment delivery. A major body of research in medical physics and radiation oncology in the past decade has been to minimize such misses through the use of image guidance to verify treatment set-up [2].

With the use of image guided radiation therapy (IGRT) throughout a patient's treatment, the potential has been observed for a significant change of the tumour region and surroundings during the time course of the multiple fractions of radiotherapy [3]. The resulting change in anatomy, which may be seen over the weeks of treatment, suggests the development of off-line approaches in which the treatment plan is re-designed (daily or weekly) to accommodate volume changes. This would maintain target coverage and healthy normal tissue sparing. Image guided adaptive radiation therapy (IGART) [4] may incorporate the daily use of kVCT or MVCT images to monitor anatomy changes and potentially for replanning purposes (where a CT simulator may not be required). In very simple terms, IGART describes a class of radiation therapy approaches in which a patient's treatment is modified during the course of care based on new information gained during the treatment (see Fig. 1). More sophisticated approaches for inter-fraction IGART [5] are not limited to corrections for tissue geometry. The potential for on-line dosimetry (perhaps via exit beam dosimetry with electronic portal imaging devices, EPIDs or tomotherapy CT detectors) during each treatment increases the feasibility of dose delivery monitoring with subsequent correction as fractions continue through the treatment course [6, 7]. This approach implies that each fraction may require the delivery of slightly different doses via modified MLC sequencing. The planning required to correct and change the subsequent dose delivery itself requires validation to ensure that the dose is delivered correctly through all of the interventions. In all of this, the IGART process involves data transfer between sophisticated advanced equipment, often with human evaluation to assess and choose between different courses of action at critical steps. Therefore, the challenge of ensuring increasingly accurate 3-D conformal dose delivery in this new adaptive IGART framework is even more complex.

2. BACKGROUND

The problem of quality assurance in radiation therapy is of great interest. New approaches are being established for IMRT delivery QA employing film [8], dosimeter arrays [9, 10], electronic portal imaging [11–14] and gel and radiochromic plastic volumetric dosimeters [15–19]. These validation techniques

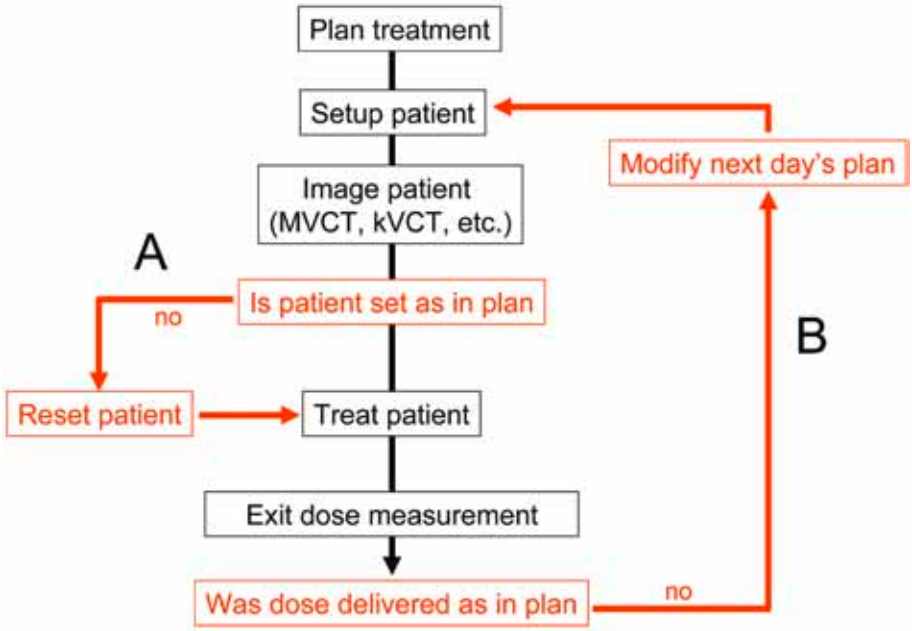

FIG. 1. An example of two potential IGART schemas. (A) the simplest IGART process may involve patient set-up verification at time of treatment (e.g. kV CBCT image registration with a simulation CT reference image from the initial treatment planning). If a discrepancy is noted by the treating therapist, the patient is moved to the correct position prior to irradiation. (B) in a more sophisticated IGART process, one might perform exit dose measurements to determine the dose delivered in a given fraction. If the dose delivery was not as intended, one could modify the next fraction to correct and bring the cumulative dose to the intended delivery over the multiple fractions.

can provide sufficient assurance of dose delivery for the well-tested and well-established day-to-day clinical practice. Similarly, various approaches have been proposed for the quality assurance of other technical components involved at different stages of IGRT. For example, there are procedures to validate the geometric integrity of the imaging systems in the radiotherapy bunker for patient localization [20, 21], to test the registration integrity for different imaging modalities used in treatment planning [22] and to perform quality assurance of treatment planning systems [23].

The Radiological Physics Centre (RPC) in the United States of America provides some indication of the success of IMRT QA approaches used to date. The RPC provided a large number of centres involved with IMRT clinical trials with anthropomorphic phantoms (of the head, thorax and pelvis) containing various dosimeters and regions of interest for irradiation. The centres were given

IMRT objectives to deliver to the phantoms using their clinically established IMRT planning and delivery processes. Initially, one third of the centres failed to achieve the goal of irradiating correctly within a 7% dose or a 4 mm distance in the high dose region near the organ at risk; this did eventually improve to 78% success [24].

The RPC experience, the results of analyses by various individuals in their clinics, and the deliberations of working groups are leading some to conclude that radiation therapy quality assurance programs need to be rethought. For example, people are suggesting that risk analysis be undertaken to identify critical points requiring greater vigilance. Also, there is an appreciation that new approaches are required to look at the complete chain inherent to modern delivery accounting for the complex interactions and connections of the various components [25–28]. According to this view, clinical QA may become more of an integrated activity.

3. PROPOSAL

The authors envision an IGART process quality assurance protocol that is not performed solely by the physics staff but by the whole clinical treatment team. Physics would prepare some test object (for example, but not limited to, a dosimeter such as a Fricke or polymer-gel or a PRESAGE radiochromic plastic dosimetry system) and insert it into some anthropomorphic phantom. The phantom would then be given to the therapy team (e.g. radiation oncologists and medical radiation treatment technologists, hereafter called therapists) to process as a patient: planning therapists would perform CT simulation; oncologists might contour structures that could be delineated in the target; planners or dosimetrists would plan the delivery on the treatment planning system; and treatment therapists would deliver the treatment using the IGART approaches being assessed. This would include whatever adaptive processes are in regular practice in the clinic. This report illustrates the concept by limiting the approach to simple patient set-up with treatment room cone beam CT (CBCT), although the process to be tested could be more challenging (see Fig. 2). In the IGART process QA:

(1) the preparation of the sample and insertion of a test tool into an appropriate phantom would be performed by the physics team as part of a regular (monthly) review at each treatment unit. The test tool would have to be appropriate for the particular IGART process being tested. In the authors' preliminary work, Fricke and polymer gel dosimeters were used as they were available in the clinic. The authors tested compliance to a patient set-up correction protocol that could have involved movement in three dimensions. The use of 3-D gel and plastic dosimeters in phantoms has

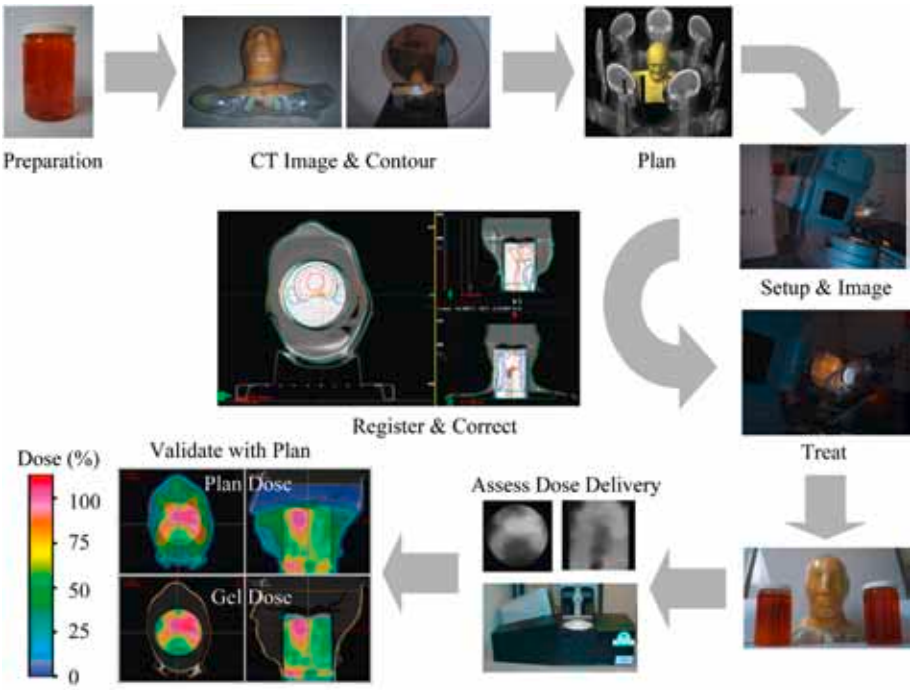

FIG. 2. An example of the implementation of a process QA protocol for an IGART procedure. Here, a Fricke-gel dosimeter was inserted into an anthropomorphic phantom for subsequent treatment by the radiation delivery team as a patient. The IGART protocol being evaluated was the simple process of patient set-up verification using on board CBCT imaging. At the end of the process, the measurements from the dosimeter are compared to the treatment plan and evaluated to determine if the delivery was as intended. The QA system could be extended easily to other IGART processes.

been well indicated [15–19]. The test tool could possibly be film, a detector array or some other device. One important feature is that it should be in an anthropomorphic phantom (preferably opaque) that would seem like a patient to the staff subsequently treating it.

(2) The CT simulation, imaging and contouring of the images would be performed as usual by the CT therapists and, it is hoped, radiation oncologists. As this IGART process QA evolves and becomes established, it may be possible to develop phantom inserts to provide contrast to direct the target and critical organ contouring. For a test of target localization by kV imaging at the treatment unit, the phantom could be designed to enable controlled and recordable perturbation of the location of the target after imaging to simulate organ motion inherent in actual patient treatment.

(3) Treatment planning would be performed by the dosimetrists/planning therapists, and the transfer of the beam data and phantom images would proceed to the treatment unit as in clinical practice. The treatment plan would also be sent to the physics department for preparation for subsequent comparison with measured data at the end of the irradiation. (This step may well involve plan transfer in to software developed for the QA.)

(4) The IGART process being tested would be implemented on the treatment unit by the treating therapists. In the illustration in Fig. 2, the test was set-up verification with the cone beam CT available on the linear accelerator with adjustment of patient set-up (in this case, through a automated table shift determined by the delivery system's registration software as per clinical practice). The test could be of any IGART process, as the phantom and test system would be designed to indicate compliance to that process. For example, a three dimensional gel dosimeter may be used to evaluate inter-fraction dose correction based on exit dose measurements from a prior fraction.

(5) At the end of the process, the removal of the test tool/dosimeter and data analysis would be performed by physics team. This would be a complex step, involving data registration and test evaluation. At this time, this would have to be performed using in-house developed software. However, if IGART process control becomes accepted by the radiation therapy community, radiation device and treatment planning vendors may enable this quality assurance step in their software environment.

Figure 3 illustrates the IGRT process control, which shows the results of two validation runs in the clinic for the testing of prostate patient repositioning using CBCT registration. The experiments were completed in a Varian environment (running Eclipse treatment planning, and an on-board imaging equipped Clinac 2100ix accelerator; Varian Medical Systems, Palo Alto, USA). The test object was an in-house prepared polymer gel dosimeter inserted into an AQUA phantom (Modus Medical Devices Inc., London, Canada).

4. CONCLUSIONS

Modern adaptive radiation therapy involves complex processes that are typically evaluated by tests at single well defined points in the treatment delivery. Such testing does not reflect that IGART is complex and involves data transfer between sophisticated advanced equipment, often with human evaluation to choose between different courses of action at critical steps. It would be beneficial

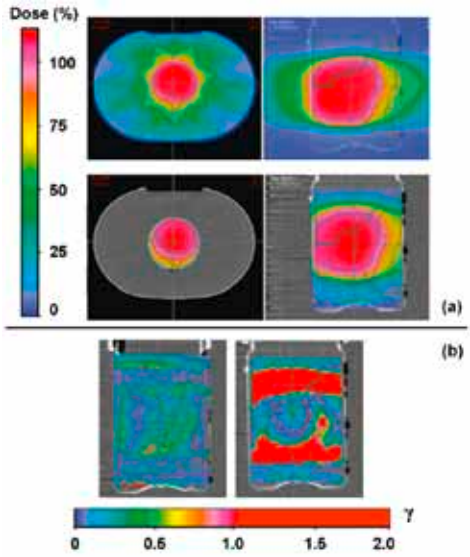

FIG. 3. In the implementation the authors used measurements with gel dosimetry to validate geometric set-up. (a) Visualizations of the treatment planning (top) and measured (bottom) doses. (b) A corresponding 3%/3 mm gamma map of the differences when the treatment fraction was delivered with (left) or without (right) a required set-up shift. The analysis can be customized to best flag failure in each specific IGART process.

to develop an IGART process QA that is more comprehensive in evaluating the whole treatment chain, including the human decision making and intervention used in some IGART techniques. While this would not replace all other tests, the regular performance of such QA in the complete IGART quality control programme would provide additional validation that patients are receiving the care intended. The testing can be easily implemented using existing dosimetry systems and dose evaluation tools standard in the clinic.

ACKNOWLEDGEMENTS

Funding from the Canadian Institutes of Health Research is appreciated.

REFERENCES

[1] KUBAN, D.A., TUCKER, S.L., DONG, L., STARKSCHALL, G., HUANG, E.H., CHEUNG, M.R., LEE, A.K., POLLACK, A., Long-term results of the M. D. Anderson randomized dose-escalation trial for prostate cancer, Int.J.Radiat.Oncol.Biol.Phys. **70** (2008) 67–74.

[2] JAFFRAY, D.A., SIEWERDSEN, J.H., WONG, J.W., MARTINEZ, A.A., Flat-panel cone-beam computed tomography for image-guided radiation therapy, Int.J.Radiat.Oncol.Biol.Phys. **53** (2002) 1337–1349.

[3] WOODFORD, C., YARTSEV, S., DAR, A.R., BAUMAN, G., VAN DYK J., Adaptive radiotherapy planning on decreasing gross tumor volumes as seen on megavoltage computed tomography images, Int.J.Radiat.Oncol.Biol.Phys. **69** (2007) 1316–1322.

[4] MARTINEZ, A.A., YAN, D., LOCKMAN, D., BRABBINS, D., KOTA, K., SHARPE, M., JAFFRAY, D.A., VICINI, F., WONG, J., Improvement in dose escalation using the process of adaptive radiotherapy combined with three-dimensional conformal or intensity-modulated beams for prostate cancer, Int.J.Radiat.Oncol.Biol.Phys. **50** (2001) 1226–1234.

[5] AHUNBAY, E.E., PENG, C., CHEN, G.P., NARAYANAN, S., YU, C., LAWTON, C., LI, X.A., An on-line replanning scheme for interfractional variations, Med.Phys. **35** (2008) 3607–3615.

[6] MACKIE, T.R., HOLMES, T., RECKWERDT, P., YANG, J., Tomotherapy: Optimized Planning and Delivery of Radiation Therapy. Int.J.Imaging Systems and Technology **6** (1995) 43–55.

[7] WELSH, J.S., PATEL, R.R., RITTER, M.A., HARARI, P.M., MACKIE, T.R., MEHTA, M.P., Helical tomotherapy: an innovative technology and approach to radiation therapy, Technol. Cancer Res.Treat. **1** (2002) 311–316.

[8] KRON, T., YARTSEV, S., MACKIE, T.R., Verification dosimetry during treatment for helical tomotherapy using radiographic film, Australas.Phys.Eng Sci.Med. **28** (2005) 232–237.

[9] KETOURNEAU, D., GULAM, M., YAN, D., OLDHAM, M., WONG, J.W., Evaluation of a 2D diode array for IMRT quality assurance, Radiother.Oncol. **70** (2004) 199–206.

[10] POPPE, B., BLECHSCHMIDT, A., DJOUGUELA, A., KOLLHOFF, R., RUBACH, A., WILLBORN, K.C., HARDER, D., Two-dimensional ionization chamber arrays for IMRT plan verification, Med.Phys. **33** (2006) 1005–1015.

[11] ANSBACHER, W., Three-dimensional portal image-based dose reconstruction in a virtual phantom for rapid evaluation of IMRT plans, Med Phys **33** (2006) 3369–3382.

[12] VIAL, P., GUSTAFSSON, H., OLIVER, L., BALDOCK, C., GREER, P.B., Direct-detection EPID dosimetry: investigation of a potential clinical configuration for IMRT verification, Phys.Med.Biol. **54** (2009) 7151–7169.

[13] MANS, A., WENDLING, M., McDERMOTT, L.N., SONKE, J.J., TIELENBURG, R., VIJLBRIEF, R., MIJNHEER, B., VAN HERK, M., STROOM, J.C., Catching errors with in vivo EPID dosimetry, Med.Phys. **37** (2010) 2638–2644.

[14] VAN ELMPT, W., NIJSTEN, S., PETIT, S., MIJNHEER, B., LAMBIN, P.M., DEKKER, A., 3D in vivo dosimetry using megavoltage cone-beam CT and EPID dosimetry. Int.J.Radiat.Oncol.Biol.Phys. **73** (2009) 1580–1587.

[15] BABIC, S., BATTISTA, J., JORDAN K., Three-dimensional dose verification for intensity-modulated radiation therapy in the radiological physics centre head-and-neck phantom using optical computed tomography scans of ferrous xylenol-orange gel dosimeters. Int.J.Radiat.Oncol.Biol.Phys. **70** (2008) 1281–1291.

[16] BRADY, S.L., BROWN, W.E., CLIFT, C.G., YOO, S., OLDHAM, M., Investigation into the feasibility of using PRESAGE/optical-CT dosimetry for the verification of gating treatments, Phys.Med.Biol. **55** (2010) 2187–2201.

[17] CEBERG, S., KARLSSON, A., GUSTAVSSON, H., WITTGREN, L., BACK, S.A., Verification of dynamic radiotherapy: the potential for 3D dosimetry under respiratory-like motion using polymer gel, Phys.Med.Biol. **53** (2008) N387–N396.

[18] CEBERG, S., GAGNE, I., GUSTAFSSON, H., SCHERMAN, J.B., KORREMAN, S.S., KJAER-KRISTOFFERSEN, F., HILTS, M., BACK, S.A., RapidArc treatment verification in 3D using polymer gel dosimetry and Monte Carlo simulation, Phys.Med.Biol. **55** (2010) 4885–4898.

[19] SAKHALKAR, H., STERLING, D., ADAMOVICS, J., IBBOTT, G., OLDHAM, M., Investigation of the feasibility of relative 3D dosimetry in the Radiologic Physics Center Head and Neck IMRT phantom using presage/optical-CT. Med.Phys. **36** (2009) 3371–3377.

[20] BALTER, J.M., ANTONUK, L.E., Quality assurance for kilo- and megavoltage in-room imaging and localization for off- and online setup error correction. Int. J Radiat.Oncol.Biol.Phys **71** (2008) S48–S52.

[21] BISSONNETTE, J.P., MOSELEY, D., WHITE, E., SHARPE, M., PURDIE, T., JAFFRAY D.A., Quality assurance for the geometric accuracy of cone-beam CT guidance in radiation therapy, Int.J.Radiat.Oncol.Biol.Phys. **71** (2008) S57–S61.

[22] ISAMBERT, A., BONNIAUD, G., LAVIELLE, F., MALANDAIN, G., LEFKOPOULOS, D., A phantom study of the accuracy of CT, MR and PET image registrations with a block matching-based algorithm, Cancer Radiother. (2008).

[23] VAN DYK, J., Quality assurance of radiation therapy planning systems: current status and remaining challenges, Int.J Radiat.Oncol.Biol.Phys **71** (2008) S23–S27.

[24] IBBOTT, G., QA in Radiation Therapy: The RPC Perspective, 6th International Conference on 3D Radiation Dosimetry (2010) 1–7.

[25] HULICK, P.R., ASCOLI, F.A., Quality assurance in radiation oncology, J Am.Coll.Radiol. **2** (2005) 613–616.

[26] HUQ, M.S., FRAASS, B.A., DUNSCOMBE, P.B., GIBBONS, J.P., Jr., IBBOTT, G.S., MEDIN, P.M., MUNDT, A., MUTIC, S., PALTA, J.R., THOMADSEN, B.R., WILLIAMSON, J.F., YORKE, E.D., A method for evaluating quality assurance needs in radiation therapy. Int.J.Radiat.Oncol.Biol.Phys. **71** (2008) S170–S173.

[27] PALTA, J.R., LIU, C., LI, J.G., Current external beam radiation therapy quality assurance guidance: does it meet the challenges of emerging image-guided technologies? Int.J Radiat.Oncol.Biol.Phys **71** (2008) S13–S17.

[28] WILLIAMSON, J.F., DUNSCOMBE, P.B., SHARPE, M.B., THOMADSEN, B.R., PURDY, J.A., DEYE, J.A., Quality assurance needs for modern image-based radiotherapy: recommendations from 2007 Interorganizational Symposium on "quality assurance of radiation therapy: challenges of advanced technology", Int.J Radiat.Oncol.Biol.Phys **71** (2008) S2–12.

COMPARATIVE STUDY OF SPECTROPHOTOMETRIC RESPONSE OF THE 270 BLOOM FRICKE GEL DOSIMETER TO CLINICAL PHOTON AND ELECTRON BEAMS

C.C. CAVINATO*, R.K. SAKURABA**, J.C. CRUZ**, L.L. CAMPOS*

* Instituto de Pesquisas Energéticas e Nucleares
Email: lcrodri@ipen.br

** Hospital Israelita Albert Einstein

São Paulo, Brazil

Abstract

This study aims to compare the spectrophotometric response of the Fricke xylenol gel (FXG) dosimeter developed at Instituto de Pesquisas Energéticas e Nucleares, prepared by using 270 Bloom gelatin from porcine skin produced in Brazil, for clinical photons 6 MV to 18 MV and electron beams with energies between 6 MeV and 16 MeV, to the reference depth using liquid and virtual water phantoms. The optical absorption spectra, dosimetric wavelengths, dose and energy dependent response, sensitivity and lower detection limits were evaluated and compared for both clinical beams. All results obtained in this study are satisfactory and indicate the viability of implementing this dosimeter in photon and electron 3-D dosimetry.

1. INTRODUCTION

Linear accelerators have been useful to treat the more differentiated tumours with clinical photon (deep seated tumours) and electron (superficial tumours) beams. The increased use of accelerators has required more efficient quality control of the treatment planning in order to optimize clinical results [1, 2]. The Fricke gel dosimeter, based on the oxidation of ferrous (Fe^{2+}) to ferric (Fe^{3+}) ions by ionizing radiation, has been widely studied for application to quality control of radiation treatments by allowing the 3-D dose distribution verification [3–19].

The High Doses Laboratory of Instituto de Pesquisas Energéticas e Nucleares (IPEN) developed a Fricke xylenol gel (FXG) dosimeter prepared using 270 Bloom gelatin from porcine skin from Brazil [20]. The 270 Bloom gelatin is low cost and easy to find on the national market, and replaces the FXG

solution produced using 300 Bloom gelatin which is imported, hard to acquire and high-priced, about forty-five times more expensive [21].

This work aims to compare the spectrophotometric response of the FXG dosimeter developed at IPEN, prepared using 270 Bloom gelatin, for clinical photons 6 MV to 18 MV and electron beams with energies between 6 and 16 MeV, at reference depths using liquid and virtual water phantoms [22]. The optical absorption spectra, appropriate wavelength for best dosimetric evaluation, dose and energy dependent response, sensitivity and lower detection limits were evaluated and compared for photon and electron clinical beams.

2. MATERIALS AND METHODS

2.1. Fricke gel solutions preparation

The FXG solutions were prepared using 5% by weight of 270 Bloom gelatin, ultrapure water, 50 mM of sulphuric acid, 1 mM of sodium chloride, 1 mM of ferrous ammonium sulphate hexahydrate and 0.1 mM of xylenol orange [4]. The samples were conditioned in polymethyl methacrylate (PMMA) cuvettes (10 mm × 10 mm × 45 mm) and stored under refrigeration (4 ± 1°C) and light protected conditions for about 12 h [4] after preparation. The FXG solutions were maintained 30 min at room temperature and light protected before irradiation.

2.2. Fricke gel samples irradiation

The samples were irradiated in the reading cuvettes with clinical photon beams 6 to 18 MV (VARIAN® linear accelerator models CLINAC 2100C and CLINAC 23EX) and electron beams with energies between 6 MeV to 16 MeV (VARIAN® linear accelerator model CLINAC 2100C) with absorbed doses between 0.05 Gy and 40 Gy at a dose rate of 400 cGy/min using radiation field size of 10 cm × 10 cm.

A MEDINTEC® liquid water phantom [PMMA walls and bottom 40 cm × 40 cm × 40 cm filled with tri-distilled water (ρ = 1.00 g/cm^3)] was used for all irradiations. All three samples sets of FXG solution were packed with polyvinyl chloride (PVC) film in order to avoid contact of the dosimetric solution with the tri-distilled water during the irradiations.

Irradiations with 6 MV photons and 12 MeV electrons were repeated using a CIVCO® virtual water (ρ = 1.03 g/cm^3) solid phantom (slabs of different thicknesses measuring 30 cm × 30 cm), to compare with the results obtained using the liquid water phantom.

To ensure the maximum dose to the centre of each FXG sample different reference depths were used (Table 1). Table 1 also presents the backscatter thicknesses used for photon and electron irradiations.

2.3. Fricke gel samples evaluation

The evaluation technique used was the optical absorption (OA) spectrophotometry and the measurements were performed using SHIMADZU Corporation® (Tokyo, Japan) spectrophotometer model UV-2101PC in the wavelength range from 190 nm to 900 nm.

All optical measurements were performed about 30 min after irradiation. Each presented value corresponds to the average of the measurement of three samples and the error bars represent the standard deviation of the mean. The background values corresponding to the optical measurements of non-irradiated FXG samples were subtracted from all absorbance values presented.

3. RESULTS AND DISCUSSION

3.1. Optical absorption spectra and dosimetric wavelength

The optical absorption spectra obtained with FXG solutions non-irradiated and irradiated with different absorbed doses in a liquid water phantom with 6 MV photon and 12 MeV electron beams are presented in Figs 1 and 2, respectively.

TABLE 1. REFERENCE DEPTHS AND BACKSCATTER THICKNESSES FOR PHOTON AND ELECTRON IRRADIATIONS

Clinical beams	Energy	Liquid water phantom (cm/liquid water)		Virtual water phantom (cm/virtual water)	
		Reference depth	Backscatter thickness	Reference depth	Backscatter thickness
Photons	6 MV	5.0	5.0	4.4	5.0
	15 MV				
	18 MV				
Electrons	6 MeV	0.8	5.0	—	—
	9 MeV	1.4		—	—
	12 MeV	2.4		2.4	5.0
	16 MeV	2.0		—	—

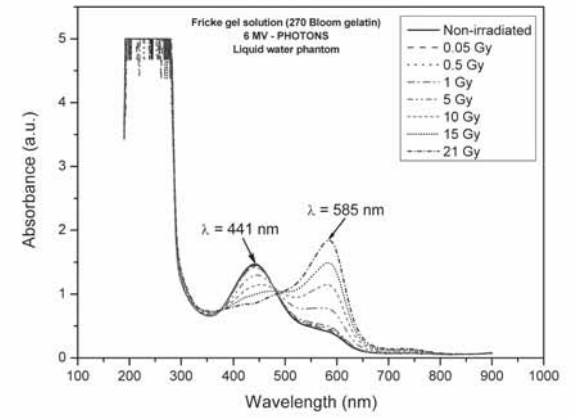

FIG. 1. Optical absorption spectra of the Fricke gel solution non-irradiated and irradiated with clinical 6 MV photon beams.

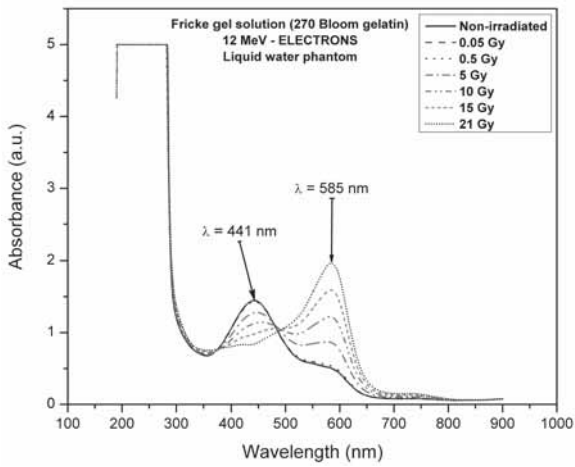

FIG. 2. Optical absorption spectra of the Fricke gel solution non-irradiated and irradiated with clinical 12 MeV electron beams.

The FXG solutions irradiated with photon and electron beams presented two absorption bands, as expected: one at 441 nm, corresponding to Fe^{2+} ions initially present in non-irradiated Fricke gel solution and other at 585 nm, corresponding to Fe^{3+} ions generated by oxidation of Fe^{2+} ions by ionizing radiation. The absorption band at 441 nm tends to disappear while the band at 585 nm increases with radiation dose.

The optical absorption spectra of the Fricke gel samples produced at IPEN with 270 Bloom gelatin irradiated with different photon and electron energies and phantom materials present the same absorption band (585 nm) as presented in the literature [5] to 300 Bloom FXG solution for clinical photons and electrons beams and ^{60}Co gamma radiation. Therefore, the dosimetric wavelength established for 270 Bloom Fricke gel solution was 585 nm.

3.2. Dose–response curves

The spectrophotometric dose–response curves of the FXG solutions irradiated with 6–18 MV photons and absorbed doses between 0.05 and 40 Gy and 6–16 MeV electrons and absorbed doses between 0.05 and 21 Gy, using liquid and virtual water phantoms, are presented in Figs 3 and 4, respectively.

The optical response of the FXG solution presented a linear behaviour in dose range from 0.05 Gy to 21 Gy (clinical dose range) for photon and electron beams. At absorbed doses greater than 20 Gy for both photons and electrons a spectrophotometric response saturation was observed.

The difference between the optical responses of the Fricke gel solution irradiated using liquid and virtual water phantoms was no more than is greater 1.0% for both 6 MV photons and 12 MeV electrons. Therefore, the spectrophotometric response was considered to be independent of the phantom material for the energy range studied.

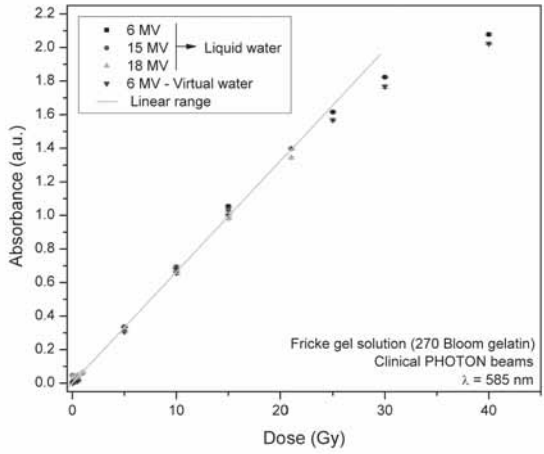

FIG. 3. Spectrophotometric dose–response curve of the Fricke gel solutions irradiated with clinical photon beams using different phantom materials.

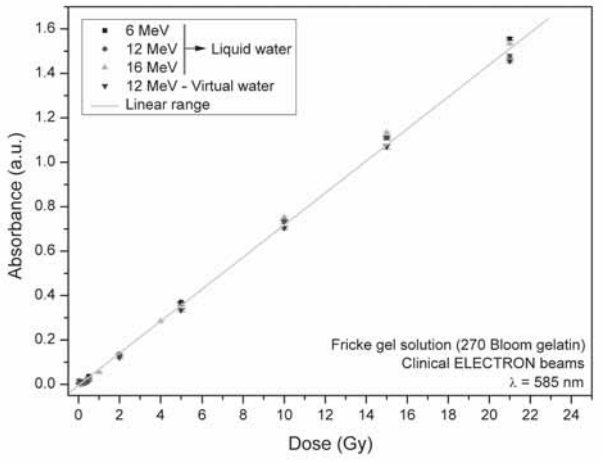

FIG. 4. Spectrophotometric dose–response curve of the Fricke gel solutions irradiated with clinical electron beams using different phantom materials.

3.3. Sensitivity and lower detection limit

The optical sensitivity for clinical photon and electron beams was 0.06 ± 0.001 au/Gy and 0.07 ± 0.001 au/Gy, respectively, for the different energies and phantom materials studied.

The lower detection limit experimentally established for photons and electrons was 0.05 Gy in the dose range studied using a clinical accelerator.

3.4. Energy dependent response

The energy dependent response curves for the FXG solutions irradiated with clinical 6–18 MV photon beams (absorbed dose of 10 Gy) relative to 18 MV photons and clinical 6–16 MeV electron beams (absorbed dose of 5 Gy) relative to 16 MeV electrons in a liquid water phantom are presented in Figs 5 and 6, respectively.

The spectrophotometric response relative to 18 MV photon beams presented a maximum variation as a function of radiation energy of about 7% and 2% for the 6 MV and 15 MV energies, respectively. The spectrophotometric response relative to 16 MeV electron beams presented a maximum variation of about 7% for 6 MeV, while the 9 and 12 MeV beams showed less of an energy dependence. According to Ibbott [23], the Fricke gel is considerably less energy dependent than thermoluminescence dosimeters, radiographic film and ionization chambers, for example.

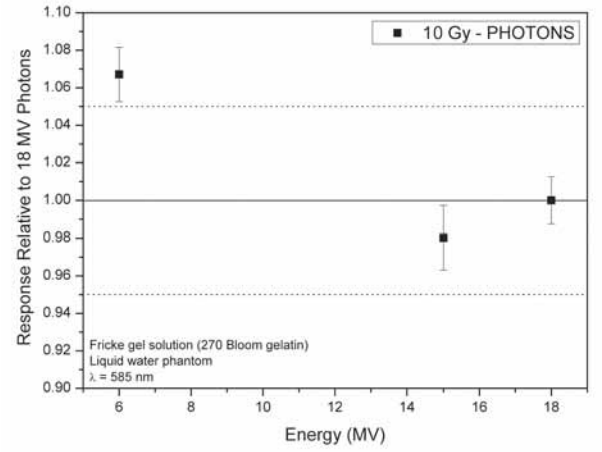

FIG. 5. Energy dependent spectrophotometric response curve of the Fricke gel solutions irradiated with clinical photon beams.

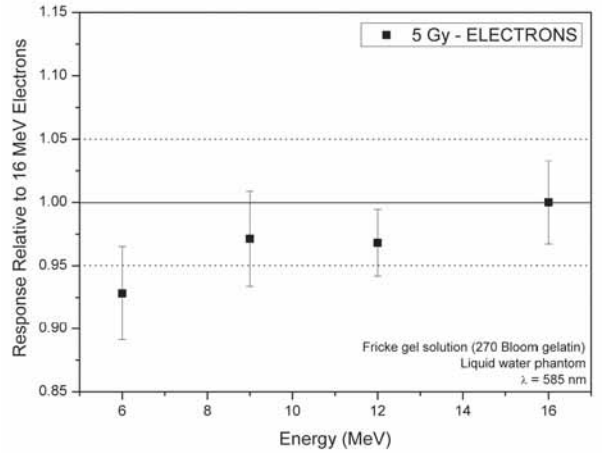

FIG. 6. Energy dependent spectrophotometric response curve of the Fricke gel solutions irradiated with clinical electron beams.

4. CONCLUSIONS

The results obtained in this study indicated that 270 Bloom FXG dosimeter developed at IPEN provided excellent results when irradiated with various clinical photon and electron beam energies and phantom materials. All results obtained were similar to those obtained for ^{60}Co gamma radiation [21] and also

indicated the viability of implementing this dosimeter for photon and electron 3-D dosimetry.

ACKNOWLEDGEMENTS

The authors are grateful to the HIAE for allowing the samples' irradiations in VARIAN® linear accelerators and to CAPES, CNPq and IPEN for financial support.

REFERENCES

[1] PODGORSAK, E.B., "External photon beams: physical aspects", Radiation Oncology Physics: a Handbook for Teachers and Students (PODGORSAK, E.B., Ed.), IAEA, Vienna (2005) 161–217.
[2] STRYDOM, W., PARKER, W., OLIVARES, M., "Electron beams: physical and clinical aspects", Radiation Oncology Physics: A Handbook for Teachers and Students, (PODGORSAK, E.B., Ed.), IAEA, Vienna (2005) 273–299.
[3] GORE, J.C., KANG, Y.S., SCHULZ, R.J., Measurement of radiation dose distributions by nuclear magnetic resonance (NMR) imaging, Phys. Med. Biol. **29** 10 (1984) 1189.
[4] OLSSON, L.E., et al., Ferrous sulphate gels for determination of absorbed dose distributions using MRI technique: basic studies, Phys. Med. Biol. **34** 1 (1989) 43.
[5] BERO, M.A., GILBOY, W.B., GLOVER, P.M., Radiochromic gel dosemeter for three-dimensional dosimetry, Radiat. Phys. Chem. **61** (2001) 433.
[6] BERO, M.A., ZAHILI, M., Radiochromic gel dosimeter (FXG) chemical yield determination for dose measurements standardization, J. Phys.: Conf. Ser. **164** (2009) 012011.
[7] KELLY, R.G., JORDAN, K.J., BATTISTA, J.J., Optical CT reconstruction of 3D dose distributions using the ferrous–benzoic–xylenol (FBX) gel dosimeter, Med. Phys. **25** 9 (1998) 1741.
[8] JORDAN, K., BATTISTA, J., Scatter measurements for optical cone-beam computed tomography, J. Phys.: Conf. Ser. **164** (2009) 012028.
[9] JORDAN, K., Optical CT scanning of cross-linked radiochromic gel without cylinder wall, J. Phys.: Conf. Ser. **164** (2009) 012029.
[10] SCHREINER, L.J., Where does gel dosimetry fit in the clinic? J. Phys.: Conf. Ser. **164** (2009) 012001.
[11] DORAN, S.J., The history and principles of optical computed tomography for scanning 3-D radiation dosimeters: 2008 update, J. Phys.: Conf. Ser. **164** (2009) 012020.
[12] SCHREINER, L.J., NMR mechanisms in gel dosimetry, J. Phys.: Conf. Ser. **164** (2009) 012032.
[13] DE DEENE, Y., Review of quantitative MRI principles for gel dosimetry, J. Phys.: Conf. Ser. **164** (2009) 012033.

[14] BÄCK, S.A.J., Clinical applications of gel dosimeters, J. Phys.: Conf. Ser. **164** (2009) 012049.
[15] MEESAT, R., et al., Evaluation of the radiation-sensitizer/protector and/or antioxidant efficiencies using Fricke and PAG dosimeters, J. Phys.: Conf. Ser. **164** (2009) 012006.
[16] LUCIANI, A.M., et al., Dosimetric performances of optically detected Fricke-agarose-Xylenol Orange gel, J. Phys.: Conf. Ser. **164** (2009) 012015.
[17] CAVINATO, C.C., et al., A dosimetric evaluation of tissue equivalent phantom prepared using 270 Bloom gelatin for absorbed dose imaging in Gamma Knife radiosurgery, J. Phys.: Conf. Ser. **164** (2009) 012016.
[18] KOEVA, V.I., et al., Preliminary investigation of the NMR, optical and x-ray CT dose-response of polymer gel dosimeters with cosolvents and increased crosslinker levels, J. Phys.: Conf. Ser. **164** (2009) 012017.
[19] SVOBODA, J., et al., Optical evaluation of Fricke xylenol orange gel by light scattered at 90 degrees, J. Phys.: Conf. Ser. **164** (2009) 012026.
[20] GALANTE, A.M.S., et al., MRI study of radiation effect on Fricke gel solutions, Radiat. Meas. **43** (2008) 550.
[21] CAVINATO, C.C., Padronização do Método de Dosimetria Fricke Gel e Avaliação Tridimensional de Dose Empregando a Técnica de Imageamento por Ressonância Magnética, Master Dissertation, Univ. of Sao Paulo, Sao Paulo (2009).
[22] INTERNATIONAL ATOMIC ENERGY AGENCY, Absorbed Dose Determination in External Beam Radiotherapy: An International Code of Practice for Dosimetry Based on Standards of Absorbed Dose to Water, Technical Reports Series No. 398, IAEA, Vienna (2000).
[23] IBBOTT, G.S., Applications of gel dosimetry, J. Phys. Conf. Ser. **3** (2004) 58.

PATIENT SPECIFIC QUALITY ASSURANCE OF WHOLE PELVIC INTENSITY MODULATED RADIOTHERAPY WITH HYPOFRACTIONATED SIMULTANEOUS INTEGRATED BOOST TO PROSTATE FOR HIGH RISK PROSTATE CANCER

E. MORETTI, M.R. MALISAN, M. CRESPI, C. FOTI, R. PADOVANI
Department of Medical Physics
University Hospital S. Maria della Misericordia,
Udine, Italy
Email: moretti.eugenia@aoud.sanita.fvg.it

Abstract

In this investigation, the results are shown of the authors' preliminary patient specific quality assurance experience in the validation of whole pelvis intensity modulated radiotherapy (WP-IMRT) with hypofractionated simultaneous integrated boost to prostate. A cohort of ten patients with localized prostate cancer (high risk) who underwent hypofractionated from March 2009 through January 2010 was included. The combination of wide fields and simultaneous delivery of three levels of dose (65, 56.25 and 50 Gy) for the prostatic gland, seminal vesicles and pelvic lymph nodes, respectively, prescribed in 25 fractions leads to the peculiarity of the final dose distribution — large regions of irradiations and a high degree of heterogeneity. The treatment verification involves 2-D measurements with a matrix of diodes and one-point measurement with a standard ionization chamber. To map properly the wide fields of WP-IMRT, successive exposures were merged with regular shifts in matrix position.

1. INTRODUCTION

The current paradigm for the quality assurance (QA) programme for intensity modulated radiotherapy (IMRT) includes QA of the treatment planning system (TPS), QA of the delivery system and patient specific QA. The aim of patient specific QA is to verify the agreement between the dose distribution calculated by the TPS and the actually delivered one. Because of complex fluence modulation, each beam often includes several small irregular off-axis subfields. Therefore, the typical resulting sharp dose gradients render the deviations between calculated and real dose critical, especially in areas close to organs at risk. Furthermore, each IMRT plan is strictly specific to the patient since the various segment configurations and monitor units (in static modality) or leaf

position and leaf speed (in dynamic modality) may be significantly different, even if the shape of the targets and organs at risk are similar. These features necessitate dosimetric verification of every IMRT plan. This study illustrates the authors' patient specific QA experience in the validation of whole pelvic IMRT (WP-IMRT) with hypofractionated simultaneous integrated boost (SIB) to the prostate. A cohort of ten patients with localized prostate cancer (high risk) who underwent IMRT hypofractionated from March 2009 to January 2010 was included. For treating the prostatic gland, seminal vesicles and pelvic lymph nodes, doses of 65, 56.25 and 50 Gy, respectively, were prescribed in 25 fractions.

2. MATERIALS AND METHODS

2.1. Dose delivery and TPS

The WP-IMRT treatments consisted of five to seven 6 MV beams from a Varian Clinac 600C linac fitted with a Millenium 120 leaf collimator (Varian Medical Systems, United States of America). The Millennium 120 Multileaf Collimator (MLC) consists of two banks of 60 leaves. The 40 central leaves have a 5 mm leaf width at the isocentre and the outer 20 leaves have a 1 cm leaf width at isocentre. The distance between the most protruding leaf and the most retracted leaf from the same bank is limited to 14.5 cm. The volumes involved in the whole pelvic treatments have typically cross-sectional dimensions greater than 14.5 cm; this implies field sizes ranging from about 8 cm × 16 cm to 10 cm × 20 cm. Thus, since the targets cannot be covered by the range of MLC motion, the fluence patterns are split into 2/3 subfluences. Typically, WP-IMRT with five fields resulted in ten split subfields in the delivery. The splitting may represent a problem in the validation of the plan: due to cumulative doses attributable to MLC scatter from split fields, calculation of dose for such fluence patterns is highly sensitive to any inadequacies of the dose calculation model and also to the uncertainties in the MLC dosimetric parameters in the TPS.

The delivery technique of the WP-IMRT plans was step-and-shoot. The most commonly used set-up encompassed five entry points with gantry angles set to 36°, 108°, 180°, 252° and 324°. Only in one case, in order to obtain a higher degree of conformance, a treatment configuration with seven gantry orientations was adopted: 0°, 51°, 103°, 155°, 206°, 258° and 309°.

The IMRT SIB plans were generated by employing the optimization module (DSS, Direct step-and-shoot) of Oncentra MasterPlan™ TPS (Nucletron, the Netherlands). The dose calculations in MasterPlan™ are performed in a two step process: in the first step, the fluence distribution exiting the treatment

machine is modelled (enhanced energy fluence algorithm); in the second step, the actual dose deposited in the patient (or phantom) is calculated by taking into account the pre-determined fluence pattern, according to different algorithms — the pencil beam employed in the current investigation and collapsed cone convolution.

The plans were transferred via DICOM-RT to the record-and-verify system DIC (Varian Medical Systems, USA). The authors performed the irradiations to the verification phantoms in the clinical mode just as for the delivery of the treatment plan to the patient. The dose rate was set to the same value (i.e. 400 MU/min at the isocentre).

2.2. Patient specific QA: Measurement tools

The pre-treatment QA strategy relied on planar and point absolute dose measurements for each treatment beam.

A 2-D phantom, a diode array (MapCheck™ model 1175, Sun Nuclear, USA) was used. It contains 445 n-type diode detectors arranged in a 22 cm octagonal grid. The grid presents two detector densities: the 10 cm × 10 cm central part contains 221 diodes spaced at 10 mm and each line of detectors is translated 5 mm with respect to the next one, so that the diagonal spacing between detectors is 7.07 mm; the outer part of the device contains 224 diodes spaced at 20 mm, and in this case, each line is shifted 1 cm and the diagonal spacing becomes 14.14 mm. The active detector area is 0.8 mm × 0.8 mm, the inherent buildup is 2 g/cm^2, while the linear depth from the top of the overlay to the diodes area is 1.35 cm and the inherent backscatter thickness is 2.27 g/cm^2. An equalization procedure is performed on a regular basis in order to determine the relative differences in sensitivity between the diodes. A dosimetric characterization of the MapCheck™ and its performance in the validation of modulated beams have been extensively discussed in the literature [2–4].

The verification set-up entailed a measurement depth of 5 cm water equivalent with the detector array at the isocentre plane. For the corresponding dose calculation, the authors applied the IMRT plan to be verified to a CT study of MapCheck™ and extracted, field by field, the 2-D dose matrix to be compared to the experimental dose distribution obtained exposing the phantom. For the field by field verification, all gantry angles were changed to vertical and the detector was normal to the central beam axis. A recalculation of the dose was performed in the MapCheck™ phantom setting a 2 mm grid calculation.

In order to increase the effective detector two dimensional density and to properly map the wide fields of WP-IMRT, successive exposures were merged with regular shifts in MapCheck™ position. The average number of the sampled

points was about 400 for every single field. This procedure with multiple irradiations of the device was demanding and workload intensive.

The verification of WP-IMRT plans was complemented with ionization chamber (IC) measurements. An NE2571 0.6 cm^3 Farmer type IC was used to assess the dose in a clinically meaningful point of a high dose region in a homogeneous PMMA phantom (30 cm × 30 cm × 18 cm), delivering all beams with their original gantry angles. The ion chamber was placed at 5 cm water equivalent depth from the front surface of the rectangular plane sided phantom. The measurement site corresponds roughly to the localization in the patient plan.

To calculate the dose to the chamber volume, a computed tomography (CT) scan was performed of the chamber in the phantom and the original plan was applied to it. The volume of interest was assumed to be the chamber sensitive volume as contoured on CT images of the chamber in PMMA phantom. The chamber material was assumed to be water equivalent. The resolution of the calculation dose matrix was 2 mm. Calculated dose statistics were averaged over each chamber's delineated pixel volume. The active volume was always located in a region of high dose and low dose gradient (less than ±5%).

For both the verification procedures, the monitor units of the original IMRT plan were kept.

At every session, the output dose of the linac was measured according to the IAEA TRS-389 Code of Practice [5] using an NE2571 Farmer IC, coupled with a secondary standard electrometer, calibrated in terms of dose to water by the National Reference Laboratory (ENEA-INMRI, Casaccia). The absolute dose calibration of Mapcheck™ was performed, correcting the experimental data for the discrepancy between the daily rate and the value used in the TPS. Furthermore, standard square fields were carried out (check fields) to monitor the output and symmetry of the beam and also to evaluate the accuracy of the position of the phantom.

2.3. Patient specific QA: Acceptance criteria

For the fluence verification method, planned versus experimental maps were compared by means of the γ function analysis [6–8], adopting a dose difference criterion of 3% and a distance to agreement (DTA) criterion of 3 mm. The γ approach combines the two above mentioned methods The user defines the dose difference and DTA pass–fail criteria: if both parameters are outside the pass–fail criteria, the agreement fails according to the γ method. In the current investigation, the γ parameter was calculated in terms of local dose by using the analysis tools of Mapcheck™ software. Dose levels under a certain threshold, corresponding to about 10% of the prescription value, were discarded. A plan was accepted if the percentage of points with γ below 1 was higher than 90%.

Concerning the IC procedure, a maximum discrepancy of 5% between predicted value and measured value was accepted. The major tolerance in this comparison technique is correlated to the considerable uncertainty in the dose assessment both by the IC and by the TPS due to the complexity of the whole procedure. Different aspects have to be taken into account. In particular, for the calculation, it is difficult to simulate accurately the experimental set-up. For the measurement, the IC large collection volume may involve the lack of lateral electron equilibrium or the position of the detector that may be outside of the field or in the penumbra regions. The fact that the IMRT conditions are radically different from the open field conditions under which the chambers are calibrated may invalidate the use of such calibration factors in modulated beams.

3. RESULTS AND DISCUSSION

For the first ten patients, all the plans satisfied the acceptance criteria.

The results of the pretreatment QA data were analysed in order to judge the goodness of the agreement between planned and delivered dose and to define confidence limits for clinical QA practice in WP-IMRT.

3.1. Comparison of two dimensional dose distributions

The planar map of γ values resulting from the comparison between the imported calculated and measured dose distributions offers a qualitative representation of the agreement between two dose distributions, as shown in Fig. 1.

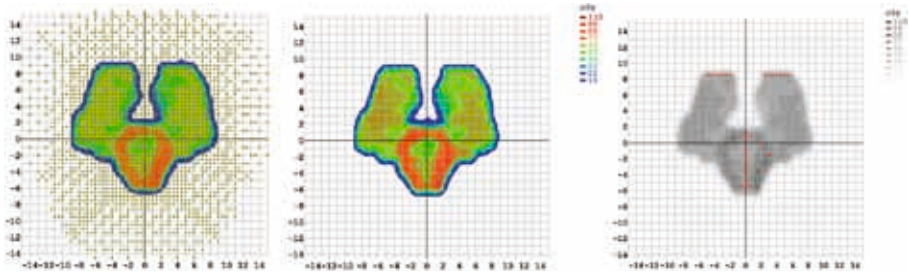

FIG. 1. Example of the comparison between dose measured (left image) by diode matrix and dose predicted by TPS (central image) in a coronal plan, for the posterior field of a WP-IMRT plan (plan no. 3). The image on the right shows the resultant match in terms of γ index (red points have values above criteria). Here, the analysis considers the whole field results from the composition of the two single parts (split fields) of the beam.

Gamma histograms, defining the percentage of γ values below a certain value, can represent an efficient pass/fail instrument in a comparison procedure. In the current investigation, it was decided to evaluate the following parameters of the γ distribution of each field of the population of plans/patients considered (ten plans for a total of 104 fields):

— mean γ value;
— percentage of points having $\gamma \leq 1$;
— percentage of points having $\gamma \leq 1.5$;
— percentage of points having $\gamma > 2$.

These γ indices are indicative of the quality of the agreement between measured-calculated plans.

The results obtained are reported in the Table 1: they show a good agreement between TPS and measurements. The average value of γ-index was: 0.46 (SD: 0.06). The mean value of percentage of points passing the criteria was observed better than 95% (96.3% with SD = 1.6). In two cases only (patients 4 and 6), the percentage of points with γ lower than unity was slightly less than 95% (93.5%, 94.3%). The average percentage of points having $\gamma \leq 1.5$ was 98.8% (SD = 0.9), while the average percentage of points with γ significantly higher than the limit value ($\gamma > 2$) was very low: 0.9 (SD = 1.2).

3.2. Comparison of point dose values

Table 2 summarizes the absolute doses for calculation and measurement. The percentage uncertainty on intra-session ionimetric measurements ranged up to 1.0% for the WP-IMRT fields.

TABLE 1. TWO DIMENSIONAL DOSE DISTRIBUTION VERIFICATION

Plan	#1	#2	#3	#4	#5	#6	#7	#8	#9	#10
#beams	5	5	5	7	5	5	5	5	5	5
#segments	99	100	131	137	131	110	116	109	119	97
average γ	**0.44**	**0.50**	**0.37**	**0.60**	**0.41**	**0.47**	**0.42**	**0.41**	**0.44**	**0.49**
SD	0.06	0.07	0.06	0.06	0.07	0.08	0.05	0.04	0.03	0.03
average % points with γ≤1	**97.7**	**95.5**	**98.4**	**93.5**	**97.7**	**94.3**	**97.1**	**96.9**	**96.1**	**95.3**
SD	1.5	2.5	1.4	3.0	2.4	3.0	1.7	2.2	1.1	1.7
average % points with γ≤1.5	**99.6**	**99.2**	**99.5**	**98.9**	**99.1**	**96.9**	**99.1**	**99.3**	**99.1**	**97.5**
SD	0.6	0.5	0.7	1.0	1.1	2.0	0.9	0.9	0.8	1.0
average % points with γ > 2	**0.4**	**0.5**	**0.4**	**1.0**	**1.2**	**4.2**	**0.5**	**0.0**	**0.1**	**0.2**
SD	0.9	0.6	0.7	1.5	1.2	3.5	0.9	0.0	0.7	1.5

Note: Results of the statistical analysis of the γ values distribution of more than 100 fields considered (corresponding to 10 WP-IMRT plans). For each plan, the following parameters were taken into account (with its SD): the average γ value, the percentage of points that pass the acceptance criterion (i.e. having γ value lower than unity), the percentage of points having $\gamma \leq 1.5$ and the percentage of points having $\gamma > 2$.

TABLE 2. POINT DOSE VALUES VERIFICATION

plan	D_{TPS} (cGy)	D_{IC} (cGy)	ratio = D_{TPS}/D_{IC}	Δ%
#1	301.0	309.0	0.974	-2.59
#2	280.1	275.1	1.018	1.82
#3	294.1	305.5	0.963	-3.73
#4	295.7	311.1	0.951	-4.94
#5	315.2	323.2	0.975	-2.47
#6	292.2	305.1	0.958	-4.22
#7	315.6	314.1	1.005	0.49
#8	331.4	334.5	0.991	-0.94
#9	314.2	307.9	1.020	2.05
#10	331.4	334.5	0.991	-0.94

Note: Results of the estimates of dose (D_{IC}) by employing IC at selected points compared with the corresponding values calculated by the TPS (D_{TPS}).

IC dose measurements agreed with the corresponding predicted values within the 5% limit. The mean ratio of absorbed dose to water from the TPS calculation to that from measurements (D_{TPS}/D_{IC}) was 0.985 (SD = 0.025). The TPS exhibited a trend to underestimate the dose compared to measurements. This could arise due to suboptimal modelling of the MLC leakage.

In practice, it is valuable to interpret the results obtained in this comparison process due to the complexity of the measurements, the type of IC employed and the operating mode of the calculation algorithm, etc. [1]. The accuracy in the TPS prediction is a function of how well the analytical model reproduces various accelerator beam geometries and components (especially MLC leaf ends and leakage). Further, the dose statistics calculated by the TPS over the IC volume are dependent upon the digitally contoured volume, which was delineated from visual inspection of the CT scan of the phantom and chamber (and was slightly larger than the manufacturer's nominal volume due to slice averaging effects present in CT images).

Uncertainties must also be considered in the measurement process when assessing IC performance. During static IMRT plan delivery on a rectangular phantom, essentially two dosimetric parameters of interest changed: field size and depth of measurement. They influence the scatter particle fluence reaching the detector. During delivery, the chamber is often positioned either outside of the field or in penumbra regions, resulting in volume averaging (especially important over gradient regions). Partial volume irradiation leads to lateral electronic disequilibrium where the non-uniform response to exposure within the detector's volume spatially affects the conversion of signal into dose to water in the detector [1]. In absorbed dose to water protocols, the calibration coefficient incorporates

fluence perturbation correction factors. However, IMRT fluences differ substantially from calibration conditions [1, 5]. It should be noted that the authors' procedure uses an all fields approach. This involves some compensation effects that could explain the observed agreement.

All these aspects render the discussion of the IC dosimetry highly critical. Thus, also considering the time factor, the authors are looking at the possibility of taking the IC dosimetric method as a secondary verification modality, to apply if unacceptable discrepancies between the 2-D dose distributions are detected.

4. CONCLUSION AND FUTURE DEVOLPMENTS

The treatment plan verification as outlined in this report based on matrix plus IC measurements was shown to be successful. The position during measurement with the IC is often critical for results because of the chamber size and the peculiarity of specific IMRT dose distributions, but is not so critical as to impair the generally good results obtained, probably due to compensation effects when the total plan is delivered.

The implemented QA procedure to check each IMRT patient is significantly time consuming and may become the bottleneck for a more intensive clinical IMRT use. Thus, to curtail the workload, the authors are investigating the possibility of using the portal imager (based on Si technology) in combination with the independent dose prediction software EPIDose™ provided by Sun Nuclear, which obtains the dose distribution from the fluence image acquired by the electronic portal imaging device (EPID). The EPID employed is a commercially available imaging device Portal Vision aS500 mounted on a Clinac 600C. The measured EPID images for each IMRT field were acquired without adding any buildup on the top of the cassette, with the detector area at a source–detector distance of 105 cm. For matching measured versus calculated dose, the γ index approach can also be used, maintaining the same routine acceptance criteria.

The preliminary results are encouraging. The two methods appear qualitatively consistent, showing a good agreement between the measured and the theoretical doses (Fig. 2). The authors validated the dose prediction performance of EPIDose™ comparing it with MapCheck™, in terms of γ parameters (average γ index, percentage of points with $\gamma \leq 1$, $\gamma \leq 1.5$ and >2). To assess quantitatively the dosimetric performance, a regression test was applied to the statistics of previous γ values. The analysis is being extended to a population of 25 WP-IMRT plans.

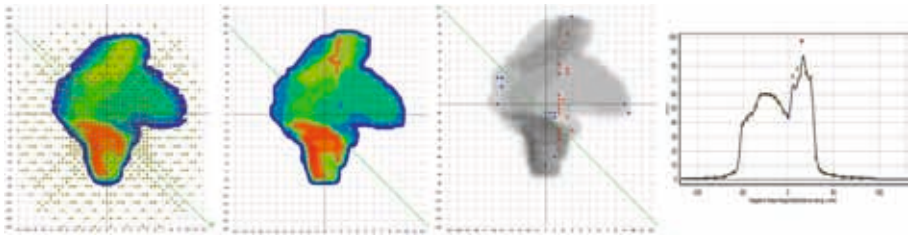

FIG. 2. Example of the comparison between dose measured (starting from the left to right) by diode matrix and EPID according to the prediction model Epidose™ for a WP-IMRT field (plan no. 5). The image in grey shows the resultant match in terms of γ index (2 mm-1%). The image on the right presents a comparison of the dose profiles along the underlined diagonal. The superior resolution power of EPID is clearly shown.

The EPID based method, still under validation, could be a useful IMRT-QA instrument, especially for the wide WP fields due to its large detector area, greater resolution and ease of use. In terms of workload at the linac, the superiority of EPID approach is evident: it was estimated that the time necessary for a verification session of the same WP-IMRT plan with EPID and Mapcheck™ is about 30 min and 90 min, respectively.

REFERENCES

[1] ALBER, M., et al., "Guidelines for the verification of IMRT", Booklet ESTRO, Brussels (2008).

[2] JURSINIC, A., NELM, B.E., A 2-D diode array and analysis software for verification of intensity modulated radiation therapy deliver, Med. Phys. **30** (2003) 870–879.

[3] LÉTOURNEAU, G.M., et al., Evaluation of a 2D diode array for IMRT quality assurance, Radiother. Oncol. **70** (2004)199–206.

[4] BANCI BUONAMICI, F., et al., An intercomparison between film dosimetry and diode matrix for IMRT quality assurance, Med. Phys. **34** (2007) 1372–1379.

[5] INTERNATIONAL ATOMIC ENERGY AGENCY, Absorbed Dose Determination in External Beam Radiotherapy: An International Code of Practice for Dosimetry Based on Standards of Absorbed Dose to Water, IAEA Technical Reports Series No. 398, IAEA, Vienna (2000).

[6] LOW, D.A, HARMS, et al., A technique for the quantitative evaluation of dose distributions, Med. Phys. **25** (1998) 656–661.

[7] LOW, D.A., DEMPSEYM J.F., Evaluation of the gamma dose distribution comparison method, Med. Phys. **30** (2003) 2455–2464.

[8] DEPUYDT, T., VAN ESCH, A., HUYSKENS, D.P., A quantitative evaluation of IMRT dose distributions: refinement and clinical assessment of the gamma evaluation, Radiother. Oncol. **62** (2002) 309–319.

PERIPHERAL DOSES IN MODERN RADIOTHERAPY TECHNIQUES: A COMPARISON BETWEEN IMRT AND TOMOTHERAPY

E. D'AGOSTINO*, R. BOGAERTS**, G. DEFRAENE**,
L. DE FREITAS NASCIMENTO*, E. LEANERTS***,
F. VAN DEN HEUVEL**, D. VERELLEN[+], F. VANHAVERE*

* Radioprotection, Dosimetry and Calibration Unit,
Belgian Nuclear Research Center, Mol
Email: edagosti@SCKCN.be

** Radiotherapy Department, University Hospital Gasthuisberg, Louvain

*** Radiotherapy Department, University Hospital Sart Tilmant, Liège

[+] Radiotherapy Department, University Hospital UZ Brussel, Brussels

Belgium

Abstract

The goal of this intercomparison is to determine the peripheral doses during treatment of prostate cancer. Two different treatment techniques are compared: (a) intensity modulated radiation therapy (IMRT — 10MV and 18MV) on a Varian Clinac 2100 C/D (Varian Medical Systems, Inc.) and (b) tomotherapy (6 MV, Tomotherapy Inc.). The treatment devices are located in the university hospitals of Louvain and Brussels. A common treatment protocol was agreed between the two clinical centres, which was used by each partner. In this case, it was possible to evaluate the performance (in terms of peripheral doses) of the different treatment techniques, when faced with the same constraints, in terms of dose distribution.

1. INTRODUCTION

Radiation therapy plays a very important role in treating about half of cancer patients. It is well known that some of the patients cured with ionizing radiations (either X ray based or with charged particles), can later develop a treatment induced secondary malignancy in organs located at a distance from the original tumour [1–7]. It is therefore extremely important to establish the doses

that are absorbed in those distant organs; these doses are also known as 'peripheral doses' [8–10].

This study presents an intercomparison designed to determine the magnitude of peripheral doses during treatment of prostate cancer. Two different techniques are considered: (a) the intensity modulated radiation therapy (IMRT) — 10 MV IMRT (now the common energy used in clinical practice) and 18 MV IMRT (both on a Varian Clinac 2100 C/D linear accelerator (Linac), Varian Medical Systems, Inc., Palo Alto, CA, USA), and (b) the TomoTherapy (TT) unit (Tomotherapy Inc., Madison, WI, USA, 6 MV). The treatment devices are located at the university hospitals of Leuven and Brussels, respectively. A common treatment protocol was agreed between the two clinical centres, which was used by each partner (though this protocol may not be optimal for all of them). The authors were able to evaluate the performance (in terms of peripheral doses) of the different units, when faced with the same constraints, in terms of dose distribution. The protocol required 74 Gy in the prostate, delivered in 2 Gy fractions. For the dosimetric study, one single fraction (i.e. 2 Gy) was to be delivered. Figure 1 shows the two radiotherapy devices included in the study.

2. MATERIALS AND METHODS

The measurements were performed with a Rando Alderson (RA) anthropomorphic phantom filled with thermoluminescent dosimeters (TLDs) (MTS-N pellets, TLD Poland) and neutron bubble detectors (in the case of 10 MV and 18 MV IMRT). For the TLD detectors, an air kerma calibration was performed with a ^{137}Cs source (0.667 MeV), exposing them to doses of 10, 70 and 200 mGy. The detectors were inserted in a Perspex (PMMA) plexiglas holder. The phantom was imaged using a CT scanner and the same conversion curve 'Hounsfield Units — electronic density' was shared across the two clinical centres, together with the CT data. The following different organs were

FIG. 1. From left to right: Linac and TT.

considered in this study: thyroid, stomach, colon, kidney, liver and lungs for neutron and photon measurements. In the case of photons, the doses to the oesophagus, spleen, red bone marrow, brain, small intestine and pancreas were monitored. Photon doses were measured by placing TLD into the RA phantom, inserted in locations corresponding to the different organs of interest. The TLDs were distributed within the different organs as uniformly as possible in order to guarantee a three dimensional coverage of the volume. In total, about 230 TLDs per irradiation were used. The final equivalent dose values were obtained by averaging over the readings in the different organs. Neutron doses were measured by placing bubble detectors, both for thermal (BDT, Bubble Technologies Industry, Ontario, Canada) and fast neutrons (BD-PND, Bubble Technologies Industry, Ontario, Canada) in holes drilled in these organs. The BDT were calibrated in a thermal nuclear reactor (BR1 at the Belgian Nuclear Research Center, SCK·CEN, located in Mol, Belgium) in terms of neutrons fluence. Conversion coefficients were used to derive equivalent doses. The BD-PND detectors were calibrated in a ^{252}Cf neutron source, in terms of equivalent dose. The read-out of the bubble detectors was performed using a home-made device, containing a camera taking pictures of the detectors from different angles. The number of bubbles was then automatically determined using in-house developed software on each projection and an average number of bubbles was determined. An uncertainty of about 30% can be expected in the neutron doses. A single treatment fraction of 2 Gy was delivered. Figure 2 shows the phantom and the detectors (TLDs and bubble detectors).

The measurements on the Linac were taken using intensity modulated fields at 10 MV and 18 MV, respectively. In both cases, five different fields were used. The RA phantom was positioned using external markers for both IMRT treatments. In the TomoTherapy device, a megavoltage CT image was used to perform the positioning.

FIG. 2. From left to right: RA phantom, TLDs and bubble detectors.

3. RESULTS AND DISCUSSION

3.1. Photon measurements

The results are presented here of the measurements taken with the same treatment protocol everywhere, including IMRT and Tomotherapy. Neutron measurements were only performed on the Linac at 10 MV and 18 MV. The contribution of neutrons to the total dose for 6 MV tomotherapy was virtually zero, as verified using bubble detectors. The TLD results are shown for all organs and also for organs partitioned into three different body regions: head and neck, thorax, pelvis. The head and neck region included: the thyroid, brain and oesophagus. The thoracic region included the following organs: the lungs, kidneys, liver, spleen, pancreas and stomach. Finally, the pelvis region included: the small intestine, colon and bladder. Red bone marrow was not assigned to any particular region, since it was spread over the three others.

As shown in Fig. 3, the highest equivalent doses (per treatment Gy) are delivered to organs/sites close to the treatment region (prostate). Note that the dose to red bone marrow is averaged over the whole body and therefore also includes regions close to the prostate. In Fig. 3, data are grouped per region, showing the head and neck (thyroid, brain and oesophagus), thorax (lungs, kidneys, liver, spleen, pancreas and stomach) and pelvis organs (small intestine and colon top; the bladder and bottom part of the colon are shown in Fig. 4).

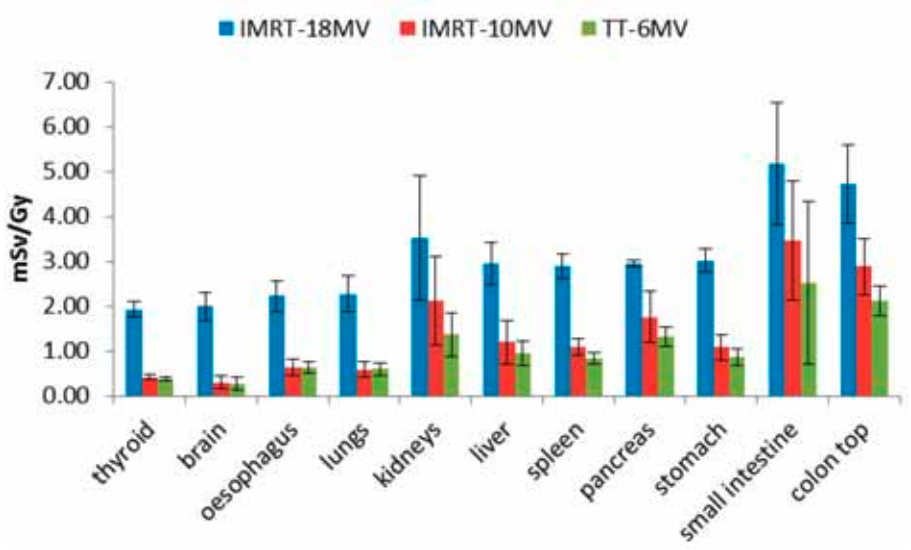

FIG. 3. Equivalent doses for photons for different peripheral organs.

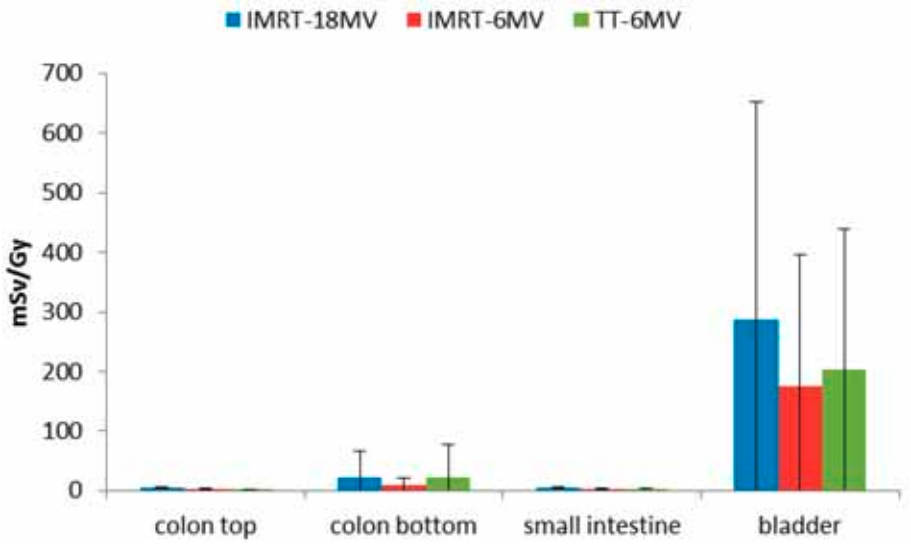

FIG. 4. Equivalent doses for photons in the pelvis region.

Table 1 shows the results obtained for the TLD measurements. Table 2 shows the average dose values, per region (head and neck, thorax and pelvis). Also, standard deviations are given per treatment technique. The mean values are obtained by averaging over the different TLD crystals, in each organ and/or each region. It can be observed that the highest equivalent doses are related to the 18 MV IMRT modality. This becomes particularly true at distances located further away from the treatment site (head and neck), where the lower energy modalities will experience a higher degree of attenuation. As seen in Fig. 3, in each of the organs/sites in the head and neck region (i.e. thyroid, brain and oesophagus), there is a significant difference between the 18, 10 and 6 MV doses. Also, a significantly higher dose, related to the 18 MV treatment, can be seen in most of the organs located in the thorax region. By contrast, 10 MV IMRT and 6 MV TT show very similar behaviour in terms of peripheral doses. The doses measured in the pelvis region (Fig. 4) are high due because part of the TLD was located very close to the irradiation volume. This also explains the large standard deviations in this region.

3.2. Neutron measurements

Figures 5 and 6 show the equivalent dose due to thermal and fast neutrons respectively, at 10 MV and 18MV. Neutron doses were measured using bubble

TABLE 1. EQUIVALENT DOSES (AND STANDARD DEVIATIONS) FOR PHOTONS FOR DIFFERENT ORGANS

mSv/Gy	18 MV	10 MV	6 MV-TT
Thyroid	1.93 ± 0.17	0.44 ± 0.06	0.38 ± 0.05
Stomach	3.01 ± 0.26	1.08 ± 0.30	0.86 ± 0.19
Colon top	4.72 ± 0.87	2.89 ± 0.63	2.12 ± 0.33
Colon bot.	21 ± 45	9 ± 11	22 ± 55
Lungs	2.27 ± 0.40	0.58 ± 0.17	0.60 ± 0.15
Kidneys	3.53 ± 1.39	2.12 ± 0.99	1.36 ± 0.49
Liver	2.94 ± 0.47	1.20 ± 0.48	0.95 ± 0.28
Oesophagus	2.23 ± 0.35	0.63 ± 0.19	0.63 ± 0.14
Spleen	2.89 ± 0.28	1.09 ± 0.19	0.84 ± 0.12
Red bone marrow	27 ± 86	31 ± 93	31 ± 94
Brain	2.00 ± 0.32	0.30 ± 0.15	0.27 ± 0.15
Small int.	5.18 ± 1.36	3.46 ± 1.33	2.52 ± 1.81
Pancreas	2.95 ± 0.07	1.76 ± 0.56	1.32 ± 0.21
Bladder	287 ± 363	175 ± 219	203 ± 234

TABLE 2. AVERAGE EQUIVALENT DOSE VALUES (AND STANDARD DEVIATIONS) IN THE DIFFERENT REGIONS

mSV/Gy	18 MV	10 MV	6 MV-TT
Head and neck	2.08 ± 0.32	0.47 ± 0.21	0.44 ± 0.20
Thorax	2.70 ± 0.71	1.02 ± 0.65	0.83 ± 0.35
Pelvis	83 ± 219	54 ± 137	66 ± 97

detectors, both for thermal (BDT) and fast neutrons (BD-PND). The bubble detectors were calibrated as explained in the previous section.

As can be seen, there is a much higher contribution of the neutrons to the total equivalent dose at 18 MV because of the higher energy of the primary photon beam and the resulting photo-neutron interaction.

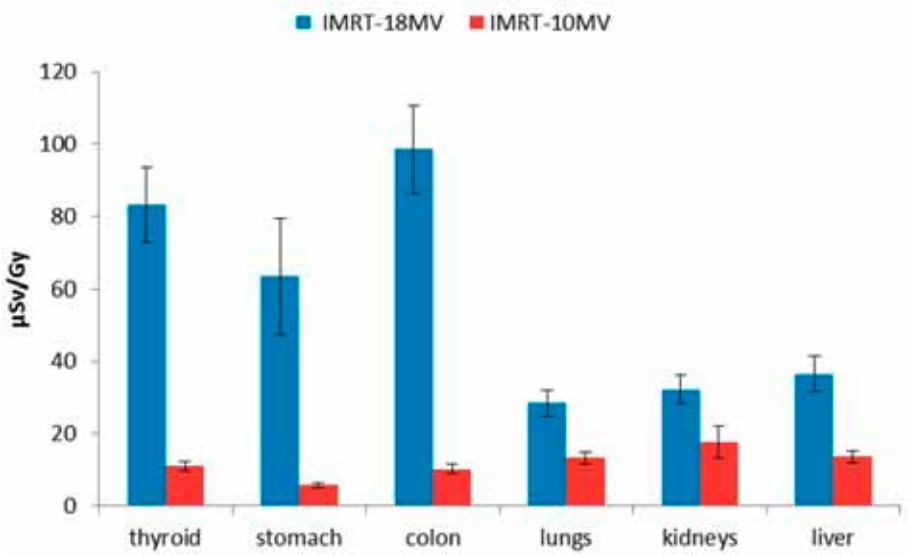

FIG. 5. Equivalent dose due to thermal neutrons.

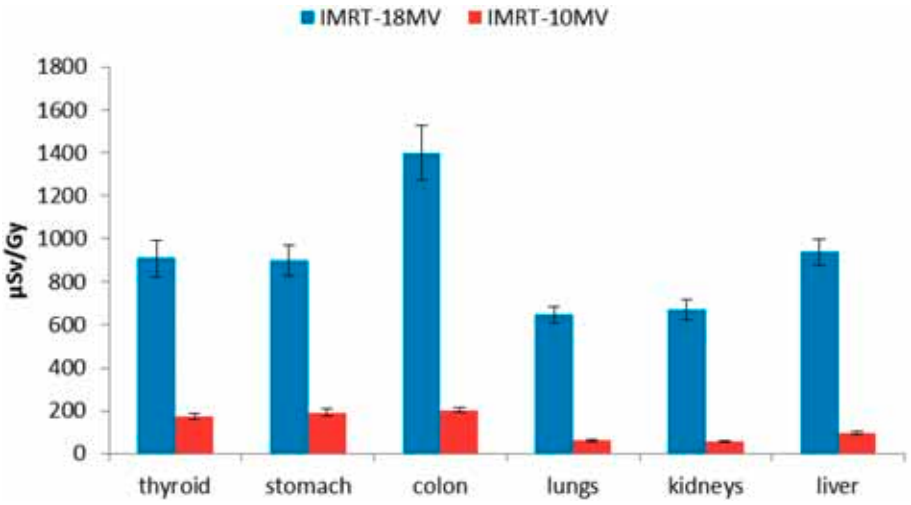

FIG. 6. Equivalent dose due to fast neutrons.

For organs distant from the irradiation field, such as the thyroid, we can see that a significant contribution to the peripheral dose comes from the neutrons, fast neutrons in particular. This is due to the important attenuation of the scattered photons, at such distances, especially at lower (10 MV) energies.

4. CONCLUSIONS

This paper presents preliminary results of a study designed to measure peripheral doses, in different organs, for two different treatment techniques at three different energies: IMRT (10 MV), IMRT (18MV) and TT (at 6 MV). The measurements were taken in two Belgian university hospitals, located in Louvain (IMRT) and Brussels (TT). For IMRT, at 10 MV and 18 MV, thermal and fast neutron doses were also measured. A common prostate treatment protocol was agreed and used by the two academic centres. The goal of this study is to compare, in terms of peripheral doses, how the different machines behave when facing the same dose constraints. In a second phase, each centre will define its own optimized treatment protocol and use it to irradiate the RA phantom. The results presented in this paper are related to the first phase of the study and include the measurement performed for the IMRT and the TT modalities.

As it has been shown, there are significantly higher photon doses related to 18 MV-IMRT, both in the head and in the thorax region. 10 MV-IMRT and TT show a similar behaviour in terms of peripheral doses. These results are in the same order of magnitude with organ doses found in the literature [4, 8].

Neutron doses (thermal and fast neutrons) were also monitored, for IMRT at 10 MV and 18 MV. The 18 MV treatment was characterized by a much higher neutron dose contribution to the total dose than the 10 MV. In particular, at distant organs (thyroid), there was a significant contribution, at 18 MV, of the (fast) neutrons doses to the total dose.

In the future, there are plans to extend the study by including a measurement on the Cyberknife. The authors also plan to complete the study by repeating the measurements where every clinical centre will use its own optimized protocol. In addition, the aim is to explicitly quantify the amount of dose that is due to the imaging used to position the phantom.

REFERENCES

[1] ALTHAR, B.S., et al., Neutron equivalent doses and associated lifetime cancer incidence risks for head & neck and spinal proton therapy, Physics in Medicine and Biology **54** (2009) 4907–4926.

[2] FONTENOT, J.D., et al., "Risk of secondary malignant neoplasms from proton therapy and intensity-modulated X-ray therapy for early-stage prostate cancer", Int. J. Radiation Oncology Biol. Phys. **74**(2) (2009) 616–622.

[3] HALL, E.J., et al., Radiation-induced second cancers: the impact of 3D-CRT and IMRT, Int. J. Radiation Oncology Biol. Phys. **56**(1) (2003) 83–88.

[4] KRY, F.S., et al., The calculated risk of fatal secondary malignancies from intensity-modulated radiation therapy, Int. J. Radiation Oncology Biol. Phys. **62(**4) (2005) 1195–1203.
[5] NEWHAUSER, D.W., et al., The risk of developing a second cancer after receiving craniospinal proton irradiation, Physics in Medicine and Biology **54**(2009) 2277–2291.
[6] SHARMA, D.S., et al., Estimation of radiation-induced carcinogenesis in adolescents with nasopharyngeal cancer treated using sliding window IMRT, Radiotherapy and Oncology **86** (2008) 177–181.
[7] XU, G.X., et al., A review of dosimetry studies on external-beam radiation treatment with respect to second cancer induction, Physics in Medicine and Biology **53**(2008) 193–241.
[8] VANHAVERE, F., et al., "Peripheral neutron and gamma doses in radiotherapy with an 18MV linear accelerator", Radiation Protection and Dosimetry **110**(1-4), (2004) 607–612.
[9] BALOG, J., et al., Helical tomotherapy radiation leakage and shielding considerations, Medical Physics **32**(3) (2005) 710–719.
[10] RAMSEY, C.R., et al., Out-of-field dosimetry measurements for a helical tomotherapy system, Journal of Applied Clinical Physics **7**(3) (2006) 1–11.

EVALUATION OF A COMMERCIAL 4-D DIODE ARRAY FOR HELICAL TOMOTHERAPY PLAN VERIFICATION

M. ZEVERINO, G. GIOVANNINI, G. TACCINI
Department of Medical Physics, National Institute for Cancer Research, Genoa, Italy
Email: Michele.zeverino@gmail.com

Abstract

The performance of a commercial 4-D diode array, the ArcCHECK (Sun Nuclear, FL, USA) has been tested for helical tomotherapy patient-specific quality assurance (QA). Seventeen helical tomotherapy plans were selected representing a variety of tumour sites. Agreement between measured and calculated dose distributions was assessed by evaluating the gamma index (γ) with criteria ranging from 2% dose differences or 2 mm distance to agreement (2%/2 mm) to 3%/3 mm. For a subset of plans, some delivery errors were voluntarily introduced in all the four rotational–translational directions to investigate the identification ability of the device. For a single plan point, dose comparison was carried out in the low dose gradient region in order to quantify the amount of dose deviation as a function of the absolute dose delivered. QA plans were also calculated and delivered to radiochromic films (GafChromic EBT2, ISP Corp., USA) within a cylindrical solid water phantom for comparison. For the 16 plans delivered, the mean percentage value of points with $\gamma < 1$ was 97.2% ± 2.2%, 94.2% ± 4.6%, 95.1% ± 3.8% and 90.8% ± 6.2% calculated with (3%/3 mm), (3%/2 mm), (2%/3 mm) and (2%/2 mm) criteria, respectively, demonstrating that the 4-D diode array can be used for rotational IMRT QA. Four of the 'wrong' measurements still had a good QA response showing a number of points >90% fulfilling $\gamma < 1$ calculated with the 3%/3 mm criterion. The number of 'false positives' decreased with tighter γ calculations (3%/2 mm and 2%/3 mm) and disappeared with 2%/2 mm. Point to point comparison showed a mean dose deviation of 1.2% ± 1.1%, 1.9% ± 1.6% and 2.1% ± 1.3% for low, medium and high dose regions, respectively. The mean percentage value of points with $\gamma < 1$ was 96.3% ± 3.3% and 91.4% ± 2.4% calculated with (3%/3 mm) for diode array and film dosimetry showing a consistent superiority of the device with respect to GafChromic film ($p < 0.05$).

1. INTRODUCTION

Intensity modulated radiation therapy (IMRT) involves the delivery of multiple beams at many angles around the patient with the aim to highly conform the dose distribution to the target while maintaining the dose to the adjacent normal structures as low as achievable. The desired fluence modulation is yielded by a computer controlled multileaf collimator whose leaves are able to sweep

across the radiation field. Submillimetre multileaf collimator positional errors may cause up to 20% dose error depending on the multileaf collimator gap width [1]. Helical tomotherapy is a particular IMRT delivery technique that simultaneously combines the motion of the binary multileaf collimator, the rotation of the gantry and the translation of the treatment couch in order to achieve the optimal dose distribution [2]. Such a complicated delivery technique requires a patient specific quality assurance (QA) programme that would allow assessing the correct beam delivery. In practice, the method of patient specific IMRT QA is to recalculate the dose distribution on a phantom that can host a detector, keeping the patient's plan properties unchanged. The calculated dose distribution is then compared to the measured dose distribution. Several detectors have been employed in such measurements ranging from 1-D (ionization chambers and diodes) to 2-D (radiographic and radiochromic films, detectors arrays) devices [3–5]. Although 2-D detector arrays offer the practical advantage of performing direct measurements (i.e. absence of typical post-processing of films), they exhibit significant angular dependency under rotational beams [6]. Recently, a new diode array (ArcCHECK, Sun Nuclear Corporation, Melbourne, FL, USA) was specifically developed for rotational therapy QA by arranging diodes on a cylindrical plane.

The purpose of this study is to evaluate the performance of the ArcCHECK device for helical tomotherapy plan verification; 16 helical tomotherapy plans representative of various tumour sites were used. Furthermore, the capability of the device in the detection of delivery errors was investigated as well as its accuracy in the determination of the absolute dose. Some selected QA plans were also measured by means of radiochromic films (GafChromic EBT2, ISP Corp, USA) for comparison.

2. MATERIALS AND METHODS

The ArcCHECK diode array consists of 1386 diodes of 0.8 mm × 0.8 mm geometrically arranged on 21 adjacent rings spaced 1 cm apart. Detector spacing is 1 cm, and each ring is rotated by 1 cm with respect to the neighbouring rings, creating a helical grid distribution of diodes which maximizes the number of non-overlapping detectors seen from a beam eye's view (BEV) perspective. The detector grid is embedded in a hollow PMMA cylinder with a 15 cm inner diameter and a 21 cm outer diameter, at a physical depth of 29 mm, corresponding to a water equivalent depth of 32.8 mm. The signal is updated every 50 ms allowing dose to time synchronization analysis [7].

The initial calibration of the device required two steps:

(i) The array calibration, which measured the differences in relative sensitivity between the detectors;
(ii) The absolute dose calibration, which assigns a known dose value to each detector corrected for its sensitivity.

Since the array calibration was provided by the vendor, the authors were limited to calibrate the device in terms of absolute dose. For this purpose, the centre of the cylinder was placed at the isocentre of a linac (Clinac 2100 C/D, Varian Medical Systems, Palo Alto, CA) for a resulting SDD of 86.27 cm and irradiated with a 6 MV, 5 cm × 5 cm field size. The exact dose value was measured using a farmer type ionization chamber positioned at the same depth of the diodes (e.g. 32.8 mm) in solid water.

CT images of the ArcCHECK were made with an 8 slice CT scanner (GE Light Speed, GE HealthCare) using 3 mm of slice thickness. Radio-opaque markers were placed at the projections of the cylindrical centre on the surface of the device for its alignment.

Dose calculations were done with the QA package included in the tomotherapy treatment planning system with a grid resolution of 2 mm. For each QA plan the ArcCHECK was placed with its centre at the isocentre of the treatment unit. The whole 3-D planned dose distribution was exported via DICOM RT and imported on the ArcCHECK software. Once the RT PLAN and RT DOSE files were loaded, the software extracted the dose plane corresponding to the detectors plane.

Sixteen plans designed for head and neck, prostate, breast and brain malignancies were calculated and then delivered to the device. Agreement between measured and calculated dose distributions was assessed by evaluating the gamma index (γ) with criteria ranging from 2% dose differences or 2 mm distance to agreement (2%/2 mm) to 3%/3 mm in order to explore the potential and the limitations of the system.

For a limited number of plans (one head and neck, one prostate and one breast), some delivery errors were voluntarily introduced in all the four rotational–translational directions by moving the device from its correct alignment prior the irradiation to investigate its identification ability [8]. Each QA plan was delivered five times: once with no shifts or rotation applied; three times with the displacements of 3 mm applied in every direction; and once with the rotation of 3° applied to the gantry, obtaining a set of 12 different measurements. Each ‘wrong’ measurement was compared to the correct one in terms of amount of points passing the γ calculation.

For one plan (a breast case), the measurement points were compared to the calculated points in low dose gradient region to quantify the amount of dose deviation as a function of the absolute (low, medium and high) dose delivered. A low dose gradient point was identified when all the surrounding calculation points lying within a square of 3 mm × 3 mm showed a dose variation of less than 5%.

Finally, for a subset of plans, QA results obtained with the diode array were compared to those obtained with radiochromic film dosimetry, although measurements were not strictly related with each other due to the different geometries of the detectors.

All ArcCHECK measurements were made in absolute dose mode using the absolute dose calibration previously described.

3. RESULTS

For the 17 plans delivered, the mean percentage value of points with $\gamma < 1$ was 97.2% ± 2.2%, 94.2% ± 4.6%, 95.1% ± 3.8% and 90.8% ± 6.2% calculated with 3%/3 mm, 3%/2 mm, 2%/3 mm and 2%/2 mm criteria, respectively. Results of the γ analysis listed by tumour site are given in Table 1. For the 12 'wrong' measurements, four of them still had a good QA response showing a number of points >90% fulfilling $\gamma < 1$ calculated with (3%/3 mm) criteria. The number of 'false positives' decreased with tighter γ calculations (3%/2 mm and 2%/3 mm) and disappeared with 2%/2 mm. Delivery errors in the X direction were more prone to give false positive with respect to all other shifts or rotations as illustrated in Table 2. An example of γ deterioration with the introduction of a rotation of 3° is given in Fig. 1 for a prostate plan. Point to point comparison carried out in low dose gradient regions showed a mean dose deviation of 1.2% ± 1.1%, 1.9% ± 1.6% and 2.1% ± 1.3% for low, medium and high dose regions, respectively. For the subset of five plans, the mean percentage value of points with $\gamma < 1$ was 96.3% ± 3.3% and 91.4% ± 2.4% calculated with (3%/3 mm) for diode array and film dosimetry, respectively.

4. DISCUSSION

Excellent agreement between measured and calculated dose was observed with (3%/3 mm) criteria, demonstrating that the 4-D diode array can be used for rotational IMRT QA. Analysis carried out with a tighter γ criteria still yielded acceptable results, showing a slight trend for better outcomes with (2%/3 mm) than with (3%/2 mm). As a consequence, the absolute dose calibration should be

TABLE 1. MEAN PERCENTAGE OF PASSING POINTS LISTED BY TUMOUR SITE OPTIMAL RESULTS FOR BONE METASTASIS WERE DUE TO THE LOW GRADE OF COMPLEXITY OF THE DOSE DISTRIBUTION

Tumour site (*n*)	γ (3%/3 mm)	γ (3%/2 mm)	γ (2%/3 mm)	γ (2%/2 mm)
	Mean percentage of passing points			
Brain (5)	98.0	93.4	97.2	91.7
Head and neck (3)	95.8	92.9	92.4	87.4
Breast (3)	94.7	93.2	90.9	87.5
Pelvis (2)	97.8	93.5	95.4	88.2
Bone metastasis (2)	99.9	99.9	99.9	99.9
Anal canal (1)	97.3	95.9	97.3	95.9
Ocular region (1)	97.5	93.3	93.5	88.3
Total (17)	97.2 (2.2)	94.2 (4.6)	95.1 (3.8)	90.8 (6.2)

TABLE 2. PERCENTAGE OF POINTS WITH Γ < 1 (AVERAGED OVER THE THREE PLANS) WITH THE INTRODUCTION OF THE DELIVERY ERRORS *(percentage of passing points greater than 85% may be regarded as 'false positive')*

	No errors	3 mm X	3 mm Y	3 mm Z	3° rotation
Mean % passing points			γ (3%/3 mm)		
	97.8%	91.3%	88.6%	85.9%	82.6%
			γ (3%/2 mm)		
	96.5%	88.0%	83.5%	84.8%	77.4%
			γ (2%/3 mm)		
	95.8%	84.9%	81.3%	78.8%	74.4%
			γ (2%/2 mm)		
	92.7%	79.2%	73.3%	71.9%	66.0%

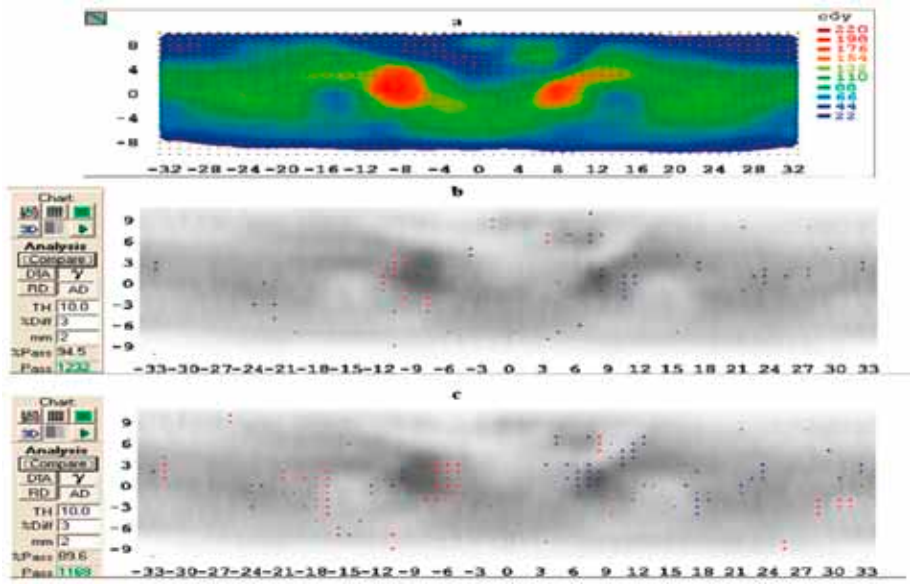

FIG. 1. γ analysis for a prostate case with 3%/2 mm criteria: (a) planned dose distribution, (b) γ analysis for the comparison with the correct measurement, note that passing rate was 94.5%, (c) γ analysis for the comparison with the 'wrong' measurement having 3° of gantry rotation. Note that the passing rate decreased to 89.6%.

carefully performed in terms of its accuracy. The treatments plans used in this work had different sonograms, indicating that the radiation entered the device from different directions as well. For instance, a head and neckplan has its fluence entering the patient more evenly spaced in the solid angle in respect to a breast plan. The optimal outcomes carried out for all the various QA plans suggested a negligible angular dependency of the diodes under the TomoTherapy beam.

Results arising from the delivery error analysis pointed out the detection ability of the device indicated by the lowering of the percentage of passing points. Nevertheless, in some cases, γ analysis was still considered acceptable, giving rise to 'false positive' measurements. In order to reduce such 'false positive' results, it may be convenient either to increase the threshold of passing points or to perform γ evaluation using a tighter criterion. The solution adopted as standard for patient specific QA by the authors involved the successful outcome of both thresholds: 97% of passing points with γ (3%/3 mm) and 90% of passing points with γ (2%/2 mm). Point dose comparison in low dose gradient region confirmed the ability of the detectors to measure absolute dose accurately within a range of 2% independently from the dose value. The γ evaluation showed a consistent

superiority of the diode array with respect to GafChromic ($p < 0.05$), suggesting that the former may represent an alternative to film dosimetry in IMRT QA tasks.

REFERENCES

[1] LOSASSO, T., CHUI, C.S., LING, C.C., Physical and Dosimetric Aspects of a Multileaf Collimation System Used in the Dynamic Mode for Implementing Intensity Modulated Radiotherapy, Medical Physics, Vol. 25, No. 10 (1998) 1919–1927.

[2] MACKIE, T.R., HOLMES, T., SWERDLOFF, S., RECKWERDT, P., DEASY, J.O., YANG, J., PALIWAL, B., KINSELLA, T., Tomotherapy: A New Concept for the Delivery of Dynamical Conformal Radiotherapy, Medical Physics, Vol. 20, No.6 |(1993) 1709–1719..

[3] JU, S.G., AHN, Y.C., HUH, S.J., YEO, I.J., Film Dosimetry for Intensity Modulated Radiation Therapy: Dosimetric Evaluation, Medical Physics, Vol. 29, No.3 (2002) 351–355.

[4] BUCCIOLINI, M., BANCI BUONAMICI, F., CASATI, M., Verification of IMRT Fields by Film Dosimetry, Medical Physics, Vol. 31, No.1 (2004) 161–168.

[5] EVIC, S., SEUNTJENS, J., SHAM, E., PODGORSAK, E.B., Precise Radiochromic Film Dosimetry using a Flat-Bed Document Scanner, Medical Physics, Vol. 32, No.7 (2005) 2245–2253..

[6] JURSINIC, P.A., SHARMA, R., REUTER, J., MapCHECK used for Rotational IMRT Measurements: Step-and-Shoot, Tomotherapy, RapidArc, Medical Physics, Vol. 37, No. 6 (2010) 2837–2846.

[7] LETOURNEAU, D., PUBLICOVER, J., KOZELKA, J., MOSELEY, D.J., JAFFRAY, D.A., Novel Dosimetric Phantom for Quality Assurance of Volumetric Modulated Arc Therapy, Medical Physics, Vol. 36, No.5 (2009) 1813–1821.

[8] BANCI BUONAMICI, F., COMPAGNUCCI, A., MARRAZZO, L., RUSSO, S., BUCCIOLINI, M., An Intercomparison between Film Dosimetry and Diode Matrix for IMRT Quality Assurance, Medical Physics, Vol. 34, No.4 (2007) 1372–1379.

INTERNAL DOSIMETRY FOR DIAGNOSTIC AND THERAPEUTIC NUCLEAR MEDICINE

(Session 6)

Chairpersons

M. LJUNGBERG
Sweden

W. BOLCH
International Commission on Radiological Protection

Co-Chairpersons

G. SGOUROS
Society of Nuclear Medicine

S. PALM
IAEA

GOOD PRACTICE OF CLINICAL DOSIMETRY REPORTING[1]

M. LASSMANN
Department of Nuclear Medicine,
University of Würzburg, Germany
Email: lassmann_m@klinik.uni-wuerzburg.de

C. CHIESA
Nuclear Medicine Unit, IRCCS Istituto Nazionale dei Tumori Foundation,
Milan, Italy

G. FLUX
Joint Department of Physics,
Royal Marsden Hospital & Institute of Cancer Research,
London, United Kingdom

M. BARDIÈS
Institut national de la santé et de la recherche médicale,
Nantes, France

Abstract

The intention of the guidance of this paper, Good Practice of Clinical Dosimetry Reporting, by the Dosimetry Committee of the European Association for Nuclear Medicine, is to guide the reader through a series of suggestions for reporting dosimetric approaches in nuclear medicine.

1. INTRODUCTION

A number of recent publications in nuclear medicine contain data on dosimetric findings for existing or new, diagnostic or therapeutic agents. In many of these articles, however, the description of the methodology applied for dosimetry is lacking or omits important details. In such a situation, it is very

[1] This paper is reproduced by courtesy of the European Association of Nuclear Medicine.

difficult to assess the reliability of the data presented, which could also prevent other scientists from reproducing or improving previously published results.

The Dosimetry Committee of the European Association for Nuclear Medicine (EANM) has recently released a guidance document on Good Practice of Clinical Dosimetry Reporting [1] (see also www.eanm.org). The authors' intention is to guide the user through a series of suggestions for reporting dosimetric approaches in nuclear medicine. At present, there are few guidelines regarding optimal practice of internal dosimetry and methods can vary widely. The validity of the results obtained from such a dosimetry study is dependent on the rigour and integrity with which such a study is reported.

The items addressed in this guidance document could also be used as a checklist by reviewers of manuscripts submitted to scientific journals or grant applications. In addition, it could be used to decide which data are useful for a documentation of dosimetry results in individual patient records.

1.1. Suggested documentation

(a) Equipment:
This includes, but is not limited to, the description of all equipment used for the study and the appropriate quality control measures taken.

(b) Image quantification:
This includes acquisition settings and the corrections performed (e.g. attenuation, scatter, dead time, reconstruction parameters for SPECT or PET, background subtraction) in addition to the calibration of all devices used.

(c) Biokinetics:
The number of data points per patient needs to be documented as well as the integration and fitting procedure of the time–activity curves. The way the data are extrapolated before the first and after the last measured data point also needs to be documented.

(d) Dosimetry calculations:
All the steps leading to a final calculation of the absorbed dose should be given for individual patients. If results are expressed in Gy/GBq, then the injected activity should also be reported. Care should be taken that the significant numbers of digits in the resulting values for absorbed doses do not exceed the errors of the underlying process. If possible, errors margins including the results of a propagation of error calculation should be included.

(e) Miscellaneous items:
In some cases confounding factors such as the use of recombinant human TSH in the case of differentiated thyroid cancer or renal protection agents (e.g. sometimes used during treatments with radiolabelled peptides) might alter the biokinetics of a given radiopharmaceutical. This information should be provided.

2. CONCLUSION

The set of recommendations given by the EANM dosimetry committee for reporting dosimetric methods and results [1] provides a comprehensive overview on the acquisition and processing of images quantitatively for dosimetric purposes and on the subsequent steps needed for a proper dosimetric assessment of nuclear medicine diagnostic and therapeutic agents. In addition, a downloadable checklist is provided as an appendix. This document and the corresponding checklist will guide the authors of reports and publications through the necessary steps so that the reproducibility of the results will be warranted; it will enable other researchers to use such information for expansion and possible improvements.

ACKNOWLEDGEMENTS

This work was developed under the supervision of the Dosimetry Committee of the EANM (K. Bacher, M. Bardiès, C. Chiesa, G. Flux, M. Konijnenberg, M. Lassmann, S. Palm (Observer for the IAEA), S.-E. Strand, L. Strigari).

REFERENCE

[1] LASSMANN, M., CHIESA, C., FLUX, G., BARDIES, M., EANM Dosimetry Committee guidance document: good practice of clinical dosimetry reporting, Eur. J. Nucl. Med. Mol. Imaging **38** (2011) 192–200.

IMAGE BASED PATIENT SPECIFIC DOSIMETRY FOR RADIONUCLIDE THERAPY

M. LJUNGBERG, K. SJÖGREEN-GLEISNER
Department of Medical Radiation Physics,
Clinical Sciences,
Lund University,
Lund, Sweden

Abstract

Therapy with radiolabelled pharmaceuticals is a systemic treatment where the absorbed dose is delivered by internally distributed radionuclides that emit electrons or α particles. Absorbed dose calculation for radionuclide therapy is a real challenge due to technical and physical limitations in the imaging process together with a physiologically governed distribution and redistribution over time. Practical issues regarding the number of measurements and patient mobility may also limit the accuracy. This paper discusses the most important factors needed to consider for patient specific image based 2-D and 3-D dosimetry.

1. INTRODUCTION

The prognosis of achieving long time remission for disseminated cancer disease is in many cases poor. A systemic treatment is often required, and treatment with radiolabelled pharmaceuticals, 'radionuclide therapy', is such a systemic treatment. Treatment of thyroid cancer with [^{131}I]-NaI is perhaps the most common targeted radionuclide therapy, which has been practised for many years. It is an effective procedure that reduces the risk of recurrence, curing a significant fraction of patients with metastatic thyroid cancer. Targeted therapies are also used to reduce severe pain in metastatic bone disease. Radionuclides successfully used in this application are ^{153}Sm, ^{186}Re and ^{89}Sr. Non-Hodgkin's lymphoma is a tumour disease with increasing incidence, which today is treated by radiolabelled antibodies expressed to the antigen CD20 on tumour cells. Approved commercial antibodies are Zevalin™ (^{90}Y) and Bexxar™ (^{131}I).

In radionuclide therapy, the absorbed dose is delivered by administration of suitable radionuclides that emit either electrons or α particles. It is assumed that the released kinetic energy is transferred by charged particle interactions to sensitive parts of the cells for activation of cell death. An accurate dosimetry is important because of radiopharmaceutical uptake in normal tissues and organs. However, absorbed dose planning for radionuclide therapy is a real challenge in

that the radionuclide source cannot be turned on or off as in external beam therapy; instead it decays exponentially. On a small scale level, the radiopharmaceutical will generally be heterogeneously distributed meaning that the energy deposition is non-uniform. Since the biokinetics is dynamic, several activity measurements need to be taken to estimate the amount of energy released in an organ or tumour. Measurement can be made by sequential planar scintillation camera measurements or by SPECT. The spatial resolution of scintillation cameras is about 10–15 mm, depending on the source location and radionuclide characteristics, which puts a limit on the detail in the spatial information obtained. The system sensitivity (cps/MBq) is another factor that, together with the acquisition time, will influence on the image noise characteristics. Practical issues regarding the number of measurements and patient mobility may thus also limit the accuracy in the calculation of the activity. Since the treatment is systemic, circulating activity may result in unnecessary absorbed doses to normal organs and tissues. Often, this puts a limit on the activity that can be administered and is one of the major reasons for the need of an accurate patient specific dosimetry. The dose rate for radionuclide therapy is much lower than in external beam therapy, and currently, an increasing number of dosimetry studies are incorporating the calculation of the biologically effective dose for ‘coupling’ to the biological effects obtained.

2. 2-D IMAGE BASED DOSIMETRY

Dosimetry using 2-D planar imaging based activity quantification has been used for many years. In a planar acquisition, the source depth in the patient is not resolved, which requires several approximate correction methods that will be described below. Despite these drawbacks, the conjugate view method has been the major choice for many dosimetric studies, mainly due to its simplicity in implementation.

2.1. Activity quantification

The most commonly employed method for obtaining quantitative measures of the activity and the residence time of organs from planar images is the conjugate view approach, in which the geometric mean is applied to 180° opposed projections, often acquired anterior–posterior. In its original formulation [1, 2], the method addresses the quantification of one or several rod sources oriented along one projection line. It is assumed that the projections are acquired in narrow beam geometry without inclusion of counts due to scatter in the patient, collimator or in the crystal. Under these circumstances, the geometric mean

gives: (a) a count rate that is independent of the source position along the projection line, (b) attenuation in the medium that can be described as the attenuation through the total patient thickness and (c) self-attenuation in the source that can be described as a function of the source extension. After applying the geometric mean and attenuation correction, division by the acquisition time and the system sensitivity will give the activity.

The implementation of the conjugate view technique includes the drawing of regions of interest (ROIs) in the images, to outline the tissues that are of interest for quantification. Often, the ROIs are defined in the raw anterior–posterior count rate images and then the respective corrections are applied. The quantification can also be performed in image space on a pixel by pixel basis, and then delineating ROIs in the resulting quantified image. The strategy used (ROI based or pixel based) has implications for the choice of correction methods, which will be discussed below.

For ROI based quantification, some studies use the first anterior–posterior count rate images, acquired pre-voiding, to determine an effective sensitivity as the ratio of the geometric mean of the count rates in an organ ROI, by the administered activity. This effective sensitivity is then assumed to implicitly include corrections for attenuation and scatter. However, such an approach does not account for the variations in the correction parameters due to redistribution of the radionuclide over time. Explicit estimations of the system sensitivity, the attenuation and scatter are preferable. The system sensitivity is experimentally determined for the camera system and energy window settings. The attenuation correction is the most important correction, as it reaches factors of 2–3 for many radionuclides. Two parameters need to be determined: the patient thickness at the location of the source, and the attenuation coefficient representing the attenuation for the patient composition along the projection line. Using a computed tomography (CT) image, the patient thickness can be measured and a representative attenuation coefficient estimated. The attenuation can also be measured by use of two transmission studies, with and without the patient in position, where the ratio between these two images describes the attenuation. The transmission measurements can be performed by utilizing an external radionuclide flood source or using an X ray CT scout [3]. In both cases, the measured attenuation must be rescaled from the transmission energy to the energy of the radionuclide. The transmission imaging approach allows for a pixel based quantification scheme, assuming that the attenuation map and the anterior–posterior images can be spatially registered. Pixel based correction may be advantageous in cases where the attenuation distribution is heterogeneous and thus difficult to represent by one value, such as for the lungs, or when the body thickness varies over the region.

A commonly applied method for scatter correction is to use an effective attenuation coefficient in the attenuation correction, with a value lower than the linear attenuation coefficient [4], which can also be described as a buildup factor [5]. The effective value is determined in phantom studies prior to application, for the radionuclide and the camera settings. This approach implicitly assumes that the scatter distribution is equivalent to the distribution of the measured counts. Another common method, that allows for assessment of the scatter distribution, is to use additional scatter energy windows in the acquisition, just beside the photopeak window [6, 7]. The measured scatter count rate is scaled to the width of the photopeak window, and subtracted from the photopeak counts. Noise may be a problem if a pixel based quantification scheme is used, since the scatter windows can be narrow. Model based approaches to scatter correction have also been applied, where deconvolution of the count rate images is applied using scatter point spread functions [8, 9]. These describe the total-to-primary ratio and the distribution of scatter, and may be determined using Monte Carlo simulation. The self-attenuation of the source induces an overestimate of the activity. The overestimate increases for increasing source thicknesses and for lower radionuclide emission energies. Most organs in the body have an average thickness in the anterior–posterior direction of 3–10 cm, giving an overestimate of about 1–8% for ^{111}In (245 keV). For ^{90}Y bremsstrahlung imaging using an energy window centred at 150 keV, effects interpreted as being related to the self-attenuation were obtained for the assessment of the total body activity, where overestimates of around 10% were obtained [9].

Overlap of activity from the background and adjacent tissues is a major factor whose magnitude depends on the distribution of the radiopharmaceutical. ‘Background’ refers to radionuclide concentration in blood or extracellular fluid, whereas ‘overlap’ refers to the activity in tissue with a radionuclide uptake that is superimposed on the tissue of interest in the image. Methods for correction of overlap and background activity have been extensively described in Ref. [5]. Background correction is generally performed by measuring the activity of a small region adjacent to the organ of interest, observing that the patient thickness should be equivalent. The background contribution is then estimated by scaling the background count density (count/pixel) to the number of pixels in the organ ROI. If possible, the background correction should be scaled to account for the thickness of the background compartment in the organ ROI, so that the volume occupied by the organ itself is not included in the background. In case of overlap, the overlapped part of the organ ROI should be treated separately. The activity residing in the overlapped part could be estimated by extrapolation from the count density in the non-overlapped part, or, if the organ that causes the overlap has already been quantified, the count density that is assumed to belong to this organ can be subtracted [8].

In addition to the conjugate view technique, planar image quantification can also be performed by using the 2-D and 3-D methods [10]. The organs of interest are delineated in a CT image and nominal activity values assigned to organ volumes. The resulting 3-D activity distribution is projected in the anterior–posterior directions. The organ activities are then determined iteratively by comparison of the calculated projections and the measured ones, assuming that they are spatially registered. The problem of overlap and background activity is thus elegantly circumvented.

2.2. Calculation of the cumulated activity

Patient imaging is performed at several times after administration to follow the radiopharmaceutical redistribution over time. At each time, the activity in the organs-of-interest is determined, giving series of time–activity data for each organ. If image registration is available, the images from all times can be spatially registered thus allowing for one single set of ROIs to be used for analysis [11]; otherwise, ROIs must be drawn for each imaging time. Curve fitting is applied to the time–activity data, often using a sum of exponential functions with the number of terms depending on the biokinetics and the number of data points available. The cumulated activity (MBq·h) is then determined as the area under the curve for each organ.

2.3. Absorbed dose calculation

Absorbed dose calculation in 2-D imaging is based on precalculated organ dose factors, ‘S values’, calculated by Monte Carlo simulation of the particle transport in a computer phantom. The S values describe the absorbed dose in a target volume per unit of cumulated activity in the source organ and are expressed in unit of $Gy \cdot MBq^{-1} \cdot h^{-1}$. The Olinda software [12] includes a large database of S values and a biokinetics module, with a user-friendly interface.

Most phantoms are geometrically stylized using mathematical shapes for representation of organs, and have been developed for estimating the risk of late effects for large populations. Therefore, they are probably not representative for a particular patient geometry. Nevertheless, owing to the lack of depth information in 2-D imaging, the use of precalculated S value has been a practical alternative. It is possible, to some degree, to scale the S values to better represent the individual patient. Scaling by the ratio of the total body weight of the phantom and the patient is the simplest solution but may be inaccurate since it scales all organs by the same fraction. A better way is to scale by the patient specific organ mass. This requires a determination of the organ mass from an anatomical CT image. In the near future, S values for more realistic phantom geometries will be

available, which will make 2-D dosimetry somewhat more accurate since the phantoms are more representative of the human anatomy [13].

3. 3-D IMAGE BASED DOSIMETRY

Although many planar quantification methods today are quite sophisticated the inherent problem with the lack of depth information remains. By use of tomographic methods such as SPECT and in some case PET, 3-D information is obtained as where each slice represents a section through the patient. Correction for various physical effects is more straightforward and can be included in the reconstruction software. Today, most quantification methods are based on the iterative MLEM algorithm. This method starts with an initial guess of a 3-D activity distribution. The algorithm includes a model of the image process for calculation of projection from the first initial guess (forward projector). In its simplest form, the model assumes straight lines to calculate the projection. The measured projection is then compared with the calculated projections by calculating the quota. This error projection is then back projected for all angles to create an error image that is multiplied with the initial image to obtain a better estimate of the radionuclide distribution (the update). This is repeated until the change in the estimated image is sufficiently low. The OSEM method [14] is very similar to MLEM except that the update is made after a subset of projections making the estimated SPECT image to converge much faster than the MLEM method.

3.1. Activity quantification

Correction for (a) non-homogeneous photon attenuation, (b) contribution to events in the image from photons that have been scattered in the patient and therefore appear at wrong positions, and (c) loss of spatial resolution due to the collimator design are necessary factors to consider in quantitative SPECT [15]. In an iterative reconstruction method, these corrections are made naturally if one can model these effects in the forward projector. Non-homogeneous attenuation correction is today best made by using a SPECT/CT system where an anatomical CT image registered to the SPECT image by hardware design can be obtained. Although CT data are produced from an X ray spectrum, it is possible to convert them into a specific discrete energy with sufficient accuracy. The CT images have a high spatial resolution and signal-to-noise ratio. The correction for scatter is somewhat difficult and several methods have been proposed. These methods are often based on multiple energy window acquisitions or on analytical models. A

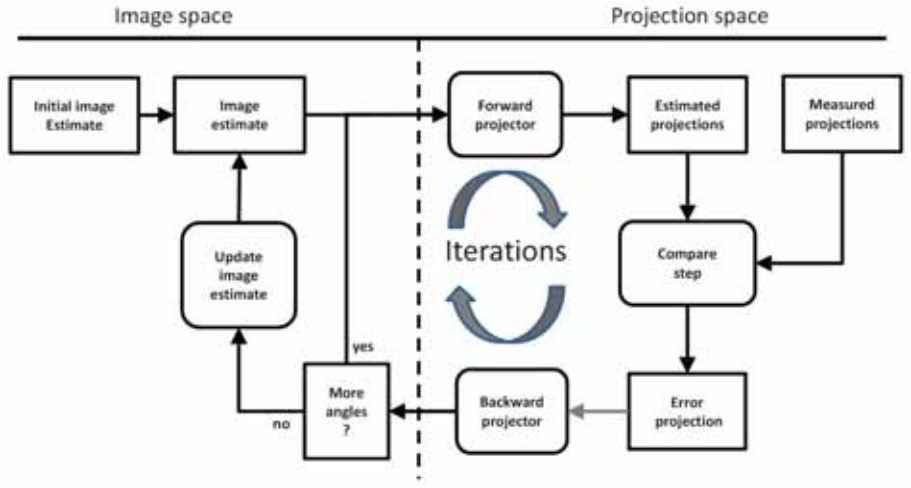

FIG. 1. The principal steps of an iterative reconstruction. The forward projector mimics the imaging process as close as possible. The difference in the various iterative methods often lies in how the comparison is made and how the error projections are calculated.

scatter estimate from a scatter window method, e.g. the triple energy window method [7], can be subtracted from the projection data prior to image reconstruction but this increases the noise and may produce negative counts. In an iterative reconstruction the scatter can be included in the forward projector as an additive component resulting in better noise characteristics. The ESSE method [16] is a model based compensation method that uses the precalculated scatter function to model scatter in the forward projector. Collimator resolution compensation can be included in the forward projector modelling the acceptance angle of the collimator holes as a distance dependent Gaussian function or, when septal penetration occurs, using tables of Monte Carlo simulated distance dependent point spread functions.

3.2. Calculation of the cumulated activity

Similar to planar based methods of calculating the cumulated activity in organs, patient imaging is performed at several times after administration. The time series of images can then be analysed by determining the activity in the whole organ by drawing volumes of interest (VOIs) in the quantified image from each time, and then by curve fitting determining the cumulated activity. If image registration is available, the time series can be spatially registered, allowing for one set of VOIs to be used for all imaging times. An advantage with combined

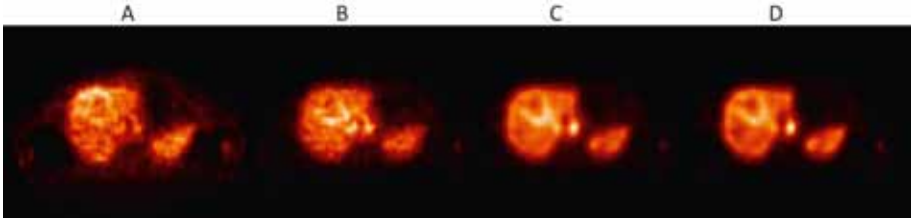

FIG. 2. An example of an SPECT study with ^{111}In-labelled antibodies distributed in the liver. The images shown from the left are (A) an uncorrected image, (B) correction for attenuation, (C) correction of attenuation and collimator response and (D) correction for attenuation, scatter (ESSE) and collimator response. All images are reconstructed using an OSEM algorithm with six iterations and six angles per subset.

SPECT/CT is that the image registration can be performed via the more detailed CT images, to determine a spatial transformation that is applied for fusion of the SPECT images [17]. For spatially registered time series of images, the calculation of the cumulated activity can also be performed on the level of each voxel, using trapezoid integration or voxel based curve fitting.

Hybrid SPECT/planar imaging has been suggested as an option when multiple SPECT/CT studies on many time points are not possible. The hybrid method combines the superior quantification accuracy of SPECT and the biokinetic information obtained from planar imaging. One SPECT study is used to determine the activity in VOIs at one time point. This is then used to normalize a time–activity curve obtained from sequential planar image based activity quantification [18].

3.3. Absorbed dose calculations

Image based absorbed dose calculations from a quantitative SPECT image can be made by: (a) assuming that released energy is locally absorbed within the voxel, (b) convolution methods with precalculated dose kernels that describe spatially the energy deposition in a uniform media from a point source, or (c) implementing a full Monte Carlo calculation using quantitative SPECT images and registered CT images to calculate the trajectories from each individual particle and score the release of energy in the voxels until particle termination. The advantage of Monte Carlo simulations compared to convolution methods is that non-homogeneities and boundaries are included in the calculation. Combined SPECT/CT studies also allow for an accurate 3-D absorbed dose calculation in that the distribution of voxel masses in the patient can be determined from the co-registered CT study. An advantage using SPECT

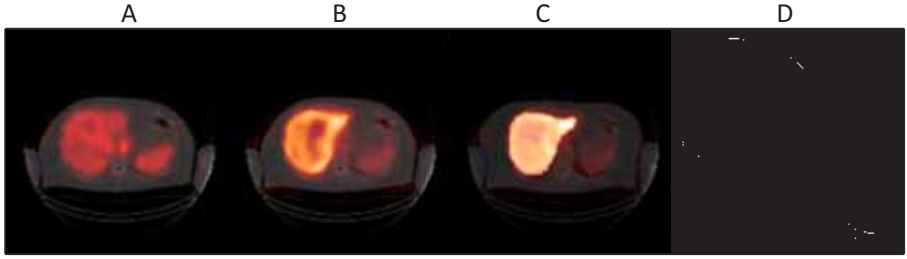

FIG. 3. This figure shows (A) the absorbed dose rate distribution for the first time point, (B) the absorbed dose distribution obtained by voxel-by-voxel integration, and (C) the region of interested for the current slice, from which (D), the integral dose–volume histogram, has been calculated.

imaging is also that absorbed dose calculations are performed on a voxel level, which reduces the need for accurate organ delineation and problems due to partial volume effects. Voxel based representations of the absorbed dose gives improved possibilities for the visualization of the absorbed dose distribution and for quantitative analysis using dose–volume histograms of target tissues and organs at risk.

4. RADIOBIOLOGICAL CONSIDERATIONS

The biologically effective dose (BED) is extensively used in external beam therapy and brachytherapy to describe the dependence of the rate of cell death (or cell repair) for different fractionation schemes and dose rates. Basically, BED can be described as the product of the physical dose (in Gy) and a relative effectiveness factor [19]. The latter is a function of the radiobiological tissue dependent parameters α/β, the rate constant for repair and the dose rate. In radionuclide therapy, the dose rate varies temporally and BED is then a useful quantity for comparison of radiation effects from different radionuclides, or other modalities [20]. A successful application of the BED was presented in kidney dosimetry for radiolabeled peptides [21]. Voxel based implementation of the BED has also been presented [22, 23], which then allows for BED maps to be visually interpreted. The equivalent uniform dose (EUD) is another radiobiological quantity, used mainly for comparison of different dose distributions in tumours [24]. In radionuclide therapy, the distribution of the absorbed dose is many times, for physiological reasons, heterogeneous. The EUD then gives the uniform biologically effective absorbed dose that would result in the same surviving fraction as the non-uniform biologically effective absorbed

dose, and has been applied, e.g. to SPECT/CT dosimetry for radiolabelled monoclonal antibodies [25].

5. EXAMPLES OF IMAGE BASED PATIENT SPECIFIC DOSIMETRY

Sgouros and Kolbert have developed the 3-D internal dosimetry programme called 3D-ID [26], which has been used for both human studies involving for example ^{131}I for thyroid cancer treatment [27] and for preclinical applications to calculate S values for dosimetry in mice [28]. Another comprehensive package for 3-D dosimetry is the RMDP developed by Guy et al. [29]. This program includes both quantitative SPECT methods and image registration and the dosimetry is calculated from β kernels or voxel S values. The imaging group at the Johns Hopkins University has been working extensively with patient specific imaged based dosimetry and methods for quantitative SPECT. Through mathematical simulations, they have evaluated the accuracy and precision for both 2-D and 3-D dosimetry procedures [30]. In recent works by Dewaraja et al., a fast Monte Carlo code [31] has been used to calculate energy deposits from both electrons and photons for accurate 3-D ^{131}I dosimetry [32]. Image quantification has been established with iterative reconstruction software that includes a full Monte Carlo simulation of the imaging process [33].

The authors developed the LundAdose Programme for dosimetry based on both 2-D and 3-D quantitative scintillation camera imaging. It is written in IDL and includes both an image reconstruction method with compensation for attenuation, scatter and collimator response [16] and a 3-D dosimetry programme using EGS4 based software based on SPECT and CT images. The authors have been involved in two clinical studies of ^{111}In/^{90}Y labelled antibodies. The first was for Non-Hodgkin's lymphoma patients that aimed to study parameters for an extracorporeal adsorption procedure [34]. Both multiple SPECT/CT and planar studies were made. In an ongoing myeloablative study including bone marrow support, the authors are performing dose planning to the secondary organ at risk, which is the liver. On the basis of a pretherapy study with ^{111}In labelled Zevalin™ the aim is to determine the necessary activity to obtain a particular absorbed dose to the liver. The dosimetry is based on seven consecutive SPECT/CT studies. From the quantitative ^{111}In SPECT images, spatially registered to each other over time by CT–CT image registration, the absorbed dose distribution is estimated for ^{90}Y by considering the differences in physical half-lives. The absorbed dose is calculated assuming local energy deposition since the range of the β particles from ^{90}Y is of the same order as the SPECT resolution. The study also includes a verification of the delivered absorbed dose by use of ^{90}Y bremsstrahlung imaging during therapy. The authors therefore developed methods for both 2-D

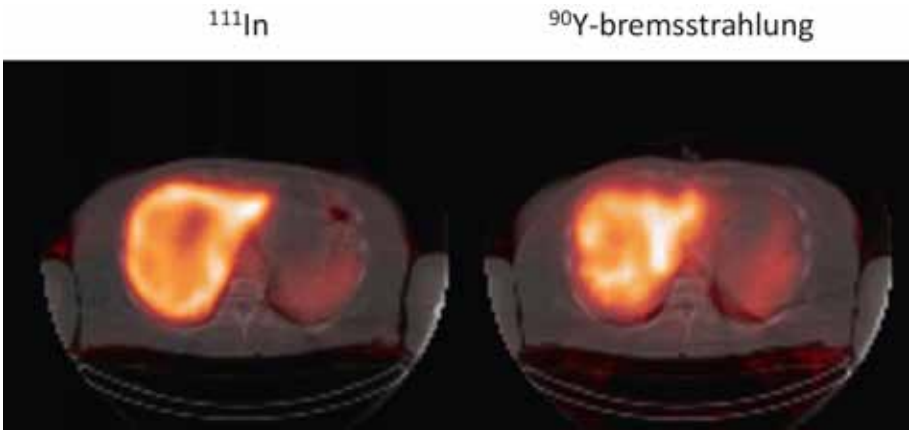

FIG. 4. Comparison between an absorbed dose ^{90}Y image as estimated from SPECT measurements of ^{111}In (left) and from SPECT measurements of ^{90}Y bremsstrahlung (right). Both images have been reconstructed using the same software but with different scatter (ESSE) and collimator kernels.

quantification [35] and 3-D SPECT quantifications [36] where both methods use Monte Carlo simulated predefined kernels to describe the scatter and penetration.

The authors also used our software for dosimetry study of ^{177}Lu-[DOTA0,Tyr3] octreotate for treatment of disseminated neuroendocrine tumours [37]. Here, it is important that the absorbed dose to the kidneys does not exceed the maximally tolerated absorbed dose. Three different methods for calculations of the kidney absorbed dose were compared involving: (a) planar activity imaging, (b) a hybrid SPECT/planar activity quantification combined with a MIRD based absorbed dose calculation using S values and (c) a hybrid SPECT/planar method where dose rate images were determined from SPECT at one time point. This study showed a large difference in calculated kidney absorbed doses depending on dosimetry method. Methods (b) and (c) gave consistent values, but method (a) gave higher absorbed dose values, which may imply that patients evaluated according this method may be undertreated.

ACKNOWLEDGEMENTS

This work was funded by the Swedish Research Council, the Swedish Cancer Foundation, the Gunnar Nilsson Foundation, the Bertha Kamprad Foundation, the Lund University Medical Faculty Foundation and from Lund University Hospital Donation Funds.

REFERENCES

[1] THOMAS, S.R., MAXON, H.R., KEREIAKES, J.G., In Vivo Quantitation of Lesion Radioactivity Using External Counting Methods, Med Phys **3** (1976) 253–255.

[2] FLEMING, J.S., A Technique for the Absolute Measurement of Activity Using a Gamma Camera and Computer, Phys Med Biol **24** (1979) 176–180.

[3] MINARIK, D., SJOGREEN, K., LJUNGBERG, M., A New Method to Obtain Transmission Images for Planar Whole-Body Activity Quantification, Cancer Biother. Radiopharm. **20** (2005) 72–76.

[4] CHIESA, C., et al., Dosimetry in Myeloablative (90)Y-Labeled Ibritumomab Tiuxetan Therapy: Possibility of Increasing Administered Activity on the Base of Biological Effective Dose Evaluation. Preliminary Results, Cancer Biother Radiopharm **22** (2007) 113–120.

[5] SIEGEL, J.A., et al., Mird Pamphlet No. 16: Techniques for Quantitative Radiopharmaceutical Biodistribution Data Acquisition and Analysis for Use in Human Radiation Dose Estimates, J Nucl Med **40** (1999) 37S-61S.

[6] JASZCZAK, R.J., GREER, K.L., FLOYD, C.E., HARRIS, C.C., COLEMAN, R.E., Improved Spect Quantification Using Compensation for Scattered Photons, J.Nucl.Med. **25** (1984) 893–900.

[7] OGAWA, K., HARATA, H., ICHIHARA, T., KUBO, A., HASHIMOTO, S., A Practical Method for Position Dependent Compton-Scatter Correction in Single Photon Emission CT, IEEE Transactions on Medical Imaging **10** (1991) 408–412.

[8] SJOGREEN, K., LJUNGBERG, M., STRAND, S.E., An Activity Quantification Method based on Registration of Ct and Whole-Body Scintillation Camera Images, with Application to ^{131}I, J.Nucl.Med. **43** (2002) 972–982.

[9] MINARIK, D., LJUNGBERG, M., SEGARS, P., GLEISNER, K.S., Evaluation of Quantitative Planar ^{90}Y Bremsstrahlung Whole-Body Imaging, Phys Med Biol **54** (2009) 5873–5883.

[10] HE, B., FREY, E.C., Comparison of Conventional, Model based Quantitative Planar, and Quantitative Spect Image Processing Methods for Organ Activity Estimation Using In-111 Agents, Phys. Med. Biol. **51** (2006) 3967–3981.

[11] SJOGREEN, K., LJUNGBERG, M., WINGARDH, K., ERLANDSSON, K., STRAND, S.E., Registration of Emission and Transmission Whole-Body Scintillation-Camera Images, J.Nucl.Med. **42** (2001) 1563–1570.

[12] STABIN, M.G., SPARKS, R.B., CROWE, E., Olinda/Exm: The Second-Generation Personal Computer Software for Internal Dose Assessment in Nuclear Medicine, Journal of Nuclear Medicine **46** (2005) 1023–1027.

[13] LEE, C., LODWICK, D., BOLCH, W.E., Nurbs based 3-D Anthropomorphic Computational Phantoms for Radiation Dosimetry Applications, Radiat Prot Dosimetry **127** (2007) 227–232.

[14] HUDSON, H.M., LARKIN, R.S., Accelerated Image Reconstruction Using Ordered Subsets of Projection Data, IEEE Trans Nucl Sci **13** (1994) 601–609.

[15] KING, M., FARNCOMBE, T., An Overview of Attenuation and Scatter Correction of Planar and Spect Data for Dosimetry Studies, Cancer Biother.Radiopharm. **18** (2003) 181–190.

[16] FREY, E.C., TSUI, B.M.W., A Practical Method for Incorporating Scatter in a Projector-Backprojector for Accurate Scatter Compensation in Spect, IEEE Transactions on Nuclear Science **40** (1993) 1107–1116.
[17] SJOGREEN-GLEISNER, K., RUECKERT, D., LJUNGBERG, M., Registration of Serial SPECT/CT Images for Three-Dimensional Dosimetry in Radionuclide Therapy, Phys Med Biol **54** (2009) 6181–6200.
[18] KORAL, K.F., et al., Initial Results for Hybrid Spect-Conjugate-View Tumor Dosimetry in ^{131}I-Anti-B1 Antibody Therapy of Previously Untreated Patients with Lymphoma, J Nucl Med **41** (2000) 1579–1586.
[19] DALE, R.G., Dose-Rate Effects in Targeted Radiotherapy, Phys Med Biol **41** (1996) 1871–1884.
[20] WESSELS, B.W., et al., Mird Pamphlet No. 20: The Effect of Model Assumptions on Kidney Dosimetry and Response--Implications for Radionuclide Therapy, J Nucl Med **49** (2008) 1884–1899.
[21] BARONE, R., et al., Patient-Specific Dosimetry in Predicting Renal Toxicity with (90)Y-Dotatoc: Relevance of Kidney Volume and Dose Rate in Finding a Dose-Effect Relationship, J.Nucl.Med. **46** Suppl 1 (2005) 99S–106S.
[22] BODEY, R.K., FLUX, G.D., EVANS, P.M., Combining Dosimetry for Targeted Radionuclide and External Beam Therapies Using the Biologically Effective Dose, Cancer Biother Radiopharm **18** (2003) 89–97.
[23] SGOUROS, G., et al., Three-Dimensional Imaging based Radiobiological Dosimetry, Semin Nucl Med **38** (2008) 321–334.
[24] O'DONOGHUE, J.A., Implications of Non-uniform Tumor Doses for Radioimmunotherapy, J Nucl Med **40** (1999) 1337–1341.
[25] DEWARAJA, Y.K., et al., ^{131}I-Tositumomab Radioimmunotherapy: Initial Tumor Dose-Response Results Using 3-Dimensional Dosimetry Including Radiobiologic Modeling, J Nucl Med **51** (2010) 1155–1162.
[26] KOLBERT, K.S., et al., Implementation and Evaluation of Patient-Specific Three-Dimensional Internal Dosimetry, J.Nucl.Med **38** (1997) 301–308.
[27] SGOUROS, G., et al., Patient-Specific Dosimetry for ^{131}I Thyroid Cancer Therapy Using ^{124}I PET and 3-Dimensional-Internal Dosimetry (3D-ID) Software, J Nucl Med **45** (2004) 1366–1372.
[28] KOLBERT, K.S., et al., Murine S Factors for Liver, Spleen, and Kidney, J Nucl Med **44** (2003) 784–791.
[29] GUY, M.J., FLUX, G.D., PAPAVASILEIOU, P., FLOWER, M.A., OTT, R.J., Rmdp: A Dedicated Package for ^{131}I SPECT Quantification, Registration and Patient-Specific Dosimetry, Cancer Biother Radiopharm **18** (2003) 61–69.
[30] HE, B., et al., Comparison of Residence Time Estimation Methods for Radioimmunotherapy Dosimetry and Treatment Planning–Monte Carlo Simulation Studies, IEEE Trans Med Imaging **27** (2008) 521-530.
[31] WILDERMAN, S.J., DEWARAJA, Y.K., Method for Fast CT/SPECT based 3D Monte Carlo Absorbed Dose Computations in Internal Emitter Therapy, IEEE Trans Nucl Sci **54** (2007) 146–151.

[32] DEWARAJA, Y.K., WILDERMAN, S.J., KORAL, K.F., KAMINSKI, M.S., AVRAM, A.M., Use of Integrated SPECT/CT Imaging for Tumor Dosimetry in I-131 Radioimmunotherapy: A Pilot Patient Study, Cancer Biother Radiopharm **24** (2009) 417–426.

[33] DEWARAJA, Y.K., LJUNGBERG, M., FESSLER, J.A., 3-D Monte Carlo based Scatter Compensation in Quantitative I-131 Spect Reconstruction, IEEE Transactions on Nuclear Science **53** (2006) 181–188.

[34] LINDEN, O., et al., A Novel Platform for Radioimmunotherapy: Extracorporeal Depletion of Biotinylated and ^{90}Y-Labeled Rituximab in Patients with Refractory B-Cell Lymphoma, Cancer Biotherapy and Radiopharmaceuticals **20** (2005) 457–466.

[35] MINARIK, D., LJUNGBERG, M., SJÖGREEN, K., Evaluation of Quantitative Planar ^{90}Y Bremsstrahlung Whole-Body Imaging Phys Med Biol **54** (2009) 5873–5883.

[36] MINARIK, D., SJÖGREEN, K., LJUNGBERG, M., Evaluation of Quantitative ^{90}Y SPECT based on Experimental Phantom Studies, Phys Med Biol **53** (2008) 5689–5703.

[37] GARKAVIJ, M., et al., ^{177}Lu-[Dota0,Tyr3] Octreotate Therapy in Patients with Disseminated Neuroendocrine Tumors: Analysis of Dosimetry with Impact on Future Therapeutic Strategy, Cancer **116** (2010) 1084–1092.

DOSIMETRY FOR NUCLEAR MEDICINE PATIENTS: FROM STANDARD TO SPECIFIC BASED APPROACHES

L. HADID*, N. GRANDGIRARD*, N. PIERRAT**, A. DESBRÉE*

* Internal Dosimetry Department,
Institute for Radiological Protection and Nuclear Safety,
Fontenay-aux-Roses
Email: aurelie.desbree@irsn.fr

** Imaging Department, Institut Curie, Paris

France

Abstract

In nuclear medicine, mean absorbed doses to organs are published for standard stylized anatomic models. To provide more realistic and detailed geometries of the human morphology, the International Commission on Radiological Protection, together with the International Commission on Radiation Units and Measurements, have recently adopted voxel phantoms to represent the reference adult. Using the OEDIPE software, an advanced tool developed at the French Institute of Radiation Protection and Nuclear Safety, and the MCNPX Monte Carlo code, dosimetric calculations were performed for the new female and male voxel phantoms. Results obtained for different radiopharmaceuticals used in nuclear medicine show that differences with the reference mathematical phantom can reach a maximum factor of 3.7 for the male and 4.1 for the female voxel phantoms. Furthermore, differences in effective doses can reach more than 50% between the published values of the mathematical phantom and the adult voxel phantom.

1. INTRODUCTION

Nuclear medicine is a discipline based on the administration of radionuclides in the human body for diagnostic or therapeutic purposes. Thus, each organ can become a source of radiation delivering a fraction of the emitted energy in tissues. Therefore, to ensure the radiation protection of the patient, accurate and realistic dosimetric studies must be achieved. In this context, the Council of the European Union in its Council Directive 97/43 Euratom distinguishes diagnostic from therapeutic procedures [1]. For diagnostic purposes, the exposure of tissues has to be evaluated and kept as low as reasonably achievable and consistent with the required diagnostic information,

taking into account economic and social factors. In this case, diagnostic reference levels of dose, which corresponds to levels of activity for radiopharmaceuticals, are established and the mean absorbed dose per unit activity administered are published for standard reference phantoms [2–4]. For therapeutic purposes, the dosimetric evaluation must be individually planned, ensuring that the exposure of healthy tissues is kept as low as possible and consistent with the therapeutic aim.

At present, most dose values available are determined on the basis of the Medical Internal Radiation Dose (MIRD) formalism [5] and standard mathematical anthropomorphic phantoms [6–9]. In the last few decades, the advances in both medical imaging and computational techniques have enabled the development of computational voxel phantoms. These are based upon three-dimensional imaging techniques such as magnetic resonance imaging (MRI) or computed tomography (CT) and provide more realistic and detailed information about the human anatomy than the MIRD type models [10]. Therefore, the International Commission on Radiological Protection (ICRP) and the International Commission on Radiation Units and Measurements (ICRU) have adopted voxel phantoms as the computational representation of the adult reference person to improve reference dosimetry [11].

Presented here are the mean absorbed doses and effective doses performed for the new ICRP/ICRU female and male voxel phantoms, using the OEDIPE software [12, 13] and the MCNPX Monte Carlo code [14]. The results obtained for different radiopharmaceuticals used in nuclear medicine are compared with the mean absorbed doses published for the Oak Ridge National Laboratory mathematical phantoms.

2. MATERIALS AND METHODS

2.1. The ICRP/ICRU adult reference voxel phantoms

The ICRP/ICRU adult male and female reference voxel phantoms [15] have been developed by the Helmholtz Zentrum München (German Center for Environmental Health, formely GSF) in collaboration with the DOCAL task group of the ICRP. The anatomy of the reference voxel phantoms is that of Rex and Regina [16], which are derived from the medical images of two individuals. The dimensions, masses and densities of the 141 anatomical regions have been adjusted to match the ICRP reference adult male and female [17]. The voxel sizes are 8 and 4.84 mm in height with in-plane resolution of 2.137 and 1.775 mm for the male and female, respectively. A detailed description of the phantoms and the

FIG. 1. Sagittal and frontal slices of the adult male voxel phantom (left) and the adult female reference voxel phantom (right).

limitations due to image resolution can be found elsewhere [15,18]. Frontal and sagittal slices of the phantoms are shown in Fig. 1.

2.2. Dosimetric formalism

The mean absorbed dose $D(r_T,T_D)$ to target tissue r_T over a defined dose integration period T_D following administration of a radionuclide to the patient is given in Ref. [19] as:

$$D(r_T, T_D) = \sum_{r_S} \tilde{A}(r_S, T_D) S(r_T \leftarrow r_S) \quad (1)$$

where

$\tilde{A}(r_S, T_D)$ is the time integrated activity (or number of nuclear transformations) in source tissue r_S over the period T_D (taken to be infinity as radionuclides of general use in nuclear medicine have relatively short physical half-lives); and

$S(r_T \leftarrow r_S)$ is the radionuclide S value.

The S value is given as:

$$S(r_T \leftarrow r_S) = \sum_i E_i Y_i \frac{\varphi(r_T \leftarrow r_S, E_i)}{M(r_T)} \quad (2)$$

where

E_i and Y_i are the mean or individual energy and yield (number per nuclear transformation), respectively, of the radiation particle i emitted by the radionuclide;

$\phi(r_T \leftarrow r_S, E_i)$ is the absorbed fraction (defined as the fraction of radiation energy E_i emitted within the source tissue r_S that is absorbed in the target tissue r_T); and

$M(r_T)$ is the mass of the target tissue r_T.

In the context of medical exposures, the effective dose E given in sievert is defined as:

$$E^{male/\,female} = \sum_T w_T H(r_T, T_D) = \sum_T w_T \sum_R w_R D_R(r_T, T_D) \quad (3)$$

where

w_T is a tissue weighting factor for target tissue r_T subject to the condition that

$$\sum_T w_T = 1$$

the w_T values used in this article are given in Table 1;

w_R is the radiation weighting factor for radiation type R; and

TABLE 1. WEIGHTING FACTORS FOR CALCULATION OF THE EFFECTIVE DOSE E ACCORDING TO THE 1990 RECOMMENDATIONS OF THE ICRP [20]

Tissue	w_T
Gonads	0.20
Colon, lung, red bone marrow, stomach	0.12
Bladder, breast, liver, oesophagus, thyroid, remainder[a, b]	0.05
Skin, bone surfaces	0.01

[a] Adrenals, brain, small intestine, kidney, muscle, pancreas, spleen, thymus and uterus.

[b] In exceptional cases where a single one of the remainder tissues or organs receives an equivalent dose in excess of the highest dose in any of the 12 organs for which a weighting factor is specified, a weighting factor of 0.025 should be applied to that tissue or organ and a weighting factor of 0.025 to the average dose in the rest of the remainder, as defined above.

$D_R(r_T,T_D)$ is the contribution of radiation type R to the mean absorbed dose in target tissue r_T. Current ICRP recommended values of w_R are 1.0 for photons, electrons, positrons and β particles.

The effective dose for protection of reference persons is based on weighting factors that are mean values representing an average over individuals of both sexes. Thus, the effective dose for the voxel adult phantom is determined using Eq. 4:

$$E = \sum_T w_T \frac{D_R(r_T,T_D)^{Male} + D_R(r_T,T_D)^{Female}}{2} \quad (4)$$

2.3. The OEDIPE software

The dose calculations are performed with the software OEDIPE, a French acronym for ‘tool for personalized internal dose assessment’. OEDIPE is a user-friendly graphical interface, developed at IRSN with the Interactive Data Language (ITT Visual Information Solutions, United States of America) [12,13]. The main purpose of this software is to estimate the dose delivered by associating voxel phantoms and the MCNPX Monte Carlo code [14]. Its global features are defined according to the following stages:

— Importation of CT or MRI images of the patient.
— Construction of a computational phantom or importation of an existing voxel phantom.
— Definition of the sources of radiation (distribution, activity, energy and type of emissions). The software includes a database of 246 radionuclides [21].
— Automatic creation of the MCNPX input file in which the geometry of the phantoms is described using repeated structures.
— Process of the MCNPX output file.

MCNPX (MCNP eXtended) is a general purpose transport code from Los Alamos National Laboratory [14] primarily based on the MCNP code [22]. Photons, electrons, neutrons, as well as 29 other particles can be considered. The version 2.6c of MCNPX was used. The cut-off energy for both photons and electrons was set at the default value of 1 keV and the energy deposited in the target regions was scored.

2.4. Monte Carlo calculations

To have a panel of radioisotopes, biodistributions, photon and electron energies, the dose calculations are achieved for the radiopharmaceuticals listed in Table 2.

Cumulated activity of a selected radiopharmaceutical was homogeneously distributed in the different source regions of the voxel phantoms following the ICRP biokinetics standard models. The term ‘total body tissues’ was defined as total body minus contents of walled organs (gall bladder, stomach, small intestine, ascending colon, transverse colon, descending colon, sigmoid colon, urinary bladder), air inside body and skin at top and bottom [15]. In addition, the term ‘other organs and tissues’ was defined as the ‘total body tissues’ minus the source organs previously identified. As described in the ICRP Publication 23 [23], the upper large intestine includes the ascending colon, the transverse colon right and left. The lower large intestine includes the descending colon, the sigmoid colon and the rectum.

The distribution of activity is realized for all the organs in a same MCNPX input file, so that the deposited energy in a target organ is obtained at once. Twenty million histories were followed so that the statistical uncertainties of the target organs do not exceed 5%. The transport of secondary particles was taken into account. The computation time for a dose calculation ranged from two hours for [^{123}I]-MIBG to 25 h for [^{131}I]-iodine uptake 55% (using two Intel (R) Xeon (TM) processors of 3.20 GHz CPU with 8 GB RAM).

The absorbed doses were calculated for 24 target organs and tissues listed in Table 2. To determine the absorbed dose to red marrow, the deposited energy was

TABLE 2. LIST OF RADIOPHARMACEUTICALS AND TARGET TISSUES USED IN THIS STUDY

Radiopharmaceuticals	Target organs and tissues	
[^{11}C]-labelled brain receptor substances ([^{11}C]-Br) [4]	Adrenals	Ovaries
L-[methyl-^{11}C]-methionine ([^{11}C]-Met) [4]	Urinary bladder wall	Pancreas
2-[^{18}F]Fluoro-2-deoxy-D-glucose ([^{18}F]-FDG) [4]	Bone surfaces/endosteum	Red marrow
[^{99m}Tc]-ECD [4]	Brain	Skin
[^{99m}Tc]-ethylenedicysteine ([^{99m}Tc]-EC) normal and abnormal renal function [4]	Breasts	Spleen
[^{99m}Tc]-MIBI resting subject and exercise [3]	Gallbladder wall	Testes
[^{111}In] [2]	Heart	Thymus
[^{123}I]-labelled brain receptor substances ([^{123}I]-Br) [4]	Kidneys	Thyroid
[^{123}I]-Metaiodobenzylguanidine ([^{123}I]-MIBG) [3]	Liver	Uterus
[^{124}I]-iodine uptake 0% and 55% [2]	Lungs	Stomach wall
[^{131}I]-iodine uptake 0% and 55% [2]	Muscles	Colon wall
	Oesophagus	Remaining organs

first determined for the 19 bones and bone groups of the reference voxel phantoms. The deposited energy in red marrow was then assumed to be proportional to the mass of red marrow in the different parts of skeleton, these data being available in ICRP Publication 110 [15]. The same method was applied for the endosteum.

3. RESULTS AND DISCUSSION

As an example of the results, Figs 1–3 show comparative values of some organ absorbed doses as well as effective doses between the reference mathematical phantom [2, 4] and the adult male and female voxel phantoms for [^{18}F]-FDG, [^{99m}Tc]-ECD and [^{123}I]-MIBG.

The maximum differences (per cent values) in absorbed doses between the reference mathematical and voxel phantoms for the different radiopharmaceuticals are given in Table 3. The mean differences for each radiopharmaceutical are also indicated with the associated standard deviation. The mean differences are higher for the female voxel phantom than for the male

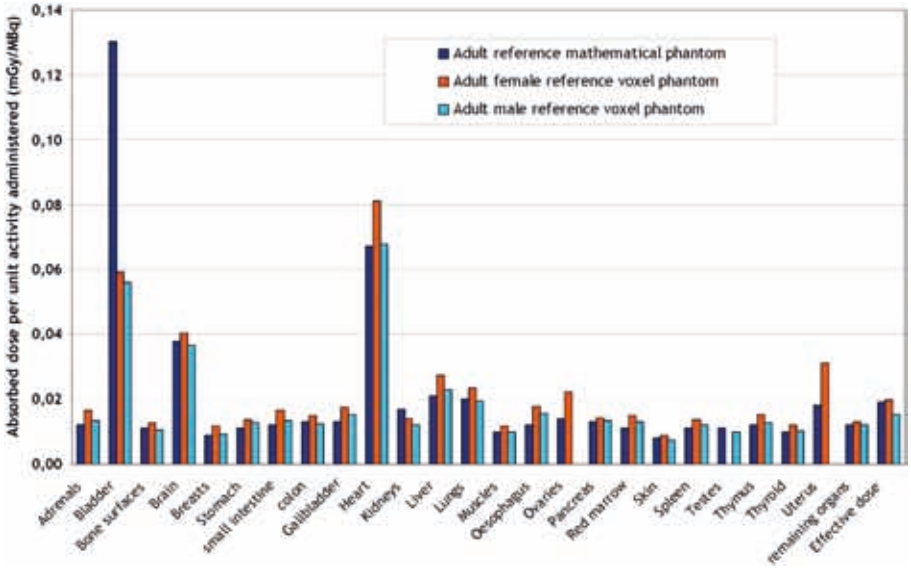

FIG. 2. Absorbed dose per unit activity administered (mGy/MBq) for [^{18}F]-FDG.

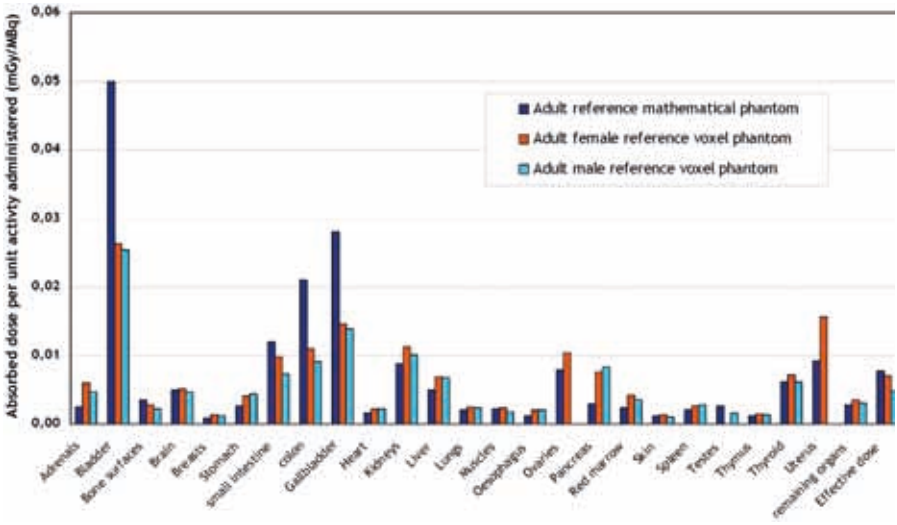

FIG. 3. Organ absorbed dose per unit activity administered (mGy/MBq) for [^{99m}Tc]-ECD.

one compared to the mathematical phantom. Indeed, the latter is hermaphrodite and its organs' masses are mostly higher than those of the female one, except for the breasts, uterus, ovaries and pancreas. The lowest mean differences are found for [^{11}C]-Br, 11.3% for the male voxel phantom, and for an [^{124}I]-iodine uptake of

TABLE 3. MAXIMUM (WITH CORRESPONDING ORGAN) AND MEAN (STANDARD DEVIATION ASSOCIATED) DIFFERENCES (%) IN ABSORBED DOSES BETWEEN REFERENCE MATHEMATICAL AND VOXEL PHANTOMS FOR THE DIFFERENT RADIOPHARMACEUTICALS

Radiopharmaceuticals	Differences between voxel male and mathematical phantom (absolute value)		Differences between voxel female and mathematical phantom (absolute value)	
	Max (%) Organs	Mean (%) SD	Max (%) Organs	Mean (%) SD
[^{11}C]-Br	59.6 Bladder	11.3 15.6	57.9 Uterus	25.0 14.4
[^{11}C]-Met	95.1 Adrenals	21.9 22.7	119.4 Adrenals	39.0 29.4
[^{18}F]-FDG	57.0 Bladder	11.4 12.9	72.9 Uterus	28.7 16.9
[^{99m}Tc]-ECD	184.7 Pancreas	41.0 38.4	163.0 Pancreas	44.6 38.2
[^{99m}Tc]-EC normal	156.4 Red marrow	32.2 39.3	166.9 Small intestine	51.3 47.5
[^{99m}Tc]-EC abnormal	72.7 Adrenals	22.3 20.2	87.2 Ovaries	42.0 22.8
[^{99m}Tc]-MIBI resting	77.6 Pancreas	31.1 21.6	82.4 Adrenals	30.0 21.2
[^{99m}Tc]-MIBI exercise	60.6 Pancreas	27.0 19.7	67.7 Adrenals	28.6 18.5
[^{111}In]	161.0 Thyroid	83.0 49.8	211.6 Thyroid	105.6 57.1
[^{123}I]-Br	179.6 Pancreas	44.9 43.0	175.5 Adrenals	54.2 46.9
[^{123}I]-MIBG	152.1 Oesophagus	65.9 34.6	175.1 Oesophagus	95.7 43.5
[^{124}I]-iodine uptake 0%	42.4 Bladder	11.4 12.0	76.3 Uterus	22.7 21.8
[^{124}I]-iodine uptake 55%	223.0 Lungs	68.9 58.3	257.0 Lungs	84.8 70.9

TABLE 3. MAXIMUM (WITH CORRESPONDING ORGAN) AND MEAN (STANDARD DEVIATION ASSOCIATED) DIFFERENCES (%) IN ABSORBED DOSES BETWEEN REFERENCE MATHEMATICAL AND VOXEL PHANTOMS FOR THE DIFFERENT RADIOPHARMACEUTICALS (cont.)

Radiopharmaceuticals	Differences between voxel male and mathematical phantom (absolute value)		Differences between voxel female and mathematical phantom (absolute value)	
	Max (%) Organs	Mean (%) SD	Max (%) Organs	Mean (%) SD
[^{131}I]-iodine uptake 0%	72.6 Bladder	12.6 18.5	70.4 Bladder	27.8 21.4
[^{131}I]-iodine uptake 55%	271.2 Lungs	79.9 72.2	307.3 Lungs	95.9 81.6

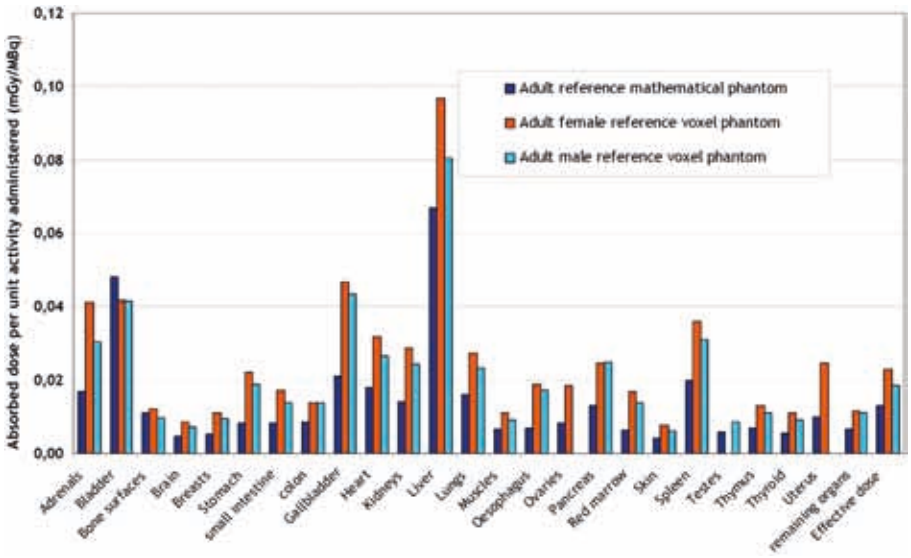

FIG. 4. Organ absorbed dose per unit activity administered (mGy/MBq) for [^{123}I]-MIBG.

0%, 22.7% for the female voxel phantom. These values reach 83.0% and 105.6% of differences for [^{111}In]. These observed discrepancies are mainly due to the mass and topology differences between organs. The maximum differences are

obtained for lungs. Indeed, in the case of [^{131}I]-iodine with an uptake of 55%, a factor of 3.7 and 4.1 for the male and female voxel phantoms, respectively, are observed. Some important differences can also be found for some walled organs such as the urinary bladder wall. These are explained by the approximations previously used for electrons in the dose calculations based on the mathematical phantom [24, 25]. Indeed, no absorbed fraction values were available; instead, it was assumed that electrons' energy was entirely absorbed in the source organs and that for activity in the contents of walled organs, the absorbed dose to the wall was half the equilibrium dose to the contents. Moreover, the differences observed can be explained by the limitation related to the voxel size of the phantoms. Indeed, voxel effects can be induced while representing small and walled organs.

The effective doses for the male and female reference voxel phantoms and the percentage differences between the adult voxel phantom and the adult mathematical phantoms are presented in Table 4 for different radiopharmaceuticals. Differences can reach more than 50% between the adult voxel and mathematical phantoms, in particular with [^{111}In], [^{123}I]-MIBG, [^{124}I]-iodine uptake 55% and [^{131}I]-iodine uptake 55%. It should however be noticed that concerning the effective doses actually published for [^{124}I]-iodine uptake 55% and [^{131}I]-iodine uptake 55%, the weighting factors used are those of ICRP publication 53 since they have not been re-evaluated with those of ICRP Publication 60. The effective dose is an interesting tool in diagnostic nuclear medicine for conveying the risk of stochastic effects in future populations of patients. Thus, the realistic and accurate determination of this parameter is important to compare patient exposures originating from different diagnostic procedures, different imaging technologies and different hospital practices. Nevertheless, as stated in the MIRD pamphlet 21 [19], the effective dose cannot be assigned as an index of stochastic risk to a single individual patient (male or female), nor can it be assigned to male or female patients of body morphometries significantly different from those of the ICRP reference individuals. Indeed, the organ doses are obtained using phantoms based on a median individual of a large population, sex and age averaged and weighted by w_T. Finally, the ICRP recently issued its 2007 Recommendations [11], superseding the 1990 Recommendations, which include updated and amended tissue weighting factor. The effective dose will therefore have to be calculated accordingly.

TABLE 4. EFFECTIVE DOSES (mSv/MBq) FOR THE MALE AND FEMALE REFERENCE VOXEL PHANTOMS AND THE DIFFERENCES (%) IN EFFECTIVE DOSE BETWEEN THE ADULT VOXEL AND MATHEMATICAL PHANTOMS FOR THE DIFFERENT RADIOPHARMACEUTICALS

Radiopharmaceuticals	Effective dose for the voxel male phantom	Effective dose for the voxel female phantom	Effective dose for the voxel adult phantom	Effective dose for the mathematical phantom	Differences between the voxel adult and mathematical phantom (%)
[^{11}C]-Br	3.26E-03	4.22E-03	3.74E-03	4.3E-03	–13.0
[^{11}C]-Met	4.45E-03	6.13E-03	5.29E-03	8.4E-03	–37.0
[^{18}F]-FDG	1.53E-02	1.99E-02	1.76E-02	1.9E-02	–7.4
[^{99m}Tc]-ECD	4.84E-03	7.05E-03	5.95E-03	7.7E-03	–22.8
[^{99m}Tc]-EC normal	3.44E-03	5.85E-03	4.64E-03	6.3E-03	–26.3
[^{99m}Tc]-EC abnormal	3.54E-03	5.00E-03	4.27E-03	4.6E-03	–7.2
[^{99m}Tc]-MIBI resting	6.63E-03	8.24E-03	7.43E-03	9.0E-03	–17.4
[^{99m}Tc]-MIBI exercise	5.68E-03	7.23E-03	6.45E-03	7.9E-03	–18.3
[^{111}In]	2.88E-01	3.64E-01	3.26E-01	2.1E-01	55.4
[^{123}I]-Br	3.70E-02	4.67E-02	4.19E-02	5.0E-02	–16.2
[^{123}I]-MIBG	1.86E-02	2.31E-02	2.08E-02	1.3E-02	60.2
[^{124}I]-iodine uptake 0%	7.49E-02	9.97E-02	8.73E-02	9.5E-02	–8.1

TABLE 4. EFFECTIVE DOSES (mSv/MBq) FOR THE MALE AND FEMALE REFERENCE VOXEL PHANTOMS AND THE DIFFERENCES (%) IN EFFECTIVE DOSE BETWEEN THE ADULT VOXEL AND MATHEMATICAL PHANTOMS FOR THE DIFFERENT RADIOPHARMACEUTICALS (cont.)

Radiopharmaceuticals	Effective dose for the voxel male phantom	Effective dose for the voxel female phantom	Effective dose for the voxel adult phantom	Effective dose for the mathematical phantom	Differences between the voxel adult and mathematical phantom (%)
[^{124}I]-iodine uptake 55%	1.95E+01	2.31E+01	2.13E+01	1.4E+01	52.1
[^{131}I]-iodine uptake 0%	3.92E-02	5.17E-02	4.54E-02	6.1E-02	–25.5
[^{131}I]-iodine uptake 55%	3.80E+01	4.47E+01	4.14E+01	2.4E+01	72.4

4. CONCLUSION

In nuclear medicine, the absorbed dose is currently established using mathematical reference phantoms and the assumption that electrons deposit their entire energy in the region where they are emitted. To improve the accuracy and realism of the simulations, the ICRP and ICRU have adopted reference voxel phantoms. Moreover, Monte Carlo calculations for electrons have been made. In this context, the authors have developed methodologies based on the OEDIPE software, an in-house developed tool, that associates voxel phantoms to the Monte Carlo code MCNPX. Thus, this method has allowed the determination of absorbed and effective doses for the new ICRP/ICRU reference voxel phantoms. Finally, the developed technique is adapted and of great interest when working on specific voxel phantoms, based on CT or MRI images, in particular to evaluate the influence of patient morphology on the absorbed doses.

REFERENCES

[1] Council Directive 97/43 Euratom of 30 June 1997 on health protection of individuals against the dangers of ionizing radiation in relation to medical exposure, and repealing Directive 84/466/Euratom, Official Journal of the European Communities of 9 July 1997, No. L 180/22-27.

[2] INTERNATIONAL COMMISSION ON RADIOLOGICAL PROTECTION, Radiation Dose to Patients from Radiopharmaceuticals, Publication 53, Pergamon Press (1987).

[3] INTERNATIONAL COMMISSION ON RADIOLOGICAL PROTECTION, Radiation Dose to Patients from Radiopharmaceuticals, Addendum to ICRP 53, Publication 80, Pergamon (1998).

[4] INTERNATIONAL COMMISSION ON RADIOLOGICAL PROTECTION, Radiation Dose to Patients from Radiopharmaceuticals, Addendum 3 to ICRP 53, Publication 106, Elsevier (2008).

[5] SNYDER, W.S., et al., “S”, absorbed dose per unit cumulated activity for selected radionuclides and organs, MIRD Pamphlet 11 (Reston, VA: Society of Nuclear Medicine) (1975) 1–258.

[6] SNYDER, W.S., et al., MIRD pamphlet no. 5: estimates of absorbed fractions for monoenergetic photon sources uniformly distributed in various organs of a heterogeneous phantom, J. Nucl. Med. **10** (1969) 1–68.

[7] SNYDER, W.S., et al., MIRD Pamphlet 5 *Revised*: Estimates of absorbed fractions for monoenergetic photon sources uniformly distributed in various organs of a heterogeneous phantom, New York: Society of Nuclear Medicine (1978).

[8] CRISTY, M., ECKERMAN, K.F., Specific absorbed fractions of energy at various ages from internal photon sources: part I. Methods ORNL/TM-8381/Vol. 1, Oak Ridge, TN: Oak Ridge National Laboratory (1987).

[9] CRISTY, M., ECKERMAN, K.F., Specific absorbed fractions of energy at various ages from internal photon sources: part VII. Adult Male ORNL/TM-8381/Volume 7, Oak Ridge, TN: Oak Ridge National Laboratory (1987).
[10] XU, X.G., ECKERMAN, K.F., Handbook of Anatomical Models for Radiation Dosimetry, Boca Raton, FL: Taylor & Francis (2010).
[11] INTERNATIONAL COMMISSION ON RADIOLOGICAL PROTECTION, Recommendations of the International Commission on Radiological Protection, Publication 103, Pergamon (2007).
[12] CHIAVASSA, S., et al., Validation of a personalized dosimetric evaluation tool (OEDIPE) for targeted radiotherapy based on the Monte Carlo MCNPX code, Phys. Med. Biol., **51** (2006) 601.
[13] CHIAVASSA, S., et al., OEDIPE: a personalized dosimetric tool associating voxel-based models with MCNPX, Cancer Biother. Radiopharm. **20** (2005) 325.
[14] WATERS, L., MCNPX user's manual version 2.4.0 Technical Report LA-CP-02-408, Los Alamos, NM: Los Alamos National Laboratory (2002).
[15] INTERNATIONAL COMMISSION ON RADIOLOGICAL PROTECTION, Adult Reference Computational Phantoms, Publication 110, Elsevier (2009).
[16] SCHLATTL, H., et al., Organ dose conversion coefficients for voxel models of the reference male and female from idealized photon exposures, Phys. Med. Biol. **52** (2007) 2123.
[17] INTERNATIONAL COMMISSION ON RADIOLOGICAL PROTECTION, Basic Anatomical and Physiological Data for Use in Radiological Protection: Reference Values, Publication **89**, Pergamon (2002).
[18] ZANKL, M., et al., Voxel-based models representing the male and female ICRP reference adult — the skeleton, Radiat. Prot. Dosim. **127** (2007) 174.
[19] BOLCH, W., et al., MIRD Pamphlet No. 21: A Generalized Schema for Radiopharmaceutical Dosimetry — Standardization of Nomenclature, J. Nucl. Med. **50** (2009) 477.
[20] INTERNATIONAL COMMISSION ON RADIOLOGICAL PROTECTION, 1990 Recommendations of the International Commission on Radiological Protection, Publication 60, Pergamon Press (1991).
[21] INTERNATIONAL COMMISSION ON RADIOLOGICAL PROTECTION, Radionuclide Transformations — Energy and Intensity of Emissions, Publication 38, Pergamon Press (1983)
[22] BRIESMEISTER, J.F., MCNP^{TM} — a general Monte Carlo N-particle transport code, version 4c LANL Memorandum LA-13709-M, Los Alamos, NM: Los Alamos National Laboratory (2000).
[23] INTERNATIONAL COMMISSION ON RADIOLOGICAL PROTECTION, Report of the Task Group on Reference Man, Publication 23, Pergamon Press (1975) 135.
[24] HADID, L., et al., Application of the ICRP/ICRU reference computational phantoms to internal dosimetry: calculation of specific absorbed fractions of energy for photons and electrons, Phys. Med. Biol. **55** (2010) 3631.
[25] ZANKL, M., et al., New calculations for internal dosimetry of beta-emitting radiopharmaceuticals, Radiat. Prot. Dosim. **139** (2010) 245.

COMPUTATIONAL PHANTOMS AND SKELETAL DOSE MODELS FOR ADULT AND PAEDIATRIC INTERNAL DOSIMETRY

W. BOLCH, M. WAYSON, D. PAFUNDI
Department of Nuclear and Radiological Engineering,
University of Florida, Gainesville, Florida,
United States of America
Email: wbolch@ufl.edu

Abstract

As outlined in Report No. 160 of the National Council on Radiation Protection and Measurement, the average value of the effective dose to exposed individual in the United States of America has increased by a factor of 1.7 over the time period 1982 to 2006, with the contribution of medical exposures correspondingly increasing by a factor of 5.7. At present, medical contributors to the effective dose include computed tomography (50% of total medical exposure), nuclear medicine (25%), interventional fluoroscopy (15%), and conventional radiography and diagnostic fluoroscopy (10%). An increased awareness of medical exposures has led to a gradual shift in the focus of radiation epidemiological studies from traditional occupational and environmental exposures to those focusing on cohorts of medical patients exposed to both diagnostic and therapeutic sources. The assignment of organ doses to patients in either a retrospective or prospective study has increasingly relied on the use of computational anatomical phantoms. This paper reviews the various phantom format types — stylized, voxel, and hybrid — as well as phantom morphometric categories — reference, patient dependent, patient sculpted, and patient specific. Specific emphasis is given to hybrid phantoms — those defined through the use of combinations of polygon mesh and NURBS surfaces. The concept of a patient dependent phantom is reviewed in which phantoms of non-50th percentile heights and weights are designed from population based morphometric databases and provided as a larger library of phantoms for patient matching and lookup of refined values of organ dose coefficients and/or radionuclide S values. This paper further outlines methods for constructing heterogeneous models of skeletal dosimetry allowing for explicit consideration for electron energy loss at both the macroscopic and microscopic dimension of the skeletal tissues. Absorbed fractions to active marrow in the reference adult male is highlighted and compared to values used in existing clinical models of marrow dose assessment.

1. INTRODUCTION

In its Report No. 160, the National Council on Radiation Protection and Measurement indicates that from 1982 to 2006, the average per capita effective

dose contributed from all radiation sources in the United States of America increased from 3.6 to 6.2 mSv [1]. The major driving force for this increase was medical exposures, which resulted in a change from 15% of total exposure in 1982 to 48% of total exposure in 2006. At present, medical contributors to the average effective dose include computed tomography (CT) (50% of total medical exposure), nuclear medicine (25%), interventional fluoroscopy (15%) and conventional radiography and fluoroscopy (10%).

A growing awareness of increased medical exposures over the past several years has had two major effects. The first is a shift in the focus of radiation epidemiological studies from traditional occupational and environmental exposure studies, to those focusing on cohorts of medical patients exposed to both diagnostic and therapeutic sources. The enhanced radiosensitivity of children makes paediatric studies of prime importance [2]. Examples include those under the Childhood Cancer Survivor Study (www.cancer.gov/cancertopics/coping/ccss), and the study of children who have undergone CT imaging (http://dceg.cancer.gov/reb/research/ionizing/medical/4). The second is an increased awareness of the need to reduce radiation exposures to current patients through optimization of image quality and patient dose in diagnostic imaging, or through maximizing tumour dose while minimizing non-target tissue dose in radiation therapy within both the near- and far-field regions of the patient. Furthermore, professional societies [3] and federal agencies [4] are increasingly advocating the recording of patient dose in imaging studies via indicator dose quantities. The ideal situation for patient dose monitoring, however, would be the ability to estimate individual organ doses for each patient and each imaging exam or therapy procedure, and record that dose in electronic form. This information would be invaluable for both prospective monitoring of cumulative exposures to seriously ill patients requiring multiple diagnostic and therapeutic procedures, as well as retrospective epidemiological studies undertaken in the future.

2. COMPUTATIONAL PHANTOMS IN MEDICAL DOSIMETRY

Estimating organ doses to medical patients, either prospectively or retrospectively, requires the use of computational anatomical models of human anatomy, although some information can be derived through physical phantoms and embedded dosimeters. A computational anatomical phantom is a computerized representation of human anatomy for use in radiation transport simulations of a medical imaging examination or a radiation therapy procedure. The need for such a phantom varies among the various medical applications for which organ dose estimates are sought. In nuclear medicine, detailed 3-D patient

anatomy is available through the CT portion of SPECT/CT or PET/CT imaging systems. However, the vast majority of nuclear medicine studies are conducted using single or dual headed planar imaging systems, and thus organ doses are generally estimated through pre-computed and phantom based S values under the MIRD system [5]. In radiography and fluoroscopy, no 3-D image of patient anatomy is generated, and essentially all organ dosimetry is accomplished through the use of computational phantoms and pre-computed organ dose conversion coefficients. In CT, 3-D anatomical data is acquired by design and can in principle be used to define the patient's own computational phantom. A major problem of this approach is that image segmentation is required to properly define tissue boundaries for reporting average organ dose or dose–volume histograms. While advances in automated image segmentation algorithms are ongoing, the vast majority of computational phantoms generated from patient CT images are performed through manual contouring. A secondary issue in CT dosimetry is that most CT images have limited anatomical coverage, and thus no anatomical information exists regarding organs and tissues that are partially imaged or are just beyond the edges of the scan field. A similar situation exists in external beam radiotherapy, where CT images of the cancer patient are used for treatment planning. While these images are more than sufficient to characterize the dose distributions within the tumour, and to establish dose gradients to near-field tissues, no anatomical information is available for characterizing radiation dose from treatment head and in-patient scatter in far-field tissue regions. The issues of photon scatter dose in intensity modulated radiation therapy (IMRT) and neutron scatter dose in proton therapy are prime examples of the need for additional anatomical information of the patient beyond that acquired during treatment planning.

2.1. Phantom format types

At present, there are three different formats for computational anatomical phantoms: stylized (or mathematical), voxel (or tomographic), and hybrid formats based on NURBS and/or polygon mesh surfaces. Stylized phantoms have been the workhorse of radiation dosimetry for over 40 years, and even today, form the basis for many reference sets of dose and risk coefficients. As shown in Fig. 1, they are composed of 3-D geometric surface equations defining both internal organs and outer body surfaces. While they are flexible in terms of allowing changes in organ size, body shape and extremity positioning, they are generally deficient with respect to anatomical realism. Voxel phantoms, in contrast, are composed of a 3-D array of volume elements, each with a unique organ identity, elemental composition and density (see Fig. 2). Voxel phantoms are assembled through segmentation (pixel tagging) of individual image slices

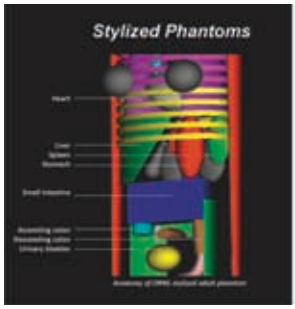

FIG. 1. Stylized phantom.

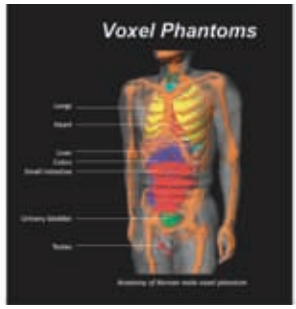

FIG. 2. Voxel phantom.

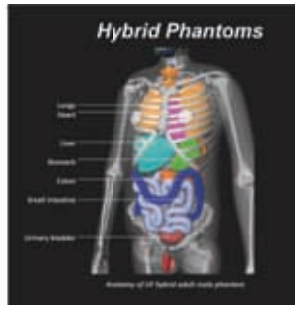

FIG. 3. Hybrid phantom.

from the CT or magnetic resonance image set, and thus they provide a high level of anatomical realism [6–8]. Their main limitation is that they are very difficult to alter in order to represent the body morphometry of subjects other than the person providing the source image. Exceptions include uniform scaling of the voxel size to represent individuals of larger or smaller stature, but of the same relative organ and body region anatomy.

Hybrid phantoms [9] — the third model format — are so named because they preserve both the anatomical realism of voxel phantoms and the mathematical flexibility of stylized phantoms as shown in Fig. 3. Various steps are followed to construct hybrid phantoms. First, image sources — typically from CT or magnetic resonance — are segmented just as would be done in the creation of a traditional voxel phantom. This step is performed at the Advanced Laboratory for Radiation Dosimetry Studies (ALRADS) at the University of Florida using the software 3D-DOCTOR™ (Able Software Corp., Lexington, MA). A resulting 3-D rendering of the subject anatomy is exported as a polygon mesh (PM) model, in which individual organs and the outer body contour are represented by a large array of triangular surfaces. For some complex structures, such as the vertebrae, this format is preferred and retained in the final hybrid phantom. For many other organs and all outer body surfaces, these polygon mesh models are subsequently converted to non-uniform rational B-spline (or NURBS) surfaces, where 3-D control points can been individually or regionally altered to permit organ reshaping and repositioning, as well as allowing for uniform enlargement or reduction. The software code RHINOERCOS™ (McNeel North America, Seattle, WA) may be used for this step. The resultant phantom is termed a hybrid-NURBS/PM phantom. However, most present-day radiation transport codes require a voxelized structure for particle tracking, and so a user defined MATLAB routine (Voxelizer™) was written to fill the NURBS/PM structures with cubic voxels of any user-defined size. This resultant anatomical model is termed a hybrid voxel phantom, where the adjective denotes that the resultant

voxel structure was derived from NURBS/PM surfaces, and not directly from a segmented medical image. An important distinction between a voxel phantom and a hybrid-voxel phantom is that while in the hybrid-NURBS/PM format, significant changes can be made to the phantom to conform to different phantom categories as defined below.

2.2. Phantom morphometric categories

Another consideration is the morphometric category of the resultant phantom. As shown in Fig. 4, four categories are possible, each moving progressively to the right along a continuum of patient specificity. The first is a reference phantom defined typically as an individual at 50th height/weight percentile from a given patient or general population. The characteristics of a reference phantom for radiation protection purposes are as defined by the International Commission on Radiological Protection (ICRP) in Publication 89 [10]. This document outlines reference values for organ masses (from which targeted organ volumes may be derived), subject height, weight, and body surface area. More specific characteristics such as extremity lengths, sitting heights and body region circumferences are not given in ICRP Publication 89, and thus additional databases must be consulted for reference phantom construction. An important point is that while ICRP specifies reference values for organ mass, analogous values for organ shape, depth, and position within the body are not defined, and thus these values generally belong to the anatomical source used for

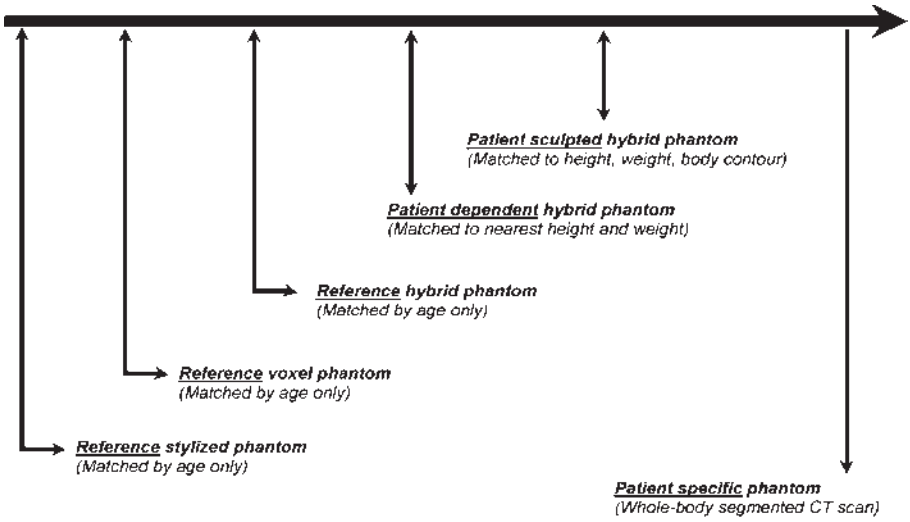

FIG. 4. Continuum of anatomical specificity.

phantom construction — cadaver, retrospective patient review, or prospective volunteer. Examples of stylized reference phantoms are those of the Oak Ridge National Laboratory (ORNL) series [11]. The ICRP reference phantoms [12] and the MAX and FAX phantoms [13] are examples of reference phantoms in voxelized formats. Three examples of reference hybrid phantoms include those of the University of Florida series [14], the RPI series [15], and the MASH and FASH phantoms of Cassola et al. [16].

Clearly, not all patients are presented at the 50th percentile height and weight at the time of treatment or imaging, and thus the use of reference phantoms, designed specifically for standardization of organ dosimetry in radiological protection, is problematic in patient medical dosimetry. One solution is simply to consider other non-50th height/weight percentiles in the relevant patient population, and then expand the available library of phantoms for patient matching. Such a concept was originally proposed by Johnson et al. [17] in defining a patient dependent phantom. In that study, the University of Florida reference adult male and female hybrid phantoms were rescaled to match 5 different height percentiles (10th, 25th, 50th, 75th and 90th) and for each height percentile, 5 different weight percentiles (also 10th, 25th, 50th, 75th and 90th). As a result, the phantoms available for patient matching expanded from only two reference phantoms to 25 male and 25 female patient dependent phantoms. As outlined in the Johnson et al. study [17], the limited series of reference paediatric phantoms were expanded from ten (newborn, 1-year, 5-year, 10-year, and 15-year male and female) to 50 males and 50 females. For paediatric patient dependent phantoms, a grid of targeted heights was established ranging from 85 to 188 cm in 11.5 cm increments for the males, and from 82 to 178 cm in 10.7 cm increments for the females. Within each age and height bin, 5 values of weight percentile were established (10th, 25th, 50th, 75th and 90th, respectively). The final series of paediatric patient dependent phantoms in the University of Florida series are thus 50 males and 50 females. The total library includes 150 phantoms. Patient matching is thus performed on a height/weight basis, and not directly by patient age. Subject age comes into play only by the assignment of a given reference hybrid phantom for rescaling to a given subset of the patient dependent phantom library. For example, the University of Florida reference 10-year female phantom was used by Johnson et al. to establish 15 additional phantoms of the female patient dependent series: phantoms at total heights of 124.9, 135.6 and 146.4 cm, each at five different weight percentiles.

Patient dependent phantoms are created through a multisteps rescaling of the starting or ‘anchor’ reference phantom. These steps include (1) matching a targeted trunk height, (2) matching a targeted total height through independent scaling of leg length, and (3) matching a targeted total body mass through scaling body circumferential parameters. As a result of the 3-D rescaling under step 1,

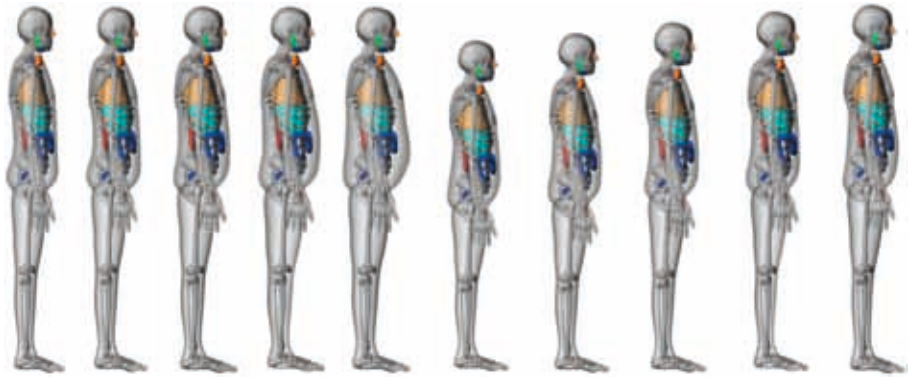

FIG. 5. Patient dependent phantoms of the University of Florida series. Five have the same height, but different weights, and five have the same weight, but different heights.

internal reference organs are similarly rescaled in 3-D, with increases in trunk height yielding larger organs and decreases in trunk height yielding smaller organs than seen in the corresponding reference phantom. These changes are broadly supported by the autopsy study by de la Grandmaison [18].

Patient dependent phantoms have the distinct advantage of improved patient specificity over reference phantoms, while at the same time, permitting organ doses to be precalculated for many medical imaging procedures. These include radionuclide S values for use in nuclear medicine, organ dose conversion coefficients for diagnostic and interventional fluoroscopy, and organ dose conversion coefficients for common CT examinations. As a result, organ doses may be assigned to the patient via software lookup tables given on only minimal patient information such as age, gender, height and weight. For even greater patient specificity, such as might be required in radionuclide and external beam therapy, one might consider the next level of anatomical model — the patient sculpted phantom. The patient sculpted phantom results from: (a) selection of a given patient dependent phantom based upon patient height and weight, and (b) readjustments to the outer body contour to explicitly match that seen in the given patient. It is conceivable that this process can be automated, and possibly utilize body surface imaging technologies. For external irradiation of the patient, such as in fluoroscopy or CT, improvements in dose accuracy will result by properly accounting for residual soft tissue attenuation and scatter. For internal irradiation of the patient, such as nuclear medicine, more modest improvement in dose accuracy would be anticipated.

On the far right side of Fig. 4 are patient specific phantoms — those that uniquely match the body morphometry and internal organ anatomy of the individual patient. Patient specific voxel phantoms are generally created through

combinations of automated and manual image segmentation. Advances in image-processing software will eventually permit the creation of patient specific hybrid phantoms where internal and exterior phantom sculpting is applied to a given patient dependent phantom. However, such phantoms require an initial set of 3-D images for their construction, and in many cases, these images will not cover all anatomical regions where a dose assessment might be sought.

2.3. ICRP reference phantoms

In late 2009, the ICRP and ICRU issued a joint report, ICRP Publication 110, describing the development and intended use of computational phantoms of the reference male and reference female [12]. In the 2007 Recommendations of the ICRP, these phantoms (shown in Fig. 6) were adopted for forthcoming updates to organ dose coefficients for internal and external radiation sources. The phantoms are given in voxelized format, and are based on medical images of selected individuals, yet are consistent with the anatomical and physiological data given in ICRP Publication 89 [10]. The phantoms were created by modification of two existing voxel models (Golem and Laura) whose body heights and weights closely resembled reference data. The report described the methods used for this process and the resulting phantom characteristics. Furthermore, to illustrate the use of these phantoms, conversion coefficients for some external and internal exposures were included.

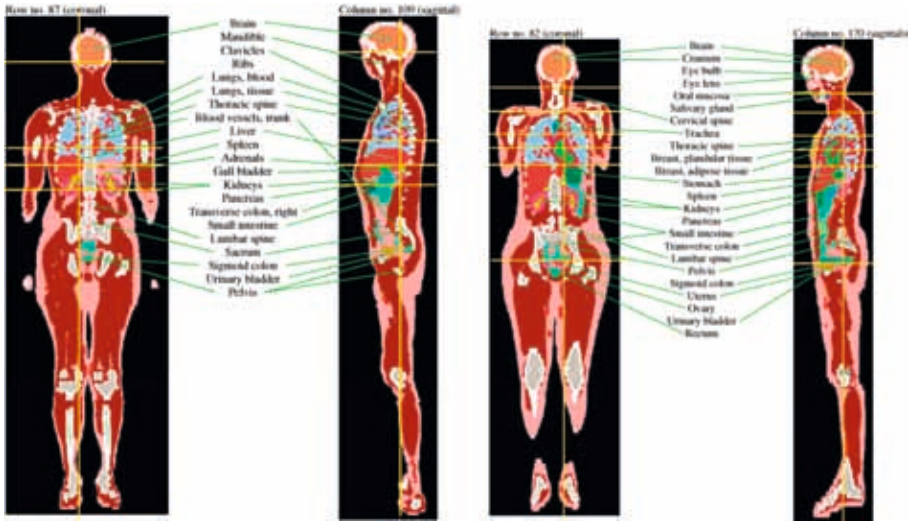

FIG. 6. Reference voxel phantoms of the ICRP adult male and adult female.

In 2008, ICRP established that its future reference phantoms for the paediatric series will be based on voxelized versions of the University of Florida hybrid phantom series [14]. These phantoms are shown in Fig. 7. In the University of Florida series, head and torso CT images of patients whose ages were close to targeted reference ages were obtained under approved protocols. Major organs and tissues were segmented and subsequently modelled as either NURBS or polygon mesh surfaces. The phantoms were matched to four reference datasets: (a) standard anthropometric data on body region sizes and circumferences, (b) reference organ masses from ICRP Publication 89, (c) reference elemental compositions from ICRU Report 46 and (d) reference data on alimentary tract organs given in ICRP Publications 89 and 100.

3. SKELETAL DOSE MODELS IN MEDICAL DOSIMETRY

The skeleton is perhaps the most difficult of all organ systems to model anatomically in the field of computational dosimetry. The relevant tissues of the bone trabeculae and marrow cavities cannot be imaged directly by clinical in vivo systems such as CT or magnetic resonance imaging. Consequently, one must rely on previously developed skeletal dosimetry models in which ex vivo microimages of excised spongiosa (acquired via contact radiography, NMR microscopy, or microCT) are used in radiation transport studies. Until recently, the only complete set of skeletal microstructural data in a format sufficient for

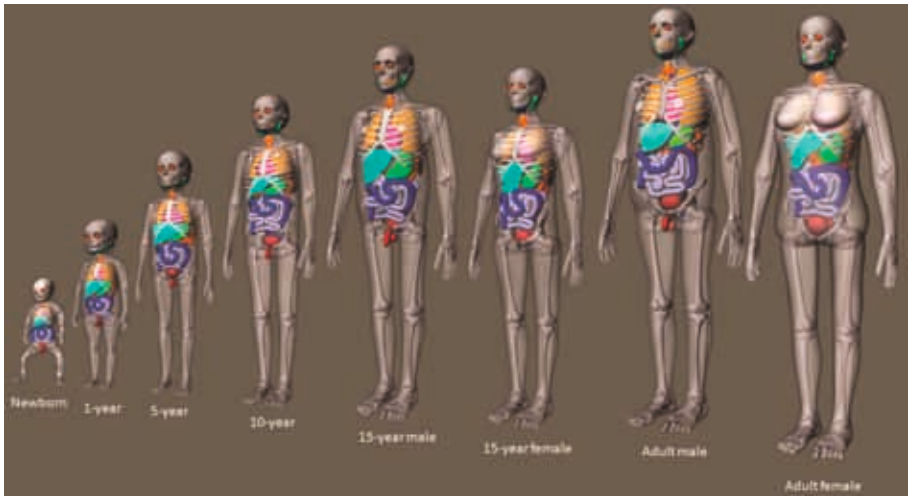

FIG. 7. The University of Florida series of reference hybrid phantoms.

radiation transport in the adult skeleton is that generated at the University of Leeds in the late 1960s to the mid-1970s. The Leeds group used optical scanning techniques to acquire linear path length distributions across the bone trabeculae and marrow cavities of the lumbar vertebrae for several subjects, as well as across several skeletal sites in a 1.7–year child (five sites), a 9-year child (five sites) and a 44-year male (seven sites) [19–20]. The bone and marrow pathlength distributions for the Leeds 44-year male subject have been used as the basis for electron (and thus beta particle and photon) absorbed fractions embodied in essentially all skeletal dosimetry models published to date. These include (1) MIRD Pamphlet No. 11 for nuclear medicine [21], (2) ICRP Publication 30 for radiation protection [22], (3) ORNL TM-8381 for photon internal dosimetry [11], (4) Bouchet et al. for nuclear medicine [23], (5) the MIRDOSE3 code [24] and (6) the OLINDA/EXM code [25].

Of equal importance are estimates of skeletal tissue mass. Unfortunately, complete tissue masses were not reported for the Leeds 44-year male subject, and thus the various skeletal dosimetry models above have had to rely on a variety of patient and/or cadaver studies as summarized in ICRP Publication 70 [26]. These studies include those by (a) Mechanik in 1926 (total marrow masses and their relative distribution within the skeleton) [27], (b) Custer in 1974 (reference marrow cellularities) [28], (c) Trotter and Hixon in 1974 (bone tissue masses) [29], and (d) Beddoe in 1976 (bone trabeculae surface–volume ratios for estimating endosteal tissue masses) [30]. The ICRP reference adult male skeletal model is thus assembled from a wide range of subject populations and measurement techniques. More fundamentally, the anatomical sources for its absorbed fractions are not the same as those from which reference tissue masses are reported.

Recent studies at the University of Florida have been focused on the construction of a comprehensive model for electron dosimetry in the adult and paediatric skeleton that specific address various limitations of existing models. These limitations include a lack of consideration of (1) electron escape from trabecular spongiosa and (2) electron cross-fire from cortical bone to spongiosa. Furthermore, the ICRP now defines the tissues at risk for radiogenic bone cancer as a 50 μm layer adjacent to the bone surfaces of the trabeculae and inner medullary cavities, but exclusive of the Haversian canals of cortical bone. The authors have previous reported on a revised skeletal dose model for the ICRP reference newborn [31]. Below is a summary of data for the ICRP reference adult male.

Candidate cadavers for skeletal model development were reviewed according the following selection criteria: (a) an age between 20 and 50 years, (b) a body mass index of between 18.5 and 30 kg/m^2, and (c) a cause of death that would preclude significant skeletal deterioration. The subject identified was a 40-year male approximately 82 kg and 170 cm at time of death. The subject died

of sudden complications associated with cardiopulmonary arrest following myocardial infarction. Prior to bone harvesting, the entire cadaver was imaged under CT at 1 mm axial resolution. Following detailed review of the in vivo CT images, bone harvesting was conducted. Thirty-eight major skeletal sites were excised from the male cadaver. These bones were cleaned of excess tissue, bagged, labelled, and stored frozen. Later, each bone was imaged under ex vivo CT scanning in order to (a) identify the location and extent of spongiosa to be sectioned for microCT imaging, and (b) quantify the fraction of bone volume associated with spongiosa, cortical bone, or medullary marrow. Following review of the ex vivo CT images, cores of marrow-intact spongiosa were strategically excised from each harvested bone sample, and subsequently imaged under microCT scanning at a 30 μm isotropic voxel size. For some bone sites, multiple cores were taken. For example, the cranial cap was sampled three times within its frontal, parietal and occipitable bones. Figure 8 shows representative images of the craniofacial bones and the sacrum at their macroscopic and microscopic scales. These image sets — voxelized heterogeneous bone models from the University of Florida adult male hybrid phantom and segmented microCT images of cored spongiosa — were used in tandem within the EGSnrc-based Paired

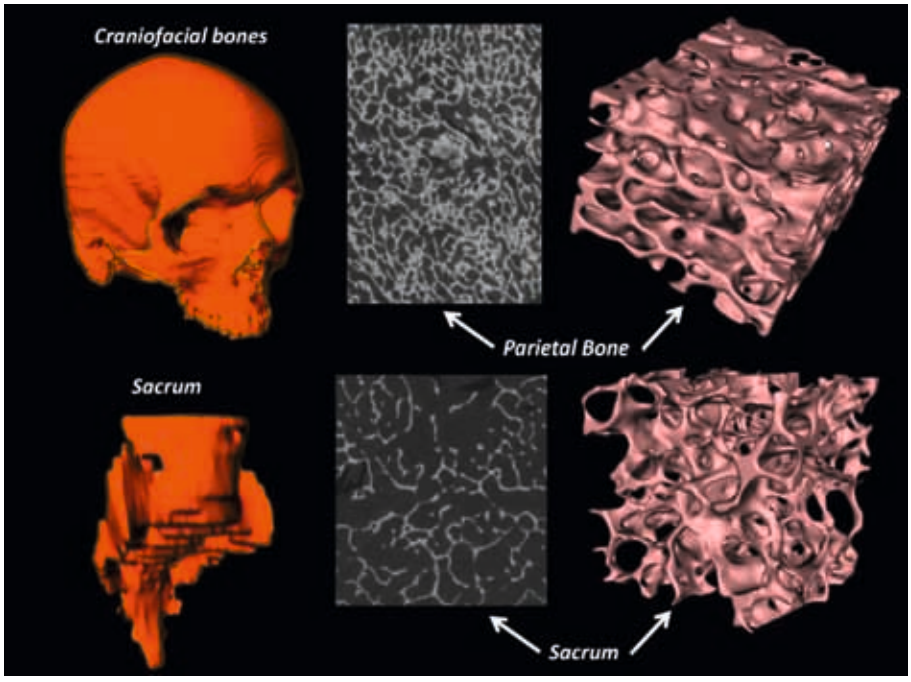

FIG. 8. Macroscopic and microscopic models for the craniofacial bones and sacrum.

Image Radiation Transport (or PIRT) model originally developed by Shah et al. [32].

Table 1 shows the partitioning of the homogeneous skeleton with in the University of Florida reference adult male hybrid phantom into its macroscopic

TABLE 1. MACROSCOPIC AND MICROSCOPIC VOLUME FRACTIONS ACROSS THE SKELETON OF THE UNIVERSITY OF FLORIDA ADULT MALE HYBRID PHANTOM

	Homogeneous	Homogeneous Bone Volume Fractions			Spongiosa Volume Fractions			ICRP 70
Skeletal Site	**Bone Volume** *(cm^3)*	*Cortical Bone*	*Spongiosa*	*Med Cavity*	*Trab Bone*	*Marrow*	*Shallow Marrow*	**Cellularity**
Craniofacial Bones	997.89	0.67	0.33	0.00				
Frontal / Facial	*249.47*				0.445	0.555	0.192	38%
Parietal	*449.05*				0.394	0.606	0.211	38%
Occipital	*299.37*				0.912	0.088	0.061	38%
Mandible	48.49	0.40	0.60	0.00	0.089	0.911	0.078	38%
Scapulae	488.91	0.35	0.65	0.00	0.153	0.847	0.100	38%
Clavicles	68.60	0.40	0.60	0.00	0.116	0.884	0.080	33%
Sternum	65.38	0.30	0.70	0.00	0.082	0.918	0.099	70%
Ribs	310.80							
Upper	*85.66*	0.40	0.60	0.00	0.103	0.897	0.072	70%
Middle	*135.25*	0.40	0.60	0.00	0.142	0.858	0.109	70%
Lower	*89.89*	0.40	0.60	0.00	0.101	0.899	0.109	70%
Cervical Vertebrae	96.67							
C3 (C1 - C3)	*42.43*	0.35	0.65	0.00	0.159	0.841	0.155	70%
C6 (C4 - C7)	*54.24*	0.35	0.65	0.00	0.194	0.806	0.140	70%
Thoracic Vertebrae	309.42							
T3 (T1 - T4)	*81.18*	0.25	0.75	0.00	0.132	0.868	0.111	70%
T6 (T5 - T8)	*98.15*	0.25	0.75	0.00	0.042	0.959	0.056	70%
T11 (T9 - T12)	*130.09*	0.25	0.75	0.00	0.111	0.889	0.106	70%
Lumbar Vertebrae	292.68							
L2 (L1 - L3)	*169.47*	0.20	0.80	0.00	0.114	0.887	0.112	70%
L4 (L4 - L5)	*123.21*	0.20	0.80	0.00	0.091	0.909	0.091	70%
Sacrum	197.17	0.25	0.75	0.00	0.118	0.882	0.111	70%
Os coxae	923.96	0.25	0.75	0.00	0.100	0.901	0.112	48%
Humeri, Proximal	180.80	0.15	0.85	0.00	0.096	0.904	0.080	25%
Humeri, Upper Shaft	91.44	0.65		0.35	0.000	1.000		25%
Humeri, Lower Shaft	81.37	0.65		0.35	0.000	1.000		0%
Humeri, Distal	110.65	0.30	0.70		0.151	0.849	0.127	0%
Radii, Proximal	18.03	0.30	0.70		0.089	0.911	0.063	0%
Radii, Upper Shaft	28.09	0.75		0.25	0.000	1.000		0%
Radii, Lower Shaft	28.09	0.75		0.25	0.000	1.000		0%
Radii, Distal	32.59	0.30	0.70		0.116	0.884	0.107	0%
Ulnae, Proximal	59.97	0.30	0.70		0.161	0.839	0.112	0%
Ulnae, Upper Shaft	34.30	0.75		0.25	0.000	1.000		0%
Ulnae, Lower Shaft	34.30	0.75		0.25	0.000	1.000		0%
Ulnae, Distal	11.29	0.25	0.75		0.139	0.861	0.133	0%
Wrists and Hands	141.62	0.65	0.35		0.151	0.849	0.127	0%
Femora, Proximal	260.72							
Head	*92.77*	0.05	0.95		0.229	0.771	0.144	25%
Neck	*167.89*	0.10	0.90		0.103	0.897	0.112	25%
Femora, Upper Shaft	194.87	0.35		0.65	0.000	1.000		25%
Femora, Lower Shaft	148.19	0.35		0.65	0.000	1.000		0%
Femora, Distal	303.72	0.10	0.90		0.146	0.854	0.118	0%
Patellae	246.65	0.10	0.90		0.146	0.854	0.118	0%
Tibiae, Proximal	113.79	0.10	0.90		0.115	0.885	0.108	0%
Tibiae, Upper Shaft	113.79	0.35		0.65	0.000	1.000		0%
Tibiae, Lower Shaft	90.75	0.35		0.65	0.000	1.000		0%
Tibiae, Distal	22.86	0.15	0.85		0.125	0.875	0.111	0%
Fibulae, Proximal	19.87	0.20	0.80		0.078	0.922	0.079	0%
Fibulae, Upper Shaft	19.87	0.70		0.30	0.000	1.000		0%
Fibulae, Lower Shaft	22.15	0.70		0.30	0.000	1.000		0%
Fibulae, Distal	35.59	0.30	0.70		0.147	0.853	0.128	0%
Ankles and Feet	508.46	0.30	0.70		0.146	0.854	0.118	0%
Total Skeleton *(cm^3)*	6753.78							
Total Skeletal Mass *(g)*	9355	*Note - based on average homogeneous bone density of 1.385 g cm-3*						
ICRP 89 Mass *(g)*	9350	*Note - ICRP 89 total skeletal mass (10,500 g) less that of cartilage (1100 g) and teeth (50 g)*						
Ratio	1.00							

and microscopic tissues. Homogeneous bone volumes are given in column 2 which fully encompass the 9350 g of total ICRP skeletal reference tissues. Columns 3 to 5 give the volume fractions of cortical bone, spongiosa, and medullary marrow as seen in the ex vivo CT scans of the 40-year male cadaver as adjusted to accommodate total reference mineral bone and total marrow. Columns 6 to 8 of Table 1 give volume fractions relevant only to cored specimens of spongiosa as seen under microCT imaging. Volume fractions for trabecular bone and marrow cavities sum to unity. The next volume fractions define the fraction of total spongiosa volume that is occupied by the marrow tissues within 50 μm of the bone surfaces — shallow marrow. Active marrow is further defined by the marrow cellularity and reference values from ICRP Publication 70 at shown in the final column of Table 1.

Tissue masses for the University of Florida adult male hybrid phantom are given in Table 2 in two sets — without and with 200 g of miscellaneous skeletal tissues. As noted at the bottom of Table 2, active and inactive marrow are matched exactly to ICRP reference values, with trabecular bone is 5% larger than reference, and cortical bone is 1% lower than reference. The ratio of trabecular to cortical bone is found to be 21%/79%, respectively, in the University of Florida adult male hybrid phantom — only slightly different than the rounded average of 20%/80% assumed by the ICRP.

Figure 9(A) shows the variation in values of the absorbed fraction for marrow self-irradiation, $\phi(AM \leftarrow AM)$ across all active marrow regions of the skeleton. These values are shown to be highest in the ribs and sacrum at energies below and above ~500 keV, respectively. They are lowest for the proximal femora/humeri and craniofacial bones below and above ~200 keV, respectively. Comparisons of skeletal averaged values of $\phi_{skel}(AM \leftarrow AM)$ are shown in Fig. 9(B) for the present study, and that given in the model of Stabin and Siegel [33]. Good agreement is seen for $\phi_{skel}(AM \leftarrow AM)$ across both models out to an energy of ~400 keV, after which the Stabin and Siegel model increasingly overestimates energy deposition to active marrow due to a lack of consideration for electron escape from spongiosa. A similar divergence in model results was seen for the ICRP reference newborn, but beginning at a much lower energy of only 10 keV [31].

Figures 10(A) and 11(A) show values of the absorbed fraction to active marrow for electron sources on the surfaces and in the volumes, respectively, of trabecular bone. Values of $\phi(AM \leftarrow TBS)$ at energies below ~100 keV are fairly constant with magnitudes dictated primarily by bone-specific variations in marrow cellularity. Maximal values of $\phi(AM \leftarrow TBS)$ and $\phi(AM \leftarrow TBV)$ are seen at energies between 500 keV and 800 keV, and are highest in the sternum and sacrum, and lowest in the proximal humeri/femora and craniofacial bones.

TABLE 2. TISSUE MASSES WITHIN THE SKELETON OF THE UNIVERSITY OF FLORIDA ADULT MALE HYBRID PHANTOM

	Tissue Masses exclusive of MST *(g)*				Tissue Masses inclusive of MST *(g)*				
Skeletal Site	**AM**	**IM**	**TBV**	**CBV**	**AM**	**IM**	**TM_{50}**	**TBV**	**CBV**
Craniofacial Bones	54.84	85.13	341.48	1233.79	56.46	87.78	52.96	346.96	1253.59
Mandible	10.08	15.65	4.76	35.79	10.38	16.13	2.27	4.83	36.36
Scapulae	102.34	158.86	89.67	315.78	105.37	163.81	31.65	91.11	320.84
Clavicles	12.02	23.21	8.78	50.64	12.37	23.94	3.28	8.92	51.45
Sternum	29.42	12.00	6.92	36.20	30.29	12.37	4.61	7.03	36.78
Ribs	115.00	46.89	41.06	229.41	118.41	48.35	18.70	41.72	233.09
Cervical Vertebrae	36.14	14.74	20.72	62.44	37.21	15.20	9.34	21.05	63.44
Thoracic Vertebrae	147.17	60.01	40.42	142.75	151.53	61.88	21.58	41.07	145.04
Lumbar Vertebrae	146.92	59.91	44.91	108.02	209.81	61.77	24.56	45.63	109.75
Sacrum	91.36	37.25	32.15	90.96	94.06	38.41	16.68	32.66	92.42
Os coxae	299.65	308.86	127.24	426.26	308.52	318.47	77.74	129.28	433.10
Humeri, Proximal	34.75	99.18	27.23	50.05	35.77	102.26	12.13	27.66	50.85
Humeri, Upper Shaft	8.00	22.85	0.00	109.68	8.24	23.56	0.46	0.00	111.44
Humeri, Lower Shaft	0.00	27.11	0.00	97.60	0.00	27.95	0.45	0.00	99.17
Humeri, Distal	0.00	62.57	21.63	61.26	0.00	64.52	9.63	21.97	62.24
Radii, Proximal	0.00	10.95	2.06	9.98	0.00	11.29	0.78	2.10	10.14
Radii, Shaft	0.00	13.37	0.00	77.75	0.00	13.78	0.39	0.00	79.00
Radii, Distal	0.00	19.20	4.88	18.04	0.00	19.79	2.39	4.96	18.33
Ulnae, Proximal	0.00	33.52	12.48	33.20	0.00	34.56	4.62	12.68	33.73
Ulnae, Shaft	0.00	16.32	0.00	94.94	0.00	16.83	0.43	0.00	96.47
Ulnae, Distal	0.00	6.94	2.17	5.21	0.00	7.16	1.11	2.21	5.29
Wrists and Hands	0.00	40.04	13.84	169.87	0.00	41.29	6.16	14.06	172.60
Femora, Proximal	50.87	145.22	66.09	39.54	52.38	149.73	29.40	67.15	40.18
Femora, Upper Shaft	31.68	90.42	0.00	125.86	32.62	93.24	1.02	0.00	127.88
Femora, Lower Shaft	0.00	91.68	0.00	95.71	0.00	94.54	1.00	0.00	97.25
Femora, Distal	0.00	222.14	73.75	56.05	0.00	229.05	31.70	74.93	56.95
Patellae	0.00	26.03	8.64	6.57	0.00	26.84	3.71	8.78	6.67
Tibiae, Proximal	0.00	186.91	47.27	45.52	0.00	192.72	23.57	48.03	46.25
Tibiae, Shaft	0.00	140.80	0.00	146.99	0.00	145.18	1.49	0.00	149.35
Tibiae, Distal	0.00	64.01	17.73	25.63	0.00	66.00	8.35	18.01	26.05
Fibulae, Proximal	0.00	16.05	2.63	8.44	0.00	16.55	1.41	2.67	8.57
Fibulae, Shaft	0.00	11.35	0.00	51.33	0.00	11.70	0.42	0.00	52.16
Fibulae, Distal	0.00	12.59	4.21	12.26	0.00	12.98	1.94	4.28	12.46
Ankles and Feet	0.00	289.25	96.03	281.49	0.00	298.25	41.27	97.57	286.01
Totals	1170	2471	1159	4355	1263	2548	447	1177	4425
								Total Skeletal Mass	9414
ICRP 89 Values	1170	2480	1100	4400				**ICRP 89 Value**	9350
Ratio	1.00	1.00	1.05	0.99				**Ratio**	1.01

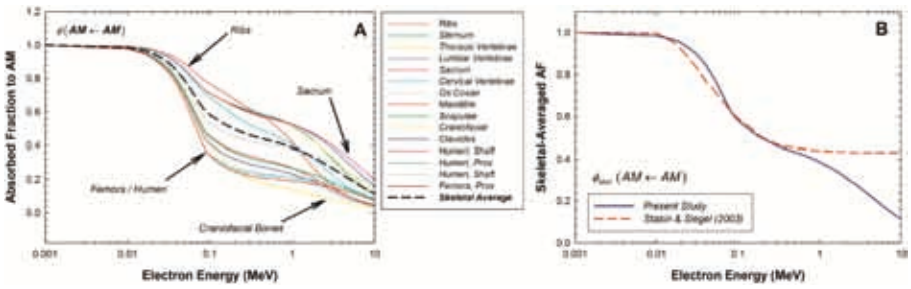

FIG. 9. Absorbed fractions for electron self-dose to active marrow (A) by bone site in the University of Florida adult male phantom, and (B) in comparison to the model of Stabin and Siegel [33].

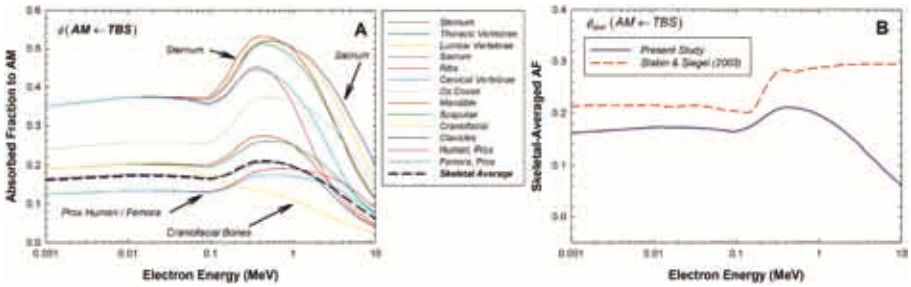

FIG. 10. Absorbed fractions to active marrow from electron sources on the trabecular surfaces (A) by bone site in the University of Florida adult male phantom, and (B) in comparison to the model of Stabin and Siegel [33].

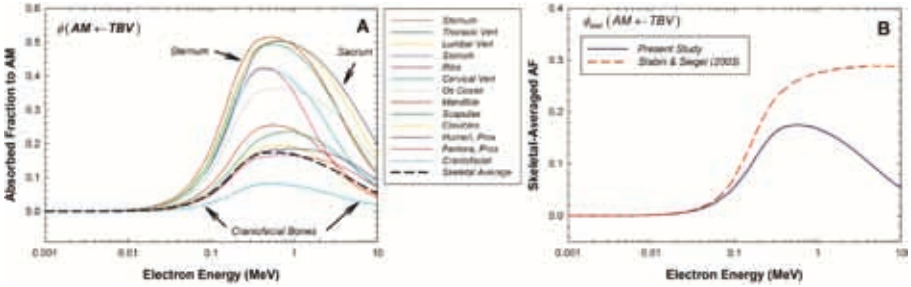

FIG. 11. Absorbed fractions to active marrow from electron sources in the trabecular volumes (A) by bone site in the University of Florida adult male phantom, and (B) in comparison to the model of Stabin and Siegel [33].

Skeletal averaged values for $\phi(AM \leftarrow TBS)$ and $\phi(AM \leftarrow TBV)$ influenced by their values seen in the craniofacial bones which account for 15.3% of total trabecular surfaces and 29.5% of total trabecular bone mass.

Skeletal averaged absorbed fractions in trabecular bone are shown in Figures 10(B) and 11(B) for the present model begin at 0.16 at low energy (product of a half-space value of 0.5 and a skeletal averaged marrow cellularity of 0.32). In contrast, values of $\phi_{skel}(AM \leftarrow TBS)$ under the Stabin and Siegel model report a value of 0.213 at 1 keV, a value not supported by ICRP reference marrow masses. Under the present model, values of $\phi_{skel}(AM \leftarrow TBS)$ begin to increase at ~100 keV and peak at ~400 keV due to electron traversal of the bone trabeculae, after which they decline owing to electron escape. In contrast, values of $\phi_{skel}(AM \leftarrow TBS)$ in the Stabin and Siegel model continue to climb and plateau at just under 0.3. for electrons born uniformly within the trabecular volumes, the curves of Figure 11(B) show a divergence of model results as low as 40 keV.

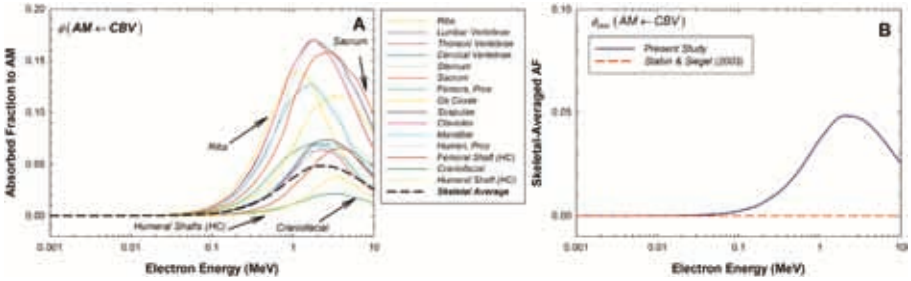

FIG. 12. Absorbed fractions to active marrow from electron sources in the cortical volumes (A) by bone site in the University of Florida adult male phantom, and (B) in comparison to the model of Stabin and Siegel [33].

Values of $\phi_{skel}(AM \leftarrow CBV)$ for cortical bone sources are shown in Fig. 12(A) across the bones of the University of Florida adult male hybrid phantom, and in Fig. 12(B) for their skeletal averaged values in the present model. The model of Stabin and Siegel does not consider irradiation of spongiosa tissues from electron sources in cortical bone (an absorbed fraction value of zero is assumed).

4. FUTURE DIRECTIONS

With the development of hybrid phantom technology and the construction of patient dependent phantom libraries, existing dosimetry software can be extended away from its historical reliance on reference phantoms. This is particular relevant for nuclear medicine and CT dosimetry, where Monte Carlo calculations of energy deposition for specified source organs and for clinically relevant body examinations can be performed and made available for patient dose assignment through simple matching by patient age, gender, height and weight. As image processing techniques become increasing automated, patient sculpted and even patient specific phantoms, coupled with real time Monte Carlo or even deterministic radiation transport simulations can be implemented in the clinic. Assessments of skeletal tissue are increasingly being refined through detailed cadaver based reference models. Challenges for the future, however, are to make these models more patient specific through adjustments for skeletal size, marrow cellularity and bone microstructure.

ACKNOWLEDGEMENTS

This work was supported in part by grants R01 CA116743 and R01 CA96441 with the National Cancer Institute, and by grant DE-FG07-06ID14773 with the US Department of Energy.

REFERENCES

[1] NATIONAL COUNCIL ON RADIATION PROTECTION AND MEASUREMENT, Ionizing radiation exposure of the population of the United States, NCRP Report No. 160, Bethesda, MD (2009).

[2] NATIONAL ACADEMY OF SCIENCES, Health risks from exposure to low-levels of ionizing radiation: BEIR II — Phase 2, National Research Council, Washington, DC (2005).

[3] AMIS, E.S. et al., American College of Radiology white paper on radiation dose in medicine, J Am. Coll. Radiol. **4** (2007) 272–284.

[4] FOOD AND DRUG ADMINISTRATION, CENTER FOR DEVICES AND RADIOLOGICAL HEALTH, Initiative to reduce unnecessary radiation exposure from medical imaging, Silver Springs, MD (2010).

[5] BOLCH, W.E., ECKERMAN, K.F., SGOUROS, G., THOMAS, S.R., MIRD Pamphlet No. 21 — A generalized schema for radiopharmaceutical dosimetry: standardization of nomenclature, J Nucl Med **50** (|2009) 477–484.

[6] ZANKL, M., VEIT, R., WILLIAMS, G., SCHNEIDER, K., FENDEK, H., PETOUSSI, N., DREXLER, G., The construction of computer tomographic phantoms and their application in radiology and radiation protection, Radiat Env Biophys **27** (1988) 153–164.

[7] ZUBAL, I.G., HARRELL, C.R., SMITH, E.O., RATTNER, Z., GINDI, G., HOFFER, P.B., Computerized three-dimensional segmented human anatomy, Med Phys **21** (1994) 299–302.

[8] ZUBAL, I.G., HARRELL, C.R., SMITH, E.O., SMITH, A.L., KRISCHLUNAS, P., High resolution, MRI-based, segmented, computerized head phantom. (S-STELSON, A.T., STABIN, M.G., SPARKS, R.B., Eds) (Proceedings of the Sixth International Radiopharmaceutical Dosimetry Symposium. Oak Ridge, Tennessee: Oak Ridge Associated Universities) (1996) 319–324.

[9] SEGARS, W.P., TSUI, B.M., Study of the efficacy of respiratory gating in myocardial SPECT using the new 4D NCAT phantom, IEEE Trans Nucl Sci **49** (2002) 675–679.

[10] INTERNATIONAL COMMISSION ON RADIOLOGICAL PROTECTION, Basic anatomical and physiological data for use in radiological protection – reference values. ICRP Publication 89, Annals of the ICRP **32** (2002) 1–277.

[11] CRISTY, M., ECKERMAN, K.F., Specific absorbed fractions of energy at various ages from internal photon sources, ORNL TM-8381, Oak Ridge National Laboratory, Oak Ridge, TN (1987).

[12] INTERNATIONAL COMMISSION ON RADIOLOGICAL PROTECTION, Adult reference computational phantoms, ICRP Publication 110, Annals of the ICRP **39** (2009) 1–165

[13] KRAMER, R., KHOURY, H.J., VIEIRA, J.W., LIMA, V.J., MAX06 and FAX06; update of two adult human phantoms for radiation protection dosimetry, Phys Med Biol **51**: (2006) 331–3346.

[14] LEE, C., LODWICK, D., HURTADO, J., PAFUNDI, D., WILLLIAMS, J.L., BOLCH, W.E., The UF family of reference hybrid phantoms for computational radiation dosimetry, Phys Med Biol **55** (2010) 339–363.

[15] ZHANG, J., NA, Y.H., CARACAPPA, P.F., XU, X,G., RPI-AM and RPI-AF, a pair of mesh-based, size-adjustable adult male and female computational phantoms using ICRP-89 parameters and their calculations for organ doses from monoenergetic photon beams, Phys Med Biol **54** (2009) 5885–5908.

[16] CASSOLA, V.F., LIMA, V.J., KRAMER, R., KHOURY, H.J., FASH and MASH: female and male adult human phantoms based on polygon mesh surfaces: I. Development of the anatomy, Phys Med Biol **55** (2010) 133–162.

[17] JOHNSON, P., WHALEN, S., WAYSON, M., JUNEJA, B., LEE, C., BOLCH, W., Hybrid patient dependent phantoms covering statistical distributions of body morphometry in the US adult and pediatric population, Proc IEEE **97** (2009) 2060–2075.

[18] DE LA GRANDMAISON, G.L., CLAIRAND, I., DURIGON, M., 2001 Organ weight in 684 adult autopsies: new tables for a Caucasoid population, Forensic Sci Int **119** (2001) 149–154.

[19] DARLEY, P.J., An investigation of the structure of trabecular bone in relation to the radiation dosimetry of bone-seeking radionuclides (Department of Medical Physics, Leeds, UK: University of Leeds) (1972) 231.

[20] BEDDOE, A.H., DARLEY, P.J., SPIERS, F.W., Measurements of trabecular bone structure in man, Phys. Med. Biol. **21** (1976) 589–607.

[21] SNYDER, W.S., FORD, M.R., WARNER, G.G., WATSON, S.B., MIRD Pamphlet No. 11: *S*, absorbed dose per unit cumulated activity for selected radionuclides and organs (New York, NY: Society of Nuclear Medicine) (1975).

[22] INTERNATIONAL COMMISSION ON RADIOLOGICAL PROTECTION, Publication 30: Limits for intakes of radionuclides by workers. (Oxford, UK: International Commission on Radiological Protection) (1980).

[23] BOUCHET, L.G., BOLCH, W.E., HOWELL, R.W., RAO, D.V., S values for radionuclides localized within the skeleton, J. Nucl. Med. **41** (2000) 189–212.

[24] STABIN, M.G., MIRDOSE: personal computer software for internal dose assessment in nuclear medicine, J. Nucl. Med. **37** (1996) 538–546.

[25] STABIN, M.G., SPARKS, R.B., CROWE, E., OLINDA/EXM: the second-generation personal computer software for internal dose assessment in nuclear medicine, J Nucl Med **46** (2005) 1023–102.

[26] INTERNATIONAL COMMISSION ON RADIOLOGICAL PROTECTION, Publication 70: Basic anatomical and physiological data for use in radiological protection: the skeleton, Ann ICRP **25** (1995) 1–180.

[27] MECHANIK, N., Studies of the weight of bone marrow in man Zeitschrift fur die Gest. Anatomy **79** (1926) (1926) 58–99.

[28] CUSTER, R., An Atlas of the Blood and Bone Marrow (Philadelphia, PA: W.B. Saunders) (1974).
[29] TROTTER, M., HIXON, B., Sequential changes in weight, density, and percentage ash weight of human skeletons from an early fetal period through old age, Anat. Rec. **179** (1974) 1–18.
[30] BEDDOE, A.H., The microstructure of mammalian bone in relation to the dosimetry of bone-seeking radionuclides (Department of Medical Physics, Leeds, UK: University of Leeds) (1976) 165.
[31] PAFUNDI, D., RAJON, D., JOKISCH, D., LEE, C., BOLCH, W., An image-based skeletal dosimetry model for the ICRP reference newborn–internal electron sources, Phys Med Biol **55** (2010) 1785–1814.
[32] SHAH, A.P., BOLCH, W.E., RAJON, D.A., PATTON, P.W., JOKISCH, D.W., A paired-image radiation transport model for skeletal dosimetry, J Nucl Med **46** (2005) 344–353.
[33] STABIN, M.G., SIEGEL, J.A., Physical models and dose factors for use in internal dose assessment, Health Phys **85** (2003) 294–310.

INVERSE TREATMENT PLANNING FOR TARGETED RADIONUCLIDE THERAPY

J.J. GONZÁLEZ-GONZÁLEZ*, C.F. CALDERÓN-MARÍN*, R. ALFONSO-LAGUARDIA**, O. DÍAZ-RIZO***, J.P. OLIVA*, R.P. BAUM[+]

* Department of Nuclear Medicine,
Institute of Oncology and Radiobiology
Email: jgg@infomed.sld.cu

** Department of Radiotherapy,
Institute of Oncology and Radiobiology

*** Institute of Applied Sciences and Technologies

Havana, Cuba

[+] Department of Nuclear Medicine,
Centre for PET,
Bad Berka Zentralklinik,
Bad Berka, Germany

Abstract

A method for inverse treatment planning was developed for patient specific targeted radionuclide therapy. The method is based on the calculation of patient-specific absorbed dose distribution using imaging data, incorporating radiobiological modelling to account for effects of dose rate distribution for prediction of tumour response. The equivalent uniform biologically effective dose concept was introduced as an additional tool for optimizing the treatment plan and evaluating its potential outcome. The inverse planning process consists in estimating the activity to be administered from the prescription of treatment in terms of tumour control probability within the accepted normal organs dose limiting toxicity for treatment schemes that use multiple activity administrations. Clinical case data were used for planning different treatment schemes with different numbers of equal amount of activity, assuming that each amount of administered activity will produce the same biological effect. The comparison of results between direct and inverse planning showed no significant differences.

1. INTRODUCTION

Nuclear medicine has a long history of systemic application of beta emitter radiopharmaceuticals for treatment of different diseases. Traditionally, the treatments are prescribed in terms of administered activity, taking into account the local and international clinical experience. One of the key challenges of targeted radionuclide therapy is the optimization of the activity to be administered and estimate in advance its potential benefit to a specific patient. For this purpose, it is necessary to quantify the relationship between administered activity and absorbed dose to tumour and normal organs that, expressed in terms of biological effects, allows estimating the radiation dose that maximizes the treatment response within the accepted tolerance for dose limiting organs. The importance of dosimetric treatment planning is that it provides the tools for these purposes.

This paper describes an inverse planning method to estimate the amount of activity to be administered from treatment prescription in terms of tumour control probabilities within the accepted normal organs dose limiting toxicity for patient specific targeted radionuclide therapy.

2. MATERIALS AND METHODS

The method proposed here is based on calculating patient specific absorbed dose distribution using imaging data, incorporating radiobiological modelling to account for effects of dose rate distribution for prediction of tumour response. Taking into account that the efficacy of targeted radionuclide therapy is affected by non-uniformity of dose and dose rate distributions in tumours, the equivalent uniform biologically effective dose (EUBED) concept was introduced as an additional tool for optimizing the treatment plan and evaluating its potential outcome. The EUBED model converts the spatial biologically effective dose (BED) distribution into an equivalent uniform biologically effective dose value that would produce a biological response similar to that expected from the original BED distribution . The EUBED describes the biological effects for non-uniform BED distribution and may be used for predicting tumour response. Accordingly, the proposed method of treatment planning quantifies the relationship between administered activity and the absorbed dose distribution that, expressed in terms of biological effect, maximizes the EUBED in tumour while the mean dose in the dose limiting normal organs is maintained within accepted values.

2.1. Inverse planning dosimetry

Considering that the tumour control probability (TCP) is one of the most relevant endpoints for treatment of tumours using ionizing radiation, a method for inverse dosimetric planning was introduced to determine the activity to be administered from treatment prescription in terms of TCP, assuming that each amount of administered activity will produce the same biological effect for treatment schemes that use multiple activity administrations that are equally time spaced .

The input data for calculations are:

— The integral dose volume histogram (iDVH) in Gy/GBq obtained from spatial absorbed dose distribution of tumour using SPECT images;
— The estimated mean absorbed
— dose of the dose limiting organ.

From the prescribed TCP, the corresponding EUBED is calculated by using the Poisson´s statistic model [3] , as follows:

$$EUBED = -\frac{1}{\alpha}\ln\left(-\frac{\ln(TCP)}{\rho V_T \Psi 2^{\frac{T}{T_d}}}\right) \quad (1)$$

where

α is the linear coefficient of the linear-quadratic model (Gy^{-1}), which is a measure of cell radiosensitivity;
ρ is the tumour cell density (cells/g), the number of cells per cm^3 of tumour;
V_T is the tumour volume, determined from CT images;
Ψ is the clonogenic fraction, the fraction of clonogenic cells from the total tumour cells;
T_d is the effective tumour doubling time, the time for tumour volume to double; and
T is the overall treatment time.

The overall treatment time is defined as:

$$T = (N - 1)t + T_c \quad (2)$$

where

N is the number of activity administrations;
t is the time interval between each administration of activity; and
T_c is the critical time at which the dose is too small to be effective.

The estimated EUBED is then divided by the number of activity administrations, N, to determine the corresponding partial $EUBED_p$ for one administration. The iDVH is converted to integral BED dose volume histogram (iBVH) from which the corresponding differential BED volume histogram (dBVH) is obtained. The BED values within the bin i of the histogram were calculated using a model based on cell repair and proliferation during the internal irradiation at low dose rate with beta emitters [6]. According to this model, for biexponential temporal behaviour of tumour dose rate [7], the BED values may be estimated as:

$$BED(T_c)_i = D_i\left\{1+\frac{T_eT_\mu D_i^2}{\tau^2\left(\frac{\alpha}{\beta}\right)}\left[\frac{T_e}{T_e+T_\mu}\left(1-\frac{2T_\mu}{T_e+T_\mu}\right)\right]-2T_u\left[\frac{1}{T_e-T_\mu}\left(\frac{T_e}{T_e+T_u}+\frac{T_\mu}{T_u+T_\mu}\right)+\frac{1}{T_u-T_\mu}\left(\frac{T_uT_\mu}{T_e(T_u+T_\mu)}+\frac{T_u}{T_e+T_u}-\frac{T_\mu}{T_e-T_\mu}-\frac{T_u}{2T_e}\right)\right]\right\}-D_c\left[1+\frac{D_c}{\left(\frac{\alpha}{\beta}\right)}\left(\frac{T_\mu}{T_e+T_\mu}\right)\right]+D_c\ln\left(\frac{\tau D_c}{T_eD_i}\right) \quad (3)$$

where

T_c is the critical time at which the dose is too small to be effective;
D_i is the mean absorbed dose (Gy) within the bin i on the iDVH;
T_e is the effective elimination half-time (h);
T_u is the effective uptake half-time (h);
τ is the effective time (h);
T_μ is the cell repair half-time (h);
α is the linear coefficient on the linear-quadratic model (Gy^{-1});
β is the quadratic coefficient on the linear-quadratic model (Gy^{-2}); and
D_c is the critical dose value from which the treatment is not effective.

$$D_c = 1.443kT_e \quad (4)$$

where k is the critical dose rate value (Gy/h) that is not effective for tumour cells sterilization.

The amount of activity that produces previously estimated partial $EUBED_p$ is determined from the dBVH by an iterative method [8]. The constraint condition is that the estimated amount of administered activity must be equal or less than maximum tolerated activity (MTA). The administered activity, A, is

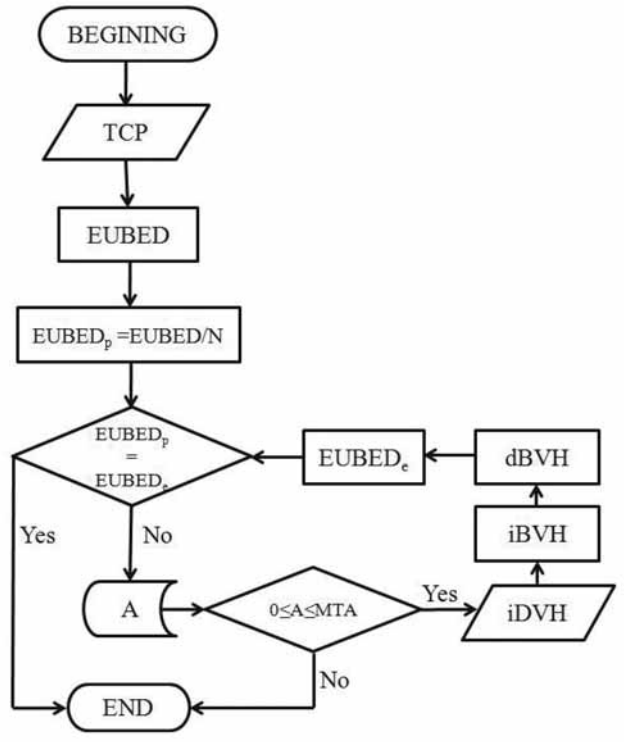

FIG. 1. Flow chart of dose of the inverse planning process.

changed within the established constraints condition to estimate the corresponding $EUBED_e$ value according to the following Eq. :

$$EUBED_e = -\frac{1}{\alpha}\ln\left(\sum_i P(\psi_i)e^{-\alpha\psi_i}\Delta\psi_i\right) \quad (5)$$

where $P(\psi)$ is the normalized probability distribution of BED, ψ_i.

The process is repeated until the $EUBED_e$ = $EUBED_p$ or when the activity, A, is greater than MTA. The treatment optimization is performed by means of varying the number of activity administrations to maximize the EUBED, while the mean dose to dose limiting organ is maintained within the accepted value. The flow chart in Fig. 1 shows the inverse planning process.

The results from inverse planning were compared with those obtained by direct planning. Briefly, the direct planning determines the dose distribution produced for a given amount of activity from which the corresponding BED distribution is calculated. The EUBED for this distribution of BED is estimated from the dBVH using Eq. (5) multiplied by the number of administrations. The

total cumulated EUBED is then used to calculate the TCP by the Poisson statistical model. An Excel spreadsheet was developed to implement the described method for inverse treatment planning.

2.2. Application to a patient study

The method was applied to scintigraphic data of a patient with inoperable liver and spleen metastases of a carcinoid tumour included on a clinical trial. The patient was injected with 110 MBq of ^{111}In-DOTATOC to assess the tumour uptake and retention before treatment with ^{90}Y-DOTATOC [9]. A previous CT study was performed to determine the volume of tumour metastases. A set of anterior and posterior whole body images and several blood samples were acquired at predefined time intervals. A SPECT study of the abdominal region was performed at 8 h after the injection of radiopharmaceutical. A set of 128 projections of 64 × 64 matrix size with 10 s per projection was acquired using circular orbit.

The van Reenen et al. method [10] was used for whole body images quantification. The SPECT projections were scatter corrected [11] using adjacent scatter windows on either side of the photopeak window placed at 172 keV, filtered with Hamming-Hann filter and reconstructed using filtered back projection method. The reconstructed images were corrected for photon attenuation using the Chang method [12].

The fraction of injected activity in the abdominal region at time t (the same region in which the SPECT study was acquired) was calculated from geometric mean counts on this region and the first whole body counts. The fraction of injected activity in the abdominal region was fitted to the sum of two exponentials functions, and the area under this curve was analytically determined and expressed as the number of disintegrations per unit of activity. This value was assigned to the segmented SPECT volume corresponding to the abdominal region of the patient. By scaling the total SPECT counts to the number of disintegrations per unit of activity in abdominal region, it is assumed that the spatial distribution measured at the time in which the SPECT study was acquired is constant, but the kinetic of radiopharmaceutical is followed by planar imaging [13]. Indeed, the relative activity concentration ratio measured in a portion of tumour or normal organ with respect to any other portion of the same tumour or normal organ is assumed constant throughout the uptake and retention of radiopharmaceutical, so that the same relationship in the number of disintegrations per unit of activity would then also be observed. This method has the advantage of minimizing the effects of background subtraction and organ superposition on the quantification of activity from planar imaging.

The tumour volumes of interest (VOIs) were created over SPECT images from an iterative selection of threshold values that best matched with the corresponding tumour volume determined by the CT study. All metastatic tumours were included in one VOI.

The tumour absorbed dose distribution was calculated by the S factor method at the voxel level [14] from SPECT images of the abdominal region. In peptide therapy with radiolabelled somatostatin analogues, the kidneys and the bone marrow are usually the dose limiting organs [19–21]. In this patient, the renal uptake of radiopharmaceutical was not observed and therefore, the bone marrow was identified as dose limiting organ. The bone marrow dose was calculated using the patient-specific method from radioactivity concentration in blood and body [19]. Owing to the small size of radiopeptide, a factor of 0.6 relating the specific activity in the red marrow to that in blood was used [20].

Since the carcinoids are slow growing radioresistant tumours [21], mean radiobiological parameters were selected for tumours with these characteristics [22]. The values of α and β were chosen to be 0.3 Gy^{-1} and 0.05 Gy^{-2}, respectively, whereas the repair half-time T_{μ} = 1.5 h, the effective doubling time T_d = 90 d and the critical dose rate k = 0.1 $Gy \cdot d^{-1}$. The values of clonogenic fraction ψ = 0.1, tumour cell density $\rho = 10^9$ cells/g were selected for calculations.

2.3. Planning strategy

The planning strategy was based on the following considerations:

— In the presence of non-uniform dose distribution, the treatment is less effective as the amount of administered activity increase [25].
— The dose fractionation is better tolerated by patients and contributes to alleviate the effects of non-uniform dose distribution on treatment efficacy [26].

Similarly to external beam radiotherapy, it was considered that a radiation treatment could be justified when a TCP $\geq$ 0.5 (50%) is reached without producing severe toxicity induced by ionizing radiation to normal organs. Accordingly, for dosimetric planning of this patient, the following problem was considered: to determine the amount of activity of ^{90}Y-DOTATOC-SMS to be injected to produce a TCP $\geq$ 0.5 (50%) without exceeding the maximum tolerate activity (MTA) for the dose limiting organ in several administrations of activity that are equally time-spaced.

For comparison and evaluation of results, different treatment schemes with different numbers of administrations were selected. The total activity was constant for each selected treatment scheme.

3. RESULTS

Table 1 shows the tumour dose statistics. Figures 2 and 3 show the obtained tumour absorbed dose distribution and the corresponding dose volume histograms. As shown, there is a high degree of non-uniformity in dose distribution with a variation coefficient equal to 54.2%.

TABLE 1. TUMOUR DOSE STATISTICS

Mean dose (Gy/GBq)	Minimum dose (Gy/GBq)	Maximum dose (Gy/GBq)	Variation coefficient (%)
7.53	2.52	19.63	52.4

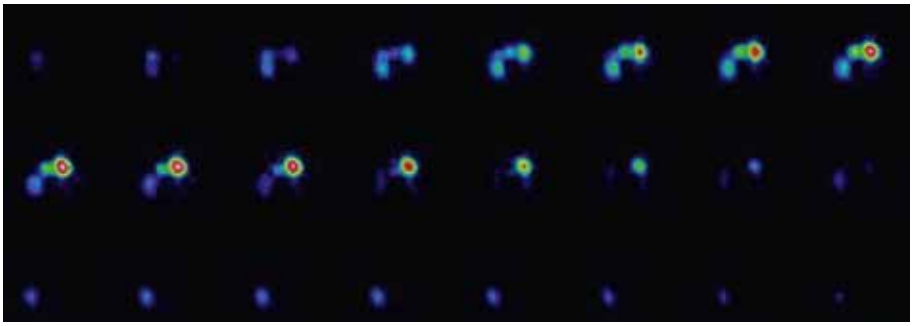

FIG. 2. Spatial distribution of tumours absorbed dose in Gy/GBq.

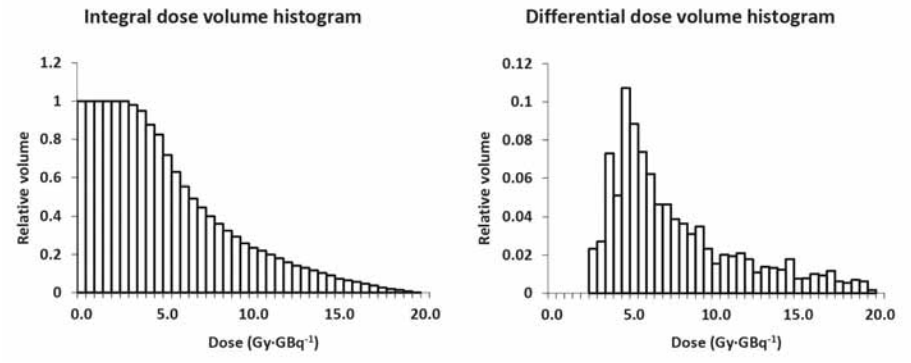

FIG. 3. Dose volume histograms.

The mean dose per unit of injected activity for bone marrow was estimated at 0.08 Gy/GBq. For this patient, the MTA was estimated at 25 GBq from MTD for bone marrow of 2 Gy [27].

Several treatment schemes with total activity of 22.2 GBq were obtained by direct planning considering six weeks intervals between each administration [18]; results are shown in Table 2. As can be seen, there are several treatment schemes that satisfied the treatment prescription (TCP ≥ 50%).

Table 3 shows the activity values estimated by inverse planning from TCP values obtained by direct planning. The comparison of both activity values shows no significant differences for each treatment scheme.

TABLE 2. TREATMENT SCHEMES OBTAINED FROM DIRECT PLANNING WITH TCP ≥ 50%

Activity (GBq)	Marrow dose (Gy)	Tumour dose (Gy)	Tumour BED (Gy)	Tumour partial EUBED (Gy)	Number of administrations	Cumulated EUBED (Gy)	TCP (%)
7.4	0.59	55.7	71.3	29.8	3	89.4	60.0
5.55	0.44	41.8	49.8	23.3	4	93.2	80.2
4.44	0.35	33.4	37.9	19.3	5	96.5	89.0
3.7	0.3	27.9	30.5	16.5	6	99.0	92.9
2.78	0.22	20.9	21.7	12.8	8	102.2	94.8
2.22	0.18	16.7	16.7	10.5	10	105.0	95.7

TABLE 3. COMPARISON OF ACTIVITY VALUES OBTAINED BY INVERSE PLANNING AND THOSE USED BY DIRECT PLANNING FOR EACH TREATMENT SCHEME

(%)	Number of administrations	Direct planning	Inverse planning
		Activity (GBq)	Activity (GBq)
60.0	3	7.40	7.40
80.2	4	5.55	5.55
89.0	5	4.44	4.44
92.9	6	3.70	3.70
94.8	8	2.78	2.77
95.7	10	2.22	2.22

4. DISCUSSION

The main consequence of non-uniform dose distribution is the loss of treatment effectiveness. The greater the non-uniformity, less effective becomes the treatment. Figure 4 shows that the EUBED does not increase in the same proportion as the mean BED with the increment of the activity. This result shows that for non-uniform dose distribution, the treatment will be proportionally less effective with the increment of activity.

In this patient, for example, one administration of 22.2 GBq of activity will produce a EUBED equal to 83 Gy. For one administration of 2.22 GBq, it is 10.5 Gy. If each administration of activity produces the same biological effects, the EUBED delivered in 10 administrations of 2.22 GBq will be equal to 105 Gy. The differences in cells kill between these two values of EUBED will be greater than a factor of 700.

Figures 5 and 6 show how the EUBED and TCP increase with the number of activity administrations. These results demonstrate that a strategy based on multiple administrations of activity contributes to optimize the treatment maximizing the EUBED in the tumour within the accepted tolerance of dose limiting organ.

According to the results shown on Table 3, there are no differences between activity estimation by inverse planning and those used by direct planning. During the direct planning, the dBVH is obtained directly from BED distribution at voxel

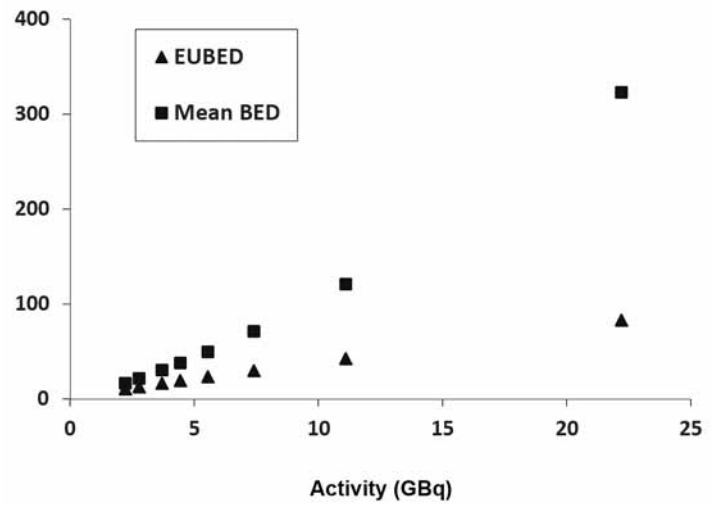

FIG. 4. Variation of mean BED and EUBED with the activity.

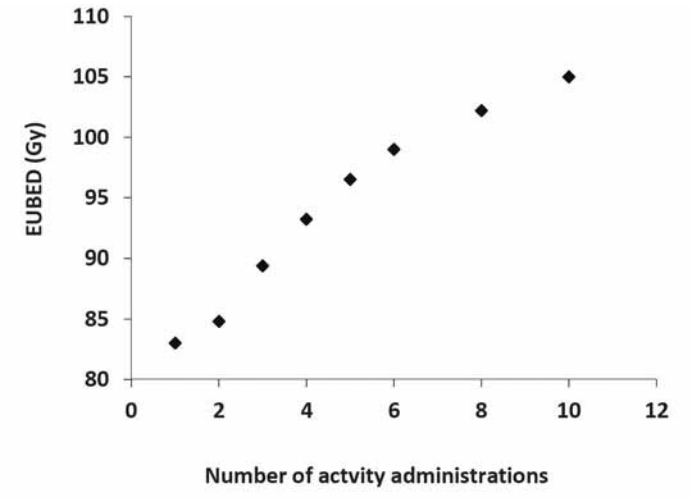

FIG. 5. Cumulated EUBED versus number of activity administrations.

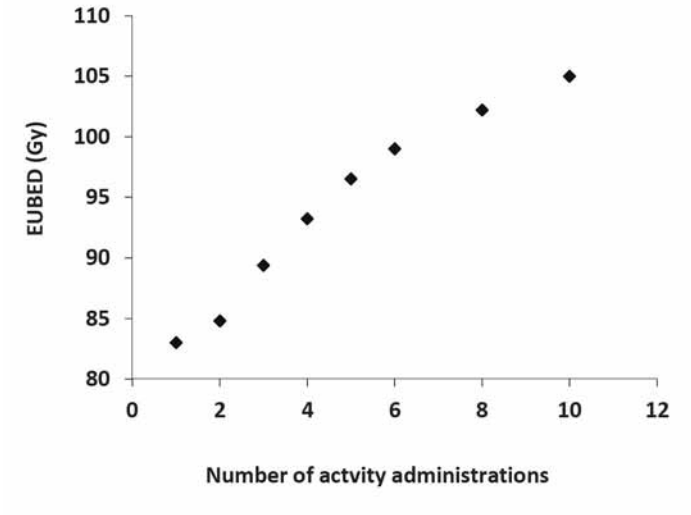

FIG. 6. TCP values versus number of activity administrations.

level, while the inverse planning is performed on the dBVH, which is derived from iDVH of absorbed dose distribution in Gy/GBq. For this reason, the EUBED estimation will be sensitive to the bin size of the dBVH during the inverse planning. To ensure relative discrepancy under 4% between the EUBED estimated by direct and inverse planning, a dose bin width of 0.5 Gy/GBq is

required for inverse planning. Consequently, the relative difference of the activity values will be less than 1%. The results presented here were obtained using a width of dose bin of 0.1 Gy/GBq.

If the planning strategy is based on mean BED rather than EUBED, the expected value of activity will be less than that obtained when the EUBED is used for treatment planning. In line with this, the delivered EUBED value will be less than expected, and the corresponding TCP value may not be relevant for tumour control. In this patient, for example, the result of dosimetric planning based on mean BED for ten administrations of activity shows a total cumulated EUBED value of 73.7 Gy, which represents a 30% loss of treatment efficacy. The TCP calculated for this EUBED value will not be relevant for tumour control. If similar calculations are performed for the other treatment schemes, it can be shown that the loss of treatment efficacy increases with the reduction of the number of administrations.

The errors associated with SPECT images quantification are mainly related to the attenuation and scatter of photons in the patient body. Several compensation methods for these effects have been developed to determine the activity in absolute units within defined VOI [28]. Partial volume effect also affects the determination of the activity in small tumour lesions and should be considered when tumour lesions are less than system spatial resolution [29]. The implementation of quantitative imaging procedures will improve the accuracy of dose calculations from SPECT imaging [28]. For these reasons, the results presented in this paper will depend of the accuracy of the quantitative imaging procedures implemented.

In the studied patient, the Chang method for attenuation correction was selected taking into account that, for the abdominal region, the attenuation coefficient may be considered constant for all tissues [28]. The triple energy window technique was used to provide accurate correction in the situation when scatter for higher energy photons ‘spill down’ into the primary photopeak window [11]. Because the tumour volumes in this patient are greater than system spatial resolution, the variation of activity inside the tumour VOI is not affected by partial volume effect.

The results presented here are valid under the assumption that equal amounts of administered activity will produce the same biological effect. However, in the course of treatment, the uptake and retention pattern of radiopharmaceutical in tumours may change from one administration to another. In clinical practice, it is recommended to perform a pretreatment study to determine the amount of activity needed to deliver the same partial EUBED before each therapeutic administration. Another approach could be to perform a pretreatment study to determine the partial EUBED produced by the same

planned amount of activity. In this case, the number of administrations needed to deliver the total planned EUBED will change.

The proposed inverse planning method takes into account the 3-D dose distribution in the tumour, incorporating the radiobiological modelling of tumour response and the EUBED concept. Also, it may help physicians to justify and to optimize treatments with beta emitter radiopharmaceutical using multiple administrations of activity.

5. CONCLUSIONS

The inverse treatment planning technique is a useful tool for estimating the amount of activity that produces an expected outcome in terms of prescribed TCP for treatment schemes based on multiple activity administrations,. It could be applied in clinical routine if tumour radiobiological parameters are available. The treatment planning based on mean BED, rather than EUBED, shows an important reduction in the likelihood of achieving tumour control when the dose distribution is non-uniform.

ACKNOWLEDGEMENTS

This work was supported by Bad Berka Centre for PET in Germany and the Institute of Oncology and Radiobiology in Cuba through the collaboration project Radionuclide Therapy of Cancer.

REFERENCES

[1] O'DONOGHUE, J.A., et al., Implications of non-uniform tumour doses for radioimmunotherapy, J Nucl Med **40** (1999) 1337.

[2] PRIDEAUX, A., et al., Three-dimensional radiobiology dosimetry: Application of radiobiologic modeling to patient-specific 3-dimensional imaging-based internal dosimetry, J Nucl Med **48** (2007) 1008.

[3] HANAN, A., et al., Methodology to incorporate biologically effective dose and equivalent uniform dose in patient-specific 3-dimensional dosimetry for Non-Hodgkin Lymphoma patients targeted with ^{131}I-Tositumomab therapy, J. Nucl Med **51** (2010) 654.

[4] DEWARAJA, Y.K., et al., ^{131}I-Tositumomab radioimmunotherapy: Initial tumor-dose response results using 3-dimensional dosimetry including radiobiologic modeling, J Nucl Med **51** (2010) 11A.

[5] O'DONOGHUE, J.A., et al., Relationships between tumour size and curability for uniformly targeted therapy with beta-emitting radionulcides, J Nucl Med **36** (1995) 1902.
[6] NAHUM, A., et al., Microdosimetric and radiocurability: modelling targeted therapy with beta emitters, Phys Med Biol **41** (1996) 1957.
[7] EBERT, M., Modelling dose response in presence of spatial variations in dose rate, Med Phys **27** 2 (2000) 393.
[8] CALDERÓN, C., GONZÁLEZ, J., "Empleo de la TCP y la NTCP para validación de la prescripción de actividad en planes de tratamiento en la radioterapia con radionucleidos emisores beta", Memorias del VIII Congreso de la Sociedad Cubana de Bioingienería (2009).
[9] GONZÁLEZ, J., CALDERÓN, C., Dose-response model for targeted radionuclide therapy, World J Nucl Med **3** (2004) 225.
[10] HOWELL, R.W., et al., Application of the Linear-Quadratic Model to radioimmunotherapy: further support for the advantage of longer-lived radionuclides, J Nucl Med **35** (1994) 1861.
[11] LASDON, L. WAREN, A., Código de optimización no lineal (GRG2), (1989) www.solver.com.
[12] CREMONESI, M., et al., Dosimetry in peptide radionuclide receptor therapy: A review. J Nucl Med **47** (2006) 1467.
[13] VAN REENEN, O., et al., Quantification of the distribution of ^{111}In-labelled platelets in organs, Eur J Nucl Med **7** (1982) 80.
[14] OGAWA, K., et al., A practical method for position-dependent Compton-scatter correction in single emission CT, IEEE Trnas Med Imag **10** (1991) 408.
[15] CHANG, L.T., A method for attenuation correction in radionuclide computer tomography, IEEE Trans Nucl Sci **25** (1978) 638.
[16] SGOUROS, G., et al., Three-dimensional dosimetry for radioinmunotherapy treatment planning. J Nucl Med **34** (1993) 1595.
[17] BOLCH, W.E., et al., MIRD Pamphlet No. 17: The dosimetry of non-uniform activity distributions-radionuclide S values at the voxel level, J Nucl Med **40** (1999) 11S.
[18] GONZÁLEZ, J., et al., Determination of radionuclide S value from any voxel size based on 3D Fourier Transform Convolution method, World J Nucl Med **6** 3 (2007) 40.
[19] BEHR, T.M., et al., Correlation of red marrow radiation dosimetry with myelotoxicity: Empirical factors influencing the radiation-induced myelotoxicity of radiolabeled antibodies, fragments and peptides in pre-clinical and clinical setting, Cancer Biotherapy & Radiopharmaceuticals **17** 4 (2002) 445.
[20] KWEKKEBOOM, D.J., Overview of results of peptide receptor radionuclide therapy with e radiolabeled somatostatin analogs, J Nucl Med **46** (2005) 62S.
[21] DE JONG M., KRENNING, E., New advances in peptide receptor radionuclide therapy, J Nucl Med **43** (2002) 617.
[22] SHEN, S., et al., Practical determination of patient-specific marrow dose using radioactivity concentration in blood and body, J Nucl Med **40** (1999) 2102.
[23] CREMONESI, M., et al., Biokinetics and dosimetry in patients administered with ^{111}In-DOTATOC: implications for internal radiotherapy with ^{90}Y-DOTATOC. J Nucl Med **26** (1999) 87.
[24] BARAKAT, M., et al., Neuroendocrine tumours, Endocrine-related cancer **11** (2004) 1.

[25] STEEL, G.G., Basic Clinic Radiobiology, Oxford Press (1997).
[26] ORTON, C., Review of radiobiological principles of radiotherapy and radiation protection. Conference, ALFIM Congress (2007).
[27] O'DONOGHUE, J.A., et al., Relationships between tumor size and curability for uniformly targeted therapy with beta-emitting radionulcides, J Nucl Med **36** (1995) 1902.
[28] INTERNATIONAL COMMISSION ON RADIATION UNITS AND MEASUREMENTS, ICRU REPORT No. 67, Absorbed dose specification in nuclear medicine, Ashford. England (2002).
[29] O'DONOGHUE, J.A., et al., Single-dose versus fractionated radioimmunotherapy: Model comparisons for uniform tumour dosimetry, J Nucl Med **41** (2000) 538.
[30] PAUWELS, S., et al., Practical dosimetry of peptide receptor radionuclide therapy with ^{90}Y-labelled with somatostatin analogs, J Nucl Med **46** (2005) 92S.
[31] SIEGEL, J.A., et al., MIRD Pamphlet No. 16: Techniques for quantitative radiopharmaceutical biodistribution data acquisition and analysis for use in human radiation dose estimates, J Nucl Med **40** (1999) 37S.
[32] GONZALEZ, J., et al., Factores físicos que afectan a la SPECT. En Neuroimagen Nuclear (2009) 71 (CASTRO-BEIRAS, J.M., J.P. OLIVA, J.P., PAREDES, Y.P. Eds), Editorial de la Comunidad autonoma de Madrid, España (2009).

VALIDATING ACTIVITY PRESCRIPTION SCHEMES IN RADIONUCLIDE THERAPY BASED ON TCP AND NTCP INDEXES CALCULATION

C.F. CALDERÓN-MARÍN, J.J. GONZÁLEZ-GONZÁLEZ,
W. QUESADA-CEPERO, R. ALFONSO-LAGUARDIA
Institute of Oncology and Radiobiology

O. DÍAZ-RIZO
High Institute of Applied Technologies and Sciences

Havana, Cuba

Abstract

The clinical application of radiobiological modelling for evaluation of treatment plans in radiotherapy is becoming more prevalent. The aim of this paper is to present a formulation for the evaluation of activity prescriptions in radionuclide therapy based on the calculation of the tumour control probabilty and normal tissue complication probability (NTCP). The dose rate functions for the calculation of the biologically effective dose are obtained from scintigraphic images. The MIRD schema is used for normal tissue dose calculations. Irradiation levels in the tumour are established from the isoeffective dose for the treatment of reference. A value of NTCP < 0.05 for critical organs was taken as the acceptance criterion during treatment planning. This article presents two examples using clinical data to ilustrate how this model can be used for biological verification of treatment plans. Although the whole body dose is commonly used as a tolerance limit, other critical organs must be carefully monitored even when the treatment may be biologically acceptable according to the 2 Gy whole body dose limit.

1. INTRODUCTION

Radiobiological models can be used to predict the biological effects of radiation treament. Although these have been mainly applied to external radiotherapy, currently, their use in radionuclide therapy is increasing as well [1–3]. Owing to the low dose rate (LDR) and biokinetic behaviour of the radiopharmaceuticals used in radionuclide therapy, a single administration is not enough to achieve acceptable levels of local control without compromising the functionality of normal tissues. Therefore, dose fractionation treatment is often used under different protocols as seen in published clinical trials [4–7].

The biological evaluation of a treatment helps verify the tumour control effectiveness and normal tissue effects of it. The organs whose functionality is potentially affected the most during treatment are commonly known as critical organs or organs at risk (OARs). The acceptance or rejection of a treatment plan is based on estimations of tumour control probability (TCP) and normal tissue complication probability (NTCP) as dose–response parameters. On the basis of data collected from external radiotherapy and peptide radiotherapy treatments, dose–response models are currently being used to perform treatment plan evaluations [8].

This paper presents a methodology for treatment plan evaluation based on TCP and NTCP calculations. TCP is calculated using the Poisson´s statistical model. The Lyman-Kutcher-Burman model is used to calculate NTCP for critical tissues. Absorbed doses in tumours and critical organs are estimated from the data obtained through nuclear medicine images. Two examples using clinical data were used to illustrate how this model could be applied during the treatment planning process.

2. METHODS

2.1. Dose rate function and internal absorbed dose calculations

For radionuclide therapy, dose rate functions are usually expressed as a sum of N exponential terms. Using the MIRD schema, the mean dose rate function in the k-th target organ $(\dot{D}_k(t))$ can be written as:

$$\dot{D}_k(t) = A_0 \sum_h \left\{ S(k \leftarrow h) \left[\sum_j^{m(h)} f_{h,j} \exp\left(-\lambda_{h,j} t\right) \right] \right\} \quad (1)$$

where

A_0 (GBq) is the injected activity;

S(k←h) (Gy·GBq^{-1}·h^{-1}) is the S value or mean absorbed dose in target k per disintigration in source h;

$f_{h,j}$ and $\lambda_{h,j}$ (h^{-1}) are the fraction of injected activity and the effective rate constant respectively for the j-th phase in the activity-time profile of the h-th source organ; and

m(h) is the number of exponential terms for the function which describes the fraction of injected activity (FIA_h) curve (term in brackets) for the h-th source organ.

The FIA_h profiles are determined from serial imaging studies. The profiles obtained with Eq. (1) should be fitted to a function of the form:

$$\dot{D}_k(t) = A_0 \sum_j \dot{D}_{0,MIRD,k,j} \exp\left(-\lambda'_{k,j} t\right) = \sum_j \dot{D}_{0,k,j} \exp\left(-\lambda'_{k,j} t\right) \tag{2}$$

where

$\dot{D}_{0,MIRD,k,j}$ (Gy·h^{-1}·GBq^{-1}) is the fitting coefficient to the dose rate profile for the h-th source organ calculated by Eq.(1); and

$\lambda'_{h,j}$ (h^{-1}) describes the j-th phase in the new dose rate function for the k-th target.

The mean total absorbed dose ($D_{T,k}$) in the k-th target organ is calculated by integration by time until the complete decay of source in Eq. (2):

$$D_{T,k} = \sum_j \frac{\dot{D}_{0,k,j}}{\lambda'_{k,j}} = A_0 \sum_j \frac{\dot{D}_{0,MIRD,k,j}}{\lambda'_{k,j}} = A_0 D_{T,MIRD,k} \tag{3}$$

where

$D_{T,MIRD,k}$ (Gy·GBq^{-1}) is the mean absorbed dose in the k-th target tissue per GBq of injected activity.

It can be demonstrated that, if the uptake fraction remains constant, when *n* sucessive administrations of equal activity amounts, $A_{0,f,}$ are given at equally spaced time intervals, τ, the dose rate profiles can be modelled as:

$$\begin{aligned} \dot{D}_{k,n}(t) &= \sum_j \dot{D}_{0,k,j} \rho_n\left(\tau, \lambda'_{k,j}\right) \exp\left(-\lambda'_{k,j} s\right) \\ &= A_{0,f} \sum_j \dot{D}_{0,MIRD,k,j} \rho_n\left(\tau, \lambda'_{k,j}\right) \exp\left(-\lambda'_{k,j} s\right) \end{aligned} \tag{4}$$

$$\rho_n\left(\tau, \lambda'_{k,j}\right) = \frac{1 - \exp\left(-n\lambda'_{k,j}\tau\right)}{1 - \exp\left(-\lambda'_{k,j}\tau\right)} \tag{5}$$

$$s = (n-1)\tau - t, \quad s \in [0, \tau] \tag{6}$$

The factor $\rho_n(\tau,\lambda'_{k,j})$ describes the effect of activity accumulation due to succesive administrations. The total absorbed dose in the k-th target is calculated as:

$$D_{T,k} = n\sum_j \frac{\dot{D}_{0,k,j}}{\lambda'_{k,j}} = nA_{0,f}\, D_{T,k,MIRD} \tag{7}$$

where

$A_{0,f}$ is the injected activity per administration. The total injected activity is $A_{0,T} = n \times A_{0,f}$.

2.2. Linear–quadratic (LQ) model: Biologically equivalent dose and 2 Gy equivalent dose

Since the target (tumour or normal tissues) is irradiated at a LDR during radionuclide therapy, the equation of the LQ model for BED calculations should be reformulated. In this case, incomplete repair must be considered in the LQ model as the LDR allows for possible repair of sub-lethal damage during the irradiation. A monoexponential kinetic repair is considered with a constant repair rate of μ. As tumour cell division could happen during LDR irradiation, the influence of cell proliferation should also be included in LQ formulation for tumour and normal tissues displaying early response, such as bone marrow. The growth cell kinetics is considered exponential. The BED at LDR ($BED_{LDR,k}$) for a multi-exponential dose rate function, including the influence of cell proliferation, (2) is given by:

$$\mathrm{BED}_{\mathrm{LDR,k}} = D_k\left(T_{eff,k}\right)\left[1 + g\left(\mu_k, T_{eff,k}\right)\frac{D_k\left(T_{eff,k}\right)}{(\alpha/\beta)_k}\right] - \frac{0.693}{\alpha_k T_{D,k}} T_{eff,k} \tag{8}$$

$$g\left(\mu_k, T_{eff,k}\right) = \frac{2}{D_k^2\left(T_{eff,k}\right)}\left[A_{1,k}\left(\mu_k, T_{eff,k}\right) - A_{2,k}\left(\mu_k, T_{eff,k}\right)\right] \tag{9}$$

$$\mathrm{A}_{1,\mathrm{k}}\left(\mu_k, T_{eff,k}\right) = \sum_i \sum_j \frac{r_{0,k,i} r_{0,k,j}}{\left(\lambda'_{k,j} - \mu\right)\left(\lambda'_{k,i} + \mu\right)}\left[1 - \exp\left[-\left(\lambda'_{k,i} + \mu_k\right) T_{eff,k}\right]\right] \tag{10}$$

$$A_{2,k}\left(\mu_k, T_{eff,k}\right) = \sum_i \sum_j \frac{r_{0,k,i} r_{0,k,j}}{\left(\lambda'_{k,j} - \mu\right)\left(\lambda'_{k,j} + \lambda'_{k,i}\right)} \times \left[1 - \exp\left[-\left(\lambda'_{k,j} + \lambda'_{k,i}\right) T_{eff,k}\right]\right] \quad (11)$$

$$D_k\left(T_{eff,k}\right) = \sum \frac{r_{0,k,j}}{\lambda'_{k,j}}\left[1 - \exp\left(-\lambda'_{k,j} T_{eff,k}\right)\right] \quad (12)$$

$$T_{eff,k} = \frac{1}{\lambda'_{k,L}} \ln\left[1.443 \alpha_k r_{0,k,L} T_{D,k}\right] \quad (13)$$

where

α_k (Gy^{-1}) is the linear radiosensitivity coefficient in the LQ model;

α/β_k (Gy) is the LQ parameter which differentiates tissues based on their response to irradiation: acute or late;

$T_{D,k}$ (h) is the potential doubling time (this is constant when the given cell population grows exponentially);

μ_k (h^{-1}) is the repair rate of sub-lethal damage;

$D_k(T_{eff,k})$(Gy) is the absorbed dose in the k-th tissue target;

$\lambda'_{k,L}$ and $r_{0,k,L}$ are the effective elimination constant rate and the dose rate coefficient respectively for the longer elimination phase for which

$$\dot{D}_{0,k,L} > \frac{0.693}{\alpha_k T_{D,k}}$$; and

$T_{eff,k}$ is the time threshold where cell kill rate is greater than cell proliferation.

For $t > T_{eff,k}$ the proliferation can overcome the toxic effect of irradiation rendering the dose delivered during this period a waste. The

$$\frac{0.693}{\alpha_k T_{D,k}}$$

ratio defines the minimum dose necessary to produce a toxic effect on the cell population.

The second term in Eq. (8) accounts for the influence of cell proliferation. This term cancels for tissues which develop late response, like the kidneys or whole body. In this case all the exponential terms in Eqs (10)–(12) go to zero.

The tolerance values for normal tissues and tumour control references are based on the data from external radiotherapy at high dose rate using a standard regime of 2 Gy per fraction. The LQ model allows the conversion of non-standard schemes to a 2 Gy equivalent dose ($ED_{2\,Gy}$). The biological equivalence between irradiation at LDR (in tumour or normal tissue) and 2 Gy standard regime is given by:

$$ED_{2Gy,k} = \frac{BED_{LDR,k}}{1 + \frac{2}{\alpha/\beta_k}} \tag{14}$$

$BED_{LDR,k}$ is calculated from Eqs (8)–(13).

2.3. Calculation of tumour control probability and normal tissue complication probability

The TCP is calculated using Poisson's statistical model; the tumour is controlled when the clonogenic cells are fully eliminated:

$$TCP = \exp\left[-\psi\rho_C \frac{\pi}{6} d_T^3 \exp\left(-\alpha BED_{LDR,T}\right)\right] \tag{15}$$

where

ψ is the clonogenic cell fraction in the tumour (0.01–0.1);
ρ_C (cells/cm^3) the cell density in the tumour (10^7–10^9);
d_T [cm] the tumour diameter; and
$BED_{LDR,T}$ is calculated using Eqs (8)–(13).

The NTCP for each normal tissue or organ at risk (OAR) can be calculated using the Lyman-Kutcher-Burman´s model [9]:

$$NTCP = \frac{1}{\sqrt{2\pi}} \int_{-\infty}^{x} \exp\left(-\frac{t^2}{2}\right) dt = \frac{1}{2}\left[1 + erf\left(\frac{x}{\sqrt{2}}\right)\right] \tag{16}$$

$$x = \frac{ED_{2Gy,k} - TD_{5/5,k}(1)}{\xi_k TD_{5/5,k}(1)} \quad (17)$$

where

$erf\left(\frac{x}{\sqrt{2}}\right)$ is the error function;

ξ_k is Lyman's parameter, which accounts for the irradiated volume effect in the k-th OAR [11]; and

$TD_{5/5,k}(1)$ is the tolerance dose for the occurrence of the effect of interest in 5% of the population in 5 years after whole organ irradiation [12].

An Excel spreadsheet was programmed to calculate $BED_{LDR,k}$, $ED_{2Gy,k}$, TCP and NTCP by direct evaluation of the corresponding equations. Iterative methods were used when necessary. The radiobiological parameters used in the calculations are shown in Table 1.

2.4. Basis for clinical applications

The methodology described here allows the user to validate if the treatment prescription (number of administrations, n, and injected activity per administration, $A_{0,f}$) is biologically acceptable. The treatment prescription is only satisfactory if TCP $\geq$ 0.5 and NTCP < 0.05 for all analysed OARs. If a treatment is rejected, it can be modified to meet the requirements. A new treatment plan can be formulated based on the n and $A_{0,f}$ necessary to achieve an absorbed dose in

TABLE 1. RADIOBIOLOGICAL PARAMETERS FOR TUMOUR AND CRITICAL ORGANS (OARs)

Parameters	Tumour	Kidneys [13]	Bone marrow [2]
α (Gy^{-1})	0.1–0.5 (0.35)	0.3	0.9
α/β (Gy)	3–15 (10)	2.5–5.0 (3.0)	10
T_D (d)	4.0–10.0 (4.0)		25
T_r (h)	0.5–2.0	0.5–3.0 (2.0)	0.5
$TD_{5/5}$ (Gy)		25.0	2.0

Note: The values in parenthesis are the base line parameters used in the calculations.

tumour, $D_{T,T}$, for which the isoeffect condition ($BED_{LDR,T} = BED_{ref,T}$) is satisfied. The isoeffect condition states that $BED_{LDR,T}$ must be equal to $BED_{ref,T}$, where $BED_{ref,T}$ is the tumour BED value for the reference irradiation scheme. This value can be calculated from the equations reported by Howell et al. in Ref. [14]. For the new scheme, the NTCP values for the OARs are calculated and the proposal is accepted if the restriction conditions are satisfied for all OARs. This process can be repeated as necessary until a satisfactory plan is reached. Therefore, treatment modifications are made by an iterative method [15].

For treatment schemes with repeated administrations, the interval between administrations (τ) is considered well-spaced if there is no activity accumulation observed due to successive administrations. Under this consideration, the expression for BED given by Eqs (8)–(13) represents the partial effect ($PE_{LDR,T}$) due to a single administration. The BED is the summation of these $PE_{LDR,T}$ and the isoeffect condition becomes $n \times PE_{LDR,T} = BED_{ref,T}$.

3. RESULTS

The dose rate functions used for radiobiological modelling may be calculated using the FIA(t) profiles obtained based on data from scintigraphic images. Figure 1 shows the dose rate ($Gy \cdot GBq^{-1}$) profiles calculated from Eq. (1) for whole body, kidneys, bone marrow and tumour. The dose rate functions for a single administration are obtained by curve fitting these dose rate profiles to Eq. (2) (solid line in Fig.1). These FIA(t) profiles were adapted from clinical data published for a ^{177}Lu-peptide [16]. The ^{177}Lu S values for the 70 kg adult male phantom were downloaded from the RADAR web site [17].

When successive administrations are given, the activity accumulation depends on the inter-administration intervals and the duration of the elimination phase. The accumulation factor $\rho_n(\tau,\lambda'_{k,j})$ given by Eq. (5) describes the contribution of the n-1 administration.

Figure 2 (left) shows the variation of $\rho_n(\tau,\lambda'_{k,j})$ as function of the inter-administration intervals for a given elimination rate constant ratio (τ/T_e). The vertical line in Fig. 2. (left) represents the 'remainder' dose rate due to the previous (n-1) administration. As τ increases, $\rho_n(\tau,\lambda'_{k,j})$ asymptotically approaches 1. On the other hand, the duration of the elimination phase increases the accumulation effect. As can be seen in Fig. 2, the effects of a longer elimination phase are greater if there is more than one elimination phase (right). Figure 3 shows the accumulation effects on the dose rate function. The assumption that there is no activity accumulation due to successive administrations is fulfilled when $\tau/T_e > 5$.

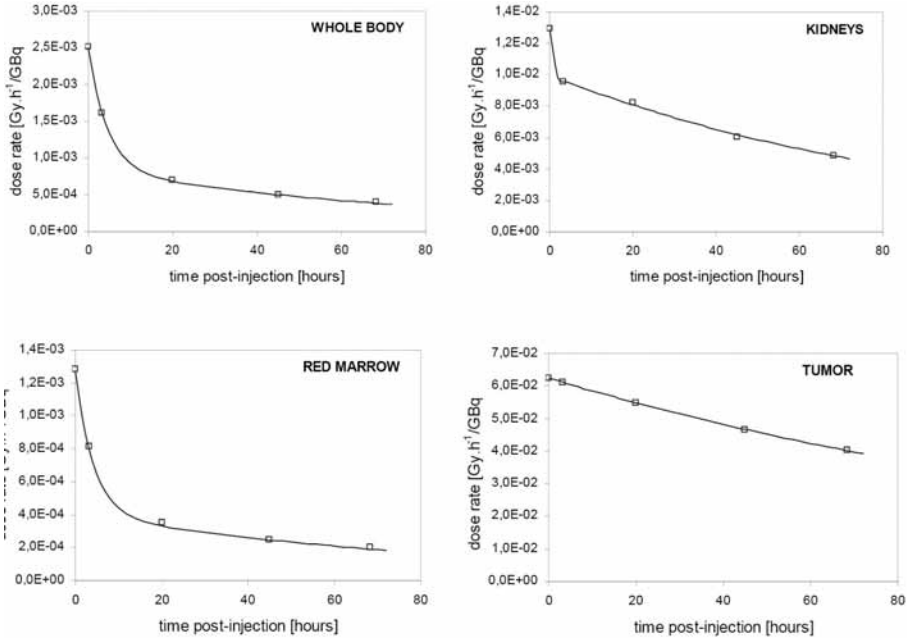

FIG. 1. Dose rate curves in critical organs and tumour calculated from FIA(t) profiles using Eq. (1). The solid lines are the fitted curves obtained from Eq. (2).

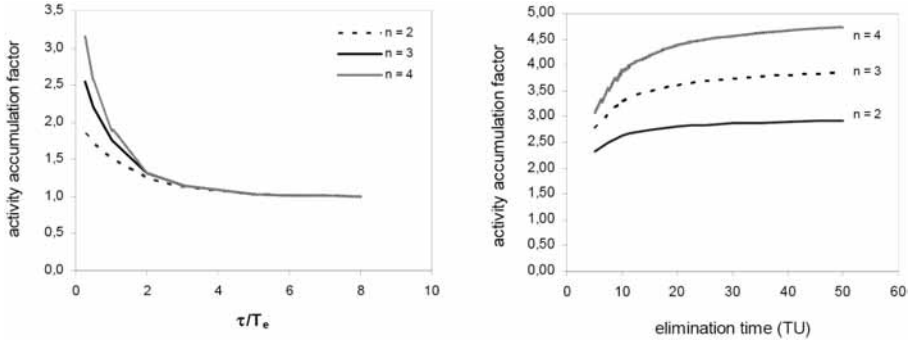

FIG. 2. Influence of interadministration and effective elimination time ratio (τ/T_e) on accumulation factor $\rho_n(\tau,\lambda'_{k,j})$(left); and influence of effective elimination phase duration on accumulation factor $\rho_n(\tau,\lambda'_{k,j})$(right).

The equations presented to calculate the BED for LDR (Eqs (8)–(13)) are the generalized version of the equations reported by González et al. [18]. This generalization allows for BED calculations of cases with more complex biokinetic profiles (i.e. two elimination phases) and for calculations of BED of

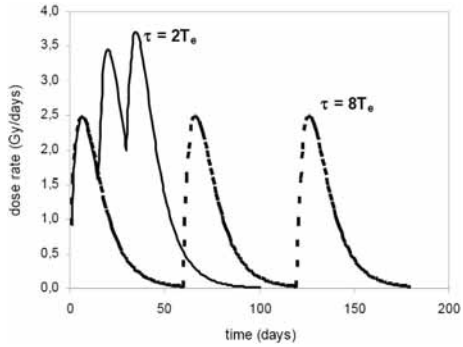

FIG. 3. Effect of interadministration interval on dose rate functions when successive administrations are given.

LDR for tumour and normal tissues for a single radiopharmaceutical administration.

The use of the proposed methodology in clinical conditions can be illustrated using a hypothetical example. The absorbed doses per GBq of injected activity in a patient, for a single administration of a ^{177}Lu-peptide, for the tumour, whole body, bone marrow and kidneys are: 9.67 Gy·GBq, 0.04 Gy·GBq, 0.041 Gy·GBq and 0.94 Gy·GBq, respectively.

Problem: Using the radiobiological data shown in Table 1, verify if the amount of activity needed to produce an acceptable biological response in the tumour is equivalent to that of a reference treatment considered as 'biologically acceptable'. Take the reference treatment to be a continuous irradiation dose rate constant with ^{222}Ra.

Solution: The treatment will be accepted if the condition NTCP < 0.05 is satisfied in all critical organs. The amount of activity that will produce the isoeffective response is calculated from the isoeffective condition for a single administration. Equations (8)–(13) must be changed by replacing $r_{0,k} = A_0 \times r_{0,MIRD}$ for any subscript *i* or *j*. This equation is derived from Eq. (2). The solution of the isoeffective equation gives that A_0 = 7.73 GBq. The absorbed dose in tumour is $D_{T,T}$ = 7.73 GBq × 9.67 Gy/GBq = 74.90 Gy and the 2 Gy equivalent dose is 57.75 Gy. The absorbed doses in the kidneys, bone marrow and whole body for the calculated activity are 6.71 Gy, 0.29 Gy and 0.28 Gy, respectively. The $ED_{2\,Gy}$ are 4.43 Gy, 0.08 Gy and 0.189 Gy, respectively. The NTCP was calculated for the kidneys using the available model parameters and the value obtained was below the threshold. Comparing the $ED_{2\,Gy}$ values for each normal tissue shown in the Table 1, it may be concluded that the treatment plan can be accepted.

However, in some patients, very low tracer uptake in the tumour is observed. In these cases, the treatment plan might have to be changed. If the uptake observed in a patient is 5 times less of what is expected, the prescribed activity will have to be increased to reach acceptable levels in the tumour, making the treatment potentially unsafe for normal tissues. The injected activity necessary to satisfy the isoeffective condition for a single administration in a patient with low tumour uptake is 38.65 GBq. Using this activity, the calculated absorbed doses in whole body, bone marrow and kidneys are 1.57 Gy, 36.38 Gy and 1.58 Gy, respectively. The 2 Gy equivalent doses are 0.95 Gy, 23.27 Gy and 1.02 Gy. The 2 Gy limit for whole body and bone marrow is not exceeded, but the treatment cannot be accepted because the $ED_{2\ Gy}$ for the kidneys exceeds the tolerance level. The corresponding NTCP value is too high. Therefore, the tolerance criterion for acceptance of the prescription must be carefully controlled. A treatment plan with multiple administrations of activity should be explored for this case. For example, an acceptable treatment course in this scenario would be to give more than six cycles of 7.0–8.0 GBq per administration.

4. DISCUSSION

The goal of treatment planning in radionuclide therapy is to estimate the optimal activity to be injected into the patient which provides satisfactory tumour control, but keeps the absorbed dose levels in OARs below the tolerance limit. In radionuclide therapy, bone marrow, whole body and kidneys are often the limiting dose organs.

It should also be noted that uncertainties in dose estimation should be taken into account during treatment planning calculations as values with high uncertainties may lead to poor dose–response correlations. Frequently, the dose estimations are based on data obtained through serial planar imaging scans, SPECT or a combination of both [19]. Some reports point out that activity quantification methods are the major contributors to uncertainty in absorbed dose estimations [20]. The scatter and photon attenuation corrections improve activity quantification estimates in planar images. Errors in organ activity estimates vary from –26% to 16% in the MIRD phantom, depending on the organ studied and the correction methods used [20]. The overlapping of anatomical structures must be carefully evaluated. Errors stemming from this issue can lead to an overestimate in dose of more than 60% [22]. Iterative reconstruction algorithm of SPECT images with scatter and attenuation corrections the preferred method [23]. He et al. reported that large differences are observed when the number of disintegrations per MBq of injected activity is estimated using only planar images versus a combination of planar and SPECT images [24]. Other error sources in

activity quantification arise from loss of counts due to deadtime when imaging high activities [25, 26] . Differences, larger than the propagation error, between the half-lives of the therapy and tracer isotopes can lead to significant discrepancies [21], as well as the activity sampling time and curve fittings [19, 21]. Activity quantification protocols must be carefully evaluated before they are used in clinical practice and methods for dosimetric verification should be explored in order to determine the instrumentation quality and assess the uncertainty in the calculations [27, 28]. Nevertheless, marked differences in the activity uptake could be observed during the course of treatment due to changes in the saturation of receptor sites or down regulation in receptor expression. The interpatient differences in receptor expression or intertumour variability in patients with multiple lesions could also produce different grades and profiles of activity uptake. Several strategies must be evaluated during treatment planning.

All the calculations in this paper were done under the assumption of uniform dose rate and absorbed dose in the tumour and normal tissues. This approach is often used for normal tissue in absence of available data demonstrating otherwise. This condition may also be assumed for small tumours and metastases. In case of non-uniform distribution more 'biologically representative' dose distribution parameters, such as the equivalent uniform distribution (EUD) [29] for normal tissue and tumour or effective dose (D_{eff}) [30] in whole irradiated normal tissue volume, can be calculated from the dose–volume distribution. However, in general clinical practice, the equations presented here are applicable.

For treatments with repeated administrations, the interval interadministration is a critical variable. It determines how the activity accumulation influences the dose rate profile. If the interval between administrations is comparable to the effective elimination time, the effect of activity accumulation will be observed. In this case the equation for calculating the BED becomes more complex than those reported in Eqs (8)–(13) [31]. The additive property of BED could be favorably used if tumour uptake changes in the course of the treatment. In that case, new activity calculations have to be performed. A large period between administrations allows tissues with early response, like bone marrow, to recover their function. There are reports of clinical trials where treatments with small interadministration intervals have been used with good results [4]. The results of the examples analysed here are in agreement with the studies where peptides labeled with ^{177}Lu [15] administered in several cycles of 4.5–7.0 GBq where well tolerated by patients. Although the second case illustrates an extreme situation, it represents a typical scenario in which activity fractionation may be a good choice. Another problem that could be solved by using the methodology presented here is the determination of the optimal number of administrations for a value of activity per administration prescribed. Updates

on the treatment plan could be performed based on the uptake profile. The new scheme must be calculated for the remainder BED fraction (partial effect).

The tolerance limits commonly used have been established from the data collected based on treatment with external radiotherapy at high dose rates. The framework of LQ model allows for the establishment of a biological correspondence between different irradiation schemes. Through the LQ model, it is possible to convert non-standard schemes to a ED_{2Gy}. This will make the reporting of tolerated doses and the communications with physicians much easier, as the information will be presented in familiar terms [12]. Additionally, the conversion to ED_{2Gy} may be useful when combining both external radiotherapy and systemic modalities.

TCP and NTCP are dose response parameters used to describe the effects of irradiation in tumour and normal tissues. The use of biological indexes like TCP and NTCP in treatment prescription ensures that the local tumour control may be achieved without complications in normal tissues. The applicability and accuracy of the tissue response estimates will depend on the quality of the available biological parameters, and on how sensible the model is to the uncertanties of the parameters used. Clinical trials with standard protocols should be performed to improve the uncertainties in the values used for calculation. Treatment effectiveness is also influenced by the shape of the dose distribution and the size of the irradiated volume. The greater the degree of heterogeneity, the more ineffective the treatment. The TCP depends on the number of clonogenic cells in the irradiated volume. More activity will be required to control larger tumour volumes. The effectiveness of heterogenous dose distributions is not improved by increasing the amount of activity administered. In these cases, the combination of external local and systemic irradiation should be explored. It is important to 'differentiate' the contribution of each OAR in the acceptance of the treatment scheme [32]. Other goal functions such as the uncomplicated tumour control probability or the function f(EUD) [33] can be used as overall predictors of treatment response. The first is a parameter based on calculation of TCP and NTCP, the second is related to the shape of the dose distribution. Such functions can also be used in treatment optimization.

5. CONCLUSION

It is possible to verify the activity prescription in radionuclide therapy based on the calculation of TCP and NTCP for a single administration schedule, as well as for prescription with fractionation of the administered activity. During verification of the prescription, the tolerance limits of all source organs, including bone marrow, must be carefully assessed.

REFERENCES

[1] STRIGRARI, L., et al., "A NTCP approach for estimating the outcome in radioiodine treatment of hyperthyroidism". Med Phys **35**(9) (2008): 3903–3910.

[2] WILDER, R.B., et al., Application of the linear-quadratic model to myelotoxicity associated with radioimmunotherapy. Eur J Nucl Med **23** (1996) 953–957.

[3] ABOU-JAOUDE, W., DALE, R., A theoretical radiobiological assessment of the influence of radionuclide half-life on tumour response in targeted radiotherapy when a constant kidney toxicity is maintained. Cancer Biother Radiopharm **19**(3) (2004) 308–321.

[4] MEREDITH, R.F., et al., Dose fractionation of radiolabeled antibodies in patients with metastatic colon cancer. J Nucl Med **33** (1992)1648–165.

[5] DENARDO, G.L., et al., Rationales, evidence and desing considerations for fractionated radioimmunotherapy. Cancer **94** (2002) 1332–1348.

[6] BUCKLEY, A.E., et al., Dosimetry for fractionated 131I-mIBG therapies in patients with primary resistant hig-risk neuroblastoma: preliminary results. Cancer Radiopharm **22**(1) (2007) 105–112.

[7] DIVGI, C.R., et al., Phase I clinical trial with fractionated readioimmunotherapy using 131I-labeled chimeric G250 in mestastatic renal cancer. J Nucl Med **45** (2004) 1412–1421.

[8] WESSELS, B.W., et al., MIRD Pamphlet 20. The effect of model assumptions on kidney dosimetry and response — implications for radionuclide therapy. J Nucl Med. **49**(11) (2008) 1884–1899.

[9] LYMAN, J.T., Complication probabilities as assessed from dose-volume histograms. Rad. Res. **104** (1985) S13-19

[10] KUTCHER, G.J., BURMAN, C., Calculation of complication probability factors for non uniform normal tissue irradiation: the effective volume method Int. J. Radiation Oncology Biol. Phys. **16**(6) (1989) 1623–1630.

[11] BURMAN, C., et al., Fitting of normal tissue tolerance data to an analytic function. Int J Radiat Oncol Biol Phys **21**(1) (1991) 123–135.

[12] EMAMI, B., et al., Tolerance of normal tissue to therapeutic irradiation. Int J Radiat Oncol Biol Phys **21**(1) (1991) 109–122.

[13] BARONE, R., et al., Patient-specific dosimetry in predicting renal toxicity with 90Y-DOTATOC: relevance of kidney volume and dose rate in finding a dose-response relationship. J Nucl Med **46** (1991) 99S-106S.

[14] HOWELL, R.W., GODDU, S.M., DANDAMUNDI, V.R., Application of the linear-quadratic model to radioimmunotherapy : further support for the advantage of longer-lived radionuclides. J. Nucl Med **35** (1994) 1861–1869.

[15] LASDON, L., WAREN, A., Código de optimización no lineal (GRG2). www.solver.com. 1989.

[16] WEHRMANN, C., et al., Results of individual patient dosimetry in peptide receptor radionuclide therapy with ^{177}Lu DOTA-TATE and ^{177}Lu DOTA-NOC. Cancer Biother Radiopharm **22**(3) (2007) 406–416.

[17] http://www.doseinfo-radar.com/RADARphan.html

[18] GONZÁLEZ, J., CALDERÓN, C., Dose response model for targeted radionuclide therapy. World J Nuc Med **3** (2004) 225–228.
[19] SIEGEL, J.A., et al., MIRD Pamphlet no 16 Techniques for quantitative radiopharmaceutical biodistribution data acquisition aand analysis for use in human radiation dose estimates. J Nucl Med **40** (1999) 37S-61S.
[20] NORRGREN, K., et al., Accuracy of the quantification of organ activity from planar gamma camera images. Cancer Biother Radiopharm **18**(1) (2003) 125–131.
[21] FLUX, G.S., et al., Estimation and implications of random error in whole body dosimetry for targeted radionuclide therapy. Phys Med Biol **47** (2002) 3211–3223.
[22] JONSSON, L., LJUNGBERG, M., STRAND, S.-E., Evaluation of accuracy in Activity Calculations for the Conjugate view method from Monte Carlo simulated scintillation camera images using experimental data in an anthropomorphic phantom. J Nucl Med **46** (2005) 1679–1686.
[23] DEWARAJA, Y.K., et al., Accurate dosimetry in 131I radionuclide therapy using patient-specific, 3-dimensional methods for SPECT reconstruction and absorbed dose calculation. J Nucl Med **46** (2005) 840–849.
[24] HE, B., et al., Comparison of organ residence time estimation methods for radioimmunotherapy dosimetry and treatment planning-patient studies. Med Phys **36**(5) (2009) 1595–1601.
[25] FERRER, L., et al., Dosimetric impact of correcting count losses due deadtime in clinical radioimmunotherapy trials involving iodine-131 scintigraphy. Cancer Biother Radiopharm 18(1) (2003) 117–124.
[26] HOBBS, R., et al., A gamma camera count rate correction method for whole-body planar imaging. Phys Med Biol **55**(3) (2010) 817.
[27] GEAR, J.I., et al., A quality-control method for SPECT-based dosimetry in targeted radionuclide therapy. Cancer Biother Radiopharm **22**(1) (2007) 166–174.
[28] COURBON, F., et al. Preparation and use of 131I magic gel as a dosimeter for targeted radionuclide therapy. Cancer Biother Radiopharm **21**(5) (2006) 427–436.
[29] NIMIERKO, A.A., A generalized concept of equivalent uniform dose (EUD). Med Phys **26** (1999) 1100.
[30] LYMAN, J.T., WOLBARST, A.B., Optimization of radiation therapy IV: A dose volume reduction histogram algorithm. Int. J. Radiation Oncology Biol. Phys. **17**(2) (1989) 433–436.
[31] CALDERÓN, C.F., et al., Modelling biological effects of repeated systemic administrations of small dose fraction in radionuclide therapy, work in press.
[32] SCHULTHEISS, T.E., ORTON, G.G., PECK, R.A., Model in radiotherapy: volume effects. Med Phys **10** (1983) 410–415.
[33] WU, Q., et al., Optimization of Intensity Modulated Radiotherapy plans based on Uniform Equivalent Dose. Int J Radiat Oncol Biol Phys **52**(1) (2002) 224–235.

EXTERNAL QUALITY AUDITS

(Session 7)

Chairperson

D. THWAITES
European Society for Therapeutic Radiology and Oncology

Co-Chairperson

J. IZEWSKA
IAEA

THE IAEA QUALITY AUDITS FOR RADIOTHERAPY

J. IZEWSKA, P. BERA, G. AZANGWE, S. VATNITSKIY*,
E. ROSENBLATT, E. ZUBIZARRETA
International Atomic Energy Agency,
Vienna
Email: j.izewska@iaea.org

Abstract

The IAEA/WHO thermoluminescent dosimetry (TLD) postal dose audit programme has been used for over 8000 radiotherapy beams throughout the world in over four decades of its operation. Records have been kept of the results of TLD audits since the inception of the programme. Analysis of these data has yielded much interesting information. In the early years, the TLD service recorded approximately 50% audited beams having adequate calibration. This percentage of acceptable results has now increased to 96%. Obviously, regular participation in dosimetry audit stimulates an improvement in dosimetry practices in radiation therapy in many hospitals worldwide. Another dosimetry audit programme for treatment planning (TPS audit) in external beam radiotherapy, which has been developed by the IAEA, assesses the radiotherapy workflow for conformal techniques, from patient data acquisition and computerized treatment planning to dose delivery. The IAEA supports national and subregional TPS audit activities to improve the quality and safety of dose calculation in radiotherapy. The third audit modality operated by the IAEA within the framework of the Quality Assurance Team for Radiation Oncology (QUATRO) is a comprehensive audit that reviews radiation oncology practices with the aim to improve quality. To date, over 50 QUATRO audits have been organized by the IAEA in radiation oncology centres in Europe, Africa, Asia and Latin America. QUATRO audits indicate and document areas for improvement and provide advice for further development of the audited centres.

1. INTRODUCTION

A high degree of accuracy, reliability and reproducibility in radiation dose delivery to cancer patients is necessary to ensure safe and high quality treatment and optimized outcome for the patient. The calibration of the radiation beam is the first and fundamental step in radiotherapy. If the radiation beam is incorrectly calibrated, radiotherapy treatment will be incorrectly delivered. In the case of large discrepancies, the consequences can be fatal. A mistake in the beam calibration will affect all patients treated with that beam.

* MedAustron, Wiener Neustadt, Austria.

Independent external quality audits, being part of a comprehensive quality assurance (QA) programme, are widely recognised as an effective method to verify the quality of practice in a radiotherapy centre. Quality audits include a range of types and levels of peer review, for example comprehensive audits review the entire radiotherapy practice and partial audits focus on specific important parts, such as dosimetry audits.

Dosimetry audits have a long tradition [1–7]. Since 1969, the IAEA jointly with the World Health Organization (WHO) has operated a dosimetry audit programme for radiotherapy using thermoluminescent dosimeters (TLDs). This paper provides a brief overview of the IAEA/WHO TLD postal dose audit programme. In addition, two more recently developed IAEA audit programmes are presented very briefly, one for treatment planning in radiotherapy (TPS audit) [8, 9] and one covering comprehensive (or clinical) audit, denoted as the Quality Assurance Team for Radiation Oncology (QUATRO) audit [10], which evaluates radiation oncology practices in cancer centres.

2. THE IAEA/WHO TLD POSTAL DOSE AUDIT SERVICE FOR RADIOTHERAPY DOSIMETRY

The IAEA/WHO TLD postal dose audit programme is one of the oldest radiotherapy dosimetry services in the world [1–6]. Initially, it was used for monitoring the calibration of ^{60}Co beams. In 1991, its scope was expanded to audits of calibration of high energy photon beams produced by clinical accelerators. Today, two thirds of beam checks are for beams generated by clinical accelerators and one third are for ^{60}Co beams.

Over the period of their operation, the IAEA/WHO TLD postal dose audits have undergone several scientific reviews, technical improvements and changes related to increasing the level of organization and efficiency of the auditing services. Automation of the TLD system in 1998 shortened the time of TLD evaluation and increased the number of hospital beams to be monitored from 100–150 to 400–500 per year (Fig. 1). Nevertheless, the requests from radiotherapy centres steadily increase and exceeded 600 beams checked in 2009.

2.1. TLD results of radiotherapy centres

Records have been kept of the results of TLD audits of radiotherapy centres since the inception of the programme. To date, the calibration of approximately 8000 radiotherapy beams (see Fig. 2) in 1700 cancer centres in 120 countries have been audited. These audits were made in radiotherapy centres in Africa, the

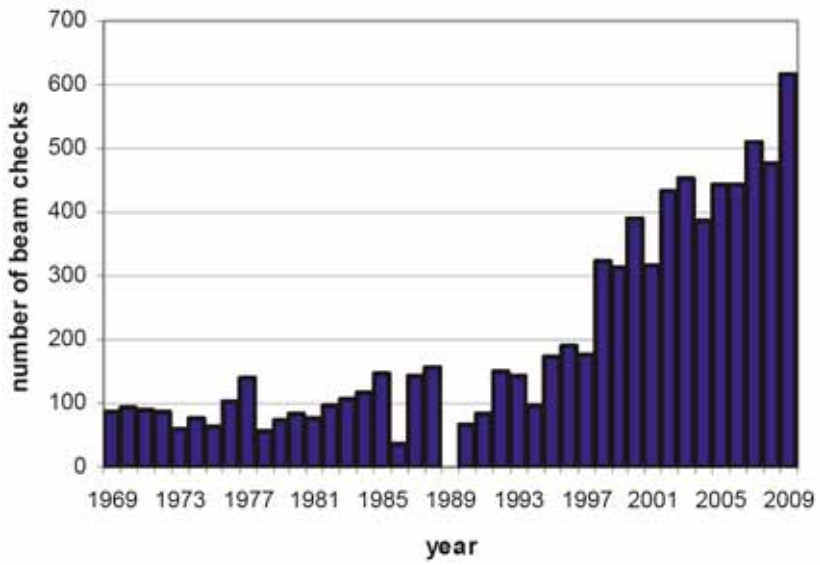

FIG. 1. Increase in the activity of IAEA/WHO TLD postal dose audits for radiotherapy centres.

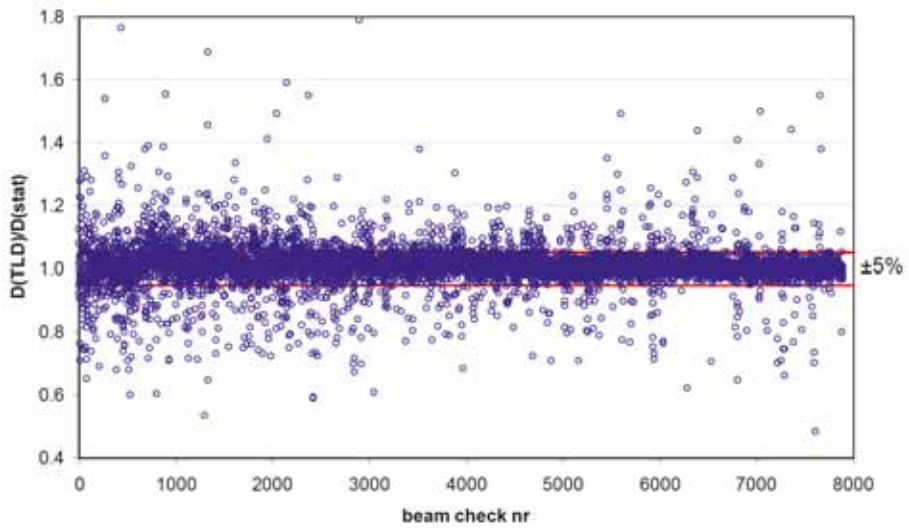

FIG. 2. Results of the IAEA/WHO TLD postal dose audits of radiotherapy centres for the delivery of absorbed dose to water under reference conditions during 1969–2009.

eastern Mediterranean, Europe, Latin America and the Caribbean, Southeast Asia and the Western Pacific. Every year, about 50 or more hospitals newly register to the TLD programme.

Differences of less than 5% between the participant stated dose and the TLD measured dose are considered acceptable. This 5% acceptance limit defines the maximum discrepancy between stated and measured doses that does not require any further investigation. For radiotherapy centres with results outside the 5% acceptance limit, the IAEA has established a follow-up procedure that uses a second TLD check to give centres the possibility to correct the discrepancy. The regular follow-up procedure of poor TLD results was introduced in 1996. Discrepancies between the TLD measured dose and the participant stated dose are resolved through direct interaction with hospital physicists and contacts with local experts where available, or by recruitment of international experts in medical physics [11] to visit the centre and assist in resolution of discrepancies. This is an important component of TLD audits that brings improvements in dosimetry practices in radiotherapy centres.

The provision of the regular audit programme over a significant time enables the IAEA to document that many radiotherapy centres have improved their abilities to accurately deliver the radiation dose. Indeed, there is a systematic growth in the fraction of acceptable TLD results, i.e. those falling within the limit of 5%. In its early years, the IAEA/WHO TLD postal dose audit service recorded approximately 50% of audited centres had adequate beam calibrations for beams used for cancer treatment [4]. In the early 1990s, less than 70% audited beams had adequate calibrations (see Fig. 3). Recently, the percentage of acceptable results has reached 96% (Fig. 3). However, 4% of the poor results remain

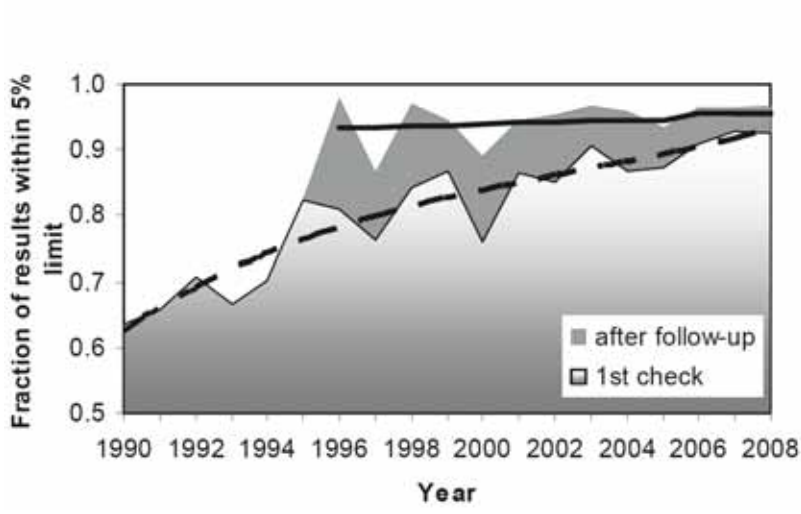

FIG. 3. Fraction of the TLD results within the 5% acceptance limit for radiotherapy hospitals. The light grey area indicates the results obtained in the first check, and the dark grey area corresponds to the percentage of results improved in the follow-up process.

uncorrected either due to a failure to respond to the IAEA/WHO efforts or due to local problems that could not be resolved without allocation of appropriate resources by local governmental bodies.

As shown in Fig. 2, large discrepancies in the beam calibration still occur. They are observed mostly in centres that engage in auditing for the first time. These centres perform less well than those centres that participate on an ongoing basis. In 2000–2009, the percentage of deviations outside the 5% acceptance limit was 80% for centres new to the audit and 91% for centres participating in an audit in a regular manner. The percentage of large deviations, exceeding 10%, was 9% for new centres compared to 4% for regular participants. The same pattern was observed for major deviations exceeding 20%, with 3% of discrepancies having occurred for new centres and 1% for regularly participating centres. This suggests that the new participants in the audit programme need to gain more experience in dosimetry in order to reach the level of well performing hospitals. This also suggests that more resources for training of medical physicists need to be allocated. As discussed above, large discrepancies still also occur in the group of regularly participating centres, although to a lesser extent. Centres with persisting deviations often work within practical limitations such as insufficient availability of qualified medical physicists or lack of adequate dosimetry equipment, which compromises quality. The clinical relevance of severe TLD deviations detected in the audit programme was confirmed in several cases [6], but, fortunately, not all poor dosimetric results reflect deficiencies in the calibration of clinical beams or machine faults. Sometimes, the TLDs receive incorrect doses due to misunderstanding of the instructions on how to perform the TLD irradiation.

2.2. Analysis of TLD results of radiotherapy centres

The analysis of recent data sheets has shown that the most common mistakes made by participants pertained to using an incorrect geometry set-up for the TLD irradiation, incorrect calculation of monitor units, irradiation time or a combination of various mistakes and errors. These are mistakes in irradiating the TLD or calculating the dose to be delivered to the TLD but they do not constitute direct evidence of incorrect patient dosimetry in the same way that an incorrectly calibrated beam would. Nevertheless, these mistakes reflect on the likelihood of various human mistakes that may impair the quality of the routine clinical dosimetry practice in these centres. Again, education and training of medical physicists in clinical dosimetry cannot be overemphasized. About 40% of deviations had reasons that could not be traced due to lack of information on the dosimetry procedures in the participants' data sheets. In particular, poor performance of some radiotherapy centres in Latin America seems to be due to an insufficient number of qualified medical physicists in the region.

Table 1 reports the deviations of TLD audit results detected in 2000–2009. In general, basic dosimetry of high energy X ray beams is observed to be more accurate compared with that of ^{60}Co beams (see Table 1), but this reflects the fact that radiotherapy centres with linacs are usually supported by better resources for medical physics services than hospitals only having ^{60}Co machines. In addition, the ^{60}Co machines in some countries exhibit performance deficiencies due to poor technical condition caused by machine age, inadequate maintenance or too low activity of ^{60}Co sources as documented by the irradiation times needed to deliver 2 Gy to the TLD. For example, over 40% of ^{60}Co machines in Eastern (non-EU) Europe are older than 20 years [12].

Different dosimetry codes of practice (CoPs) are used in countries around the world, ranging from old exposure (N_X) based CoPs of the early 1970s, through air kerma (N_K) based CoPs developed in the 1980s, up to the recently developed modern absorbed dose to water ($N_{D,w}$) based CoPs. TLD results of 2000–2009 grouped by the code of practice reported by centres participating in audits are given in Table 2. The distribution of results shows the smallest standard deviation (last column) for participants using the absorbed dose to water ($N_{D,w}$) based CoPs, such as TRS 398 [13], while results from participants with empty or incompletely filled data sheets have the largest standard deviation. Also, the mean of the distribution is close to 1.000 for users of $N_{D,w}$ and N_K CoPs, while for users of old codes of practice and those with incomplete or empty data sheets, the mean D_{TLD}/D_{stat} deviates from 1.000 by 1–2%, indicating problems with traceability to the International System of Units. The number of major discrepancies, greater than 20%, is large for the group with no or incomplete dosimetry data. In Table 2, 75 major discrepancies (>20%) were excluded from the statistics, 42 of which were from this group.

TABLE 1. RESULTS OF TLD AUDITS IN 2000–2009

	^{60}Co beams (2013)	High energy X ray beams (2427)
Deviations outside the 5% limit:	18%	6%
5–10%	9%	4%
10–20%	6%	1%
>20%	3%	1%
Results within the 5% limit	82%	94%

TABLE 2. THE MEAN RATIO OF TLD MEASURED DOSE TO THE DOSE STATED BY THE PARTICIPANT, $D_{TLD}/D_{STAT,}$ AND THE STANDARD DEVIATION OF THE DISTRIBUTION OF TLD RESULTS GROUPED ACCORDING TO THE DOSIMETRY CoPs USED BY PARTICIPANTS IN TLD AUDITS (2000–2009)

Code of practice	Number of beams checked	Mean D_{TLD}/D_{stat}	Standard deviation (%)
N_{Dw}	1875 (13)[a]	1.003	2.6
N_K	1162 (13)	1.005	3.3
N_X	340 (7)	1.020	4.7
Ion chamber details only	129 (3)	1.020	5.4
No dosimetry data	858 (39)	1.011	5.1

[a] Discrepancies greater than 20% were excluded from the statistics. Number of excluded results is shown in parentheses.

The data reported by the participants show that there is a substantial increase in the use of modern absorbed dose to water codes of practice since 2000. In 2008–2009, about 84% of participants use CoPs based on absorbed dose to water standards. There has been a notable decrease in the use of N_K and old N_X based CoPs, especially in hospitals in the Latin America region. However, in the Western Pacific region, 32% of the hospitals participating in TLD audits are still using outdated CoPs based on exposure standards.

2.3. Uncertainties in radiotherapy machine calibrations

On the basis of the TLD audit results, the uncertainty of calibration of treatment machines can be derived for various countries. In 2000–2009, 100 countries participated in the IAEA/WHO TLD postal dose audits at least once. Figure 4 shows the mean and standard deviation of the distribution of the TLD results for 82 countries participating with more than five beams[1] in this period.

Data shown in Fig. 4 demonstrate that approximately 75% of the countries have the mean of the distributions of TLD results between 0.99–1.01 and 95%

[1] A low (<5) number of participations in TLD audits is not considered statistically significant and therefore such data were excluded from the analysis.

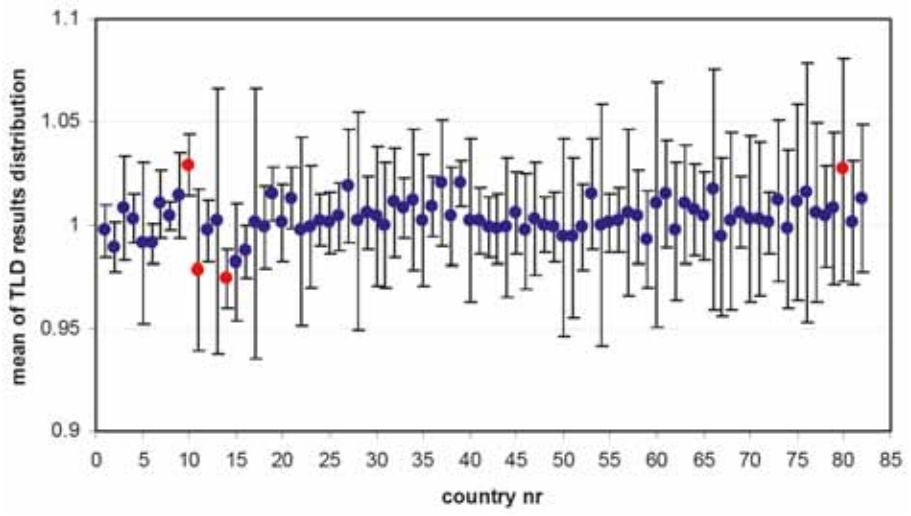

FIG. 4. Results in the IAEA/WHO TLD postal dose audit presented as the mean of the distributions of TLD results for 82 countries participating in TLD audits in 2000–2009 with more than 5 beams. The error bars correspond to the standard deviation of the distributions of results for individual countries. Red circles indicate countries with a mean <0.98 or >1.02. Extreme deviations exceeding 20% have been excluded from the statistics.

countries within 0.98–1.02, whereas 5% (4/82) of the countries have the mean outside 2%. The latter value is a sign of poor traceability to the International System of Units for these countries. This can be attributed to insufficient access to reliable dosimeter calibrations by the national SSDL, lack of such an SSDL in some of these countries, lack of dosimetry equipment in some hospitals, and problems with the implementation of dosimetry CoPs.

The standard deviation of the distributions of TLD results in various countries shown in Fig. 4 is smaller than 5% for hospitals in 90% (74/82) of countries. It is smaller than 3% for 62% (51/82) of countries, which suggests that the basic dosimetry practices in radiotherapy centres are generally adequate. However, hospitals in 10% (8/82) of countries perform less adequately, as their TLD results show larger spread, with the standard deviation exceeding 5%.

2.4. The IAEA/WHO TLD audits for secondary standards dosimetry laboratories (SSDLs)

In addition to auditing the beam calibration at radiotherapy centres, since 1981, TLD audits have also been used to monitor the consistency of dosimetry practices by members of the IAEA/WHO network of SSDLs [14, 15]. Results of

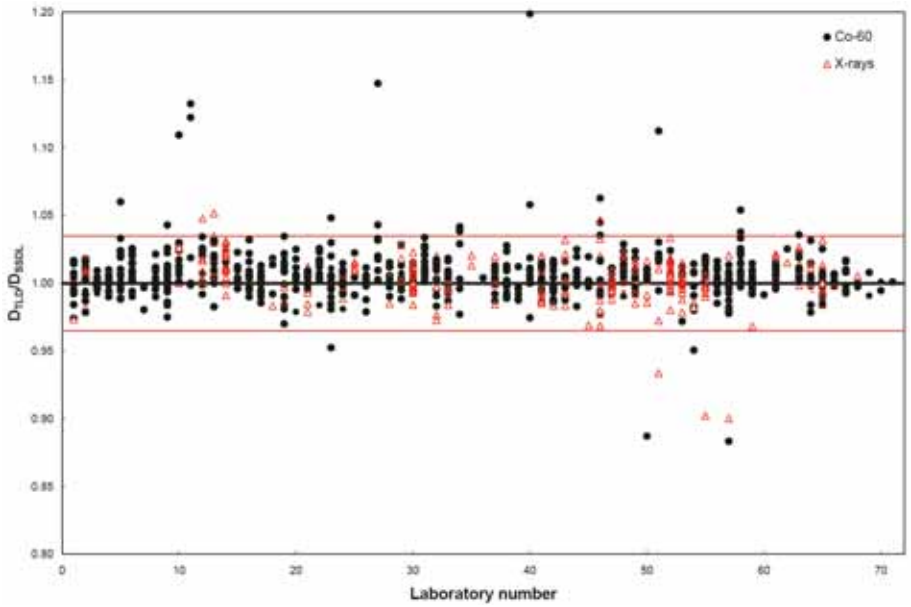

FIG. 5. Results of the IAEA/WHO TLD batches 1997–2009. A total of 988 beam calibrations were checked in 71 laboratories, which include 684 ^{60}Co (circles) and 304 high energy X ray beams (triangles); 29 deviations outside the 3.5% acceptance limit were detected.

this programme in 1997–2009 (Fig. 5) indicate that about 97% of the results of SSDLs that have participated in the TLD audits were within the acceptance limit of 3.5%.

For laboratories with deviations outside the acceptance limit, a follow-up programme has been established to resolve the discrepancies. Those laboratories are assisted by the IAEA to understand and resolve the problem. A repeat (follow-up) TLD set is sent to each of these SSDLs and deviations outside the 3.5% limit are explained and corrected.

3. THE IAEA TPS AUDIT METHODOLOGY

The dosimetry audits gradually evolve from the basic beam calibration audit that is the most essential step, by including other beam parameters, progressing to complex treatment techniques, verifying treatment planning, and finally auditing the complete process of dose planning and delivery. These developments bring the dosimetry audit closer to the patient treatment and therefore have the potential to increase potential benefits.

One of the newer audit modalities operated by the IAEA involves audits of treatment planning systems in radiotherapy [8, 9]. The objective of the TPS audit is to ensure the optimal usage of treatment planning systems and hence safer radiotherapy. The TPS audit reviews the dosimetry, treatment planning and radiotherapy delivery processes in radiotherapy centres using 'end to end' approach, i.e. following the pathway similar to that of the patient, through imaging, treatment planning and dose delivery. This audit is implemented at the national level with IAEA assistance and is currently operated in some European countries. The IAEA provides equipment (a dosimetry phantom) and the detailed audit methodology, as well as expert services to help national auditing organizations to introduce the TPS audit in their country. The national counterparts conduct the TPS audit at local radiotherapy centres.

To date, two pilot TPS audit exercises have been completed for 3-D conformal radiotherapy, in the Baltic States and among Hungarian radiotherapy centres [16]. Issues related to treatment preparation, planning and delivery were identified, and opportunities for improvement outlined. The TPS audit in the Baltic States showed mostly acceptable results with a few exceptions related to TPS algorithm limitations for heterogeneities. The deviations of up to 20% between the measured and the calculated dose were discovered for points located in the lung. A number of small discrepancies related to beam modelling were also observed. In Hungary, four TPSs of ten audited had all results within the acceptance criteria, whereas six others had one or more measurement points showing discrepancies between the TPS calculated and measured doses. Generally, better agreement between the TPS calculations and measurements was observed for 6 MV X ray beams than for 15 MV and 18 MV beams. Following the TPS audit, areas for improvement were identified, for example TPS data input, CT calibration, beam calibration, and they were discussed with local physicists. Further TPS audits in other European countries have been scheduled.

4. COMPREHENSIVE AUDIT IN RADIOTHERAPY: QUATRO

In order to optimize outcomes of radiation treatment, it is equally important that the clinical aspects as well as the physical and technical aspects of patient treatment are audited, because, though essential for the radiotherapy process, accurate beam dosimetry and treatment planning alone cannot guarantee the required outcome. A comprehensive audit methodology has been developed and described by the IAEA [10], known as the QUATRO methodology.

The IAEA QUATRO audits assemble teams of professionals (radiation oncologist, medical physicist, radiation therapist (RTT)) to peer review radiotherapy practices and management at radiation oncology centres with the

aim to improve quality. QUATRO audits include the assessment of the radiotherapy infrastructure; patient and equipment procedures; radiation protection aspects; and staffing levels and professional training programmes for the local radiotherapy staff. QUATRO audits aim to help radiotherapy centres attain the best level of practice possible for their country.

By 2010, QUATRO had conducted approximately 50 audits on request, in radiotherapy centres from Central and Eastern Europe, Asia, Africa, and Latin America. Auditors identify gaps in technology, human resources and procedures, allowing the audited centres to document areas for improvement. Some centres have been acknowledged for operating at a high level of competence, while others have received sets of recommendations. Most common recommendations concerned the staffing levels, which were found insufficient in a few centres; in particular, the numbers of medical physicists were found too low. In addition, the numbers of radiotherapy technologists (RTTs) were found inadequate in some centres. QUATRO also identified issues related to staff training, in particular RTTs, as well as the need to increase the institutional support to staff continuous education. Some centres were recommended to revise and update radiation treatment protocols and many received recommendations on strengthening various aspects of QA programmes and procedures, in particular for patient related QA. In several centres the audit identified equipment shortages and it documented the need for additional radiation treatment units, imaging and treatment planning equipment. At the same time, the use of existing equipment required optimisation and improved scheduling for extended operational time. Other recommendations concerned the structure, management and organization of cancer centres that needed improvements in order to optimize the workflow, achieve efficiency gains and ensure smooth cooperation among departments. Some common issues, which were observed in QUATRO audits, such as the need for RTT staff training, have been addressed internationally. A few radiotherapy centres who have already implemented QUATRO recommendations, received re-audits. Several developments and considerable enhancement of quality in radiotherapy practices were recorded in these centres.

5. CONCLUSION

The IAEA/WHO TLD audit programme has witnessed significant improvements in dosimetry practices worldwide in four decades of its operation. However, discrepancies in beam calibrations are still observed. This suggests that without an audit, these errors may not have been discovered and radiation treatments would not have been correctly delivered to patients. Discrepancies recorded in audits are monitored by the IAEA/WHO, and their causes are traced,

analysed and corrected. Several issues that hamper quality of basic dosimetry in radiotherapy have been identified, such as insufficient number of qualified medical physicists, lack of dosimetry equipment, and obsolete treatment machines. These issues have to be addressed locally.

Dosimetry audits in radiotherapy have been demonstrated to be a useful tool for the improvement of practices in individual radiotherapy centres as well as helping to raise the overall quality and status of radiotherapy dosimetry worldwide. Audits help in reducing uncertainties and in increasing the precision and consistency of radiotherapy dosimetry between centres. Overall, they raise awareness of problems and raise the general level of dosimetry quality. Therefore, it is of importance for any radiotherapy centre to have regular access to, and to participate in, dosimetry audit programmes. All radiation beams used clinically should be independently checked through an audit before the patient treatments start and further, they should be audited on regular basis.

The IAEA transfers the TPS audit methodology to the national level with the aim of improving the quality and safety of dose calculation in radiotherapy. The IAEA TPS audit methodology focuses on conformal techniques using semi-anthropomorphic phantom and 'end-to-end' procedure including phantom imaging, treatment planning and dose delivery. Although the TPS audit programme has only recently been initiated, first audits have drawn the attention of radiotherapy physicists to issues in basic dosimetry, treatment planning and dose delivery thus bringing improvements in clinical dosimetry and the use of TPSs.

QUATRO focuses on reviewing overall quality of the whole multidisciplinary process, management and infrastructure of radiotherapy centres. It assesses the ability of a centre to maintain its radiotherapy practices at the level corresponding to the best clinical practice in the specific economic setting of a given country. QUATRO identifies and documents any operational and structural inadequacies and weak links, and provides advice for quality improvement of radiotherapy services. Overall, QUATRO has contributed to important developments at centres, and it identified common issues of concern that are addressed internationally.

REFERENCES

[1] EISENLOHR, H.H., ABEDIN-ZADEH, R., Checking dosimetry accuracy by post, IAEA Bulletin **15** (1973) 40–43.

[2] EISENLOHR, H.H., JAYARAMAN, S., IAEA-WHO cobalt-60 teletherapy dosimetry programme using mailed LiF dosimeters: A survey of results obtained during 1970-75, Phys Med Biol. **22** (1977) 18–28.

[3] BOYD, A.W., EISENLOHR, H.H., IAEA/WHO Co-60 teletherapy dosimetry programme using mailed LiF dosimeters: A survey of results obtained during 1975–1982, Med. Phys. **10** (1983) 491–92.
[4] SVENSSON, H., HANSON, G.P., ZSDANSKY, K., The IAEA/WHO TL dosimetry programme for radiotherapy centres 1969–1987, Acta Oncol. **29** (1990) 461–467.
[5] IZEWSKA, J., ANDREO, P., The IAEA/WHO TLD postal programme for radiotherapy hospitals, Radiother. Oncol., **54** (2000) 65–72.
[6] IZEWSKA, J., ANDREO, P., VATNITSKY, S., SHORTT, K.R., The IAEA/WHO TLD postal dose quality audits for radiotherapy: a perspective of dosimetry practices at hospitals in developing countries, Radiother Oncol., **69** (2003) 91–97.
[7] AGUIRRE, J.F., TAILOR, R.C., IBBOTT, G., STOVALL, M., HANSON, W.F., "Thermoluminescence dosimetry as a tool for the remote verification of output for radiotherapy beams: 25 years of experience", Standards and Codes of Practice in Medical Radiation Dosimetry (Proc. Int. Symp. Vienna, 2002), IAEA, Vienna (2003) 191–199.
[8] GERSHKEVITCH, E., et al., Dosimetric Verification of Radiotherapy Treatment Planning Systems: Results of IAEA Pilot Study, Radioth. Oncol. **89** (2008) 338–346.
[9] INTERNATIONAL ATOMIC ENERGY AGENCY, Commissioning of Radiotherapy Treatment Planning Systems: Testing for Typical External Beam Treatment Techniques, IAEA-TECDOC-1583, IAEA, Vienna (2008).
[10] INTERNATIONAL ATOMIC ENERGY AGENCY, Comprehensive Audits of Radiotherapy Practices: A Tool for Quality Improvement, IAEA, Vienna (2007).
[11] INTERNATIONAL ATOMIC ENERGY AGENCY, On-Site Visits to Radiotherapy Centres: Medical Physics Procedures, IAEA-TECDOC-1543, IAEA, Vienna (2007).
[12] INTERNATIONAL ATOMIC ENERGY AGENCY, Directory of Radiotherapy Centres — DIRAC, www-naweb.iaea.org/nahu/dirac.
[13] INTERNATIONAL ATOMIC ENERGY AGENCY, Absorbed Dose Determination in External Beam Radiotherapy: An International Code of Practice for Dosimetry Based on Standards of Absorbed Dose to Water, Technical Reports Series No. 398, IAEA, Vienna (2000).
[14] BOYD, A., EISENLOHR, H., GIRZIKOWSKY, R., Postal dose intercomparison of Co-60 dosimetry using thermoluminescence dosimeters among secondary standard dosimetry laboratories, Med Phys. **9** (1982) 112–113.
[15] SVENSSON, H., ZSDANSKY, K., NETTE, P., Dissemination, transfer and intercomparison in radiotherapy dosimetry: the IAEA concept, Measurement assurance in dosimetry: Proc. IAEA International Symposium, Vienna, 24–27 May 1993, Vienna, IAEA (1994) 165–176.
[16] GERSHKEVITSH, E., PESZNYAK, C., VATNITSKY, S., Audit of 3 D conformal radiotherapy treatment planning systems, SSDL Newsletter No. **58** (2010) 40–42.

CREDENTIALING INSTITUTIONS FOR ADVANCED TECHNOLOGY CLINICAL TRIALS

G.S. IBBOTT, A. MOLINEU, J. LOWENSTEIN-LEIF, P. ALVAREZ, J.F. AGUIRRE, D.S. FOLLOWILL
Department of Radiation Physics, M.D. Anderson Cancer Center,
The University of Texas, Houston,
Texas, United States of America
Email: gibbott@mdanderson.org

Abstract

The Radiological Physics Center (RPC) is charged with assuring the consistent delivery of radiation doses to patients on NCI sponsored clinical trials. To accomplish this, the RPC conducts annual mailed audits of machine calibration, dosimetry audit visits to institutions, reviews of treatment records, and credentialing procedures requiring the irradiation of anthropomorphic phantoms. Through these measurements, the RPC has gained an understanding of the level of quality assurance (QA) practised in this cohort of institutions, and a database of measurements of beam characteristics of a large number of treatment machines. The results of irradiations of phantoms have yielded insight into the delivery of advanced technology treatment procedures.

1. INTRODUCTION

Perhaps the first published criticism of US healthcare appeared in 1910 and was written by an educator called Abraham Flexner. Flexner had been recruited to the Carnegie Foundation to study and report on professional education systems of all types, including medicine. The Flexner Report on Medical Education in the United States of America and Canada is well known for his statement condemning the quality of medical education and the broad disparity in quality of the services provided [1]:

> "We have indeed in America medical practitioners not inferior to the best elsewhere; but there is probably no other country in the world in which there is so great a distance and so fatal a difference between the best, the average, and the worst."

It is likely that the situation is improved considerably today, in the US as well as in other countries. But at the same time, the wide and disturbing range in quality of healthcare throughout the world is well known and frequently reported

on. Questions are raised regularly in the press about the appropriate use of imaging, the perceived lack of quality of hospital care, and the high and rapidly increasing cost of health services [2]. Reforming the US healthcare system is again a national priority, and it seems to be agreed that reform must occur soon before the system collapses.

The requirements of quality assurance (QA) were brought to the attention of the US public in 2000 when a report from the Institute of Medicine highlighted the frequency of patient deaths from medical errors [3]. While the magnitude of the problem was shocking — as many as 98 000 patients dying each year from such errors — practitioners of radiation therapy were probably better aware of both the problem and potential solutions than those of many other medical fields. QA has a lengthy and solid foundation in radiation therapy, resulting at least in part from its quantitative nature.

During the past few years, a number of significant radiation therapy errors have been reported worldwide [4–9]. Among the reasons postulated are the introduction of, and increasing dependence upon, advanced technologies [10, 11]. Some errors were blamed specifically on the introduction of the technologies [12, 13]. Other publications reported that the introduction of advanced technology equipment permitted errors to occur that might otherwise have been detected [9]. The demands of advanced technologies on department resources might have drawn resources from simpler or basic functions [14]. It is also believed that, in some cases, the demands on department resources caused a reduction in effort devoted to fundamental QA functions [4, 15].

Clearly, larger errors have a significant impact on the success of radiation therapy. But smaller errors, while having no discernible effect on the treatment of an individual patient, are very likely to influence the overall success of treatments of large numbers of patients [16–18].

2. THE ROLE OF THE RADIOLOGICAL PHYSICS CENTER (RPC)

The idea of an independent quality assurance review office did not begin with the RPC although the RPC is one of the longest continually operating offices of this type. In 1926, Rolf Sievert described a system for quality assurance and a ‘circulating department’ for standardizing a QA programme [19]. He listed a number of critical parameters describing the equipment (e.g. ‘The reliability of the kilovolt-meter’) and individual patient treatments (e.g. ‘The primary dosage of the skin’). Sievert noted, “With standardization it would be possible to make comparisons between the results obtained at different hospitals. A good deal of experience would soon accumulate through people annually visiting the different

roentgen departments all over the country, and this would be of assistance when fitting up new roentgen wards and purchasing new apparatuses and tubes."

In 1950, Thoraeus described the experiences of the 'circulating department' established by Sievert since its creation in 1925 [20]. The department was at that time visiting about 60 facilities and inspecting 137 therapy units. Visits were made twice each year, and included measurements of timer function, kV and mA, dose rates and radiation protection. No specifics were given in the article, but it was reported that "inconsistent, and thus unreliable" dose meters were found during the visits. Thoraeus discusses the compilation of depth dose data from measurements at a number of institutions, which were then provided to all institutions to be used as a means of standardizing treatments. He also describes the increasing use of "modern protective equipment" during the course of the inspections, in part as a result of inadequacies uncovered during the inspections.

The RPC was established in 1968 to contribute to the development, conduct, and QA of multi-institutional cooperative group clinical trials. A description of clinical trials and the role of several of the QA offices can be found in a report published by the American Association of Physicists in Medicine (AAPM) [21]. The mission of the RPC is to assure NCI and the cooperative groups that institutions participating in clinical trials deliver prescribed radiation doses that are clinically comparable and consistent.

In 1999, the RPC joined with several other QA offices to form the Advanced Technologies Consortium (ATC) [22]. The ATC currently consists of the RPC, the Image Guided Therapy QA Center (ITC) in St. Louis, the Quality Assurance Resource Center (QARC) in Providence, RI and the headquarters dosimetry group of the Radiation Therapy Oncology Group (RTOG), located in Philadelphia. The role of the ATC is to support the development and conduct of advanced technology clinical trials, and to facilitate communications among the four QA offices.

2.1. Remote audits

The RPC initiated a programme of mailed thermoluminescent dosimeters (TLDs) in 1977 [23]. The uncertainty of the TLD system to measure output of accelerators remotely was evaluated and found to be 1.5% [24]. Consequently, the RPC's measurement of an institution's output can be stated at an uncertainty of less than 5% using a 99% confidence interval. When the TLD measurement disagrees with an institution's stated dose by more than 5%, the RPC initiates a series of activities to resolve the discrepancy. If the discrepancy cannot be resolved through telephone calls and the review of procedures and documentation, an on-site dosimetry visit is scheduled. The RPC recently

replaced the TLD system with one based on optically stimulated luminescence dosimetry (OSLD) [25].

2.2. On-site dosimetry review visits

An on-site audit has been recommended by several organizations, including the AAPM and the IAEA [26, 27]. An independent audit is especially important for solo practitioners, and is a valuable exercise for all practising clinical medical physicists. It need not be extensive, but should address key activities such as basic calibrations, the overall QA programme and documentation.

The RPC visit procedure consists of: a review of the institution's QA procedures and documentation; a review of treatment records to ascertain the consistency of the procedures used for treatment planning and monitor unit calculations; and measurements of the radiation beams and radioactive sources. The measurements include mechanical alignment and accuracy of position readout devices, light versus radiation field congruency, calibration of treatment machine output and brachytherapy source strength, relative field size dependence, percent depth dose, off-axis ratio, some asymmetric jaw and irregular field parameters, and accessory transmission factors. Several measurements are designed to evaluate the basic data required for delivery of intensity modulated radiation therapy (IMRT). Procedures for evaluating image guided radiation therapy (IGRT) are under development, and procedures for visits to proton beam facilities are currently being implemented.

The RPC has conducted on-site dosimetry audits during its 42 year history, and has accumulated extensive measured data from 2350 photon beams into 81 separate tables classified by manufacturer, model and beam energy. This database of 'standard data' enables the RPC to compare an institution's measured data with the standard data. Differences often help to identify measurement errors as well as explain the source of calibration errors detected by a mailed audit.

2.3. Credentialing for advanced technology clinical trials

Clinical trials that require the use of advanced technologies such as IMRT and prostate brachytherapy are considered sufficiently challenging so that institutions are required to demonstrate their ability to use these technologies before being permitted to register patients. Credentialing for such clinical trials generally involves most or all of the following procedures:

(a) Previous patients treated with technique
Institutions must demonstrate that they are familiar with the technique and have used it to treat at least some minimum number of patients.

(b) Facility questionnaire
This questionnaire asks institutions to describe relevant aspects of their treatment planning and delivery equipment, their QA procedures, and in some cases, the personnel who will be participating in protocol patient treatments.

(c) Knowledge assessment questionnaire
The physician is asked to take a simple open book quiz to indicate that he or she is familiar with the protocol and its requirements.

(d) Benchmark case or phantom
For the more complex technologies, the institution may be required to submit a treatment plan generated for a standardized geometry or CT data set, or simulate, plan and treat an anthropomorphic phantom. If the protocol requires a benchmark treatment plan, the RPC reviews the institution's plan and recalculates the doses at key locations to evaluate the accuracy of the planning system. When anthropomorphic phantoms are used, the RPC sends a phantom to the institution, with instructions to treat the phantom in exactly the same manner that patients are treated in the department. The institution will image the phantom, develop a treatment plan using the technique to be tested (e.g. IMRT or stereotactic body radiation therapy, or SBRT), perform the customary QA procedures, then deliver the treatment to the phantom. The phantom is returned to the RPC where dosimeters (TLD capsules and radiochromic film) are removed and analysed. The RPC then compares the delivered dose to the institution's plan to determine the agreement.

Several phantom models have been developed including one that mimics the brain, the head and neck, the thorax, the abdomen, the pelvis and the spine (see Fig. 1 [28, 29]).

(e) Electronic data submission
Many clinical trials involving advanced technology radiation therapy are now requiring institutions to submit the treatment plans for protocol patients digitally to the ITC. The plans performed for irradiation of the RPC's anthropomorphic phantoms also must be submitted digitally.

(f) RPC QA and dosimetry review
The RPC often reviews the institution's QA and dosimetry procedures and records.

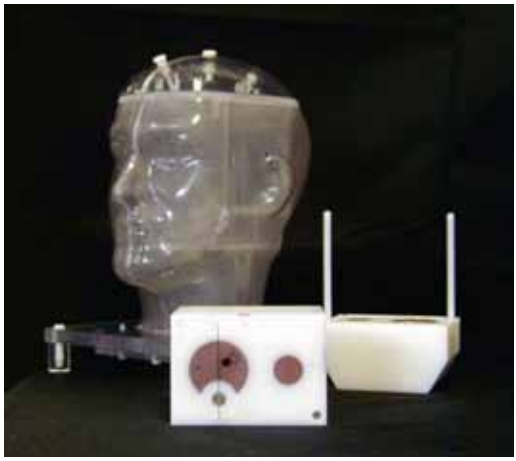

FIG. 1. The RPC's head-and-neck phantom. The phantom is representative of all RPC phantoms and consists of a water filled shell containing inserts with imageable structures representing target volumes and organs at risk. The inserts also contain radiochromic film and TLDs to evaluate the delivered dose.

(g) Clinical review by a radiation oncologist
In some cases, the protocol requires that the institution submit representative treatment plans performed for patients treated previously using the technology being tested by the protocol, and techniques at least similar to those required by the protocol. The plans are reviewed by the study chair or a radiation oncologist who works with the RPC to ensure that they conform to the intentions of the study chair or his/her designee.

2.4. Reviews of patient treatment records

In some cases, the RPC (or another QA office) reviews the treatment plans prepared by participating institutions for patients registered on the clinical trial. When the number of patients to be registered is relatively small, and the protocol is complex, the study chair may require that institutions submit their treatment plans for review before the patients are treated. The RPC often participates in such 'rapid reviews' to ensure that the treatment plans meet the dosimetric requirements of the protocol. An example of a recent protocol that requires rapid reviews is the joint trial of accelerated partial breast irradiation conducted by the National Surgical Adjuvant Breast and Bowel Project (NSABP) and RTOG.

In other cases, the RPC performs retrospective reviews. The RPC relies on measurements made at the institution through the TLD programme and on-site dosimetry reviews, or if a visit has not yet been made, its database of measured

'standard' data. Using these data and the treatment parameters (field size, depth, MU setting, etc.), the RPC can independently calculate the dose received by the patient.

3. RESULTS FROM RPC QA AUDITS

3.1. Annual calibration checks

Nearly 1800 institutions are currently participating in clinical trials and are enrolled in the RPC's audit programmes, of which approximately 1650 are located in North America, and represent roughly 65% of all radiotherapy facilities in this region. Approximately 230 new machines are installed each year at the facilities audited by the RPC. New machines are subject to calibration errors as they are put into clinical service, with potentially serious results. Over the years, 5–6% of the US megavoltage beams audited with TLD have fallen outside of the RPC's ±5% dose or 5 mm electron depth dose criteria on the first measurement (see Fig. 2). With 3200 machines being monitored today, this represents approximately 700 beams that fall outside the RPC's criteria for acceptability. Among these institutions, nearly 20% or roughly 350 institutions have one or more beams outside the RPC's criteria on an annual basis that require an investigation by the RPC (see Fig. 3).

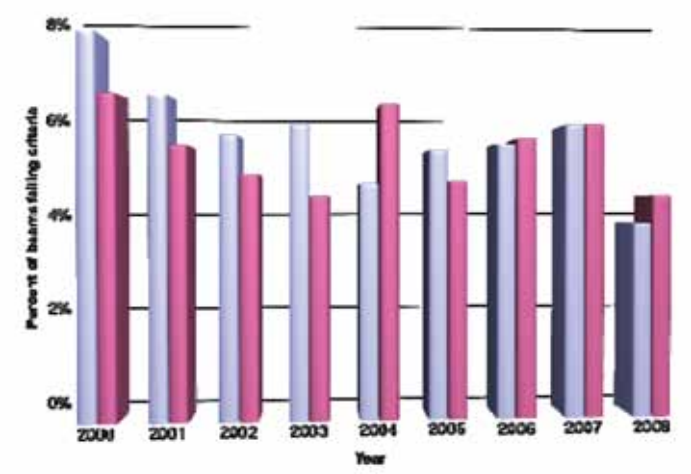

FIG. 2. The percentage of megavoltage radiation beams at US institutions that fail to meet the RPC's 5%/5 mm criteria for acceptability. The blue bars indicate the proportions at institutions visited by the RPC.

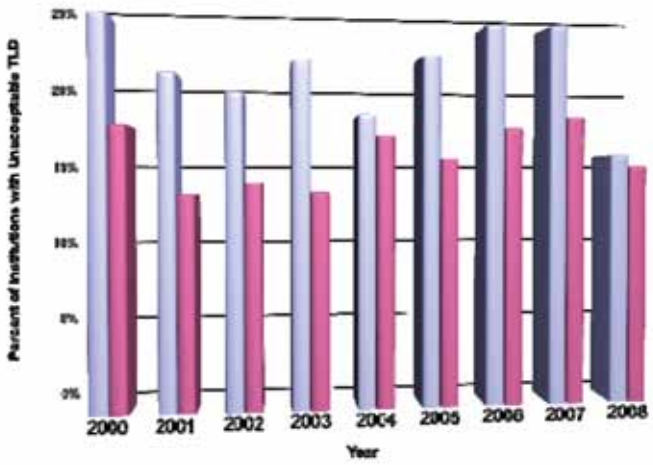

FIG. 3. The percentage of institutions irradiating TLDs in any year that had at least one beam failing the RPC's 5%/5 mm criteria for acceptability.

An annual independent audit coincides with the QA standard requirement in most states that each beam be calibrated annually to ascertain that the output has not changed. The precedent for performing the TLD audit annually was established by the RPC many years ago and all current trial data and results are based on having this level of QA. A review of trial results from the European Organization for Research and Treatment of Cancer (EORTC) indicated that decreases in tumour control probability were associated with discrepancies in the beam calibration, as measured by a TLD audit programme [16]. At the same time, increases in normal tissue morbidity were associated with discrepant high TLD measurements. This article also indicated that sequential TLD audits improved the uniformity of the clinical outcome and that small deviations in beam output might lead to clinically important variations in outcome. Mailed TLD audits were deemed to be an integral part of quality assurance for trials.

3.2. Measurements of beam parameters

Following a dosimetry review visit, the RPC generates a detailed report describing the observations made and measurements taken, as well as the level of agreement with the institution's planning data. The report clearly indicates any measurements that disagree by a significant amount with the institution's data, and when the disagreements exceed appropriate thresholds, the report includes recommendations to the institution for improvement. These recommendations then demonstrate areas that require attention by the institution. When considered

in aggregate, these recommendations form an indication of the areas of general concern at the visited institutions. The common recommendations and the frequency with which institutions receive them are shown in Table 1. Of note are the recommendations indicated by asterisks, which are considered important dosimetry parameters. Overall, 70% of visited institutions received one or more of these recommendations.

3.3. Reviews of QA programmes

The RPC judges the quality of an institution's QA programme against the AAPM's TG-40 and TG-142 Recommendations [31, 32]. A list of common failures or lapses in QA programmes found by the RPC is shown in Table 2.

3.4. Observations from reviews of patient records

Over a five year period, from 2005 to 2009, the RPC found systematic errors in 1% of charts, individual errors in 8% of charts, and transcription errors in 27% of the charts. In each case, the error was corrected by the RPC and reported to the study group so that correct information could be used for evaluation of the clinical trial. The results of these reviews were also reported to the institutions promptly in order to enable the institutions to take corrective action.

TABLE 1. SELECTED DISCREPANCIES DETECTED DURING 2004–2008 DURING RPC DOSIMETRY REVIEW VISITS TO 165 INSTITUTIONS [30]

Errors regarding:	Number of institutions (%)
Review QA programme	127 (84%)
Wedge transmission	53 (32%)
Photon FSD (small fields)	46 (28%)
Off-axis factors, beam symmetry	42 (25%)
Photon depth dose	34 (21%)
Electron calibration	25 (15%)
Photon calibration	22 (13%)
Electron depth dose	19 (12%)

TABLE 2. COMMON QA LAPSES AND DEFICIENCIES FOUND AT INSTITUTIONS DURING RPC VISITS [30]

— QA records not available or maintained
— Annual calibrations or monthly checks not performed timely
— No record of comparison to clinical values on institution's annual QA report
— No record of comparison of daily and monthly checks against annual baseline values
— Physicist review of daily checks not documented
— No record of corrective actions and repeat measurements
— Daily check of electron beam energy not performed
— Output or field flatness constancy with gantry angle not checked during annual calibration

TABLE 3. PASSING RATES FOR THE RPC ANTHROPOMORPHIC PHANTOMS

Phantom	Head & neck	Prostate	Spine	Lung	Liver
Irradiations	752	174	19	174	23
Pass	585	143	13	124	12
Pass (%)	78%	82%	68%	71%	52%
Criteria	7%/4 mm	7%/4 mm	5%/3 mm	5%/5 mm	7%/4 mm
Year introduced	2001	2004	2009	2004	2005

Note: The criteria for agreement are shown in the fifth row of the table.

3.5. Results of anthropomorphic phantom reviews

During the time period from 2001 to 2009 the RPC mailed IMRT head-and-neck phantoms to 472 distinct institutions. See Table 3 and Fig. 4. A total of 752 irradiations were analysed. Of these, 585 irradiations or 78% successfully met the accreditation criteria shown in Table 3. More than 350 institutions failed to meet the irradiation criteria on the first attempt and had to repeat the phantom irradiation. Of those failing to meet the accreditation criteria, the majority failed only the dose criterion. The remaining unsuccessful irradiations failed the distance to agreement (DTA) criterion or both the dose and DTA criteria.

Institutions irradiating the phantoms submitted their treatment plans digitally to facilitate comparison with the measured data. The achievable agreement between the plan and the measured dose distribution was determined for each phantom by conducting a pilot test with eight to ten institutions. These data then were presented to the clinical trials study group and criteria for phantom

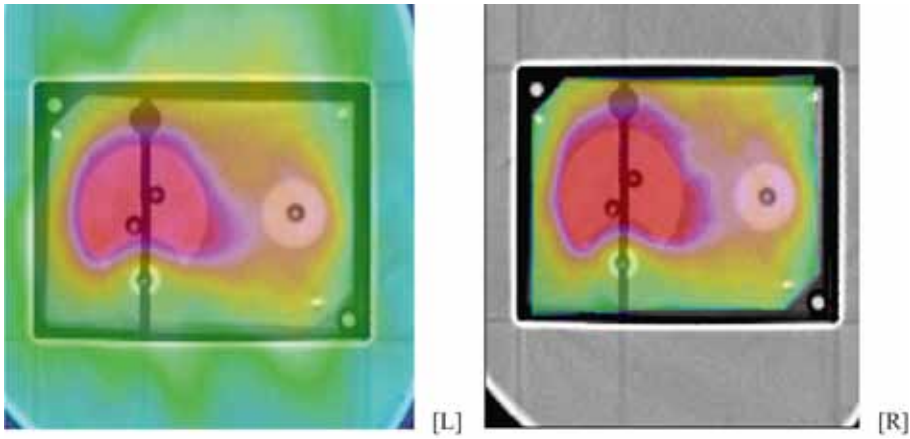

FIG. 4. A comparison between an institution's treatment plan (left) and the delivered dose (right) showing good agreement.

evaluation were decided on. Consequently, the different criteria reflect differences in the challenges posed by the phantoms, the goals of the clinical trial, and a compromise between establishing stringent criteria and encouraging participation in the trials.

The average TLD/institution ratio for the planning target volumes was 0.99 with a standard deviation of 5%. The range of the measurements was large, with ratios extending from 0.44 to 1.26. The DTA for the high dose gradient region between the primary planning target volume and the organ at risk averaged 0.2 mm with a standard deviation of 3.1 mm. The majority of the phantoms met the 4 mm criterion. The range of the DTAs was from –15 mm to +17 mm. A negative DTA meant that an institution delivered dose posteriorly beyond the planned distribution and delivered a higher than intended dose to the organ at risk.

4. SUMMARY AND CONCLUSIONS

As described above, the majority of institutions audited by the RPC meet well accepted criteria established by organizations such as the AAPM and RTOG. However, a significant number of institutions fail to meet these standards. The RPC's mailed TLD programme found reference calibration discrepancies at 15–20% of the audited institutions for the past eight years. During dosimetry audit visits, measurements with an ionization chamber in a water phantom were made of several significant dosimetry parameters; 70% of the institutions visited

had discrepancies in one or more of them. In particular, the RPC disagreed with the institution's calibration of one or more photon beams during audit visits to 13% of the institutions visited during the past five years. During reviews of treatment records, the RPC has disagreed with calculations performed by the audited institutions in as many as 9% of the reviewed charts. Measurements of tumour dose delivered to anthropomorphic phantoms demonstrated that institutions delivered the intended tumour dose within the 7%/4 mm DTA criteria for 75–80% of the time. Where possible, institutions whose irradiations failed the RPC's criteria were contacted and efforts were made to understand the causes. In some cases, the specific cause could be identified and those causes are listed in Table 4. A frequent cause of discrepancy was inadequate modelling of the radiation beams in the treatment planning computer [33]. It is suspected that, in some cases, institutions failed to follow the RPC's instructions to treat the phantom as if it were an actual patient, and did not use their customary staff and procedures when imaging, planning and treating the phantom.

The RPC endeavours to understand the reasons for such discrepancies, and to educate the institutions in the procedures needed to resolve them. Follow-up output audits, calibration and QA record reviews, and re-reviews of treatment

TABLE 4. CONFIRMED CAUSES OF DISCREPANCIES WITH THE RPC ANTHROPOMORPHIC PHANTOMS FROM A STUDY OF A LIMITED SERIES OF DISCREPANCIES

Explanation	Minimum no. of occurrences
Incorrect output factors in TPS	1
Incorrect PDD in TPS	1
IMRT technique	3
Software error	1
Inadequacies in beam modelling at leaf ends	14
QA procedures	3
Errors in couch indexing with Peacock system	3
Equipment performance	2
Se-tup errors	7

Note: The frequency with which each cause occurred is given.

records are all intended to confirm that discrepancies are corrected. However, RPC records indicate that additional discrepancies and errors occur each year. This suggests that without an independent review, the number of errors would be greater, and both the time elapsed before their discovery and the number of patients treated incorrectly would also be greater.

4.1. The need for routine QA

The pressure to adopt new technologies such as IMRT, IGRT and brachytherapy pulls resources away from routine, and more mundane but still very important procedures. Physicists must not forget that advanced technologies, as well as more conventional treatment techniques, depend on basic measurements and routine QA procedures. While such procedures are less exciting to perform, and rarely generate patient revenue, they are the foundation of accurate and successful treatment.

An important component of a radiation therapy QA programme is an independent review. It cannot be assumed that software such as spreadsheets can always be relied on for a second check. Likewise, if another physicist in the same institution performs calculation checks, different procedures and reference data should be used to ensure that the checks are truly independent.

4.2. The need for patient specific QA

It is occasionally voiced in open forums that patient specific QA procedures are performed for IMRT only, because in the USA at least, it is a requirement for reimbursement. The experience of the RPC suggests that since procedures such as IMRT are still sufficiently challenging, treatment accuracy cannot be taken for granted. Even IMRT procedures performed frequently, such as prostate therapy, are subject to unexpected errors. While some savings in QA effort can undoubtedly be achieved by performing extensive QA of only a selection of records and calculations, many modern techniques such as IMRT are particularly difficult to develop a ‘feel’ for, and it may be possible to develop an unwarranted level of comfort with the technique. Until extensive experience is achieved with such techniques, it is recommended that patient specific QA be performed routinely.

REFERENCES

[1] FLEXNER, A., Medical Education in the United States and Canada, Carnegie Foundation for Higher Education (1910).

[2] BOGDANICH, W., "THE RADIATION BOOM: Radiation Offers New Cures, and Ways to Do Harm" (2010), http://www.nytimes.com/2010/01/24/health/24radiation.html,and http://www.nytimes.com/2010/01/27/us/27radiation.html

[3] KOHN, L.T., et al., "To err is human: Building a safer health system". Washington, DC: National Academy Press (2000).

[4] DUNSCOMBE, P., et al., The Ottawa Orthovoltage Incident: Report of the Panel of Experts convened by Cancer Care Ontario (2008), http://www.ottawahospital.on.ca/about/reports/orthovoltage-cco-e.pdf.

[5] DONALDSON, L., Towards Safer Radiotherapy, The Royal College of Radiologists, Society and College of Radiographers, Institute of Physics and Engineering in Medicine, National Patient Safety Agency, British Institute of Radiology, London, (2008).

[6] INTERNATIONAL ATOMIC ENERGY AGENCY, Lessons Learned from Accidental Exposures in Radiotherapy, Safety Reports Series No. 17, IAEA, Vienna (2000).

[7] INTERNATIONAL COMMISSION ON RADIATION PROTECTION, "Prevention of Accidental Exposures to Patients Undergoing Radiation Therapy". Annals of the ICRP, Vol. 30, Issue 3, Sep (2000).

[8] ROGERS, L., "Over 200 hurt or killed by botched radiation", The Times (London) Online: http://www.timesonline.co.uk/tol/news/uk/article711360.ece?token=null&offset=12&page=1.

[9] WAtoday, "Cancer patients 'given excess radiation'", http://www.watoday.com.au/breaking-news-national/cancer-patients-given-excess-radiation-20090131-7u9o.html

[10] BARTHELEMY-BRICHANT, N., et al., Evaluation of frequency and type of errors detected by a computerized record and verify system during radiation treatment. Radiother. Oncol **53** (1999) 149–154.

[11] PERROW, C., Normal Accidents: Living with High Risk Technologies, Princeton University Press, Princeton, New Jersey (1999).

[12] MACKLIS, R.M., MEIER, T., WEINHOUS, M.S., Error rates in clinical radiotherapy, J Clin Oncol **16** (1998) 551–556.

[13] HUANG, G., et al., Error in the delivery of radiation therapy: Results of a quality assurance review, Int. J. Radiat. Oncol. Bio. Phys. **61** (2005) 1590–1595.

[14] PATTON, G.A., et al., Facilitation of radiotherapeutic error by computerized record and verify systems, Int J Radiat Oncol Biol Phys. **56** (2003) 50–57.

[15] MARKS, L.B., et al., The impact of advanced technologies on treatment deviations in radiation treatment delivery, Int J Radiat Oncol Biol Phys. **69** (2007) 1579–1586.

[16] BENTZEN, S.M., et al., Clinical impact of dosimetry quality assurance programmes assessed by radiobiological modeling of data from the thermoluminescent dosimetry study of the European Organization for Research and Treatment of Cancer, European J. Cancer **36** (2000) 615–620.

[17] BOYER, A., SCHULTHEISS, T., Effects of dosimetric and clinical uncertainty on complication-free local tumor control. Radiotherapy and Oncology **11** (1988) 65–71.
[18] PETTERSEN, M.N., et al., Quality assurance of dosimetry and the impact on sample size in randomized clinical trials, Radiotherapy and Oncology **86** (2008) 195–199.
[19] SIEVERT, R.M., A circulating physical department for standardizing the Roentgen radiation used in therapy, Acta Radiol **5** (1926) 457–467.
[20] THORAEUS, R., Features of the system of periodical inspection adopted for Roentgen therapy installations in Sweden, and some experiences of the inspection work, Acta Radiol **33** (1950) 253–280.
[21] OLCH, A., et al., "Quality Assurance for Clinical Trials: A Primer for Physicists, Prepared by AAPM Subcommittee on QA for Clinical Trials", AAPM Report No. 86, American Institute of Physics, College Park, MD (2004).
[22] PURDY, J., et al., The Advanced Technology QA Consortium (ATC), Med. Phys. **31** (2004) 1833.
[23] KIRBY, T.H., et al., Mailable TLD system for photon and electron therapy beams, Int. J. Radiat. Oncol. Biol. Phys. **12** (1986) 261–265.
[24] KIRBY, T.H., et al., Uncertainty analysis of absorbed dose calculations from thermoluminescensce dosimeters, Med. Phys. **19** (1992) 1427–1433.
[25] HOMNICK, J., et al., Optically Stimulated Luminescence (OSL) Dosimeters Can Be Used for Remote Dosimetry Services, Med. Phys. **35**(6) (2008) 2994.
[26] HALVORSEN, P.H., et al., AAPM Task Group 103 report on peer review in clinical radiation oncology physics, J Appl Clin Med Phys **6** (2005) 50–64.
[27] INTERNATIONAL ATOMIC ENERGY AGENCY, Comprehensive Audits of Radiotherapy Practices: A Tool for Quality Improvement, IAEA, Vienna (2007).
[28] MOLINEU, A., et al., Design and Implementation of an Anthropomorphic Quality Assurance Phantom for Intensity Modulated Radiation Therapy for the Radiation Oncology Group, Int. J. of Radiat. Oncol. Biol. Phys. **63** (2005) 577–83.
[29] FOLLOWILL, D.S., et al., Design, development, and implementation of the Radiological Physics Center's pelvis and thorax anthropomorphic quality assurance phantoms, Med. Phys. **34**(6) (2007) 2070-6.
[30] IBBOTT, G.S., "QA for clinical dosimetry, with emphasis on clinical trials" (ROGERS, D.W.O., CYGLER, J.E., Eds) Clinical Dosimetry Measurements in Radiotherapy, Medical Physics Publishing, Madison, WI (2009).
[31] KUTCHER, G.J., et al., Comprehensive QA for Radiation Oncology, Med. Phys. **21** (1994) 581–618
[32] KLEIN, E.E., et al., Task Group 142 Report: Quality assurance of medical accelerators, Med. Phys. **36** (2009) 4197–4212.
[33] CADMAN, P., et al., Dosimetric considerations for validation of a sequential IMRT process with a commercial treatment planning system, Phys Med Biol **47**(16)(2002) 3001–10.

PRELIMINARY RESULTS FROM A DOSIMETRIC AUDIT PERFORMED AT SWEDISH RADIOTHERAPY CENTRES

T. KNÖÖS, J. MEDIN
Skåne University Hospital Lund and Lund University,
Lund
Email: tommy.knoos@med.lu.se

L. PERSSON
Swedish Radiation Safety Authority,
Stockholm

Sweden

Abstract

A dosimetry audit was performed during 2010 in Sweden, initiated by the medical physics group in Lund and supported by the national authority for radiation safety. There are 18 departments delivering with about 65 linear accelerators, but for this study only one or in a few exceptions two units have been included per department. The audit covered: (a) input CT data to treatment planning, (b) beam calibration under reference conditions, (c) delivery of a standard set of beams, and (d) delivery of a five field prostate type treatment plan. The first 13 departments will be included in this report. The measurements were performed with a commercial phantom covering most types of tissues present in the body for the CT input data. Dose determination in reference geometry was accomplished with an ionization chamber/electrometer combination according to the International Code of Practice TRS-398. For the two final parts, an electronic semi-quasi three dimensional diode detector system was used to sample 1069 dose points, which then were used for evaluation against the dose distribution from the local treatment planning system. The visited institutes are equipped with one of two different brands of treatment planning systems, and most of the users do not have the possibility to change the transfer of CT number/Hounsfield units to electron density to be used in the dose calculations. The transfer function at each department however, has been checked; thus, any changes from the default settings have been recorded. The preliminary data for the reference dosimetry show an excellent agreement between the absorbed dose determined by the local user and the audit group (1.003 ± 0.005, $k = 1$); the small spread should particularly be noted.

1. INTRODUCTION

An external audit of radiotherapy is a method of identifying systematic errors both in data and in procedures implemented at the local department. Audits can cover several steps in the radiotherapy process, e.g. beam calibration, target definition, dose calculations and the delivery of treatment. Several national audits have been performed in many European countries during the last decades, e.g. the United Kingdom [1], Poland [2] and Germany [3]. There have also been international audits, for example, one initiated by the European Society for Therapeutic Radiology and Oncology (ESTRO) covering nine European countries with 66 participating centres [4]. This study included beam calibration under reference conditions, but several other studies have also included dose measurements in other geometries. The European Organisation for Research and Treatment of Cancer (EORTC) organized an audit for departments participating in clinical trials, which was reported in three papers, the latter of which included dosimetric data from more anatomical shaped geometries [5]. The ESTRO–EQUAL study of 1998 included beam calibration, but also percent depth doses, output factors as well as wedge transmission factors [6]. One of the most comprehensive external audit programmes is available from the Radiological Physics Center (RPC) at the M.D. Anderson Cancer Center established by the American Association of Physicists in Medicine (AAPM) and funded by, e.g. the National Cancer Institute in the United States.[1]

The previous national inter-institutional audit in Sweden was performed 28 years ago [7], although some departments have been participating in the above-mentioned international audits. Therefore, a project was initiated by the Lund Medical Physics Group and the Swedish Radiation Safety Authority during 2008–2009 to perform a dosimetry audit of the radiotherapy centres in Sweden. External audits can, in principle, be performed in two ways, as mailed service or by site visits. In this project, it was decided to carry out site visits, which started late 2009.

2. METHODS AND MATERIALS

The present audit covers three steps in the radiotherapy chain. The first was the input data to the treatment planning system (TPS) consisting of computerized tomography (CT) attenuation distributions, i.e. CT numbers or Hounsfield units (HUs), which are the basis for dose calculation. The second sub-process was the

[1] More information is available at http://rpc.mdanderson.org.

absorbed dose calibration of the linear accelerator under reference conditions [8]; and the last step was the validation of the local commissioning of algorithm input data (see definition by the IAEA [9]), facilitated through measurements of absorbed dose distributions in discrete points for simple beam configurations evaluated against calculations with the local TPS.

2.1. CT data

A plastic phantom with cylinders of different electron densities reproducing various tissue properties was scanned using a common planning protocol in the local CT scanner and transferred to the local TPS in order to analyse the conversion of HUs to densities (or electron densities).

A commercial phantom was used (Electron Density Phantom 062, by Computerized Imaging Reference Systems, CIRS, Inc, VA, United States of America), which includes insert covering the most common tissues (see Table 1).

2.2. Beam calibration

Absorbed dose measurements under reference conditions according to the IAEA TRS 398 [8] were performed in a water phantom with PMMA walls. This phantom was designed and built at the audit group's workshop with dimensions 25 cm × 25 cm × 35 cm with two tubes for ionisation chambers of Farmer 0.6 cm^3 type. One chamber was for the measured charge and the second for monitoring the stability of the beam. All measurements in the audit phantom were performed

FIG. 1. The density phantom positioned on the CT scanner couch ready to be scanned.

TABLE 1. TISSUE SUBSTITUTES IN THE CT PHANTOM FOR EVALUATION OF HOUNSFIELD UNIT TO DENSITY CONVERSION

Tissue/material	Physical density (g/cm^3)	Electron density ($electrons/cm^3 \times 10^{23}$)	Relative electron density to water
H_2O syringe	1.00	3.340	1.000
Lung (inhale)	0.20	0.634	0.190
Lung (exhale)	0.50	1.632	0.489
Breast (50/50)	0.99	3.261	0.976
Dense bone 800 mg/cm^3	1.53	4.862	1.456
Trabecular bone 200 mg/cm^3	1.16	3.730	1.117
Liver	1.07	3.516	1.052
Muscle	1.06	3.483	1.043
Adipose	0.96	3.170	0.949

with the gantry at 0° defined according to IEC 61217 [10], i.e. the beam was vertical and enters the water without passing any PMMA.

All measurements by the audit group were performed using the reference geometry of the visited hospital, i.e. either with a set-up where the centre of the ionization chamber was positioned at the isocentre (SAD) or with the isocentre at the surface of the water and the chamber at the reference depth (SSD). Both the local physicists (using their own equipment) and the audit group determine the absorbed dose in the reference geometry at the visit as close as possible in time to each other.

The audit team determined the $TPR_{20,10}$ for studied beams and the corrections factors for the polarity effect k_{pol}, ion recombination k_s and the ambient correction factor $k_{t,p}$ considering the difference in conditions compared to the calibration at the SSDL[2]. All equipment used by the audit team was calibrated biennially by the standard laboratories in Sweden. This includes a barometer, thermometer, electrometer and ionization chambers.

[2] Secondary standard dosimetry laboratory (SSDL).

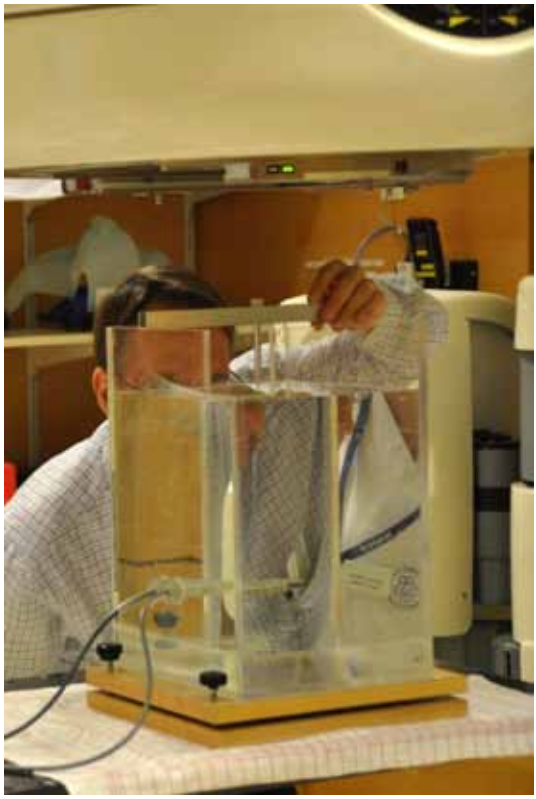

FIG. 2. The audit group's water phantom positioned for irradiation. Fixed distance rods were used to determine the distance from the upper edge of the phantom down to the water level while the ionization chambers have a fixed position, thus assuring the correct depth of measurement. The phantom was placed on a dual plate with three adjustment screws to facilitate the levelling.

2.3. Validation of treatment data

A crucial step regarding accuracy in the radiotherapy process is the commissioning of data to the TPS and maintaining them throughout the lifetime of the linear accelerator. Several methods are used and different data sets or algorithm input data are required for the various TPS on the market. Independent of the methodologies and contents, the accuracy of the delivered treatment to the patient depends on the agreement of the predicted/calculated dose from the TPS and the output of the treatment unit.

TABLE 2. LIST OF THE STANDARD FIELDS EVALUATED WITH THE DIODE ARRAY DETECTOR SYSTEM

Field size (cm^2)	Gantry angle	Collimator rotation	Open or wedged beam
10×10	0°, 90°, 270°	0°	Open
10×10	0°	0°, 90°, 270°	Open
5×5, 5×20, 20×5	0°	0°	Open
10×20	0°	0°	Wedge 20°, wedge 60°

In this audit, a set of standard fields (see Table 2) calculated in the local TPS was compared with measurements using a semi-quasi 3-D diode array detector (Delta4, ScandiDos AB, Uppsala, Sweden). The fields calculated with the local dose planning system were exported to the detector system software, the fields were delivered, and the resulting dose distribution was sampled. This type of detector has recently been introduced to the community and a few reports have been published showing its accuracy to verify highly complex treatment modalities [11–13].

As the final check during this audit, a typical 3-D conformal plan for prostate was sent to all participating departments, transferred to the local TPS onto the PMMA phantom representing the diode array detector.

3. RESULTS AND DISCUSSION

When this report was written, 13 out of the 18 institutes had been visited covering 14 different linear accelerators and 27 different beams between 4 MV and 18 MV X rays. The remaining sites are scheduled for autumn 2010 or early spring 2011.

3.1. CT data

Among the visited sites, only two brands of TPSs were represented (Varian Eclipse and Nucletron Oncentra), and most users were using the default settings for importing and transferring the CT data to density maps for the dose calculation, i.e. both dose planning systems in fact used the same data [14]. The two systems are available at the auditor's department; thus, the authors collected all scanned CT data in DICOM format, and the HU for each included density was

evaluated directly from the images. During the present audit, it was found that the default transfer function had been changed at one department (A), resulting in erroneous results for the high density regions. After this audit, the local physics group went back to the default settings.

3.2. Beam calibration

All visited sites followed the IAEA TRS 398 Code of Practice with a 50/50 choice of SAD or SSD set-up except for two sites, which performed all beam calibrations with an SSD of 95 cm and with the chamber centre positioned at 5 cm depth for all energies. The TRS 398 gives the possibility to perform measurements at 5 cm for energies where the $TPR_{20,10}$ is less than 0.7; however, these sites are violating the Code of Practice for the higher energies.

For the first 27 checked beams from 14 different accelerators, the average ratio between the local (or stated) and the audit reference absorbed dose (measured) is 1.003 ± 0.005 (k = 1). The very small spread among the Swedish departments is most remarkable.

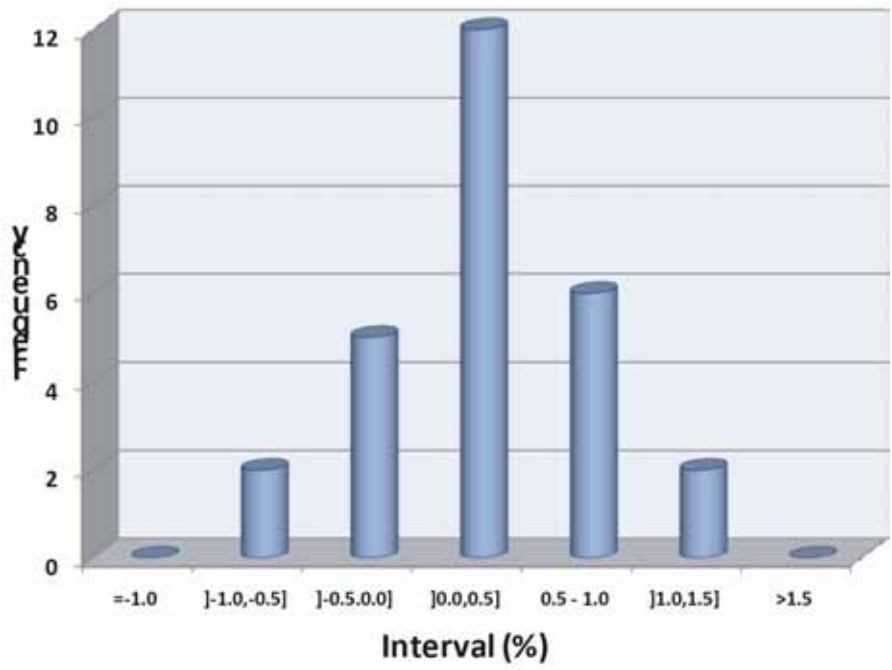

FIG. 3. Distribution of deviations (%) between stated absorbed dose to measured dose at reference conditions from 27 beams.

3.3. Validation of treatment data

In this preliminary report, only data for the five field prostate treatment will be reported. A gamma analysis [15, 16] was performed for these prostate beams both for the composite treatment and for each individual field, using preliminary criteria of 3% and 3 mm. A more in-depth analysis of the uncertainties involved in the measurement must be performed before the final analysis. In Fig. 4, a screen dump from the biplanar diode detector system is shown for one of the irradiations. A summary of both the composite agreement and, when available, beam individual beam gamma analysis agreement is shown in Table 3 below.

All departments except one had results where the fraction of measurements having gamma values less than unity (conforming fraction) was well above 90%. Site A is where they had introduced their own conversion function for HU to electron density in their TPS (c.f. CT data above). It should be noted that this error only resulted in erroneous dose values for density above 1.1 relative to water, and the worst case is actually for PMMA phantoms as used in this audit.

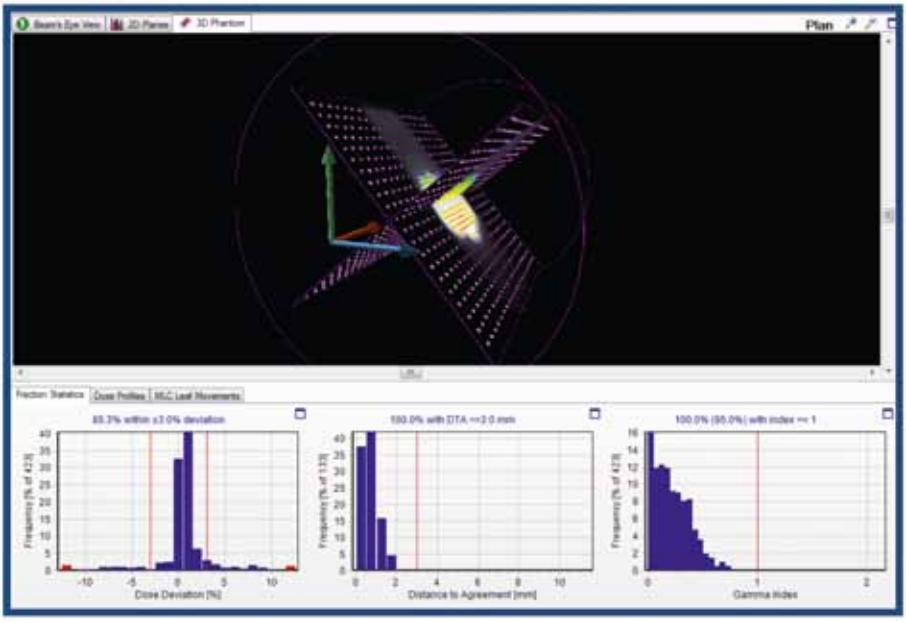

FIG. 4. Example of an evaluation of a measurement with the diode array detector. In the upper panel, the two diode planes are shown with the dose distribution. In the lower, from left to right; dose deviation, distance-to-agreement, and gamma distribution with dose and distance criteria of 3% and 3 mm, respectively.

TABLE 3. FRACTION OF MEASUREMENTS WITH GAMMA LESS THAN UNITY WITH AN EVALUATION CRITERIA OF 3% AND 3 mm FOR THE FIVE FIELD PROSTATE-LIKE TREATMENT

Site	Field No. 1	Field No. 2	Field No. 3	Field No. 4	Field No. 5	Composite
A	—	—	—	—	—	29.9
B	—	—	—	—	—	97.4
C	99.0	99.0	98.9	97.7	98.1	99.3
D	100.0	85.5	100.0	100.0	100.0	100.0
E	96.5	94.2	99.4	96.1	98.4	98.2
F	100.0	99.8	100.0	100.0	100.0	100.0
G	100.0	95.2	100.0	99.5	100.0	100.0
H	100.0	99.2	100.0	98.2	100.0	100.0
I	93.7	70.6	98.8	93.4	95.4	93.8
J	95.2	96.2	97.5	93.8	94.8	97.9
K	96.5	96.0	99.1	95.2	100.0	99.3
L	99.4	88.2	100.0	86.3	95.8	97.9
M	99.3	77.1	97.1	79.6	94.1	98.7
					Average	98.5

Note: The average value excludes site A.

Points failing are most commonly positioned at the edges of the dose distributions, which could be due to several factors, including the positioning system at the local clinic, i.e. the isocentre mark-up system — the positioning lasers, which directly influence the placement of the detector system. Another major contributor could be the modelling of the penumbra in the TPS; in particular, since all these beam are shaped by the multileaf collimators (MLCs), this could be of great uncertainty. Both the MLC modelling and their calibration on the accelerator may contribute to these disagreements.

4. CONCLUSIONS

The audit process at each hospital was performed either during two afternoons/evenings or during a full day where the machine was available to both the local and the audit teams; a total of 7–8 h have been spent on each unit. A very

short time was spent on the CT scanners, less than 15 min, which was easily accomplished at all departments.

For this preliminary report, the following conclusions can be made:

— For the CT transfer to density, no user corrections were applied, ensuring that the transfer was performed according to international standards. One case was found where user interference resulted in an erroneous transfer for densities above about 1.2 relative to water. The transfer function was subsequently corrected.
— Reference dosimetry is performed according to the TRS 398 at all departments except for two. In these two cases the selected geometry does not conforms to the TRS 398 recommendations. In practice, this has no significant consequence for the patient dosimetry with the specific type of linacs used at these two departments. However, from a fundamental point of view and in order to guarantee a high accuracy in clinical dosimetry, it must be considered very important to follow the international standards for dosimetry.
— The agreement between the local and the audit team regarding reference dosimetry is very good, with a small average deviation (1.003) and, in particular, a rather small spread (1 SD = 0.004).
— The five field prostate plans were delivered with high agreement between measurements and treatment planning calculations. The conforming fraction for the gamma analysis with criteria of 3%/3 mm averaging 98.5% [93.8–100], except for one institute where the error in the HU conversion resulted in a very low conformity.

This study has shown the value of external audits where systematic errors can be detected. It has also shown that the dosimetry procedures at the visited department are performed at high quality.

ACKNOWLEDGEMENTS

This project was supported by grants from Swedish Radiation Safety Authority, SSM 2009/2554. All physicists and other staff members at the visited departments are highly acknowledged for making this audit possible. This preliminary report includes data from the departments in Borås, Göteborg, Karlstad, Linköping, Malmö, Stockholm (two sites), Uppsala, Västerås, Växjö and Örebro.

REFERENCES

[1] THWAITES, D.I., WILLIAMS, J.R., AIRD, E.G., KLEVENHAGEN, S.C., WILLIAMS, P.C., A dosimetric intercomparison of megavoltage photon beams in UK radiotherapy centres, Phys. Med. Biol. **37** (1992) 445–461.

[2] IZEWSKA, J., GAJEWSKI, R., GWIAZDOWSKA, B., KANIA, M. ROSTKOWSKA, J., TLD postal dose intercomparison for megavoltage units in Poland, Radiother. Oncol. **36** (1995) 143–152

[3] FERREIRA, I.H., RICHTER, J., DUTREIX, A., BRIDIER, A., CHAVAUDRA, J., SVENSSON, H., The ESTROEQUAL Quality assurance network for photon and electron radiotherapy beams in Germany, Strahlenther. Onkol. **177** (2001) 383–393.

[4] DUTREIX, A., DERREUMAUX, S., CHAVAUDRA, J. VAN DER SCHUEREN, E., Quality control of radiotherapy centres in Europe: beam calibration, Radiother. Oncol. **32** (1994) 256–264.

[5] JOHANSSON, K.A., HORIOT, J.C. VAN DER SCHUEREN, E., Quality assurance control in the EORTC cooperative group of radiotherapy. 3. Intercomparison in an anatomical phantom, Radiother. Oncol. **9** (1987) 289–298.

[6] FERREIRA, I.H., DUTREIX, A., BRIDIER, A., CHAVAUDRA, J., SVENSSON, H., The ESTRO-QUALity assurance network (EQUAL). Radiother. Oncol. **55** (2000) 273–284.

[7] JOHANSSON, K.A., MATTSSON, L.O., SVENSSON, H., Dosimetric intercomparison at the Scandinavian radiation therapy centres, I. Absorbed dose intercomparison, Acta Radiol Oncol. **21**(1) (1982) 1–10.

[8] INTERNATIONAL ATOMIC ENERGY AGENCY, Absorbed Dose Determination in External Beam Radiotherapy: An International Code of Practice for Dosimetry Based on Standards of Absorbed Dose to Water, Technical Reports Series No. 398, Vienna, IAEA (2000).

[9] INTERNATIONAL ATOMIC ENERGY AGENCY, Commissioning and Quality Assurance of Computerized Planning Systems for Radiation Treatment of Cancer, Technical Reports Series No. 430, IAEA, Vienna (2004).

[10] INTERNATIONAL ELECTROTECHNICAL COMMISSION, IEC 61217 (2008-04) Ed. 1.2 Radiotherapy equipment – Coordinates, movements and scales (2008).

[11] BEDFORD, J.L., LEE, Y.K., WAI, P., SOUTH, C.P., WARRINGTON, A.P., Evaluation of the Delta4 phantom for IMRT and VMAT verification, Phys Med Biol. (2009) 54(9) N167–76. Epub.

[12] KORREMAN, S., MEDIN, J., KJAER-KRISTOFFERSEN, F., Dosimetric verification of RapidArc treatment delivery, Acta Oncol. 48(2)12009) 85–91.

[13] SADAGOPAN, R., BENCOMO, J.A., MARTIN, R.L., NILSSON, G., MATZEN, T., BALTER, P.A., Characterization and clinical evaluation of a novel IMRT quality assurance system, J Appl Clin Med Phys. **10**(2) (2009) 2928.

[14] KNÖÖS, T., NILSSON, M., AHLGREN, L., A method for conversion of Hounsfield number to electron density and prediction of macroscopic pair production cross-sections, Radiother Oncol. **5**(4) (1986) 337–45.

[15] LOW, D.A., DEMPSEY, J.F., Evaluation of the gamma dose distribution comparison method, Med Phys. **30**(9) (2003) 2455–64.

[16] LOW, D.A., HARMS, W.B., MUTIC, S., PURDY, J.A., A technique for the quantitative evaluation of dose distributions, Med Phys. **25 (%)** (1998) 656–61.

BEL*d*ART: IMPLEMENTATION OF A QUALITY ASSURANCE AUDIT FOR PHOTON AND ELECTRON BEAMS BASED ON ALANINE/EMR DOSIMETRY

B. SCHAEKEN[*,**,***], S. LELIE[*,***], R. CUYPERS[*], W. SCHROEYERS[*], F. SERGENT[+], S. VYNCKIER[++], A. RIJNDERS[+++], D. VERELLEN[***,§], H. JANSSENS[*], S. SCHREURS[*]

[*] NuTeC-EMR Dosimetry Laboratory,
XIOS Hogeschool Limburg,
Technologiecentrum, Diepenbeek
Email: bob.schaeken@zna.be

[**] ZNA-Middelheim,
Department of Radiotherapy,
Antwerp

[***] Vrije Universiteit Brussel,
Brussels

[+] Clinique et Maternité Ste-Elisabeth,
Department of Radiotherapy,
Namur

[++] UCL, St-Luc University Hospital,
Department of Radiation Oncology,
Brussels

[+++] Europe Hospitals,
Deptartment of Radiotherapy,
Brussels

[§] UZBrussel,
Department of Radiotherapy,
Brussels

Belgium

Abstract

The Belgian dosimetry audit in radiotherapy, BEL*d*ART, was initiated to verify, on a national base, the compliance of the dose stated by the centre with the measured dose of all beams in clinical use. On-site visits comprise basic mechanical tests and dosimetric verification of the dose measured in reference and non-reference conditions, including irregular fields with a multileaf collimator for photon beams and beam output measurements for electron beams. To date, about 60% of the beams were audited comprising 101 clinical beams from 32 linacs. Overall, in 92% of the cases the ratio of the alanine measured to stated dose was within optimal level ($|\delta| \leq 3\%$). In 7% of the results, deviations out of the optimal level but within the tolerance level ($3\% < |\delta| \leq 5\%$) were observed and could be mainly attributed to: inaccurately modelled depth dose at 20 cm depth (24%), output of rectangular fields and collimator exchange effect (25%) and output for irregular fields (25%). Three measurements (0.7%) were notified out of tolerance level, but no emergency situation occurred ($|\delta| > 10\%$). For the first time, alanine/electron magnetic resonance dosimetry was used as the transfer dosimeter in a large scale audit.

1. INTRODUCTION

The importance of quality assurance in radiotherapy has long been recognized [1–2] and guidelines have been given in national and international recommendations [3–5]. The implementation of a systematic dose audit can detect/correct errors occurring in the complex process of radiotherapy and directly leads to improvements in the overall quality of radiotherapy dosimetry, contributing to an improved clinical outcome. In the past, mailed dosimetry audits organized on a large scale were all based on (mailed) thermoluminescent dosimetry [1, 2, 6–11]. The Belgian dosimetry audit in radiotherapy (BEL*d*ART) project was set up by the Federal Agency of Nuclear Control (FANC) to verify, on a national basis, the compliance of the dose stated by the centre with the measured dose. The on-site visit encompasses basic mechanical tests and dosimetric verification of the dose delivered in reference and non-reference conditions, including irregular fields with the multileaf collimator (MLC) for photon beams and beam output measurements in electron beams. Absorbed dose to water is measured in water with alanine dosimeters and read out with electron magnetic resonance (EMR). The audit was initiated in February 2009 and for each linac, all photon beams in clinical use, as well as two electron beams, are subjected to the audit.

2. MATERIALS AND METHODS

BEL*d*ART is organized as an on-site visit audit over a period of three years. The audit includes a basic mechanical test (position of isocentre, optical distance indicator, laser lines and correspondence between the radiation field and light field) and a verification of the absorbed dose at the beam axis in water under various conditions. For the mechanical tests, tolerances specified by the NCS-9 were adopted [12]. Prior to the on-site visit, the local physicist is asked to prepare all tests (MU calculations) with the treatment planning system (TPS) in the same clinical setting as would be used for a patient. As a result, the complete dosimetric chain is audited.

2.1. Dosimetry tests

For high energy X rays, various dosimetric parameters are checked at the beam axis in reference and non-reference conditions. The audit includes checks of the reference beam output, the beam quality index (QI) (TPR_{10}^{20}) of open and wedged beams, the wedge and tray factor, beam output variation with symmetric collimator openings including the collimator exchange effect and beam output for a symmetrical irregular open field shaped with an MLC (MLC1) or blocks; asymmetric irregular open field (MLC2) and an asymmetric irregular field in combination with a wedge, representing the most complicated case (MLC3). These tests are equivalent to the EQUAL programme [2], except that beam output as a function of collimator opening is measured at the depth of 8 cm. In addition, for participants working with a fixed source–skin distance, the absorbed dose is checked at 8 cm depth in an irradiation at fixed source–axis distance and vice versa. A total of 11 tests were performed using 13 sets of four detectors for each photon beam. For electron beams, the output is measured under reference conditions for one high and one low energy beam. The relative deviation between measured and stated dose $\delta \equiv (D_{measured} - D_{centre})/D_{centre}$ is classified into four levels and reported to the participating centre:(a) ‘within optimal level’: $|\delta| \leq 3\%$, no further actions are taken, (b) out of optimal level but ‘within tolerance level’: $3\% < |\delta| \leq 5\%$, with the proposal to evaluate the deviations, (c) ‘out of tolerance level’: $5\% < |\delta| \leq 10\%$, a second run is organized, and (d) ‘alarm level’: $|\delta| > 10\%$ with immediate consultation.

2.2. The alanine/EMR system

In each experiment, the measured dose to water is expressed as the average reading of four detectors (Harwell, $\varnothing$ = 4.8 mm, h = 2.7 mm, $\bar{m}$ = 59.8 mg). The alanine detectors are read out at the NuTeC-XIOS EMR dosimetry laboratory

with a Bruker EMX^{micro} spectrometer (9” magnet, X-band) equipped with a high sensitivity resonator ER4119HS-W1. EMR spectra are acquired as the first derivative of the absorption spectrum using the following spectrometer settings: centre magnetic field = 348 mT; sweep width = 30 mT; microwave power = 0.25 mW; field modulation = 0.5 mT; modulation frequency = 100 kHz; 2048 channels each sweep, conversion time = 40.96 ms. A fully automated positioning device has been installed, allowing (a) motorized quartz pedestal to control height into the cavity, (b) pneumatic fixation of the detector, and (c) five automated rotations over72° of the detector prior to each scan. The spectrometer is operating in an air-conditioned room in which temperature and relative humidity (RH) are permanently monitored (T = 21°C, RH ≤ 40%). Temporal variations in the spectrometer sensitivity are taken into account by recording the irradiated alanine spectra simultaneously with a reference substance. Dose to water is determined using the ‘individual base function’ methodology developed by Anton [13,14]. Measured EMR spectra are fitted with a pure alanine base function obtained from detectors irradiated at 0 Gy and 20 Gy in the ^{60}Co reference beam at PTB [15]. Dose to water is expressed as ‘dose normalized amplitude’ (A_D). The readings are corrected for:temperature: (1) $k_T = (1.9 \pm 0.2) \times 10^{-3}$ K^{-1}; (2) energy: $k_Q^{MV} = 1.0030 \pm 0.0032$ and (3) fading: $k_{fading} = e^{-ct.\Delta t}$, $c_t = 7.10^{-5} \pm 4 \times 10^{-5}$ d^{-1}. For measurements in electron beams, the same methodology was followed as for photon beams, except that the alanine readings were corrected for electron energy response (k_Q^{MeV}). Some ambiguity exists in published results for the response of alanine in electron beams. Several authors reported a flat energy response within measurement uncertainty for electron energies in the range of 6–28 MeV [16–18] and a variation of less than 2% was estimated by cavity theory [19]. More recently, the energy dependence was studied by comparing the slopes of dose–response curves for different energies [20] and by comparing experimental results with Monte Carlo calculations [21]. To rule out possible systematic errors in the BEL*d*ART audit, it was decided not to use the published values. The energy dependence of the alanine response per unit absorbed dose to water for each beam relative to ^{60}Co was measured in reference conditions at a dose level of 8 Gy. The alanine readings were referenced to a Roos chamber, which was cross-calibrated to a Farmer type graphite walled ionization chamber in an 18 MeV beam, following NCS-18 [22].

The standard uncertainty on the amplitude measurement was estimated by repeated amplitude measurements of the calibration set as $u(A_D)$ = 30 mGy and is independent of dose. The relative combined standard uncertainty on a dose measurement under the experimental conditions of BEL*d*ART, is estimated as $u_r(D_w)$ = 1.1 % (k = 1)in the worst case. For details concerning the analysis of the spectra and uncertainty budget,refer to Anton [23]. An example of the

implementation of the alanine dose measuring procedure can be found elsewhere [24].

2.3. Internal quality assurance and traceability

A set of alanine dosimeters irradiated to a known dose in the range between 0 Gy and 25 Gy in the Co-60 reference beam at PTB against water calorimetry is obtained every year or at the purchase of a new batch of alanine dosimeters. Each measuring session, the 0 Gy and 20 Gy pellets of this calibration set are used to determine the pure alanine base function and the set of 3, 15 and 25 Gy pellets are used to check the consistency of the alanine/EMR dosimetry system. At four month intervals, the complete calibration set is read out to monitor changes in the uncertainty of amplitude measurements, should the need arise. In addition, the alanine dose measurements are benchmarked periodically with ionometry (Farmer chamber) in reference conditions as well as for the complete set of BEL*d*ART tests.

3. RESULTS

To date, 32 linacs (Varian, Siemens, Elekta, Novalis, BrainLabAB/MHI 'Vero') have been subjected to the audit. For the mechanical control:all results are found within tolerance, except for one linac (mismatch of light field and radiation field by 4 mm in the gantry-target direction and fixed by the manufacturer). Dose was measured in 762 tests involving 3048 alanine pellets.

3.1. High energy photon beams

For benchmarking purposes, alanine dose measurements were compared to the dose measured with a Farmer ionization chamber (IC), In reference conditions, the average ratio of alanine to IC measured dose was $D_{\text{alanine}}/D_{\text{Farmer}} = 0.998$ with a spread of 0.005 (1s). In addition, the outcome of the alanine dose measurements for the set of BEL*d*ART tests was compared to IC measurements in 6, 15 and 18 MV photon beams from different linacs (Fig. 1).

The average ratio of alanine to IC measurements was 1.001, $s = 0.006$; $N = 92$, which is comparable to the measurements in reference conditions. In all tests, deviations from the stated dose of 4 Gy were confirmed by IC measurements within measurement uncertainty.

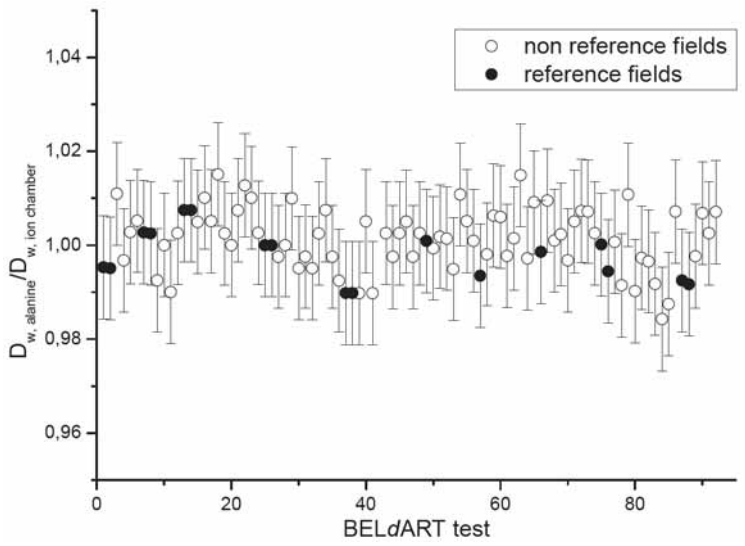

FIG. 1. Dose ratio of alanine to Farmer chamber measurements for the set of BELdART tests in sequential order (open circles) in 6, 15 and 18 MV photon beams. Closed circles refer to measurements in reference conditions. Error bars are at the k = 2 level.

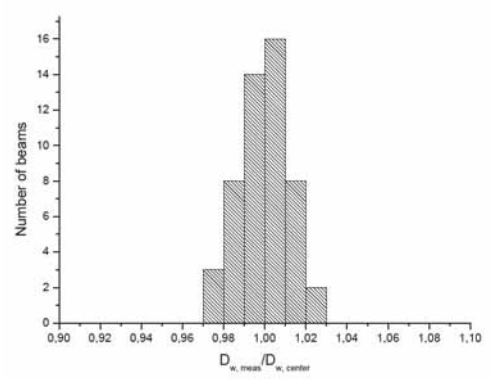

FIG. 2. Frequency distribution of the ratio of the dose ($D_{w,m}$) measured under reference conditions to the dose stated by the hospital ($D_{w,s}$) for 55 high energy photon beams. The mean of the distribution is 1.000 with a standard deviation of 0.015 and the range is 0.974–1.030.

Dosimetry parameters were checked in 59 photon beams (4 MV–18 MV). For a total of 738 tests, the average ratio of measured dose to stated dose D_w/D_{centre} was 0.998 with a standard deviation, *s*, of 0.018.

The results for the reference beam output are shown in Fig. 2. For the 59 beams, the mean of the distribution is 1.000, *s* is 0.015 and the range is 0.974 to 1.030.

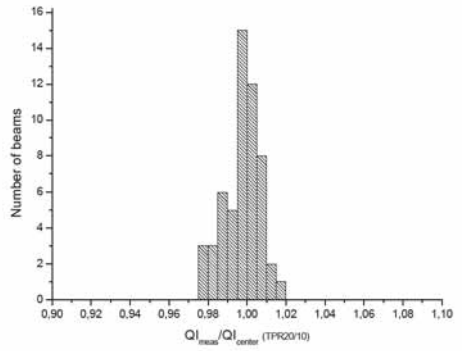

FIG. 3. Frequency distribution of the ratio of the measured QI (TPR_{10}^{20}) to the QI stated by the hospital for 55 high energy photon beams. The mean distribution is 0.997 with a standard deviation of 0.009 and the range is 0.976–1.018.

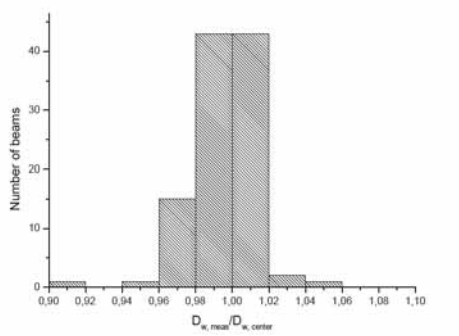

FIG. 4. Frequency distribution of the ratio of the measured dose ($D_{w,m}$) to the dose stated by the hospital ($D_{w,s}$) for 106 measurements in wedged photon beams. The mean distribution is 0.995 with a standard deviation of 0.017 and the range is 0.916–1.045.

Regarding depth doses, all output measurements were within the optimal level for checks at 10 cm depth, both for open and wedged fields. The average ratio is 0.99 with s = 1.4% for the open fields and 0.995 with s = 1.3% for the wedged fields. At the depth of 20 cm, most of the results (90%) are still within the optimal level, both for open and wedged fields, but in the remainder of the cases, the deviations are more pronounced but still within the acceptable level ($\delta \leq 5\%$). For all photon beams, the stated QI corresponds with the measured QI within optimal level (Fig. 3).

Considering the beam output for wedged fields (Fig. 4), the frequency distribution is wider with an average of 0.995, s = 1.7% and the range is 0.916 to 1.045. Figure 5 presents the variation in beam output corresponding to regular

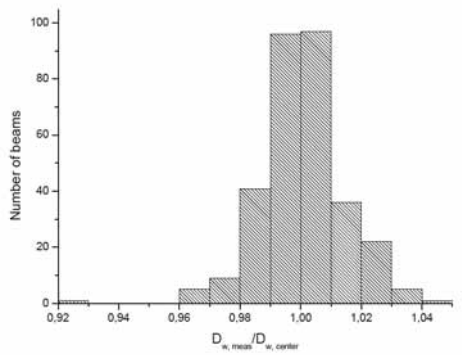

FIG. 5. Frequency distribution of the ratio of the measured beam output ($\dot{D}_{w,m}$) at 8 cm depth for various regular collimator openings to the beam output stated by the hospital ($\dot{D}_{w,s}$). For 331 measurements, the mean distribution is 0.999 with a standard deviation of 0.015 and the range is 0.925–1.040.

collimator opening, including small (6 cm × 6 cm) and large (20 cm × 20 cm) field openings, as well as elongated collimator openings to check the collimator exchange effect. The mean of the distribution is 0.999, s = 0.015 and the range is 0.925–1.040.

For the group of irregular shaped open fields (Fig. 6), 85% of the checks are within optimal level and no out of tolerance ratios were encountered. For the most complicated test of the audit (MLC3) only two deviations were out of tolerance level which occurred on the same linac:a systematic underestimation of the beam output for all experiments with –2.8% and –3.5% was observed for the low and high energy respectively. After a second check, all deviations were within the optimal level for this linac.

On the whole, in 93% of the cases the ratio of alanine measured to stated dose was within the optimal level ($|\delta| \leq 3\%$). In 6% of the results, deviations out of optimal level but within the tolerance level ($3\% < |\delta| \leq 5\%$) were observed and could be mainly attributed in equal shares to: inaccurate PDD at 20 cm depth, output of rectangular fields and collimator exchange effect, and output for irregular fields. Three measurements (0.8%) exceed the tolerance level.

3.2. Electron beams

The alanine readings in electron beams were corrected with experimentally determined energy correction factors, listed in Table 1. The relative standard uncertainty is estimated 1.8%.

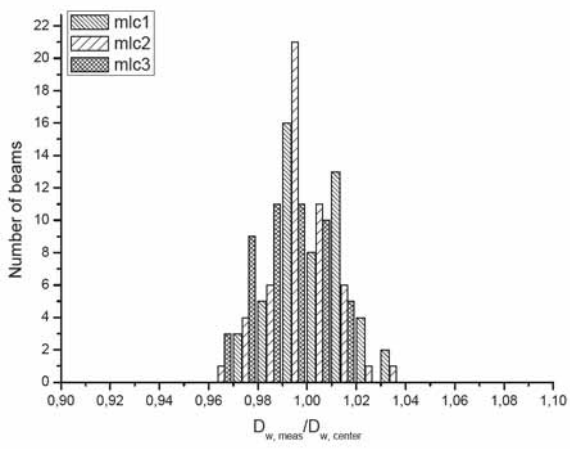

FIG. 6. Frequency distribution of the ratio of the measured dose to water ($D_{w,m}$) at 8 cm depth on the beam axis for irregular fields to the dose stated by the hospital ($D_{w,s}$) for 51 measurements. For MLC1: the mean distribution is 1.004 with standard deviation 0.014 and the range is 0.976 to 1.034. For MLC2: the mean distribution is 0.997 with standard deviation 0.013 and the range is 0.967 to 1.031. For MLC3: the mean distribution is 0.991 with a standard deviation of 0.014 and the range is 0.966–1.019.

TABLE 1. ENERGY CORRECTION FACTORS k_Q^{MeV} FOR HIGH ENERGY ELECTRON BEAMS EXPERIMENTALLY DETERMINED WITH TWO TYPES OF ALANINE DETECTOR HOLDER

MeV	4	6	8	10	12	15	18	20	22
R_{50} (cm)	1.64	2.43	3.22	3.99	5.01	5.98	7.19	7.85	8.85
BELdART holder	1.031	1.017	1.018	1.016	1.005	0.997	1.002	0.993	0.962
PMMA disk holder	1.025	1.013	1.017				1.002		

The output in water was measured in 48 electron beams (4–25 MeV) at reference conditions. The ratio of measured to stated dose D_w/D_{centre} was 1.002 with s = 0.024 (Fig. 7). No differences between the results of low energy electron beams and high energy beams are observed:for low energy electron beams (R_{50} < 7 cm), the mean of the distribution is 0.997 with a standard deviation of 0.022 and the range is 0.963–1.028; for high energy electron beams, the mean of the distribution is 1.006 with a standard deviation of 0.026 and the range is

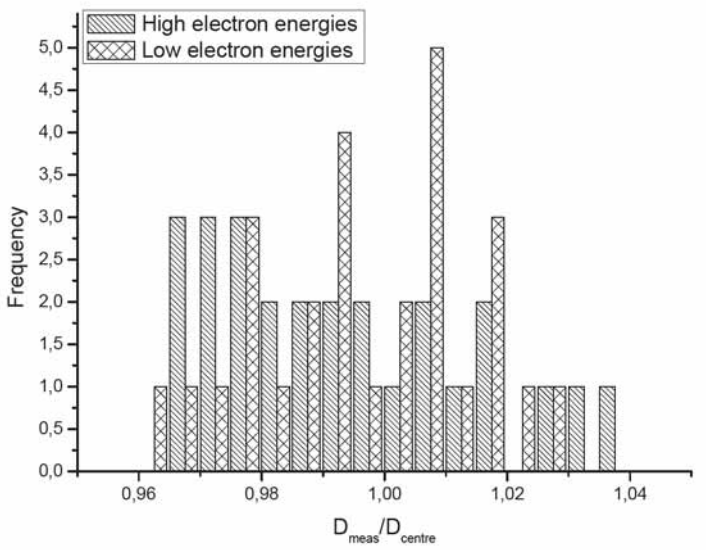

FIG. 7. Frequency distribution of the ratio of the beam output measured at reference depth to the beam output stated by the hospital for high energy electron beams. For 48 measurements, the mean distribution is 1.002 with a standard deviation of 0.024 and a range of 0.963–1.036.

0.965–1.036. All deviations were found within the optimal level ($\delta \leq 3\%$), except for one beam (out of tolerance deviation, $\delta > 5\%$) and two beams out of optimal level but within tolerance ($\delta \leq 5\%$).

4. DISCUSSION

In this work, the alanine/EMR system is not calibrated in the usual way i.e. by establishing a dose–response curve. Contrary to other authors, the EMR absorption spectra were fitted with a pure alanine base function obtained from pellets of the same batch, irradiated to a well known dose, from which the dose normalized amplitude A_D was derived. This system was calibrated with one set of four alanine pellets irradiated to a dose of 25 Gy, $u_r(D_w) = 0.6\%$ ($k = 2$) in the ^{60}Co reference beam at PTB against water calorimetry [15]. This set of four pellets (and one set for background measurement) was used at every measurement session, i.e. the amplitude of each individual pellet was compared with the same well known amplitude which is sufficient for accurate dose measurements [12]. The use of a calibration curve $\bar{A}_D = aDw + b$ and derivation of the 'calculated' dose $D_w^c = (\alpha \bar{A}_D - D_0)$ with ($\alpha = a^{-1}$, $D_0 = b/a$; ideally $\alpha = 1$; $D_0 = 0$) would not

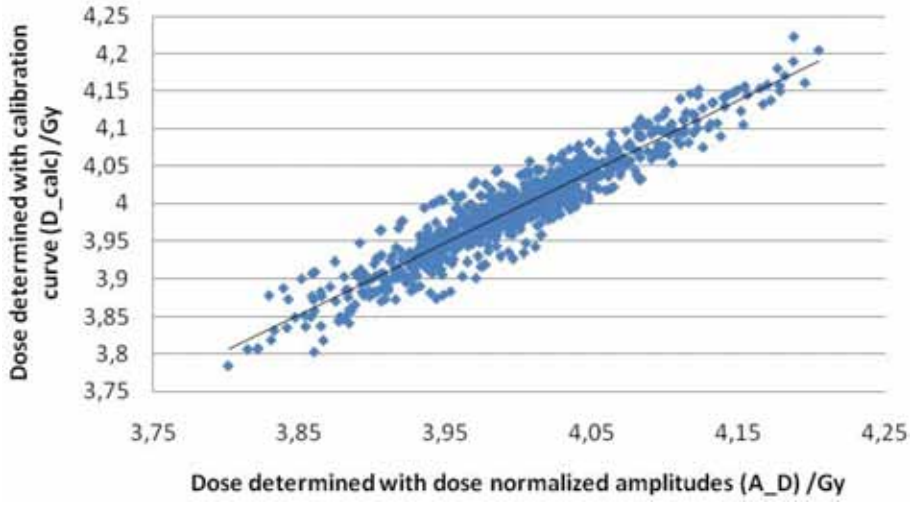

FIG. 8. Comparison of alanine-measured dose (N=847) determined with dose normalized amplitudes to dose calculated using the linear calibration curve.

alter the results (Fig. 8); in fact, it would increase the measurement uncertainty, and as a result, no calibration curve was established.

For the specific purpose of internal control, additional dosimeters from the calibration set (3 Gy, 10 Gy) were read out at each session to check the underlying hypothesis that the alanine pellets undergo the same temporal evolution. The calibration set of detectors is stored at a RH < 30% and out of light, together with the BEL*d*ART dosimeters, which are read out within ten days after irradiation. In these conditions, signal fading is absent within a time span of 14 months [25]; however, long term follow-up is ongoing.

Because alanine/EMR dosimetry is used here for the first time as the transfer dosimeter in an audit programme, it was decided to benchmark its results at regular intervals against ionization measurements with a Farmer chamber, which is still considered the gold standard for dose measurements in radiotherapy. The output of MV photon beams was measured in reference conditions over a time span of two years and directly compared with IC measurements: all alanine dose measurements are confirmed with Farmer chamber measurements within measurement uncertainty. This is in accordance with the results of an intercomparison of primary standards for absorbed dose to water for PTB relative to the LSDL in Belgium [26].

For electron beams, the measured beam output in reference conditions corresponds well with the hospital stated beam output, although the spread in results is larger compared with photon beams, as was also observed in other audit

programmes [1, 2]. By the choice of energy correction factors, the potential exists to introduce systematic errors. There seems to be a consensus in the literature that the energy dependence of the alanine response per unit absorbed dose to water between electron energies is weak or not significantly different and that the dependence relative to ^{60}Co is more pronounced. Different average values for the energy correction factor were published: 1.012 [16], 1.000 ± 0.01 [18], 1.008 [17], 1.030 ± 0.012 [20], 1.013 ± 0.012 [21]. The effect of the type of binder is less critical [21]. Contrary to earlier measurements [20], we observed an increase of alanine response relative to ^{60}Co with increasing electron energy and the BEL*d*ART measurements were corrected for accordingly. To rule out holder effects, alanine measurements were carried out with the BEL*d*ART holder and with a PMMA disc shaped pellet holder with the same dimensions as the Roos chamber. At the dose of 8 Gy, the measurement uncertainty for the alanine/EMR system in electron beams is of the order of 2 %, the Roos chamber readings contributing most to the combined standard uncertainty (1.8%) [22]. The ambiguity in the energy dependence of alanine could probably be overruled when using water calorimetry as a reference for dose to water determination in electron beams.

Compared to the existing transfer dosimeters, the alanine system offers some practical advantages in this field for different reasons: (a) the compactness of the dosimeter: a stack of four pellets were used, representing a volume of 0.05 cm^3, which is considerably smaller than a reference ionization chamber (≈0.6 cm^3), offering more flexibility (small field sizes). Moreover, the number of pellets could be reduced at the expense of increased measurement uncertainty. The use of one pellet in a photon beam would double the standard uncertainty $u_r(D_w)$ to 2.2% (k = 1) and is comparable to thermoluminescent dosimetry as it has been implemented in existing audits [1, 2, 27], (b) increasing the reference dose would lower the measurement uncertainty at the expense of increased irradiation time which might be undesirable. The number of alanine pellets and requested dose can be matched to meet the desired measurement uncertainty and the combination of four pellets and a dose of 4 Gy was considered a comfortable compromise for this audit programme, (c) owing to the non-destructive character of the readings, the alanine dosimeters can be stored for future readings if necessary or for intercomparisons between different laboratories. Upon reading, all pellets are archived in sealed and air evacuated bags to protect them from ambient conditions (RH) in order to minimize/cancel fading effects, allowing repeated readouts at a later time, as alanine/EPR readings are non-destructive.

Globally, the results indicate that for the number of beams being audited, the beam calibration and basic beam parameters are generally correctly implemented for routine patient treatments.

5. CONCLUSION

Alanine/EMR dosimetry has been successfully introduced as a transfer dosimetry system in a national dosimetry audit programme for radiotherapy in Belgium. Dose to water can be measured with high accuracy and the dose measurement uncertainty is at least as small as for reference ionization chambers practiced in modern dose protocols. The relative absence of signal fading in combination with a non-destructive readout opens new perspectives in inter-institutional comparison and taking of evidence.

ACKNOWLEDGEMENTS

The BEL*d*ART project is financed by the Belgian Federal Agency of Nuclear Control. H. Beutjens is acknowledged for reading out all detectors.

REFERENCES

[1] IZEWSKA, J., et al., The IAEA/WHO TLD postal programme for radiotherapy hospitals, Radiother. Oncol. **54** (2000) 65.
[2] FERREIRA, I., et al., The ESTRO Quality Assurance Network (EQUAL)", Radiother. Oncol. **55** (2000) 273.
[3] ALETTI, P., et al., Recommendations for a quality assurance programme in external radiotherapy (ALETTI, P., BEY, P., Eds.) Physics for clinical radiotherapy, Booklet $N^0$2, 1st edition, Leuven: Apeldoorn, Garant (1995).
[4] KUTCHER, G., et al., Comprehensive QA for radiation oncology: report of the AAPM Radiation Therapy Committee Task Group 40, Med. Phys. **21** (1994) 581.
[5] THWAITES, D., et al., Quality assurance in radiotherapy (ESTRO Advisory Report to the Commission of the European Union for the 'Europe Against Cancer Programme, Radiother. Oncol. **35** (1995) 61.
[6] IZEWSKA, J., et al., TLD postal dose intercomparison for megavoltage units in Poland, Radiother. Oncol. **36** (1995) 143.
[7] AMIES, C., et al., Multicentre dosimetry study of mantle treatment in Australia and New Zeeland, Radiother. Oncol. **40** (1996) 171.
[8] HAZLE, J., Quality assurance for intraoperative electron radiotherapy clinical trials: ionization chamber and mailable thermoluminescent dosimeter results, Int. J. Radiat. Oncol. Biol. Phys. **24** (1992) 559.
[9] KROUTILIKOVA, D., et al., Thermoluminescent dosimeters (TLD) quality assurance network in the Czech Republic, Radiother. Oncol. **66** (2003) 235.
[10] THWAITES, D., A dosimetric intercomparison of megavoltage photon beams in UK radiotherapy centers, Phys. Med. Biol. **37** (1992) 445.

[11] FOLLOWILL, D.S., et al., Design, development and implementation of the Radiological Physics Center's pelvis and thorax anthropomorphic quality assurance phantoms, Med. Phys. **43** (2007) 2070.
[12] THE NETHERLANDS COMMISSION ON RADIATION DOSIMETRY, Quality Control of Medical Linear Accelerators: current practice and minimum requirements, Report 9, NCS, Delft (1996).
[13] ANTON, M., Development of a secondary standard for the absorbed dose to water based on the alanine EPR dosimetry system, Appl. Rad. Isot. **62** (2005) 779.
[14] ANTON, M., Uncertainties in alanine/ESR dosimetry at the Physikalisch-Technische Bundesanstalt, Phys. Med. Biol. **51** (2006) 5419.
[15] KRAUSS, A., The PTB water calorimeter for the absolute determination of absorbed dose to water in Co-60 radiation, Metrologia **43** (2006) 259.
[16] ONORI, S., et al., Dosimetric characteristics of alanine-based ESR detectors in electron beams used in radiotherapy, Rad. Prot. Dosim. **34** (1990) 282.
[17] SHARPE, P., et al., The relative response of fricke, dichromate and alanine dosimeters to ^{60}Co and high energy electron beam radiation, Radiat. Phys. Chem. **46** (1995) 1274.
[18] OLSON, K., Response of the alanine radiation dosimeter to high-energy photon and electron beams, Phys. Med. Biol. **35** (1990) 43.
[19] CIESIELSKI, B., Energy response of agar-alanine radical dosimetry to therapeutic electron beams, Med. Phys. **20** (1993) 1453.
[20] BERGSTRAND, E., et al., An experimental investigation of the electron energy dependence of the EPR alanine dosimetry system, Rad. Meas. **39** (2005) 21.
[21] ZENG, G., et al., An experimental and Monte Carlo investigation of the energy dependence of alanine / EPR dosimetry: II.Clinical electron beams, Phys. Med. Biol. **50** (2005) 1119.
[22] THE NETHERLANDS COMMISSION ON RADIATION DOSIMETRY, Code of practice for the absorbed dose determination in high energy photon and electron beams, Report 18, NCS, Delft (2008).
[23] ANTON, M., et al., Alanine dosimetry uncertainty components, PTB-DOS-55, Braunschweig (2009).
[24] SCHAEKEN, B., et al., Alanine/EPR dosimetry applied to the verification of a total body irradiation protocol and treatment planning dose calculation using a humanoid phantom, Med. Phys. Accepted [DOI:b 101118/1.3496355] (2010).
[25] ANTON, M., Post-irradiation effect in alanine dosimeter probes of two different suppliers, Phys. Med. Biol. **53** (2008) 1241.
[26] KESSLER, C., et al., Comparison of the standards for absorbed dose to water of the PTB, Germany and the BIPM for ^{60}Co γ rays, Metrologica **43**, Tech. Suppl. 06005 (2006)
[27] KIRBY, T., Uncertainty analysis of absorbed dose calculations from thermoluminescence dosimeters, Med. Phys. **19**, (1992) 1427.

DOSIMETRY AUDITS IN RADIOTHERAPY USING A RADIOPHOTOLUMINESCENT GLASS DOSIMETER IN JAPAN

H. MIZUNO, A. FUKUMURA
National Institute of Radiological Sciences,
Chiba
Email: h_mizuno@nirs.go.jp

Y. KUSANO
Kanagawa Cancer Center,
Yokohama

S. SAKATA
Association for Nuclear Technology in Medicine,
Chiba

Japan

Abstract

Although over 800 linear accelerators have been used clinically in about 700 radiation therapy facilities in Japan, no external audit system existed for many years. A postal dosimetry audit system was established by the National Institute of Radiological Sciences (NIRS; Secondary Standards Dosimetry Laboratory). Instead of a thermoluminescent detector (TLD), the authors chose a radiophotoluminescent glass dosimeter (RGD). RGDs and a water equivalent solid phantom were sent to radiotherapy departments, where the RGDs were irradiated with 1 Gy in the reference conditions of the high energy X ray beam (field size 10 cm × 10 cm, depth 10 cm) in a solid phantom. Irradiated RGDs were then sent back to NIRS for evaluation. The tolerance level was set to ±5% considering the RGD measurement uncertainty of ±1.6% (1 standard deviation). The NIRS group conducted a postal audit run with 106 hospitals from 2006 to 2007 and achieved a 1.3% standard deviation for 191 beams. On the basis of this successful trial, the postal dose audit service was initiated in November 2007 and is now operated by the Association for Nuclear Technology in Medicine. As of March 2010, 113 hospitals have participated in the audit. This includes 127 linear accelerators and 224 beams checked (4–15 MV). The results are presented as ratios of the NIRS RGD read dose to that stated by the user, D_{RGD}/D_{stat}. The mean ratio was 1.005, its standard deviation 0.9%, and the results ranged between a minimum of 0.974 and a maximum of 1.036. To make the audit more practical, an audit for the dose delivery in non-reference conditions has also been studied. This includes checks of dose variations with field size and wedge transmission. A small correction factor was found necessary for field size variation. The dose audit in non-reference conditions began in April 2010.

1. INTRODUCTION

Although over 800 linear accelerators have been clinically used in about 700 radiation therapy facilities in Japan [1], no external audit system existed for many years. Only a few small group dose comparisons among centres were performed by certain scientific groups [2–3]. More interest in the dosimetry audit was triggered by severe radiation therapy accidents caused by erroneous irradiation doses that have been made public in Japan in 2001. The main reason for these accidents was the incorrect use of new treatment planning systems. The demand for quality assurance in radiation therapy was highlighted due to these accidents and a pilot external audit study was initiated based on a national group funded by the Ministry of Health, Labour and Welfare [4]. For a detector suitable for postal audit, this group chose a radiophotoluminescent glass dosimeter (RGD) rather than a thermoluminscent detector (TLD). The new RGD system, the Dose Ace (Asahi Glass Co.), commercially available in Japan, had a stable output, adequate reproducibility and negligible fading effects. The pilot study to test the RGD based audit system was undertaken by the National Institute of Radiological Sciences (NIRS; Secondary Standards Dosimetry Laboratory) and the postal dosimetry audits have finally been established in Japan [5]. The NIRS group initially conducted a postal audit trial with 106 hospitals from 2006 to 2007 and achieved consistent results with a 1.3% standard deviation for 191 beams [5]. On the basis of this successful pilot study, the postal dose audit service was initiated in November 2007 and is now operated by the Association for Nuclear Technology in Medicine (ANTM). This paper presents the audit results from 2007 to 2009 and discusses ongoing developments.

2. MATERIALS

2.1. RGD

The RGD is a silver activated phosphate glass with the following weight composition: 11.0% Na, 31.55% P, 51.16% O, 6.12% Al and 0.17% Ag [6]. The dosimeter dimensions are 1.5 mm in diameter and 12 mm in length. The physical phenomenon used to operate the RGD system is radiophotoluminescence (RPL). The irradiation of the glass produces RPL centres, which in turn will emit the orange luminescence under UV ray excitation. After emitting the luminescence, they return to the stable RPL centre state. Therefore, the number of RPL centres remains constant, allowing an infinite numbers of readings. An FDG-1000 (ATG) reader is shown in Fig. 1.

FIG. 1. RGD system (RGD, reader and operating PC).

TABLE 1. PHYSICAL CHARACTERISTICS OF THE TOUGH WATER PHANTOM AND WATER

Material	Density (g/cm^3)	Mean atomic number	Electron density (cm^3)
Tough water phantom	1.01	7.42	3.25×10^{23}
Water	1.00	7.42	3.34×10^{23}

2.2. Tough Water Phantom

A water equivalent solid phantom, the Tough Water Phantom (Kyoto Kagaku Co.), was used. It consists mainly of C, O and H. Its physical characteristics are shown in Table 1. It is a 30 cm × 30 cm slab phantom with varying slab thicknesses. Its central region was prepared to incorporate an insert with the RGD elements (Fig. 2).

3. DOSIMETRY AUDIT SYSTEM

The RGDs and a Tough Water Phantom were sent to radiotherapy hospitals, where the RGDs were irradiated with 1 Gy in the reference conditions (field size

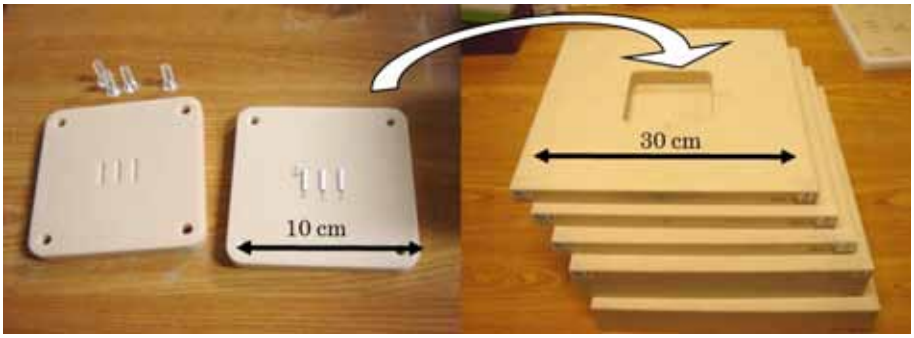

FIG. 2. Three RGDs are contained in the Tough Water Phantom.

10 cm × 10 cm, depth 10 cm) in the phantom. After the irradiation, the RGDs were sent back to the NIRS for evaluation, where the RGD signals were read by an RGD reader. The RGDs were calibrated using a ^{60}Co γ ray beam. The participant's dose was derived from the following equation:

$$D = \sum_{\text{X-ray}} (X_i \times I_i) \times E_q \times P_q \times \frac{Dose_{^{60}\text{Co}}}{\sum_{^{60}\text{Co}} (X_i \times I_i)} \quad (1)$$

where

X_i is the raw reading of the RGD element whose ID number is i;

I_i is the sensitivity correction factor of the RGD element whose ID number is i (derived by uniform irradiation using ^{60}Co γ rays), where

$$I_i = \frac{D_{^{60}\text{Co}}}{X_i} \quad (2)$$

E_q is the energy correction factor of beam quality 'q' (RGD elements were irradiated by ^{60}Co γ rays and 4–20 MV X rays. A correction factor was derived from the ionization chamber measurements, D(^{60}Co) and D(q), performed in the same geometry set-up as that used for the RGD);

$$E_q = \left[\frac{\sum_i X_i (^{60}\text{Co}) \times I_i}{\sum_i X_i (q) \times I_i} \right]^{\text{Glass}} \times \left[\frac{D(q)}{D(^{60}\text{Co})} \right]^{\text{IC}} \quad (3)$$

P_q is the phantom correction factor for the beam quality, q, where

$$P_q = \frac{D_w}{D_T} \tag{4}$$

where

D_w is the absorbed dose to water determined from the readings of the ionization chamber for the X ray beam quality, q, in 10 cm deep water;

D_T is the absorbed dose to water determined from the readings of the ionization chamber for the same X ray beam quality, q, 10 cm deep in the Tough Water Phantom;

Dose ^{60}Co is the absorbed dose to water determined from the readings of the ionization chamber for ^{60}Co γ rays taken just before the irradiation of control RGD elements in the same geometry set-up.

The tolerance level for the participant results was set to ±5% considering the measurement uncertainty of ±1.6% (1 standard deviation). Since 2008, inter-laboratory comparisons have been performed annually with the IAEA Dosimetry Laboratory operating the IAEA/WHO TLD postal dose quality audit. The comparison results confirmed the RGD system performance within the expected uncertainties every year.

As there is neither mandatory regulation nor financial support for an operating dosimetry audit programme in Japan, the hospitals that participate in the audit have to pay a fee of about US $1000 for the audit which involves the calibration of two high energy X ray beams in reference conditions. The authors recommend the participation in the audit every three years.

4. THE AUDIT RESULTS OF THE PAST TWO YEARS

From its inception in November 2007 up to March 2010, 113 hospitals participated in the audit. This included a total of 127 linear accelerators and a total of 224 checked beams, including 60 beams of 4 MV, 67 beams of 6 MV, 94 beams of 10 MV and 3 beams of 15 MV. The distribution of the results is shown in Fig. 3. The results correspond to the ratios of the NIRS RGD determined dose to that stated by the user, D_{RGD} /D_{stat}. The mean ratio was 1.005, its standard deviation was 0.9% and the reults ranged between a minimum of 0.974 and a maximum of 1.036.

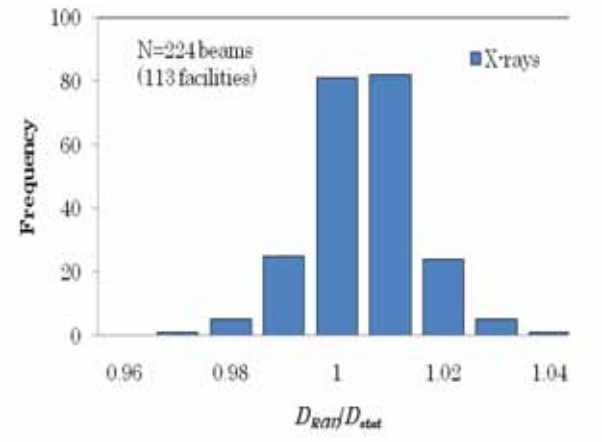

FIG. 3. Distribution of the results of postal dose audits of radiotherapy hospitals for the delivery of absorbed dose to water under reference condition during 2007–2009.

5. APPLICATION TO NON-REFERENCE CONDITIONS

To make the audit more practical, an audit for non-reference conditions was also studied. This included checks of dose variations with field size and wedge transmission. Experimentally, the effect of both conditions was tested. A range of field sizes, from 5 cm × 5 cm to 25 cm × 25 cm, were applied. The depth (10 cm) and the SSD (90 cm) were fixed, and only the field size was changed. The measurements using the ionization chamber were made under the same conditions. Similar measurements were performed with a set of wedges (15°, 30°, 45° and 60°) using a 10 cm × 10 cm field size. The percentage ratios of the RGD readings to the beam output determined with the ionization chamber insignificantly increased with the increase in field size. This might have been caused by a change in the energy spectrum. The mean energy of X rays increases in a smaller field because of the decrease in scattered photons within the field. A correction factor for the field size was derived by fitting the achieved data. Regarding wedged field, no systematic tendency was observed. Although RGD has strong energy dependence for low energy photon levels below 100 keV, the irradiation condition of the authors' audit system is 10 cm depth. Spectral change due to insertion of a metal wedge seemed to have a small effect on RGD readings at that depth. The correction factor for the wedged field was determined to be negligible. On the these studies, the authors initiated an audit of non-reference conditions for different field sizes and wedged beams in April 2010.

ACKNOWLEDGEMENTS

The authors would like to thank their NIRS and ANTM colleagues for their support in RGD irradiation and reading.

REFERENCES

[1] TESHIMA, T., et al., Japanese structure survey of radiation oncology in 2007 (First report), J Jpn Soc Ther Radiol Oncol **21** (2009) 113–125. *In Japanese*

[2] HAYAMI, A., et al., Mailed TLD dose intercomparison at a reference point of high energy photon beams among 11 institutions in Japan, J Jpn Soc Ther Radiol Oncol **9** (1997) 139–145. *In Japanese*

[3] ENOKIDO, Y., et al., Field survey results on output for x-ray therapeutic accelerators in radiotherapy institutions of Saitama and Tochigi prefectures, Igaku Butsuri **27**(2) (2007) 71–7, *in Japanese*

[4] SHIMBO, M., Developing postal dose audit system in Japan (Proc. of The World Congress on Medical Physics and Biomedical Engineering 2006) (2006) 5297.

[5] MIZUNO, H., et al., Feasibility study of glass dosimeter postal dosimetry audit of high-energy radiotherapy photon beams, Radiother Oncol **86** (2008) 258–263.

[6] TSUDA, M., A few remarks on photoluminescence dosimetry with high energy x-rays. Igaku Butsuri **20**(3) (2000) 131–139, *in Japanese*

THE ROLE OF DOSIMETRY AUDITS IN RADIOTHERAPY QUALITY ASSURANCE: EIGHT YEARS OF EXPERIENCE IN GREEK EXTERNAL BEAM RADIOTHERAPY AND BRACHYTHERAPY CENTRES

C.J. HOURDAKIS, A. BOZIARI
Greek Atomic Energy Commission,
Agia Paraskevi,
Athens, Greece
Email: khour@gaec.gr

Abstract

The Greek Atomic Energy Commission (GAEC) runs dosimetry audits through on-site visits for photon and electron beams and for ^{192}Ir brachytherapy high dose rate systems in all Greek radiotherapy centres. In audits, absolute and relative dosimetry measurements are being performed. The deviation, expressed as the percentage difference of the measured values by the GAEC to the respective stated values by the radiotherapy centre of absorbed dose to water or air kerma strength were recorded and compared to the action levels of ±3% (preventive actions needed) and ±5% (immediate corrective actions needed). The results of the subsequent audit rounds, each one lasting for approximately four years, are presented in this work. During the first round, 79.2% of photon beams exhibited deviations of less than 3%, while during the second round this photon beam percentage increased to 96.9%. During the first round, 76.4% of the electron beams recorded deviations less than 3% and 12.9% higher than 5%. All brachytherapy sources showed deviations less than 3%. An improvement in dose accuracy was recorded during the subsequent rounds of the audits.

1. INTRODUCTION

The ICRU and other investigators [1–3] suggest that in radiotherapy, an accuracy of at least 5% should be achieved (at 1.5 standard deviations) in the overall delivery of absorbed dose to the target volume in the patient, considering the effect of doses on the local tumour control probability and on the normal tissue complication probability.

In April 2010, Greece had 26 radiotherapy centres at public or private hospitals/clinics, where 36 linacs and 8 ^{60}Co teletherapy units were in operation, producing 64 photon beams (^{60}Co, 6–23 MV) and 126 electron beams (4–21 MeV) in total. Furthermore, 7 high dose rate (HDR) ^{192}Ir and 2 medium dose rate (MDR)/low dose rate (LDR) ^{137}Cs remote afterloading brachytherapy

systems are operating. The Greek Atomic Energy Commission (GAEC) runs dosimetry audits in all Greek radiotherapy centres by means of on-site visits in order to assess the dose accuracy, identify and resolve problems in dosimetry and disseminate the IAEA TRS 398 protocol [4, 5]. Additionally, the GAEC's Ionizing Radiation Calibration Laboratory (IRCL) calibrates the reference dosimetry equipment of all radiotherapy centres, in terms of absorbed dose to water at ^{60}Co beam quality and air kerma strength at ^{192}Ir qualities [6, 7]. The GAEC's dosimetry audit is a continuous process: the first round for photon beams (2002–2006), electrons (2002–2008) and brachytherapy (2006–2009) are completed. The second round is at the final stage for photons (2006–2010) and in progress for electrons and brachytherapy, while the third round for photons has already been initiated. The first audit round results for the photons have been published in Ref. [8]. This work presents the results of these audits and focuses on the improvements of radiotherapy centres' dosimetry during the subsequent audit rounds.

2. MATERIAL AND METHODS

The dosimetry audits were conducted through on-site visits. The functional performance characteristics of the irradiation units (linacs and ^{60}Co) were assessed through mechanical and radiation tests [8]. Relative dosimetry measurements, i.e. tissue–phantom ratio at 20 and 10 cm depths in water, $TPR_{20,10}$, (for photons), half–value depth for electrons, R_{50} and per cent depth dose and depth in water at dose maximum, d_{max} (for both), were performed using the IBA Scanditronix Wellhofer RFA-200 water phantom (60 cm × 50 cm × 40 cm). For radiotherapy photon and electron beams, the absorbed dose to water $D_w(z)$ was determined according to the IAEA TRS 398 code of practice for dosimetry using the IBA Scanditronix Wellhofer FC65-P Farmer type and the PTW W 23343 Marcus or the TW 34045 Advance Marcus ionization chambers connected to the PTW UNIDOS 10002 electrometer. The dosimetry equipment used for the measurements has been calibrated at IRCL against the reference equipment, which provides traceability to the Bureau International des Poids et Measures. For brachytherapy sources, the air kerma strength was measured using the Standard Imaging HDR 1000 well type ionization chamber connected to the CDX 2000B electrometer; the dosimetry equipment has been calibrated at the Laboratoire National Henri Becquerel/Commissariat à l'energie atomique (LNE-LNHB) primary standard laboratory.

For each photon or electron beam, the measured dose at the reference depth in water (D_M) was compared to the relevant dose value stated by the radiotherapy centre (D_S) and the ratio $r = D_S/D_M$ as well as the per cent relative deviation,

$d_r = [(D_S/D_M) - 1] \times 100\%$, were recorded. For brachytherapy, the air kerma strength values were recorded. The deviations, d_r, were compared to the actions levels of ±3% (preventive actions needed) and ±5% (immediate corrective actions needed). The uncertainties of measurements for photons, electrons and brachytherapy were 0.8, 1.0 and 1.5%, respectively, at 1 SD (k = 1, at 68% confidence level approximately).

3. RESULTS AND DISCUSSION

At the beginning of the dosimetry audits (2002), several dosimetry protocols were used in Greek radiotherapy centres (Fig. 1), resulting in an inconsistent approach to dose calculations and relative dosimetry. At that time, the choice of dosimetry protocol used in Greek hospitals had been made according to the dosimetry equipment calibration (in terms of air kerma or absorbed dose in water), as well as the training and the experience of the medical physicists.

After the completion of the first audit round, all radiotherapy centres have adopted the IAEA TRS 398 dosimetry protocol for both photon and electron beams. The step by step procedures followed by the GAEC staff during the on-site visits, as well as the continuous cooperation and assistance to the hospital staff, helped to achieve better consistency in clinical dosimetry in Greece. Additionally, the IRCL provided all necessary calibrations in terms of the $N_{D,w}$ of

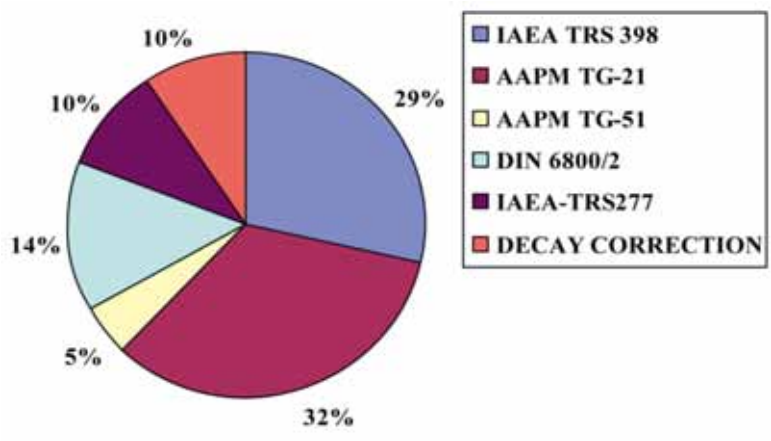

FIG. 1. The dosimetry protocols for photon and electron beams used by the Greek radiotherapy centres at the beginning of the audits, 2002. Since 2006, all centres have been using the IAEA TRS 398 protocol [5].

the user's dosimeters as well as assistance and training, in order that the IAEA TRS 398 protocol be adopted smoothly by the hospitals.

3.1. Photon beams

For the three audit rounds, the ratios of the $TPR_{20,10}$ value stated by the radiotherapy centre to those measured by GAEC were close to 1.000 and varied within narrow ranges, as shown in Table 1. This fact reflects good performance with respect to the photon energy and the maintenance of the linacs since, in most cases, the stated $TPR_{20,10}$ values were measured by the radiotherapy centre staff several days or even weeks prior to the audit. The results also showed that, irrespective of the linac model, the $TPR_{20,10}$ values were similar for the same nominal photon energy, i.e. 0.678 ± 0.008 (range 0.031) for 6 MV, 0.758 ± 0.007 (range 0.03) for 15 MV and 0.775 ± 0.006 (range 0.006) for 18 MV. The variation of $TPR_{20,10}$ values between different linac models is presented in Table 1 for 6 MV and 18 MV photon beams.

Figure 2 presents the ratios, *r*, of the dose, D_w, stated by the radiotherapy centre to the dose, D_w, measured by GAEC for all photons beams that were audited during the first and the second rounds (the results from the third round are not shown, due to the limited number of data). It is evident that the second round distribution is narrower than that of the first round, the peak values are more uniformly spread and are closer to unity, while extreme values (low or high) have

TABLE 1. $TPR_{20,10}$ VALUES FOR DIFFERENT LINAC MODELS AT 6 MV AND 18 MV

Linac model and MV	$TPR_{20,10}$ values		
	Average	Minimum	Maximum
Electa series, 6 MV	0.683	0.670	0.690
Philips SL series, 6 MV	0.676	0.668	0.680
Siemens Primus series, 6 MV	0.672	0.662	0.688
Varian Clinac series, 6 MV	0.666	0.660	0.670
Electa series, 18 MV	0.777	0.774	0.780
Siemens Primus series, 18 MV	0.768	0.759	0.777
Varian Clinac series, 18 MV	0.781	0.780	0.782

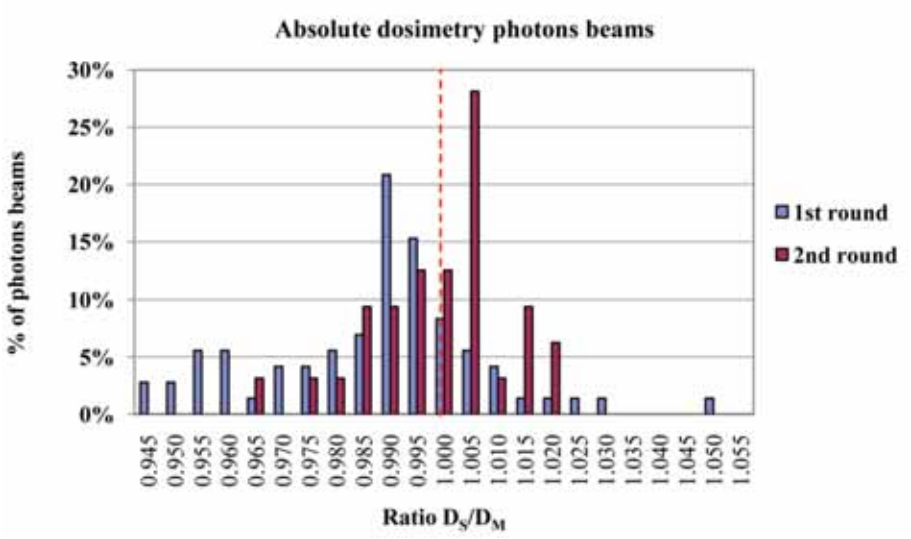

FIG. 2. The distribution of the ratios of the dose stated (by the user) and the dose measured by GAEC for the photon beams, assessed during the first and the second audit rounds.

not recurred. The average values of the ratios, *r*, of the stated to measured doses and the respective ranges (i.e. $r_{min} - r_{max}$) are given in Table 1. The range of *r* values decreased between the subsequent audit rounds and the average ratios, *r*, were closer to 1.000.

At the second audit round, only four of the photon beams showed significant (i.e. over the 0.8% uncertainty of the measurement) decrease in dose accuracy compared to the dose accuracy recorded at the first round (i.e. larger ratio, *r*, values in the second round than in the first). Nonetheless, for these beams, the maximum difference of the ratios, *r*, in the second rounds and in first rounds was 1.6%.

Table 2 also presents the percentages of the photon beams that exhibited deviations d_r relevant to the actions levels of ±3% (preventive action needed) and ±5% (immediate corrective action needed). It is evident that the large majority (97%) of the Greek radiotherapy centres fulfilled the requirements of dosimetry accuracy, thus no immediate actions were required. Two of the beams exceeding ±5% dose accuracy, a ^{60}Co and a 6 MV, were used at the same hospital, showing deviations of +5.38% and –5.26%, respectively. The errors were attributed to the malfunctioning of the optical distance indicator (for the ^{60}Co) and to the inappropriate determination of the dose rate at d_{max} using the per cent depth dose curves (for the 6 MV). The deviation at the 18 MV beam, produced by the same linac, was 2.5%. A third beam with a deviation of –5.08%, referred to a ^{60}Co,

TABLE 2. PHOTON BEAMS: THE AVERAGE VALUES (±SD) AND THE RANGE OF THE RATIO OF THE STATED TO MEASURED $TPR_{20,10}$ AND D_W, AND THE PERCENTAGE OF PHOTON BEAMS EXHIBITING PER CENT RELATIVE DEVIATIONS (D_R) WITHIN THE SPECIFIED RANGES

	First round (72 beams)	Second round (68 beams)	Third round[a] (6 beams)
$TPR_{20,10}$ ratio (±SD)	0.999 ± 0.008	0.998 ± 0.010	0.999 ± 0.004
Range of $TPR_{20,10}$ ratio (min–max)	0.982–1.022	0.979–1.017	0.991–1.002
Ratio of D_w, r (±SD)	0.990 ± 0.021	0.996 ± 0.013	1.000 ± 0.057
Range of r ($r_{min} - r_{max}$)	0.947–1.054	0.961–1.020	0.993–1.007
$\|d_r\| \leq 3\%$	79.2%	96.9%	100%
$3\% < \|d_r\| < 5\%$	16.7%	3.1%	0%
$\|d_r\| \geq 5\%$	3.1%	0.0%	0%

[a] The third round has recently been initiated and includes data from about 10% of the photon beams.

where the stated dose rate at the reference depth had not been measured for many months and the current value had been derived from the ^{60}Co decay data.

As concluded from the audits, the main sources of discrepancies in photon dosimetry were: the lack of recent check/calibration of photon beams; the malfunctioning of optical distance indicator and lasers; errors in positioning the chamber's reference point to the reference depth; and the lack of recent $TPR_{20,10}$ measurement, which resulted in the failure to detect a photon energy shift. The overall results showed that the repeated audits contributed to the improvement of dosimetry accuracy.

3.2. Electron beams

During the first and the second audit rounds, 140 and 38 electron beams were assessed, respectively, whereas the second round is still in progress. The average and the range of the ratios of the R_{50} values stated by the radiotherapy centre and those measured by GAEC, for all electron energies, are shown in Table 1. Discrepancies in R_{50} measurements were observed, especially at lower and higher energy electron beams. This was mainly due to the lack of recent R_{50} measurement by the radiotherapy centre staff as well as to the drift of the electron

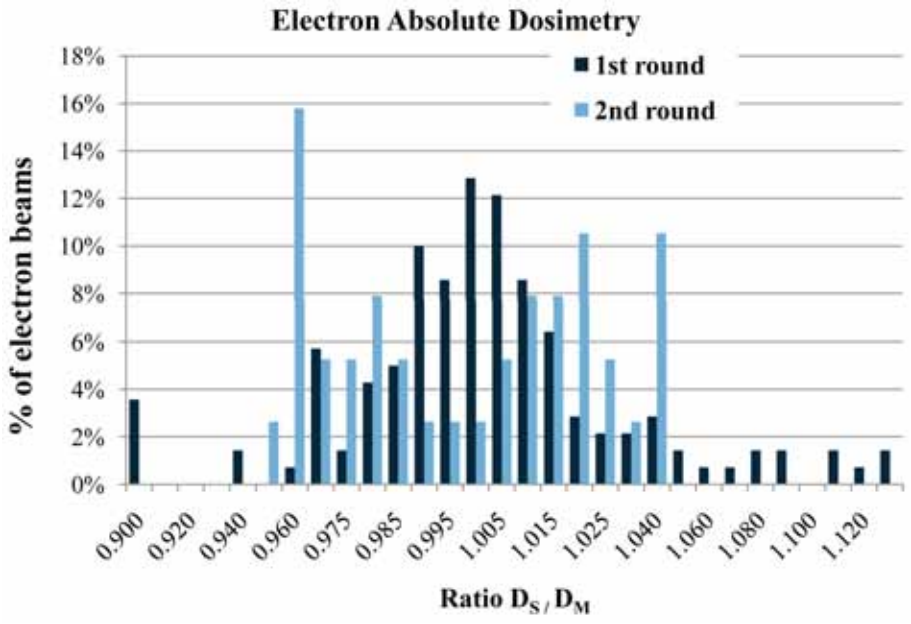

FIG. 3. The distribution of the ratios of the stated (by the user) to the measured absolute doses in water for the electron beams as assessed during the first and the second audit rounds.

energy of the linac. Since the R_{50} value determines the reference depth of the D_w measurement, z_{ref}, these R_{50} ratio (stated to measured) discrepancies contributed significantly to the deviations of D_w between the GAEC and the radiotherapy centre.

Figure 3 presents the distribution of the ratios of the dose stated by the radiotherapy centre to the dose measured by GAEC, *r*, the electron beams. The average values and the respective ranges (i.e. $r_{min} - r_{max}$) of the ratios, *r*, are shown in Table 2.

Table 3 also shows the percentages of the electron beams that showed deviations, d_r, relevant to the action levels of ±3% (preventive action needed) and ±5% (immediate corrective action needed). The large majority of electron beams showed acceptable results within the limits of ±3%. Most of the major deviations (i.e. $|d_r| > 5\%$) that were recorded during the first audit round were corrected or eliminated. It is worthwhile to mention that at three radiotherapy centres, all of the electron beams (12 in total) showed absolute deviations of greater than 5%. At these centres, systematic and consistent errors occurred, which concerned both dosimetric procedures (determination of the per cent depth dose, R_{50} and

TABLE 3. ELECTRON BEAMS: THE AVERAGE VALUES (±SD) AND THE RANGE OF THE RATIOS OF THE STATED TO MEASURED R_{50} AND D_W, R, AND THE PERCENTAGE OF ELECTRON BEAMS SHOWING PER CENT RELATIVE DEVIATIONS (D_R) WITHIN THE SPECIFIED RANGES

	First round (148 beams)	Second round (38 beams)
R_{50} ratio (±SD)	0.972 ± 0.026	0.964 ± 0.032
Range of R_{50} ratio (min–max)	0.899–1.029	0.874–1.003
Ratio of D_w, r (±SD)	0.998 ± 0.047	0.994 ± 0.028
Range of r ($r_{min} - r_{max}$)	0.720–1.128	0.948–1.040
$\|d_r\| \leq 3\%$	76.4%	65.8%
$3\% < \|d_r\| < 5\%$	10.7% (15 beams)	31.6% (12 beams)
$\|d_r\| \geq 5\%$	12.9% (18 beams)	2.6% (1 beam)

reference depth) and linac performance (lack of recent adjustment and calibration) and, therefore, affect the dose accuracy of all electron beams.

Although the second round is only at the initial stage (10% of the beams were assessed), it appears that the overall accuracy was not improved significantly, as was the case for the photon beams. Ten electron beams out of 38 exhibited significantly (i.e. over the 1.0% uncertainty of the measurement) higher discrepancies in the second round than in the first, which in one case was –5.2%. The main sources of discrepancies in electron dosimetry were: the conversion of ionization to depth–dose curves; the measurement of R_{50}; the determination of the reference depth, z_{ref}; and the point of dose maximum, d_{max}. These parameters may change due to variation of the linac performance. Small changes of those parameters may affect the electron dosimetry significantly. Therefore, frequent checks and calibration of linac electron beams are necessary.

The difference in dose accuracy at various electron energies was also assessed. Figure 4(a) presents the distribution of electron beams exhibiting deviations outside the ±3% and ±5% limits in respect of the nominal electron energy. The data referred to all electron beams as assessed during the first audit round. It is clear that lower and higher energy electron beams were more prone to dose inaccuracies than middle energy beams. This was mainly due to the uncertain determination of the reference depth, the depth of dose maximum and the positioning of the chamber's reference point at those depths. In Fig. 4(b), the

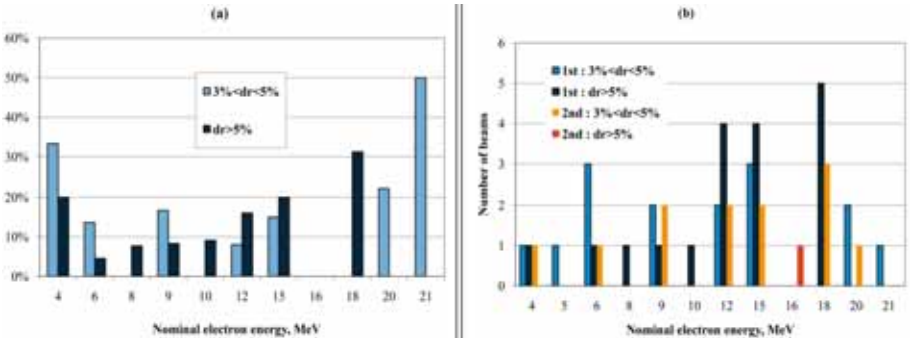

FIG. 4. (a) The percentage distribution of the electron beams (148 in total) exhibiting deviations, d_r, outside the ±3% and ±5% limits during the first audit round, and (b) the number of electron beams at the corresponding nominal electron energy showing deviations, d_r, outside the ±3% and ±5% limits during the first and second audit rounds.

total number of beams at the corresponding energy and deviation, d_r, are shown for the two audit rounds.

3.3. Brachytherapy

During the first dosimetry audit, seven HDR ^{192}Ir and two MDR/LDR ^{137}Cs brachytherapy systems were assessed, while at the continuing second round, three HDR ^{192}Ir had already been measured. Figure 5 presents the ratios, *r*, of the stated (by the user) to the measured air kerma strengths ($mGy \cdot h^{-1} \cdot m^{-2}$) for these systems. All of the clinics measured the air kerma strength ($mGy \cdot h^{-1} \cdot m^{-2}$) using well type ionization chambers, except one (no. 3 in Fig. 5), where a Farmer type ionization chamber is placed at four fixed positions around the ^{192}Ir source.

During the first round, the average values of the ratio, *r*, for the ^{192}Ir and ^{137}Cs systems were 1.002 ± 0.009 and 1.002 ± 0.009, respectively; the ranges of the *r* values were 0.028 and 0.007, respectively. The results show that all systems exhibited acceptable air kerma strength accuracy within the limits of ±3%.

Taking into account the uncertainty of the measurements (±1.5%), all three systems assessed during the second round showed similar *r* values to those in the first round.

4. CONCLUSION

The dosimetry quality audits with on-site visits have proved to be a very useful tool for improving the quality in radiotherapy. Guidance and

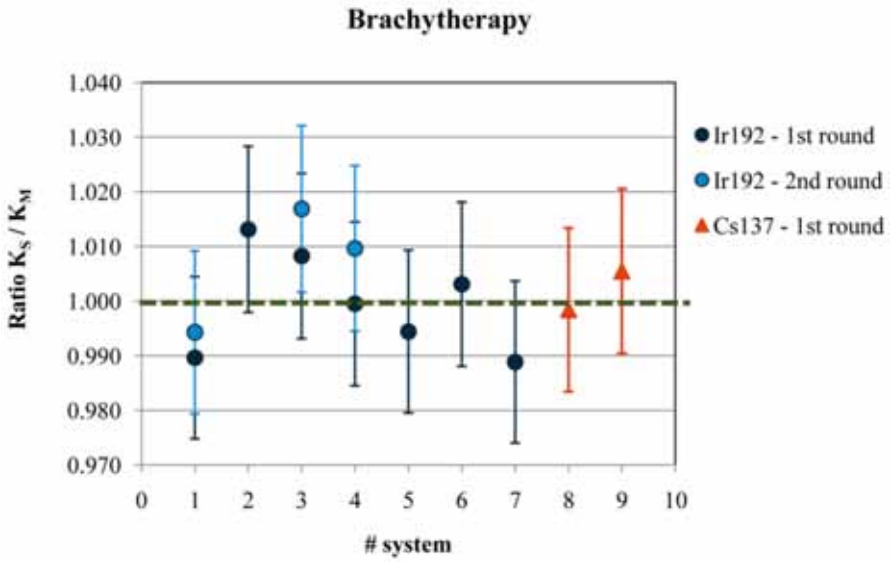

FIG. 5. The ratios of the stated (by the user) to the measured air kerma strengths for the HDR Ir192 and the MDR/LDR ^{137}Cs brachytherapy systems, assessed during the first and second audit rounds.

recommendations have been provided to the hospitals to improve accuracy, correct pitfalls and eliminate sources of errors. An improvement in dose accuracy was recorded during the subsequent rounds of the audit. These audits succeeded in disseminating the IAEA TRS 398 dosimetry protocol at all radiotherapy centres, achieving homogenization and consistency of dosimetry within the country. Regular checks and calibration of the linac radiation output, especially for electron beams, are essential for maintaining high dose accuracy on a daily basis.

REFERENCES

[1] INTERNATIONAL COMMISSION ON RADIATION UNITS AND MEASUREMENTS, Determination of Absorbed Dose in a Patient Irradiated by Beams of X or Gamma Rays in Radiotherapy Procedures**,** Report **24**, Bethesda MD (1976).

[2] BRAHME, A., Dosimetric precision requirements in radiation therapy, Acta Radiol. Oncol. **23** (1984) 379–391.

[3] MIJNHEER, B., BATTERMANN, J.J., WAMBERSIE, A., What degree of accuracy is required and can be achieved in photon and neutron therapy, Radioth. Oncol. **8** (1987) 237–251.

[4] INTERNATIONAL ATOMIC ENERGY AGENCY, Absorbed Dose Determination in External Beam Radiotherapy: An International Code of Practice for Dosimetry Based on Standards of Absorbed Dose to Water, Technical Reports Series No. 398, IAEA, Vienna (2000).

[5] INTERNATIONAL ATOMIC ENERGY AGENCY, Implementation of the International Code of Practice on Dosimetry in Radiotherapy (TRS 398): Review of Testing Results, IAEA-TECDOC-1455, IAEA, Vienna (2005).

[6] INTERNATIONAL ATOMIC ENERGY AGENCY, Calibration of Photon and Beta Ray Sources Used in Brachytherapy, IAEA-TECDOC-1274, IAEA, Vienna (2002).

[7] INTERNATIONAL ATOMIC ENERGY AGENCY, Implementation of Microsource High Dose Rate (mHDR) Brachytherapy in Developing Countries, IAEA-TECDOC-1257, IAEA, Vienna (2001).

[8] HOURDAKIS, C.J., BOZIARI, A., Radiother Oncol. **87**(1) (2008) 132–41.

TESTING, COMMISSIONING AND VALIDATING AN OPTICALLY STIMULATED LUMINESCENCE (OSL) DOSIMETRY SYSTEM FOR MAILED DOSIMETRY AT THE RADIOLOGICAL PHYSICS CENTER

J.F. AGUIRRE, P. ALVAREZ, G.S. IBBOTT, D.S. FOLLOWILL
M.D. Anderson Cancer Center, Radiological Physics Center,
University of Texas, Houston,
Texas, United States of America
Email: faguirre@mdanderson.org

Abstract

The Radiological Physics Center (RPC) commissioned a dosimetry system based on the microStar® reader and a single production batch of optically stimulated luminescence dosimeters (OSLDs), nanoDot™ (Landauer Inc.). The procedures for the determination of dose with OSLDs were designed to resemble those followed with thermoluminescent dosimetry (TLD) as used by the RPC for remote dosimetry audits of photon and electron radiotherapy beams. As with TLD, the dosimeters are irradiated in acrylic phantoms under standardized geometric conditions. The steps for a reading session, the criteria for the number of dosimeters, readings per dosimeter, interspersing of 'standard' and 'control' dosimeters, and important quality control procedures have been subsequently determined. The methodology defined for dose determination based on OSLD requires the determination of individual correction factors. A method was developed and tested for the determination of the correction factors that accounted for the large number of dosimeters under commissioning (10 000) and the small number of dosimeters read per session (~125). Validation of the process and an assessment of the accuracy of the system were performed through comparisons with TLD banking on the RPC's long experience with the latter. TLD and OSLD were irradiated sequentially multiple times with photon and electron beams of a range of energies at our own facility as well as at several other institutions. The results from both dosimeters were compared. The results from the TLD versus OSLD comparison based on irradiations done at our facility were within 2%. The results from irradiations done at multiple institutions were also within 2%. Photon energies from cobalt to 18 MV and electrons from 5 MeV to 23 MeV were verified.

1. INTRODUCTION

Thermoluminescent dosimetry (TLD) has been used by the Radiological Physics Center (RPC) for more than 30 years [1] for remote audits of standard output verification for photon beams, as well as output and energy verification for electron beams using lithium fluoride (LiF) TLD-100 disposable powder positioned in acrylic blocks. With acceptance criteria of ±5% for beam output and

5 mm for depth, the RPC has evaluated treatment units on an annual basis. The data show that the agreement between the measured dose versus that stated by the institutions has a standard deviation of 1.7%, and under very controlled conditions, the agreement is within 0.7%. The data from this experience provides a justification to use the dosimeter to flag units with beam output outside 5%, although the system may be more reliable than that, as the standard deviation above suggests. TLD powder has a uniformity of dose response better than 1.5%, a non-linearity correction of up to 10% over the range of 50–400 cGy, fading of the stored signal up to 5.5% in 25 d and energy dependence requiring corrections of up to 7% [2]. Under the best controlled circumstances, the data show that the agreement between measured and predicted dose for a cobalt beam is better than 1%. The confidence on these results is maintained through a quality assurance (QA) programme covering readers, powder, sessions and customer results.

Optically stimulated luminiscence dosimeters (OSLDs) have been previously used for personnel dosimetry and tested for measurements in the therapeutic range [3]. The general characteristics of the microStar System™ with InLight™ dosimeters to be used by the RPC were studied with favourable results [4] and a decision was made to purchase two readers and a batch of InLight nanoDot™ dosimeters, a smaller version of the previous design, with the purpose of accepting, commissioning and validating it for regular use. Commissioning an OSLD system included the design of a methodology to irradiate the dosimeters, the steps of a reading session, criteria for the number of dosimeters to be read per session, readings per dosimeter, interspersing of ‘standard’ and ‘control’ dosimeters, quality control steps, an algorithm to calculate dose, annealing and reading cycles, and identification of the properties of the dosimeters such as signal depletion, reader dependence, individual dosimeter correction factors, dose response characteristics, signal fading and energy/block corrections. The validation of the process and an assessment of the accuracy of the system were performed through comparisons with TLD.

2. MATERIALS AND METHODS

2.1. The basic model

Crystalline dielectric materials with impurities form crystal lattice imperfections that become traps for electrons or holes under irradiation. Later, these act as luminescent centres emitting light when they recombine under stimulation from heat for TLD or from light for OSL. The phenomenological model describing the luminescent properties of these materials has been explained in the literature [2–4].

The InLight nanoDot™ dosimeters consist of a disc of Al_2O_3:C material encased within a lightfast envelope, which prevents any signal fading from light exposure. They are coupled with a microStar System™ reader. Stimulated with a green light from an LED within the reader the dosimeter emits blue light that is converted into current by a PMT and automatically stored in the system memory.

The amount of emitted light has a quasi linear relation with the dose received by the dosimeter after several factors are accounted for in the measurement process. First, the emitted light is related to the intensity of the stimulating laser beam and the duration of the stimulus. These are factors controlled by preset conditions on the reader. Second, the reader may have some variability from day to day that needs to be accounted for through the use of standard dosimeters irradiated to a known dose and used to calibrate the reader every session. Third, the emitted light from the dosimeter is affected by the individual properties of each dosimeter as well as the general properties of any OSLD related to the lack of linearity with dose, the different response to different energies, the loss of signal from irradiation to reading time and the depletion of the signal after every reading.

2.2. Methodology

The preset conditions of the reader were studied during the period of evaluation of the system [4]. A seven second reading time was established using factory settings. It was agreed that the methodology for the determination of dose to a dosimeter would consist of the following steps:

(a) The relative sensitivity of the whole batch of OSLD is to be determined by irradiation to the same dose and by comparing the reading to the average signal.
(b) For irradiation under a photon beam, OSLDs are embedded in small acrylic blocks that, while providing electronic equilibrium, do not produce significant backscatter. For electrons, the dosimeters are placed in a block that is large enough to provide full scatter but small enough to be easily mailed. Both these blocks are identical to those used for TLD redesigned for the OSLD dosimeter but with equivalent geometric characteristics. Each point of measurement in the block has two dosimeters.
(c) A group of dosimeters defined as standards is irradiated under known conditions in a cobalt beam to allow the calibration of the system at every reading session.
(d) Dosimeters to measure dose under photon or electron beams are irradiated in specified geometric conditions by customers.

(e) The signal from both standards and customer dosimeters is to be corrected for the sensitivity of each nanodot, depletion of signal of the nanodot after each reading, dose non-linearity characteristics of the batch, loss of accumulated signal by the dosimeters from irradiation to reading time and the dependence of the signal with energy or type of block.

(f) The sensitivity of the system using standards is calculated using Eq. (1):

- Sensitivity = Dose to standards/(Reading × ECF × Depl × K_E × K_F × K_L)$_{std}$ (1)

where

ECF is the element (dosimeter) correction factor;
Depl is the correction for depletion of signal;
K_E is the correction for energy/block dependence;
K_F is the correction for fading of the signal;
K_L is the correction for the lack of linearity of the signal with dose.

- The dose to a customer's dosimeter is calculated using Eq. (2):

Dose = Sensitivity × (Reading × ECF × Depl × K_E × K_F × K_L)$_{customer}$ (2)

- To reduce uncertainties in the process, both standards and customer's dosimeters are irradiated preferably to the same dose and on the same dates or as close as possible.
- The dose to an OSL dosimeter was set at 100 cGy to keep it at clinical radiotherapy levels and yet to allow for numerous irradiations to be given to a maximum cumulative dose of 10 Gy.

2.3. The correction parameters

2.3.1. Element correction factor (ECF)

The ECF is a measure of the relative response of each dosimeter compared to the whole population of dosimeters. The determination of the ECF for each OSLD as part of a group of 10 000 dosimeters, all coming from the same production, was done based on irradiations at ^{60}Co energy. The dose level was 25 cGy and the set-up a 25 cm × 25 cm field size allowing the irradiation of a set of approximately 30 dosimeters simultaneously. The reading sessions were

organized to read three groups of 30 OSLD irradiated the same day plus some reference dosimeters for normalization and quality assurance purposes.

The determination of the ECFs was performed for each group of 100 OSLD read in one session. The ECF was defined as the ratio between the average reading of the whole set and the average of the reading per each OSLD. The ECF were found to have a range of variation of up to ±10%. Dosimeters with ECF no larger than 8% were considered acceptable.

ECFs were also calculated for the whole group of 4000 dosimeters as the ratio between the average of averages of all the sessions readings and the average reading for each dosimeter with good agreement with the previous methodology.

2.3.2. Depletion correction

The signal diminishes every time a reading is taken thus a correction is applied. It was decided that three readings should be taken for each dosimeter unless the maximum to minimum of them was larger than 1% when two more readings would be taken. If the dosimeter then failed to be within 1%, the measurement would be considered questionable and unusable.

2.3.3. Linearity correction

The equation to calculate dose assumes linear response of the dosimeter; there is a small non-linearity in the response that needs to be accounted for. The deviation from linearity as a function of dose normalized at the dose of 100 cGy is applied as a correction to the reading.

2.3.4. Fading correction

The signal loses its value over time due to recombination of electrons and holes. A correction can be applied to restore the reading to what it would have been immediately after irradiation.

2.3.5. Energy/block correction

Although other experiments report that the signal for the same amount of radiation exposure is the same for different energies, the dosimeters are embedded in acrylic phantoms of different geometrical characteristics for each energy. Further, although they have been designed to allow an irradiation to a miniphantom in air, there is the possibility of different response by the dosimeter dependent on size of the block. The loaded OSLD blocks are irradiated to the same dose as those irradiated in a ^{60}Co beam. The ratios of the response between

the reference dosimeters in ^{60}Co and those irradiated at other energies provide correction factors for energy and/or block dependence of the system.

2.4. The logistics of a reading session

The sequence to read an OSLD session was kept as close as possible to that of TLD. Standard dosimeters are read at the beginning and at the end of the session. The session is divided in four segments of around 25 dosimeters that are read after a control dosimeter is read. Controls are dosimeters irradiated to a known dose in another cobalt unit at our institution that serve the purpose of monitoring the changes in the reader through the session as well as a verification that measurements were stable through the session. A session of 115 dosimeters will last around two hours.

There are some checks of background reading as well as a built in light reading that are performed at the beginning and end of the session but are only analysed to look for gross changes in the system over time.

2.5. QA

The TLD system has had QA procedures that were replicated for OSLD.

The following components have been implemented for the QA programme on OSLD:

— Acceptance and commissioning of instruments;
— Characterization of dosimeters as a batch from the same production;
— Per session QA;
— Per individual result QA;
— Quarterly and other QA;
— Maintenance and repair;
— Training of personnel.

2.5.1. Written procedures

The procedures defining OSLD activities have been written and are available to the staff.

2.5.2. Commissioning of the reader

Two readers were tested for reproducibility of the readings, depletion characteristics, and a baseline was established for the background and test signal values. The manufacturer's software is designed to have two reading modes for

low and high doses that trigger automatically. The trigger point between low and high dose was verified to avoid automatic change of mode at doses within our range (25–350 cGy).

2.5.3. Characterization of a batch

The dosimeters are purchased from the provider with the request that all belong to the same production and upon commissioning of the batch, dosimeters that respond outside 8% from the average signal are discarded. Also, after a dosimeter has received a cumulative dose of 10 Gy, it is decommissioned.

2.5.4. Quality control per session

Each reading session is checked for background and test signal, controls are read and the measured dose is compared to the dose that can be predicted from calculations. Changes in the controls through the session are monitored to verify the stability of the session. The spread of the readings per dosimeter are evaluated.

2.5.5. Quality control of individual results

The ratio between measured and institution stated dose is evaluated against previous results for that beam at that institution. Significant discrepancies are discussed with the physicist at each institution and repeats are sent to verify the result.

2.5.6. Quarterly and other controls

On a periodic basis, the RPC compares measurements with TLD measurements done by Radiation Dosimetry Services, a sister company at MDACC, the IAEA and other TLD programmes.

2.5.7. Training of personnel

Personnel receive specific training on irradiation of standard and controls, reading procedures and interpretation of flags that may suggest irregularities in the process.

2.6. Validation of the system

To validate the system, simultaneous irradiations were performed with TLD and OSLD. The results from both dosimeters were compared for photon energies (^{60}Co-18 MV) and electron energies (5–23 MeV). This was performed with the authors' own linear accelerator as well as with a group of institutions. Given the authors' long experience and accumulated data for TLD, they consider this comparison to be strong evidence of the reliability of our OSLD system.

3. RESULTS

3.1. Element correction factor (ECF)

The difference between ECF per reading session of 100 OSLD and ECF from the whole group was less than 1%. The decision of determination of ECF of a batch by session of 100 dosimeters was taken based on these results.

3.2. Depletion correction

The depletion correction was done for each reader and at different dose levels. The behaviour was studied up to 50 readings. Figure 1 shows the depletion curve for one of the readers based on the setting used by the RPC. The depletion is dependent on the illumination intensity and reading time; it does not depend on dose level or batch, but it is shown to be reader dependent.

3.3. Linearity correction

The linear response of the OSLD was studied between 25 and 350 cGy. Figure 2 presents the relation between dose and K_L. The reference dose is 100 cGy. This correction is batch dependent.

3.4. Fading correction

The study was conducted between 1 and up to 120 d after irradiation. Figure 3 presents the behaviour of the fading factor.

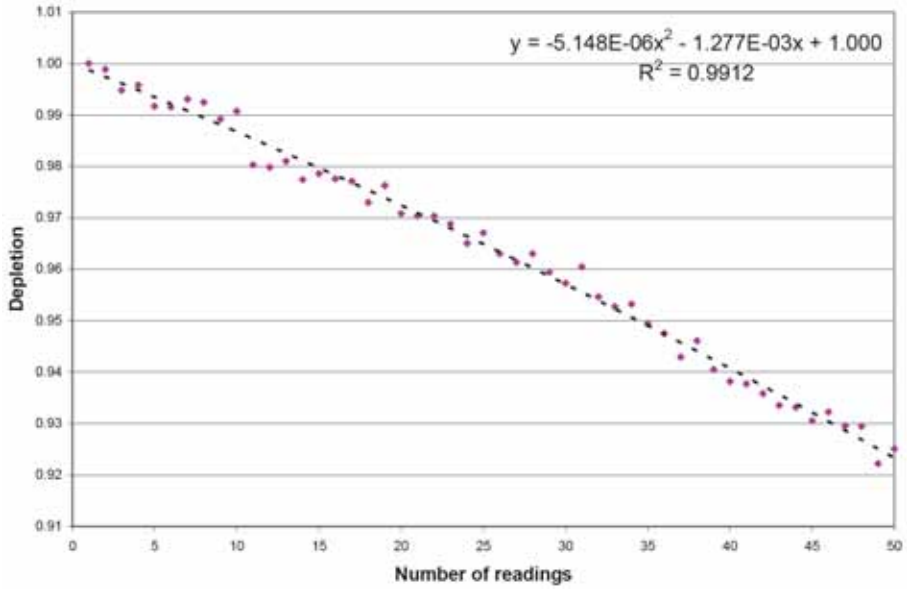

FIG. 1. Depletion curve for OSLD on microStar reader based on settings used by the RPC.

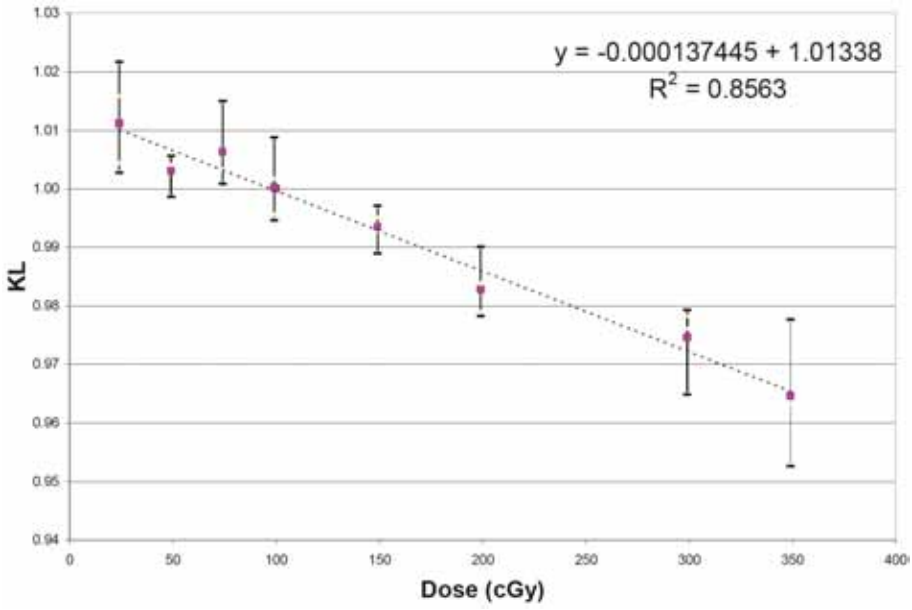

FIG. 2. Linearity correction factor as function of dose for OSLD.

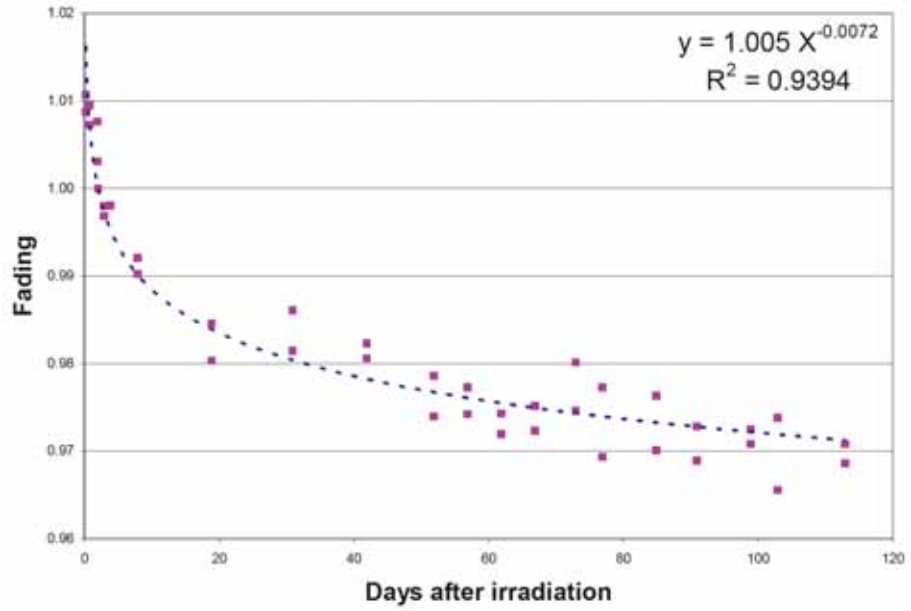

FIG. 3. Fading correction for OSLD up to almost four months after irradiation.

3.5. Energy/block correction

Irradiations were performed for photon beams between 6 and 18 MV and electron beams from 6 MeV to 20 MeV. Conventional linear accelerators were used. Rates of 300 MU/min or less were used during irradiation. Correction for the combination of energy/block ranged from 1.000 to 1.058 for photon beams, and 1.027 to 1.035 for electron beams.

3.6. Validation

For a total of 11 institutions and a range of 16 photon and electron energies, OSLD and TLD irradiations on the same date showed an agreement between both dosimeter systems from 0.994 to 1.011 for institutions, and 0.985 to 1.024 for energy comparison.

4. CONCLUSIONS

The OSLD system has been commissioned and validated as a remote audit tool for the RPC for verification of output and energy of photon and electron beams in the radiotherapy range.

ACKNOWLEDGEMENTS

The work was supported by PHS CA010953 and CA081647 awarded by NCI, DHHS.

REFERENCES

[1] AGUIRRE, J., et al., "Thermoluminescence Dosimetry as a Tool for the Remote Verification of Output for Radiotherapy Beams: 25 Years of Experience", Standards and Codes of Practice in Medical Radiation Dosimetry (Proc. Int. Symp. Vienna, 2002), IAEA, Vienna (2003) 191–199.

[2] KIRBY, T., et al., Mailable TLD system for photon and electron therapy beams, Int. J. Radiat. Oncol. Biol. Phys. **12** (1986) 261–265.

[3] JURSINIC, P., Characterization of optically stimulated luminescent dosimeters, OSL for clinical measurements, Med. Phys. **34** (12) (2007) 4594.

[4] HOMNICK, J., et al., Optically Stimulated Luminescence (OSL) Dosimeters Can Be Used for Remote Dosimetry Services, Med. Phys. **35** (6) (2008) 2994.

[5] YUKIHARA, E.G., et al., Optically stimulated luminescence (OSL) dosimetry in medicine, Phys. Med. Biol. **53** (2008).

[6] AGUIRRE, J., et al., Optically Stimulated Light Dosimetry: Commissioning of an OSL System for Remote Dosimetry Audits: The Radiological Physics Center Experience, Med. Phys. **36** (2009) 2591.

A SYSTEM FOR MAILED DOSE AUDIT IN RADIOTHERAPY USING LITHIUM FORMATE EPR DOSIMETRY

S. OLSSON*, Z. MALKE**, P. LARSSON*,
Å. CARLSSON TEDGREN**,***

* Department of Radiation Physics,
Linköping University Hospital,
Linköping
Email: sarakolsson@yahoo.se

** Department of Medical Radiation Physics,
Linköping University,
Linköping

*** Swedish Radiation Safety Authority,
Stockholm

Sweden

Abstract

A mailed audit system for dose verification using lithium formate electron paramagnetic resonance dosimetry was designed and evaluated. For this purpose, a semi-anthropomorphic phantom was manufactured, inserted with pellet shaped lithium formate dosimeters and treated with an intensity modulated radiotherapy plan. The measurement results agreed with the planned doses within the estimated standard uncertainties.

1. INTRODUCTION

The aim of radiation therapy is to deliver high doses to the target to achieve local tumour control while protecting the surrounding healthy tissue. The dose needed for local control and the dose tolerated by healthy tissue give a narrow therapeutic window [1, 2]. Therefore, high accuracy in the delivered dose is critical. As radiation therapy techniques are becoming more advanced, quality assurance of machines, delivery techniques and clinical routines become more important. The absorbed dose given in external radiation treatments is related to measurements for determination of absorbed dose to water under reference

conditions using a calibrated ionization chamber traceable to a standard laboratory [3]. When delivering a radiation treatment several factors, other than accelerator output in reference conditions, contribute to the uncertainties in the dose delivered to the tumour and healthy tissue. Therefore, an effective audit system where influences from the whole treatment chain are taken into account, from computed tomography (CT) scanning to contouring of structures, treatment planning and treatment delivery, would be of great value.

There are systems for dose audits for the whole treatment chain or parts of it utilizing anthropomorphic or multipurpose phantoms and thermoluminescent (TL) dosimetry [4–6]. The aim of the present work is to design and evaluate a mailed dosimetry audit system where influences from the whole treatment chain are taken into account, using EPR dosimetry with lithium formate. Experimental details are found in an MSc thesis by Malke [7]. The strategy was to let a phantom undergo the treatment chain for intensity modulated radiotherapy (IMRT) treatment and perform measurements in the phantom to evaluate the dose in relevant points. For this purpose, an audit phantom was designed to be relevant for the head-and-neck region with target and organs at risk (OARs) and inserts for electron paramagnetic resonance (EPR) dosimeters. Point doses in the target and OARs were determined and results compared to planned doses. The IMRT treatment was delivered to the audit phantom using dynamic multileaf collimator technique. All doses stated in this work refer to absorbed dose to water in the medium. This is also valid for the dose values obtained from the treatment planning system.

EPR dosimetry is a method available today with the potential to become a complement to TL dosimetry, which has been used for clinical applications for many years with its advantages of high sensitivity, dosimeter reusability and low energy dependence. However, most TL materials show a supralinearity in the dose response, typically for doses above 1 Gy. Within EPR dosimetry, most dosimeter materials have a linear dose response over a very large dose range. EPR dosimetry with alanine is accepted as a standard dosimetry method, especially for measurements of high doses for industrial applications. Alanine is nearly water equivalent [8] with a lower energy dependence than the common TL dosimetry material lithium fluoride, but has a low sensitivity, which is a drawback for its usefulness in radiotherapy applications [9].

Polycrystalline lithium formate monohydrate (HCO_2LiH_2O — referred to as ‘lithium formate’) [10] is 2–6 times more sensitive than alanine (depending on read out procedure) and exhibits no zero-dose signal. The dose response is linear for doses up to 1000 Gy. This gives a wide measurement dose range, which facilitates simultaneous measurements in points corresponding to both OARs and target. The readout of the dosimeters is performed with an EPR spectrometer and is non-destructive to the signal, which allows for several readouts to improve the

statistics. Lithium formate is even more water equivalent than alanine regarding mass energy absorption coefficient and mass collision stopping power. The dosimeters used in this study contain 10% paraffin and 90% lithium formate, and have a density of 1.32 g/cm^3. The response of the dosimeters is independent of the dose rate and the beam quality in the ranges that are relevant for the accelerator produced high energy photon beams [11].

In an earlier study [11], no significant signal fading (instability of the radiation induced radicals over time) was found during the first 28 d. However, experiences from several investigations indicate that the fading properties of lithium formate are complex, requiring controlled readout and storing conditions regarding temperature and air humidity. For alanine, the signal dependence of the read out temperature is 0.135–0.190% per K for doses between 20–100 kGy [12]. To the authors' knowledge, there are no published investigations of a possible temperature and humidity dependence for lithium formate, but it is likely that lithium formate has a readout temperature dependency of the same order of magnitude as alanine. There is a concern for how the dosimeters are affected by temperature during the transport between the clinics for the mailed dose audit. Higher temperature could result in higher thermal motion and hence faster fading. Lithium formate is also mildly hygroscopic at high air humidities. This has a significant influence on the signal stability at relative humidities above 55–60%. An air tight encapsulation during storage is therefore essential.

Nevertheless, in this work, all irradiations including calibration were performed on one day and all readouts were performed two days later, which made the results insensitive to fading. Before the system is used for a mailed dose audit, the signal fading due to temperature and humidity will be further investigated in order to find routines and corrections to minimize its influence.

Lithium formate has already been used for clinical applications such as pretreatment IMRT verification [11], high dose rate brachytherapy [13] and stereotactic radiosurgery [14]. Since the dosimeters are useful for a wide dose range and are expected to have a stable signal under controlled conditions, it should be a well suited system for mailed dosimetry audits.

2. MATERIALS AND METHODS

2.1. Phantom and dosimeters

An anthropomorphic phantom (Fig. 1) was designed and constructed at Linköping University Hospital after an idea derived from an IMRT phantom designed for a remote monitoring programme [4]. The cylindrical phantom has a diameter of 20 cm and a length of 24 cm. For manufacturing reasons, it consists

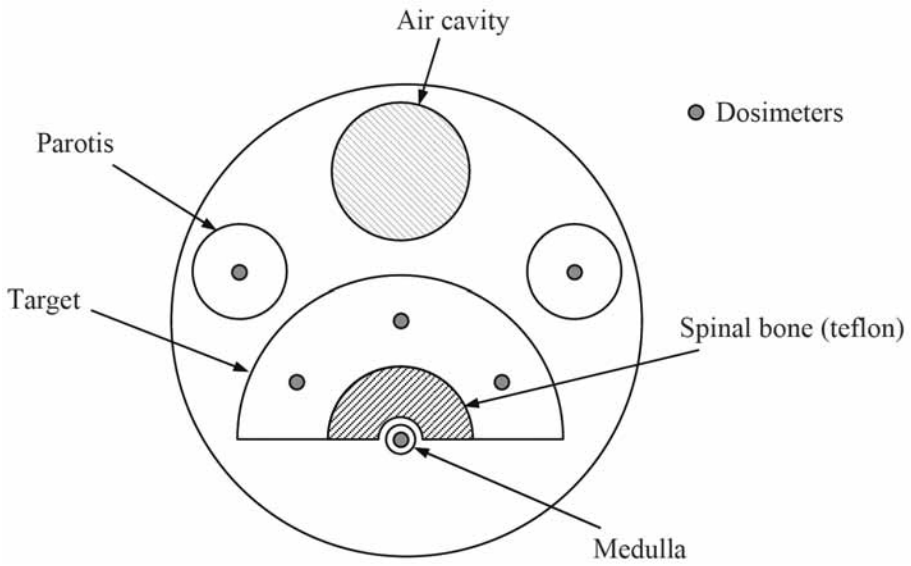

FIG. 1. A transversal slice of the audit phantom.

of eight slices tacked together with three rods throughout the phantom. The first and the last slices rest on braces.

The inside of the phantom was designed to mimic the head-and-neck region with the tumour (target) partially encompassing the medulla (OAR). Other OARs are the salivary glands adjacent to the tumour. PMMA (polymethyl methacrylate) was the choice of material since it is near tissue equivalent and readily available. A structure made of Teflon resembling the spinal bones and an inhomogeneity in the form of an air cavity were also included. The air cavity was also treated as an OAR corresponding to lung tissue or trachea. The structures go through the four cylindrical slices in the middle. Three holes were drilled in the target, and one hole each in the salivary glands and the medulla. Cylindrical PMMA tubes with an inner diameter of 5 mm were inserted into the holes for dosimeter placement.

In order to eliminate the dependency on the person contouring the organs, the structures were accommodated to fit tightly in, and to be easily discriminated from, the surrounding material.

The dosimeters were produced with a manual tabletop pellet press following a standardized method [11] giving cylindrical pellets of 5 mm height and 4.5 mm diameter, with a weight of 100 ± 2 mg. The dosimeters consist of 90% lithium formate (Sigma-Aldrich, 98%), which is the active material, and 10% solid household paraffin, which is used as a binder. No encapsulation was needed.

2.2. EPR measurements and readout

A BRUKER EleXsys E 580 spectrometer was utilized for all EPR measurements. The spectrometer was equipped with a standard cavity ER 4102ST. The measured signal is defined as the peak to peak amplitude of the first derivative of the absorption spectrum, divided by the mass of the dosimeter. Every dosimeter was read out five times. In order to reduce uncertainties due to spectrometer response variation over time, the five readings were spread out over the day and the whole batch including calibration dosimeters was read out in one day. The EPR signal was not smoothed, filtered or manipulated in any way and was determined as the mean of all five readings. A quartz glass sample tube with an inner diameter of 5 mm and flat bottom was employed for dosimeter placement in the cavity. To ensure identical and reproducible positioning of the dosimeters in the cavity, the sample tube containing the dosimeter was placed on the notch of an in-cavity pedestal. For the present work, the spectrometer settings in Table 1 were used.

2.3. Dosimeter batch quality control

It is important to check that all dosimeters respond equally to radiation before use. An upper limit for the relative standard deviation of the mean signal of the batch was set to 1%. Dosimeters not fulfilling that condition are excluded from the batch. In this case, the standard deviation of the mean signal was 0.87%.

All dosimeters of the batch were irradiated, ten at a time in a stack, in a cubic PMMA phantom. The dosimeters were irradiated at 7 cm depth in PMMA in a field of area 10 cm × 10 cm at a source–surface distance (SSD) of 100 cm in a 6 MV photon beam using a Varian Clinac 600 C/D linear accelerator. To account for possible inhomogeneities in the radiation field, the dose was given in

TABLE 1. SPECTROMETER SETTINGS

Microwave power:	20 mW
Modulation amplitude:	1.2 mT
Sweep width:	3 mT
Sweep center:	346 mT
Time constant:	327.68 ms
Sweep time:	167.77 s

ten fractions and the dosimeters were translocated in the stack after each fraction. Thus, the dosimeters were given a total dose of 3 Gy. The signal corresponding to this dose is considered as the background signal, *b*, of the batch.

2.4. Measurements

All irradiations described below were performed in a 6 MV photon beam using a Varian Clinac iX linear accelerator at Linköping University Hospital.

The audit phantom was CT scanned using a Siemens SOMATOM Sensation Open. During the scan, the dosimeters were replaced with PMMA inserts to avoid measuring the dose from the CT scan. The treatment planning system (TPS) used for contouring the phantom structures, and optimizing and calculating the IMRT treatment plan was Helios/Eclipse (Varian) with AAA (analytical anisotropic algorithm). The resulting treatment plan consisted of seven coplanar beams separated by 51–52º. Six EPR dosimeters were placed in the phantom, one in each parotis and the medulla, and three in the target. The phantom was irradiated according to the IMRT treatment plan giving the target a dose of 5 Gy. The absorbed doses in the different structures of the phantom, determined with EPR dosimetry, were compared to the corresponding planned doses from the TPS.

In order to check the quality of the IMRT treatment plan compared to other clinical plans, a verification measurement was performed according to the plan verification method normally used in the clinic. The accelerator output and the attenuation in the treatment table were corrected for in the determination of the planned doses.

Two groups of five dosimeters each were used to establish a calibration curve for the batch according to the method described in earlier studies [11, 13]. In order to test the precision and accuracy of the current dosimetric method, three groups containing three dosimeters each, were irradiated simultaneously with an ionization chamber to doses in the interval 1–9 Gy, unknown to the person responsible for readout. Results were compared to doses determined with the ionization chamber. Both the calibration and blind test measurements were performed in a PMMA phantom at a depth of 8 cm, in a 6 MV photon beam with a 10 cm × 10 cm field and an SSD of 100 cm. An NE 2571 ionization chamber with a calibration coefficient traceable to a standards laboratory was used as a reference. To compare the TPS with the measurements in a simple homogeneous set-up, a treatment plan describing the blind test was created on a virtual PMMA phantom with the same dimensions as the calibration phantom.

The fact that the reference conditions are not completely fulfilled, using a PMMA phantom instead of water, were taken into account as an increased uncertainty in the beam quality correction factor. To ensure the same dose to each dosimeter independently of position and inhomogeneities within the radiation

field, the calibration dosimeters were rotated in the phantom as described for the batch quality control.

3. RESULTS

The results from the blind tests and the audit phantom measurements are presented in Tables 2 and 3, respectively. The relative standard uncertainty of the absorbed dose values determined by ionization chamber measurements was assumed to be 1.5%, and the corresponding value for the planned doses were taken to be 3.1% according to a review by Ahnesjö and Aspradakis [15], where 'future values' with a 2% relative standard uncertainty in the dose calculation

TABLE 2. RESULTS FROM THE BLIND TESTS, COMPARED WITH IONIZATION CHAMBER VALUES AND PLANNED DOSES

	Dose, ion chamber (Gy)	Dose, EPR Gy)	Relative difference, EPR–ion chamber (%)	Dose, TPS (Gy)
Group 1	1.53 ± 0.02	1.51 ± 0.03	–1.2 ± 2.4	1.56 ± 0.05
Group 2	3.58 ± 0.05	3.54 ± 0.07	–1.1 ± 2.4	3.63 ± 0.11
Group 3	7.66 ± 0.15	7.68 ± 0.16	0.3 ± 2.9	7.77 ± 0.24

TABLE 3. RESULTS FROM MEASUREMENTS IN THE AUDIT PHANTOM, COMPARED WITH PLANNED DOSES

	Planned dose (Gy)	Dose, EPR (Gy)	Relative difference (%)
Target 1	5.13 ± 0.15	5.03 ± 0.10	–1.9 ± 3.7
Target 2	4.92 ± 0.15	4.74 ± 0.09	–3.7 ± 3.7
Target 3	5.16 ± 0.15	5.03 ± 0.11	–2.4 ± 3.7
Medulla	2.87 ± 0.09	2.83 ± 0.06	–1.4 ± 3.7
Parotis DX	1.19 ± 0.04	1.21 ± 0.02	1.7 ± 3.5
Parotis SIN	1.21 ± 0.04	1.20 ± 0.02	–0.8 ± 3.5

were assumed to be relevant. The relative differences between EPR and ionization chamber measurements are well below the calculated uncertainties in the EPR measurements. A description of these uncertainty calculations are given in the MSc thesis by Malke [7].

4. CONCLUSIONS

This work shows promising initial results for an audit system where influences from imaging, planning and treatment delivery are taken into account. The present project will continue for two years as a regional dose audit project between three or four clinics, and further investigation and measurements will be performed.

For the blind tests, the doses obtained from the EPR dosimeters agreed with the results obtained from the ionization chamber and from the TPS within the estimated standard uncertainties. The absorbed doses from the audit phantom measurements also agree with the planned doses within the estimated standard uncertainties. The experiment will be repeated using three dosimeters in each measurement point for higher precision.

There are several general recommendations of uncertainty limits in the delivered dose, but according to the IAEA [3], the uncertainty in the delivered absorbed dose to a target volume should be less than ±5%. For audit measurements performed in the reference conditions using TL dosimeters, an agreement within 5% is often considered satisfactory.

ACKNOWLEDGEMENTS

This work was partly financed by the Medical Research Council of Southeast Sweden (project: FORSS-86231). The authors wish to thank B. Frost at Linköping University Hospital for manufacturing the phantom.

REFERENCES

[1] BRAHME, A., Dosimetric precision requirements in radiation therapy, Acta Radiol. Oncol. **23** (1984) 379.

[2] CHETTY, I.J., et al., Report of the AAPM Task Group No. 105: Issues associated with clinical implementation of Monte Carlo based electron external beam treatment planning, Med. Phys. **34** (2007) 4818.

[3] INTERNATIONAL ATOMIC ENERGY AGENCY, Absorbed Dose Determination in External Beam Radiotherapy: An International Code of Practice for Dosimetry Based on Standards of Absorbed Dose to Water, Technical Reports Series No. 398, IAEA, Vienna (2000).
[4] HAN, Y., et al., Dosimetry in an IMRT phantom designed for a remote monitoring program, Med. Phys. **35** (2008) 2519.
[5] SWINNEN, A., et al., The use of a multi purpose phantom for mailed dosimetry checks of therapeutic photon beams: OPERA, Radiother. Oncol. **64** (2002) 317.
[6] BRIDIER, A., et al., A comparative description of three mulipurpose phantoms (MPP) for external audits of photon beams in radiotherapy: the water MPP, the Umeå MPP and the EC MPP, Radiother. Oncol. **55** (1999) 285.
[7] MALKE, Z., System for dose audit for external radiation therapy based on EPR dosimetry with Lithium Formate, MSc Thesis, Stockholm University, Sweden (2010), (http://su.diva-portal.org/smash/record.jsf?searchId=1&pid=diva2:373798
[8] BERGSTRAND, E.S., et al., An investigation of the photon energy dependence of the EPR alanine dosimetry system, Phys. Med. Biol. **48** (2003) 1753.
[9] NAGY, V., et al., Uncertainties in alanine dosimetry in the therapeutic dose range, Appl. Radiat. Isot. **56** (2002) 917.
[10] VESTAD, T.A., et al., EPR dosimetric properties of formats, Appl. Radiat. Isot. **59** (2003) 181.
[11] GUSTAFSSON, H., et al., Lithium formate EPR dosimetry for verifications of planned dose distributions prior to intensity-modulated radiation therapy, Phys. Med. Biol. **53** (2008) 4667.
[12] NAGY, V., et al., Advancements in accuracy of the alanine dosimetry system. Part 2: The influence of the irradiation temperature, Radiat. Phys. Chem. **57** (2000) 1.
[13] ANTONOVIC, L., et al., Evaluation of a lithium formate EPR dosimetry system for dose measurements around Ir-192 brachytherapy sources, Med. Phys. **23** (2009) 2236.
[14] WALDELAND, E., et al., Dosimetry of stereotactic radiosurgery using lithium formate EPR dosimeters, Phys. Med. Biol. **55** (2010) 2307.
[15] AHNESJÖ, A., ASPRADAKIS, M.M., Dose calculations for external photon beams in radiotherapy, Phys.Med.Biol **44** (1999) R99.

USE OF AN ANTHROPOMORPHIC PHANTOM TO IMPROVE THE EXTERNAL BEAM QUALITY AUDITS IN RADIOTHERAPY

J.L. ALONSO SAMPER
National Control Center for Medical Devices
Email: pepe.samper@infomed.sld.cu

R. ALFONSO-LAGUARDIA, F. GARCIA YIP,
E. LARRINAGA-CORTINA, J.L. MORALES-LOPEZ,
I. SILVESTRE-PATALLO
Department of Radiotherapy, Institute of Oncology and Radiobiology

Havana, Cuba

Abstract

The present paper describes the Cuban experience in the implementation of an external quality audit system for high energy radiotherapy photon beams (^{60}Co and linac) in non-reference conditions using a thorax (CIRS) phantom. By comparing the calculated and actually delivered doses for four test cases, it is possible to check the quality of the entire planning chain from prescription to delivery as well as the integrity of the beam data modelled into the treatment planning system (TPS). The test cases were taken/modified from IAEA TRS 430 and include direct, tangential, wedged, blocked and multiple fields, all commonly used in clinic. According to the available insertion holes in the phantom, a number of dose points were defined and calculated with four different clinical TPSs used in our environment. Subsequently the dose was measured at these points with an ionization chamber. A set of audit results with on-site measurement are shown to demonstrate the practicability of the method. The points were classified by regions according to their position with respect to the beam axis. The 90% of measured points were found within tolerance. For the failing 10% we found no correlation with TPS (centre) or with the complexity of the case. For all test cases, except the simplest one, at least one department/TPS prediction falls outside tolerance. There is no significant difference among the audited departments.

1. INTRODUCTION

The Cuban National Audit Program in Radiotherapy (NAPRAT) started in 2000 and is based on standardized on-site visits to the radiotherapy services. During the visit, the entire radiotherapy process is reviewed from the clinical and physical points of view. From the latter perspective, some predefined test cases

are evaluated to check for any significant discrepancy between prescribed and delivered dose.

In the first years of the programme, a fixed depth water phantom was used to check the output of each therapy beam and other relative dosimetric parameters. With time, a number of test cases were added to the audit to detect mechanical problems of the machines.

Based on the outcome of the IAEA coordinated research project E2.40.13, Development of Procedures for Quality Assurance for Dosimetry Calculation in Radiotherapy [1–4], the authors started to use an anthropomorphic phantom (CIRS thorax phantom) to check a broader range of treatment's techniques. In general, the methodology for the physical aspects of an audit visit was based on QUATRO recommendations [5], but a number of dosimetry clinical test cases were added.

In 2007, national guidelines for the audits were developed, based on QUATRO type audits recommendations, which allowed to quantify the audit results [6] within three categories: clinical, safety and quality control aspects.

The aim of the on-site visit is twofold: first, to promptly find weakness within the performances of the radiotherapy services of the kind that would lead to potential radiological risk situations related to patients, occupational workers or members of public; and second, to aid with its recommendations to the continuous improvement of the treatment quality.

2. MATERIAL AND METHODS

The phantom used was a CIRS thorax phantom model 002LFC (Computerized Imaging Reference Systems Inc., Norfolk, Virginia, United States of America) received through an IAEA Technical Cooperation project. This model was previously used by IAEA CRP E2.40.13 for clinical commissioning of treatment planning systems (TPSs).

When NAPRAT started in 2000, a fixed depth slab shaped water phantom was used for on-site TPS calculation and treatment delivery accuracy audits [7]. The acquisition of new technologies by the Cuban public health system, such as linear accelerators with multileaf collimators (MLC) and electronic portal imaging devices (EPIDs), computed tomography (CT) image based TPSs, access to CT scanners for treatment planning purposes, and more sophisticated immobilization devices, allowed the radiotherapy services to embark on a comprehensive transition to 3-D conformal radiotherapy following international recommendations [8]. Consequently, more complex test cases were required in order to evaluate the particular performance of 3-D image based treatment planning.

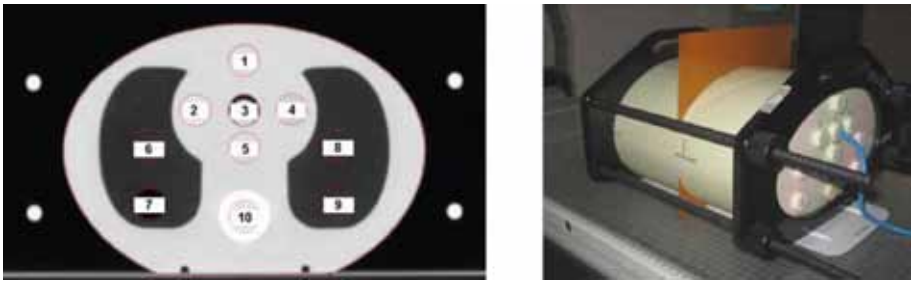

FIG. 1. CT slice of CIRS thorax phantom model 002LFC, showing the 10 insert positions. Labelling of holes and the recommended arrangement of the certified electron density reference plugs for CT scan: Plug 1 — water equivalent, plug 2 — muscle substitute, plug 3 — syringe filled with water, plug 4 — adipose substitute, plug 5 — water equivalent, plug 6 — lung substitute, plug 7 — should be empty to represent air, plugs 8 and 9 — lung substitutes, plug 10 — bone substitute.

The CIRS thorax phantom allows absolute and relative measurements with ionization chambers (IC) in ten different drilled positions, as well as the use of film in the sliced section, as shown in Fig. 1. The shape of the phantom is human torso-like and a CT calibration is possible using its tissue substitute inserts. The phantom provides IC holders made from lung, soft tissue and bone equivalent materials in order to perform measurements inside these materials. The IC holders of the CIRS phantom are designed to hold cylindrical, semiflexible type ICs. For auditing purposes, the semiflexible PTW 31010 (0.125 cm^3) was available. This IC ensures a good compromise between small size for reasonable spatial resolution and large sensitive volume for precise dose measurements. Its semispherical sensitive volume results in a flat angular response, which is a useful feature considering the different beam incidence angles used in the audit test cases.

Radiotherapy centres with high energy photon beams (^{60}Co, 6 MV and 15 MV) were audited. Four different TPSs were included in the study to calculate irradiation parameters and doses for the test cases: AMEPLAN v4.1 (in-house), Theraplan Plus v3.8 (NUCLETRON, Veenendaal, Netherlands), Precise Plan v2.16 (ELEKTA, Crawley, United Kingdom) and WIN-PLT (Nuclemed, Buenos Aires, Argentina).

A set of test cases was adopted from those proposed by the IAEA TRS 430 and adapted according to the authors' experiences. The tolerances and action levels were established in accordance with the complexity of the case and with the region of the beam profile where the measurement point was located. In

general, the accepted tolerance of the measurement was 2–3%, and in the penumbra region, it reached up to 2 mm.

2.1. Description of test cases

Prior to the TPS verification, during the EQAV, a redundant check of the absolute calibration is performed in a water phantom by the audit team. Once the agreement between the reference output established by the local physicist and the audit team is confirmed, then the audit of the treatment planning process can be performed.

The CT images of the phantom are loaded into the TPS. Before performing any planning, it is necessary to check the correctness of the CT number versus relative electron density curve. Based on the CT number, the TPS may report the densities of various inserts, which are checked against certificate; this is the test case '0'.

The test cases are designed in increasing complexity starting with test case 1, the purpose of which is to tune the IC calibration factor in the conditions of the phantom used.

Test case 1a is a simple 10 cm × 10 cm field, at source–surface distance (SSD) equal source–axis distance (SAD). Gantry 0°. Measurements are performed in holes 1, 3, 5, 9 and 10 of the phantom. The purpose of this test is to verify relative depth–dose data.

Test case 1b is a 30° wedged 10 cm × 10 cm field, gantry 0°, at SSD set-up. Measurements are performed in holes 1, 2, 3 and 4. The purpose is to verify wedge filter factor and wedged isodoses.

Test case 2a is a 15 cm × 10 cm tangential field, gantry 90°, SAD set-up. Measurements are taken in holes 1 and 3. The purpose is to verify off-axis profiles and the lack of lateral dispersion in the frequent tangential breast fields.

Test case 2b is a 10 W × 15 cm^2 tangential field, with a 30° wedge filter, gantry 90° and collimator of 270°. Measurements are performed in holes 1 and 3 of the phantom. The purpose is to verify the effect the lack of lateral dispersion in the presence of a wedge filter.

Test case 3 is a four field box, SAD set-up. AP and PA fields are 15 cm × 10 cm and the laterals 15 cm × 8 cm. Measurements are taken in the holes 5, 6 and 10 of the phantom. This is a frequently used treatment technique in our clinical practice and the purpose of this test is to verify the dose delivered by each field taking into account the heterogeneities that every of them passes through. The total dose from all the four fields is reported.

Test case 4 is a single 18 cm × 20 cm irregular field with a central block of 18 cm × 5 cm, gantry 0° at SSD set-up. Measurements are taken in the holes number 2, 3 and 8 of the phantom. The goal of this test is to verify the TPS

performance in conditions with lack of lateral scatter and to check the dose calculation accuracy both in the irradiated and blocked regions.

The dose comparison criteria between measured and calculated doses were adopted from the IAEA TRS 430, Table 18. The dose deviation was calculated using the following equation:

$$\text{Deviation [\%]} = 100*(D_{cal} - D_{meas})/D_{meas,ref} \quad (1)$$

where $D_{meas,ref}$ is the measured dose at the reference point (prescription).

3. RESULTS

The following are the results from four audit visits to radiotherapy centres that utilize the different TPSs previously mentioned. Figure 2 shows the dose distribution for the four test cases.

The results shown in Table 1 are relative to the value measured in point 3 of test case 1a, which serves as a reference output. Consequently, the difference

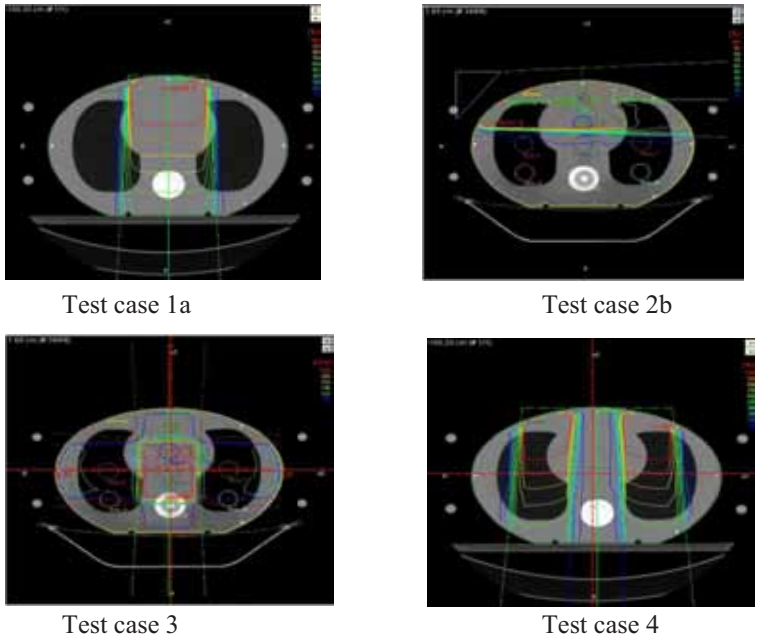

FIG. 2. Dose distributions obtained with TPS on the CIRS phantom with test cases.

TABLE 1. DISCREPANCIES BETWEEN MEASURED AND PRESCRIBED DOSES PER HOLE PER TEST CASE, ACCORDING TO THE TPS USED

Case	Hole	Hospital[a] w/ TPS-1	Hospital w/ TPS-2	Hospital w/ TPS-3	Hospital w/ TPS-4	Type[b]	Tolerance[c]	No. of results outside tolerances
1a	1	0.3	–1.7	0.52	–0.3	Central axis	2	0
	3	0.0	0.0	0.0	0.0	Central axis	2	0
	5	–0.1	0.6	–0.3	–0.1	Central axis	2	0
	9	–1.6	2.9	–1.5	4.7	Outside beam edges/in lung	5	0
	10	1.1	–0.3	0.4	1.6	Central axis/in bone	3	0
1b	1	–1.7	2.3	3.5	–0.3	Central axis/wedge	3	1
	3	0.0	0.0	2.1	–0.9	Central axis/wedge	3	0
	2	–2.7	–1.2	3.5	–0.3	Off-axis/wedge	4	0
	4	–0.1	–1.0	4.8	–0.1	Off-axis/wedge	4	1
2a	1	6.6	4.3	–0.2	0.5	Central axis/lack of scatter	3	2
	3	–3.3	1.9	0.8	1.5	Penumbra/beneath lung	15	0
2b	1	4.5	1.8	–3.3	0.2	Central axis/wedged/lack of scatter	4	1
	3	4.9	7.1	–3.9	2.1	Penumbra/wedged/beneath lung	15	0

TABLE 1. DISCREPANCIES BETWEEN MEASURED AND PRESCRIBED DOSES PER HOLE PER TEST CASE, ACCORDING TO THE TPS USED (cont.)

Case	Hole	Hospital[a] w/ TPS-1	Hospital w/ TPS-2	Hospital w/ TPS-3	Hospital w/ TPS-4	Type[b]	Tolerance[c]	No. of results outside tolerances
3	5	0.1	0.1	0.5	1.6	Central axis/inhomogeneities.	3	0
	6	0.2	1.7	–1.4	1.2	Central axis/inhomogeneities	3	0
	10	–1.7	1.7	6.8	0.4	Central axis/inhomogeneities	3	1
4	2	–0.9	0.9	3.7	0.4	Off-axis/irregular/lack of scatter	3	1
	3	4.6	0.4	–1.5	0.6	Off axis/irregular/blocked/lack of scatter	5	0
	8	–3.0	9.8	1.5	1.4	Off-axis/irregular/in lung	3	1

[a] TPS number refers to the four different TPS audited.
[b, c] Taken from Table 18, Ref. [7].

between the calculated and measured dose in this point is zero. In all cases, the dose to the prescription point is 100 cGy.

The four test cases also evaluated relative doses at points different from the prescription one, assisting in the detection of problems in the whole treatment chain. These problems could be divided into the following categories:

— Mechanical problems inherent to the treatment unit.
— Patient data acquisition (CT) (tissue relative electronic density errors assignment).
— Input data in the TPS. (PDD, profile, output factors, wedge factors, etc.).
— Calculation algorithms, tissue inhomogeneities, lateral dispersion approximation, block transmission, field shape considerations, etc.
— Data transmission/communication between the TPS and the treatment machine.
— Human error during planning.
— Human error during positioning and immobilization.

All TPSs were commissioned before their clinical use and the results of these processes were within the allowed tolerance. This is assured by the clinical acceptance report provided by the National Control Center for Medical Devices.

Thus, in general, no significant discrepancies were found in the measured dosimetry data (absolute calibration, relative dose factor, wedge factors, etc.), nor in the actual beam data used in the TPSs. This reflects the accumulated experience of the medical physicists, the impact of several years of systematic on-site and postal audits, as well as the fact that the commissioning of every treatment unit and TPS is redundantly reviewed by an independent physics team, which performs several end-to-end tests.

The numerical values do not reflect all the discrepancies associated with mechanical inaccuracies of the audited treatment unit, since some were corrected during the auditing process. Nevertheless, this has been an important source of discrepancies, since in some cases, the mechanical faults of the machines caused differences of over 2% between measurement and calculation.

The most demanding test is probably the 2b, because it combines difficulties such as the lack of tissue, heterogeneities, lack of lateral scatter and off-axis measurement. The measurement at point 1 of this test is critical because this hole falls in the penumbra region.

One of the TPSs uses only predefined bulk density inhomogeneity corrections, so it does not consider the actual CT based electron density of the phantom. The discrepancies found, in the hospital with the TPS 1, between the prescribed and measured dose, were mainly due to TPS 1 not considering the lack in lateral dispersion and therefore, the results of the calculations failed in complex situations. Based on this finding, the TPS 1 is gradually being replaced.

The main source of error was the human factor during planning and the phantom set-up. These activities were not independently doubled checked during the EQAV. It must be mentioned that, in daily practice, the treatment plans are checked redundantly. This is not the case for the patient set-up, since portal images are not acquired and an independent check of the patient positioning by another therapist is not performed either, although according to the procedures for patient set-up, the presence of a second therapist within the treatment room is mandatory.

To check the DICOM plan data transfer from TPS to the control console, a printout of the plan is produced and visually compared by the auditor against the parameters displayed by the treatment console. Errors related to this data transmission were not found.

The phantom set-up was critical in several points where a 2 mm difference can create a discrepancy of about 5% for linacs and 10% for cobalt units.. In addition, a source of uncertainty is attributable to calculating the dose value at a single point, instead of the averaged dose over a region of interest that is representative of the IC volume. This would be considered in future developments of this research.

The measured doses in the prescription point showed discrepancies no greater than 2%, but in other points, some discrepancies exceeded the permissible values, as shown in column 8 of Table 1. This allowed a better understanding of the weaknesses of the method in a particular TPS and provided further information about potential corrections to reported doses in complex points of interest (regions as lung, bone, lack of lateral dispersion, etc.).

4. CONCLUSIONS

The authorshave followed the IAEA recommendations for radiotherapy quality audits (IAEA-TECDOC-1543), but have extended the recommended benchmark test cases to dosimetry measurements in conditions closer to the clinical practice. Other audit groups have implemented similar procedures [3].

Since its implementation four years ago, the quantification of the discrepancies between prescribed and delivered doses using the CIRS phantom during the EQAV has improved the clinical dosimetry of the treatments, the radiation protection of patients and the quality assurance of the treatment process.

Additional test cases are being designed and evaluated to check modern techniques implemented in the audited radiotherapy services, such as IMRT, stereotactic body radiotherapy and HDR applications.

REFERENCES

[1] GERSHKEVITSH, E., et al., Dosimetric Verification of Radiotherapy Treatment Planning Systems: Results of IAEA Pilot Study, Radioth. Oncol. **89** (2008) 338–346.

[2] INTERNATIONAL ATOMIC ENERGY AGENCY, Commissioning of Radiotherapy Treatment Planning Systems: Testing for Typical External Beam Treatment Techniques, IAEA-TECDOC-1583, IAEA, Vienna (2008).

[3] GERSHKEVITSH, E., PESHNYAK, C., VATNITSKY, S., Audit of 3D conformal radiotherapy treatment planning systems, SSDL Newsletter No. 58, June 2010, IAEA (2010) 40–42.

[4] IZEWSKA, J., BERA, P., AZANGWE, G., VATNITSKY, S., ROSENBLATT, E., ZUBIZARRETA, E., "The IAEA quality audits for radiotherapy", Standards, Applications and Quality Assurance in Medical Radiation Dosimetry (Proc. Int. Symp. Vienna, 2010) (this Proceedings).

[5] INTERNATIONAL ATOMIC ENERGY AGENCY, On-site Visits to Radiotherapy Centres: Medical Physics Procedures, IAEA-TECDOC-1543, IAEA, Vienna (2007).

[6] ALONSO-SAMPER, J.L., ALFONSO-LAGUARDIA, R., GARCIA-YIP, F., Quantification of Results of External Quality Audit Visits in Radiotherapy, Proc. 4th Latin American Congress on Medical Physics, Cartagena de Indias, Colombia (2007).

[7] INTERNATIONAL ATOMIC ENERGY AGENCY, Commissioning and Quality Assurance of Computerized Planning Systems for Radiation Treatment of Cancer, Technical Reports Series No. 430, IAEA, Vienna (2004).

[8] INTERNATIONAL ATOMIC ENERGY AGENCY, Transition from 2-D Radiotherapy to 3-D Conformal and Intensity Modulated Radiotherapy, IAEA-TECDOC-1588, IAEA, Vienna (2008).

IAEA SUPPORT TO NATIONAL TLD AUDIT NETWORKS FOR RADIOTHERAPY DOSIMETRY

J. IZEWSKA, P. BERA, G. AZANGWE
International Atomic Energy Agency,
Vienna
Email: j.izewska@iaea.org

D. THWAITES
Leeds University Hospital,
Leeds, United Kingdom

D. GEORG
Medical University of Vienna,
Vienna, Austria

D.S. FOLLOWILL
Radiological Physics Center, M.D. Anderson Cancer Center,
University of Texas, Houston,
Texas, United States of America

Abstract

For several years, the IAEA has supported the development of methodology and establishment of national quality audit networks for radiotherapy dosimetry. The main objective was to extend the availability of radiotherapy dosimetry audits to as many radiotherapy centres as possible throughout the world. Since 1995, a series of three coordinated research projects (CRPs) has been conducted by the IAEA to assist its Member States to develop such national audit programmes. The first CRP focused on the basic beam calibration audits. The basic programme was extended to audits in non-reference conditions through a second CRP. The third CRP initiated in 2009 is expanding the dosimetry audit tools for more complex techniques used for treatment of cancer patients. The national audit networks participating in these CRPs have incorporated in their programmes procedures for auditing hospital dosimetry for these techniques.

1. INTRODUCTION

For about 15 years, the IAEA has encouraged and supported the development of methodology, establishment and operation of national activities

for dosimetry audit in radiotherapy [1]. The main objective is to ensure that dosimetry audits are made available to the largest possible number of radiotherapy centres in the world due to the considerable advantages of participating in the audit [2]. Audits verify whether the quality of dosimetry practices in a radiotherapy centre is adequate; they also contribute to quality improvement and increased safety of radiation treatments.

National auditing activities complement the IAEA/WHO postal dose audit service using the thermoluminescent dosimeter (TLD) [3–4] that the IAEA Dosimetry Laboratory has been providing for over four decades [5] to about 1700 radiotherapy centres in 120 countries worldwide. The national developments in dosimetry audit allow the IAEA to utilize the resources in cost effective manner and focus on providing the IAEA/WHO audits to the centres that do not have, other than the IAEA, access to verification of their dosimetry practices.

Since 1995, a series of three coordinated research projects (CRPs) has been conducted by the IAEA to assist in developing such national dosimetry audit programmes, initially for beam calibration audits in reference conditions [1, 6]. This work was then extended for audits in non-reference conditions [7], to further improve independent verification of radiotherapy dosimetry in hospitals. Current work focuses on expanding the dosimetry audit tools to be suitable for complex techniques used for radiation treatments of cancer patients. The methodologies for verifying the dose at these different complexity levels have been developed at the IAEA and tested in pilot study in conjunction with CRP participants. The IAEA's Dosimetry Laboratory contributed to these developments and provided external quality control of the national TLD systems by exchanging dosimeters with the national laboratories. These developments are described below.

2. IAEA CRPS ON DOSIMETRY AUDIT IN RADIOTHERAPY

2.1. CRP–1: Setting-up national external audit groups for a basic dosimetry audit

CRP–1 entitled Development of a Quality Assurance Programme for Radiation Therapy Dosimetry in Developing Countries was initiated in 1995. It had the aim of transferring TLD postal audits methodology to the national level using the long standing IAEA experience in this area. Through participation in this initial CRP, 12 countries established External Audit Groups (EAGs) for radiotherapy dosimetry: Algeria, Argentina, China, Colombia, Cuba, Czech Republic, India, Israel, Malaysia, Philippines, Poland and Vietnam. The CRP–1 provided a framework for setting up a national structure within which it was possible to establish and manage radiotherapy dosimetry audits and other linked

quality assurance activities. A standardized methodology for measurements, the same for all participating countries, was developed [6].

This initial CRP–1 was focused on the most basic level of radiotherapy dosimetry audit, i.e. the beam output check in reference conditions for high energy photon beams. The basis for the measurements retained the IAEA audit approach of using the most cost effective method of carrying out an external audit for large number of radiotherapy centres and for large geographic areas, i.e. using mailed TLD as well as the IAEA holders and procedures. A structure for a technical backup to the national EAG work was also established at the IAEA Dosimetry Laboratory. The countries set up their TLD systems with technical support from the IAEA. Initial pilot TLD runs were conducted with a few local hospitals to test methods, instructions and data sheets, and later the audit programme was extended to all hospitals in the country.

2.2. CRP–2: Dosimetry audits in non-reference conditions

Following the closure of the CRP–1, the IAEA continued the support of the national EAGs in 2001–2006 by conducting a second project (CRP–2) Development of TLD-Based Quality Audits for Radiotherapy Dosimetry in Non-Reference Conditions. This project grew naturally from the work of the earlier CRP–1 and also from the clear evidence available from other audit systems [8, 9] that it is necessary to check other additional parameters, in order to further improve the quality of radiotherapy in participating centres. The objective of the CRP–2 was then to extend the scope of activities of the national audit programmes from the basic beam output check to more complex audit measurements in clinically relevant regular irradiation geometries, i.e. in non-reference conditions, and also to provide the initial basis for auditing other radiotherapy modality beams. The aims included assisting the national EAGs in developing a systematic approach for these audits, with a structured programme gradually increasing the complexity of the dosimetry parameters audited. It aimed to address the specific needs of individual participating countries in order to provide models and experience for a range of different national situations. The participants of the CRP–2 were the EAGs of Algeria, Argentina, Bulgaria, China, Cuba, India and Poland.

2.3. CRP–3: Dosimetry audits for complex treatment techniques

Further development has subsequently progressed within the IAEA framework and the still ongoing CRP–3 Development of Quality Audits for Radiotherapy Dosimetry for Complex Treatment Techniques was initiated in 2009 as an extension of the audit steps previously developed and tested. It is

developing and testing another three levels of radiotherapy dosimetry audit to cover the initial essential stages for more complex treatments. This was set up recognizing that more treatment machines are being installed in the IAEA Member States with the capability of providing new treatment techniques such as intensity modulated radiotherapy (IMRT); such increasingly complex treatments require more sophisticated modelling by the treatment planning system (TPS) and more complex dosimetry, quality assurance (QA) and verification of treatment dose delivery. The national EAGs involved as participants in the CRP–3 are those of Algeria, Argentina, Brazil, China, Czech Republic and Poland.

2.4. Common methodology for dosimetry audits in radiotherapy developed under the three CRPs

The audit methodology developed under the three CRPs follows the overall philosophy of the IAEA audit programme of step by step extension of audits for increasing levels of complexity of radiotherapy dosimetry. Each audit step considers critical and significant clinical radiotherapy dosimetry parameters and builds on the experience of the previous audit steps. In each case, the approach ensures that basic dosimetry parameters are audited successfully before more complex audit levels are launched. The fully developed and tested dosimetry audit steps 1–3 from CRP–1 and CRP–2 are summarized below, together with the audit steps 4–6 for complex treatment techniques still under development and test in the current CRP–3:

Step 1: Postal dose audits for high energy photon beams in reference conditions. It is necessary for any of the audit systems to successfully implement this initial step before beginning any subsequent audit step.

Step 2: Postal dose audits for photon and electron beams in reference and non-reference conditions, on the beam axis. This includes checks of dose variation with field size and wedge transmission for photon beams, checks of electron beam output as well as dose variation with field size and treatment distance for electron beams.

Step 3: Postal dose audits for photon beams in reference conditions and in non-reference conditions off-axis. This includes checks on selected points in beam profiles, with and without wedges, for both symmetric and asymmetric fields in these beams.

Step 4: Postal dose audits for photon beams shaped with a multileaf collimator (MLC). This entails checks on the beam axis of dose variation with field size and shape for a range of MLC shaped regular and irregular fields, including wedged fields. It also includes auditing of the hospital method to calculate these dosimetric parameters; this is to be performed with the local TPS.

Step 5: Postal dose audits for photon beams in the presence of heterogeneities. This will include checks in solid phantoms of doses, both on and off the beam axis, and both inside and beyond heterogeneities, in order to test TPS and local implementation of approaches for dosimetry modelling and calculation of corrections for the presence of lung and bone in treatment beams.

Step 6: Postal dose audits of two dimensional small field distributions. This will include checks using radiochromic film in solid phantoms of dose profiles, particularly penumbra, to test the local TPS modelling for small fields as a necessary parameter for accurate modelling for IMRT.

Considering the developments of radiotherapy technology and treatment techniques, and the request by participating EAGs, it is anticipated that future developments within this framework will use solid phantoms and 2-D dosimetry to propose new methodology for subsequent audit levels to check IMRT and other advanced delivery technology.

2.5. National studies to implement the TLD audit methodology

In order to implement the TLD based quality audits for radiotherapy dosimetry at the national level as developed within the three IAEA CRPs, the EAGs of each participating country conducted several studies to adapt the CRP procedures to their own specific situation. Each EAG has developed a procedural manual outlining the specific steps and measurements, instructions, data forms and logistics of operating the quality audit. In addition, each EAG conducted its own feasibility studies to assess the functionality and accuracy of the TLD holders used for the audit and of the documentation to measure the dosimetry parameters proposed within the CRPs. These feasibility studies encompassed several tests to determine the full set of parameters for the national TLD audit systems. In this process, any pitfalls of the proposed approach to these quality audits were identified and corrected. In parallel to the above activities, comparisons of the EAG TLD systems with the IAEA's Dosimetry Laboratory were conducted. Finally, the national EAGs launched the now tested and agreed quality audit programme for radiotherapy dosimetry in their own countries, first on a pilot basis, and then including several local radiotherapy centres.

3. SUPPORT TO THE NATIONAL AUDIT ACTIVITIES BY THE IAEA DOSIMETRY LABORATORY

The IAEA Dosimetry Laboratory has actively participated in the experimental part of the programme above, developed new TLD holders and dosimetry phantoms, and conducted feasibility studies, as well as multicentre

pilot studies to test the newly developed dosimetry audit methodologies before they were tested at the national level.

An example illustrating such work is the multicentre pilot study for audit step 3: photon beam checks in non-reference conditions off-axis utilizing a modified IAEA TLD holder with a horizontal arm [7, 10]. The results of the recently performed multicentre pilot study for the audit step 4, i.e. MLC checks on-axis, are given in Fig. 1. The CRP participants irradiated TLDs as per newly developed instructions using high energy photon beams available in their centres and several MLC field arrangements. They calculated the dose to TLD using their TPSs. They reported the irradiation details in newly developed datasheets and returned TLDs to the IAEA for evaluation together with comments regarding the clarity of instructions and data forms. Following this study, the participants adopted the methodology to the national level and organized pilot exercises involving a few local radiotherapy centres and the local TLD laboratory.

The EAG network of auditing systems closely cooperates with the IAEA Dosimetry Laboratory for these developments and also it exchanges dosimeters and carries out cross-measurements for on-going quality control of the local TLD systems. The IAEA provides EAGs with TLDs for irradiation within the framework of the regular IAEA dosimetry audit programme for secondary standards dosimetry laboratories. In addition, EAGs are encouraged to send to the IAEA their TLDs for reference irradiation and 'blind check'. The IAEA irradiates

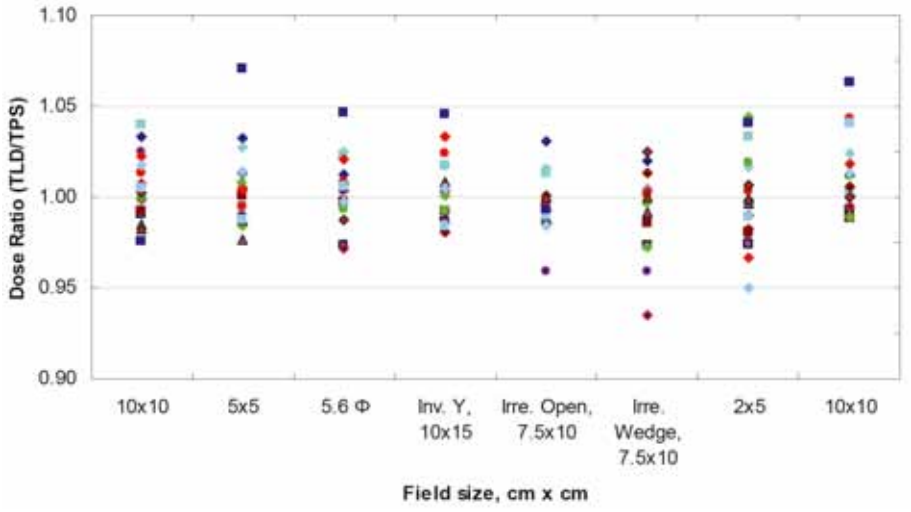

FIG. 1. Results of a multicentre pilot study for the audit step 4. Individual symbols correspond to the results by different CRP participants. The high energy X ray beams used are 6, 10 , 15 and 18 MV.

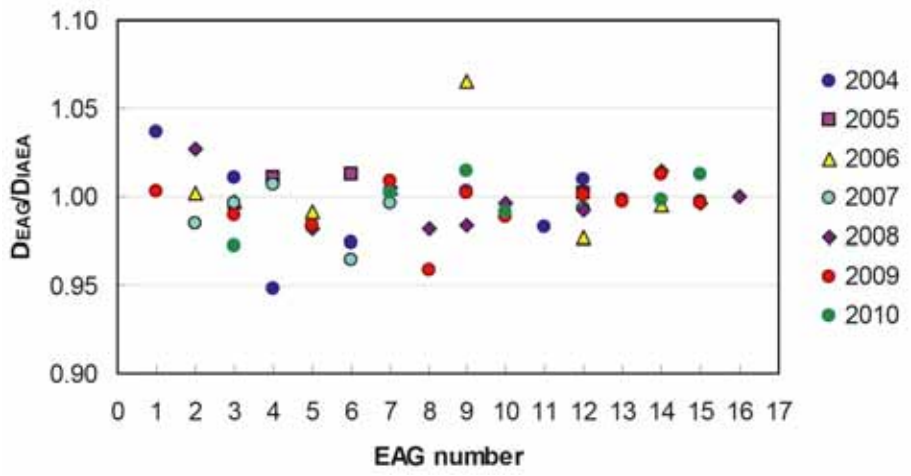

FIG. 2. The results of the EAG blind checks in 2004–2010.

a few TLD sets with a range of well defined doses and an additional TLD set with a dose that is not communicated to the EAG (blind check). The EAGs use the reference TLDs irradiated with known doses for the calibration of their TLD systems and evaluate the 'blind TLDs' based on this calibration. Upon reporting the 'blind doses' to the IAEA, the actual dose delivered to the TLDs is communicated back to the EAG.

The results of blind checks in 2004–2010 are shown in Fig. 2. To date, 16 national EAGs participated in this programme with different frequencies. In all, 53 blind check irradiations were provided by the IAEA with the mean of the D_{EAG}/D_{IAEA} distribution of 0.997 and the relative standard deviation of 0.018. On a few occasions, this programme revealed problems with the performance of local TLD systems and with the implementation of TLD evaluation methodology. All discrepancies between the EAG evaluated dose (D_{EAG}) and the IAEA delivered dose (D_{IAEA}) were discussed with the EAGs. Most problems were caused by poor stability of TLD readers at the time of the measurements, which increased uncertainties temporarily. However, on two occasions, laboratories used inadequate TLD readout and evaluation procedures. Some laboratories, where problems were observed initially, have been able to rectify them in subsequent participations (see Fig. 2).

4. CONCLUSION

The IAEA has a long standing history providing support and assistance for radiotherapy dosimetry audits in Member States. It has supported the development of methodology and establishment of national TLD based QA audit networks for radiotherapy dosimetry in order to cost effectively utilize IAEA resources and to extend the availability of radiotherapy dosimetry audits to as many hospitals as possible throughout the world.

Since 1995, a series of CRPs has been conducted by the IAEA to assist in developing such national dosimetry audit programmes. The overall radiotherapy dosimetry audit approach established and developed throughout these CRPs is based on a process of increasingly complex steps and parameters being checked. This approach was developed in order to have a clear rationale, relevant to radiotherapy accuracy, quality and safety, in the use of resources and efforts. It was also developed so that experience of previous levels is used to inform development, implementation and analysis of results for subsequent levels.

Through the link with the IAEA Dosimetry Laboratory, the national audit networks closely cooperate at the consecutive stages of developing the dosimetry audit methodology locally and by carrying out cross-measurements. In this way, the EAG systems are interlinked to ensure that international and national radiotherapy dosimetry audit networks are working to the consistent levels and standards. Currently, the cross-measurement programme is regularly carried out between the IAEA Dosimetry Laboratory and several national and international audit programmes. When broadly implemented, the network of national audit groups for radiotherapy dosimetry will significantly contribute to ensuring the consistency of quality in dosimetry in radiotherapy centres worldwide.

ACKNOWLEDGEMENTS

The development of dosimetry audit procedures for national TLD networks has been conducted through a series of IAEA consultancies. Special contributions to these developments have been provided by A. Dutreix (France) in the first CRPs. National EAGs are acknowledged for their work, local developments and testing the new TLD audit methods and phantoms.

REFERENCES

[1] IZEWSKA, J., THWAITES, D.I., "IAEA supported national thermoluminescence dosimetry audit networks for radiotherapy dosimetry: Summary of the posters presented in session 12b", Standards and Codes of Practice in Medical Radiation Dosimetry (Proc. Int. Symp. Vienna, 2002), IAEA, Vienna (2003) 249–267.

[2] THWAITES, D.I., The significance and impact of dosimetry audits in radiotherapy, IAEA/WHO Vienna, Austria, SSDL Newsletter **58** (2010) 7–9.

[3] SVENSSON, H., HANSON, G.P., ZSDANSKY, K., The IAEA/WHO TL dosimetry programme for radiotherapy centres 1969–1987, Acta Oncol. **29** (1990) 461–467.

[4] IZEWSKA, J., ANDREO, P., The IAEA/WHO TLD postal programme for radiotherapy hospitals, Radiother. Oncol. **54** (2000) 65–72.

[5] IZEWSKA, J., AZANGWE, G., BERA, P., 40 years of the IAEA/WHO TLD postal dose audits for radiotherapy, IAEA/WHO Vienna, Austria, SSDL Newsletter **58** (2010) 17–23.

[6] IZEWSKA, J., et al., Guidelines for the Preparation of a Quality Manual for External Audit Groups on Dosimetry in Radiotherapy, IAEA/WHO Vienna, Austria, SSDL Newsletter **46** (2002) 2–13.

[7] IZEWSKA, J., et al., A methodology for TLD postal dosimetry audit of high-energy radiotherapy photon beams in non-reference conditions, Radiotherapy and Oncology, **84** (2007) 67–74.

[8] FERREIRA, I.H., DUTREIX, A., BRIDIER A., SVENSSON, H., "ESTRO European assurance programme for radiation treatments (the EQUAL network)", Standards and Codes of Practice in Medical Radiation Dosimetry (Proc. Int. Symp. Vienna, 2002), IAEA, Vienna (2003) 157–165.

[9] MOLINEU, A., FOLLOWILL, D.S., BALTER, P.A., et al., Design and implementation of an anthropomorphic quality assurance phantom for intensity-modulated radiation therapy for the Radiation Therapy Oncology Group, Int. J. Rad. Onc. Biol. Phys. **63** (2005) 577–583.

[10] HULTQVIST, M., FERNANDEZ-VAREA, J.M., IZEWSKA, J., Monte Carlo simulation of correction factors for IAEA TLD holders, Phys. Med. Biol. **55** (2010) N161–N166.

RADIATION PROTECTION DOSIMETRY

(Session 8)

Chairperson

Z. KNEZEVIC
Croatia

Co-Chairperson

R. CRUZ-SUÁREZ
IAEA

ESTIMATION OF HAND DOSES FROM POSITRONS DURING FDG MANIPULATION

M. FÜLÖP
Slovak Medical University
Email: marko.fulop@szu.sk

I. MAKAIOVÁ
OUSA

P. POVINEC, D. BACEK, P. VLK
BIONT

P. RAGAN
ÚVZ SR

Bratislava, Slovakia

I. GOMOLA
IBA Dosimetry,
Schwarzenbruck, Germany

V. HUŠÁK
University Hospital Olomouc,
Czech Republic

Abstract

A method of positron dose estimation is based on measurements performed with two thermoluminescent dosimeters (TLDs) with different detection sensitivity to positrons and photons. Detection efficiencies of both dosimeters were determined by experiments with a plane source of ^{18}F shielded by polyethylene layers of various thicknesses. The contribution of positrons to the skin dose during preparation and administration of FDG to patients was investigated by measuring dose distribution on the hands of nuclear medicine staff. A significant decrease of the skin dose caused by positron irradiation of the hands can be achieved by an additional local shielding of infusion tubes and syringes by a plastic material of a thickness of 1.5 mm. The use of silicon thimbles with a thickness of 1.5 mm applied to the tips of index fingers and thumbs is also recommended, as these areas are usually exposed to the highest dose levels, with a significant component of positron irradiation. The proposed radiation protection measures may decrease the maximum hand skin doses by approximately 30%.

1. INTRODUCTION

During manipulation with FDG (^{18}F-FDG), the hands of nuclear medicine staff are often irradiated by positrons that penetrate the walls of syringes or infusion tubes, or are emitted from surfaces contaminated by ^{18}F-FDG. A skin dose due to positrons is much more localized than a dose due to gamma radiation; therefore, in a mixed positron–gamma radiation field, it is necessary to measure both components separately. This is not an easy task, because dosimeters designed to measure positrons dose are also sensitive to photons.

2. MATERIALS AND METHODS

A method of positron dose estimation is based on measurements with two different types of commercially available thermoluminescent dosimeter (TLDs (Poland)), each with a different detection sensitivity to positrons and photons. The first type is the MCP-Ns (LiF: Mg, Cu, P) with an active layer thickness of 0.05 mm (tissue equivalent thickness of 0.07 mm), designed to measure $H_p(0.07)$; the second TLD is the MCP-7 (LiF: Mg,Cu,P) type with a thickness of 0.9 mm. Both TLDs are in the form of circular pellets with a diameter of 4.5 mm. Differences in the detection sensitivities between the two different types of TLD exposed by ^{18}F-FDG are caused by various thicknesses of their sensitive layers, as described in Refs [1] and [2]. According to this study, the thermoluminescent (TL) signal for various thicknesses of TLD irradiated by beta particles is given by the following equation:

$$TL = C \cdot \left(1 - e^{-bd}\right) \tag{1}$$

where C is a proportionality constant, b is a constant dependent on dosimeter material properties for a given beta source and the geometry of the irradiator, and d is the thickness of the sensitive layer. Taking into account the differences in the thickness of the active layers of the tested TLDs, MCP-Ns and MCP-7, differences in their positron detection efficiency are assumed.

The value of parameter b for a positron source ^{18}F was determined experimentally by using pairs of TLDs MCP-7 and MCP-Ns, which were placed at the same positions on the fingers of the hand phantoms, as shown in Fig. 1. Between TLDs and the positron source layers of polyethylene of thicknesses

FIG. 1. Measurement of skin dose by pairs of TLDs MCP-7 and MCP-Ns placed on the finger phantom. The plane source of positron ^{18}F-FDG is at a distance of 2 cm under the finger.

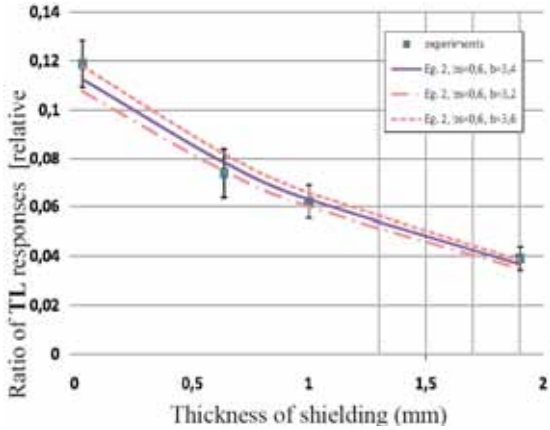

FIG. 2. Ratios of TL responses of MCP-Ns to MCP-7 with respect to the polyethylene shielding thickness.

0.032 mm, 0.635 mm, 1 mm and 1.9 mm were inserted. Ratios of MCP-Ns to MCP-7 TL responses are shown in Fig. 2.

By modifying Eq. (1), taking into account the attenuation of positrons in the shielding material, the measured data in Fig. 2 can be approximated by the equation:

$$\frac{TL^{MCP-Ns}}{TL^{MCP-7}} = C \cdot e^{-b_s d_s} \cdot \frac{1-e^{-0.05b}}{1-e^{-0.9b}} \qquad (2)$$

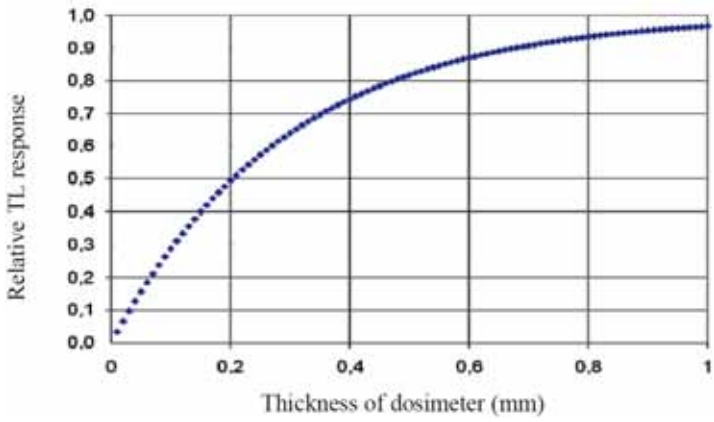

FIG. 3. TL response to positrons emitted by ^{18}F versus thickness of TLD material of LiF: Mg,Cu,P.

where $b_s = 0.6$ is constant dependent on the shielding material properties for the positron source and the geometry of irradiation, d_s is the thickness of the shielding, constants 0.05 and 0.9 are thicknesses of MCP-Ns and MCP-7, and $b = 3, 4$ for both types of TLD.

Relative differences between measured data and approximation relation (2) (for $b = 3, 4$) in Fig. 2 are less than 10%.

TL response versus detector thickness calculated by using Eq. (1) for $b = 3, 4$ is shown in Fig. 3.

From Fig. 3, the ratio of TL sensitivities of MCP-7 to MCP-Ns for positron detection is 6.0. The TL sensitivities of MCP-7 and MCP-Ns for detection of positrons are significantly different. Thus by the use of pair MCP-7 and MCP-Ns on the hands of nuclear medicine staff, measurement of both gamma and positron components of hand irradiation during manipulation with ^{18}F-FDG could be performed.

In positron and gamma mixed fields the value of gamma (γ) and positron (p) components can be assessed from measured TL responses of MCP-7 ($TL_{\gamma+p}^{MCP-7}$) and MCP-Ns ($TL_{\gamma+p}^{MCP-Ns}$) and by solving the following equations:

$$TL_{\gamma+p}^{MCP-7} = TL_{\gamma}^{MCP-7} + TL_{p}^{MCP-7} \tag{3}$$

$$TL_{\gamma+p}^{MCP-Ns} = TL_{\gamma}^{MCP-Ns} + TL_{p}^{MCP-Ns} \tag{4}$$

$$TL_{p}^{MCP-7} = 6.0 \cdot TL_{p}^{MCP-Ns} \tag{5}$$

$$TL_{\gamma}^{MCP-7} = 27 \cdot TL_{\gamma}^{MCP-Ns} \quad (6)$$

$$TL_{p}^{MCP-Ns} = 0.95 \cdot TL_{p}^{MCP-Ns} \quad (7)$$

The coefficient of 27 is the ratio of TL sensitivities of MCP-7 to MCP-Ns for photons using a ^{137}Cs calibration source. The last equation is based on beta energy response with respect to ^{60}Co of MCP-Ns irradiated with ^{147}Pm, ^{204}Tl and ^{90}Sr/^{90}Ir sources [3].

3. EXPERIMENTAL RESULTS

The TLDs were calibrated with ^{137}Cs gamma source with a dose close to 5 mGy, and the readout was performed with a Harshaw-Bicron 3500 reader in a nitrogen atmosphere.

TLDs MCP-7 and MCP-Ns, in close proximity, were encapsulated into a polyethylene foil with a thickness of 0.03 mm and attached to latex gloves. Twelve various locations on both hands, including those that usually receive the highest skin dose (i.e. underneath the tips and the nails of index fingers and thumbs), were chosen for placing the TLD pairs to estimate the skin doses during a real preparation and administration of ^{18}F-FDG to patients in a nuclear medicine department (see Fig. 4).

Differences of the dose responses in the pairs of TLDs of the same type (MCP-7) reached up to approximately 25% (Fig. 5).

These differences are, for example, due to various positions of TLDs, energy and angular dependences, batch uniformity and calibration procedure. The

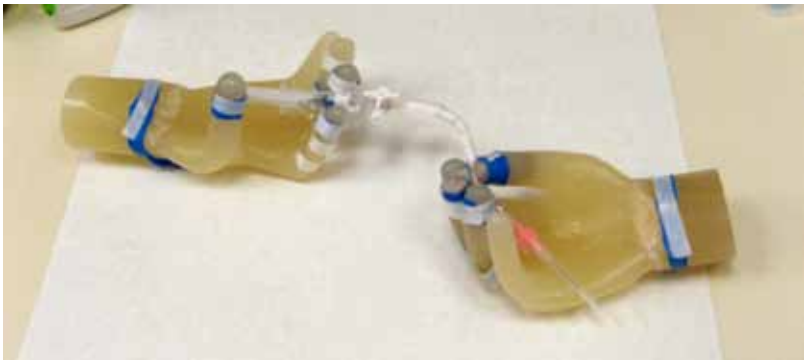

FIG. 4. Measurement of skin dose by pairs of TLDs MCP-7 and MCP-Ns on hands with an unshielded syringe (left) and with an infusion tube (right), both filled by ^{18}F-FDG.

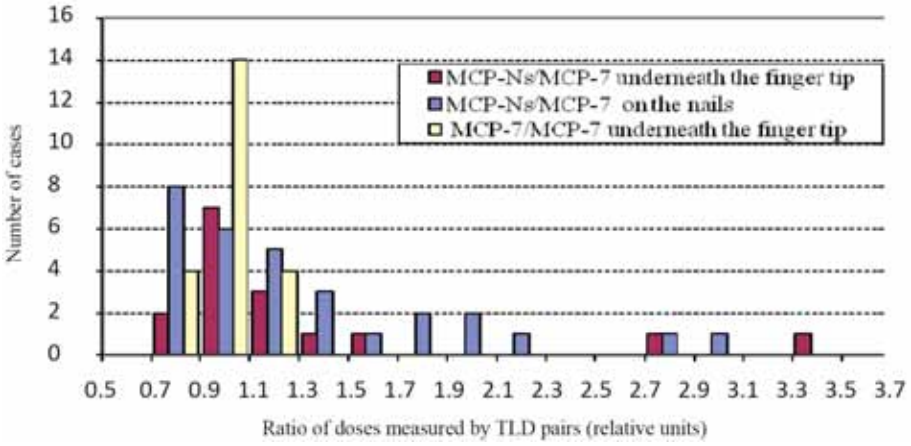

FIG. 5. Frequency distribution of the ratios of the doses measured by TLD pairs at the tips of the index fingers.

contribution of positrons to the total dose can be considered only if the ratio MCP-Ns/MCP-7 is higher than 1.25. Taking this into account, the authors observed that a positron dose contributed to the total skin dose in about 30% of monitored cases (15 monitored cases out of 46). A 'monitored case' is one monitored by a physician or radiopharmacist at a PET department during two working days.

The contributions of positrons to the total skin dose given in Table 1 were determined from measurements using TLD pairs on hand phantoms holding an unshielded syringe, distribution vent and infusion tube. The last row of Table 1 contains the ratio and contribution of positron skin dose using measurements on a finger phantom contaminated by ^{18}F-FDG. Experimental determination of the contribution of positron dose from an infusion tube to the total skin dose $H_p(0.07)$ is in a good agreement with theoretical calculations published in Ref. [4].

4. CONCLUSIONS

A method for estimating skin doses due to positron and photon components of radiation fields around positron sources ^{18}F by using TLDs with different detection efficiencies for positrons was introduced. Measurements of skin dose on the hands of nuclear medicine staff handling ^{18}F -FDG showed significant contributions of a positron component.

TABLE 1. CONTRIBUTION OF POSITRONS TO THE SKIN DOSE ON HANDS DURING PREPARATION AND ADMINISTRATION OF ^{18}F-FDG TO PATIENTS

Handling	Shielding material		Ratio of skin doses MCP-Ns/MCP-7	Contribution of positrons to the total skin dose $H_p(0.07)$
	Thickness (mm)	Density (g/cm^3)		
With unshielded syringe	1.03	0.95	1.2	21%
With distribution vent	0.69–1.5	1.10	1.4	36%
With infusion tube	0.69	1.10	1.8	56%
Contamination by ^{18}F-FDG	0.03	0.95	3.0	85%

The skin dose caused by positron irradiation of hands can be decreased by an additional local shielding of infusion tubes and syringes by a plastic material of a thickness of 1.5 mm. The use of silicon thimbles of a thickness of 1.5 mm applied to the tips of index fingers and thumbs (which are usually exposed to the highest dose levels) is also recommended. The proposed radiation protection measures may decrease the maximum hand skin doses by approximately 30%.

ACKNOWLEDGEMENT

This work was supported by the Ministry of Health of Slovakia, Project No. 2005/26-SZU-04.

REFERENCES

[1] SOARES, C.G., VYNCKIER, S., JÄRVINGEN, H., CROSS, W.G., SIPILÄ, P., FLÚHS, D., SCHACKEN, B., MOURTADA, F.A., BASS, G.A., WILLIAMS, T.T., Dosimetry of beta ray ophthalmic applicators: comparison of different measurement methods, Med. Phys **28**(7) (2001) 1371–1384.

[2] GAZA, R., BULUR, E., McKEEVER, S.W.S., SOARES, C.G., Experimental Determination of the Dose Deposition Profile of a 90Sr Beta Source, Radiation Protection Dosimetry, Vol. 120, No. 1–4 (2006) 33–37.

[3] BILSKI, P., OLKO, P., BURGKHARDT, B., PIESCH, E., Ultra-thin LiF:Mg,Cu,P detectors for beta dosimetry, Proceedings of the International Symposium on Luminescent Detectors and Transformers of Ionizing Radiation, Radiation Measurements (1995), Vol. 24, Issue 4, (1995) 439–443.

[4] COVENS, P., BERUS, D., VANHAVERE, F., CAVELIERS, V., The introduction of automated dispensing and injection during PET procedures: a step in the optimisation of extremity doses and whole-body doses of nuclear medicine staff, Radiation Protection Dosimetry (2010) 10.1093/rpd/ncq110.

EVALUATION OF RADIATION PROTECTION STATUS IN SOME HEALTH CENTRES IN SUDAN

A. SULIEMAN, S. KHALIFA, M. ELFADIL
College of Medical Radiologic Science,
Sudan University of Science and Technology,
Khartoum, Sudan
Email: abdelmoneim_a@yahoo.com

Abstract

This study aims to evaluate the radiation protection status in some health centres, in Omdurman city in Sudan. It was carried out in four health care centres: (Aldaw-Hajoj (A), Abo-Sed (B), Alrakha (C) Wad-Nobawi (D)). The following parameters were investigated: X ray machine performance, ambient dose, patient dose, X ray room design, and radiation protection knowledge for technologists and medical doctors. Thermoluminescence dosimeters (TLDs) were used to measure patients' entrance skin dose (ESD). All the centres investigated are equipped with mobile X ray machines. Radiation exposure surveys were carried out using survey meters and quality control test tools. Knowledge level of doctors concerning radiation doses received by patients when they undergo commonly requested radiological examinations were investigated using questionnaires. The patient dose was measured in 108 patients in four centres in Omdurman city. The mean ESDs were 0.25 mGy for the chest, 0.3 mGy for the upper limbs and 0.4 mGy for the lower limbs. The results of the tests were acceptable in all parameters except the test of filtration, which showed that the filtration was insufficient. The machines at centres A and D were lacking a light beam to check the collimations. The knowledge of medical doctors and technologists in the field of radiation protection concepts is insufficient and in agreement with previous studies.

1. INTRODUCTION

In recent years, there has been increasing concern among patients and radiological workers that unnecessary high levels of radiation are delivered for common X ray examinations should be reduced due to radiation risks. The medical applications of ionizing radiation are accepted worldwide as being essential tools for improving human health. However, they also represent by far the largest manmade source of radiation exposure to the population. It has been estimated that 98.80% of the dose due to artificial sources comes from diagnostic procedures [1].

In the United Kingdom, an estimated 100–250 deaths occur each year from cancers directly related to medical exposure to radiation [2, 3]. Therefore, greater

need for radiation protection seems justified. The growing use of imaging procedures in Sudan has raised concerns about exposure to low dose ionizing radiation in the general population. These departments receive over 1000 patients per month; therefore, there is an imperative need to evaluate the radiation protection status.

Furthermore, no study has been published concerning radiation protection practice in Khartoum State health centres in the literature.

Previous investigations proved that doctors' knowledge of radiation safety is insufficient and hundreds of unnecessary examinations are performed every year [4–7].

The purpose of this study was to investigate the level of protection in four health care centres in Omdurman city concerning the following: (a) the evaluation of the departmental design, shielding and availability of radiation protection accessories (Lead aprons, thyroid shields, etc), (b) the evaluation of the quality control programme and radiation protection status and the method and criteria of equipment selection, (c) and the measurement of the patient radiation dose in common investigations.

2. DESCRIPTION OF SCENARIO SELECTION PROCEDURES

2.1. Dosimeter

TLD GR200A (made up of LiF(Mg,Cu,P)) circular type to measure the patients' doses for different investigations. The high sensitivity to photons and excellent linearity down to few μGy makes it suitable for accurate measurements. In this study, a total of 30 Thermoluminescence dosimeter (TLD) chips were calibrated under reproducible reference conditions using Toshiba Rotande model (T6-6TL-6) against ionization chamber PTW.CONNY II connected to radiation monitor controller at 100 cm SSD, 75 kV and 20 mAs. Both the chamber and electrometer were calibrated for the energy ranges 30–120 kVp at the national standard laboratory. The TLD signal was read using an automatic TLD reader (Fimel PCL3, France) in an atmosphere of inert nitrogen. The readout was at a 155°C, preheat temperature and the signal was acquired from 155–260°C with a heating rate of 11°C/s.

2.2. Patient dose measurements

A total of 108 patients were investigated in this study. The measurements include chest–upper limbs–lower limbs investigations. The entrance skin dose (ESD) was directly measured for the radiographic procedures using three TLDs

(one envelope) placed on the patients' skin surface at the point of insertion of the central axis beam using a very thin envelope made of white polyethylene plastic foil, each containing three TLDs. During the radiographic procedure, the TLDs are kept in the required position and are fixed in place with sticky tape.

2.3. X ray machines

All of these centres are equipped with mobile machines and serve the local community because these departments dedicated to routine (plain) films. The types of machine in all centres are:

Centre	Manufacturer	Filtration (mm Al)	Date of manufacture
Aldaw-Hajoj (A)	ShimadzuR-0CA	1.5	2004
Abou-Sed (B)	ShimadzuR-0CA	1.5	2004
Alraha (C)	ShimadzuR-0CA	1.5	2004
Wad-Noubawi (D)	Siemens	2.0	2006

2.4. Quality control of radiographic units

The three types of quality control tests implemented were visual inspection and performances testing to evaluate the performance of X ray generator and X ray tube. These parameters include reproducibility of exposure factors, radiation output and filtration. Ambient doses were measured using a calibrated survey meter (RDS-120, Universal Survey Meter, range of 0.05–10 μSv/h, Rados Tech, Finland) Measurements were performed at the following locations: the control unit, the door and a dark room. The X ray tube output (mGy/mAs) used a Unfors Xi dosimeter with an accuracy better than 5%.

2.5. The questionnaires

A questionnaire was circulated to 18 medical doctors and 15 technologists working at these centres. Participants were asked about the radiation dose from radiation dose units of measurements, the annual dose from background radiation, biological effects of radiation and methods of radiation protection.

The first questionnaire (for the technologists) was designed to collect data regarding the following parameters: shielding, radiation protection accessories (lead apron, etc.). The second questionnaire was designed to collect the data from the doctors in order to evaluate the justification criteria. The answers were evaluated according to the United Nations Scientific Committee on the Effects of Atomic Radiation (UNSCEAR) 2000 report [1] and were considered correct within a 20% deviation.

3. RESULTS

3.1. Patient dose measurements

This study aimed to evaluate the current status of radiation protection in different centres in Omdurman. Radiation dose measurements were performed in 108 patients (chest–upper and lower limbs–skull).The mean ESDs were 0.25 mGy for the chest, 0.3 mGy for the upper limbs and 0.4 mGy for the lower limbs, as shown in Table 1.

The lowest radiation dose was in centre B (mean of 0.22 mGy) and the highest dose was in centre A (mean of 0.33 mGy). These doses are higher than the DRL suggested by the NRPB [8].

The protection status associated with co-patients was good in the three centres (B, C and D) and high in centre A where the dose rate at the reception reached 100 μSv/h. The radiation dose to the technologists was within the annual limits recommended by ICRP [9] and high in one centre (centre D: 21.12 mGy/a).

3.2. Quality control of radiographic units

The result shows there was radiation leakage in centres A (reception) and centre D (control unit). Measurements were not taken at centre B due to administrative obstacles (Table 1).

3.3. The questionnaires

All the 33 questionnaires were returned. The knowledge of medical doctors in the field of radiation protection concepts was very poor. Therefore, unnecessary exposure and optimization and justification principles were hard to apply. The results of this study showed that all the centres lacked protection accessories (gonad shields, thyroid shield), three centres without lead glass, no radiation protection officer or medical physicist in all centres and as a consequence, no quality control programme or occupational dose monitoring.

TABLE 1. THE MEAN, STANDARD DEVIATION AND RANGE (in parentheses) FOR ALL THE VARIABLES MEASURED FOR ALL THE PATIENTS

Projection	*n*.pt	kVp	mAs	BMI	ESD (mGy)
Chest (PA)	56	62 ± 3.6 (55–73)	12 ± 3.6 (2–20)	29 ± 3.3 (15–32)	0.25 ± 0.04 (0.14–0.36)
Wrist	4	58 ± 4 (55–63)	4.1 ±1.4 (2.5–5)	20.6 ± 5.3 (16.4–24.9)	0.21 ± 0.05 (0.05–25)
Hand	9	52 ± 3.7 (48–60)	7.5 ± 1.8 (3.6–8)	32 ± 2.1 (30.5–33.6)	0.24 ± 0.07 (0.17–0.40)
Forearm	3	56 ± 8.4 (50–62)	7.5 ± 2 (6–9)	32 ± 2.1 (30.5–33.6)	0.40 ± 0.2 (0.27–0.55)
Elbow	8	56.4 ± 5.8 (48–64)	7.1 ± 3.9 (3.6–14)	31 ± 8.2 (22–44)	0.36 ± 0.7 (0.14–0.58)
Shoulder	5	63.6 ± 3.6 (60–68)	7.7 ± 3.6 (3.6–12)	32.2 ± 3.2 (28.3–35.7)	0.25 ± 0.08 (0.16–0.36)
Foot	5	58.4 ± 3.2 (55–62)	8.4 ± 3.2 (5–12)	28 ± 4.4 (23.4–33.4)	0.36 ± 0.13 (0.25–0.6)
Ankle	2	55.5 ± 2.1 (5457)	5.7 ± 0.9 (5–6.4)	30.6 ± 6.5 (26–35.2)	0.26 ± 0.03 (0.24–0.28)
Knee	12	57 ± 4.8 (48–68)	8.4 ± 3 (5–14)	23.4 ± 0.53 (18–26.1)	0.43 ± 0.15 (0.24–0.74)
Skull	1	65.0	12.0	21.4	0.55
Hip	1	80.0	12.0	33.2	0.44
Leg	2	55.5 ± 2.5 (54–57)	12–8 (5.7 ± 0.8) (5–6.4)	30.5 ± 4.5 (26–35)	0.26 ± 0.02 (0.23–0.28)

TABLE 2. THE RESULTS OF THE RADIATION DOSE RATE (μSv/h) AT DIFFERENT LOCATIONS IN THE X RAY ROOM

Centre	Door and reception	Dark room	Control unit
A	100	1	1.0
B	—	—	—
C	0.0[a]	0.0[a]	10
D	0.0[a]	0.0[a]	1.0

[a] Below the detection limit of the survey meter.

Further, 95% of doctors underestimated the radiation risks for paediatric patients, which might lead them to request radiological examinations more often than is necessary and safe. This means increased risk for patients.

4. DISCUSSION

Radiation dose measurement in diagnostic radiology is considered to be a critical factor for optimizing radiation protection to the health care practitioners, the patient and the public. In diagnostic radiology, there is a need to measure patient doses because X rays are potentially harmful. Patient dose must be assessed at least once every three years in order to compare the typical dose for an average sized patient with the DRL [9], which have been expressed in terms of ESD.

4.1. Patient dose measurements

Patient dose depends on many parameters and exposure factors. Although patient dose increases with weight, individual variations can be great (Table 1). ESD was 40% higher than the NRPB study [8]. This result indicates that a low degree of patient dose optimization was achieved in this study. The mean ESD centre A ranged from 0.74 mGy to 0.2 mGy; centre B ranged from 0.44 to 0.14 mGy; centre C ranged from 0.56 mGy to 0.2 mGy; and centre D ranged from 0.55 mGy to 0.19 mGy in all the examinations.

In centres A and B, the ESD were up to 70% higher than the DRL, because there is a light beam collimator.

Patient dose in radiography can be reduced by a number of factors without losing the necessary information for diagnosis; one of these factors is collimation.

Reducing the size of the X ray beam to the minimum size needed to image the object of interest is an obvious means of limiting dose to patients. Limiting beam area on the skin surface also limits the volume of the irradiated patient. In addition to the importance of 'field size' on the patient's skin, the X ray source to skin distance plays a role in limiting doses. Because of the divergence of the X ray beam, increasing this distance reduces the divergence within the patient and therefore reduces the volume irradiated [10].

Increasing the speed class of the film–screen combination will affect both the ESD and effective dose by the same factor. The higher the sensitivity class, the lower the dose, but image quality requirements ultimately limit the range of acceptable sensitivities. In order to obtain an adequate level of patient dose and good image quality, screens must also be matched with the appropriate type of film (green or blue sensitive film). The sensitivity class of the film–screen combination used should be selected according to the type of examination. The quality of the image and the radiation dose depend on the characteristics and condition of the film and intensifying screens used. Therefore, it is important that the screens are carefully handled and kept clean using the manufacturer's recommended products [11].

The optimal choice of energy spectrum depends primarily on patient thickness, contrasting detail, characteristics of the antiscatter grid used, and image receptor and display method. While a 'high kilovolt technique' is desirable in some types of examination, in general, high kilovolt techniques cannot be recommended in cases where high contrast performance is needed. The usual approach is to use the highest kVp that is compatible with the imaging performance required to ensure a diagnostic image [10]. Higher kilovoltages reduce skin dose, but lead to higher 'depth' dose and a greater scattering of X rays [9, 11]

Filtration is used to remove the low energy components of the X ray spectrum which do not contribute to image formation but are absorbed by superficial layers of the tissues.

The minimum total filtration present in a standard general radiographic X ray tube for use up to 100 kVp is not less 2.5 mm of aluminium (in the centres in question, the filtration is 1–2 mm Al), which increases the ESD. If too much additional filtration is used, image quality can be compromised by the reduction in contrast that arises from the harder quality of the incident X ray beam. Also, too much filtration reduces the amount of radiation reaching the film.

Reductions in mAs affect both ESD and effective dose by the same factor. In some cases, there is scope to keep the same mAs by increasing the mA and reducing the time. This also may yield image quality improvements by reducing motion blurring due to shorter exposure time.

In general, reduction of the patient dose can be achieved by using collimation–fast speed screen–high kilovolt techniques. Periodical monitoring of patient doses should be performed every three years as recommended at international levels. Quality control tests are crucial in radiation dose optimization and diagnostic reference levels. Continuous training in radiation protection is vital for medical doctors and technologists.

4.2. Quality control test

Since this study was the first in the field of radiation dose and radiation protection, at the beginning, quality control tests were performed in all X ray departments in order to obtain baseline data for these machines; Table 3 shows the results of quality control tests. The entire test is acceptable except for the filtration.

4.3. Ambient dose

Readings of the survey meter showed that the dose for the worker in centres A and D were (1 μSv/h). Thus, the annual dose can be easily calculated using the working load for staff. Therefore, the annual effective dose for staff ranged from 2.11 mSv to 2.49 mSv, which is acceptable. All the areas surrounding these departments were no radiation leakage accept the reception of centre A, which has the highest dose to the co-patient (100 μSv).

TABLE 3. RESULTS OF QUALITY CONTROL TESTS IN THE CENTRES

Name of test/centre	A	B	C	D
Reproducibility of exposure	<0.05	<0.05	<0.05	<0.05
Radiation output	< 10%	< 10%	< 10%	< 10%
Filtration check	<0.5	<0.5	<0.5	<0.5
kVp accuracy	<4 of each other	<4 of each other	<4 of each other	<4 of each other
mAs linearity	0.0008	0.0007	0.005	0.001
Perpendicularity	—	Acceptable	—	Acceptable
Beam restriction system	—	Acceptable	—	Acceptable

4.4. The questionnaire

The level of doctors' knowledge concerning radiation doses received by patients when they undergo commonly requested radiological investigations is insufficient to protect them from unjustified radiation. For example, only 3% of the doctors had radiation protection courses. The basic rule of radiation protection is not considered during patient imaging; for example, only 18% of the sample asked about the ten day rule (pregnancy); 16% of the images were performed without a suitable request, and the rejection and repetition ratio of the radiograph could reach 30%.

5. CONCLUSION

The knowledge of medical doctors in this study in radiation protection concepts is insufficient and in agreement with previous studies. Therefore, unnecessary exposure, optimization and justification principles are not easily applied. Continuous training in radiation protection is vital for medical doctors and technologists

The results of patient dose measurements indicate that the current pattern of use of diagnostic imaging in these centres is exposing patients to substantial higher doses of ionizing radiation. Strategies for optimizing and ensuring appropriate use of these procedures in the general population should be developed.

REFERENCES

[1] UNITED NATIONS SCIENTIFIC COMMITTEE ON EFFECTS OF ATOMIC RADIATION. SOURCES AND EFFECTS OF IONIZING RADIATION, UNSCEAR 2000, Vol. 1, Report to the General Assembly, UN, New York (2000).

[2] ROYAL COLLEGE OF RADIOLOGISTS, NATIONAL RADIOLOGICAL PROTECTION BOARD, Patient dose reduction in diagnostic radiology. Documents of the National Radiological Protection Board; 1: No 3. (1990).

[3] SHIRALKAR, S., RENNIE, A., SNOW, M., GALLAND, R.B., LEWIS, M.H., GOWER-THOMAS, K., Doctors' knowledge of radiation exposure: Questionnaire study, BMJ **327** (2003) 371–2.

[4] ARSLANOĞLU, A., BILGIN, S., KUBAL., Z., CEYHAN, M., İLHAN, M., MARAL, I., Doctors' and intern doctors' knowledge about patients' ionizing radiation exposure doses during common radiological examinations. Diagn Interv Radiol. **13** (2007) 53–55.

[5] QUINN, A.D., TAYLOR, C.G., SABHARWAL, T., SIKDAR, T., Radiation protection awareness in non-radiologists, Br J Radiol. **70** (1997) 102–106.
[6] JACOB, K., VIVIAN, G., STEEL, J.R., X ray dose training: Are we exposed to enough? Clin Radiol **59** (2004) 928–934.
[7] SOYE, J.A., PATERSON, A., A survey of awareness of radiation dose among health professionals in Northern Ireland, The British Journal of Radiology **81** (2008) 725–729.
[8] HART, D., WALL, B., Radiation exposure of UK population from medical and dental X ray examination, NRPB (2002) 30–31.
[9] INTERNATIONAL COMMISSION OF RADIOLOGICAL PROTECTION. ICRP 103. The 2007 Recommendations of the International Commission on Radiological Protection, Ann, ICRP **103** (2007).
[10] INTERNATIONAL COMMISSION ON RADIOLOGICAL PROTECTION, ICRP Publication 60, Annals Vol. 21, No. 1–3, Pergamon, Oxford, UK (1991).
[11] INTERNATIONAL ATOMIC ENERGY AGENCY, Radiation Doses in Diagnostic Radiology and Methods for Dose Reduction, IAEA-TECDOC-796, IAEA, Vienna (1995).

CHAIRPERSONS OF SESSIONS

Session 1	P.J. ALLISY-ROBERTS	BIPM
	H.M. KRAMER	Germany
	P. ANDREO	Sweden
	A. MEGHZIFENE	IAEA
	K. ROSSER	United Kingdom
	J. SEUNTJENS	AAPM
Session 2	S. HUQ	AAPM
	J. MEDIN	Sweden
	H. PALMANS	United Kingdom
	D.T.L. JONES	ICRU
Session 3	J. VENSELAAR	ESTRO
	D. VAN DER MERWE	South Africa
Session 4	A. TORRESIN	EFOMP
	K. FAULKNER	EFOMP
	J. BOONE	ICRU
	D.R. DANCE	EFOMP
	F. SHANNOUN	WHO
	D. McLEAN	IAEA
Session 5	G.S. IBBOTT	AAPM
	J. VAN DYK	IAEA
Session 6	M. LJUNGBERG	Sweden
	W. BOLCH	ICRP
	G. SGOUROS	SNM
	S. PALM	IAEA
Session 7	D. THWAITES	ESRO
	J. IZEWSKA	IAEA
Session 8	Z. KNEZEVIC	Croatia
	R. CRUZ-SUÁREZ	IAEA

SECRETARIAT OF THE SYMPOSIUM

A. MEGHZIFENE	Scientific Secretary
M. KHAELSS	Conference Services
D. UMGEHER	Conference Services
J. INCE	Administrative Support
S. STEYSKAL	Administrative Support
E. POSTA	Administrative Support
B. HALL	Proceedings Editor
R.J. BENBOW	Coordinating Editor

PROGRAMME COMMITTEE

P.J. ALLISY-ROBERTS	BIPM
H. AMOLS	AAPM
P. ANDREO	Sweden
R. CRUZ-SUÁREZ	IAEA
K. FAULKNER	EFOMP
D.S. FOLLOWILL	AAPM
D. GEORG	IOMP
O. HOLMBERG	IAEA
J. IZEWSKA	IAEA
D.T.L. JONES	ICRU
A. KESNER	IAEA
M. KRAMER	Germany
D. McLEAN	IAEA
A. MEGHZIFENE	IAEA
S. PALM	IAEA
G. SGOUROS	SNM
F. SHANNOUN	WHO
H. SVENSSON	IOMP
D. THWAITES	ESTRO
A. TORRESIN	EFOMP
D. VAN DER MERWE	South Africa
J. VAN DYK	IAEA
J. VENSELAAR	ESTRO

AUTHOR INDEX

IAEA
International Atomic Energy Agency

Where to order IAEA publications

In the following countries IAEA publications may be purchased from the sources listed below, or from major local booksellers. Payment may be made in local currency or with UNESCO coupons.

AUSTRALIA
DA Information Services, 648 Whitehorse Road, MITCHAM 3132
Telephone: +61 3 9210 7777 • Fax: +61 3 9210 7788
Email: service@dadirect.com.au • Web site: http://www.dadirect.com.au

BELGIUM
Jean de Lannoy, avenue du Roi 202, B-1190 Brussels
Telephone: +32 2 538 43 08 • Fax: +32 2 538 08 41
Email: jean.de.lannoy@infoboard.be • Web site: http://www.jean-de-lannoy.be

CANADA
Bernan Associates, 4501 Forbes Blvd, Suite 200, Lanham, MD 20706-4346, USA
Telephone: 1-800-865-3457 • Fax: 1-800-865-3450
Email: customercare@bernan.com • Web site: http://www.bernan.com

Renouf Publishing Company Ltd., 1-5369 Canotek Rd., Ottawa, Ontario, K1J 9J3
Telephone: +613 745 2665 • Fax: +613 745 7660
Email: order.dept@renoufbooks.com • Web site: http://www.renoufbooks.com

CHINA
IAEA Publications in Chinese: China Nuclear Energy Industry Corporation, Translation Section, P.O. Box 2103, Beijing

CZECH REPUBLIC
Suweco CZ, S.R.O., Klecakova 347, 180 21 Praha 9
Telephone: +420 26603 5364 • Fax: +420 28482 1646
Email: nakup@suweco.cz • Web site: http://www.suweco.cz

FINLAND
Akateeminen Kirjakauppa, PO BOX 128 (Keskuskatu 1), FIN-00101 Helsinki
Telephone: +358 9 121 41 • Fax: +358 9 121 4450
Email: akatilaus@akateeminen.com • Web site: http://www.akateeminen.com

FRANCE
Form-Edit, 5, rue Janssen, P.O. Box 25, F-75921 Paris Cedex 19
Telephone: +33 1 42 01 49 49 • Fax: +33 1 42 01 90 90
Email: formedit@formedit.fr • Web site: http://www. formedit.fr

Lavoisier SAS, 145 rue de Provigny, 94236 Cachan Cedex
Telephone: + 33 1 47 40 67 02 • Fax +33 1 47 40 67 02
Email: romuald.verrier@lavoisier.fr • Web site: http://www.lavoisier.fr

GERMANY
UNO-Verlag, Vertriebs- und Verlags GmbH, Am Hofgarten 10, D-53113 Bonn
Telephone: + 49 228 94 90 20 • Fax: +49 228 94 90 20 or +49 228 94 90 222
Email: bestellung@uno-verlag.de • Web site: http://www.uno-verlag.de

HUNGARY
Librotrade Ltd., Book Import, P.O. Box 126, H-1656 Budapest
Telephone: +36 1 257 7777 • Fax: +36 1 257 7472 • Email: books@librotrade.hu

INDIA
Allied Publishers Group, 1st Floor, Dubash House, 15, J. N. Heredia Marg, Ballard Estate, Mumbai 400 001,
Telephone: +91 22 22617926/27 • Fax: +91 22 22617928
Email: alliedpl@vsnl.com • Web site: http://www.alliedpublishers.com

Bookwell, 2/72, Nirankari Colony, Delhi 110009
Telephone: +91 11 23268786, +91 11 23257264 • Fax: +91 11 23281315
Email: bookwell@vsnl.net

ITALY
Libreria Scientifica Dott. Lucio di Biasio “AEIOU”, Via Coronelli 6, I-20146 Milan
Telephone: +39 02 48 95 45 52 or 48 95 45 62 • Fax: +39 02 48 95 45 48
Email: info@libreriaaeiou.eu • Website: www.libreriaaeiou.eu

JAPAN
Maruzen Company, Ltd., 13-6 Nihonbashi, 3 chome, Chuo-ku, Tokyo 103-0027
Telephone: +81 3 3275 8582 • Fax: +81 3 3275 9072
Email: journal@maruzen.co.jp • Web site: http://www.maruzen.co.jp

REPUBLIC OF KOREA
KINS Inc., Information Business Dept. Samho Bldg. 2nd Floor, 275-1 Yang Jae-dong SeoCho-G, Seoul 137-130
Telephone: +02 589 1740 • Fax: +02 589 1746 • Web site: http://www.kins.re.kr

NETHERLANDS
De Lindeboom Internationale Publicaties B.V., M.A. de Ruyterstraat 20A, NL-7482 BZ Haaksbergen
Telephone: +31 (0) 53 5740004 • Fax: +31 (0) 53 5729296
Email: books@delindeboom.com • Web site: http://www.delindeboom.com

Martinus Nijhoff International, Koraalrood 50, P.O. Box 1853, 2700 CZ Zoetermeer
Telephone: +31 793 684 400 • Fax: +31 793 615 698
Email: info@nijhoff.nl • Web site: http://www.nijhoff.nl

Swets and Zeitlinger b.v., P.O. Box 830, 2160 SZ Lisse
Telephone: +31 252 435 111 • Fax: +31 252 415 888
Email: infoho@swets.nl • Web site: http://www.swets.nl

NEW ZEALAND
DA Information Services, 648 Whitehorse Road, MITCHAM 3132, Australia
Telephone: +61 3 9210 7777 • Fax: +61 3 9210 7788
Email: service@dadirect.com.au • Web site: http://www.dadirect.com.au

SLOVENIA
Cankarjeva Zalozba d.d., Kopitarjeva 2, SI-1512 Ljubljana
Telephone: +386 1 432 31 44 • Fax: +386 1 230 14 35
Email: import.books@cankarjeva-z.si • Web site: http://www.cankarjeva-z.si/uvoz

SPAIN
Díaz de Santos, S.A., c/ Juan Bravo, 3A, E-28006 Madrid
Telephone: +34 91 781 94 80 • Fax: +34 91 575 55 63
Email: compras@diazdesantos.es, carmela@diazdesantos.es, barcelona@diazdesantos.es, julio@diazdesantos.es
Web site: http://www.diazdesantos.es

UNITED KINGDOM
The Stationery Office Ltd, International Sales Agency, PO Box 29, Norwich, NR3 1 GN
Telephone (orders): +44 870 600 5552 • (enquiries): +44 207 873 8372 • Fax: +44 207 873 8203
Email (orders): book.orders@tso.co.uk • (enquiries): book.enquiries@tso.co.uk • Web site: http://www.tso.co.uk

On-line orders
DELTA Int. Book Wholesalers Ltd., 39 Alexandra Road, Addlestone, Surrey, KT15 2PQ
Email: info@profbooks.com • Web site: http://www.profbooks.com

Books on the Environment
Earthprint Ltd., P.O. Box 119, Stevenage SG1 4TP
Telephone: +44 1438748111 • Fax: +44 1438748844
Email: orders@earthprint.com • Web site: http://www.earthprint.com

UNITED NATIONS
Dept. I004, Room DC2-0853, First Avenue at 46th Street, New York, N.Y. 10017, USA
(UN) Telephone: +800 253-9646 or +212 963-8302 • Fax: +212 963-3489
Email: publications@un.org • Web site: http://www.un.org

UNITED STATES OF AMERICA
Bernan Associates, 4501 Forbes Blvd., Suite 200, Lanham, MD 20706-4346
Telephone: 1-800-865-3457 • Fax: 1-800-865-3450
Email: customercare@bernan.com · Web site: http://www.bernan.com

Renouf Publishing Company Ltd., 812 Proctor Ave., Ogdensburg, NY, 13669
Telephone: +888 551 7470 (toll-free) • Fax: +888 568 8546 (toll-free)
Email: order.dept@renoufbooks.com • Web site: http://www.renoufbooks.com

Orders and requests for information may also be addressed directly to:

Marketing and Sales Unit, International Atomic Energy Agency
Vienna International Centre, PO Box 100, 1400 Vienna, Austria
Telephone: +43 1 2600 22529 (or 22530) • Fax: +43 1 2600 29302
Email: sales.publications@iaea.org • Web site: http://www.iaea.org/books

11-15861

The use of properly calibrated dosimeters, together with approved codes of practice and peer reviewed quality assurance programmes, is essential for ensuring safe and effective diagnosis and treatment of patients with ionizing radiation. Owing to its dual role in disseminating radiation measurement standards and verifying the accuracy of dosimetry applied at the hospital level, the IAEA is well positioned to convene international meetings focused on dosimetry and relevant quality assurance programmes. The International Symposium on Standards, Applications and Quality Assurance in Medical Radiation Dosimetry (IDOS), which was held at the IAEA in Vienna on 9–12 November 2010, provided a unique opportunity to review advances in radiation dosimetry during the last decade, since the previous international symposium on the same topic was held in 2002. These proceedings present the conclusions reached at the end of the symposium as well as a refereed selection of papers that were given at the symposium. Emphasis was placed on dosimetry standards and implementation of dosimetry protocols in therapeutic and imaging applications of radiation in medicine. A key 'take home' message was that advances in technology for radiation therapy dose delivery require vigilance to ensure adequate quality control. In the future, advances in diagnostic capabilities may lead to better therapy planning. Certainly, the coupling between diagnostic information and therapy delivery is expected to strengthen. In this case, many challenges in dosimetry remain to be solved.

INTERNATIONAL ATOMIC ENERGY AGENCY
VIENNA
ISBN 978–92–0–116210–6
ISSN 0074–1884